

Master of Science in
Computacional Mechanics

Erasmus Mundos
Master Course

INTRODUCTION TO
THE FINITE ELEMENT METHOD

Lectures

EUGENIO OÑATE
PEDRO DÍEZ
FRANCISCO ZÁRATE
ANTONIA LARESE

October 2008

Contents

1	INTRODUCTION TO THE FINITE ELEMENT METHOD	1
1.1	WHAT IS THE FINITE ELEMENT METHOD?	1
1.2	ANALYTICAL AND NUMERICAL METHODS	1
1.3	WHAT IS A FINITE ELEMENT?	2
1.4	STRUCTURAL MODELLING AND FEM ANALYSIS	3
1.4.1	Classification of the problem	3
1.4.2	Structural model	3
1.4.3	Structural analysis by the FEM	5
1.4.4	Verification and validation of FEM results	6
1.5	DISCRETE SYSTEMS. BAR STRUCTURES	9
1.5.1	Basic concepts of matrix analysis of bar structures	10
1.5.2	Analogy with the matrix analysis of other discrete systems	13
1.5.3	Basic steps for matrix analysis of discrete systems	15
1.6	DIRECT ASSEMBLY OF THE GLOBAL STIFFNESS MATRIX	17
1.7	DERIVATION OF THE MATRIX EQUILIBRIUM EQUATIONS FOR THE BAR ELEMENT USING THE PRINCIPLE OF VIRTUAL WORK	19
1.8	DERIVATION OF THE BAR EQUILIBRIUM EQUATIONS VIA THE MINIMUM TOTAL POTENTIAL ENERGY PRINCIPLE	20
1.9	PLANE PIN-JOINTED FRAMEWORKS	22
1.10	TREATMENT OF PRESCRIBED DISPLACEMENTS AND COMPUTATION OF REACTIONS	24
1.11	INTRODUCTION TO THE FINITE ELEMENT METHOD FOR ANALYSIS OF CONTINUUM SYSTEMS	27

Contents

2	FEM ANALYSIS OF 1D PROBLEMS. APPLICATION TO THE POISSON EQUATION	33
2.1	INTRODUCTION	33
2.2	THE POISSON EQUATION	34
2.3	WEIGHTED RESIDUAL METHOD	40
2.3.1	Approximation of the unknown. Weighted Residuals	42
2.3.2	Application of the WRM for the solution of the 1D heat conduction equation	43
2.3.3	Global definition of the shape functions	45
2.3.4	Point Collocation Method	48
2.3.5	Subdomain collocation method	51
2.3.6	Galerkin method	53
2.3.7	Least square method	55
2.4	GENERAL SOLUTION PROCEDURE	59
2.4.1	Conclusions	61
2.5	INTEGRABILITY CONDITION	62
2.6	WEAK FORM OF THE WEIGHTED RESIDUAL METHOD	62
2.6.1	Natural boundary condition	64
2.6.2	Discretization of the weak form	64
2.7	DERIVATION OF THE PRINCIPLE OF VIRTUAL WORK FROM THE WEIGHTED RESIDUAL METHOD	71
2.8	THE PVW IN POISSON PROBLEMS	73
2.9	THE FEM IN 1D POISSON PROBLEMS	73
2.9.1	Discretization of the problem. Local definition of the shape functions	75
2.9.2	Derivation of the algebraic equation systems. Solution of the 1D Poisson problem using one 2-noded 1D element	77
2.9.3	Solution of the 1D Poisson problem using two 2-noded elements	81
2.10	GENERALIZATION OF THE SOLUTION FOR A MESH OF TWO-NODED ELEMENTS	85

Contents

3	1D FINITE ELEMENTS FOR AXIALLY LOADED RODS	87
3.1	INTRODUCTION	87
3.2	AXIALLY LOADED ROD	87
3.3	AXIALLY LOADED ROD OF CONSTANT CROSS SECTIONAL AREA. DISCRETIZATION IN ONE LINEAR ROD ELEMENT	89
3.4	DERIVATION OF THE DISCRETIZED EQUATIONS FROM THE GLOBAL DISPLACEMENT INTERPOLATION FIELD	94
3.5	AXIALLY LOADED ROD OF CONSTANT CROSS SECTIONAL AREA. DISCRETIZATION IN TWO LINEAR ROD ELEMENTS	97
3.6	GENERALIZATION OF THE SOLUTION WITH N LINEAR ROD ELEMENTS	102
3.7	EXTRAPOLATION OF THE SOLUTION FROM TWO DIFFERENT MESHES	106
3.8	MATRIX FORMULATION OF THE ELEMENT EQUATIONS	108
	3.8.1 Shape function matrix	109
	3.8.2 Strain matrix	109
	3.8.3 Constitutive matrix	109
	3.8.4 Principle of Virtual Work	110
	3.8.5 Stiffness matrix and equivalent nodal force vector	110
3.9	SUMMARY OF THE STEPS FOR THE ANALYSIS OF A STRUCTURE USING THE FEM	112
3.10	ADVANCED ROD ELEMENTS AND REQUIREMENTS FOR THE NUMERICAL SOLUTION	113
	3.10.1 INTRODUCTION	113
3.11	ONE DIMENSIONAL C^0 ELEMENTS. LAGRANGE ELEMENTS	114
3.12	ISOPARAMETRIC FORMULATION AND NUMERICAL INTEGRATION	117
	3.12.1 Introduction	117
	3.12.2 The concept of parametric interpolation	118
	3.12.3 Isoparametric formulation of the two-noded rod element	120
	3.12.4 Isoparametric formulation of the 3-noded quadratic rod element	121

3.13	NUMERICAL INTEGRATION	123
3.14	STEPS FOR THE COMPUTATION OF MATRICES AND VEC- TORS FOR AN ISOPARAMETRIC ROD ELEMENT	125
3.14.1	Interpolation of the axial displacement	126
3.14.2	Geometry interpolation	126
3.14.3	Interpolation of the axial strain	126
3.14.4	Computation of the axial force	127
3.14.5	Element stiffness matrix	127
3.14.6	Equivalent nodal force vector	128
3.15	BASIC ORGANIZATION OF A FINITE ELEMENT PROGRAM	129
3.16	SELECTION OF ELEMENT TYPE	129
3.17	REQUIREMENTS FOR CONVERGENCE OF THE SOLUTION	133
3.17.1	Continuity condition	133
3.17.2	Derivativity condition	133
3.17.3	Integrability condition	133
3.17.4	Rigid body condition	134
3.17.5	Constant strain condition	134
3.18	ASSESSMENT OF CONVERGENCE REQUIREMENTS. THE PATCH TEST	135
3.19	OTHER REQUIREMENTS FOR THE FINITE ELEMENT AP- PROXIMATION	137
3.19.1	Compatibility condition	137
3.19.2	Condition of complete polynomial	137
3.19.3	Stability condition	138
3.19.4	Geometric invariance condition	139
3.20	SOME REMARKS ON THE COMPATIBILITY AND EQUILIB- RIUM OF THE SOLUTION	139
3.21	CONVERGENCE REQUIREMENTS IN ISOPARAMETRIC EL- EMENTS	141
3.22	ERROR TYPES IN THE FINITE ELEMENT SOLUTION	142
3.22.1	Discretization error	142
3.22.2	Error in the geometry approximation	143
3.22.3	Error in the computation of the element integrals	144
3.22.4	Errors in the solution of the global equation system	144
3.22.5	Errors associated with the constitutive equation	146

Contents

7	SHAPE FUNCTIONS FOR 2D AND 3D ELEMENTS WITH C^o CONTINUITY	183
7.1	INTRODUCTION	183
7.2	DERIVATION OF THE SHAPE FUNCTIONS FOR C^o TWO DIMENSIONAL ELEMENTS	183
7.2.1	Complete polynomials in two dimensions. Pascal's triangle	183
7.2.2	Shape functions of C^o rectangular elements. Natural coordinates in two dimensions	184
7.3	LAGRANGE RECTANGULAR ELEMENTS	186
7.3.1	Four-noded Lagrange rectangle	186
7.3.2	Nine-noded quadratic Lagrange rectangle	186
7.3.3	Sixteen-noded cubic Lagrange rectangle	190
7.3.4	Other Lagrange rectangular elements	190
7.4	SERENDIPITY RECTANGULAR ELEMENTS	191
7.4.1	Eighth-noded quadratic Serendipity rectangle	192
7.4.2	Twelve-noded cubic Serendipity rectangle	194
7.4.3	Seventeen-noded quartic Serendipity rectangle	195
7.5	SHAPE FUNCTIONS FOR C^o CONTINUOUS TRIANGULAR ELEMENTS	196
7.5.1	Area coordinates	196
7.5.2	Derivation of the shape functions for C^o continuous triangles	198
7.5.3	Shape functions for the 3-noded linear triangle	198
7.5.4	Shape functions for the six-noded quadratic triangle	199
7.5.5	Shape functions for the ten-noded cubic triangle	200
7.5.6	Natural coordinates for triangles	201
7.6	ANALYTIC COMPUTATION OF INTEGRALS OVER RECTANGLES AND STRAIGHT SIDE TRIANGLES	201
7.7	SHAPE FUNCTIONS FOR 3D ELEMENTS	205
7.8	RIGHT PRISMS	205
7.8.1	Right prisms of the Lagrange family	206
7.8.2	Serendipity prisms	209
7.9	STRAIGHT EDGED TETRAHEDRA	215
7.9.1	Shape functions for the 10-noded quadratic tetrahedron	219

7.9.2	Shape functions for the 20-noded quadratic tetrahedron .	220
7.10	COMPUTATION OF THE ELEMENT INTEGRALS	221
7.10.1	Analytical computation of element integrals	221

Contents

9	2D SOLIDS. LINEAR TRIANGULAR AND RECTANGULAR ELEMENTS	259
9.1	INTRODUCTION	259
9.2	TWO DIMENSIONAL ELASTICITY THEORY	260
9.2.1	Displacement field	260
9.2.2	Strain field	261
9.2.3	Stress field	262
9.2.4	Stress-strain relationship	262
9.2.5	Virtual work expression	270
9.3	FINITE ELEMENT FORMULATION. THREE-NODED SOLID TRIANGULAR ELEMENT	270
9.3.1	Discretization of the displacement field	271
9.3.2	Discretization of the strain field	273
9.3.3	Discretization of the stress field	275
9.3.4	Discretized equilibrium equations	275
9.3.5	Stiffness matrix and equivalent nodal force vectors for the 3-noded solid triangular element	278
9.4	THE FOUR NODED SOLID RECTANGULAR ELEMENT	282
9.4.1	Basic formulation	282
9.4.2	Some remarks on the behaviour of the 4-noded solid rectangle	286
9.5	PERFORMANCE OF THE 3-NODED SOLID TRIANGLE AND THE 4-NODED SOLID RECTANGLE	289
9.6	GENERAL PERFORMANCE OF TRIANGULAR AND RECTANGULAR ELEMENTS	291
9.7	CONCLUDING REMARKS	293
10	REFERENCES	295

Chapter 1

INTRODUCTION TO THE FINITE ELEMENT METHOD

1.1 WHAT IS THE FINITE ELEMENT METHOD?

The finite element method (FEM) is a procedure for the numerical solution of the equations which govern problems found in nature. Usually the behaviour of nature can be described by equations expressed in differential or integral form. For this reason the FEM is understood in mathematical circles as a numerical technique for solving partial differential or integral equations. Generally, the FEM allows to obtain the evolution in space and/or time of one or more variables representing the behaviour of a physical system.

When referred to the analysis of structures the FEM is a powerful method for computing the displacements, stresses and strains in a structure under a set of loads. This is precisely what we aim to study in this book.

1.2 ANALYTICAL AND NUMERICAL METHODS

The conceptual difference between analytical and numerical methods is that the former search for the universal mathematical expressions representing the general and “exact” solution of a problem governed typically by mathematical equations. Unfortunately exact solutions are only possible for a few particular cases which frequently represent coarse simplifications of reality.

On the other hand, numerical methods, such as the FEM aim to providing a solution, in the form of a set of numbers, to the mathematical equations governing a problem. The strategy followed by most numerical methods is to transform the mathematical equations into a set of algebraic equations which depend on a finite set of parameters. These equations in the practical case involve many thousands (or even millions) of unknowns and therefore the final system of algebraic equations can only be solved with the help of computers. This explains why even though many numerical methods have been known

since the XVIII century, their development and popularity has occurred in tandem to the progress of modern computers in the XX century. The term *numerical method* is synonym of *computational method* in this text.

Numerical methods represent, in fact, the return of numbers as the true protagonists in the solution of a problem. The loop initiated by Pythagoras some 25 centuries ago has been closed in the last few decades with the evidence that, with the help of numerical methods, we can find precise answers to any problem in science and engineering.

We should keep in mind that numerical methods for structural engineering are inseparable from mathematics, material modelling and computer science. Nowadays it is unthinkable to attempt the development of a new numerical method for the solution of a structural problem without referring to those disciplines. As an example, any numerical method for solving large scale structural problems has to take into account the hardware environment where it will be implemented (most probably using parallel computing facilities). Also a modern computer program for structural analysis should be able to incorporate the continuous advances in the modelling of new materials.

The word which perhaps best synthesizes the immediate future of numerical methods is “computational multiphysics”. The solution of problems will not be attempted from the perspective of a single physical field and it will involve all the couplings which characterize the complexity of reality. For instance, the design of a structural component for a vehicle (an automobile, an aeroplane, etc.) will take into account the manufacturing process and the function which the component will play throughout its life time. Structures in civil engineering will be studied considering the surrounding environment (soil, water, air). Similar examples are found in mechanical, naval and aeronautical engineering and indeed in practically all branches of engineering science. Accounting for the non-deterministic character of data will be essential for estimating the probability that the new products and processes conceived by men behave as planned. The huge computational needs resulting from a “stochastic multiphysics” viewpoint will demand better numerical methods, new material models and, indeed, faster computers.

It is only through the integration of a deep knowledge of the physical and mathematical basis of a problem and of numerical methods and informatics, that effective solutions will be found for the mega-structural problems of the twenty-first century.

1.3 WHAT IS A FINITE ELEMENT?

A finite element can be visualized as a small portion of a continuum (i.e. a structure). The word “finite” distinguishes such a portion from the “infinitesimal” elements of a differential calculus. The geometry of the continuum is considered to be formed by the assembly of a collection of non-overlapping domains with simple geometry termed finite elements (i.e. triangles and quadri-

laterals in 2D, or tetrahedra and hexahedra in 3D). It is usually said that a “mesh” of finite elements “discretizes” the continuum (Figure 1.1). The space variation of the problem parameters (i.e. the displacements in a structure) is expressed within each element by means of a polynomial expansion. Given that the “exact” analytical variation of such parameters is more complex (and generally unknown), the FEM only provides an *approximation* to the exact solution.

1.4 STRUCTURAL MODELLING AND FEM ANALYSIS

1.4.1 Classification of the problem

The first step in the solution of a problem is the identification of the problem itself. Hence, before we can analyze a structure we must ask ourselves the following questions: Which are the more relevant physical phenomena influencing the structure? Is the problem of static or dynamic type? Are the kinematics or the material properties linear or non-linear? Which are the key results requested? What is the level of accuracy sought? The answers to these questions are essential for selecting a structural model and the adequate computational method.

1.4.2 Structural model

Computational methods, such as the FEM, are applied to “models” of a real problem, and not to the actual problem itself. Even experimental methods in structural laboratories make use of scale physical models, unless the actual structure is tested in real size, which rarely occurs. Models can be developed once the physical nature of a problem is clearly understood. In the derivation of a model we should aim to exclude superfluous details and include all the relevant features of the problem under consideration so that the model can describe reality with enough accuracy.

A *structural model* must include three fundamental aspects. The *geometric description* of the actual structure by means of its specific geometrical components (points, lines, surfaces, volumes), the *mathematical expression* of the basic physical laws governing the behaviour of the structure (i.e. force-equilibrium equations) usually written in terms of differential and/or integral equations, and the specification of the *properties of the materials* in the structure. Note that the same structure can be analyzed using different structural models depending on the accuracy and/or simplicity sought in the analysis. As an example, a beam can be modelled using the more general 3D elasticity theory, the 2D plane stress theory or the simpler beam theory. Each model provides a different set out for the analysis of the actual structure. We should bear in mind that the solution taking as its starting point an incorrect structural model, even if obtained with the most accurate numerical method, will



Fig. 1.1: Discretization of different solids and structures into finite elements

be a wrong solution, far from correct physical values.

In this book we will study the analysis by the FEM of a number of structural models, each one applicable to one or more practical structural types. The material properties in all cases will be considered to be *linear elastic*.

Furthermore the analysis will be restricted to *linear kinematics* and to *static loading*. The structures are therefore analyzed under ***linear static conditions***. Despite their simplicity, these assumptions are applicable to most of the situations found in the everyday practice of structural analysis and design.

The structural models considered in this book are classified as *solid models* (2D/3D solids and axisymmetric solids), *beam and plate models* and *shell models* (faceted shells, axisymmetric shells and curved shells). Figure 1.2 shows the general features of a typical member of each structural model family. The structures that can be analyzed with these models cover the main problems in structural engineering and include frames, dams, retaining walls, tunnels, bridges, cylindrical tanks, shell roofs, ship hulls, mechanical parts, airplane fuselages, vehicle components, etc.

1.4.3 Structural analysis by the FEM

The geometry of a structure is *discretized* when it is split into a mesh of finite elements of a certain accuracy. Clearly the discretization introduces another approximation. With respect to reality we have therefore to account for two error sources from the outset: the *modelling error* and the *discretization error*. The former can be reduced by improving the structural model which describes the actual behaviour of the structure, as previously explained. The discretization error, on the other hand, can be reduced by using a finer mesh (i.e. more elements), or else by increasing the accuracy of the finite elements chosen using higher order polynomial expansions for approximating the displacement field within each element. We have to recall that even if we could reduce the discretization error to zero, we would not be able to reproduce accurately the actual behaviour of the structure, unless the structural model was perfect.

Additionally, the use of computers introduces *numerical errors* associated with the ability of the computer to represent data accurately with numbers of finite precision. The numerical error is usually small, although it can be large in some problems, such as when some parts of the structure have very different physical properties. The sum of discretization and numerical errors contribute to the *error of the computational method*.

Figures 1.3(a) and (b) show schematically the discretization of some geometrical models of structures using specific finite elements. Figure 1.4 shows the actual image of a car panel, the geometrical definition of the panel surface by means of NURBS (non-uniform rational b-splines) patches using computer-aided design (CAD) tools, the discretization of the surface by a mesh of 3-noded shell triangles and some numerical results of the FEM analysis. The differences between the real structure of the panel, the geometrical description and the analysis mesh can be seen clearly. A similar example of the FEM analysis of an office building is shown in Figure 1.5.

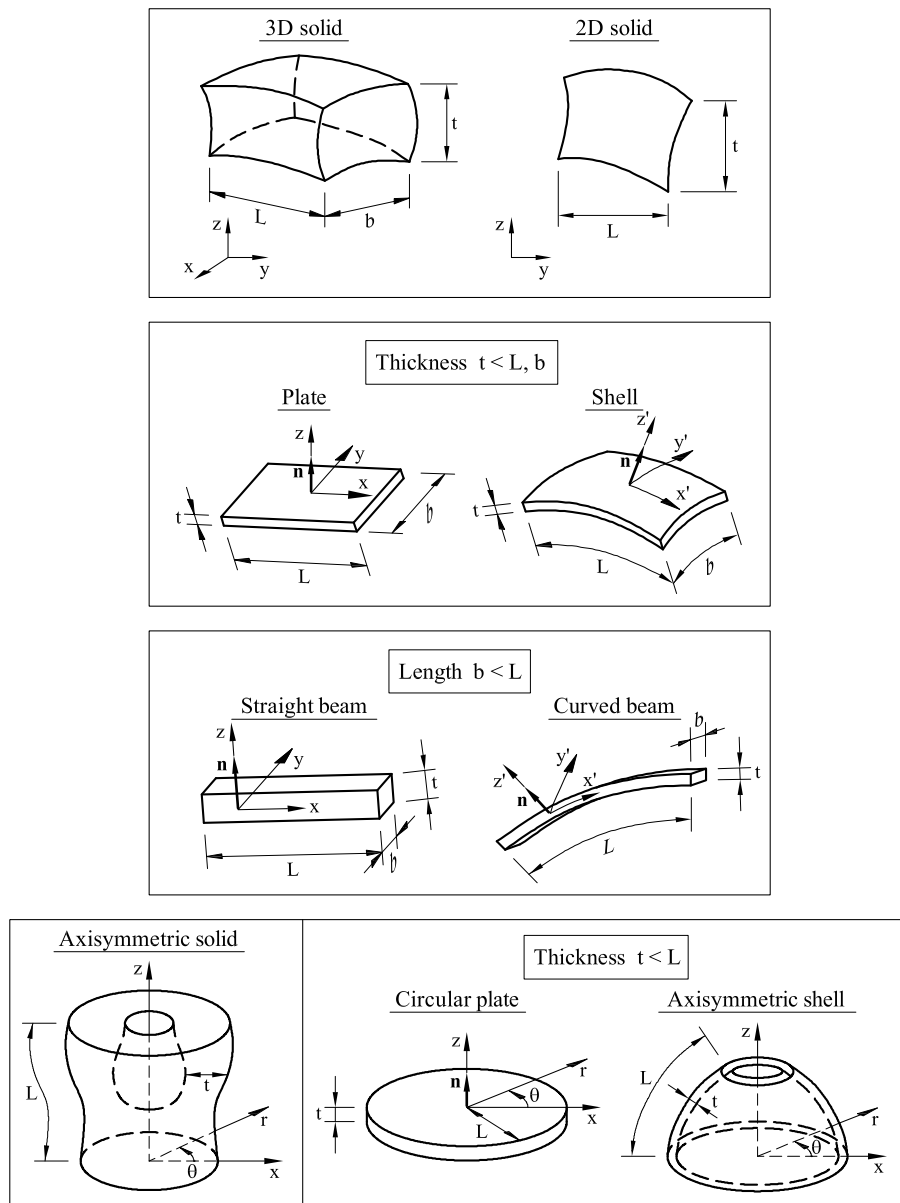


Fig. 1.2: Structural models for some structures

1.4.4 Verification and validation of FEM results

Developers of structural finite element computer codes, analysts who use the codes and decision makers who rely on the results of the analysis face a critical question: How should confidence in modelling and computation be critically assessed? *Validation* and *verification* of FEM computations are the primary methods for building and quantifying this confidence. In essence, validation is the assessment of the accuracy of both the structural and computational models by comparison of the numerical results with *experimental data*. Experiments can be performed in laboratory using scale models of a structure

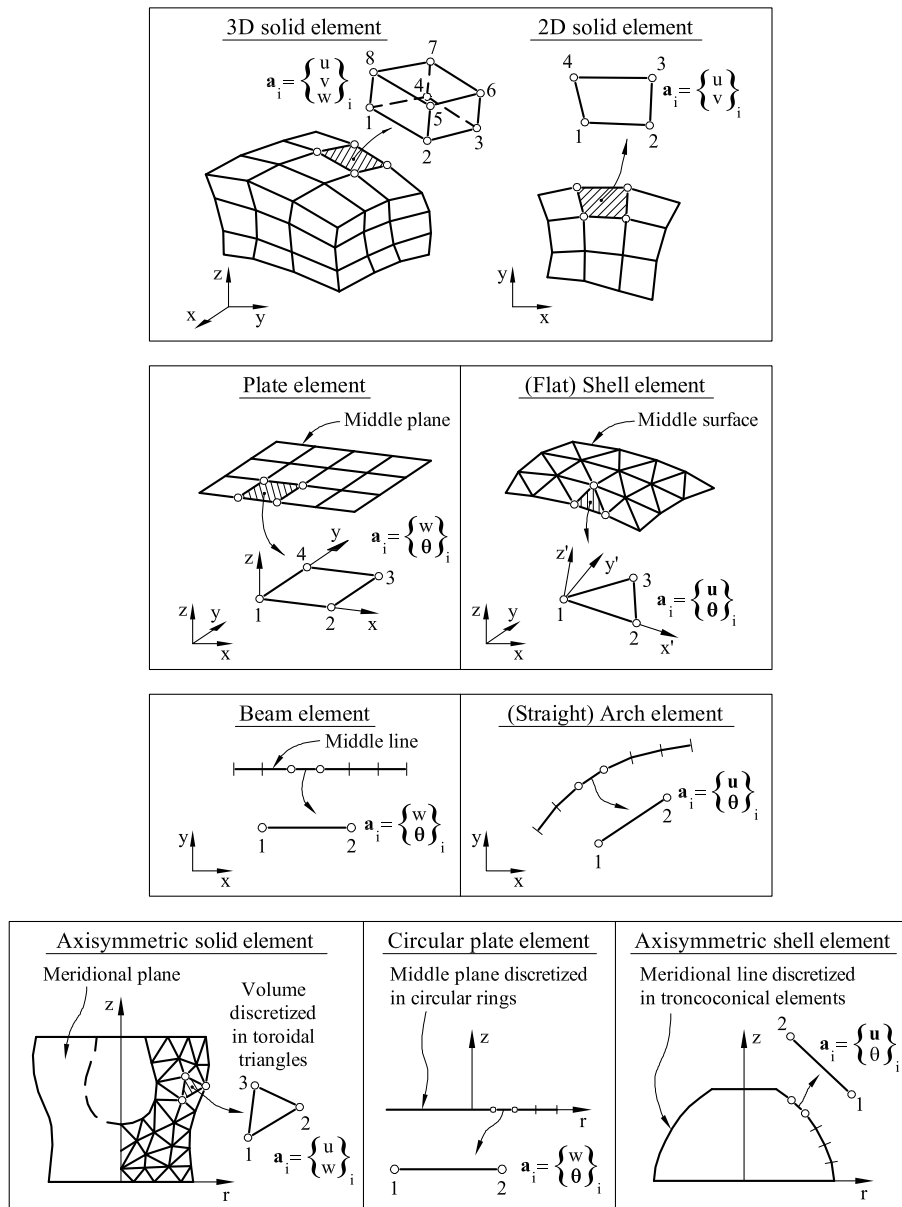


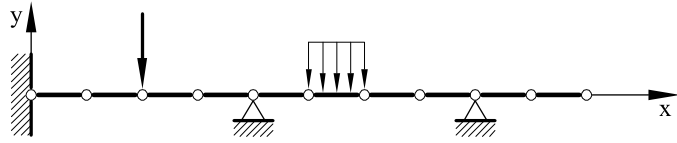
Fig. 1.3: (a) Discretization of structural models into finite elements

or on actual structures. The correct definition of the experimental tests and the reliability of the experimental results are crucial issues in the validation process.

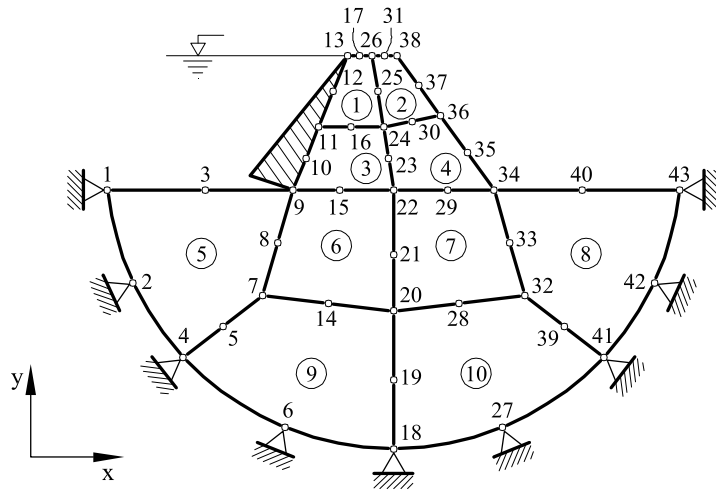
In verification, on the other hand, the relationship between the numerical results to the real world is not an issue. The verification of FEM computations is usually made by comparing the numerical results for simple benchmark problems with “exact” solutions obtained analytically, or using more accurate numerical methods.

Figure 1.6 shows a scheme of the validation and verification procedures.

a) Beam discretized with 1D finite elements



b) Gravity dam and soil discretized with 2D finite elements



c) Double curvature dam and soil discretized with 3D solid finite elements

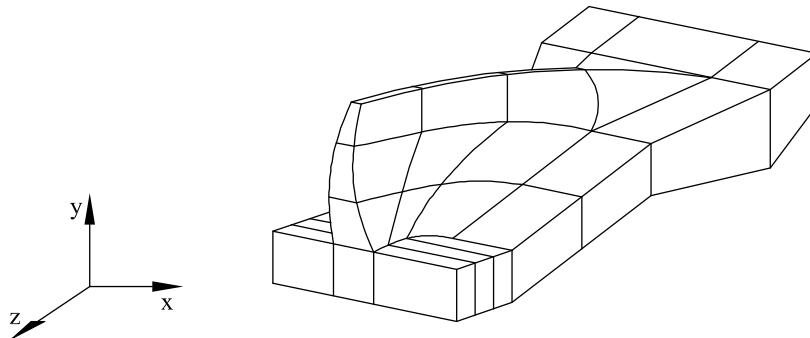


Fig. 1.3: (b) Discretization of structural models in one-, two- and three-dimensional finite elements

The verification process is typically performed first in order to evaluate and reduce the possible sources of numerical error (i.e. discretization error, numerical errors, etc.). These errors can be appraised using error estimation techniques. A more accurate numerical solution can be found with a finer discretization or by using higher order elements (Chapter 0). The subsequent experimental validation provides insight on the capacity of the overall structural model to

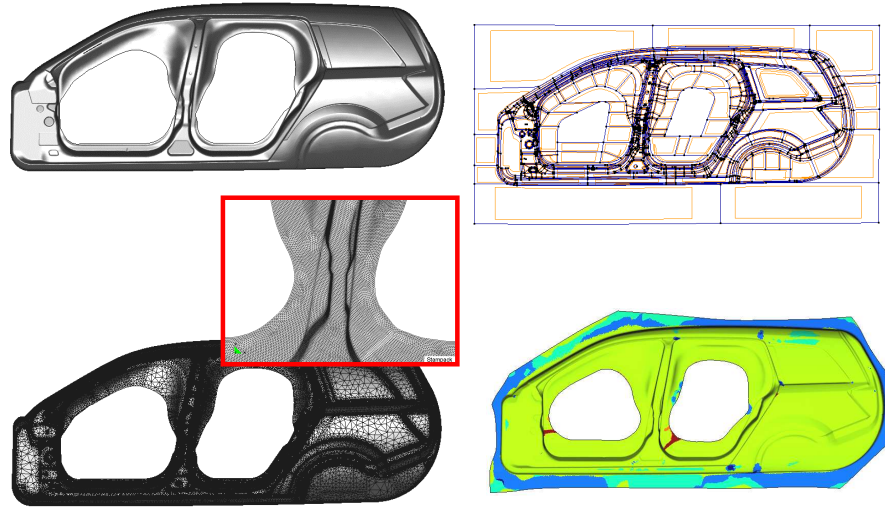


Fig. 1.4: (a) Actual geometry of an automotive panel. (b) CAD geometrical description by NURBS patches. (c) Finite element mesh of 3-noded shell triangles discretizing the panel geometry. (d) FEM numerical results of the structural analysis showing the equivalent strain distribution (Images by courtesy of Quantech ATZ SA, www.quantech.es)

reproduce the behaviour of a real structure with enough precision. Although both the accuracy of the structural model and the computational method are assessed in a validation exercise, a large validation error for an already verified code typically means that the structural model chosen is not adequate and that a more refined structural model should be used. In summary, verification serves to check that we are solving structural problems accurately, while validation tell us that we are solving the right problem. The issue of verification and validation of FEM codes is treated extensively in [1].

In the following sections we will revisit the basic concepts of the matrix analysis of bar structures, considered here as a particular class of the so-called “discrete systems”. Then we will summarize the general steps in the analysis of “continuous” structures by the FEM. The interest of classical matrix structural analysis is that it provides a general solution framework which reassembles very closely that followed in the FEM.

1.5 DISCRETE SYSTEMS. BAR STRUCTURES

The solution of a many technical problems requires the analysis of a network system formed by different “elements” connected by their extremities or joints, and subjected to a set of “loads” which are usually external to the system. Examples of such systems, which we will call *discrete systems*, are common in structural engineering (pin-jointed bar structures, frames, grillages, etc.) and in many other different engineering problems, e.g.: hydraulic piping networks,

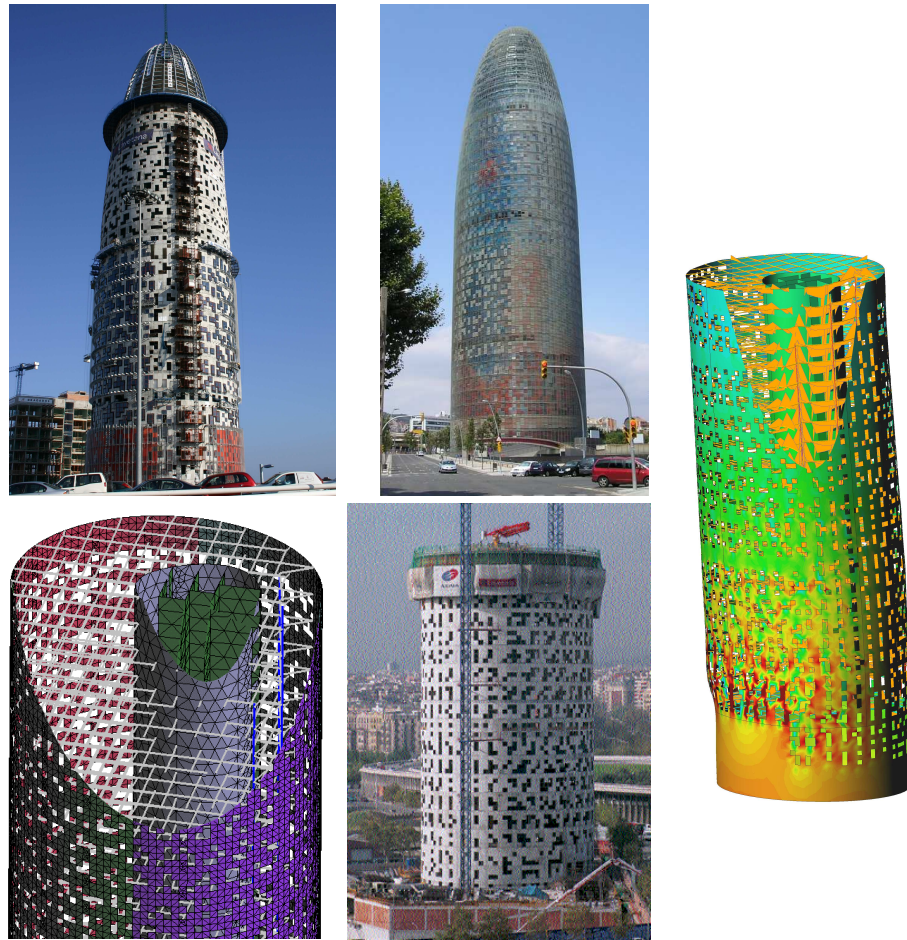


Fig. 1.5: FEM analysis of the Agbar tower (Barcelona). Actual structure and discretization into shell and 3D beam elements. Deformed mesh (amplified) under wind loads (Images courtesy of Compass Ingeniería y Sistemas SA, www.compassis.com)

electric networks, transport planning networks, production organization systems (PERT, etc) amongst others. Figure 1.7 shows some of these discrete systems.

Most discrete systems can be studied using *matrix analysis* procedures which have a very close resemblance to the Finite Element Method (FEM). In Appendix I the basic concepts of matrix algebra are summarized. An outline of the matrix analysis techniques for bar structures and other discrete systems such as electric and hydraulic networks is presented in the next section.

1.5.1 Basic concepts of matrix analysis of bar structures

Matrix analysis is the most popular technique for the solution of bar structures [L3], [P14]. Matrix analysis also provides a general methodology for the FEM analysis of other structural problems. A good knowledge of this technique is

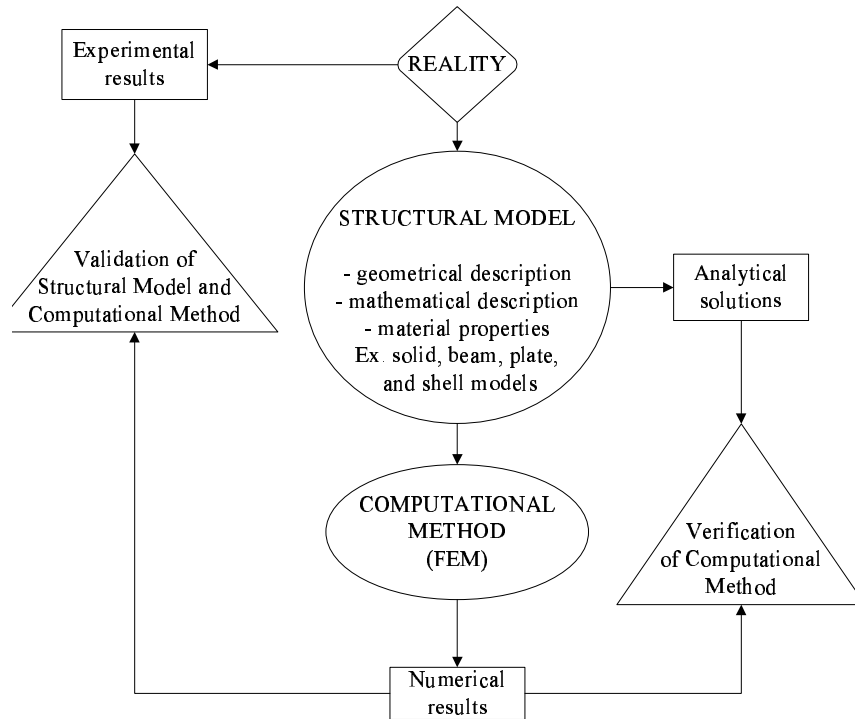


Fig. 1.6: Schematic view of the verification and validation processes in the FEM

essential for the study of this book.

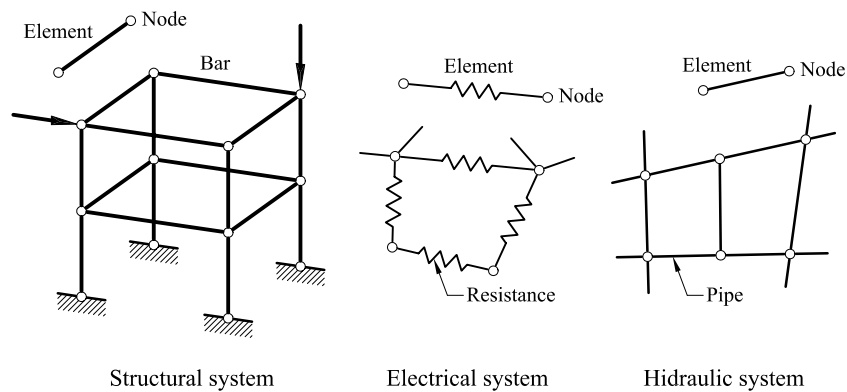


Fig. 1.7: Some discrete systems

The matrix equations for a bar structure are obtained from the study of the “equilibrium” of the different individual bars. We will consider first the case of an isolated bar, e , of length $l^{(e)}$ subjected to axial end forces $R_1^{(e)}$ and $R_2^{(e)}$ only (Figure 1.8). Strength of Materials defines the strain at any point

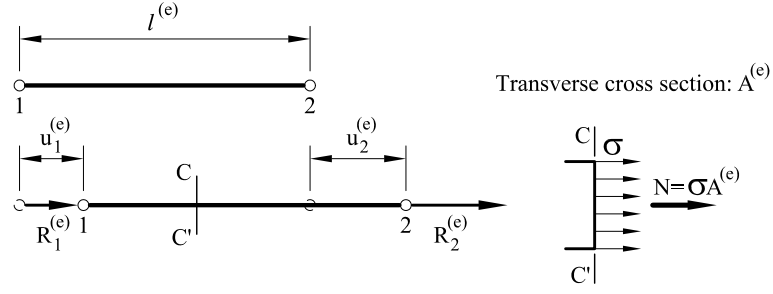


Fig. 1.8: Deformation of a bar subjected to axial forces

along the bar by the relative elongation [T7,10], i.e.

$$\varepsilon = \frac{\Delta l^{(e)}}{l^{(e)}} = \frac{u_2^{(e)} - u_1^{(e)}}{l^{(e)}} \quad (1.1)$$

where $u_1^{(e)}$ and $u_2^{(e)}$ are the displacements of the end points 1 and 2, respectively. In Eq.(1.1) and the following the superindex denotes values associated to an individual bar.

The axial stress σ is related to the strain ε by Hooke's law [T6,7] as

$$\sigma = E^{(e)}\varepsilon = E^{(e)}\frac{u_2^{(e)} - u_1^{(e)}}{l^{(e)}} \quad (1.2)$$

where $E^{(e)}$ is the Young modulus of the material. The *axial force* N at each section is obtained by integrating the stress over the cross sectional area. The axial force is transmitted to the adjacent bars through the joints. In the case of a homogeneous material we have

$$N = A^{(e)}\sigma = (EA)^{(e)}\frac{u_2^{(e)} - u_1^{(e)}}{l^{(e)}} \quad (1.3)$$

The equilibrium equation for the bar of Figure 1.8 is simply

$$R_1^{(e)} + R_2^{(e)} = 0 \quad (1.4a)$$

with

$$R_2^{(e)} = N = (EA)^{(e)}\frac{u_2^{(e)} - u_1^{(e)}}{l^{(e)}} = k^{(e)}(u_2 - u_1) \quad (1.4b)$$

where $k^{(e)} = \left(\frac{EA}{l}\right)^{(e)}$. Eqs.(1.4) can be written in matrix form as

$$\mathbf{q}^{(e)} = \begin{Bmatrix} R_1^{(e)} \\ R_2^{(e)} \end{Bmatrix} = k^{(e)} \begin{bmatrix} 1 & -1 \\ -1 & 1 \end{bmatrix} \begin{Bmatrix} u_1^{(e)} \\ u_2^{(e)} \end{Bmatrix} = \mathbf{K}^{(e)} \mathbf{a}^{(e)} \quad (1.5a)$$

where

$$\mathbf{K}^{(e)} = k^{(e)} \begin{bmatrix} 1 & -1 \\ -1 & 1 \end{bmatrix} \quad (1.5b)$$

$\mathbf{K}^{(e)}$ is the *stiffness matrix* of the bar, which depends on the geometry of the bar ($l^{(e)}, A^{(e)}$) and its mechanical properties ($E^{(e)}$) only; $\mathbf{a}^{(e)} = [u_1^{(e)}, u_2^{(e)}]^T$ and $\mathbf{q}^{(e)} = [R_1^{(e)}, R_2^{(e)}]^T$ are the joint displacements and the joint equilibrium force vectors for the bar, respectively.

The effect of a uniformly distributed external axial load of intensity $b^{(e)}$ can easily be taken into account by adding one half of the total external load to each axial force at the bar ends. The equilibrium equation now reads

$$\mathbf{q}^{(e)} = \begin{Bmatrix} R_1^{(e)} \\ R_2^{(e)} \end{Bmatrix} = k^{(e)} \begin{bmatrix} 1 & -1 \\ -1 & 1 \end{bmatrix} \begin{Bmatrix} u_1^{(e)} \\ u_2^{(e)} \end{Bmatrix} - \frac{(bl)^{(e)}}{2} \begin{Bmatrix} 1 \\ 1 \end{Bmatrix} = \mathbf{K}^{(e)}\mathbf{a}^{(e)} - \mathbf{f}^{(e)} \quad (1.6)$$

where $\mathbf{f}^{(e)} = \frac{(bl)^{(e)}}{2} \begin{Bmatrix} 1 \\ 1 \end{Bmatrix}$ is the vector of joint forces due to the distributed loading.

The equilibrium equations for the whole structure are obtained by imposing the equilibrium of forces at each of the n joints. This condition can be written as

$$\sum_{e=1}^{n_e} R_i^{(e)} = R_j \quad , \quad j = 1, n \quad (1.7)$$

The sum on the left hand side (l.h.s.) of Eq.(1.7) extends over all bars n_e sharing the joint point with global number j and R_j^{ext} represents the external load acting on that joint. The values of the bar end forces $R_i^{(e)}$ of Eq.(1.7) are expressed in terms of the joint displacements using Eq.(1.6). This process leads to the following global equilibrium equation

$$\begin{bmatrix} K_{11} & K_{12} & \cdots & K_{1n} \\ K_{21} & K_{22} & \cdots & K_{2n} \\ \vdots & & & \\ \vdots & & & \\ K_{n1} & K_{n2} & \cdots & K_{nn} \end{bmatrix} \begin{Bmatrix} u_1 \\ u_2 \\ \vdots \\ u_n \end{Bmatrix} = \begin{Bmatrix} f_1 \\ f_2 \\ \vdots \\ f_n \end{Bmatrix} \quad (1.8a)$$

$$\mathbf{K}\mathbf{a} = \mathbf{f} \quad (1.8b)$$

where \mathbf{K} is the global stiffness matrix of the structure and \mathbf{a} and \mathbf{f} are the global joint displacement vector and the global joint force vector respectively. The derivation of Eq.(1.8a) is termed the *assembly process*. The solution of Eq.(1.8a) yields the displacements at all joint points from which the values of the internal axial forces in the bars can be computed.

1.5.2 Analogy with the matrix analysis of other discrete systems

The steps between Eqs.(1.1) and (1.8) are very similar for many discrete systems. For instance, the study of a single resistance element 1-2 in an electric network (Figure 1.9a) yields the following relationship between the currents

entering the resistance element and the voltages at the end points (Ohm's law)

$$I_1^{(e)} = -I_2^{(e)} = \frac{1}{R^{(e)}}(V_1^{(e)} - V_2^{(e)}) = k^{(e)}(V_1^{(e)} - V_2^{(e)}) \quad (1.9)$$

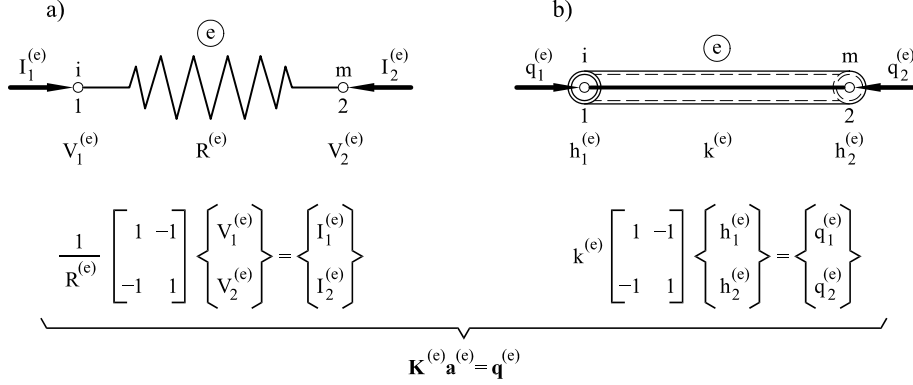


Fig. 1.9: a) Electrical resistance, b) Fluid carrying pipe. Equations of equilibrium

We note that this equation is identical to Eq.(1.4) for the bar element if the current intensities and the voltages are replaced by the joint forces and the joint displacements, respectively, and $1/R^{(e)}$ by $\left(\frac{EA}{l}\right)^{(e)}$. Indeed, if uniformly distributed external currents $b^{(e)}$ are supplied along the length of the element, the force term $\mathbf{f}^{(e)}$ of Eq.(1.6) is found. The ‘‘assembly rule’’ is the well known Kirchhoff's law stating that the sum of all the current intensities arriving at a joint must be equal to zero, i.e.

$$\sum_{e=1}^{n_e} I_i^{(e)} = I_j \quad , \quad j = 1, n \quad (1.10)$$

where I_j is the external current intensity entering joint j . Note the analogy between Eqs.(1.10) and (1.7).

The same analogy can be found in the study of fluid carrying pipe networks. The equilibrium equation relating fluid flow q and hydraulic head h at the ends of a single pipe element can be written as (Figure 1.5b)

$$q_1^{(e)} = -q_2^{(e)} = k^{(e)}(h_1^{(e)} - h_2^{(e)}) \quad (1.11)$$

where $k^{(e)}$ is a parameter which is a function of the pipe roughness and the hydraulic head. This implies that the terms of the stiffness matrix $\mathbf{K}^{(e)}$ for a pipe element are known functions of the joint heads $h_i^{(e)}$. The equilibrium equation for each pipe element is written in an identical manner to Eq.(1.6) where $u_i^{(e)}$ and $R_i^{(e)}$ are replaced by $h_i^{(e)}$ and $q_i^{(e)}$, respectively and $b^{(e)}$ represents the input of a uniformly distributed flow source along the pipe length.

The assembly rule simply states that at each of the n pipe joint the sum of the flow contributed by the adjacent pipe elements should equal the external flow source, i.e.

$$\sum_{e=1}^{n_e} q_i^{(e)} = q_j \quad , \quad j = 1, n \quad (1.12)$$

The global equilibrium equations are assembled similarly as for the bar element yielding the system of Eqs.(1.8). In the general problem matrix \mathbf{K} will be a function of the nodal hydraulic head via the $k^{(e)}$ parameter. Iterative techniques for the solution of the resulting non-linear system of equations are needed in this case.

1.5.3 Basic steps for matrix analysis of discrete systems

What we have seen thus far leads us to conclude that the analysis of a discrete system (i.e. a bar structure) involves the following steps:

- a) Definition of a network of discrete elements (bars) connected among themselves by joints adequately numbered. Each element e has known geometrical and mechanical properties. All these characteristics constitute the problem *data* and should be defined in the simplest possible way (preprocessing step).
- b) Computation of the stiffness matrix $\mathbf{K}^{(e)}$ and the joint force vector $\mathbf{f}^{(e)}$ for each element of the system.
- c) Assembly and solution of the resulting global matrix equilibrium equation ($\mathbf{K}\mathbf{a} = \mathbf{f}$) to compute the unknown parameters at each joint (i.e. the displacements for the bar system).
- d) Computation of other relevant parameters for each element (i.e. the axial strains and forces) in terms of the joint parameters.

The results of the analysis should be presented in a clear graphical form to facilitate the assessment of the system's performance (postprocessing step).

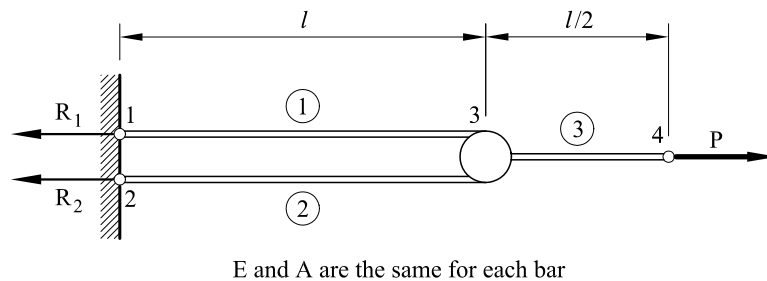


Fig. 1.10: Analysis of a simple three-bar structure under an axial load

Example: 1.1 Compute the displacements and axial forces in the three bar structure of Figure 1.10 subjected to an horizontal force P acting at its right hand end.

- **Solution**

The equilibrium equations for each joint are (see Eq.(1.5))

$$\text{Bar 1} \quad \begin{Bmatrix} R_1^{(1)} \\ R_2^{(1)} \end{Bmatrix} = k^{(1)} \begin{bmatrix} 1 & -1 \\ -1 & 1 \end{bmatrix} \begin{Bmatrix} u_1^{(1)} \\ u_2^{(1)} \end{Bmatrix}$$

$$\text{Bar 2} \quad \begin{Bmatrix} R_1^{(2)} \\ R_2^{(2)} \end{Bmatrix} = k^{(2)} \begin{bmatrix} 1 & -1 \\ -1 & 1 \end{bmatrix} \begin{Bmatrix} u_1^{(2)} \\ u_2^{(2)} \end{Bmatrix}$$

$$\text{Bar 3} \quad \begin{Bmatrix} R_1^{(3)} \\ R_2^{(3)} \end{Bmatrix} = k^{(3)} \begin{bmatrix} 1 & -1 \\ -1 & 1 \end{bmatrix} \begin{Bmatrix} u_1^{(3)} \\ u_2^{(3)} \end{Bmatrix}$$

with $k^{(1)} = k^{(2)} = \frac{EA}{l}$ and $k^{(3)} = \frac{2EA}{l}$.

The compatibility equations between local and global displacements are

$$u_1^{(1)} = u_1 \quad ; \quad u_2^{(1)} = u_3 \quad ; \quad u_1^{(2)} = u_2$$

$$u_2^{(2)} = u_3 \quad ; \quad u_1^{(3)} = u_3 \quad ; \quad u_2^{(3)} = u_4$$

Applying the assembly equation (1.7) to each of the four joints we have

$$\text{joint 1:} \quad \sum_{e=1}^3 R_i^{(e)} = -R_1$$

$$\text{joint 2:} \quad \sum_{e=1}^3 R_i^{(e)} = -R_2$$

$$\text{joint 3:} \quad \sum_{e=1}^3 R_i^{(e)} = 0$$

$$\text{joint 4:} \quad \sum_{e=1}^3 R_i^{(e)} = P$$

Substituting the values of $R_i^{(e)}$ from the equilibrium equation of each bar, we obtain

$$\text{joint 1:} \quad k^{(1)}(u_1^{(1)} - u_2^{(1)}) = -R_1$$

$$\text{joint 2:} \quad k^{(2)}(u_1^{(2)} - u_2^{(2)}) = -R_2$$

$$\text{joint 3:} \quad k^{(1)}(-u_1^{(1)} + u_2^{(1)}) + k^{(2)}(-u_1^{(2)} + u_2^{(2)}) + k^{(3)}(u_1^{(3)} + u_2^{(3)}) = 0$$

$$\text{joint 4:} \quad k^{(3)}(-u_1^{(3)} + u_2^{(1)}) = P$$

Above equations can be written in matrix form using the displacement compatibility conditions as

$$\begin{array}{cccc}
 & 1 & 2 & 3 & 4 \\
 \begin{array}{l} 1 \\ 2 \\ 3 \\ 4 \end{array} & \begin{bmatrix} k^{(1)} & 0 & -k^{(1)} & 0 \\ 0 & k^{(2)} & -k^{(2)} & 0 \\ -k^{(1)} & -k^{(2)} & (k^{(1)} + k^{(2)} + k^{(3)}) & -k^{(3)} \\ 0 & 0 & -k^{(3)} & k^{(3)} \end{bmatrix} & \begin{Bmatrix} u_1 \\ u_2 \\ u_3 \\ u_4 \end{Bmatrix} & = & \begin{Bmatrix} -R_1 \\ -R_2 \\ 0 \\ P \end{Bmatrix}
 \end{array}$$

Substituting the values of $k^{(e)}$ for each bar and imposing the boundary conditions $u_1 = u_2 = 0$, the previous system can be solved to give

$$u_3 = \frac{Pl}{2EA} ; \quad u_4 = \frac{Pl}{EA} ; \quad R_1 = R_2 = \frac{P}{2}$$

The axial forces in each bar are finally obtained as

$$\text{Bar 1 : } N^{(1)} = \frac{EA}{l}(u_3 - u_1) = \frac{P}{2}$$

$$\text{Bar 2 : } N^{(2)} = \frac{EA}{l}(u_3 - u_2) = \frac{P}{2}$$

$$\text{Bar 3 : } N^{(3)} = \frac{2EA}{l}(u_4 - u_3) = P$$

1.6 DIRECT ASSEMBLY OF THE GLOBAL STIFFNESS MATRIX

The stiffness contribution of each individual bar can be *directly* assembled in the global stiffness matrix by the following procedure. Consider a bar e connecting two joints with global numbers i and m . Each term (i, m) of the bar stiffness matrix contributes to the same position (i, m) of the global stiffness matrix (Figure 1.11). Thus, the global stiffness matrix terms can be directly computed by systematically adding the contributions from the different bars using information from the nodal numbers. This assembly process can be programmed in a simple and general form [H5].

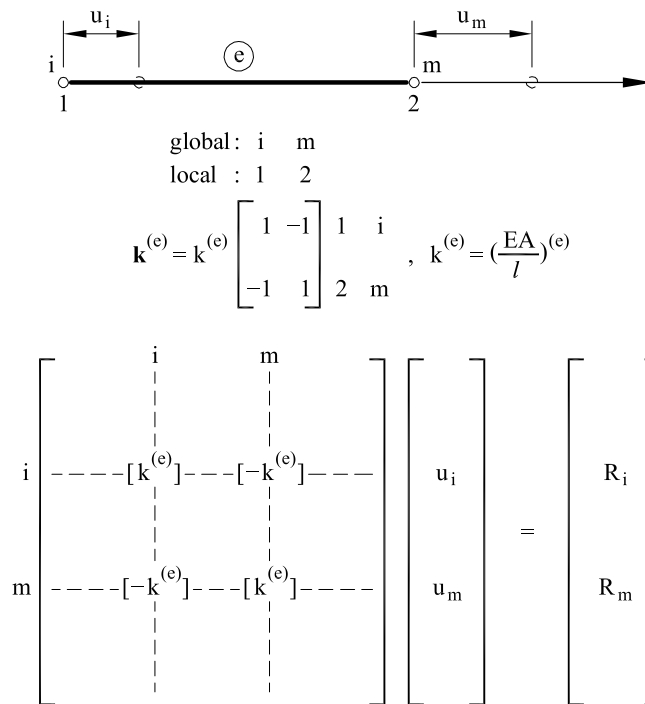
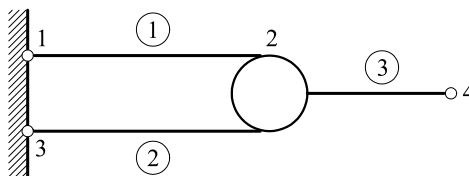


Fig. 1.11: Contributions to the global stiffness matrix from an individual bar

Example: 1.2 Obtain the bandwidth of the stiffness matrix of the structure of Figure 1.4 with the node numbering indicated below.

- **Solution**

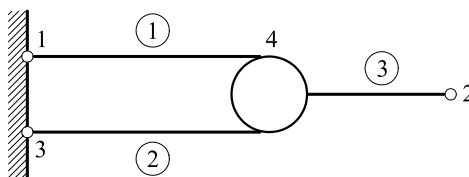
Numbering a)



The local numbering of each bar element is always taken from left to right

$$\mathbf{K}^{(e)} = \begin{bmatrix} k_{11}^{(1)} & k_{12}^{(1)} & 0 & 0 \\ k_{21}^{(1)} & (k_{22}^{(1)} + k_{22}^{(2)} + k_{11}^{(3)}) & k_{21}^{(2)} & k_{12}^{(3)} \\ 0 & k_{12}^{(2)} & k_{11}^{(2)} & 0 \\ 0 & k_{21}^{(3)} & 0 & k_{22}^{(3)} \end{bmatrix}$$

Numbering b)



$$\mathbf{K}^{(e)} = \begin{bmatrix} k_{11}^{(1)} & 0 & 0 & k_{12}^{(1)} \\ 0 & k_{22}^{(3)} & 0 & k_{21}^{(3)} \\ 0 & 0 & k_{11}^{(2)} & k_{12}^{(2)} \\ k_{21}^{(1)} & 0 & k_{21}^{(2)} & (k_{11}^{(1)} + k_{22}^{(2)} + k_{11}^{(3)}) \end{bmatrix}$$

It is observed that in numbering (a) the bandwidth is 4, whereas in numbering (b) the banded structure is lost and the bandwidth coincides with the number of terms of the main diagonal (=6). These differences, although of little relevance in this simple example, can be very significant in practical problems.

1.7 DERIVATION OF THE MATRIX EQUILIBRIUM EQUATIONS FOR THE BAR ELEMENT USING THE PRINCIPLE OF VIRTUAL WORK

One of the main steps in the matrix analysis of bar structures is the derivation of the matrix equations for the single bar element. These equations express the equilibrium between the loads acting at the bar joints and the displacements of the joint points (Eq.(1.5)). For the simple axially loaded bar these equations can be directly obtained using concepts from Strength of Materials. For complex structures more general procedures are needed. Among these, the Principle of Virtual Work (PVW) is the more powerful and widespread technique. This well known principle states that: “A structure is in equilibrium under a set of external loads if after imposing to the structure arbitrary (virtual) displacements compatible with the boundary conditions, the work performed by the external loads on the virtual displacements equals the work performed by the actual stresses on the strains induced by the virtual displacements”.

The PVW is a necessary and sufficient condition for the equilibrium of the whole structure or any of its parts [T7], [Z6]. Next, we will apply this technique to the axially loaded bar of Figure 1.2. The PVW in this case is written as

$$\int \int \int_{V^{(e)}} \delta \varepsilon \sigma dV = \delta u_1^{(e)} R_1^{(e)} + \delta u_2^{(e)} R_2^{(e)} \quad (1.13)$$

where $\delta u_1^{(e)}$ and $\delta u_2^{(e)}$ are, respectively, the virtual displacements of ends 1 and 2 of a bar with volume $V^{(e)}$, and $\delta \varepsilon$ is the corresponding virtual strain which can be obtained in terms of $\delta u_1^{(e)}$ and $\delta u_2^{(e)}$ as

$$\delta \varepsilon = \frac{\delta u_2^{(e)} - \delta u_1^{(e)}}{l^{(e)}} \quad (1.14)$$

Substituting the values of σ and $\delta\varepsilon$ of Eqs.(1.2) and (1.14) into (1.13) and integrating the stresses over the cross sectional area of the bar gives

$$\int_{l^{(e)}} \frac{1}{l^{(e)}} [\delta u_2^{(e)} - \delta u_1^{(e)}] (EA)^{(e)} \frac{1}{l^{(e)}} [u_2^{(e)} - u_1^{(e)}] dx = \delta u_1^{(e)} R_1^{(e)} + \delta u_2^{(e)} R_2^{(e)} \quad (1.15)$$

Integrating over the bar length, assuming the Young modulus $E^{(e)}$ and the area $A^{(e)}$ to be constant, yields

$$\begin{aligned} \left(\frac{EA}{l}\right)^{(e)} [u_1^{(e)} - u_2^{(e)}] \delta u_1^{(e)} + \left(\frac{EA}{l}\right)^{(e)} [u_2^{(e)} - u_1^{(e)}] \delta u_2^{(e)} &= \\ &= \delta u_1^{(e)} R_1^{(e)} + \delta u_2^{(e)} R_2^{(e)} \end{aligned} \quad (1.16)$$

Since the virtual displacements are *arbitrary*, the satisfaction of Eq.(1.16) for any value of $\delta u_1^{(e)}$ and $\delta u_2^{(e)}$ requires that the terms multiplying each virtual displacement at each side of the equation should be identical. This leads to the following system of two equations

$$\text{For } \delta u_1^{(e)} : \left(\frac{EA}{l}\right)^{(e)} [u_1^{(e)} - u_2^{(e)}] = R_1^{(e)} \quad (1.17a)$$

$$\text{For } \delta u_2^{(e)} : \left(\frac{EA}{l}\right)^{(e)} [u_2^{(e)} - u_1^{(e)}] = R_2^{(e)} \quad (1.17b)$$

which are the equilibrium equations we are looking for.

We can check that these equations, written in matrix form, coincide with Eqs.(1.5) directly obtained using more physical arguments. The effect of a distributed load can easily be taken into account by adding to the right hand side (r.h.s.) of Eq.(1.13) the term $\int_{l^{(e)}} \delta u b dx$. Assuming a linear distribution of the virtual displacements in terms of the end values, the expression of Eq.(1.6) is recovered.

The PVW will be used throughout this book to derive the matrix equilibrium equations for the different structures studied.

1.8 DERIVATION OF THE BAR EQUILIBRIUM EQUATIONS VIA THE MINIMUM TOTAL POTENTIAL ENERGY PRINCIPLE

The equilibrium equations for a structure can also be derived via the principle of Minimum Total Potential Energy (MTPE). The resulting equations are identical to those obtained via the PVW. The applications of the MTPE principle are generally limited to elastic materials for which simple forms of the total potential energy can be derived. The PVW is more general as it is applicable to non linear problems (including both material and geometrical

non linearities) and it is usually chosen as the starting variational form for deriving finite element equations.

The total potential energy for a single bar e under point forces $R_i^{(e)}$ at the two ends is

$$\Pi^{(e)} = \frac{1}{2} \int_{l^{(e)}} \varepsilon N dx - \sum_{i=1}^2 u_i^{(e)} R_i^{(e)} \quad (1.18)$$

Substituting into Eq.(1.18) the expression for the elongation ε and the axial forces in terms of the end displacements, i.e.

$$\varepsilon = \frac{u_2^{(e)} - u_1^{(e)}}{l^{(e)}} \quad , \quad N = (EA)^{(e)} \frac{u_2^{(e)} - u_1^{(e)}}{l^{(e)}} \quad (1.19)$$

gives

$$\Pi^{(e)} = \frac{1}{2} \int_{l^{(e)}} \left(\frac{u_2^{(e)} - u_1^{(e)}}{l^{(e)}} \right) (EA)^{(e)} \left(\frac{u_2^{(e)} - u_1^{(e)}}{l^{(e)}} \right) dx - \left(u_1^{(e)} R_1^{(e)} + u_2^{(e)} R_2^{(e)} \right) \quad (1.20)$$

The MTPE principle states that a structure is in equilibrium for values of the displacement making Π stationary. The MTPE also holds for the equilibrium of any part of the structure. The equilibrium condition is written for the single bar as

$$\frac{\partial \Pi^{(e)}}{\partial u_i^{(e)}} = 0 \quad i = 1, 2 \quad (1.21)$$

i.e.

$$\begin{aligned} \frac{\partial \Pi^{(e)}}{\partial u_1^{(e)}} &= -\frac{1}{l^{(e)}} \int_{l^{(e)}} (EA)^{(e)} \left(\frac{u_2^{(e)} - u_1^{(e)}}{l^{(e)}} \right) dx - R_1^{(e)} = 0 \\ \frac{\partial \Pi^{(e)}}{\partial u_2^{(e)}} &= \frac{1}{l^{(e)}} \int_{l^{(e)}} (EA)^{(e)} \left(\frac{u_2^{(e)} - u_1^{(e)}}{l^{(e)}} \right) dx - R_2^{(e)} = 0 \end{aligned} \quad (1.22)$$

For a linear material, the above equations simplify to

$$\begin{aligned} \left(\frac{EA}{l} \right)^{(e)} [u_1^{(e)} - u_2^{(e)}] &= R_1^{(e)} \\ \left(\frac{EA}{l} \right)^{(e)} [u_2^{(e)} - u_1^{(e)}] &= R_2^{(e)} \end{aligned} \quad (1.23)$$

Note the coincidence between the above end force-displacement equilibrium equations and those obtained via the PVW (Eqs.(1.17)).

Eq.(1.20) can be rewritten as

$$\Pi^{(e)} = \frac{l}{2} [\mathbf{a}^{(e)}]^T \mathbf{K}^{(e)} \mathbf{a}^{(e)} - [\mathbf{a}^{(e)}]^T \mathbf{q}^{(e)} \quad (1.24)$$

where $\mathbf{K}^{(e)}$, $\mathbf{a}^{(e)}$ and $\mathbf{q}^{(e)}$ are respectively the stiffness matrix, the joint displacement vector and the joint equilibrium force vector for the single bar (see Eqs.(1.5)).

The stationarity of $\Pi^{(e)}$ with respect to the joint displacements gives

$$\frac{\partial \Pi^{(e)}}{\partial \mathbf{a}^{(e)}} = \mathbf{0} \quad \rightarrow \quad \boxed{\mathbf{K}^{(e)} \mathbf{a}^{(e)} = \mathbf{q}^{(e)}} \quad (1.25)$$

Eq.(1.25) is the same matrix equilibrium equation between the forces and the displacements at the bar joints obtained in the the previous section (see Eq.(1.5a)).

The total potential energy for a bar structure can be written in a form analogous to Eq.(1.24) as

$$\Pi = \frac{1}{2} \mathbf{a}^T \mathbf{K} \mathbf{a} - \mathbf{a}^T \mathbf{f} \quad (1.26)$$

where \mathbf{K} , \mathbf{a} and \mathbf{f} are respectively the stiffness matrix, the joint displacement vector and the external joint force vector for the *whole structure*. The stationarity of Π with respect to \mathbf{a} gives

$$\frac{\partial \Pi}{\partial \mathbf{a}} = \mathbf{0} \quad \rightarrow \quad \boxed{\mathbf{K} \mathbf{a} = \mathbf{f}} \quad (1.27)$$

Eq.(1.27) is the global matrix equilibrium equation relating the displacements and the external forces at all the joints of the structure. The global matrix equations can be obtained by assembly of the contributions from the individual bars, as previously explained.

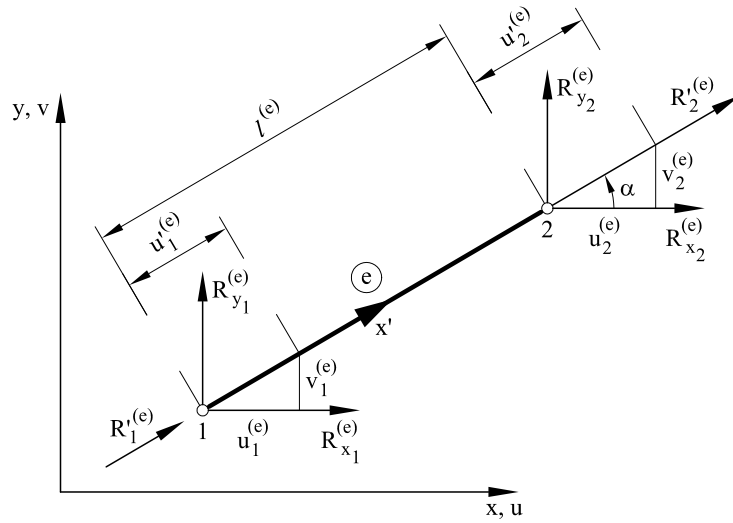


Fig. 1.12: Forces and displacements at the end points of a plane pin-jointed bar

1.9 PLANE PIN-JOINTED FRAMEWORKS

We will briefly treat the case of plane pin-jointed frameworks as an extension of the concepts previously studied. Each joint has now two degrees of freedom (d.o.f.) corresponding to the displacements along the two cartesian axes.

Eqs.(1.4) relating the joint displacements and the axial forces in *local axes* still holds. However, the sum of the joint forces for the different bars sharing a joint requires the force-displacement relationships to be expressed in a global cartesian system x, y .

Let us consider a bar 1-2 inclined an angle α with respect to the global axis x , as shown in Figure 1.12. For joint 1 we have

$$\begin{aligned} R_1^{(e)} &= R_{x_1}^{(e)} \cos \alpha + R_{y_1}^{(e)} \sin \alpha \\ u_1^{(e)} &= u_1^{(e)} \cos \alpha + v_1^{(e)} \sin \alpha \end{aligned} \quad (1.28)$$

where the primes denote the components in the direction of the local axis x' . In matrix form

$$\begin{aligned} R_1^{(e)} &= [\cos \alpha, \sin \alpha] \begin{Bmatrix} R_{x_1} \\ R_{y_1} \end{Bmatrix}^{(e)} = \mathbf{L}^{(e)} \mathbf{q}_1^{(e)} \\ u_1^{(e)} &= [\cos \alpha, \sin \alpha] \begin{Bmatrix} u_1 \\ v_2 \end{Bmatrix}^{(e)} = \mathbf{L}^{(e)} \mathbf{u}_1^{(e)} \end{aligned} \quad (1.29)$$

where $\mathbf{u}_1^{(e)}$ and $\mathbf{q}_1^{(e)}$ contain the two displacements and the two forces of joint 1 expressed in the global cartesian system x, y , respectively and $\mathbf{L}^{(e)} = [\cos \alpha, \sin \alpha]$.

Analogous expressions can be found for node 2 as

$$R_2^{(e)} = \mathbf{L}^{(e)} \mathbf{q}_2^{(e)} \quad \text{and} \quad u_2^{(e)} = \mathbf{L}^{(e)} \mathbf{u}_2^{(e)} \quad (1.30)$$

with

$$\mathbf{q}_2^{(e)} = [R_{x_2}, R_{y_2}]^T \quad \text{and} \quad \mathbf{u}_2^{(e)} = [u_2^{(e)}, v_2^{(e)}]^T$$

From Figure 1.6, we deduce

$$R_1^{(e)} = -R_2^{(e)} = k^{(e)} [u_1^{(e)} - u_2^{(e)}] \quad \text{with} \quad k^{(e)} = \left(\frac{EA}{l} \right)^{(e)} \quad (1.31)$$

Multiplying Eq.(1.31) by $[\mathbf{L}^{(e)}]^T$ and using Eqs.(1.29) and (1.30) the following two equations are obtained

$$\begin{aligned} \mathbf{q}_1^{(e)} &= [\mathbf{L}^{(e)}]^T k^{(e)} \mathbf{L}^{(e)} \mathbf{u}_1^{(e)} - [\mathbf{L}^{(e)}]^T k^{(e)} \mathbf{L}^{(e)} \mathbf{u}_2^{(e)} \\ \mathbf{q}_2^{(e)} &= -[\mathbf{L}^{(e)}]^T k^{(e)} \mathbf{L}^{(e)} \mathbf{u}_1^{(e)} + [\mathbf{L}^{(e)}]^T k^{(e)} \mathbf{L}^{(e)} \mathbf{u}_2^{(e)} \end{aligned} \quad (1.32)$$

In matrix form

$$\begin{Bmatrix} \mathbf{q}_1^{(e)} \\ \mathbf{q}_2^{(e)} \end{Bmatrix} = \begin{bmatrix} \mathbf{K}_{11}^{(e)} & \mathbf{K}_{12}^{(e)} \\ \mathbf{K}_{21}^{(e)} & \mathbf{K}_{22}^{(e)} \end{bmatrix} \begin{Bmatrix} \mathbf{u}_1^{(e)} \\ \mathbf{u}_2^{(e)} \end{Bmatrix} \quad (1.33a)$$

where

$$\begin{aligned} \mathbf{K}_{11}^{(e)} &= \mathbf{K}_{22}^{(e)} = -\mathbf{K}_{12}^{(e)} = -\mathbf{K}_{21}^{(e)} = [\mathbf{L}^{(e)}]^T k^{(e)} \mathbf{L}^{(e)} = \\ &= k^{(e)} \begin{bmatrix} \cos^2 \alpha & \sin \alpha \cos \alpha \\ \sin \alpha \cos \alpha & \sin^2 \alpha \end{bmatrix} \end{aligned} \quad (1.33b)$$

The assembly of the contributions of the individual bar members into the global stiffness matrix follows precisely the steps explained in Section 1.2. Note that each joint contributes a 2×2 matrix as shown in Figure 1.13. An example of the assembly process is presented in Figure 1.14.

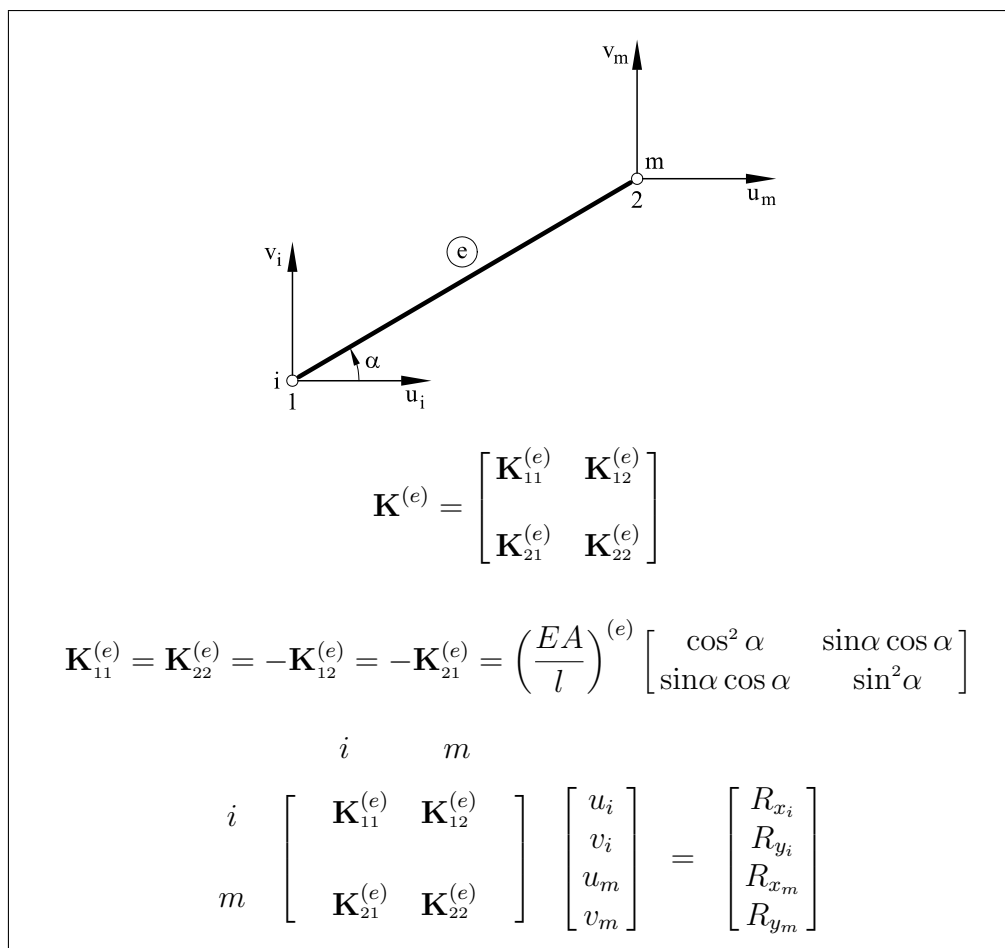


Fig. 1.13: Contributions to the global stiffness matrix from a general member of a pin-jointed framework

1.10 TREATMENT OF PRESCRIBED DISPLACEMENTS AND COMPUTATION OF REACTIONS

In this book we will not enter into the details of techniques for solving the system of algebraic equations $\mathbf{Ka} = \mathbf{f}$. This is a problem typical of matrix algebra and many well known solution procedures are available (i.e.: Gauss reduction, Choleski, modified Choleski, Frontal; Profile, etc.) [H4], [P13], [R2]. We will just treat here briefly the problem of prescribed displacements and the computation of the corresponding reactions, as these are issues of general interest for the study of this book.

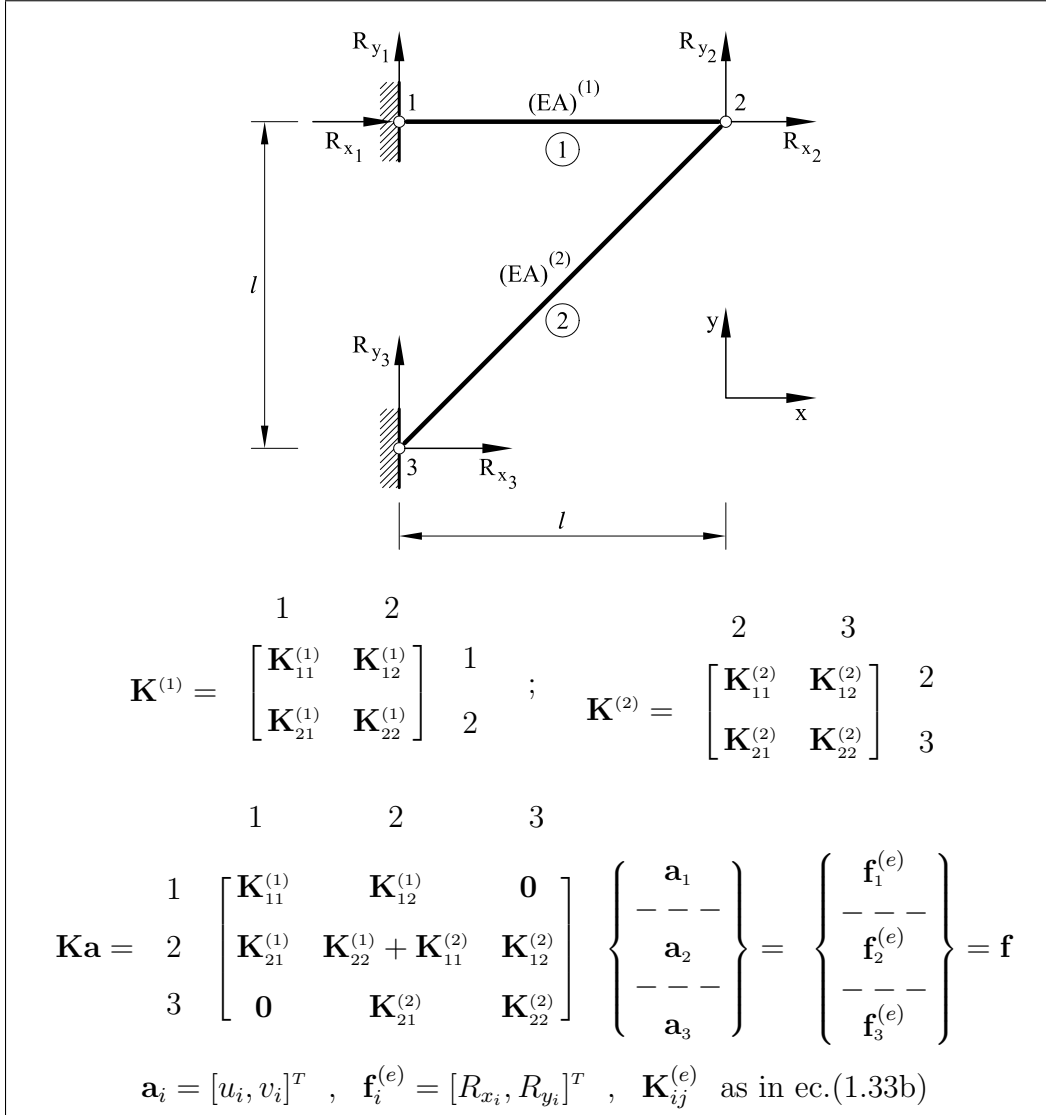


Fig. 1.14: Plane pin-jointed framework. Equation of global equilibrium

Let us consider the following system of equations

$$\begin{aligned}
 k_{11}u_1 + k_{12}u_2 + k_{13}u_3 + \dots + k_{1n}u_n &= f_1 \\
 k_{21}u_1 + k_{22}u_2 + k_{23}u_3 + \dots + k_{2n}u_n &= f_2 \\
 k_{31}u_1 + k_{32}u_2 + k_{33}u_3 + \dots + k_{3n}u_n &= f_3 \\
 \vdots & \\
 k_{n1}u_1 + k_{n2}u_2 + k_{n3}u_3 + \dots + k_{nn}u_n &= f_n
 \end{aligned} \tag{1.34}$$

where f_i are external forces (which can be equal to zero) or reactions in points where the displacement is prescribed.

Let us assume that a displacement, for example u_2 , is prescribed to the

value \bar{u}_2 , i.e.

$$u_2 = \bar{u}_2 \quad (1.35)$$

There are two basic procedures to introduce this condition in the above system of equations:

- a) The second row and column of Eq.(1.34) are eliminated and the values of f_i in the right hand side are substituted by $f_i - k_{i2}\bar{u}_2$. That is, the system of n equations with n unknowns is reduced in one equation and one unknown as follows

$$\begin{array}{cccccc} k_{11}u_1 & + & k_{13}u_3 & + & \dots & + & k_{1n}u_n & = & f_1 & - & k_{12}\bar{u}_2 \\ k_{31}u_1 & + & k_{33}u_3 & + & \dots & + & k_{3n}u_n & = & f_3 & - & k_{32}\bar{u}_2 \\ \vdots & & \vdots & & & & \vdots & & \vdots & & \vdots \\ k_{n1}u_1 & + & k_{n3}u_3 & + & \dots & + & k_{nn}u_n & = & f_n & - & k_{n2}\bar{u}_2 \end{array} \quad (1.36)$$

Once the values of u_1, u_3, \dots, u_n are obtained, the reaction f_2 is computed by the following equation (in the case that the external force acting at node 2 is equal to zero)

$$f_2 = k_{21}u_1 + k_{22}\bar{u}_2 + k_{23}u_3 + \dots + k_{2n}u_n \quad (1.37)$$

If u_2 is zero, the procedure remains the same, although the values of f_i are not modified and f_2 is obtained by Eq.(1.37) with $\bar{u}_2 = 0$.

- b) An alternative procedure which does not require the original system of equations to be modified substantially, is to add a very large number to the term of the main diagonal corresponding to the prescribed displacements. The force term in the modified row is substituted by the value of the prescribed displacement multiplied by the large number chosen. Thus, if we have $u_2 = \bar{u}_2$ we substitute k_{22} by $k_{22} + 10^{15}k_{22}$ (for instance), and f_2 by $10^{15}k_{22} \times \bar{u}_2$. The final system of equations is

$$\begin{array}{cccccc} k_{11}u_1 & + & k_{12}u_2 & + & k_{13}u_3 & + & \dots & + & k_{1n}u_n & = & f_1 \\ k_{21}u_1 & + & (1 + 10^{15})k_{22}u_2 & + & k_{23}u_3 & + & \dots & + & k_{2n}u_n & = & 10^{15}k_{22}\bar{u}_2 \\ k_{31}u_1 & + & k_{32}u_2 & + & k_{33}u_3 & + & \dots & + & k_{3n}u_n & = & f_3 \\ \vdots & & \vdots & & \vdots & & & & \vdots & & \vdots \\ k_{n1}u_1 & + & k_{n2}u_2 & + & k_{n3}u_3 & + & \dots & + & k_{nn}u_n & = & f_n \end{array} \quad (1.38)$$

In this way, the second equation is equivalent to

$$10^{15}k_{22}u_2 = 10^{15}k_{22}\bar{u}_2 \quad \text{or} \quad u_2 = \bar{u}_2 \quad (1.39)$$

which is the prescribed condition. The value of the reaction f_2 is computed ‘‘a posteriori’’ by Eq.(1.37).

1.11 INTRODUCTION TO THE FINITE ELEMENT METHOD FOR ANALYSIS OF CONTINUUM SYSTEMS

Most problems in science and engineering are of *continuous* nature and can not be naturally modelled by a collection of discrete element. Examples of “continuous” problems in structural analysis are standard in civil, mechanical, aeronautical and naval engineering. Amongst the more common we can list: plates, foundations, roofs, containers, bridges, dams, airplane fuselages, car bodies, ship hulls, mechanical components, etc. (Figure 1.15).

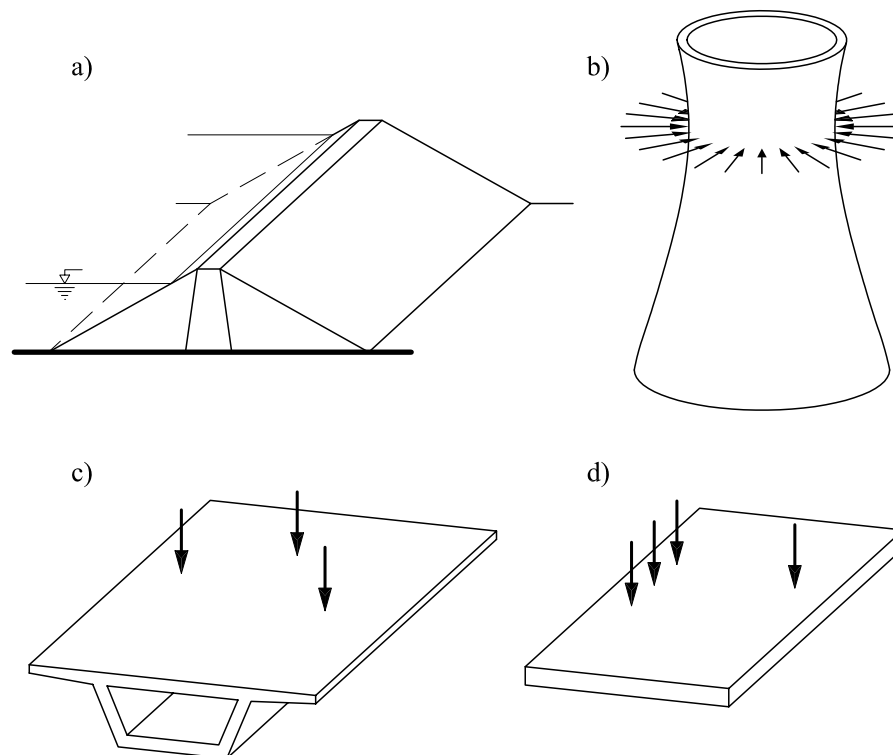


Fig. 1.15: Continuous structures: a) Dam, b) Shell, c) Bridge, d) Plate

Although a continuous system is inherently three-dimensional (3D), its behaviour can be accurately described in some cases by one- (1D) or two-dimensional (2D) structural models. This occurs, for instance, in the analysis of plates in bending, where only the deformation of the plate mid-plane is considered. Other examples are the case of prismatic bodies analyzed with 2D or axisymmetric models.

The analytical solution of a “continuous” system is very difficult (generally impossible), due to the complexities of the geometry, the boundary conditions, the material properties, the type of loading, etc. This explains the need for computational methods to analyse continuous systems.

The FEM is the simpler and more powerful computational procedure for the analysis of continuous systems with arbitrary geometry and general material

properties subjected to any type of loading.

The FEM allows one the behaviour of a continuous system with an infinite number of d.o.f. to be modelled by that of another one with approximately the same geometrical and mechanical properties, but with a finite number of d.o.f. The latter are related to the external forces by a system of algebraic equations expressing the equilibrium of the system. We will find that the basic finite element methodology is analogous to the matrix analysis techniques studied for bar structures. These analogies between matrix analysis can be clearly visualized in the analysis of the bridge shown in Figure 1.16. Without entering into too the details, the basic steps in the finite element analysis are the following:

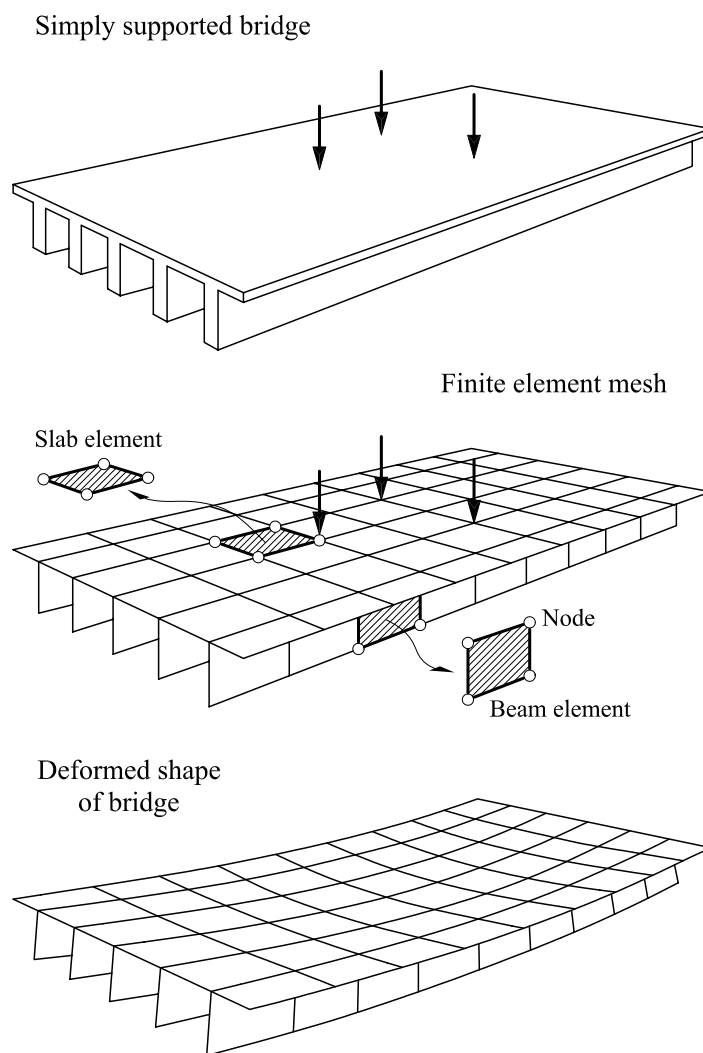


Fig. 1.16: Analysis of a bridge by the finite element method

Step 1: Starting with the geometrical description of the bridge, its supports and the loading, the first step is to select a *structural model*. For example, we

could use a stiffened plate model (Chapter 13), a facet shell model (Chapter 10), or a 3D solid model (Chapter 7). The material properties must also be defined, as well as the scope of the analysis (small or large displacements, static or dynamic analysis, etc.). As mentioned earlier in this book we will focus on linear static analysis only.

Step 2: The structure is subdivided into a mesh of non-intersecting domains termed finite elements (*discretization process*). The problem variables (displacements) are interpolated within each element in terms of their values at a known set of points of the element called *nodes*. The number of nodes defines the approximation of the solution within each element. Some nodes are placed at the element boundaries and they can be interpreted as linking points between adjacent elements. However, nodes in the interior of the elements are needed for higher-level approximations and, hence, the nodes do not have a physical meaning as the connecting joints in bar structures. The mesh can include elements with different geometries, such as 2D plate elements coupled with 1D beam elements. The *discretization* process is an essential part of the *preprocessing* step which includes the definition of all the analysis data. The preprocessing step typically consumes a considerable amount of human effort. The use of efficient preprocessing tools is therefore essential for the analysis of practical structures in competitive times [F2,F,H,G].

Step 3: The stiffness matrices $\mathbf{K}^{(e)}$ and the load vectors $\mathbf{f}^{(e)}$ are obtained for each element. The computation of $\mathbf{K}^{(e)}$ and $\mathbf{f}^{(e)}$ is more complex than for bar structures and it usually requires the evaluation of integrals over the element domain.

Step 4: The element stiffness and the load terms are assembled into the overall stiffness matrix \mathbf{K} and the load vector \mathbf{f} for the structure.

Step 5: The global system of linear simultaneous equations $\mathbf{K}\mathbf{a} = \mathbf{f}$ is solved for the unknown displacement variables \mathbf{a} .

Step 6: Once the displacements \mathbf{a} are computed, the strains and the stresses are evaluated within each element. Reactions at the nodes restrained against movement are also computed.

Step 7: Solving steps 3-6 requires a *computer implementation* of the FEM by means of a standard or specially developed program.

Step 8: After a successful computer run, the next step is *the interpretation and presentation of results*. Results are presented graphically to aid their interpretation and checking (*postprocessing step*). The use of specialized graphic software is essential in practice [F2,F,G,H].

Step 9: Having assessed the finite element results, the analyst may consider several modifications which may be introduced at various stages of the analysis. For example, it may be found that the structural model selected is inappropriate and hence it should be adequately modified. Alternatively, the finite element mesh chosen may turn out to be too coarse to capture the expected stress distributions and must therefore be refined or a different, more accurate element used. Round-off problems arising from ill-conditioned equations, the equation solving algorithm and the computer word length employed in the analysis may cause difficulties and can require the use of double-precision arithmetic or some other techniques. Input data errors which occur quite frequently must be also corrected.

All these possible modifications are indicated by the feedback loop shown in Figure 1.17 taken from [H5].

From the structural engineer's point of view, the FEM can be considered as an extension to continuous systems of the matrix analysis procedures for bar structures. The origins of the FEM go back to the early 1940's with the first attempts to solve problems of 2D elasticity using matrix analysis techniques by subdividing the continuum into bar elements [H11,M6]. In 1946 Courant [C16] introduced for the first time the concept of "continuum element" to solve 2D elasticity problems using a subdivision into triangular elements with an assumed displacement field. The arrival of digital computers in the 1960's contributed to the fast development of matrix analysis based techniques, free from the limitations imposed by the need to solve large systems of equations. It was during this period what the FEM rapidly establish itself as a powerful approach to solve many problems in mathematics and physics. It is interesting that the first applications of the FEM were related to structural analysis and, in particular, to aeronautical engineering [A10], [T12]. It is acknowledged that Clough first used the name "finite elements" in relation to the solution of 2D elasticity problems in 1960 [C8]. Since then the FEM had a tremendous expansion in its application to many different fields. Supported by the continuous upgrading of computers and by the increasing complexity of many areas in science and technology, today the FEM enjoys a unique position as a powerful technique for solving the most difficult problems in engineering and applied sciences.

It would be an impossible task to list here all the significant published work since the origins of the FEM. Only in 2006, scientific publications in this field were estimated to number in excess of 25,000. The reader interested in the historical aspects of the FEM should consult the reference list in Zienkiewicz and Taylor [Z15] and the Encyclopedia of Computational Mechanics [].

Within the fields of engineering, applied mathematics and physics the problems to which the FEM is applied are basically the following:

1. *Stationary equilibrium problems:* those problems where the properties of

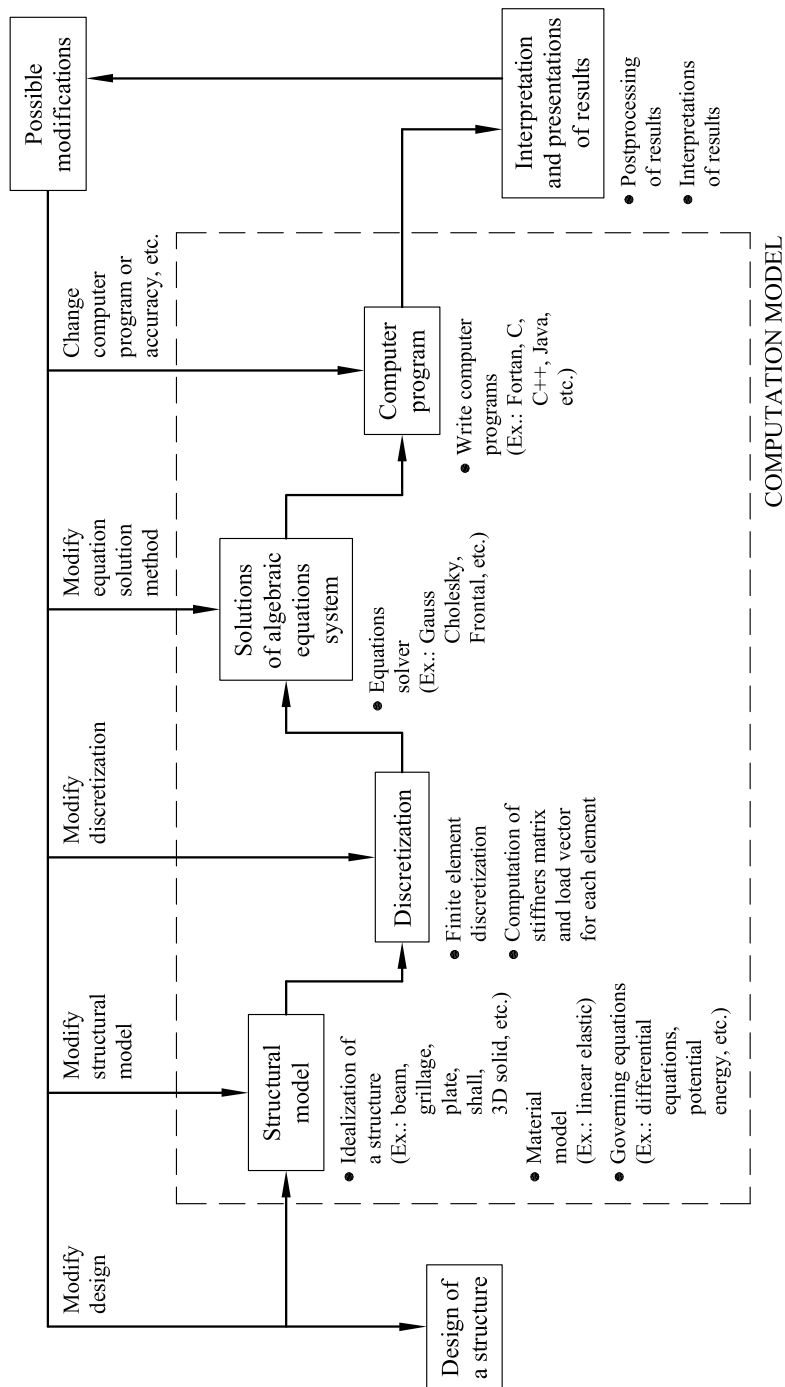


Fig. 1.17: Flow chart of the analysis of a structure by the FEM

the system do not vary with time.

2. *Eigenvalue problems.* They are an extension of the stationary equilibrium problems for which some critical values of certain parameters are obtained.

Chapter 2

FEM ANALYSIS OF 1D PROBLEMS. APPLICATION TO THE POISSON EQUATION

2.1 INTRODUCTION

The behaviour of continuum systems can in general be expressed in terms of differential equations with their adequate boundary conditions. The objective of this chapter is to present an overview of the solution of one-dimensional (1D) partial differential equations with the FEM.

There are two general procedures for solving a differential equation: a) the direct integration of the equation, which yields the so called analytical solution (*exact method*), and the *approximate solution* using numerical methods.

Numerical solution procedures for partial differential equations (PDE) be classified as: a) those which are applied on the original PDE (for example, the finite difference method), and b) those which work with an equivalent integral expression. The FEM belongs to this second class of methods. The two standard approaches of this kind are: a) variational methods, and b) residual formulations.

The variational method is based on the search for the solution to the problem by solving an integral equation which represents a general property of the system. A typical example is the integral expression obtained from the minimum energy principle.

The residual formulations are based on Weighted Residual (WR) methods such as the Point Collocation method, the Subdomain Collocation method, the Galerkin method, the Minimum Least Squares method, etc.

The FEM can therefore be viewed as a procedure for solving the PDEs governing a physical problem via a residual or variational formulation. Typically, residual methods are more general and advantageous than variational methods and they will be the focus of this chapter.

This chapter presents different weighted residual techniques for solving a

PDE with the FEM. The model problem considered is the Poisson equation in 1D.

2.2 THE POISSON EQUATION

The Poisson equation expresses in mathematical form the behaviour of many physical problems. For this reason it has been chosen here as the model problem for introducing the basis of the FEM.

The simplest form of the Poisson equation is as follows:

$$\left. \begin{array}{l} \text{In 1D: } k \frac{d^2\phi}{dx^2} + Q(x) = 0 \\ \text{In 2D: } k \frac{d^2\phi}{dx^2} + k \frac{d^2\phi}{dy^2} + Q(x, y) = 0 \\ \text{In 3D: } k \frac{d^2\phi}{dx^2} + k \frac{d^2\phi}{dy^2} + k \frac{d^2\phi}{dz^2} + Q(x, y, z) = 0 \end{array} \right\} \boxed{k \nabla^2 \phi + Q = 0} \quad (2.1)$$

where ϕ is the problem unknown, k is a parameter expressing a physical property of the system, Q is a source term and ∇^2 is the Laplace operator, i.e. $\nabla^2 = \frac{\partial^2}{\partial x^2} + \frac{\partial^2}{\partial y^2}$ in 2D. In general the parameter k can be different for each of the space directions. The simplest isotropic form is chosen here.

Table 2.1 presents the meaning of the terms in Eq.(2.2) for some physical problems.

	Unknown, ϕ	k	Q
Heat conditions	temperature	heat conductivity	internal heat source
Flow through porous media	pressure head	permeability	water source
1D elasticity	displacement	Young modulus x Area	body force
Potential flow	velocity potential	density	–
Magnetostatics	magnetic potential	reductivity	–
Torsion	warping function	shear modulus	–
Torsion	stress function	(shear modulus) -1	twist
Gass diffusion	concentration	diffusivity	–
Reynolds film lubrication	pressure	(film thickness) ³ /viscosity	lubricant supply

Table 2.1: Meaning of the terms in the Poisson equation for some problems

The form of the Poisson equation given in Eq.(2.2) assumes that k is constant. In fact k can be a function of the position and even of the problem unknown ϕ and its derivatives, as it happens in non-linear problems.

We present next examples of the derivation of the Poisson equation for three specific problems: 1) heat transfer in a bar, 2) bar under axial forces and 3) seepage in a porous media.

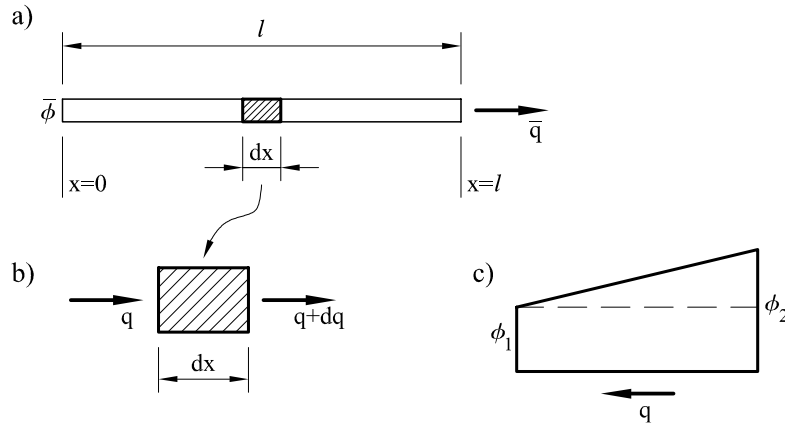


Figure 2.1: Heat conduction in a bar. Heat flow balance in an infinitesimal domain.

Example 2.1 *Steady state heat conduction in a bar*

Solution

Let us consider the bar of Figure 2.1 representing a 1D domain through which heat is transferred via conduction effects in a steady manner. The temperature $\bar{\phi}$ at $x = 0$ is known, i.e.

$$\phi = \bar{\phi}|_{x=0} \quad (a)$$

and also the heat flux \bar{q} at $x = l$

$$q = \bar{q}|_{x=l} \quad (b)$$

The balance of heat flux in a differential domain of the bar is expressed as (Figure 2.2b)

$$\underbrace{(q + dq)}_{\text{out going flux}} - \underbrace{q}_{\text{in-coming flux}} = 0$$

$$\boxed{dq = 0} \quad (c)$$

The relationship between the heat flux q and the temperature is expressed by Fourier's law

$$\boxed{q = -k \frac{d\phi}{dx}} \quad (d)$$

where k is the thermal conductivity parameter.

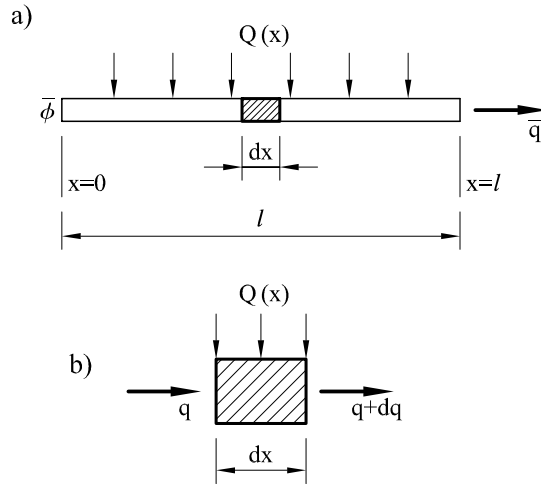


Figure 2.2: a) Bar under a heat source $Q(x)$; b) Heat balance in an infinitesimal domain.

Derivation of (d) gives

$$dq = \frac{dq}{dx} dx = -\frac{d}{dx} \left(k \frac{d\phi}{dx} \right) dx$$

Substituting this equation into (c) gives

$$\boxed{\frac{d}{dx} \left(k \frac{d\phi}{dx} \right) = 0} \quad \text{heat balance equation} \quad (e)$$

Note that the mathematical problem is well defined as we know

1. The governing differential equation (e)
2. The boundary conditions (a) and (b)

Let us now assume that the bar is subjected to an external heat source per unit length Q (Figure 2.2a). A similar heat balance procedure on an infinitesimal domain (Figure 2.2b) leads to the following equations

$$(q + dq) - q - Qdx = 0 \quad (f)$$

$$\frac{dq}{dx} - Q = 0 \quad (g)$$

Substituting (d) into (g) gives

$$\boxed{\frac{d}{dx} \left(k \frac{d\phi}{dx} \right) + Q = 0} \quad (h)$$

Expressions (e) and (h) are two forms of the Poisson equation. The form (e) (with $Q = 0$) is usually known as the Laplace equation.

Note that for k being constant, the simplified form of the Poisson equation of Eq.(2.1) is obtained.

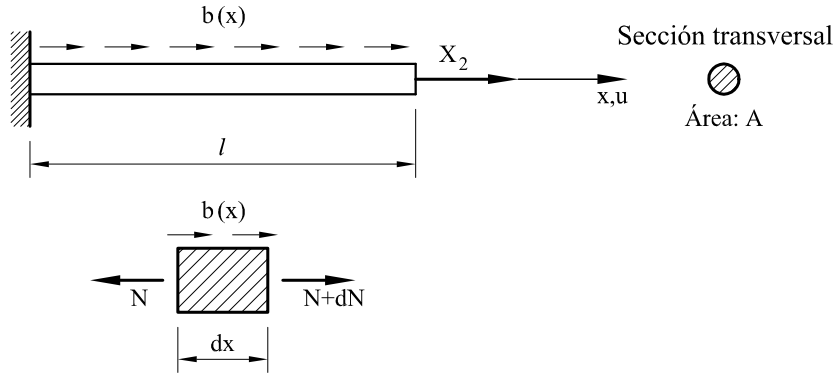


Figure 2.3: Bar under axial forces. Equilibrium of force in an infinitesimal domain.

The boundary conditions (a) and (b) completing the definition of the problem can be summarized as

$$\text{Boundary conditions} \begin{cases} \text{Prescribed temperature: } \phi - \bar{\phi} = 0 \text{ at } x = 0 & (i) \\ \text{Prescribed heat flux} \begin{cases} q - \bar{q} = 0 & \text{at } x = l \\ \text{or} \\ k \frac{d\phi}{dx} + \bar{q} = 0 & \text{at } x = l \end{cases} & (j) \end{cases}$$

Condition (i) are known in mathematics a *Dirichlet boundary condition*, while condition (j) is known as *Neumann boundary condition*.

Example 2.2 Bar under axial forces

Solution

Let us consider the clamped bar of Figure 2.3, under an horizontal force \bar{x}_2 acting in the free end and distributed axial forces $b(x)$.

The governing equations of the problem are obtained following a similar process as in Example 2.1. The equilibrium of axial forces is established in an infinitesimal domain (Figure 2.3b), i.e.

$$\frac{dN}{dx} + b(x) = 0 \quad (a)$$

The stress-strain relationship is expressed by Hooke's law

$$\sigma = E\varepsilon = E \underbrace{\frac{du}{dx}}_{\varepsilon} \quad (b)$$

The axial force N is obtained by integrating the stress over the transverse cross-section as

$$N = \sigma A \quad (c)$$

In (a) and (b) σ is the normal stress, E is the Young's modulus, ε is the axial strain, u the horizontal displacement and A the area of the transverse cross section.

From (b) and (c)

$$N = \sigma A = EA \frac{du}{dx} \quad (d)$$

Substituting (d) into (a) gives

$$\boxed{\frac{d}{dx} \left(EA \frac{du}{dx} \right) + b = 0} \quad (e)$$

The above equation expresses the equilibrium (or balance) of forces at each point of the bar. It is therefore named the equilibrium equation for the bar.

The boundary conditions are

Prescribed displacement: $u = 0$ at $x = 0$

$$\text{Prescribed force} \begin{cases} N = X_2 & \text{in } x = l \\ EA \frac{du}{dx} - X_2 = 0 & \text{in } x = l \end{cases} \quad (f)$$

Eqs.(e) and (f) define the governing equations of the problem.

Note the analogy of Eq.(e) with Eq.(h) of the previous example. Both are Poisson equations in 1D. The following lines show the analogies between the structural and thermal problems.

Thermal problem – Axially loaded bar

temperature	$\phi \leftarrow u \rightarrow$	displacement
conductivity	$k \leftarrow EA \rightarrow$	axial stiffness
heat source	$Q \leftarrow b \rightarrow$	distributed force
prescribed heat flow	$\bar{q} \leftarrow X_2 \rightarrow$	point force

The only difference in the analysis between the equation parameters in the thermal problem and the axially loaded bar is the negative sign in the point force X_2 . This is a consequence of the proportionality between the displacement gradient and the stress in structures, whereas in thermal problems the heat flux goes in the opposite direction of the gradient, i.e.

$$N = \underbrace{EA}_k \frac{du}{dx} = k \frac{du}{dx}$$

$$q = -k \frac{d\phi}{dx}$$

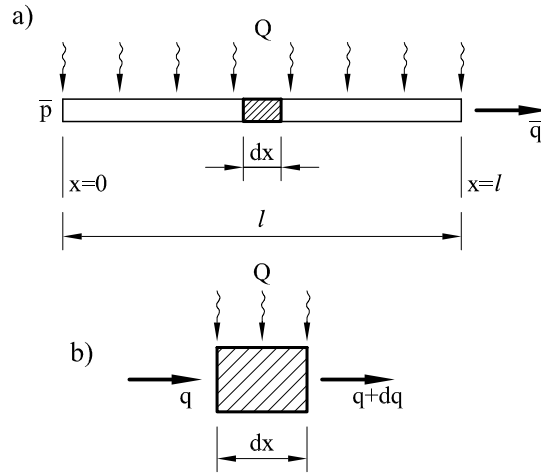


Figure 2.4: a) Water flow through a porous bar.; b) Balance of water fluxes in an infinitesimal domain

Example 2.3 *Water flow in a porous medium*

Solution

The balance of water flow in the infinitesimal domain of Figure 2.4 gives

$$(q + dq) - Qdx - q = 0$$

$$\frac{dq}{dx} - Q = 0 \tag{a}$$

In (a) q and Q represent the internal water flux and the external source of water per unit length, respectively.

The relationship between the water flow q and the pressure p is expressed by means of Darcy law

$$q = -k \frac{dp}{dx} \tag{b}$$

where k is the permeability of the porous medium.

Note the analogy of above equations with the equivalent ones in the thermal and structural problems. Substituting (b) into (a) gives

$$\frac{d}{dx} \left(k \frac{dp}{dx} \right) + Q = 0 \tag{c}$$

Boundary conditions

$$\begin{aligned} \text{Prescribed pressure} \quad p - \bar{p} = 0 & \quad \text{at } x = 0 \\ \text{Prescribed flux} \quad q - \bar{q} = 0 & \quad \text{at } x = l \\ & \quad \text{or} \\ k \frac{dp}{dx} + \bar{q} = 0 & \quad \text{at } x = l \end{aligned} \tag{d}$$

There is a perfect analogy between the governing equations in the thermal and porous media flow problems, as expressed in the following lines:

Thermal problem – Porous media flow

temperature	ϕ	\leftrightarrow	water pressure
conductivity	k	\leftrightarrow	permeability
heat source	Q	\leftrightarrow	water source
heat flux	q	\leftrightarrow	water flux

2.3 WEIGHTED RESIDUAL METHOD

The weighted residual method (WRM) is based on transforming the differential equation which governs the problem in an equivalent integral expressions.

Let $A(\phi)$ be the governing differential equation (i.e. the Poisson equation)

$$A(\phi) = \frac{d}{dx} \left(k \frac{d\phi}{dx} \right) + Q = 0 \quad \text{in } \Omega \quad (2.2)$$

where Ω is the analysis domain.

Also, let $B(\phi)$ be the equation expressing the boundary conditions

$$B(\phi) : \begin{cases} \phi - \bar{\phi} = 0 & \text{in } \Gamma_\phi \\ k \frac{d\phi}{dx} + \bar{q} = 0 & \text{in } \Gamma_q \end{cases} \quad (2.3)$$

where Γ_ϕ is the Dirichlet boundary where the unknown function is prescribed and Γ_q is the Neumann boundary where the flux incoming or outgoing the domain is prescribed. The unknown ϕ and the parameters k , Q and q have adequate meanings for each physical problem, as explained in the previous section.

For instance, for the problem of Figure 2.1, we have

$$\begin{aligned} \Omega: & \quad 0 \leq x \leq l \text{ (the bar length)} \\ \Gamma_\phi: & \quad x = 0 \text{ (left hand end point)} \\ \Gamma_q: & \quad x = l \text{ (right hand end point)} \end{aligned}$$

The integral form equivalent to the governing equations given above is obtained by multiplying the differential expressions A and B by arbitrary weighting functions and integrating over the domain of each equation. Thus

$$\int_{\Omega} W(x)A(\phi)d\Omega + \int_{\Gamma} \bar{W}(x)B(\phi)d\Gamma = 0 \quad (2.4)$$

where $W(x)$ and $\bar{W}(x)$ are the weighting functions.

It is clear that if above integral equation is satisfied for each pair of weighting functions W and \bar{W} , the following conditions must be satisfied

$$A(\phi) = 0 \quad \text{in } \Omega$$

$$B(\phi) = 0 \quad \text{in } \Gamma$$

Conversely, satisfaction of Eq.(2.2) and (2.3) indicates necessarily that the integral equation (2.4) is satisfied for any weighting function.

This heuristic proof indicates that Eq.(2.4) is a necessary and sufficient condition for the satisfaction of the governing equations. In other words, function ϕ satisfying the differential equations (2.2) and (2.3) also satisfies the equivalent integral form (2.4). The solution of the problem via Eq.(2.4) or via (2.2) and (2.3) are the starting point for method such as finite difference or finite point procedures based on the satisfaction of the differential equations in a finite set governing of points in the analysis domain. On the other hand, Eq.(2.4) is the basis of the so-called integral methods, such as the finite element method (FEM).

An interesting feature of Eq.(2.4) is the additive property of the integral. This, if the integrals of Eq.(2.4) are computable, the integral from of Eq.(2.4) can be written as

$$\sum_e \int_{\Omega^e} W A(\phi) dx + \sum_e \int_{\Gamma^e} \bar{W} B(\phi) d\Gamma = 0 \quad (2.5)$$

where the sum extends over the collection of non-interesting domains (elements) covering the domain Ω and its boundary Γ . Eq.(2.5) is the basis of the assembly process in the FEM.

2.3.1 Approximation of the unknown. Weighted Residuals

The numerical solution of the problem sought for an approximate value of the unknown $\hat{\phi}$ such that

$$\phi(x) \cong \hat{\phi}(x) \quad (2.6)$$

The usual way for expressing the approximate solution is via a linear combination of functions as

$$\hat{\phi}(x) = \sum_{i=0}^n N_i(x) a_i \quad (2.7)$$

where a_i are the unknown parameters and $N_i(x)$ are functions of the independent variable x . Typical choices for N_i , are

1. *Monomials* ($N_i(x) = x^i$):

$$\hat{\phi}(x) = \sum_{i=0}^n a_i x^i = a_0 + \sum_{i=1}^n a_i x^i \quad (2.8a)$$

2. *Fourier series functions* ($N_i(x) = \sin ix, \cos ix$):

$$\hat{\phi}(x) = \sum_{i=0}^n a_i \cos ix + \sum_{i=0}^n \beta_i \sin ix = a_0 + \sum_{i=1}^p a_i \cos ix + \sum_{i=1}^p \beta_i \sin ix \quad (2.8b)$$

3. *Exponential functions* ($N_i(x) = e^{bix}$):

$$\hat{\phi}(x) = \sum_0^n a_i e^{bix} \quad (2.8c)$$

Substituting the approximate function $\hat{\phi}$ into the integral expression (2.4) gives

$$\int_{\Omega} W A(\hat{\phi}) d\Omega + \oint_{\Gamma} \bar{W} B(\hat{\phi}) d\Gamma = 0 \quad (2.9)$$

The above expression is an approximation of the integral form (2.4) and it is usually called *weighed residual* expression. This name comes after observing that $A(\hat{\phi})$ and $B(\hat{\phi})$ are the “residuals” of the approximate solution in the domain and the boundary, respectively. Thus, substituting $\hat{\phi}$ into the governing equations we have

$$A(\hat{\phi}) = r_{\Omega} \quad \text{in } \Omega$$

$$B(\hat{\phi}) = r_{\Gamma} \quad \text{in } \Gamma$$

Hence, Eq.(2.9) can be written as

$$\int_{\Omega} W r_{\Omega} d\Omega + \oint_{\Gamma} \bar{W} r_{\Gamma} d\Gamma = 0 \quad (2.10a)$$

Obviously, if $\hat{\phi}$ is the exact solution, i.e. of $\phi = \hat{\phi}$, then $r_{\Omega} = 0$ in Ω and $r_{\Gamma} = 0$ in Γ .

The value of the residuals r_{Ω} and r_{Γ} indicate the error in the satisfaction of the governing differential equations due to the choice of the approximate function $\hat{\phi}$.

Expressions (2.9) or (2.10a) can be therefore be interpreted as the integral of the residuals of the differential equations weighted by the functions $w(x)$ and $\bar{w}(x)$. This explains the name of the weighted residual method.

The approximate solution is found by choosing a *finite set* of weighted functions. Thus, by choosing a number of weighting functions equal to the terms of the expansion (3), the following system of equations is obtained

$$\int_{\Omega} W_i A(\sum_j N_j a_j) d\Omega + \oint_{\Gamma} \bar{W}_i B(\sum_j N_j a_j) d\Gamma = 0; \quad i = 1, n \quad (2.11)$$

The above expression can be written in matrix form, after an adequate ordering, as

$$\mathbf{K}\mathbf{a} = \mathbf{f} \quad (2.12)$$

where \mathbf{K} is a square matrix which elements depend on the geometrical and physical properties of the problem, \mathbf{a} is the vector containing the n unknown parameters and \mathbf{f} is a vector depending on the prescribed value of the fluxes and the unknown function in the boundary.

Solution of the algebraic equation system (2.12) yields the value of the unknowns a_i . The derivation of Eq.(2.12) for some specific problems will be presented in the following sections.

2.3.2 Application of the WRM for the solution of the 1D heat conduction equation

The more typical particular cases of the WRM are

1. Point collocation method
2. Subdomain collocation method
3. Galerkin method
4. Least square method

Let us consider the solution of the 1D Poisson equation for $k = \text{constant}$, i.e.

$$A(\phi) = k \frac{d^2 \phi}{dx^2} + Q = 0 \quad \text{in } \Omega \quad (2.13)$$

More specifically, let us consider the solution of a heat conduction problem in 1D, where k is the heat conductivity, Q is the external heat source per unit length and ϕ is the temperature.

In the example to be solved (Figure 2.5) we will take

$$k = 1$$

$$Q: \begin{cases} 1 & \text{for } 0 \leq x < l/2 \\ 0 & \text{for } l/2 < x \leq l \end{cases} \quad (2.14)$$

Boundary conditions

$$B(\phi): \begin{cases} \phi = 0 & \text{in } x = 0 \\ \phi = 0 & \text{in } x = l \end{cases} \quad (2.15)$$

The solution process via the WRM follows the steps previously explained, i.e.

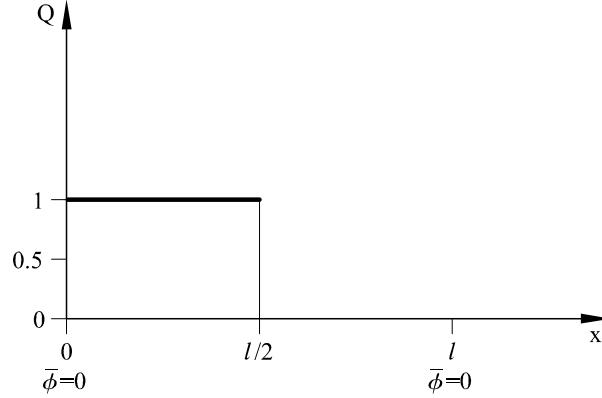


Figure 2.5: Heat conduction in a bar of length l . Piece-wise distribution of the heat source Q and prescribed temperature at the ends

- We define the governing differential equations of the problem

$$A(\phi) = 0 \quad \text{in the domain } \Omega$$

- and the boundary conditions

$$B(\phi) = 0 \quad \text{in the boundary } \Gamma \text{ of } \Omega$$

The solution process is as follows

1. The unknown $\phi(x)$ is approximated by a function $\hat{\phi}(x)$ as

$$\phi \cong \hat{\phi} = \sum_{i=1}^n N_i(x) a_i \quad (2.16)$$

where $N_i(x)$ is a known “shape functions” and a_i $i = 1, n$ are n the unknown parameters. Substituting Eq.(2.16) into Eqs.(2.15) yields the residuals (errors) in the domain and the boundary, i.e.

$$\begin{aligned} A(\hat{\phi}) &= r_\Omega \neq 0 & \text{in } \Omega \\ B(\hat{\phi}) &= r_\Gamma \neq 0 & \text{in } \Gamma \end{aligned}$$

2. We impose that the integral of the residuals, weighted with n test functions W_i and \bar{W}_i is zero, i.e.

$$\boxed{\int_{\Omega} W_i(x) A(\hat{\phi}) d\Omega + \int_{\Gamma} \bar{W}_i(x) B(\hat{\phi}) d\Gamma = 0} \quad i = 1, 2, \dots, n \quad (2.17)$$

3. the parameters a_i are found by solving the algebraic system of n equations with n unknowns resulting from Eq.(2.17) and written as

$$\mathbf{K}\mathbf{a} = \mathbf{f}$$

2.3.3 Global definition of the shape functions

The shape functions $N_i(x)$ can be defined “globally” over the whole domain Ω , or else “locally” in subdomains Ω_i . Next we will consider the global definition of $N_i(x)$.

For the solution of Eqs.(2.13)–(2.15) we will assume first an approximation of ϕ using Fourier series

$$\phi(x) \simeq \hat{\phi}(x) = \sum_{i=1}^n a_i \sin \frac{\pi x i}{l}; \quad i = 1, 2, \dots, n \quad (2.18)$$

$$N_i(x) = \sin \frac{\pi x i}{l} \quad (2.19)$$

From the expression of $N_i(x)$ we observe that

- they are continuous over the domain Ω ,
- they satisfy the boundary conditions (2.15), i.e.

$$\left. \begin{array}{l} N_i(0) = \sin(0) = 0 \\ N_i(l) = \sin(i\pi) = 0 \end{array} \right\} \forall_i$$

Hence

$$\begin{aligned} \hat{\phi}(0) &= \sum_{i=1}^n a_i N_i(0) = 0 \\ \hat{\phi}(l) &= \sum_{i=1}^n a_i N_i(l) = 0 \end{aligned}$$

This gives

$$B(\hat{\phi}) = r_{\Gamma}(x) = 0 \quad \text{in the boundary } \Gamma \ (x = 0, x = l) \quad (2.20)$$

Also, from Eqs.(2.13) and (2.18)

$$\begin{aligned} A(\hat{\phi}) &= A \left(\sum_{i=1}^n a_i \sin \frac{\pi x i}{l} \right) = k \frac{d^2}{dx^2} \left(\sum_{i=1}^n a_i \sin \frac{\pi x i}{l} \right) + Q = \\ &= \sum_{i=1}^n \left[-a_i \left(\frac{i\pi}{l} \right)^2 \sin \frac{\pi x i}{l} \right] + Q \end{aligned} \quad (2.21)$$

Eq.(2.18) are re-written (for $r_{\Gamma} = 0$) as

$$\int_0^l \underbrace{W_i(x)}_{r_{\Omega}} \left(\frac{d^2 \hat{\phi}}{dx^2} + Q \right) dx = 0; \quad i = 1, 2, \dots, n$$

Substituting Eq.(2.18) into above integral gives

$$\int_0^l \left[\sum_1^n - \left(\frac{\pi j}{l} \right)^2 a_j \sin j \frac{\pi x}{l} + Q \right] W_i(x) dx = 0; \quad i = 1, 2, \dots, n$$

$$\sum_{j=1}^n \left[\underbrace{a_j \left(j \frac{\pi}{l} \right)^2 \int_0^l W_i(x) \sin j \frac{\pi x}{l} dx}_{K_{ij}} \right] = \underbrace{\int_0^l W_i(x) Q dx}_{f_i}, \quad i = 1, 2, \dots, n \quad (2.22)$$

In compact form

$$\boxed{\sum_{j=1}^n K_{ij} a_j = f_i} : \quad i = 1, 2, \dots, n \quad (2.23)$$

which leads to a system of n linear equation with n unknowns.

For $i = 1$

$$a_1 \left(\frac{\pi}{l} \right)^2 \int_0^l W_1 \sin \frac{\pi x}{l} dx + a_2 \left(\frac{2\pi}{l} \right)^2 \int_0^l W_1 \sin \frac{2\pi x}{l} dx + \dots$$

$$\dots + a_n \left(\frac{n\pi}{l} \right)^2 \int_0^l W_1 \sin \frac{n\pi x}{l} dx = \int_0^l W_1 Q dx$$

For $i = 2$

$$a_1 \left(\frac{\pi}{l} \right)^2 \int_0^l W_2 \sin \frac{\pi x}{l} dx + a_2 \left(\frac{2\pi}{l} \right)^2 \int_0^l W_2 \sin \frac{2\pi x}{l} dx + \dots$$

$$\dots + a_n \left(\frac{n\pi}{l} \right)^2 \int_0^l W_2 \sin \frac{n\pi x}{l} dx = \int_0^l W_2 Q dx$$

For $i = n$

$$a_1 \left(\frac{\pi}{l} \right)^2 \int_0^l W_n \sin \frac{\pi x}{l} dx + a_2 \left(\frac{2\pi}{l} \right)^2 \int_0^l W_n \sin \frac{2\pi x}{l} dx + \dots$$

$$\dots + a_n \left(\frac{n\pi}{l} \right)^2 \int_0^l W_n \sin \frac{n\pi x}{l} dx = \int_0^l W_n Q dx$$

The above equations can be written in matrix form as

$$\frac{\pi^2}{l^2} \begin{bmatrix} \int_0^l W_1 \sin \frac{\pi x}{l} dx & 4 \int_0^l W_1 \sin \frac{2\pi x}{l} dx & \dots & n^2 \int_0^l W_1 \sin \frac{n\pi x}{l} dx \\ \int_0^l W_2 \sin \frac{\pi x}{l} dx & 4 \int_0^l W_2 \sin \frac{2\pi x}{l} dx & \dots & n^2 \int_0^l W_2 \sin \frac{n\pi x}{l} dx \\ \vdots & \vdots & \vdots & \vdots \\ \int_0^l W_n \sin \frac{\pi x}{l} dx & 4 \int_0^l W_n \sin \frac{2\pi x}{l} dx & \dots & n^2 \int_0^l W_n \sin \frac{n\pi x}{l} dx \end{bmatrix} \begin{Bmatrix} a_1 \\ a_2 \\ \vdots \\ a_n \end{Bmatrix} =$$

$$= \begin{Bmatrix} \int_0^l QW_1 dx \\ \int_0^l QW_2 dx \\ \vdots \\ \int_0^l QW_n dx \end{Bmatrix}$$

or

$$i \rightarrow \underbrace{\begin{pmatrix} K_{11} & K_{12} & \dots & K_{1n} \\ K_{21} & K_{22} & \dots & K_{2n} \\ \vdots & \vdots & \boxed{K_{ij}} & \vdots \\ K_{n1} & K_{n2} & \dots & K_{nn} \end{pmatrix}}_{\mathbf{K}} \underbrace{\begin{Bmatrix} a_1 \\ a_2 \\ a_i \\ a_n \end{Bmatrix}}_{\mathbf{a}} = \underbrace{\begin{Bmatrix} f_1 \\ f_2 \\ f_i \\ f_n \end{Bmatrix}}_{\mathbf{f}} \quad (2.24)$$

$$\mathbf{Ka} = \mathbf{f} \quad (2.25)$$

where a term K_{ij} of \mathbf{K} can be expressed as

$$K_{ij} = \left(\frac{j\pi}{l}\right)^2 \int_0^l W_i(x) \sin j \frac{\pi x}{l} dx \quad (2.26)$$

Similarly a term f_i of \mathbf{f} is

$$f_i = \int_0^l W_i(x) Q(x) dx \quad (2.27)$$

Expressions (2.26) and (2.27) are a generic form of the terms of \mathbf{K} and \mathbf{f} , respectively, which favours the programming of all the expressions.

The remaining step is the evaluation of all matrices and vectors after defining the weighted functions W_i . The selection of W_i yields different forms of the Weighted Residual Method.

2.3.4 Point Collocation Method

This method consists in defining n points in the analysis domain and choosing the Dirac Delta functions as the weighting function. Thus,

$$W_i(x) = \delta(x - x_i), \quad i = 1, 2, \dots, n \quad (2.28)$$

Function δ has the property that for $x \neq x_i$, $\delta_i(x) = 0$ and satisfies the conditions

$$\int_{-\infty}^{\infty} \delta(x - x_i) dx = 1 \quad (2.29a)$$

$$\int_0^l f(x) \delta(x - x_i) dx = f(x_i) \quad (2.29b)$$

Thus

$$\int_0^l W_i(x) A(\hat{\phi}) dx = \int_0^l \delta(x - x_i) A(\hat{\phi}) dx = A(\hat{\phi}) \Big|_{x=x_i} = 0, \quad i = 1, 2, \dots, n \quad (2.30)$$

Choosing the Dirac Delta functions as the weighting function, it is equivalent to making $A(\hat{\phi})$ equal to zero at each point $x = x_i$ ($i = 1, \dots, n$). Hence, the procedure is equivalent to imposing the vanishing of the residual at each one of the sampling points chosen. From Eq.(2.30) we deduce that there is no need to perform an integration for obtaining the system of algebraic equations.

We will solve the previous problem for one and two terms of the Fourier series expansions (2.18).

Solution with $W_i = \delta_i$ for $n = 1$

$$\hat{\phi} = N_1(x) a_1$$

We take

$$x_i = x_1 = l/2$$

From Eq.(2.28)

$$W_1(x) = \delta(x - l/2)$$

From Eq.(2.27)

$$f_i = f_1 = \int_0^l \delta(x - l/2) Q(x) dx = Q\left(\frac{l}{2}\right) = \frac{1}{2}$$

This value is deduced from Figure 2.5. At a point infinitely close to $x = l/2$ from the left Q takes a unit value, where $Q = 0$ for a point to the right of $x = l/2$. This difficulty is overcome by taking $Q = l/2$ for $x = l/2$.

On the other hand

$$K_{11} = \left(\frac{\pi}{l}\right)^2 \int_0^l \delta\left(\frac{x-l}{2}\right) \sin \frac{\pi x}{l} dx = \left(\frac{\pi}{l}\right)^2 \sin \frac{\pi l}{l 2} = \left(\frac{\pi}{l}\right)^2$$

From (2.24)

$$K_{11}a_1 = f_1$$

$$\frac{\pi^2}{l^2}a_1 = \frac{1}{2} \implies \boxed{a_1 = l^2/2\pi^2}$$

The approximate function sought is therefore

$$\boxed{\hat{\phi}(x) = \underbrace{\frac{l^2}{2\pi^2}}_{a_1} \underbrace{\sin \frac{\pi}{l}x}_{N_1(x)}} \longrightarrow \hat{\phi} = 0,0507 l^2 \sin \frac{\pi x}{l}$$

We can verify that the residual r_Ω vanishes at $x_1 = l/2$

$$\begin{aligned} A(\hat{\phi}) \Big|_{x=x_1=l/2} &= \frac{d^2 \hat{\phi}}{dx^2} + Q = \frac{d^2}{dx^2} \left(\frac{l^2}{2\pi^2} \sin \frac{\pi}{l}x \right) \Big|_{x=l/2} + Q(x) \Big|_{x=l/2} = \\ &= -\frac{l^2}{2\pi^2} \frac{\pi^2}{l^2} \sin \frac{\pi}{l}x \Big|_{x=l/2} + Q \left(\frac{l}{2} \right) = -\frac{1}{2} + \frac{1}{2} = 0 \end{aligned}$$

Solution with $W_i = \delta_i$ for $n = 2$

$$\hat{\phi}(x) = N_1(x)a_1 + N_2(x)a_2$$

Taking

$$\begin{aligned} x_1 &= l/4 \\ x_2 &= 3/4l \end{aligned}$$

$$W_1(x) = \delta(x - l/4)$$

$$W_2(x) = \delta(x - 3/4l)$$

From Eq.(2.23) we obtain

For $i = 1$

$$K_{11}a_1 + K_{12}a_2 = f_1$$

For $i = 2$

$$K_{21}a_1 + K_{22}a_2 = f_2$$

The algebraic equation system is

$$\begin{bmatrix} K_{11} & K_{12} \\ K_{21} & K_{22} \end{bmatrix} \begin{Bmatrix} a_1 \\ a_2 \end{Bmatrix} = \begin{Bmatrix} f_1 \\ f_2 \end{Bmatrix}$$

For $i = 1$

$$K_{11} = \frac{\pi^2}{l^2} \int_0^l W_1 \sin \frac{\pi x}{l} dx = \frac{\pi^2}{l^2} \int_0^l \delta \left(x - \frac{l}{4} \right) \sin \frac{\pi x}{l} dx = \frac{\pi^2}{l^2} \sin \frac{\pi l}{4} = \frac{\sqrt{2} \pi^2}{2 l^2}$$

$$K_{12} = \frac{4\pi^2}{l^2} \int_0^l W_1 \sin \frac{2\pi x}{l} dx = \frac{4\pi^2}{l^2} \int_0^l \delta \left(x - \frac{l}{4} \right) \sin \frac{2\pi x}{l} dx = \frac{4\pi^2}{l^2} \sin \frac{2\pi}{4} l = \frac{4\pi^2}{l^2}$$

$$f_1 = \int_0^l Q(x) W_1(x) dx = \int_0^l Q \delta \left(x - \frac{l}{4} \right) dx = Q \left(\frac{l}{4} \right) = 1$$

For $i = 2$

$$K_{21} = \frac{\pi^2}{l^2} \int_0^l W_2 \sin \frac{\pi x}{l} dx = \frac{\pi^2}{l^2} \int_0^l \delta \left(x - \frac{3l}{4} \right) \sin \frac{\pi x}{l} dx = \frac{\pi^2}{l^2} \sin \frac{3\pi l}{4} = \frac{\sqrt{2} \pi^2}{2 l^2}$$

$$K_{22} = \frac{4\pi^2}{l^2} \int_0^l W_2 \sin \frac{2\pi x}{l} dx = \frac{4\pi^2}{l^2} \int_0^l \delta \left(x - \frac{3l}{4} \right) \sin \frac{2\pi x}{l} dx = \frac{4\pi^2}{l^2} \sin \frac{2\pi}{4} \frac{3l}{l} = -\frac{4\pi^2}{l^2}$$

$$f_2 = \int_0^l Q(x) W_2(x) dx = \int_0^l Q \delta \left(x - \frac{3l}{4} \right) dx = Q \left(\frac{3l}{4} \right) = 0$$

Therefore

$$\frac{\pi^2}{l^2} \begin{bmatrix} \frac{\sqrt{2}}{2} & 4 \\ \frac{\sqrt{2}}{2} & -4 \end{bmatrix} \begin{Bmatrix} a_1 \\ a_2 \end{Bmatrix} = \begin{Bmatrix} 1 \\ 0 \end{Bmatrix} \Rightarrow \begin{cases} a_1 = l^2 / \sqrt{2} \pi^2 \\ a_2 = l^2 / 8\pi^2 \end{cases}$$

The approximate solution is

$$\hat{\phi}(x) = \underbrace{\frac{1}{\sqrt{2}} \frac{l^2}{\pi^2}}_{a_1} \underbrace{\sin \frac{\pi x}{l}}_{N_1(x)} + \underbrace{\frac{l^2}{8\pi^2}}_{a_2} \underbrace{\sin \frac{2\pi x}{l}}_{N_2(x)}$$

We can verify that

$$A(\hat{\phi}) = 0 \Big|_{\substack{x_1=l/4 \\ x_2=3/4l}}$$

$$A(\hat{\phi}) = \frac{d^2 \hat{\phi}}{dx^2} + Q(x) = - \left\{ \frac{1}{\sqrt{2}} \frac{l^2}{\pi^2} \frac{\pi^2}{l^2} \sin \frac{\pi}{l} x + \frac{1}{8} \frac{l^2}{\pi^2} \frac{4\pi^2}{l^2} \sin \frac{2\pi}{l} x \right\} + Q(x) \Big|_{x_1, x_2}$$

$$A(l/4) = - \left(\frac{1}{\sqrt{2}} \frac{\sqrt{2}}{2} + \frac{1}{2} 1 \right) + Q(l/4) = -1 + 1 = 0$$

$$A(3/4l) = - \left(\frac{1}{\sqrt{2}} \frac{\sqrt{2}}{2} + \frac{1}{2} (-1) \right) + Q \left(\frac{3}{4} l \right) = -0 + 0 = 0$$

2.3.5 Subdomain collocation method

The method consists in subdividing the domain Ω into as many subdomains as unknown parameters a_i . The test functions W_i are then chosen so that they take a unit value in each subdomain Ω_i and zero in the rest. Thus,

$$\begin{aligned} W_i(x) &= 1 & \forall x \in \Omega_i \\ W_i(x) &= 0 & \forall x \notin \Omega_i \end{aligned} \quad (2.31)$$

Applying the WRM gives

$$\int_{\Omega_i} A(\hat{\phi}) dx = 0, \quad i = 1, 2, \dots, n \quad (2.32)$$

The previous equation is equivalent to making zero the integral of the residual in each subdomain Ω_i .

As in the previous case we will find $\hat{\phi}(x)$ for one and two terms of the Fourier series expansion (2.18)

Solution for $n = 1$

$$\begin{aligned} \hat{\phi}(x) &= N_1(x)a_1 \\ \Omega_i &\equiv \Omega \end{aligned}$$

i.e., the subdomain Ω_i is taken to coincide with the whole domain $\Omega : [0, l]$

$$W_1 = 1 \quad 0 \leq x \leq l$$

From Eq.(2.32) we deduce

$$K_{11}a_1 = f_1$$

where

$$K_{11} = \frac{\pi^2}{l^2} \int_0^l W_1 \sin \frac{\pi x}{l} dx = \frac{\pi^2}{l^2} \int_0^l \sin \frac{\pi x}{l} dx = \frac{2\pi}{l}$$

$$f_1 = \int_0^l W_1 Q(x) dx = \int_0^l Q(x) dx = \int_0^{l/2} \underbrace{Q(x)}_1 dx + \int_{l/2}^l Q(x) dx = l/2$$

Therefore

$$\frac{\overbrace{\frac{K_{11}}{2\pi}}}{l} a_1 = \frac{\overbrace{f_1}}{l} \implies \boxed{a_1 = \frac{l^2}{4\pi}}$$

and

$$\hat{\phi}(x) = \underbrace{\frac{l^2}{4\pi}}_{a_1} \underbrace{\sin \frac{\pi x}{l}}_{N_1(x)}$$

Solution for $n = 2$

$$\hat{\phi}(x) = N_1(x)a_1 + N_2(x)a_2$$

We take as subdomains the two intervals

$$[0, l/2] \quad \text{and} \quad [l/2, l]$$

hence

$$W_1(x) : \begin{cases} 1 & 0 \leq x \leq l/2 \\ 0 & l/2 < x \leq l \end{cases}$$

$$W_2(x) : \begin{cases} 0 & 0 \leq x \leq l/2 \\ 1 & l/2 < x \leq l \end{cases}$$

The above is equivalent to imposing that the integral of the residual is zero in each of the two subdomains chosen.

In Eq.(2.23) we have for $n = 2$, $i = 1, 2$

$$\begin{array}{l} i = 1; \\ i = 2; \end{array} \quad \begin{array}{l} K_{11}a_1 + K_{12}a_2 = f_1 \\ K_{21}a_1 + K_{22}a_2 = f_2 \end{array} \quad \Bigg| \quad \Longrightarrow \quad \begin{bmatrix} K_{11} & K_{12} \\ K_{21} & K_{22} \end{bmatrix} \begin{Bmatrix} a_1 \\ a_2 \end{Bmatrix} = \begin{Bmatrix} f_1 \\ f_2 \end{Bmatrix}$$

For $i = 1$

$$K_{11} = \frac{\pi^2}{l^2} \int_0^l W_1 \sin \frac{\pi x}{l} dx = \frac{\pi^2}{l^2} \int_0^{l/2} \sin \frac{\pi x}{l} dx = \frac{\pi}{l}$$

$$K_{12} = \frac{4\pi^2}{l^2} \int_0^l W_1 \sin \frac{2\pi x}{l} dx = \frac{4\pi^2}{l^2} \int_0^{l/2} \sin \frac{2\pi x}{l} dx = \frac{4\pi}{l}$$

$$f_1 = \int_0^l W_1 Q dx = \int_0^{l/2} Q dx = \frac{l}{2}$$

For $i = 2$

$$K_{21} = \frac{\pi^2}{l^2} \int_0^l W_2 \sin \frac{\pi x}{l} dx = \frac{\pi^2}{l^2} \int_{l/2}^l \sin \frac{\pi x}{l} dx = \frac{\pi}{l}$$

$$K_{22} = \frac{4\pi^2}{l^2} \int_0^l W_2 \sin \frac{2\pi x}{l} dx = \frac{4\pi^2}{l^2} \int_{l/2}^l \sin \frac{2\pi x}{l} dx = -\frac{4\pi}{l}$$

$$f_2 = \int_0^l W_2 Q dx = \int_{l/2}^l Q dx = 0$$

Hence

$$\frac{\pi}{l} \begin{bmatrix} 1 & 4 \\ 1 & -4 \end{bmatrix} \begin{Bmatrix} a_1 \\ a_2 \end{Bmatrix} = \begin{Bmatrix} l/2 \\ 0 \end{Bmatrix} \Rightarrow \begin{cases} a_1 = l^2/4\pi \\ a_2 = l^2/16\pi \end{cases}$$

The approximate solution is now

$$\hat{\phi}(x) = \underbrace{\frac{l^2}{4\pi}}_{a_1} \underbrace{\sin \frac{\pi x}{l}}_{N_1(x)} + \underbrace{\frac{l^2}{16\pi}}_{a_2} \underbrace{\sin \frac{2\pi x}{l}}_{N_2(x)}$$

2.3.6 Galerkin method

This popular method consists in taking as weighting functions the approximation functions N_i , i.e.

$$W_i(x) \equiv N_i(x) \quad (2.33)$$

The WRM is written as

$$\int_{\Omega} N_i A(\hat{\phi}) d\Omega + \int_{\Gamma} N_i B(\hat{\phi}) d\Gamma = 0 \quad (2.34)$$

In the problem we are solving the integral over the boundary Γ is zero. Next we will solve the problem by taking one and two terms of the approximation (2.18) as in the previous cases.

Solution for $n = 1$

$$\begin{aligned} \hat{\phi}(x) &= N_1(x) a_1 \\ W_1(x) &= N_1(x) = \sin \frac{\pi x}{l} \end{aligned}$$

Hence

$$K_{11} = \frac{\pi^2}{l^2} \int_0^l W_1 \sin \frac{\pi x}{l} dx = \frac{\pi^2}{l} \int_0^l \sin^2 \frac{\pi x}{l} dx = \frac{\pi^2}{2l}$$

$$f_1 = \int_0^l W_1 Q dx = \int_0^{l/2} \sin \frac{\pi x}{l} 1 dx = l/\pi$$

Therefore

$$\underbrace{\frac{\pi^2}{2l}}_{K_{11}} a_1 = \underbrace{\frac{l}{\pi}}_{f_1} \rightarrow a_1 = \frac{2l^2}{\pi^3}$$

The final result is

$$\hat{\phi}(x) = \underbrace{\frac{2l^2}{\pi^3}}_{a_1} \underbrace{\sin \frac{\pi x}{l}}_{N_1(x)}$$

Solution for $n = 2$

$$\begin{aligned}\hat{\phi}(x) &= N_1(x)a_1 + N_2(x)a_2 \\ W_1(x) &= N_1(x) = \sin \frac{\pi x}{l} \\ W_2(x) &= N_2(x) = \sin \frac{2\pi x}{l}\end{aligned}$$

The terms of the system (2.23) are

For $i = 1$

$$\begin{aligned}K_{11} &= \frac{\pi^2}{l^2} \int_0^l W_1 dx \sin \frac{\pi x}{l} = \frac{\pi^2}{l^2} \int_0^l \sin^2 \frac{\pi x}{l} dx = \frac{\pi^2}{2l} \\ K_{12} &= \frac{4\pi^2}{l^2} \int_0^l W_1 \sin \frac{2\pi x}{l} dx = \frac{4\pi^2}{l^2} \int_0^l \sin \frac{\pi x}{l} \sin \frac{2\pi x}{l} dx = 0 \\ f_1 &= \int_0^l W_1 Q dx = \int_0^{l/2} \sin \frac{\pi x}{l} 1 dx = \frac{l}{\pi}\end{aligned}$$

For $i = 2$

$$\begin{aligned}K_{21} &= \frac{\pi^2}{l^2} \int_0^l W_2 \sin \frac{\pi x}{l} dx = \frac{\pi^2}{l^2} \int_0^l \sin \frac{2\pi x}{l} \sin \frac{\pi x}{l} dx = 0 \\ K_{22} &= \frac{4\pi^2}{l^2} \int_0^l W_2 \sin \frac{2\pi x}{l} dx = \frac{4\pi^2}{l^2} \int_0^l \sin^2 \frac{2\pi x}{l} dx = 2\frac{\pi^2}{l} \\ f_2 &= \int_0^l W_2 Q dx = \int_0^{l/2} \sin \frac{2\pi x}{l} 1 dx = \frac{l}{\pi}\end{aligned}$$

The resulting matrix expression is

$$\frac{\pi^2}{l} \begin{bmatrix} 1/2 & 0 \\ 0 & 2 \end{bmatrix} \begin{Bmatrix} a_1 \\ a_2 \end{Bmatrix} = \begin{Bmatrix} l/\pi \\ l/\pi \end{Bmatrix} \Rightarrow \begin{cases} a_1 = 2l^2/\pi^3 \\ a_2 = l^2/2\pi^3 \end{cases}$$

The approximate solution is

$$\hat{\phi}(x) = \underbrace{\frac{2l^2}{\pi^3}}_{a_1} \underbrace{\sin \frac{\pi x}{l}}_{N_1(x)} + \underbrace{\frac{l^2}{2\pi^3}}_{a_2} \underbrace{\sin \frac{2\pi x}{l}}_{N_2(x)}$$

2.3.7 Least square method

The least square (LSQ) method consists in finding the unknown parameters by minimizing the integral of the residual squared in the analysis domain. The minimization process implies the derivation of the integral with respect to each unknown. This leads to an algebraic system of n equations with n unknowns, as in the previous methods.

The LSQ method can be interpreted as a particular case of the WRM with $W = A(\phi)$ and $\hat{W} = B(\phi)$.

The expression to be minimized is

$$I = \int_{\Omega} [A(\hat{\phi})]^2 d\Omega + \int_{\Gamma} [B(\hat{\phi})]^2 d\Gamma \quad (2.35)$$

Making

$$\delta I = \frac{\partial I}{\partial a_1} \delta a_1 + \frac{\partial I}{\partial a_2} \delta a_2 + \dots + \frac{\partial I}{\partial a_n} \delta a_n = 0 \quad (2.36)$$

Satisfaction of this equation implies

$$\begin{cases} \frac{\partial I}{\partial a_1} = 0 \\ \frac{\partial I}{\partial a_2} = 0 \\ \vdots \\ \frac{\partial I}{\partial a_n} = 0 \end{cases} \quad (2.37)$$

For the 1D heat conduction problem in hand the minimization process can be written as

$$\frac{\partial}{\partial a_i} \int_0^l [A(\hat{\phi})]^2 dx = 0; \quad i = 1, 2, \dots, n$$

or

$$\begin{aligned} \frac{\partial}{\partial a_i} \int_0^l \left[\frac{d^2 \hat{\phi}}{dx^2} + Q \right]^2 dx &= \int_0^l 2 \left[\frac{d^2 \hat{\phi}}{dx^2} + Q \right] \frac{\partial}{\partial a_i} \left[\frac{d^2 \hat{\phi}}{dx^2} \right] dx \\ &= \int_0^l \underbrace{2 \frac{\partial}{\partial a_i} \left[\frac{d^2 \hat{\phi}}{dx^2} \right]}_{W_i(x)} \underbrace{\left[\frac{d^2 \hat{\phi}}{dx^2} + Q \right]}_{A(\hat{\phi})} dx \\ &= \int_0^l W_i(x) A(\hat{\phi}) dx = 0 \quad i = 1, 2, \dots, n \end{aligned}$$

The outcome of the minimization process can be interpreted as a form of the WRM with

$$\begin{aligned} W_i &= 2 \frac{\partial}{\partial a_i} \left[\frac{d^2 \hat{\phi}}{dx^2} \right] = 2 \frac{\partial}{\partial a_i} \left[\frac{d^2}{dx^2} \left(\sum_1^n a_j \sin \frac{j\pi x}{l} \right) \right] = \\ &= 2 \frac{\partial}{\partial a_i} \left[-a_1 \left(\frac{\pi}{l} \right)^2 \sin \frac{1\pi x}{l} - a_2 \left(\frac{2\pi}{l} \right)^2 \sin \frac{2\pi x}{l} - \dots \right. \\ &\quad \left. - a_i \left(\frac{i\pi}{l} \right)^2 \sin \frac{i\pi x}{l} - \dots - a_n \left(\frac{n\pi}{l} \right)^2 \sin \frac{n\pi x}{l} \right] = \\ &= -2 \left(\frac{i\pi}{l} \right)^2 \sin \frac{i\pi x}{l} \end{aligned}$$

Solution for $n = 1$

$$\begin{aligned} \hat{\phi}(x) &= N_1(x)a_1 \\ W_1 &= -\frac{2\pi^2}{l^2} \sin \frac{\pi x}{l}; \quad i = 1 \end{aligned}$$

After a little algebra we find

$$K_{11} = \frac{\pi^2}{l^2} \int_0^l W_1 \sin \frac{\pi x}{l} dx = \frac{\pi^2}{l^2} \int_0^l -\frac{2\pi^2}{l^2} \sin^2 \frac{\pi x}{l} dx = -\frac{\pi^4}{l^3}$$

$$f_1 = \int_0^l W_1 Q dx = \int_0^{l/2} -\frac{2\pi^2}{l^2} \sin \frac{\pi x}{l} dx = -\frac{2\pi}{l}$$

Finally we obtain

$$-\frac{\pi^4}{l^3} a_1 = -2 \frac{\pi}{l} \Rightarrow a_1 = \frac{2l^2}{\pi^3}$$

Hence

$$\hat{\phi}(x) = \underbrace{\frac{2l^2}{\pi^3}}_{a_1} \underbrace{\sin \frac{\pi x}{l}}_{N_1(x)}$$

Solution for $n = 2$

$$\begin{aligned} \hat{\phi}(x) &= N_1(x)a_1 + N_2(x)a_2 \\ W_1 &= -2 \frac{\pi^2}{l^2} \sin \frac{\pi x}{l}; \quad i = 1 \\ W_2 &= -\frac{8\pi^2}{l^2} \sin \frac{2\pi x}{l}; \quad i = 2 \end{aligned}$$

After some algebra we find

For $i = 1$

$$K_{11} = \frac{\pi^2}{l^2} \int_0^l W_1 \sin \frac{\pi x}{l} dx = \frac{\pi^2}{l^2} \int_0^l -\frac{2\pi^2}{l^2} \sin^2 \frac{\pi x}{l} dx = -\frac{\pi^4}{l^3}$$

$$K_{12} = \frac{4\pi^2}{l^2} \int_0^l W_1 \sin \frac{2\pi x}{l} dx = \frac{4\pi^2}{l^2} \int_0^l -\frac{2\pi^2}{l^2} \sin \frac{\pi x}{l} \sin \frac{2\pi x}{l} dx = 0$$

$$f_1 = \int_0^l W_1 Q dx = \int_0^{l/2} -\frac{2\pi^2}{l^2} \sin \frac{\pi x}{l} 1 dx = -\frac{2\pi}{l}$$

For $i = 2$

$$K_{21} = \frac{\pi^2}{l^2} \int_0^l W_2 \sin \frac{\pi x}{l} dx = \frac{\pi^2}{l^2} \int_0^l -\frac{8\pi^2}{l^2} \sin \frac{2\pi x}{l} \sin \frac{\pi x}{l} dx = 0$$

$$K_{22} = \frac{4\pi^2}{l^2} \int_0^l W_2 \sin \frac{2\pi x}{l} dx = \frac{4\pi^2}{l^2} \int_0^l -\frac{8\pi^2}{l^2} \sin^2 \frac{2\pi x}{l} dx = -16 \frac{\pi^4}{l^3}$$

$$f_2 = \int_0^l W_2 Q dx = \int_0^{l/2} -\frac{8\pi^2}{l^2} \sin \frac{2\pi x}{l} 1 dx = -\frac{8\pi}{l}$$

The final system of equations is

$$\frac{\pi^4}{l^3} \begin{bmatrix} -1 & 0 \\ 0 & -16 \end{bmatrix} \begin{Bmatrix} a_1 \\ a_2 \end{Bmatrix} = \begin{Bmatrix} -2\pi/l \\ -8\pi/l \end{Bmatrix} \Rightarrow \begin{cases} a_1 = 2l^2/\pi^3 \\ a_2 = l^2/2\pi^3 \end{cases}$$

The approximate solution is

$$\hat{\phi}(x) = \frac{2l^2}{\pi^3} \sin \frac{\pi x}{l} + \frac{l^2}{2\pi^3} \sin \frac{2\pi x}{l}$$

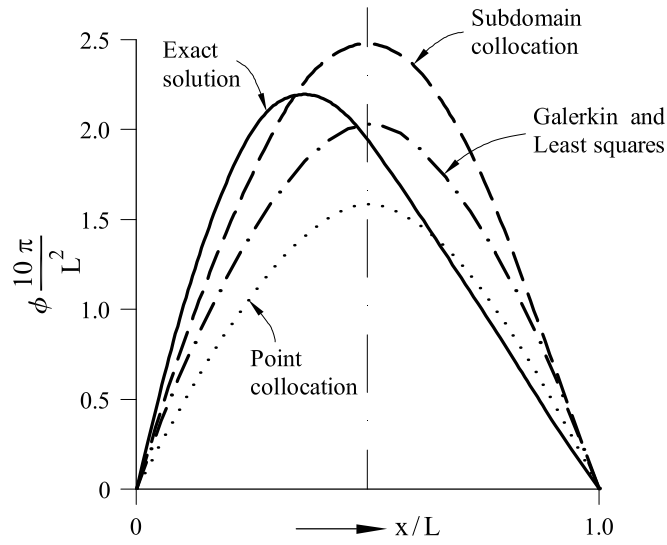
Note that the solution coincides with that obtained with the Galerkin method. This coincidence is fortuitous and it can not be generalized to other problems.

Figures 2.6 and 2.7 show the results obtained with the different WRM presented using one and two terms of the Fourier series used for the approximation (Eq.2.18). Note the best accuracy of the Galerkin method, which explains its popularity of this method for application with the FEM.

2.4 GENERAL SOLUTION PROCEDURE

Let is consider the equation

$$A(\phi) = \frac{d}{dx} \left(k \frac{d\phi}{dx} \right) + Q = 0 \quad \text{en } \overbrace{0 \leq x \leq l}^{\Omega} \quad (2.38)$$



	a_1	$\phi(l/4)$	$\phi(l/2)$	$\phi(3l/4)$
Exact solution		$0.0625 l^2$	$0.0625 l^2$	$0.0313 l^2$
Subdomain collocation	$0.0796 l^2$	$0.0563 l^2$	$0.0796 l^2$	$0.0563 l^2$
Point collocation	$0.0507 l^2$	$0.0359 l^2$	$0.0507 l^2$	$0.0359 l^2$
Galerkin	$0.0645 l^2$	$0.0456 l^2$	$0.0645 l^2$	$0.0456 l^2$
Least squares	$0.0645 l^2$	$0.0456 l^2$	$0.0645 l^2$	$0.0456 l^2$

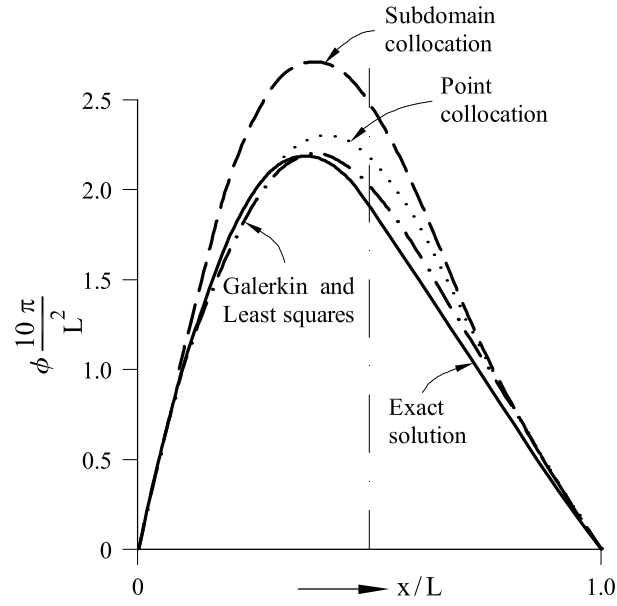
Figure 2.6: Exact and approximate solution using Fourier series (one term) for the 1D heat conduction problem of Figure 2.4

which governs the heat conduction problem of Figure 2.8 with the boundary conditions

$$B(\phi) \begin{cases} \phi - \bar{\phi} = 0; & \text{en } x = 0 (\Gamma_\phi) \\ k \frac{d\phi}{dx} + \bar{q} = 0; & \text{en } x = l (\Gamma_q) \end{cases} \quad (2.39)$$

The unknown ϕ is approximated by

$$\phi \simeq \hat{\phi} = \sum_{i=1}^n N_i(x) a_i \quad (2.40)$$



	a_1	a_2	$\phi(l/4)$	$\phi(l/2)$	$\phi(3l/4)$
Exact solution			$0.0625 l^2$	$0.0625 l^2$	$0.0313 l^2$
Subdomain collocation	$0.0796 l^2$	$0.0199 l^2$	$0.0762 l^2$	$0.0796 l^2$	$0.0364 l^2$
Point collocation	$0.0716 l^2$	$0.0127 l^2$	$0.0633 l^2$	$0.0796 l^2$	$0.0379 l^2$
Galerkin	$0.0645 l^2$	$0.0161 l^2$	$0.0617 l^2$	$0.0645 l^2$	$0.0295 l^2$
Least squares	$0.0645 l^2$	$0.0161 l^2$	$0.0617 l^2$	$0.0645 l^2$	$0.0295 l^2$

Figure 2.7: Exact and approximate solution using Fourier series (two terms) for the 1D heat conduction problem of Figure 2.4

Application of the WRM gives

$$\int_0^l W_i \underbrace{\left[\frac{d}{dx} \left(k \frac{d\hat{\phi}}{dx} \right) + Q \right]}_{A(\hat{\phi})} dx + \left[\underbrace{\bar{W}_i \left(k \frac{d\hat{\phi}}{dx} + \bar{q} \right)}_{B(\hat{\phi})} \right]_{x=l} = 0 \quad (i = 1, 2, \dots, n) \quad (2.41)$$

Note that we have not included in above expression the term in the Dirichlet boundary $\Gamma_{(x=0)}$. The reason is that in the following we will choose functions $\hat{\phi}$ that satisfy the Dirichlet boundary condition.

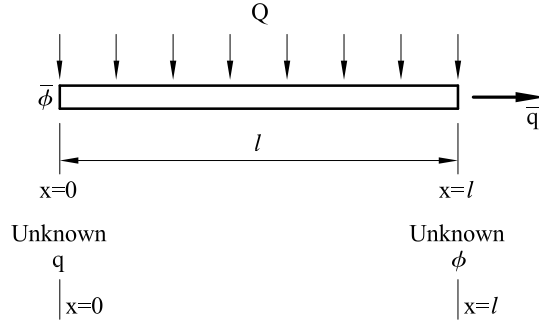


Figure 2.8: The 1D heat conduction problem in a bar

Introducing Eq.(2.40) into (2.41) gives

$$\begin{aligned} & \int_0^l W_i \frac{d}{dx} \left[k \left(\frac{dN_1}{dx} a_1 + \frac{dN_2}{dx} a_2 + \dots + \frac{dN_n}{dx} a_n \right) \right] dx + \\ & + \left[\bar{W}_i k \left(\frac{dN_1}{dx} a_1 + \frac{dN_2}{dx} a_2 + \dots + \frac{dN_n}{dx} a_n \right) + \bar{q} \right]_{x=l} + \\ & + \int_0^l W_i Q dx = 0 \quad (i = 1, 2, \dots, n) \end{aligned}$$

The above equations is a system of n equations with n unknowns that can be written in matrix form as

$$\underbrace{\begin{bmatrix} K_{11} & K_{12} & \dots & K_{1n} \\ K_{21} & K_{22} & \dots & K_{2n} \\ \vdots & & & \\ K_{n1} & K_{n2} & \dots & K_{nn} \end{bmatrix}}_{\mathbf{K}} \underbrace{\begin{bmatrix} a_1 \\ a_2 \\ \vdots \\ a_n \end{bmatrix}}_{\mathbf{a}} = \underbrace{\begin{bmatrix} f_1 \\ f_2 \\ \vdots \\ f_n \end{bmatrix}}_{\mathbf{f}} \quad (2.42)$$

where

$$\begin{aligned} K_{ij} &= \int_0^l W_i \frac{d}{dx} k \left(\frac{dN_j}{dx} \right) dx + \left[\bar{W}_i k \frac{dN_j}{dx} \right]_{x=l} \\ f_i &= - \int_0^l W_i Q dx - [\bar{W}_i \bar{q}]_{x=l} \end{aligned} \quad (2.43)$$

The selection of the test functions W_i leads to the different modalities of the WRM. For $W_i = N_i$ we obtain the Galerkin method. Note that in general

$$K_{ij} \neq K_{ji}$$

and, therefore, matrix \mathbf{K} is non symmetrical.

Application of the Galerkin method in the example of previous section lead to a symmetric expression of \mathbf{K} . This a consequence of the particular form of the Fourier expansion chosen for the approximation.

2.4.1 Conclusions

We point out some key aspects of the solution process explained in the previous section.

1. The unknown function is approximated by the sum of product of known functions $N_i(x)$ and unknown parameters a_i

$$\phi(x) \cong \hat{\phi}(x) = \sum_{i=1}^n N_i(x)a_i \quad (2.44)$$

2. The governing equations of the problem are written in an integral form via the WRM as

$$\int_{\Omega} W_i A(\hat{\phi}) dx + \int_{\Gamma} \bar{W}_i B(\hat{\phi}) dx = 0 \quad (2.45)$$

3. Substituting the approximation of the unknown into the previous integral form leads to a system of algebraic equations

$$\mathbf{K}\mathbf{a} = \mathbf{f}$$

Solution of above system gives the value of the parameters a_i , which define the approximate expression of the unknown function ϕ .

2.5 INTEGRABILITY CONDITION

Integration of the m th-derivative of a function $f(x)$ requires the continuity of its first $m - 1$ derivatives. In other words, the integral $\int_{\Omega} \frac{d^m f(x)}{dx^m} dx$ will be compatible if the derivative $\frac{d^{m-1} f(x)}{dx^{m-1}}$ is continuous.

This property is clarified in the example of Figure 2.9. The figure shows a linear function $f(x)$. The integral exists in the interval $[0, x_i + 1]$ and coincides with the area of the triangular region shown. Figure 2.9b shows the first derivative $f'(x)$. Note that this function is discontinuous and its integral is equal to the sum of the areas of the two rectangular regions shown. Figure 2.9c shows $f''(x)$. The function is not integrable and this is a consequence of $f'(x)$ not being continuous, in agreement with the integrability criterium stated above.

A function is C^m continuous if the function and its m first derivatives are continuous. This C^1 continuous function implies that both the function and its first derivatives are continuous, C^0 continuity indicates that just the function is continuous. C^{-1} continuity implies that the function is discontinuous.

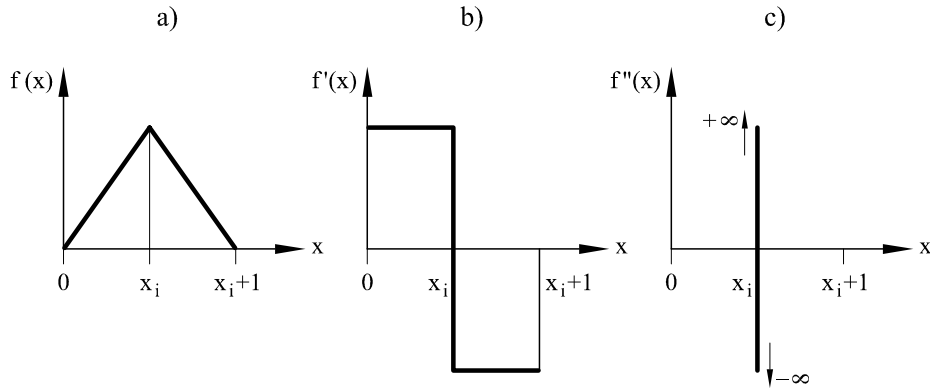


Figure 2.9: Integral of a linear function and its two first derivative

2.6 WEAK FORM OF THE WEIGHTED RESIDUAL METHOD

Let us consider once more the 1D Poisson equation

$$\frac{d}{dx} \left(k \frac{d\phi}{dx} \right) + Q = 0$$

with boundary conditions

$$\begin{aligned} \phi - \bar{\phi} &= 0 \quad \text{en } x = 0 \\ k \frac{d\phi}{dx} + \bar{q} &= 0 \quad \text{en } x = l \end{aligned}$$

The integral form is obtained by multiplying the above equations by test functions and integrating over the domain. Thus

$$\int_0^l W \left[\frac{d}{dx} \left(k \frac{d\phi}{dx} \right) + Q \right] dx + \left[\bar{W} \left(k \frac{d\phi}{dx} + \bar{q} \right) \right]_l = 0 \quad (2.46)$$

From this expression we note

- The derivative of ϕ is of order 2. This requires C^1 continuity for ϕ and, therefore, the shape functions must also be C^1 continuous.
- The derivative of k appears in the integral. This requires that k is continuous (C^0 continuity). This is an obvious inconvenience for problems where the analysis domain contains material with different properties.
- No derivative is applied on W . This implies that W can be discontinuous (C^{-1} continuity). Above requirements are clearly non-symmetrical with request to ϕ and W . Thus, while continuity of the first derivative is required for ϕ , no continuity requirement is demanded for W . This lack of symmetry leads generally to a non symmetric expression of the algebraic equation system resulting from the discretization process.

This “problem” can be overcome by an integration by parts of the second derivative term in the integral expression of the WRM. Recalling the integration by parts rule

$$\int_0^l u dv = [uv]_0^l - \int_0^l v du$$

and applying this rule to the term involving the second derivative of ϕ in the expression of the WRM (Eq.(2.46)) gives (for $u = W$ and $v = k \frac{d\phi}{dx}$)

$$\int_0^l W \frac{d}{dx} \left(k \frac{d\phi}{dx} \right) dx = \left[W k \frac{d\phi}{dx} \right]_0^l - \int_0^l \frac{dW}{dx} k \frac{d\phi}{dx} dx \quad (2.47a)$$

Substituting this expression into the WRM gives

$$\boxed{-\int_0^l \frac{dW}{dx} k \frac{d\phi}{dx} dx + \int_0^l W Q dx + \left[W k \frac{d\phi}{dx} \right]_0^l + \left[\bar{W} \left(k \frac{d\phi}{dx} + \bar{q} \right) \right]_l = 0} \quad (2.47b)$$

Note that the continuity requirements for ϕ , W and k have changed. Thus, the first derivatives of ϕ and W are just now involved, which simply requires C^0 continuity for these two functions.

Also, the derivative of the k has disappeared and k can now be a discontinuous function. The changes in the continuity requirement are summarized in Table 2.2.

Continuity requirements		
	Original integral form	Weak integral form
ϕ	C	C^0
W	C^{-1}	C^0
k	C^0	C^{-1}

Table 2.2: Continuity requirements for ϕ , W and k in the original integral form and the weak form

We recall that C^{-1} continuity means that the function can be discontinuous.

Eq.(2.47b) is called the weak integral form (or simply the *weak form*). This name comes from the fact that we have restricted the field for selecting the test functions W . Note that the original integral form we allowed any choice for W , while the weak form is restricted to functions W which are continuous.

2.6.1 Natural boundary condition

Let us choose for convenience $\bar{W} = -W$ in the weak form (2.47b). Simplification and rearranging of terms leads to

$$\int_0^l \frac{dW}{dx} k \frac{d\phi}{dx} dx = \int_0^l W Q dx - \left[W k \frac{d\phi}{dx} \right]_0^l - [W \bar{q}]_l \quad (2.48)$$

Recalling that $q = -k \frac{d\phi}{dx}$ gives

$$\boxed{\int_0^l \frac{dW}{dx} k \frac{d\phi}{dx} dx = \int_0^l W Q dx + [Wq]_0 - [W\bar{q}]_l} \quad (2.49)$$

We note the following points:

1. The variable ϕ has disappeared from the Neumann boundary where the heat flux is prescribed ($x = l$).
2. If the heat flux at $x = l$ is prescribed to a zero value ($\bar{q} = 0$), then all the Neumann boundary terms disappear from the weak form (2.49). The conditions of zero prescribed flux at the boundary are typically termed *natural* boundary condition.
3. q_0 is the incoming flux into the domain by the left end ($x = 0$) where the value of ϕ is prescribed. Thus q_0 can be interpreted as an end “reaction” (using a terminology from structural mechanics) corresponding to the prescribed value of the unknown. The value of q_0 can be computed “a posteriori”, once the approximate solution for ϕ has been found.

2.6.2 Discretization of the weak form

The weak form will be in the following the starting expression for deriving the discretized equation in the FEM. Thus, substituting the approximation for ϕ defined as

$$\phi \cong \hat{\phi} = \sum_{j=1}^n N_j a_j$$

into the weak form (2.49) and choosing n test functions W_i , $i = 1, 2, \dots, n$ gives

$$\boxed{\int_0^l \frac{dW_i}{dx} k \sum_{j=1}^n \frac{dN_j}{dx} a_j dx = \int_0^l W_i Q dx + [W_i q]_{x=0} - [W_i \bar{q}]_{x=l}} \quad (2.50)$$

$i = 1, 2, \dots \quad n$

The algebraic system of n equations and n unknowns is obtained by giving values to W_i in above expression from $i = 1$ to n .

For $i = 1$

$$\int_0^l \frac{dW_1}{dx} k \left(\frac{dN_1}{dx} a_1 + \frac{dN_2}{dx} a_1 + \dots + \frac{dN_n}{dx} a_n \right) dx = \int_0^l W_1 Q dx + (W_1 q)_0 - (W_1 \bar{q})_l \quad (2.51)$$

For $i = 2$

$$\int_0^l \frac{dW_2}{dx} k \left(\frac{dN_1}{dx} a_1 + \frac{dN_2}{dx} a_2 + \cdots + \frac{dN_n}{dx} a_n \right) dx = \int_0^l W_2 Q dx + (W_2 q)_0 - (W_2 \bar{q})_l$$

For $i = n$

$$\int_0^l \frac{dW_n}{dx} k \left(\frac{dN_1}{dx} a_1 + \frac{dN_2}{dx} a_2 + \cdots + \frac{dN_n}{dx} a_n \right) dx = \int_0^l W_n Q dx + (W_n q)_0 - (W_n \bar{q})_l$$

Above equations can be written in matrix form as

$$\begin{bmatrix} K_{11} & K_{12} & \cdots & K_{1n} \\ K_{21} & K_{22} & \cdots & K_{2n} \\ \vdots & & & \vdots \\ K_{n1} & K_{n2} & \cdots & K_{nn} \end{bmatrix} \begin{Bmatrix} a_1 \\ a_2 \\ \vdots \\ a_n \end{Bmatrix} = \begin{Bmatrix} f_1 \\ f_2 \\ \vdots \\ f_n \end{Bmatrix}$$

$$\mathbf{K}\mathbf{a} = \mathbf{f}$$

where

$$\begin{aligned} K_{ij} &= \int_0^l \frac{dW_i}{dx} k \frac{dN_j}{dx} dx \\ f_i &= \int_0^l W_i Q dx + (W_i q)_0 - (W_i \bar{q})_l \end{aligned} \tag{2.52}$$

We are still free to choose an appropriate expression for W_i . Choosing the Galerkin form ($W_i = N_i$) gives

$$\boxed{\begin{aligned} K_{ij} &= \int_0^l \frac{dN_i}{dx} k \frac{dN_j}{dx} dx \\ f_i &= \int_0^l N_i Q dx + (N_i q)_0 - (N_i \bar{q})_l \end{aligned}} \tag{2.53}$$

Note that matrix \mathbf{K} is *symmetrical*, which is advantageous for the computations. This symmetry is one of the key properties of the so-called *Galerkin weak form*.

We point out again that f_i contains the incoming flux q_0 at the boundary where ϕ is prescribed. The flux is an unknown that can be computed “a posteriori” once the value of the unknown parameters have been found. This process is explained in the example given next.

Example 2.4 *Solution of 1D Poisson equation via the Galerkin weak form and a polynomial approximation*

Solution

Let us consider the Poisson equation

$$A(\phi): \frac{d^2\phi}{dx^2} + 3 = 0 \quad \text{en } \Omega \quad (a)$$

The boundary conditions are

$$B(\phi): \begin{cases} \phi - 1 = 0, & x = 0 \quad (\Gamma)_\phi \\ \frac{d\phi}{dx} + 2 = 0, & x = l \quad (\Gamma)_q \end{cases} \quad (b)$$

From (a) and (b) we deduce $k = 1$, $Q = 3$, $\bar{\phi} = 1$ and $\bar{q} = 2$.

We define a polynomial approximation of the unknown such that the boundary conditions for the temperature prescribed at $x = 0$ is satisfied, i.e.

$$\phi(x) \cong \hat{\phi}(x) = 1 + \sum_{j=1}^n a_j x^j \quad (c)$$

Note that $x = 0$, $\phi = 1$.

From (c) we deduce $N_j = x^j$ ($i = 1, 2, \dots, n$).

Let us find now the solution for $n = 2$

$$\begin{aligned} \hat{\phi}(x) &= 1 + a_1 x + a_2 x^2 \\ N_1(x) &= x, \quad N_2(x) = x^2 \end{aligned} \quad (d)$$

where a_1 and a_2 are the unknowns.

The Galerkin weak form leads to an algebraic system with two equations that can be expressed as

$$\begin{bmatrix} K_{11} & K_{12} \\ K_{21} & K_{22} \end{bmatrix} \begin{Bmatrix} a_1 \\ a_2 \end{Bmatrix} = \begin{Bmatrix} f_1 \\ f_2 \end{Bmatrix} \quad (e)$$

where

$$\begin{aligned} K_{11} &= \int_0^l \frac{dN_1}{dx} \frac{dN_1}{dx} dx = \int_0^l dx = l \\ K_{12} &= \int_0^l \frac{dN_1}{dx} \frac{dN_2}{dx} dx = \int_0^l 2x dx = l^2 = K_{21} \\ K_{22} &= \int_0^l \frac{dN_2}{dx} \frac{dN_2}{dx} dx = \int_0^l 4x^2 dx = \frac{4}{3} l^3 \\ f_1 &= \int_0^l N_1 Q dx + (N_1 q)_0 - (N_1 \bar{q})_l = \int_0^l 3x dx - 2l = \frac{3}{2} l^2 - 2l \\ f_2 &= \int_0^l N_2 Q dx + (N_2 q)_0 - (N_2 \bar{q})_l = \int_0^l 3x^2 dx - 2l^2 = l^3 - 2l^2 \end{aligned} \quad (f)$$

Substituting into (e) gives

$$\underbrace{\begin{bmatrix} l & l^2 \\ l^2 & \frac{4}{3}l^3 \end{bmatrix}}_{\mathbf{K}} \underbrace{\begin{Bmatrix} a_1 \\ a_2 \end{Bmatrix}}_{\mathbf{a}} = \underbrace{\begin{Bmatrix} \frac{3l^2}{2} - 2l \\ l^3 - 2l^2 \end{Bmatrix}}_{\mathbf{f}} \quad (g)$$

Solution of the system gives $a_1 = 3l - 2$, $a_2 = -3/2$.

The approximate solution is

$$\hat{\phi}(x) \equiv \phi(x) = 1 + (3l - 2)x - \frac{3}{2}x^2 \quad (h)$$

Let us find out as an exercise the analytical solution. Integration of the original differential equation gives

$$\begin{aligned} \frac{d\phi}{dx} &= -3x + A \\ \phi &= -\frac{3}{2}x^2 + Ax + B \end{aligned}$$

Constants A and B are found by using the boundary conditions

$$\begin{aligned} (\phi)_0 &= 1 \implies B = 1 \\ \left(\frac{d\phi}{dx}\right)_l &= -2 \implies -3l + A = -2; \quad A = 3l - 2 \end{aligned}$$

The exact solution is therefore

$$\phi = -\frac{3}{2}x^2 + (3l - 2)x + 1 \quad (i)$$

Note that the approximate solution coincides with the exact one. This is a consequence of the quadratic approximation chosen that coincides with the exact one.

The incoming flux q_0 is found as

$$q_0 = -k \frac{d\phi}{dx} \Big|_{x=0} = -(a_1 + 2a_2x) \Big|_{x=0} = -a_1 = 2 - 3l$$

This shows that the flux at the Dirichlet boundary where the unknowns is prescribed can be computed “a posteriori” in terms of the parameters of the approximation. Note the analogy with the computation of the reaction at the support of a structure from the displacements at the joints of the structure.

Example 2.5 Solve the 1D heat conduction equation accounting for heat conduction losses via the Galerkin weak form and a polynomial approximation.

Solution

Let us consider the heat balance equation in a bar where heat is generated due to a distributed source Q and heat is lost along the bar length due to the difference between the temperature of the bar and that of the external medium (heat conduction loss).

The heat balance equation in an infinitesimal element of the bar is written as

$$q + Qdx - (q + dq) - h(\phi - \phi_e)dx = 0$$

Simplifying and using Fourier's law ($q = -k\frac{d\phi}{dx}$), we obtain

$$\frac{d}{dx} \left(k \frac{d\phi}{dx} \right) + Q - h(\phi - \phi_e) = 0 \quad (a)$$

where h is the convection parameter and ϕ_e the external temperature.

The third term expresses the heat loss due to convection along the bar.

Let us assume a problem with $k = 1$, $Q = 0$, $h = 1$ and $\phi_e = 0$, i.e.

$$A(\phi): \frac{d^2\phi}{dx^2} - \phi = 0 \quad \text{in } \Omega \quad (b)$$

with the following boundary conditions

$$B(\phi): \begin{cases} \phi = 0; & x = 0 \quad (\Gamma_\phi) \\ \frac{d\phi}{dx} - 20 = 0 & ; \quad x = l \quad (\Gamma_q) \end{cases} \quad (c)$$

The integral expression of the previous equation is obtained in the usual way as

$$\int_0^l W_i \left(\frac{d^2\phi}{dx^2} - \phi \right) dx + \left[\bar{W}_i \left(\frac{d\phi}{dx} - 20 \right) \right]_{x=l} = 0 \quad (d)$$

The weak form is obtained integrating by parts the second derivative term. This

$$\int_0^l W_i \frac{d^2\phi}{dx^2} dx = - \int_0^l \frac{dW_i}{dx} \frac{d\phi}{dx} dx + \left[W_i \frac{d\phi}{dx} \right]_0^l \quad (e)$$

Substituting (e) into (d) and making $\bar{W}_i = -W_i$, gives

$$- \int_0^l \frac{dW_i}{dx} \frac{d\phi}{dx} dx + \left[W_i \frac{d\phi}{dx} \right]_0^l - \int_0^l W_i \phi dx - \left[W_i \left(\frac{d\phi}{dx} - 20 \right) \right]_l = 0 \quad (f)$$

After little algebra we obtain

$$\int_0^l \left(\frac{dW_i}{dx} \frac{d\phi}{dx} + W_i \phi \right) dx = (W_i q)_0 + 20(W_i)_l \quad (i = 1, 2, \dots, n) \quad (g)$$

where

$$q_0 = -k \left. \frac{d\phi}{dx} \right|_0$$

Note that the effect of convection leads to a new term in the l.h.s. of (g) which obviously affects the stiffness matrix. Also note that $\phi_e \neq 0$ introduces an additional term in the flux vector.

Let us assume the following expansion

$$\begin{aligned} \phi &\cong \hat{\phi} = \sum_{j=1}^2 a_j x^j = a_1 x + a_2 x^2 \\ N_1 &= x; \quad N_2 = x^2 \end{aligned} \quad (h)$$

Substituting Eq.(h) into (g) and applying the Galerkin method ($W_i = N_i$) gives

$$\int_0^l \left(\frac{dN_i}{dx} \frac{d\hat{\phi}}{dx} + N_i \hat{\phi} \right) dx = (N_i q)_0 + 20(N_i)_l; \quad (i = 1, 2) \quad (i)$$

Substituting the approximation for ϕ gives

$$\int_0^l \left[\frac{dN_i}{dx} \left(\sum_{j=1}^2 \frac{dN_j}{dx} a_j \right) + N_i \left(\sum_{j=1}^2 N_j a_j \right) \right] dx = (N_i q)_0 + 20(N_i)_l; \quad (i = 1, 2) \quad (j)$$

The expressions for the stiffness matrix and the flux vector are

$$K_{ij} = \int_0^l \left(\frac{dN_i}{dx} \frac{dN_j}{dx} + N_i N_j \right) dx \quad (k)$$

where $\frac{dN_i}{dx} \frac{dN_j}{dx}$ is the conduction term and $N_i N_j$ is the term due to convection.

$$f_i = (N_i q)_0 + 20(N_i)_l \quad (l)$$

The numerical expressions for K_{ij} and f_i are

$$\begin{aligned} K_{11} &= \int_0^1 (1 + x^2) dx \Rightarrow K_{11} = 4/3 \\ K_{12} &= \int_0^1 (2x + x^3) dx \Rightarrow K_{12} = 5/4 = K_{21} \\ K_{22} &= \int_0^1 (4x^2 + x^4) dx \Rightarrow K_{22} = 23/15 \\ f_1 &= (xq)_0 + 20x|_l = 20 \\ f_2 &= (x^2 q)_0 + 20x^2|_l = 20 \end{aligned}$$

The system of equations is written in matrix form as

$$\begin{bmatrix} 4/3 & 5/4 \\ 5/4 & 23/15 \end{bmatrix} \begin{Bmatrix} a_1 \\ a_2 \end{Bmatrix} = \begin{Bmatrix} 20 \\ 20 \end{Bmatrix}$$

From above we obtain

$$\begin{cases} 4/3a_1 + 5/4a_2 = 20 \\ 5/4a_1 + 23/15a_2 = 20 \end{cases} \Rightarrow \begin{cases} a_1 = 11,7579 \\ a_2 = 3,4582 \end{cases}$$

The solution is

$$\hat{\phi} = \overbrace{11,7579}^{a_1} x + \overbrace{3,4582}^{a_2} x^2$$

The heat flux q_0 at $x = 0$ is

$$q_0 = -\left. \frac{d\hat{\phi}}{dx} \right|_{x=0} = -11,7579$$

Let us verify the approximation of the flux computed at $x = 1$ with the exact value

$$q_l = -\left. \frac{d\hat{\phi}}{dx} \right|_{x=1} = -11,7579 - 2 \times 3,4582 = -18,67$$

The minus sign denotes that the flux *goes out* the domain, as expected.

Using a single term in the approximation (h), gives $\hat{\phi} = 15$ and $q_l = -15$.

We can plot the approximate solution for comparison with the exact solution. The following tables show the approximate and exact values of ϕ at $x = 0,5$ and $x = 1$, and of the flux $\left(\frac{d\phi}{dx}\right)$ at $x = 1$.

	$\hat{\phi}$		ϕ (exact)
	$n = 1$	$n = 2$	
$x = 0,5$	7,5	6,7435	6,7540
$x = 1$	15	15,2161	15,2319

$\frac{d\hat{\phi}}{dx}$		$\frac{d\phi}{dx}$ (exact)
	$n = 1$	$n = 2$
$\left. \frac{d\hat{\phi}}{dx} \right _1$	-15	-18,67
$\left. \frac{d\phi}{dx} \right _1$		-20

Table 2.3: Comparison of the approximate and exact values for ϕ y $\left. \frac{d\hat{\phi}}{dx} \right|_1$
(Example 2.5)

Note that the accuracy for ϕ is greater than that for the flux at the end point. This is due to the computation of the flux as the first derivative of the approximate function $\hat{\phi}$. Recall that the derivatives of an approximate function introduces an additional error. Consequently, the fluxes computed from the numerical solution are an order less accurate than the values of $\hat{\phi}$. This conclusion also extends to the FEM.

2.7 DERIVATION OF THE PRINCIPLE OF VIRTUAL WORK FROM THE WEIGHTED RESIDUAL METHOD

Let us consider the bar under traction forces of Figure 2.3.

The governing equation is

$$A(u): \frac{d}{dx} \left(EA \frac{du}{dx} \right) + b = 0 \quad (2.54)$$

and the boundary conditions

$$B(u): \begin{cases} \text{Prescribed displacement} & u = 0 & x = 0 \\ \text{Prescribed forces} & EA \frac{du}{dx} - \bar{H} = 0 & x = l \end{cases}$$

The equivalent integral form is derived via the WRM

$$\int_0^l W \left[\frac{d}{dx} \left(EA \frac{du}{dx} \right) + b \right] dx + \left[\bar{W} \left(EA \frac{du}{dx} - \bar{H} \right) \right]_{x=l} = 0 \quad (2.55)$$

The weak form is obtained integrating by parts the term

$$\int_0^l W \left[\frac{d}{dx} \left(EA \frac{du}{dx} \right) \right] dx = - \int_0^l \frac{dW}{dx} EA \frac{du}{dx} dx + \left[\bar{W} EA \frac{du}{dx} \right]_0^l \quad (2.56)$$

Substituting above expressions into the WRM and making $\bar{W} = -W$, gives

$$- \int_0^l \frac{dW}{dx} EA \frac{du}{dx} dx + \left[W EA \frac{du}{dx} \right]_0^l - \left[W \left(EA \frac{du}{dx} - \bar{H} \right) \right]_l + \int_0^l W b dx = 0 \quad (2.57)$$

Let us recall that

$$N = \sigma A = E \epsilon A = EA \frac{du}{dx} \quad (2.58)$$

Hence, the weak form can be written as

$$\int_0^l \frac{dW}{dx} \underbrace{(EA) \frac{du}{dx}}_N dx = \int_0^l W b dx + (W \bar{H})_l - (W N)_0 \quad (2.59)$$

Let us denote, for convenience, the arbitrary test functions as *virtual displacement* δu . Hence,

$$W(x) \equiv \delta u(x) \quad (2.60)$$

The term $(W N)_0$ is eliminated by imposing that the virtual displacement δu satisfies the kinematic boundary conditions, i.e.

$$\delta u(x)|_{x=0} = 0 \quad (2.61)$$

Substituting W by δu into the weak form and noting (2.60) leads to

$$\int_0^l \frac{d(\delta u)}{dx} N dx = \int_0^l \delta u b dx + (\delta u \bar{H})_l \quad (2.62)$$

The *virtual strain* is defined as

$$\delta \varepsilon = \frac{d(\delta u)}{dx} \quad (2.63)$$

Substituting this expression into the weak form leads finally to

$$\boxed{\int_0^l \delta \varepsilon N(x) dx = \int_0^l \delta u b dx + \delta u_l \bar{H}} \quad (2.64)$$

The terms $\delta u b$ can be interpreted as the work (per unit length) performed by the distributed force b over the virtual displacement δu . Also, the term $\delta u_l \bar{H}$ is the work of the force \bar{H} over the virtual displacement of the bar end. Finally the integral of the l.h.s. of Eq.(2.63) represents the work of the axial forces over the virtual strains (elongations) along the bar.

The previous integral expression is known in practice as the *Principle of Virtual Work* (PVW). The definition of PVW is as follows:

“A body is in equilibrium if, for any virtual displacement δu that satisfies the kinematic boundary conditions, the work performed by the stresses over the virtual strains equals the work performed by the external forces over the virtual displacement”.

As the starting point for the derivation of the PVW is the equilibrium equation, the PVW is an equilibrium expression. Also, starting from the PVW and integrating by parts the l.h.s. and taking into account that the virtual displacement are arbitrary, we recover the original governing equations. The PVW is therefore a *necessary* and *sufficient* condition for the equilibrium of a structure

The PVW has advantages versus the governing differential equations expressing the equilibrium of a body, as it has a simple physical meaning. The PVW is the starting point for the solution via FEM of most problems in structural mechanics.

2.8 THE PVW IN POISSON PROBLEMS

The PVW has an analogous expression in Poisson problems. Thus making

$$\begin{aligned} W(x) &= \delta \phi(x) \\ N &= -q \\ \frac{d(\delta \phi)}{dx} &= \delta \left(\frac{d\phi}{dx} \right) = \delta g \\ b(x) &= Q(x) \\ \bar{H} &= -\bar{q} \end{aligned}$$

In above $\delta\phi$ or δg are the virtual variables (i.e. temperature, pressure, etc.) and the virtual gradient, respectively. The PVW is written in this case as,

$$\boxed{\int_0^l \delta g(-q)dx = \int_0^l \delta\phi Q dx - (\delta\phi)_l \bar{q}}$$

The minus sign in the above expression comes from the fact that the flux direction is the opposite to that of the gradient of ϕ .

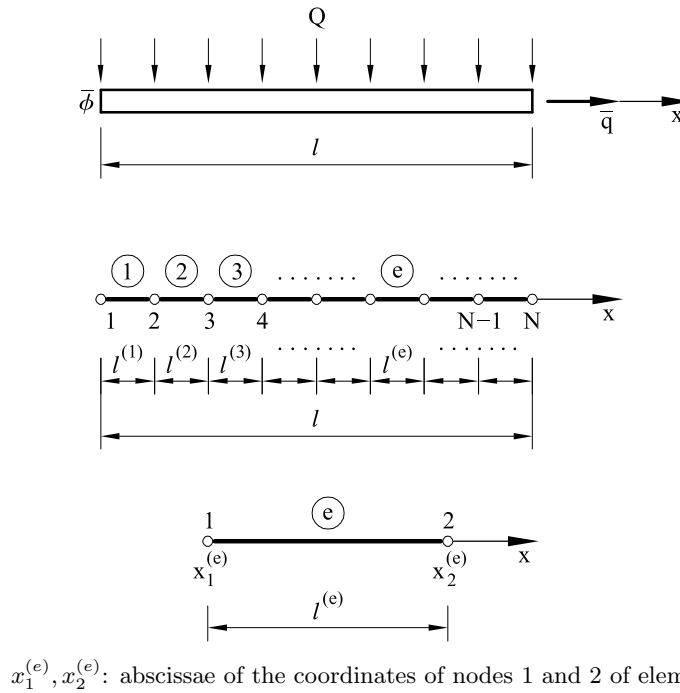


Figure 2.10: Discretization of a bar into 1D two-noded finite element

2.9 THE FEM IN 1D POISSON PROBLEMS

We will study next the general solution of 1D Poisson problems with the FEM.

Let us consider a discretization of the analysis domain (the 1D domain) in non-overlapping sub-domains, termed hereafter “finite elements” (Figure 2.10).

Among the many choice for approximately the unknown function ϕ we will choose the simplest one, using polynomial functions locally defined within each finite element as

$$\phi(x) \simeq \hat{\phi}(x) = a_0 + a_1x + a_2x^2 + \cdots + a_nx^n = \sum_{i=0}^n a_i x^i \quad (2.64)$$

where n is the number of points within the element where the value of ϕ is assumed to be known. Such points are called *nodes*. Also, a_o, a_1, \dots, a_n are constant parameters depending on the value of ϕ at the nodes *only*. The above expression is typically written as

$$\hat{\phi}(x) = N_1^{(e)}(x)\phi_1^{(e)} + N_2^{(e)}(x)\phi_2^{(e)} + \dots + N_n^{(e)}(x)\phi_n^{(e)} = \sum_{i=1}^n N_i^{(e)}(x)\phi_i^{(e)} \quad (2.65)$$

where $N_1^{(e)}(x), \dots, N_n^{(e)}(x)$ are the polynomial functions that interpolate ϕ within the element domain (they are called *shape functions*) and $\phi_i^{(e)}$ is the value of the approximate function ϕ at the node i . In the follows for simplicity we will skip the hat over $\hat{\phi}$. This means that we will make no distinction between the exact and approximate expressions of the unknown ϕ .

The shape function $N_i^{(e)}(x)$ interpolates within the element the unknown corresponding to node i only and, therefore, it is called the *shape function of node i* . It is easy to note that $N_i^{(e)}(x)$ takes the unit value at the node and zero at the other nodes.

Substituting the approximate expression from $\phi(x)$ for each element into the integral form of the WRM leads, after simple algebra, to a system of algebraic equations expressing the equilibrium of the problem in terms of the nodal values of unknown ϕ at the nodes of the finite element mesh. Such equations can be written in matrix form as

$$\mathbf{K} \mathbf{a} = \mathbf{f} \quad (2.66)$$

with

$$\mathbf{K} = \begin{bmatrix} K_{11} & K_{12} & \dots & K_{1n} \\ \vdots & & & \vdots \\ \vdots & & & \vdots \\ K_{N1} & K_{N2} & \dots & K_{NN} \end{bmatrix}; \quad \mathbf{a} = \begin{Bmatrix} \phi_1 \\ \phi_2 \\ \vdots \\ \phi_N \end{Bmatrix}; \quad \mathbf{f} = \begin{Bmatrix} f_1 \\ f_2 \\ \vdots \\ f_N \end{Bmatrix} \quad (2.67)$$

where N is the total number of nodes in the finite element mesh.

By analogy with matrix analysis of structures, \mathbf{K} is called the *stiffness matrix* of the finite element mesh and \mathbf{a} and \mathbf{f} are called the nodal unknown vector and the vector of equivalent nodal fluxes, respectively. \mathbf{K} and \mathbf{f} can be obtained by assembling the individual contributions from each element as in matrix analysis of bar structures. The solution of the global system of algebraic equations gives the value of ϕ at the nodes from which the gradient and the flux within each element can be found.

For the sake of clarity we will study in a subsequent section the solution of the 1D Poisson problem using two meshes of one and two two-noded linear finite elements, respectively.

2.9.1 Discretization of the problem. Local definition of the shape functions

Let us define the distribution of the unknown function ϕ within each element. The bar is discretized into two-noded 1D finite element. Within each element the unknown function $\phi(x)$ is approximated using a linear polynomial as (Figure 2.11)

$$\phi^{(e)}(x) \cong \hat{\phi}^{(e)}(x) = \sum_{i=0}^1 \alpha_i x^i = \alpha_0 + \alpha_1 x \quad (2.68)$$

Taking into account that at the end node of each element the unknown function values coincide with those of the nodal unknowns we can write

$$\begin{aligned} \hat{\phi}^{(e)}(x_1) &= \phi_1^{(e)} = \alpha_0 + \alpha_1 x_1^{(e)} \\ \hat{\phi}^{(e)}(x_2) &= \phi_2^{(e)} = \alpha_0 + \alpha_1 x_2^{(e)} \end{aligned} \quad (2.69)$$

Solving the above equation system with two unknowns gives

$$\begin{aligned} \alpha_0 &= \phi_1^{(e)} - \frac{\phi_2^{(e)} - \phi_1^{(e)}}{x_2^{(e)} - x_1^{(e)}} x_1^{(e)} \\ \alpha_1 &= \frac{\phi_2^{(e)} - \phi_1^{(e)}}{x_2^{(e)} - x_1^{(e)}} \end{aligned}$$

Substituting α_0 and α_1 into (2.68) gives

$$\hat{\phi}^{(e)}(x) = \left(\phi_1^{(e)} - \frac{\phi_2^{(e)} - \phi_1^{(e)}}{x_2^{(e)} - x_1^{(e)}} x_1^{(e)} \right) + \left(\frac{\phi_2^{(e)} - \phi_1^{(e)}}{x_2^{(e)} - x_1^{(e)}} \right) x$$

After some rearranging we obtain

$$\begin{aligned} \hat{\phi}^{(e)}(x) &= \underbrace{\frac{x_2^{(e)} - x}{x_2^{(e)} - x_1^{(e)}}}_{N_1^{(e)}(x)} \phi_1^{(e)} + \underbrace{\frac{x - x_1^{(e)}}{x_2^{(e)} - x_1^{(e)}}}_{N_2^{(e)}(x)} \phi_2^{(e)} \\ &= N_1^{(e)}(x) \phi_1^{(e)} + N_2^{(e)}(x) \phi_2^{(e)} = \sum_{i=1}^2 N_i^{(e)}(x) \phi_i^{(e)} \end{aligned} \quad (2.70)$$

from which the expression of the shape functions $N_i^{(e)}$ is deduced as

$$\begin{aligned} N_1^{(e)}(x) &= \frac{x_2^{(e)} - x}{x_2^{(e)} - x_1^{(e)}} = \frac{x_2^{(e)} - x}{l^{(e)}} \\ N_2^{(e)}(x) &= \frac{x - x_1^{(e)}}{x_2^{(e)} - x_1^{(e)}} = \frac{x - x_1^{(e)}}{l^{(e)}} \end{aligned} \quad (2.71)$$

Note that

$$x = x_1^{(e)} \rightarrow \begin{cases} N_1^{(e)}(x_1) = 1 \\ N_2^{(e)}(x_1) = 0 \end{cases} \quad x = x_2^{(e)} \rightarrow \begin{cases} N_1^{(e)}(x_2) = 0 \\ N_2^{(e)}(x_2) = 1 \end{cases}$$

The above expressions show that the shape functions of a node take a unit value at that node and zero at the other node.

Figure 2.11 shows the graphic representation of the shape functions of the two-noded bar element.

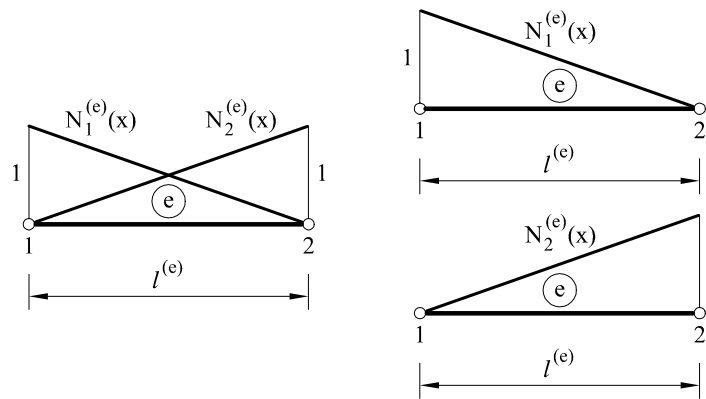


Figure 2.11: Linear shape functions for the 1D two-noded bar element

The interpolation (2.70) allows us to obtain the value of the unknown ϕ at any point of the element in terms of the nodal values $\phi_1^{(e)}$ and $\phi_2^{(e)}$, which become now the problem unknowns.

The linear interpolation chosen within each element provides a linear-wise approximation of ϕ over the analysis domain. If the nodal values coincide with the exact ones (which only occurs in exceptional cases), we will have the situation of Figure 2.12a. Clearly the coincidence of the approximate and the exact solution will only occur when the exact solution varies also linearly. In the most general case the nodal unknown values will not coincide with the exact ones (Figure 2.12b), neither the exact solution will vary linearly along the analysis domain. The error can be corrected with a finer discretization or using higher order finite elements.

2.9.2 Derivation of the algebraic equation systems. Solution of the 1D Poisson problem using one 2-noded 1D element

Let us retake the problem of the heated bar of Figure 2.8. The governing equations for the heat conduction problem are

$$A(\phi) = \frac{d}{dx} \left(k \frac{d\phi}{dx} \right) + Q = 0 \quad 0 \leq x \leq l$$

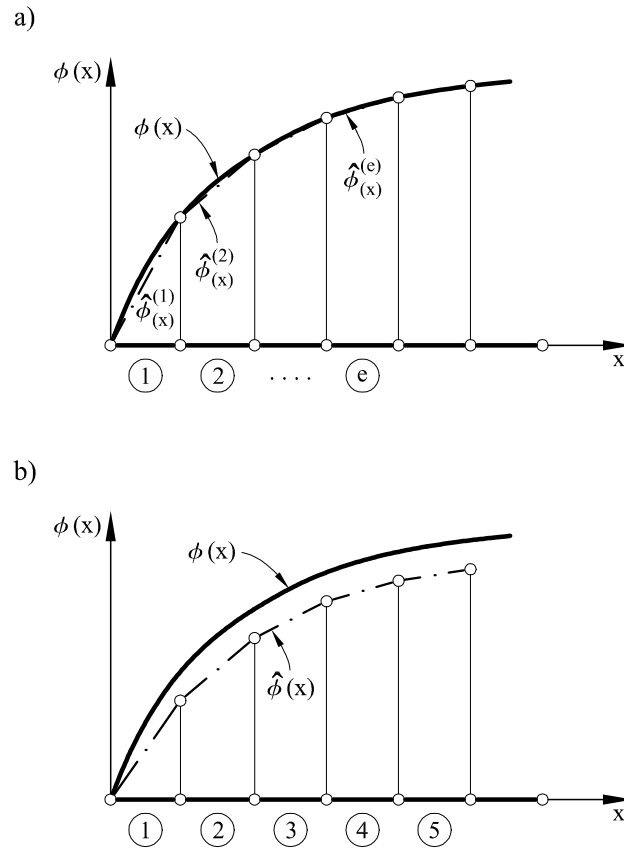


Figure 2.12: Approximation of the solution via linear finite elements. a) Nodally exact solution; b) Nodally approximate solution

$$B(\phi): \begin{cases} \phi - \bar{\phi} = 0 & x = 0 \\ k \frac{d\phi}{dx} + \bar{q} = 0 & x = l \end{cases}$$

The analytical solution of this problem (for k constant) is obtained as follows:

$$k \frac{d\phi}{dx} = -Qx + A$$

$$\phi = -\frac{Q}{2k}x^2 + \frac{Ax}{k} + B$$

From the boundary conditions we deduce

$$\begin{aligned} B &= \bar{\phi} \\ k \frac{d\phi}{dx} \Big|_l &= -Ql + A \\ A &= -Ql - \bar{q} \end{aligned}$$

Substituting into the expression for ϕ gives

$$\phi = -\frac{Q}{2k}x^2 + (Ql - \bar{q})\frac{x}{k} + \bar{\phi} \quad (2.72)$$

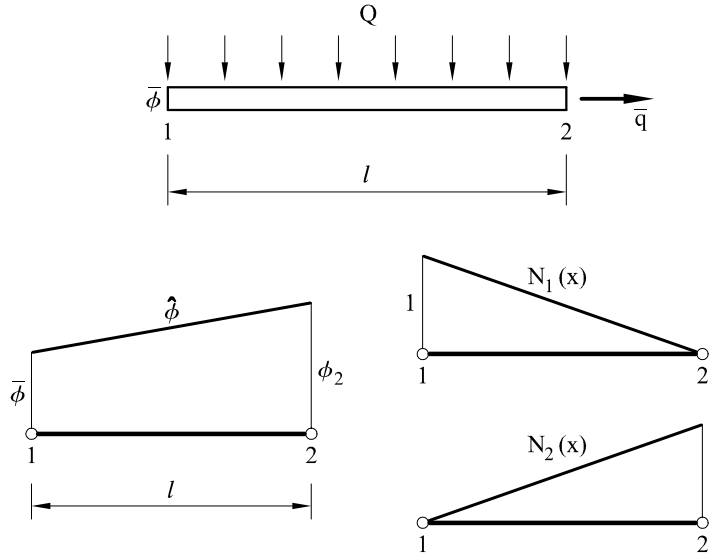


Figure 2.13: Solution of the 1D problem of Figure 2.8 using one 2-noded linear element

The weak form is written as

$$\int_0^l \frac{dW_i}{dx} k \frac{d\hat{\phi}}{dx} dx = \int_0^l W_i Q dx + W_i q \Big|_{x=0} - W_i \bar{q} \Big|_{x=l} \quad (2.73)$$

We will now solve the FEM problem with a single 2-noded element (Figure 2.13). The temperature ϕ is approximated within the element as

$$\hat{\phi}(x) = N_1(x)\phi_1 + N_2(x)\phi_2 \quad (2.74)$$

where the upper index e has been omitted as we only have one element.

Let us recall that ϕ_1 and ϕ_2 are temperatures at nodes 1 and 2, respectively. Derivating the above expression gives

$$\frac{d\hat{\phi}(x)}{dx} = \frac{dN_1(x)}{dx}\phi_1 + \frac{dN_2(x)}{dx}\phi_2 \quad (2.75)$$

Substituting (2.74) into the weak form (2.73) and applying the Galerkin WR method ($W_i = N_i$), gives

$$\int_0^l \frac{dN_i}{dx} k \left[\frac{dN_1}{dx}\phi_1 + \frac{dN_2}{dx}\phi_2 \right] dx = \int_0^l N_i(x) Q dx + [N_i(x)q]_0 - [N_i(x)\bar{q}]_l, \quad i = 1, 2$$

For $i = 1$

$$\int_0^l \frac{dN_1}{dx} k \left[\frac{dN_1}{dx}\phi_1 + \frac{dN_2}{dx}\phi_2 \right] dx = \int_0^l N_1 Q dx + q_0$$

as

$$\begin{aligned} N_1(0) &= 1 \\ N_1(l) &= 0 \end{aligned}$$

For $i = 2$

$$\int_0^l \frac{dN_2}{dx} k \left[\frac{dN_1}{dx} \phi_1 + \frac{dN_2}{dx} \phi_2 \right] dx = \int_0^l N_2 Q dx - \bar{q}$$

as

$$\begin{aligned} N_2(0) &= 0 \\ N_2(l) &= 1 \end{aligned}$$

The above equations define a system of two equations with two unknowns that can be written as

$$\begin{bmatrix} K_{11} & K_{12} \\ K_{21} & K_{22} \end{bmatrix} \begin{Bmatrix} \phi_1 \\ \phi_2 \end{Bmatrix} = \begin{Bmatrix} f_1 \\ f_2 \end{Bmatrix}$$

where the elements of the stiffness matrix are

$$K_{ij} = \int_0^l \frac{dN_i}{dx} k \frac{dN_j}{dx} dx$$

Similarly we obtain for the components of the equivalent flux vector

$$f_1 = \int_0^l N_1 Q dx + q_0$$

$$f_2 = \int_0^l N_2 Q dx - \bar{q}$$

The above expressions are completely general and applicable to any 1D heat conduction element. It is easy to particularize the expressions for the 2-noded element.

Note that

$$\frac{dN_1}{dx} = \frac{-1}{l^{(e)}}, \quad \frac{dN_2}{dx} = \frac{1}{l^{(e)}}$$

Thus gives

$$\begin{aligned} K_{11}^{(e)} &= K_{22}^{(e)} = \frac{k}{l} \\ K_{21}^{(e)} &= K_{12}^{(e)} = \frac{-k}{l} \\ f_1 &= \frac{Ql}{2} + q_0 \\ f_2 &= \frac{Ql}{2} - \bar{q} \end{aligned}$$

The system of algebraic equations to be solved in this simple case is

$$\frac{k}{l} \begin{bmatrix} 1 & -1 \\ -1 & 1 \end{bmatrix} \begin{Bmatrix} \phi_1 \\ \phi_2 \end{Bmatrix} = \begin{Bmatrix} \frac{Ql}{2} + q_0 \\ \frac{Ql}{2} - \bar{q} \end{Bmatrix}, \quad \phi_1 = \bar{\phi} \quad (2.76)$$

The approximate solution for the end value ϕ_2 is

$$\phi_2 = \frac{Ql^2}{2k} - \frac{\bar{q}l}{k} + \bar{\phi} \quad (2.77)$$

Note that the value ϕ_2 coincides with that given by the exact analytical solution. This is remarkable as the exact parabolic solution differs from the linear approximation chosen for the element. This coincidence only occurs for some special 1D problems.

The end flux “ q_0 ” (considered here as a nodal “reaction”) can be obtained by substituting ϕ_2 into the first equation giving

$$q_0 = \bar{q} - Ql \quad (2.78)$$

Note that the end flux satisfies the flux balance equation, i.e.

$$\underbrace{(q_0 + Ql)}_{\text{incoming flux}} - \underbrace{\bar{q}}_{\text{outgoing flux}} = 0$$

2.9.3 Solution of the 1D Poisson problem using two 2-noded elements

We will now solve the problem using a discretization of the bar into two linear elements as shown in Figure 2.14. The approximation of ϕ over the whole bar can be written as

$$\phi \simeq \hat{\phi} = N_1\phi_1 + N_2\phi_2 + N_3\phi_3 \quad (2.79)$$

where N_i are called *global shape function*. From Figure 2.14 we deduce

$$\left. \begin{aligned} N_1 &= N_1^{(1)} \\ N_1 &= 0 \end{aligned} \right\} \begin{aligned} 0 \leq x \leq l/2 \\ l/2 < x \leq l \end{aligned}$$

$$\left. \begin{aligned} N_2 &= N_2^{(1)} \\ N_2 &= N_1^{(2)} \end{aligned} \right\} \begin{aligned} 0 \leq x \leq l/2 \\ l/2 < x \leq l \end{aligned} \quad (2.80)$$

$$\left. \begin{aligned} N_3 &= 0 \\ N_3 &= N_2^{(2)} \end{aligned} \right\} \begin{aligned} 0 \leq x < l/2 \\ l/2 \leq x \leq l \end{aligned}$$

We can see that each global shape function N_i coincides with a local shape function $N_j^{(e)}$ within each element. Note also that the global shape function of a node taking a unit value at the node and zero at the other node in the mesh. This means that the “influence domain” of each node in the mesh extends only over the element that share the node.

The discretized weak form is written now as

$$\int_0^l \frac{dN_i}{dx} k \left[\frac{dN_1}{dx} \phi_1 + \frac{dN_2}{dx} \phi_2 + \frac{dN_3}{dx} \phi_3 \right] dx = \int_0^l N_i Q dx + [N_i q]_0 - [N_i \bar{q}]_l$$

$i = 1, 2, 3$ “global” numbering

(2.81)

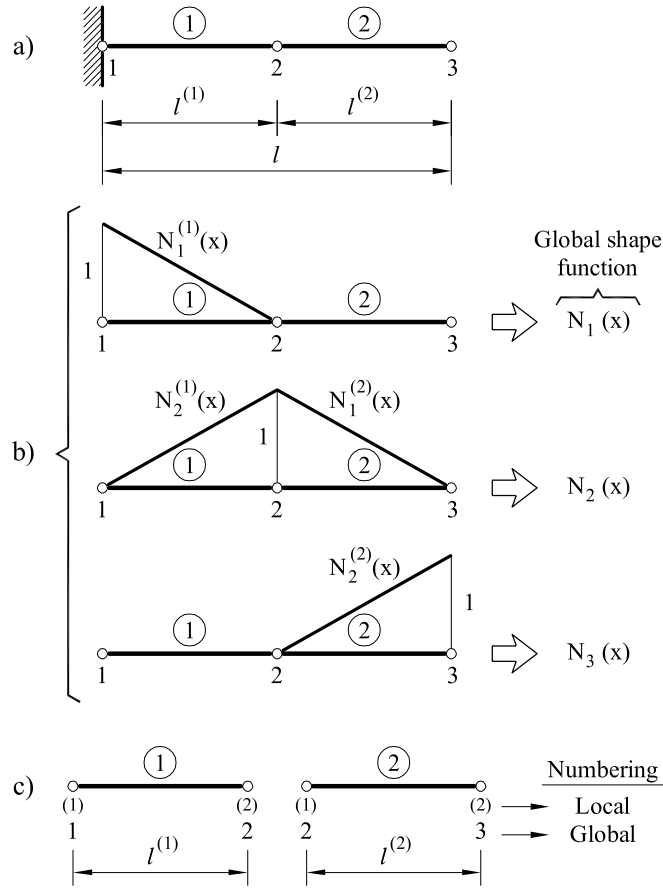


Figure 2.14: Discretization of a bar with two 1D linear elements. Global shape functions

We particularize above expression for different values of i .

For $i = 1$

$$\int_0^{l/2} \frac{dN_1^{(1)}}{dx} k \left[\frac{dN_1^{(1)}}{dx} \phi_1 + \frac{dN_2^{(1)}}{dx} \phi_2 \right] dx = \int_0^{l/2} N_1^{(1)} Q dx + [N_1 q]_0 - [N_1 \bar{q}]_l =$$

$$= \underbrace{\int_0^{l/2} N_1^{(1)} Q dx}_{f_1^{(1)}} + q_0 \quad (2.82a)$$

Note that it makes no sense to include $\frac{dN_3}{dx} \phi_3$ within the bracket term in the l.h.s., as N_3 takes a zero value within the first element ($0 \leq x < l/2$).

For the derivation of the r.h.s. of (2.82a) we have used that $N_1 = 1$ at $x = 0$ and $N_1 = 0$ at $x = l$.

For $i = 2$

$$\begin{aligned}
& \int_0^{l/2} \frac{dN_2^{(1)}}{dx} k \left[\frac{dN_1^{(1)}}{dx} \phi_1 + \frac{dN_2^{(1)}}{dx} \phi_2 \right] dx + \int_{l/2}^l \frac{dN_1^{(1)}}{dx} k \left[\frac{dN_1^{(2)}}{dx} \phi_2 + \frac{dN_2^{(2)}}{dx} \phi_3 \right] dx = \\
& = \underbrace{\int_0^{l/2} N_2^{(1)} Q dx}_{f_2^{(1)}} + \underbrace{\int_{l/2}^l N_1^{(2)} Q dx}_{f_1^{(2)}}
\end{aligned} \tag{2.82b}$$

Note that the boundary terms are zero as $N_2 = 0$ at $x = 0$ and $x = l$.

For $i = 3$

$$\begin{aligned}
& \int_{l/2}^l \frac{dN_2^{(2)}}{dx} k \left[\frac{dN_1^{(2)}}{dx} \phi_2 + \frac{dN_2^{(2)}}{dx} \phi_3 \right] dx = \int_{l/2}^l N_2^{(2)} Q dx + \\
& + [N_3 q]_0 - [N_3 \bar{q}]_l = \underbrace{\int_{l/2}^l N_2^{(2)} Q dx}_{f_2^{(2)}} - \bar{q}
\end{aligned} \tag{2.82c}$$

The above expressions can be written in matrix form as

$$\underbrace{\begin{bmatrix} K_{11}^{(1)} & K_{12}^{(1)} & 0 \\ K_{21}^{(1)} & K_{22}^{(1)} + K_{11}^{(2)} & K_{12}^{(2)} \\ 0 & K_{21}^{(2)} & K_{22}^{(2)} \end{bmatrix}}_{\mathbf{K}} \underbrace{\begin{Bmatrix} \phi_1 = \bar{\phi} \\ \phi_2 \\ \phi_3 \end{Bmatrix}}_{\mathbf{a}} = \underbrace{\begin{Bmatrix} f_1^{(1)} + q_0 \\ f_2^{(1)} + f_1^{(2)} \\ f_2^{(2)} - \bar{q} \end{Bmatrix}}_{\mathbf{f}}$$

with

$$K_{ij}^{(e)} = \int_{l^{(e)}} \frac{dN_i^{(e)}}{dx} k \frac{dN_j^{(e)}}{dx} dx$$

$$f_i^{(e)} = \int_{l^{(e)}} N_i^{(e)} Q dx$$

We see that the global stiffness matrix can be obtained by assembling the individual element matrices $\mathbf{K}^{(e)}$, as we did for the assembly of the stiffness matrices in bar structures. Also note the banded structure of \mathbf{K} . The bandwidth size depends on the numbering of the nodes in the finite element mesh

The components of the global equivalent nodal flux vector can be also obtained by assembling the contributions from each element. Note that at the end nodes 1 and 3 we should add the global flux components q_0 and \bar{q} . As

usual the sign of the end flux is positive is heat comes *into* the body, whereas it is negative for heat fluxes that originate heat losses in the body.

Note again the coincidence of the assembly process for \mathbf{K} and \mathbf{f} with that followed for the matrix analysis of bar structures.

The expressions of $\mathbf{K}^{(e)}$ and $\mathbf{f}^{(e)}$ given above are general and applicable to any 1D heat conduction element. We particularize next these expressions for the 2-noded element. From the expression of the shape function we obtain

$$\frac{dN_1^{(e)}(x)}{dx} = -\frac{1}{l^{(e)}}$$

$$\frac{dN_2^{(e)}(x)}{dx} = \frac{1}{l^{(e)}}$$

Substituting the above expressions into $K_{ij}^{(e)}$, we obtain

$$K_{11}^{(e)} = \int_{l^{(e)}} \left(-\frac{1}{l^{(e)}}\right) \left(-\frac{1}{l^{(e)}}\right) k dx = \left(\frac{k}{l}\right)^{(e)} = K_{22}^{(e)}$$

where k has been assumed to be constant within each element. Also

$$K_{12}^{(e)} = K_{21}^{(e)} = \int_{l^{(e)}} \left(-\frac{1}{l^{(e)}}\right) k \left(\frac{1}{l^{(e)}}\right) dx = -\left(\frac{k}{l}\right)^{(e)}$$

Assuming a uniform distribution of Q over the bar gives

$$\begin{aligned} f_1^{(e)} &= \int_{l^{(e)}} \frac{x_2^{(e)} - x}{l^{(e)}} Q dx = \int_{l^{(e)}} \frac{x_2^{(e)}}{l^{(e)}} Q dx - \int_{l^{(e)}} \frac{x}{l^{(e)}} Q dx = \\ &= Q[x]_0^{l^{(e)}} - \frac{Q}{l^{(e)}} \left[\frac{x^2}{2}\right]_0^{l^{(e)}} = \frac{Ql^{(e)}}{2} \end{aligned}$$

$$f_2^{(e)} = \int_{l^{(e)}} \frac{x - x_1^{(e)}}{l^{(e)}} dx = \frac{Q}{l^{(e)}} \left[\frac{x^2}{2}\right]_0^{l^{(e)}} = \frac{Ql^{(e)}}{2}$$

The global matrix equation is therefore written as

$$\begin{bmatrix} \left(\frac{k}{l}\right)^{(1)} & \left(-\frac{k}{l}\right)^{(1)} & 0 \\ \left(-\frac{k}{l}\right)^{(1)} & \left(\frac{k}{l}\right)^{(1)} + \left(\frac{k}{l}\right)^{(2)} & \left(-\frac{k}{l}\right)^{(2)} \\ 0 & -\left(\frac{k}{l}\right)^{(2)} & \left(\frac{k}{l}\right)^{(2)} \end{bmatrix} \begin{Bmatrix} \phi_1 \\ \phi_2 \\ \phi_3 \end{Bmatrix} = \begin{Bmatrix} \frac{Ql^{(1)}}{2} + q_0 \\ \frac{Ql^{(1)}}{2} + \frac{Ql^{(2)}}{2} \\ \frac{Ql^{(2)}}{2} - \bar{q} \end{Bmatrix}$$

For k constant over the bar and an uniform mesh ($l^{(e)} = l/2$) we obtain

$$\frac{2k}{l} \begin{bmatrix} 1 & -1 & 0 \\ -1 & 2 & -1 \\ 0 & -1 & 1 \end{bmatrix} \begin{Bmatrix} \phi_1 \\ \phi_2 \\ \phi_3 \end{Bmatrix} = \begin{Bmatrix} \frac{Ql}{4} + q_0 \\ \frac{Ql}{2} \\ \frac{Ql}{4} - \bar{q} \end{Bmatrix}, \quad \phi_1 = \bar{\phi}$$

The solution of the above system gives

$$\begin{aligned} \phi_3 &= \frac{Ql^2}{2k} - \frac{\bar{q}l}{k} + \bar{\phi} \\ \phi_2 &= \frac{3Ql^2}{8k} - \frac{\bar{q}l}{2k} + \bar{\phi} \\ \phi_0 &= \bar{q} - Ql \end{aligned} \tag{2.83}$$

Note that the solution for ϕ_2 and ϕ_3 coincides again with the exact values (eq. (2.72)). Also, we obtain again $q_0 = \bar{q} - Ql$ which balances the sum of heat fluxes over the bar.

2.10 GENERALIZATION OF THE SOLUTION FOR A MESH OF TWO-NODED ELEMENTS

We summarize next the steps to be followed for solving the 1D Poisson problem with 2-noded linear elements.

1. Obtain the stiffness matrix $\mathbf{K}^{(e)}$ and the equivalent nodal flux vector $\mathbf{f}^{(e)}$ for each element.

For the 2-noded element the expressions are

$$\mathbf{K}^{(e)} = \begin{bmatrix} K_{11}^{(e)} & K_{12}^{(e)} \\ K_{21}^{(e)} & K_{22}^{(e)} \end{bmatrix} \quad \mathbf{f}^{(e)} = \begin{Bmatrix} f_1^{(e)} \\ f_2^{(e)} \end{Bmatrix}$$

with

$$K_{ij}^{(e)} = \int_{l^{(e)}} \frac{dN_i^{(e)}(x)}{dx} k \frac{dN_j^{(e)}(x)}{dx} dA = (-1)^{i+j} \left(\frac{k}{l} \right)^{(e)} \tag{2.84}$$

$$f_i^{(e)} = \int_{l^{(e)}} N_i^{(e)} Q dx = \frac{(Ql)^{(e)}}{2}$$

Note that $\mathbf{K}^{(e)}$ has a many rows and columns as degrees of freedom (d.o.f.) has the element. Recall that for the 1D Poisson problem we just have a single d.o.f. per node.

3. *Propagation problems.* They include all non-stationary problems where the evolution of some variables depends on time.

Table I lists different applications of the FEM in different engineering disciplines related to the three types of problems mentioned above.

Discipline	STATIONARY PROBLEMS	EIGENVALUE PROBLEMS	PROPAGATION PROBLEMS
Civil, Aerospace and Naval Engineering	Static analysis of structures. Stationary porous media flow	Structural stability problems	Seismic and dynamic analysis of structures. Fluid dynamics analysis
Mechanical Engineering	Stress analysis of mechanical systems. Stationary heat transfer	Modal and vibration analysis of mechanical components	Dynamic analysis of mechanical systems. Transient heat transfer
Geotechnical Engineering	Stress analysis in soils and rocks. Flow through porous media	Modal and vibration analysis of soils	Wave propagation in soils and rocks
Nuclear Engineering	Stress and heat transfer analysis in nuclear structures. Fracture mechanics	Modal and vibration analysis of nuclear structures	Seismic and dynamic analysis of nuclear structures. Transient heat transfer
Electrical and Telecommunication Engineering	Stationary analysis of Maxwell equations	Frequency analysis of Maxwell equations	Transient solution of Maxwell equations

From the practical point of view of the analyst it should never be forgotten that the FEM is a very powerful technique to obtain *approximate solutions* for continuous problems. In the hands of a careful and expert user the FEM is an indispensable tool for the analysis of complex problems which cannot be studied otherwise. However, being an approximate method it involves a certain *error* in the numerical values and users should always consider FEM results with a critical eye. In this course we will try to facilitate the understanding of the theoretical and applied aspects of the FEM for analysis of continuum systems.

Chapter 3

1D FINITE ELEMENTS FOR AXIALLY LOADED RODS

3.1 INTRODUCTION

The objective of this chapter is to introduce the basic concepts of the FEM in its application to the analysis of simple one-dimensional (1D) axially loaded rods via the principle of virtual work (PVW).

The organization of the chapter is as follows. In the first section the analysis of axially loaded rods using 2-noded rod elements is presented. Particular emphasis is put in the analogies with the solution of the same problem using the standard matrix analysis techniques studied in the Chapter 1 for bar structures. Here some examples of application are given. Then the chapter the matrix finite element formulation which will be adopted throughout this course is presented. In the final part of the chapter the general derivation of the one-dimensional (1D) shape functions is presented. Such functions are very useful for obtaining the shape functions of two- (2D) and three- (3D) dimensional elements in the next chapters. The concepts of isoparametric element and numerical integration are explained. These concepts are essential for the study of high-order 2D and 3D elements. Finally, the requirements for the convergence of the numerical solution are discussed, together with a description of the more usual solution errors.

3.2 AXIALLY LOADED ROD

Let us consider a rod of length l subjected to a uniformly distributed axial load per unit length $b(x)$ and a set of axial point loads X_i acting at p different points x_i (Figure 3.1). The rod can also have prescribed displacements \bar{u}_j at m points x_j . The displacement of the rod points produces the corresponding strains $\varepsilon(x) = \frac{du}{dx}$ and stresses σ in the rod which are related by Hooke's law, i.e.

$$\sigma = E\varepsilon = E \frac{du}{dx} \quad (3.1)$$

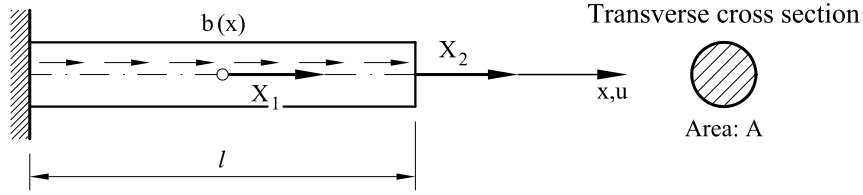


Fig. 3.1: Axially loaded rod

where E is the Young modulus of the material.

In the equilibrium configuration the stresses and the external forces satisfy the *Principle of Virtual Work* (PVW) defined in Section 1.7. The PVW for the rod is written as

$$\iiint_V \delta \varepsilon \sigma dV = \int_0^l \delta u b dx + \sum_{i=1}^p \delta u_i X_i \quad (3.2)$$

where δu and $\delta \varepsilon$ are the virtual displacement and the virtual strain of an arbitrary point of the rod center line δu_i is the virtual displacement of the point where the point load X_i acts, and V is the rod volume. The left- and right-hand sides of Eq.(3.2) represent the internal and external virtual work carried out by the actual stresses and the external loads, respectively.

Eq.(3.2) can be rewritten after integration over the cross section of area A (note that $dV = dA \cdot dx$) and using Eq.(3.1) as

$$\int_0^l \delta \varepsilon EA \frac{du}{dx} = \int_0^l \delta u b dx + \sum_{i=1}^p \delta u_i X_i \quad (3.3)$$

It can be proved [T7] that the equilibrium solution of the rod problem is reduced to finding a displacement field $u(x)$ satisfying Eq.(3.3) and the displacement boundary conditions (kinematic conditions). The approximate solution using the FEM is set as follows: find an alternative displacement field $\hat{u}(x)$ which approximates $u(x)$ and which also satisfies Eq.(3.3) and the kinematic conditions.

Among the different options available to express the approximate displacement field $\hat{u}(x)$ we will choose the simplest one using polynomials locally defined for each element. Thus, after discretization we can write for each element

$$u(x) \simeq \hat{u}(x) = a_o + a_1 x + a_2 x^2 + \dots + a_n x^n = \sum_{i=1}^n a_i x^i \quad (3.4)$$

In Eq.(3.4) n is the number of points of the element where the displacement is assumed to be known. These points are called *nodes*. The parameters a_o, a_1, \dots, a_n depend on the nodal displacements only. In the following we will skip the hat over the approximate solution and write Eq.(3.4) in the form

$$u(x) = N_1^{(e)}(x)u_1^{(e)} + N_2^{(e)}(x)u_2^{(e)} + \dots + N_n^{(e)}(x)u_n^{(e)} = \sum_{i=1}^n N_i^{(e)}(x)u_i^{(e)} \quad (3.5)$$

where $N_1^{(e)}(x), \dots, N_n^{(e)}(x)$ are the polynomial interpolating functions defined over the domain of each element e (termed hereafter *shape functions*) and $u_i^{(e)}$ is the value of the (approximate) displacement of node i . The shape function $N_i^{(e)}(x)$ interpolates within each element the displacements of node i only and for this reason it is called the *shape function of node i* . Note from Eq.(3.5) that $N_i^{(e)}(x)$ is equal to one at node i and equal to zero at all other nodes. These concepts will be extended in the next section.

Substituting the displacement approximation for each element in the PVW allows us to express the equilibrium equations in terms of the nodal displacements of the finite element mesh. These algebraic equations can be written in the standard matrix form

$$\mathbf{K} \mathbf{a} = \mathbf{f} \quad (3.6)$$

where, by analogy with bar systems, \mathbf{K} is termed the *stiffness matrix* of the finite element mesh, and \mathbf{a} and \mathbf{f} are the *vectors of nodal displacements* and of *equivalent nodal forces*, respectively. Both \mathbf{K} and \mathbf{f} are obtained by assembling the contributions from the individual elements as in matrix analysis of bar structures. Solving Eq.(3.6) yields the values of the displacements at all the nodes in the mesh from which the strains and stresses within each element can be found.

These concepts will be illustrated in the next section for the analysis of an axially loaded rod with constant cross sectional area using two meshes of one and two linear rod elements, respectively.

3.3 AXIALLY LOADED ROD OF CONSTANT CROSS SECTIONAL AREA. DISCRETIZATION IN ONE LINEAR ROD ELEMENT

Let us consider the bar in Figure 3.2. The bar is first discretized in a single element with two nodes which define a linear interpolation of the displacement field as

$$u(x) = a_o + a_1x \quad (3.7)$$

Naturally, $u(x)$ must take the values $u_1^{(1)}$ and $u_2^{(1)}$ at nodes 1 and 2, i.e.

$$u(x_1^{(1)}) = u_1^{(1)} \quad \text{and} \quad u(x_2^{(1)}) = u_2^{(1)} \quad (3.8)$$

where $x_1^{(1)}$ and $x_2^{(1)}$ are the coordinates of nodes 1 and 2, respectively. The superindex 1 in Eq.(3.8) denotes that all the parameters refer to the element number one.

From Eqs.(3.8) and (3.7) the following system of equations is obtained

$$\begin{aligned} u_1^{(1)} &= a_o + a_1x_1^{(1)} \\ u_2^{(1)} &= a_o + a_1x_2^{(1)} \end{aligned} \quad (3.9)$$

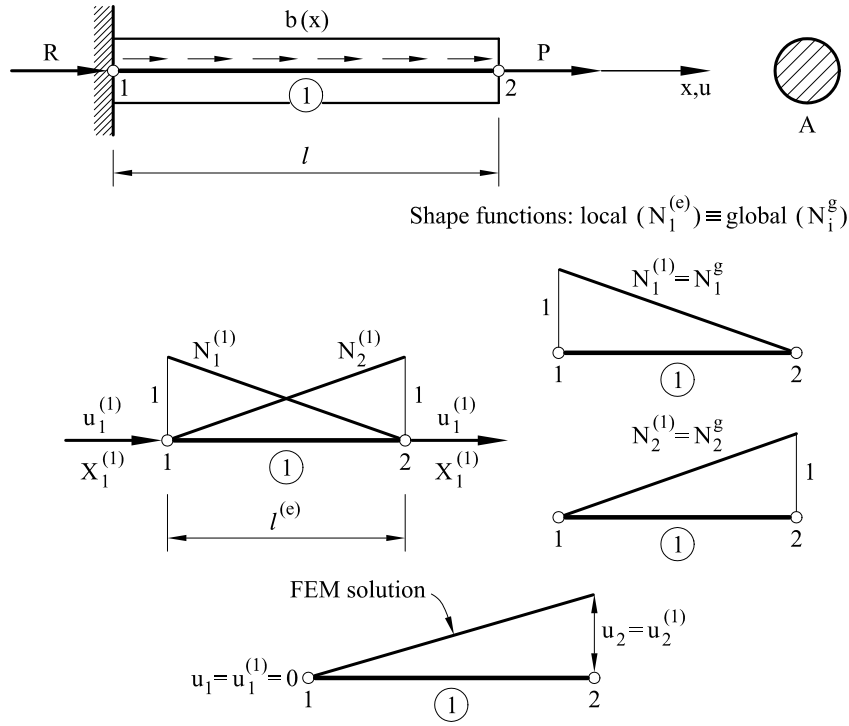


Fig. 3.2: Axially loaded rod of constant cross section. Discretization in a single 2-noded rod element

from which the parameters a_o and a_1 are found as

$$a_o = \frac{u_1^{(1)} - u_2^{(1)}}{x_1^{(1)} - x_2^{(1)}} \quad \text{and} \quad a_1 = \frac{x_2^{(1)}u_1^{(1)} - x_1^{(1)}u_2^{(1)}}{x_2^{(1)}x_1^{(1)}} \quad (3.10)$$

Substituting Eq.(3.10) into (3.7) allows us to rewrite the latter as

$$u = N_1^{(1)}(x)u_1^{(1)} + N_2^{(1)}(x)u_2^{(1)} \quad (3.11)$$

where $N_1^{(1)}$ and $N_2^{(1)}$ are the shape functions of nodes 1 and 2, respectively given by

$$N_1^{(1)}(x) = \frac{x_2^{(1)} - x}{l^{(1)}} \quad ; \quad N_2^{(1)}(x) = \frac{x - x_1^{(1)}}{l^{(1)}} \quad (3.12)$$

where $l^{(1)} = x_2^{(1)} - x_1^{(1)}$ is the element length. It is deduced from Eq.(3.12) that the shape functions $N_i^{(1)}$ ($i = 1, 2$) vary linearly within the element and take the value one at node i and the value zero at the other node. This is a general property which is a consequence of the local definition of the finite element interpolation chosen. This lets us anticipate in most cases the geometry of the shape functions, as will be frequently seen throughout this book.

Before we proceed any further it is important to clarify the differences between local and global numbering. Table 3.1 shows an example of both numberings for

the nodes, the coordinates and the nodal displacements for the example in Figure 3.2.

Element	nodes		coordinates		displacement	
	local	global	local	global	local	global
1	1	1	$x_1^{(1)}$	x_1	$u_1^{(1)}$	u_1
	2	2	$x_2^{(1)}$	x_2	$u_2^{(1)}$	u_2

Table 3.1: Local and global parameters for the example in Figure 3.2

Note that since we have taken in this case a single element, the local and global numbers coincide.

The derivatives of the shape functions are computed as

$$\frac{dN_1^{(1)}}{dx} = -\frac{1}{l^{(1)}} \quad \text{and} \quad \frac{dN_2^{(1)}}{dx} = \frac{1}{l^{(1)}} \quad (3.13)$$

In this way the axial strain can be obtained at each point within the element as

$$\varepsilon = \frac{du}{dx} = \frac{dN_1^{(1)}}{dx} u_1^{(1)} + \frac{dN_2^{(1)}}{dx} u_2^{(1)} = -\frac{1}{l^{(1)}} u_1^{(1)} + \frac{1}{l^{(1)}} u_2^{(1)} \quad (3.14)$$

Obviously, the linear shape functions yield a constant strain (and stress) field over the element.

The forces between elements are transmitted across the nodes only. These forces are termed *equilibrating nodal forces* and can be obtained for each element using the PVW. For the single element of Figure 3.2 we can write

$$\int_{x_1^{(1)}}^{x_2^{(1)}} \delta\varepsilon EA \cdot \varepsilon dx = \int_{x_1^{(1)}}^{x_2^{(1)}} \delta u \cdot b dx + \delta u_1^{(1)} X_1^{(1)} + \delta u_2^{(1)} X_2^{(1)} \quad (3.15)$$

where $\delta u_1^{(1)}$, $\delta u_2^{(1)}$, $X_1^{(1)}$ and $X_2^{(1)}$ are the virtual displacements and the equilibrating nodal forces of nodes 1 and 2 of the element, respectively. The virtual displacement can also be linearly interpolated in terms of the nodal values as

$$\delta u = N_1^{(1)} \delta u_1^{(1)} + N_2^{(1)} \delta u_2^{(1)} \quad (3.16)$$

The virtual strain is now expressed in terms of the virtual nodal displacements as

$$\delta\varepsilon = \frac{d}{dx}(\delta u) = \frac{dN_1^{(1)}}{dx} \delta u_1^{(1)} + \frac{dN_2^{(1)}}{dx} \delta u_2^{(1)} \quad (3.17)$$

Eq.(3.15) is rewritten, after substitution of (3.11), (3.16) and (3.17), as

$$\begin{aligned} & \int_{x_1^{(1)}}^{x_2^{(1)}} \left[\frac{dN_1^{(1)}}{dx} \delta u_1^{(1)} + \frac{dN_2^{(1)}}{dx} \delta u_2^{(1)} \right] (EA) \left[\frac{dN_1^{(1)}}{dx} \delta u_1^{(1)} + \frac{dN_2^{(1)}}{dx} \delta u_2^{(1)} \right] dx - \\ & - \int_{x_1^{(1)}}^{x_2^{(1)}} \left[N_1^{(1)} \delta u_1^{(1)} + N_2^{(1)} \delta u_2^{(1)} \right] b dx = \delta u_1^{(1)} X_1^{(1)} + \delta u_2^{(1)} X_2^{(1)} \end{aligned} \quad (3.18)$$

Grouping terms gives

$$\begin{aligned} & \delta u_1^{(1)} \left[\int_{x_1^{(1)}}^{x_2^{(1)}} \left(\frac{dN_1^{(1)}}{dx} (EA) \frac{dN_1^{(1)}}{dx} u_1^{(1)} + \frac{dN_1^{(1)}}{dx} (EA) \frac{dN_2^{(1)}}{dx} u_2^{(1)} \right) dx - \right. \\ & - \left. \int_{x_1^{(1)}}^{x_2^{(1)}} N_1^{(1)} b dx - X_1^{(1)} \right] + \delta u_2^{(1)} \left[\int_{x_1^{(1)}}^{x_2^{(1)}} \left(\frac{dN_2^{(1)}}{dx} (EA) \frac{dN_1^{(1)}}{dx} u_1^{(1)} + \right. \right. \\ & \left. \left. + \frac{dN_2^{(1)}}{dx} (EA) \frac{dN_2^{(1)}}{dx} u_2^{(1)} \right) dx - \int_{x_1^{(1)}}^{x_2^{(1)}} N_2^{(1)} b dx - X_2^{(1)} \right] = 0 \end{aligned} \quad (3.19)$$

Since the virtual displacements are arbitrary, satisfying of Eq.(3.19) leads to the following system of two equations

$$\begin{aligned} & \int_{x_1^{(1)}}^{x_2^{(1)}} \left(\frac{dN_1^{(1)}}{dx} (EA) \frac{dN_1^{(1)}}{dx} u_1^{(1)} + \frac{dN_1^{(1)}}{dx} (EA) \frac{dN_2^{(1)}}{dx} u_2^{(1)} \right) dx - \\ & - \int_{x_1^{(1)}}^{x_2^{(1)}} N_1^{(1)} b dx - X_1^{(1)} = 0 \end{aligned} \quad (3.20)$$

$$\begin{aligned} & \int_{x_1^{(1)}}^{x_2^{(1)}} \left(\frac{dN_2^{(1)}}{dx} (EA) \frac{dN_1^{(1)}}{dx} u_1^{(1)} + \frac{dN_2^{(1)}}{dx} (EA) \frac{dN_2^{(1)}}{dx} u_2^{(1)} \right) dx \\ & - \int_{x_1^{(1)}}^{x_2^{(1)}} N_2^{(1)} b dx - X_2^{(1)} = 0 \end{aligned}$$

From Eq.(3.20) the values of the equilibrating nodal forces are obtained. In matrix form

$$\begin{aligned} & \left(\int_{x_1^{(1)}}^{x_2^{(1)}} \left[\begin{array}{cc} \left(\frac{dN_1^{(1)}}{dx} (EA) \frac{dN_1^{(1)}}{dx} \right) & \left(\frac{dN_1^{(1)}}{dx} (EA) \frac{dN_2^{(1)}}{dx} \right) \\ \left(\frac{dN_2^{(1)}}{dx} (EA) \frac{dN_1^{(1)}}{dx} \right) & \left(\frac{dN_2^{(1)}}{dx} (EA) \frac{dN_2^{(1)}}{dx} \right) \end{array} \right] dx \right) \begin{Bmatrix} u_1^{(1)} \\ u_2^{(1)} \end{Bmatrix} - \\ & - \int_{x_1^{(1)}}^{x_2^{(1)}} \begin{Bmatrix} N_1^{(1)} \\ N_2^{(1)} \end{Bmatrix} b dx = \begin{Bmatrix} X_1^{(1)} \\ X_2^{(1)} \end{Bmatrix} \end{aligned} \quad (3.21)$$

or

$$\mathbf{K}^{(1)} \mathbf{a}^{(1)} - \mathbf{f}^{(1)} = \mathbf{q}^{(1)} \quad (3.22a)$$

with

$$\begin{aligned}\mathbf{K}_{ij}^{(1)} &= \int_{x_1^{(1)}}^{x_2^{(1)}} \frac{dN_i^{(1)}}{dx} (EA) \frac{dN_j^{(1)}}{dx} dx & (3.22b) \\ \mathbf{f}_i^{(1)} &= \int_{x_1^{(1)}}^{x_2^{(1)}} N_i^{(1)} b dx & i, j = 1, 2 \\ \mathbf{a}^{(1)} &= [u_1^{(1)}, u_2^{(1)}]^T & ; \quad \mathbf{q}^{(1)} = [X_1^{(1)}, X_2^{(2)}]^T\end{aligned}$$

Eq.(3.22a) expresses the balance between the equilibrating nodal forces $\mathbf{q}^{(1)}$, the distributed forces $\mathbf{f}^{(1)}$, and the nodal displacements $\mathbf{a}^{(1)}$. In Eq.(3.22a) $\mathbf{K}^{(1)}$ is the element stiffness matrix and $\mathbf{f}^{(1)}$ is the *equivalent nodal force* vector for the element.

If the Young modulus, the cross sectional area and the distributed loading are constant over the element, the following is obtained

$$\mathbf{K}^{(1)} = \left(\frac{EA}{l}\right)^{(1)} \begin{bmatrix} 1 & -1 \\ -1 & 1 \end{bmatrix} ; \quad \mathbf{f}^{(1)} = \frac{(bl)^{(1)}}{2} \begin{Bmatrix} 1 \\ 1 \end{Bmatrix} \quad (3.23)$$

Note the coincidence between these expressions and those obtained for the axially loaded bar in Chapter 1. This coincidence could have been anticipated if we had observed that in both cases the same linear displacement field is assumed. This obviously leads, via the PVW, to the same expressions for the element stiffness matrix and the nodal load vector.

The global equilibrium equations are obtained by the same nodal load balancing procedure explained for bar structures in the previous chapter. Thus, for each of the N nodes in the mesh we have

$$\sum_e X_i^{(e)} = X_j^{\text{ext}} \quad , \quad j = 1, N \quad (3.24)$$

where the sum is extended over all the elements sharing the node with global number j , $X_i^{(e)}$ is the equilibrating nodal force contributed by each element, X_j^{ext} is the external point load acting at the node.

For the single element mesh considered, Eq.(3.24) is written as (see Figure 3.2)

$$\begin{aligned}\text{node 1 : } & X_1^{(1)} = R_1 \\ \text{node 2 : } & X_2^{(1)} = P\end{aligned}$$

Substituting the values of the equilibrating nodal forces from Eq.(3.21) and making use of Table 3.1 the global equilibrium equations are obtained as

$$\left(\frac{EA}{l}\right) \begin{bmatrix} 1 & -1 \\ -1 & 1 \end{bmatrix} \begin{Bmatrix} u_1 \\ u_2 \end{Bmatrix} = \begin{Bmatrix} R_1 + \frac{bl}{2} \\ P + \frac{bl}{2} \end{Bmatrix}$$

or

$$\mathbf{K} \mathbf{a} = \mathbf{f} \quad (3.25)$$

where, as usual, \mathbf{K} , \mathbf{a} and \mathbf{f} are, respectively, the global stiffness matrix, the vector containing the displacements of all nodes in the mesh and the global equivalent nodal force vector. Eq.(3.25) is solved after imposing the condition $u_1 = 0$, to give

$$u_2 = \frac{l}{EA} \left(P + \frac{bl}{2} \right) \quad ; \quad R_1 = -(P + bl) \quad (3.26)$$

The axial strain ε and the axial stress N in the element are given by

$$\begin{aligned} \varepsilon^{(1)} &= \frac{dN_1^{(1)}}{dx} u_1^{(1)} + \frac{dN_2^{(1)}}{dx} u_2^{(1)} = -\frac{u_1^{(1)}}{l_1^{(1)}} = \frac{P + \frac{bl}{2}}{EA} \\ N^{(1)} &= (EA)^{(1)} \varepsilon^{(1)} = P + \frac{bl}{2} \end{aligned} \quad (3.27)$$

The exact solution for this simple problem is [T7]

$$\begin{aligned} u &= \frac{1}{EA} \left[-\frac{bx^2}{2} + (P + bl)x \right] \\ \varepsilon &= \frac{1}{EA} [P + b(l - x)] \end{aligned} \quad (3.28)$$

The finite element and the exact solutions are compared in Figure 3.3 for $P = 0$ and $b = 1T/m$. Note that the value of the end displacement is the exact solution. This is a coincidence and it should be considered as an exception which only occurs for a few occasions only.¹ Within the rod the single element approximation yields a linear displacement field very different from the exact quadratic solution. Also note that the constant axial stress value obtained differs substantially from the linear exact solution. As expected, the numerical solution improves as the mesh is refined and this is shown in Section 3.5 for a mesh of two elements.

3.4 DERIVATION OF THE DISCRETIZED EQUATIONS FROM THE GLOBAL DISPLACEMENT INTERPOLATION FIELD

It is interesting that a general expression for the displacement interpolation field *for the whole mesh* can be obtained by simple superposition of the local approximations for each element. This lets us define *global shape functions* which naturally should coincide with the original local expressions within each element. The use of global shape functions leads to identical results as with the simpler local functions. However, its study has an academic interest.

¹It has been proved [Z7] that the finite element solution coincides with the exact one for 1D problems if the interpolation chosen satisfies exactly the homogeneous form of the differential equation of equilibrium. This is written for the rod problem as $\frac{d^2u}{dx^2} = 0$, which is obviously satisfied by the linear approximation chosen.

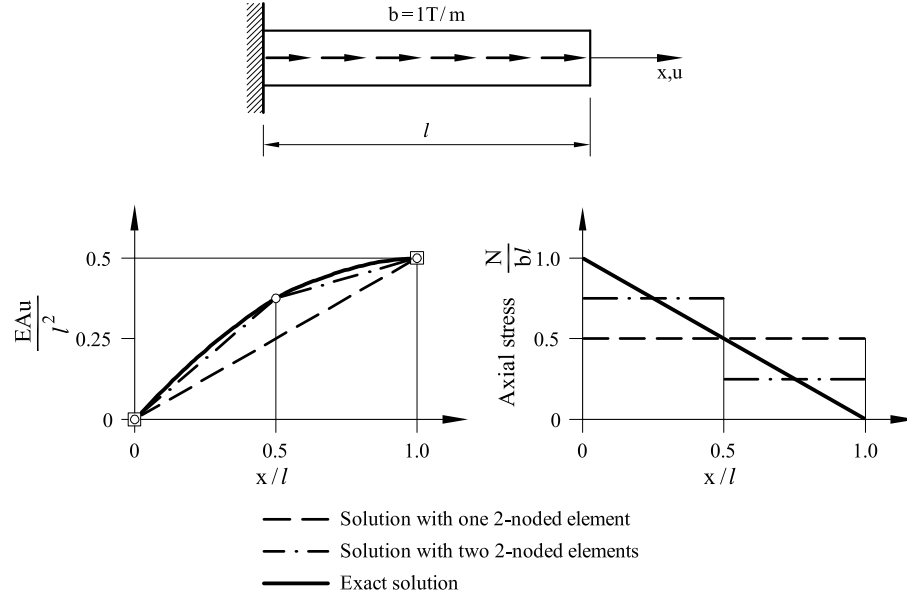


Fig. 3.3: Axially loaded rod under uniformly distributed loading. Exact and approximate solutions using one and two linear rod elements

The conceptual differences between global and local shape functions will be clarified by repeating the single rod element problem using a global interpolation for the displacement field.

The axial displacement can be written in the single element mesh as

$$u(x) = N_1^g(x) u_1 + N_2^g(x) u_2 \quad (3.29)$$

where $N_1^g(x)$ and $N_2^g(x)$ are the *global shape functions* of nodes 1 and 2, respectively, and u_1 and u_2 are the displacements of these nodes. Note that for the global displacements we skip the superindex e . We deduce from Eq.(3.29) that the global function of a node takes the value *one* at that node and *zero* at all other nodes. This provides the relationship between global and local shape functions as

$$\begin{aligned} N_i^g(x) &= N_i^{(e)}(x) && \text{if } x \text{ belongs to element } e \\ &= 0 && \text{if } x \text{ does not belong to element } e \end{aligned} \quad (3.30)$$

For the single element case considered, the global and local shape functions coincide (Figure 3.2). Thus,

$$N_1^g(x) = N_1^{(1)}(x) \quad \text{and} \quad N_2^g(x) = N_2^{(1)}(x) \quad (3.31)$$

The axial strain in the rod of Figure 3.2 can be obtained as

$$\varepsilon = \frac{du}{dx} = \frac{dN_1^g}{dx} u_1 + \frac{dN_2^g}{dx} u_2 \quad (3.32)$$

The virtual displacement and the virtual axial strain are expressed as

$$\delta u = N_1^g \delta u_1 + N_2^g \delta u_2 \quad , \quad \delta \varepsilon = \frac{dN_1^g}{dx} \delta u_1 + \frac{dN_2^g}{dx} \delta u_2 \quad (3.33)$$

The PVW is written for the rod as

$$\begin{aligned} & \int_0^l \left[\frac{dN_1^g}{dx} \delta u_1 + \frac{dN_2^g}{dx} \delta u_2 \right] (EA) \left[\frac{dN_1^g}{dx} u_1 + \frac{dN_2^g}{dx} u_2 \right] dx - \\ & - \int_0^l [N_1^g \delta u_1 + N_2^g \delta u_2] b dx = \delta u_1 R_1 + \delta u_2 P \end{aligned} \quad (3.34)$$

After eliminating the virtual displacements, Eq.(3.34) leads to

$$\begin{aligned} & \left(\int_0^l \begin{bmatrix} \frac{dN_1^g}{dx} (EA) \frac{dN_1^g}{dx} & \frac{dN_1^g}{dx} (EA) \frac{dN_2^g}{dx} \\ \frac{dN_2^g}{dx} (EA) \frac{dN_1^g}{dx} & \frac{dN_2^g}{dx} (EA) \frac{dN_2^g}{dx} \end{bmatrix} dx \right) \begin{Bmatrix} u_1 \\ u_2 \end{Bmatrix} - \\ & - \int_0^l \begin{Bmatrix} N_1^g \\ N_2^g \end{Bmatrix} b dx = \begin{Bmatrix} R_1 \\ P \end{Bmatrix} \end{aligned} \quad (3.35)$$

The following relationships are important for the computation of the integrals in Eq.(3.35)

$$\left. \begin{aligned} N_1^g &= N_1^{(1)} \\ N_2^g &= N_2^{(1)} \\ \frac{dN_1^g}{dx} &= \frac{dN_1^{(1)}}{dx} \\ \frac{dN_2^g}{dx} &= \frac{dN_2^{(1)}}{dx} \end{aligned} \right\} 0 \leq x \leq l \quad (3.36)$$

Using Eq.(3.36) we obtain

$$\begin{aligned} \int_0^l \frac{dN_1^g}{dx} \frac{dN_1^g}{dx} dx &= \int_0^{l^{(1)}} \left(\frac{dN_1^{(1)}}{dx} \right)^2 dx = \frac{1}{l} \\ \int_0^l \frac{dN_1^g}{dx} \frac{dN_2^g}{dx} dx &= \int_0^{l^{(1)}} \frac{dN_1^{(1)}}{dx} \frac{dN_2^{(1)}}{dx} dx = -\frac{1}{l} \\ \int_0^l \frac{dN_2^g}{dx} \frac{dN_2^g}{dx} dx &= \int_0^{l^{(1)}} \left(\frac{dN_2^{(1)}}{dx} \right)^2 dx = \frac{1}{l} \\ \int_0^l N_i^g dx &= \int_0^{l^{(1)}} N_i^{(1)} dx = \int_0^{l^{(1)}} N_2^{(1)} dx = \frac{l}{2} \end{aligned} \quad (3.37)$$

Substituting Eq.(3.37) into the PVW expression (3.34) yields the *global equilibrium equation* (3.25) directly. Recall that in the previous section this equation

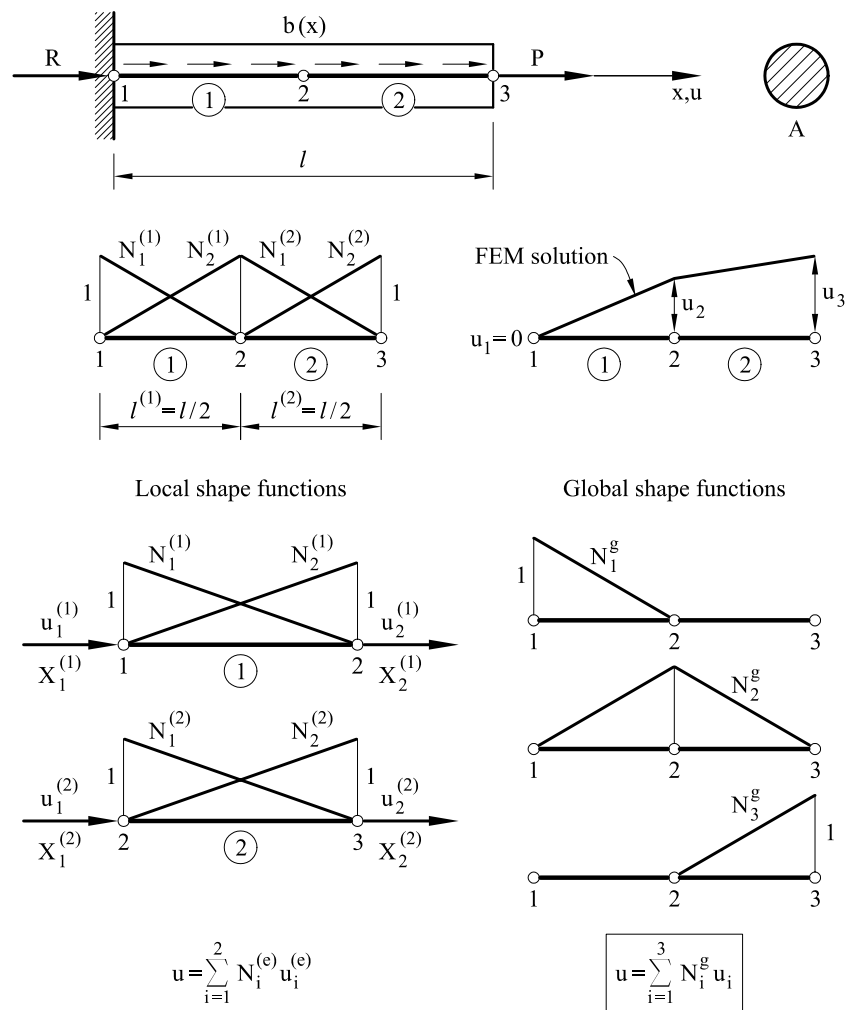


Fig. 3.4: Axially loaded rod. Discretization in two linear rod elements

was obtained from the assembly of the element contributions. From this point onwards the solution process is identical to that explained in Eqs.(3.25)-(3.27) and it will not be repeated here.

In the next section the same problem is solved using a mesh of two linear elements.

3.5 AXIALLY LOADED ROD OF CONSTANT CROSS SECTIONAL AREA. DISCRETIZATION IN TWO LINEAR ROD ELEMENTS

The same rod as for the previous example is discretized now in two linear rod elements as shown in Figure 3.4 where the differences between local and global shape functions are also shown.

The discretized equilibrium equations will be obtained first using the local description of the shape functions.

The displacements within each element are interpolated as

$$\begin{array}{c} \text{Element 1} \\ u(x) = N_1^{(1)}(x)u_1^{(1)} + N_2^{(1)}(x)u_2^{(1)} \end{array} \quad \left| \quad \begin{array}{c} \text{Element 2} \\ u(x) = N_1^{(2)}(x)u_1^{(2)} + N_2^{(2)}(x)u_2^{(2)} \end{array} \right. \quad (3.38)$$

The shape functions and their derivatives are

$$\begin{array}{c} N_1^{(1)} = \frac{x_2^{(1)} - x}{l^{(1)}} ; \quad \frac{dN_1^{(1)}}{dx} = -\frac{1}{l^{(1)}} \\ N_2^{(1)} = \frac{x - x_1^{(1)}}{l^{(1)}} ; \quad \frac{dN_2^{(1)}}{dx} = \frac{1}{l^{(1)}} \end{array} \quad \left| \quad \begin{array}{c} N_1^{(2)} = \frac{x_2^{(2)} - x}{l^{(2)}} ; \quad \frac{dN_1^{(2)}}{dx} = -\frac{1}{l^{(2)}} \\ N_2^{(2)} = \frac{x - x_1^{(2)}}{l^{(2)}} ; \quad \frac{dN_2^{(2)}}{dx} = \frac{1}{l^{(2)}} \end{array} \right. \quad (3.39)$$

The axial strain in each element is

$$\varepsilon = \frac{du}{dx} = \frac{dN_1^{(1)}}{dx}u_1^{(1)} + \frac{dN_2^{(1)}}{dx}u_2^{(1)} \quad \left| \quad \varepsilon = \frac{du}{dx} = \frac{dN_1^{(2)}}{dx}u_1^{(2)} + \frac{dN_2^{(2)}}{dx}u_2^{(2)} \quad (3.40)$$

The matrix form of the discretized equilibrium equations is obtained using the PVW as explained in the previous section for the single element case (see Eqs.(3.12)-(3.20)). We find that

$$\mathbf{q}^{(1)} = \mathbf{K}^{(1)}\mathbf{a}^{(1)} - \mathbf{f}^{(1)} \quad ; \quad \mathbf{q}^{(2)} = \mathbf{K}^{(2)}\mathbf{a}^{(2)} - \mathbf{f}^{(2)} \quad (3.41a)$$

where

$$\begin{aligned} \mathbf{K}^{(1)} &= \int_{x_1^{(1)}}^{x_2^{(1)}} (EA) \begin{bmatrix} \frac{dN_1^{(1)}}{dx} & \frac{dN_1^{(1)}}{dx} & \frac{dN_1^{(1)}}{dx} & \frac{dN_2^{(1)}}{dx} \\ \frac{dN_2^{(1)}}{dx} & \frac{dN_1^{(1)}}{dx} & \frac{dN_2^{(1)}}{dx} & \frac{dN_2^{(1)}}{dx} \end{bmatrix} dx \\ \mathbf{f}^{(1)} &= \int_{x_1^{(1)}}^{x_2^{(1)}} \begin{bmatrix} N_1^{(1)} & N_2^{(1)} \end{bmatrix}^T b^{(1)} dx \\ \mathbf{q}^{(1)} &= \begin{bmatrix} X_1^{(1)} & X_2^{(1)} \end{bmatrix}^T, \quad \mathbf{a}^{(1)} = \begin{bmatrix} u_1^{(1)} & u_2^{(1)} \end{bmatrix}^T \\ \mathbf{K}^{(2)} &= \int_{x_1^{(2)}}^{x_2^{(2)}} EA \begin{bmatrix} \frac{dN_1^{(2)}}{dx} & \frac{dN_1^{(2)}}{dx} & \frac{dN_1^{(2)}}{dx} & \frac{dN_2^{(2)}}{dx} \\ \frac{dN_2^{(2)}}{dx} & \frac{dN_1^{(2)}}{dx} & \frac{dN_2^{(2)}}{dx} & \frac{dN_2^{(2)}}{dx} \end{bmatrix} dx \\ \mathbf{f}^{(2)} &= \int_{x_1^{(2)}}^{x_2^{(2)}} \begin{bmatrix} N_1^{(2)} & N_2^{(2)} \end{bmatrix}^T b^{(2)} dx \\ \mathbf{q}^{(2)} &= \begin{bmatrix} X_1^{(2)} & X_2^{(2)} \end{bmatrix}^T, \quad \mathbf{a}^{(2)} = \begin{bmatrix} u_1^{(2)} & u_2^{(2)} \end{bmatrix}^T \end{aligned} \quad (3.41b)$$

are respectively the stiffness matrices, the equivalent nodal force vectors, the equilibrating nodal force vectors and the nodal displacement vectors of elements 1 and 2.

The integrals in Eqs.(3.41b) are computed keeping in mind the relationships between the local and global numbering of the element parameters summarized in Table 3.2.

Element	nodes		coordinates		displacement	
	local	global	local	global	local	global
1	1	1	$x_1^{(1)}$	x_1	$u_1^{(1)}$	u_1
	2	2	$x_2^{(1)}$	x_2	$u_2^{(1)}$	u_2
2	1	2	$x_1^{(2)}$	x_2	$u_1^{(2)}$	u_2
	2	3	$x_2^{(2)}$	x_3	$u_2^{(2)}$	u_{32}

Table 3.2: Local and global parameters for the example of Figure 3.4

Substituting Eq.(3.39) into (3.41) and using Table 3.2 the following expressions are obtained for the case of homogeneous material and uniformly distributed loading:

$$\begin{aligned} \mathbf{K}^{(1)} &= \left(\frac{EA}{l}\right)^{(1)} \begin{bmatrix} 1 & -1 \\ -1 & 1 \end{bmatrix} ; & \mathbf{K}^{(2)} &= \left(\frac{EA}{l}\right)^{(2)} \begin{bmatrix} 1 & -1 \\ -1 & 1 \end{bmatrix} \\ \mathbf{f}^{(1)} &= \frac{(bl)^{(1)}}{2} [1, 1]^T ; & \mathbf{f}^{(2)} &= \frac{(bl)^{(2)}}{2} [1, 1]^T \end{aligned} \quad (3.42)$$

The equilibrium of nodal forces is written as (see Eq.(3.24) and Figure 3.4)

$$\begin{aligned} \text{Node 1 : } & X_1^{(1)} &= R_1 \\ \text{Node 2 : } & X_2^{(1)} + X_1^{(2)} &= 0 \\ \text{Node 3 : } & X_2^{(2)} &= P \end{aligned} \quad (3.43)$$

Substituting $X_i^{(e)}$ from Eq.(3.42) into (3.43) the following matrix equilibrium equation is obtained

$$\begin{bmatrix} \left(\frac{EA}{l}\right)^{(1)} & -\left(\frac{EA}{l}\right)^{(1)} & 0 \\ -\left(\frac{EA}{l}\right)^{(1)} & \left[\left(\frac{EA}{l}\right)^{(1)} + \left(\frac{EA}{l}\right)^{(2)}\right] & \left(\frac{EA}{l}\right)^{(2)} \\ 0 & -\left(\frac{EA}{l}\right)^{(2)} & \left(\frac{EA}{l}\right)^{(2)} \end{bmatrix} \begin{Bmatrix} u_1 \\ u_2 \\ u_3 \end{Bmatrix} = \begin{Bmatrix} \frac{bl}{4} + R_1 \\ \frac{bl}{2} \\ \frac{bl}{4} + P \end{Bmatrix} \quad (3.44a)$$

$$\mathbf{Ka} = \mathbf{f} \quad (3.44b)$$

The element stiffness matrix is deduced from Eqs.(3.42) and (3.44) as

$$\begin{aligned} \mathbf{K}^{(e)} &= \begin{bmatrix} K_{11}^{(e)} & K_{12}^{(e)} \\ K_{21}^{(e)} & K_{22}^{(e)} \end{bmatrix} = \int_{x_1^{(e)}}^{x_2^{(e)}} (EA)^{(e)} \begin{bmatrix} \frac{dN_1^{(e)}}{dx} & \frac{dN_1^{(e)}}{dx} & \frac{dN_1^{(e)}}{dx} & \frac{dN_2^{(e)}}{dx} \\ \frac{dN_2^{(e)}}{dx} & \frac{dN_1^{(e)}}{dx} & \frac{dN_2^{(e)}}{dx} & \frac{dN_2^{(e)}}{dx} \end{bmatrix} dx = \\ &= \left(\frac{EA}{l} \right)^{(e)} \begin{bmatrix} 1 & -1 \\ -1 & 1 \end{bmatrix} \end{aligned} \quad (3.45)$$

Note that the assembly process is identical to that explained in the previous chapter for bar structures.

The same assembly process applies to the global vector of equivalent nodal forces. The elemental expression of this vector is

$$\mathbf{f}^{(e)} = \begin{Bmatrix} f_1^{(e)} \\ f_2^{(e)} \end{Bmatrix} = \int_{x_1^{(e)}}^{x_2^{(e)}} \begin{Bmatrix} N_1^{(e)} \\ N_2^{(e)} \end{Bmatrix} b^{(e)} dx = \left(\frac{bl}{2} \right)^{(e)} \begin{Bmatrix} 1 \\ 1 \end{Bmatrix} \quad (3.46)$$

Substituting $\left(\frac{EA}{l} \right)^{(1)} = \left(\frac{EA}{l} \right)^{(2)} = \frac{2EA}{l}$ into Eq.(3.44a) and solving the equation system we find that

$$\begin{aligned} u_1 &= 0 \quad ; \quad u_2 = \frac{l}{2EA} \left(P + \frac{3bl}{4} \right) \\ u_3 &= \frac{l}{2EA} (2P + bl) \quad ; \quad R_1 = -(P + bl) \end{aligned} \quad (3.47)$$

The axial strain and the axial force are constant within each element and are obtained as

$$\begin{array}{c} \mathbf{Element\ 1} \\ \varepsilon^{(1)} = \left(\frac{du}{dx} \right)^{(1)} = \frac{u_2}{l^{(1)}} = \frac{P + \frac{3bl}{4}}{EA} \\ N^{(1)} = (EA)^{(1)} \varepsilon^{(1)} = P + \frac{3bl}{4} \end{array} \left| \begin{array}{c} \mathbf{Element\ 2} \\ \varepsilon^{(2)} = \left(\frac{du}{dx} \right)^{(2)} = \frac{u_3 - u_2}{l^{(2)}} = \frac{1}{EA} \left(\frac{bl}{4} + P \right) \\ N^{(2)} = (EA)^{(2)} \varepsilon^{(2)} = \frac{bl}{4} + P \end{array} \right. \quad (3.48)$$

The distribution within each element of the displacement u and the constant axial force N is shown in Figure 3.3. Note that for the same reasons explained in Section 3.3 the nodal displacements coincide with the exact values. Some improvement in the approximation of the global displacement field is also observed. However, the error in the axial force is still considerable and its reduction requires a finer discretization and the nodal smoothing of the constant axial forces over each element. This can be done by simply averaging the nodal forces.

The results obtained for the axial forces (and strains) are more inaccurate than those for the displacement field. This is a general rule which is explained by the fact that the strains and the stresses are computed from the derivatives of

the approximate displacement field. This, naturally, increases the solution error for those values.

The same problem is now solved using the global description of the shape functions.

The axial displacement can be expressed globally over the two elements mesh as (see Figure 3.4)

$$u(x) = N_1^g(x)u_1 + N_2^g(x)u_2 + N_3^g(x)u_3 \quad (3.49)$$

and the axial strain is given by

$$\varepsilon = \frac{du}{dx} = \frac{dN_1^g}{dx}u_1 + \frac{dN_2^g}{dx}u_2 + \frac{dN_3^g}{dx}u_3 \quad (3.50)$$

The discretized form of the PVW is written using above equations as

$$\begin{aligned} & \int_0^l \left(\frac{dN_1^g}{dx} \delta u_1 + \frac{dN_2^g}{dx} \delta u_2 + \frac{dN_3^g}{dx} \delta u_3 \right) (EA) \\ & \left(\frac{dN_1^g}{dx} u_1 + \frac{dN_2^g}{dx} u_2 + \frac{dN_3^g}{dx} u_3 \right) dx - \\ & - \int_0^l \left(N_1^g \delta u_1 + N_2^g \delta u_2 + N_3^g \delta u_3 \right) b dx = \delta u_1 R_1 + \delta u_3 P \end{aligned} \quad (3.51)$$

This leads, after eliminating the virtual displacements, to the following matrix system of equations

$$\begin{aligned} & \left(\int_0^l \begin{bmatrix} \frac{dN_1^g}{dx} \frac{dN_1^g}{dx} & \frac{dN_1^g}{dx} \frac{dN_2^g}{dx} & \frac{dN_1^g}{dx} \frac{dN_3^g}{dx} \\ \frac{dN_2^g}{dx} \frac{dN_1^g}{dx} & \frac{dN_2^g}{dx} \frac{dN_2^g}{dx} & \frac{dN_2^g}{dx} \frac{dN_3^g}{dx} \\ \frac{dN_3^g}{dx} \frac{dN_1^g}{dx} & \frac{dN_3^g}{dx} \frac{dN_2^g}{dx} & \frac{dN_3^g}{dx} \frac{dN_3^g}{dx} \end{bmatrix} (EA) dx \right) \begin{Bmatrix} u_1 \\ u_2 \\ u_3 \end{Bmatrix} - \\ & - \int_0^l \begin{Bmatrix} N_1^g \\ N_2^g \\ N_3^g \end{Bmatrix} b dx = \begin{Bmatrix} R_1 \\ 0 \\ P \end{Bmatrix} \end{aligned} \quad (3.52)$$

The computation of the integrals in Eq.(3.52) requires a correspondence between the global and local shape functions. The following relationships are de-

duced from Table 3.2 and Figure 3.4

$$\left. \begin{array}{l} N_1^g = N_1^{(1)} \\ \frac{dN_1^g}{dx} = \frac{dN_1^{(1)}}{dx} \\ N_2^g = N_2^{(1)} \\ \frac{dN_2^g}{dx} = \frac{dN_2^{(1)}}{dx} \\ N_3^g = 0 \\ \frac{d\bar{N}_3}{dx} = 0 \end{array} \right\} 0 \leq x \leq \frac{l}{2} ; \left. \begin{array}{l} N_1^g = 0 \\ \frac{dN_1^g}{dx} = 0 \\ N_2^g = N_1^{(2)} \\ \frac{dN_2^g}{dx} = \frac{dN_1^{(2)}}{dx} \\ N_3^g = N_2^{(2)} \\ \frac{dN_3^g}{dx} = \frac{dN_2^{(2)}}{dx} \end{array} \right\} \frac{l}{2} \leq x \leq l \quad (3.53)$$

Making use of the expressions (3.53) in (3.52) the *global* equilibrium equation is directly obtained. The reader can easily verify the coincidence of this equation with Eq.(3.44a) obtained by assembly of the element contributions.

This example clearly shows that the use of the global shape functions is less systematic and requires more detailed computations than the element by element approach. These differences are even more apparent for finer meshes. As a consequence, the assembly of the global equations from the elemental expressions derived via the local shape functions is recommended in practice.

3.6 GENERALIZATION OF THE SOLUTION WITH N LINEAR ROD ELEMENTS

The solution process explained in the previous sections can be easily generalized for a discretization using a mesh of n 2-noded (linear) rod elements. The stiffness matrix and the equivalent nodal force vector for each element are given by

$$\mathbf{K}^{(e)} = \int_{x_1^{(e)}}^{x_2^{(e)}} (EA)^{(e)} \begin{bmatrix} \frac{dN_1^{(e)}}{dx} & \frac{dN_1^{(e)}}{dx} & \frac{dN_1^{(e)}}{dx} & \frac{dN_2^{(e)}}{dx} \\ \frac{dN_2^{(e)}}{dx} & \frac{dN_1^{(e)}}{dx} & \frac{dN_2^{(e)}}{dx} & \frac{dN_2^{(e)}}{dx} \end{bmatrix} dx \quad (3.54)$$

$$\mathbf{f}^{(e)} = \int_{x_1^{(e)}}^{x_2^{(e)}} \begin{Bmatrix} N_1^{(e)} \\ N_2^{(e)} \end{Bmatrix} b^{(e)} dx$$

which after substitution of the shape functions and their derivatives

$$\begin{aligned} N_1^{(e)} &= \frac{x_2^{(e)} - x}{l^{(e)}} \quad ; \quad \frac{dN_1^{(e)}}{dx} = -\frac{1}{l^{(e)}} \\ N_2^{(e)} &= \frac{x - x_1^{(e)}}{l^{(e)}} \quad ; \quad \frac{dN_2^{(e)}}{dx} = \frac{1}{l^{(e)}} \end{aligned} \quad (3.55)$$

gives (for homogeneous material and uniformly distributed loading)

$$\mathbf{K}^{(e)} = \left(\frac{EA}{l} \right)^{(e)} \begin{bmatrix} 1 & -1 \\ -1 & 1 \end{bmatrix} \quad ; \quad \mathbf{f}^{(e)} = \frac{(bl)^{(e)}}{2} \begin{Bmatrix} 1 \\ 1 \end{Bmatrix} \quad (3.56)$$

The assembly process leads, after some algebra, to the following global matrix equation

$$\underbrace{\begin{bmatrix} k^{(1)} & -k^{(1)} & 0 & \dots & 0 \\ -k^{(1)} & [k^{(1)} + k^{(2)}] & -k^{(2)} & \dots & 0 \\ 0 & -k^{(2)} & [k^{(2)} + k^{(3)}] & \dots & 0 \\ 0 & 0 & -k^{(3)} & \dots & \vdots \\ \vdots & \vdots & \ddots & \dots & \vdots \\ 0 & 0 & \dots & [k^{(n-1)} + k^{(n)}] & -k^{(n)} \\ 0 & 0 & \dots & -k^{(n)} & k^{(n)} \end{bmatrix}}_{\mathbf{K}} \underbrace{\begin{Bmatrix} u_1 \\ u_2 \\ u_3 \\ \vdots \\ u_{n-1} \\ u_n \end{Bmatrix}}_{\mathbf{a}} =$$

$$= \underbrace{\begin{Bmatrix} \frac{(bl)^{(1)}}{2} + P_1 \\ \frac{(bl)^{(1)}}{2} + \frac{(bl)^{(2)}}{2} + P_2 \\ \frac{(bl)^{(2)}}{2} + \frac{(bl)^{(3)}}{2} + P_3 \\ \vdots \\ \frac{(bl)^{(n-1)}}{2} + \frac{(bl)^{(n)}}{2} + P_{n-1} \\ \frac{(bl)^{(n)}}{2} + P_n \end{Bmatrix}}_{\mathbf{f}} \quad \text{with} \quad k^{(e)} = \left(\frac{EA}{l} \right)^{(e)} \quad (3.57)$$

Note that matrix \mathbf{K} depends on the geometrical (l and A) and material (E) parameters of each element, while vector \mathbf{f} depends on the intensity of the distributed load $b^{(e)}$, the element length and the point loads P_i acting at the nodes. The unknown reactions at the prescribed nodes are treated as point loads and they are computed “a posteriori” following standard procedures of structural matrix analysis (see Section 1.4) [L3], [T9].

Example: 3.1 Analyse the axially loaded rod with exponentially varying cross sectional area of Figure 3.5 using three meshes of one, two and three linear rod elements.

- Solution

The change in cross sectional area is defined by $A = A_o e^{-\frac{x}{l}}$ where A_o is the cross sectional area at the clamped end and l is the rod length. The rod is subjected to an axial force acting at the free end. The exact solution for this simple problem is

$$\sigma = \frac{F}{A} = \frac{F}{A_o} e^{\frac{x}{l}} \quad , \quad \varepsilon = \frac{\sigma}{E} = \frac{F}{EA_o} e^{\frac{x}{l}}$$

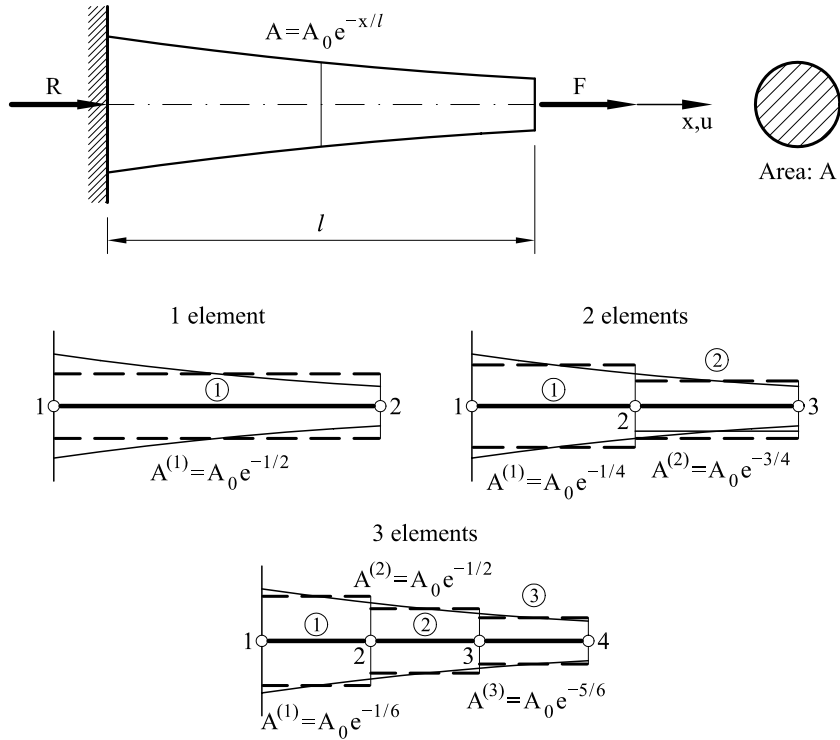


Fig. 3.5: Axially loaded rod with exponentially varying cross section. Discretization in 3 meshes of two-noded rod elements

$$u(x) = \int_0^x \varepsilon dx = \int_0^x \frac{F}{EA_0} e^{x/l} dx = \frac{Fl}{EA_0} (e^{x/l} - 1)$$

$$u(l) = \frac{Fl}{EA_0} (e - 1) = 1.71828 \frac{Fl}{EA_0} \quad ; \quad R_1 = -F$$

Two options are possible for the finite element solution: a) to use the exact expression of the cross sectional area, and b) to assume a constant cross sectional area within each element. The second option has been chosen here for simplicity. The reader is encouraged to repeat this problem as an exercise using the first alternative.

One elements solution

The cross sectional area is assumed to be constant and equal to $A = A_0 e^{-1/2}$. The element stiffness matrix is directly given by Eq.(3.56), i.e.

$$\mathbf{K}^{(1)} = \frac{EA_0}{l} e^{-1/2} \begin{bmatrix} 1 & -1 \\ -1 & 1 \end{bmatrix} = \frac{EA_0}{l} 0.60653 \begin{bmatrix} 1 & -1 \\ -1 & 1 \end{bmatrix}$$

The equilibrium equation is deduced from Eq.(3.57) (noting that the distributed loads $b^{(e)}$ are zero) as

$$\frac{EA_0}{l} 0.60653 \begin{bmatrix} 1 & -1 \\ -1 & 1 \end{bmatrix} \begin{Bmatrix} u_1 \\ u_2 \end{Bmatrix} = \begin{Bmatrix} R_1 \\ F \end{Bmatrix} \quad ; \quad u_1 = 0$$

which when solved gives

$$u_2 = \frac{1}{0.60653} \frac{Fl}{EA_o} = 1.6487 \frac{Fl}{EA_o} \quad ; \quad R_1 = -F$$

The percentage of error with respect to the exact solution is 4.21%. This can be considered acceptable given the simplicity of the mesh.

Two elements solution

Now $A^{(1)} = A_o e^{-1/4}$ and $A^{(2)} = A_o e^{-3/4}$. The equilibrium equations for each element (Figure 3.5) are obtained as explained in Section 3.5.

Element 1

$$1.5576 \left(\frac{EA_o}{l} \right) \begin{bmatrix} 1 & -1 \\ -1 & 1 \end{bmatrix} \begin{Bmatrix} u_1 \\ u_2 \end{Bmatrix} = \begin{Bmatrix} X_1^{(1)} \\ X_2^{(1)} \end{Bmatrix}$$

Element 2

$$0.9447 \left(\frac{EA_o}{l} \right) \begin{bmatrix} 1 & -1 \\ -1 & 1 \end{bmatrix} \begin{Bmatrix} u_2 \\ u_3 \end{Bmatrix} = \begin{Bmatrix} X_1^{(2)} \\ X_2^{(2)} \end{Bmatrix}$$

After global assembly we have

$$\frac{EA_o}{l} \begin{bmatrix} 1.5576 & -1.5576 & 0 \\ -1.5576 & 2.5023 & -0.9447 \\ 0 & -0.9447 & 0.9447 \end{bmatrix} \begin{Bmatrix} u_1 \\ u_2 \\ u_3 \end{Bmatrix} = \begin{Bmatrix} R_1 \\ 0 \\ F \end{Bmatrix} \quad u_1 = 0$$

which gives

$$\begin{aligned} u_3 &= 1.7005 \frac{Fl}{EA_o} \quad (\text{Error} = 1.04\%) \\ u_2 &= 0.377541 u_3 = 0.6419 \frac{Fl}{EA_o} \\ R_1 &= -F \end{aligned}$$

Three elements mesh

For the three elements mesh (Figure 3.5) $A^{(1)} = A_o e^{-1/6}$, $A^{(2)} = A_o e^{-1/2}$ and $A^{(3)} = A_o e^{-5/6}$. The equilibrium equations for each element are

Element 1

$$2.5394 \frac{EA_o}{l} \begin{bmatrix} 1 & -1 \\ -1 & 1 \end{bmatrix} \begin{Bmatrix} u_1 \\ u_2 \end{Bmatrix} = \begin{Bmatrix} X_1^{(1)} \\ X_2^{(1)} \end{Bmatrix}$$

Element 2

$$1.8196 \frac{EA_o}{l} \begin{bmatrix} 1 & -1 \\ -1 & 1 \end{bmatrix} \begin{Bmatrix} u_2 \\ u_3 \end{Bmatrix} = \begin{Bmatrix} X_1^{(2)} \\ X_2^{(2)} \end{Bmatrix}$$

Element 3

$$1.3028 \frac{EA_o}{l} \begin{bmatrix} 1 & -1 \\ -1 & 1 \end{bmatrix} \begin{Bmatrix} u_3 \\ u_4 \end{Bmatrix} = \begin{Bmatrix} X_1^{(3)} \\ X_2^{(3)} \end{Bmatrix}$$

The global equilibrium equation after assembly is

$$\frac{EA_o}{l} \begin{bmatrix} 2.5394 & -2.5394 & 0 & 0 \\ -2.5394 & 4.3590 & -1.8196 & 0 \\ 0 & -1.8196 & 3.1234 & -1.3038 \\ 0 & 0 & -1.3038 & 1.3038 \end{bmatrix} \begin{Bmatrix} u_1 \\ u_2 \\ u_3 \\ u_4 \end{Bmatrix} = \begin{Bmatrix} R_1 \\ 0 \\ 0 \\ F \end{Bmatrix} \quad u_1 = 0$$

and the solution is

$$\begin{aligned} u_4 &= 1.71036 \frac{Fl}{EA_o} \quad (\text{Error} = 0.46\%) \\ u_3 &= 0.55156 \quad u_4 = 0.9432 \frac{Fl}{EA_o} \\ u_2 &= 0.230241 \quad u_4 = 0.3938 \frac{Fl}{EA_o} \\ R_1 &= -F \end{aligned}$$

Once the nodal displacements have been obtained, the axial strain and the axial stress can be computed for each element. For example, at the central point of element number 2 in the three elements mesh we have

$$\begin{aligned} u(l/2) &= N_1^{(2)}\left(x^{(2)} = \frac{l^{(2)}}{2}\right) u_1^{(2)} + N_2^{(2)}\left(x^{(2)} = \frac{l^{(2)}}{2}\right) u_2^{(2)} = \\ &= \frac{1}{2} 0.23024 u_4 + \frac{1}{2} 0.55156 u_4 = 0.3909 u_4 = 0.6686 \frac{Fl}{EA_o} \end{aligned}$$

$$(\text{Exact value} = 0.6487 \frac{Fl}{EA_o}. \text{ Error : } 3.07\%).$$

$$\begin{aligned} \varepsilon(l/2) &= \left(\frac{dN_1^{(2)}}{dx}\right)_{x^{(2)}=\frac{l^{(2)}}{2}} u_1^{(2)} + \left(\frac{dN_2^{(2)}}{dx}\right)_{x^{(2)}=\frac{l^{(2)}}{2}} u_2^{(2)} = 1.6491 \frac{F}{EA_o} \\ &= \left(-\frac{3}{l} 0.2302 + \frac{3}{l} 0.5516\right) u_4 = 0.9642 \frac{u_4}{l} \end{aligned}$$

$$\sigma(l/2) = E\varepsilon_A = 1.649 \frac{F}{A_o} \quad (\text{Exact value: } 1.6487 \frac{F}{A_o}. \text{ Error: } 0.02\%)$$

The convergence of the end displacement value with the number of elements is shown in Figure 3.6. We see that the simple assumption of constant cross sectional area leads to percentage errors of less than 1% for meshes finer than two elements.

The displacement and stress distribution along the rod for the three meshes are plotted in Figure 3.7 together with the exact solution. Note that the nodal displacements and even the linear displacement field within each element are very accurate for the three meshes. However, the convergence of the constant stress field for each element to the exact exponential solution is quite slow.

3.7 EXTRAPOLATION OF THE SOLUTION FROM TWO DIFFERENT MESHES

Expanding in Taylor series the displacement in the vicinity of a node i gives

$$u = u_i + \left(\frac{\partial u}{\partial x}\right)_i (x - x_i) + \left(\frac{\partial^2 u}{\partial x^2}\right)_i (x - x_i)^2 + \dots \quad (3.58)$$

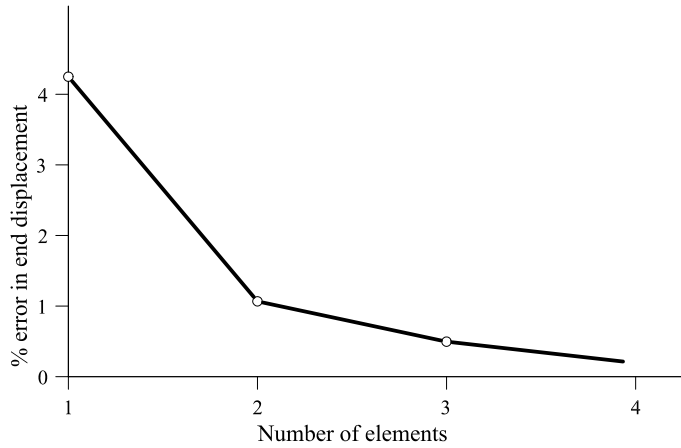


Fig. 3.6: Axially loaded rod with varying cross sectional area. Convergence of the end displacement value and the stress distribution with the number of elements

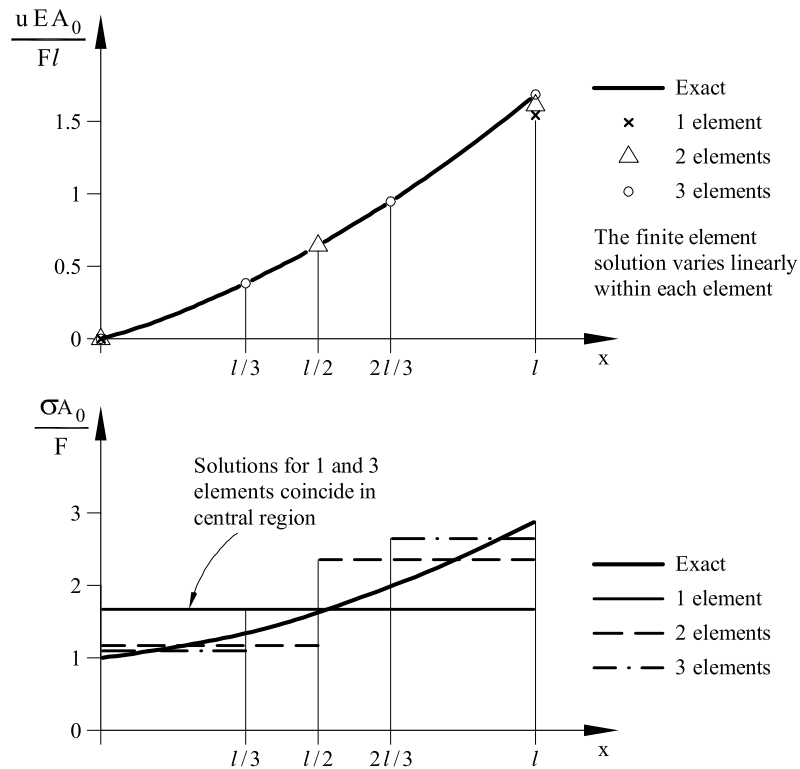


Fig. 3.7: Nodal displacements and stress distribution along the rod for the three meshes

If the shape functions $N_i(x)$ are polynomials of p th degree it is obvious that only the first p terms of the Taylor expansion can be approximated exactly as the derivatives of order $p + 1$, $p + 2$, etc. are zero. The error of this approximation is then of the order of the first term disregarded in the above expansion, i.e.

$$\text{error} = u_{\text{exact}} - u_{\text{approx}} = O(x - x_i)^{p+1} \simeq O(l^{p+1}) \quad (3.59)$$

where $O(l^{p+1})$ is read as “of the order of l^{p+1} ” and l is the element length.

Let us now consider two solutions u^1 and u^2 obtained with two meshes of uniform element sizes l and l/d , respectively. We can write

$$\begin{aligned} u_{\text{exact}} - u^1 &= O(l^{p+1}) \\ u_{\text{exact}} - u^2 &= O\left[\left(\frac{l}{d}\right)^{p+1}\right] \end{aligned} \quad (3.60)$$

The approximate value of u_{exact} is obtained in terms of u^1 and u^2 from Eqs.(3.60) as

$$u_{\text{exact}} \cong \frac{(d^{p+1})u^2 - u^1}{(d^{p+1}) - 1} \quad (3.61)$$

This technique is known as Richardson extrapolation [R2]. For the rod of Figure 3.5 we obtain for the end displacement value:

1. Extrapolated solution from meshes 1 and 2 ($d = 2$)

$$u(l) = \frac{4u^2 - u^1}{3} = 1.7178 \frac{Fl}{EA_o} \quad (\text{Error: } 0.03\%)$$

2. Extrapolated solution using meshes 1 and 3 ($d = 3$)

$$u(l) = \frac{9u^2 - u^1}{8} = 1.71807 \frac{Fl}{EA_o} \quad (\text{Error: } 0.012\%)$$

3. Extrapolated solution using meshes 2 and 3 ($d = 1.5$)

$$u(l) = \frac{(9.5)^2 u^2 - u^1}{(1.5)^2 - 1} = 1.71825 \frac{Fl}{EA_o} \quad (\text{Error: } 0.002\%)$$

We see that Richardson's extrapolation is an effective technique to improve the displacement solution obtained from two meshes using elements of the same type. This simple procedure is also applicable for 2D and 3D problems. Obviously, the enhanced nodal displacement values can be used to obtain an improved solution for the stress field. Unfortunately the improvement is not so relevant as for the nodal displacements.

3.8 MATRIX FORMULATION OF THE ELEMENT EQUATIONS

The methodology explained in the previous sections is very useful for introducing the basic steps of the FEM. However, for problems with more than one displacement variable per node a matrix formulation is much more convenient as it allows all variables and algebraic operations to be grouped together in a compact form. The matrix formulation also provides a systematic finite element methodology for *all* the structural problems treated in this book. The basic concepts of the matrix formulation will be presented next.

Most expressions used henceforth will be referred to an individual element only. Therefore, superindex “e” denoting element values will be omitted hereafter for simplicity, with the exception of a few significative element parameters such as the main geometrical dimensions ($l^{(e)}$, $A^{(e)}$ and $V^{(e)}$), the nodal displacement vector $\mathbf{a}^{(e)}$, the nodal coordinates vector $\mathbf{x}^{(e)}$, the nodal force vectors ($\mathbf{f}^{(e)}$, $\mathbf{q}^{(e)}$), the stiffness matrix $\mathbf{K}^{(e)}$, and other relevant elemental parameters. All other parameters, vectors and matrices appearing in the text should be interpreted, unless otherwise mentioned, as belonging to an individual element.

3.8.1 Shape function matrix

Let us consider a general 2-noded rod element. The displacement field is expressed within the element as

$$u = N_1 u_1 + N_2 u_2 \quad (3.62)$$

Eq.(3.62) is written in matrix form as

$$\mathbf{u} = \{u\} = [N_1, N_2] \begin{Bmatrix} u_1 \\ u_2 \end{Bmatrix} = \mathbf{N} \mathbf{a}^{(e)} \quad (3.63)$$

where

$$\mathbf{N} = [N_1, N_2] \quad ; \quad \mathbf{a}^{(e)} = \begin{Bmatrix} u_1 \\ u_2 \end{Bmatrix} \quad (3.64)$$

are the *shape function matrix* and the *nodal displacement vector* of the element. As mentioned above, the superindex “e” denoting element values has been omitted from most terms in Eqs.(3.62)-(3.64).

3.8.2 Strain matrix

The strain vector is written as

$$\boldsymbol{\varepsilon} = \{\varepsilon\} = \left\{ \frac{dN_1}{dx} u_1 + \frac{dN_2}{dx} u_2 \right\} = \left[\frac{dN_1}{dx}, \frac{dN_2}{dx} \right] \begin{Bmatrix} u_1 \\ u_2 \end{Bmatrix} = \mathbf{B} \mathbf{a}^{(e)} \quad (3.65)$$

where

$$\mathbf{B} = \left[\frac{dN_1}{dx}, \frac{dN_2}{dx} \right] \quad (3.66)$$

is the *strain matrix* of the element.

3.8.3 Constitutive matrix

The *stress vector* is written as

$$\boldsymbol{\sigma} = [N] = (EA) \boldsymbol{\varepsilon} = [EA] \boldsymbol{\varepsilon} = \mathbf{D}\mathbf{B}\mathbf{a}^{(e)} \quad (3.67)$$

where

$$\mathbf{D} = [EA] \quad (3.68)$$

is the matrix of mechanical properties of the material, also called hereafter *constitutive matrix*.

For the axial rod problem vectors $\boldsymbol{\varepsilon}$ and $\boldsymbol{\sigma}$ and matrix \mathbf{D} have a single component only. In general $\boldsymbol{\sigma}$ and $\boldsymbol{\varepsilon}$ will have t components. Thus, if n is the number of nodes of an individual finite element and d the number of d.o.f. of each node, the dimensions of the vectors and matrices in the constitutive equation are

$$\underset{t \times 1}{\boldsymbol{\sigma}} = \underset{t \times t}{\mathbf{D}} \cdot \underset{[t \times (n \times d)]}{\mathbf{B}} \cdot \underset{[(n \times d) \times 1]}{\mathbf{a}^{(e)}} \quad (3.69)$$

3.8.4 Principle of Virtual Work

The PVW for an individual element is written in matrix form as

$$\int_{l^{(e)}} \delta \boldsymbol{\varepsilon}^T \boldsymbol{\sigma} \, dx = \int_{l^{(e)}} \delta \mathbf{u}^T \mathbf{b} \, dx + [\delta \mathbf{a}^{(e)}]^T \mathbf{q}^{(e)} \quad (3.70)$$

Note that the PVW is a *scalar equation*, i.e. both sides of Eq.(3.70) are numbers representing the internal and external virtual work, respectively. This explains the organization of the terms in Eq.(3.70), as a scalar number is obtained as product of a row vector times a column vector, i.e. if s is a scalar number we can write

$$s = a_1 b_1 + \cdots + a_n b_n = [a_1, a_2, \dots, a_n] \begin{Bmatrix} b_1 \\ b_2 \\ \vdots \\ b_n \end{Bmatrix} = \mathbf{a}^T \mathbf{b} \quad (3.71)$$

Naturally, if vectors $\boldsymbol{\varepsilon}$ and $\boldsymbol{\sigma}$ have a single term, as in the axially loaded rod problem, the vector product (3.71) reduces to multiplying two numbers. However, for most of the problems studied in this book, vectors $\boldsymbol{\varepsilon}$ and $\boldsymbol{\sigma}$ have several components and the matrix form of the PVW will be used.

3.8.5 Stiffness matrix and equivalent nodal force vector

From Eqs.(3.63) and (3.65) we have

$$\begin{aligned} [\delta \mathbf{u}]^T &= [\delta \mathbf{a}^{(e)}]^T \mathbf{N}^T \\ [\delta \boldsymbol{\varepsilon}]^T &= [\delta \mathbf{a}^{(e)}]^T \mathbf{B}^T \end{aligned} \quad (3.72)$$

Substituting now Eqs.(3.65), (3.67) and (3.72) into the PVW *written for a single element* gives

$$\int_{l^{(e)}} [\delta \mathbf{a}^{(e)}]^T \mathbf{B}^T \mathbf{D} \mathbf{B} \mathbf{a}^{(e)} dx - \int_{l^{(e)}} [\delta \mathbf{a}^{(e)}]^T \mathbf{N}^T \mathbf{b} dx = \delta \mathbf{a}^{(e)} \mathbf{q}^{(e)} \quad (3.73)$$

where $\mathbf{b} = \{b\}$ is the vector of distributed loads acting on the element. Eliminating the virtual displacements from Eq.(3.73) yields

$$[\delta \mathbf{a}^{(e)}]^T \left[\left(\int_{l^{(e)}} \mathbf{B}^T \mathbf{D} \mathbf{B} dx \right) \mathbf{a}^{(e)} - \int_{l^{(e)}} \mathbf{N}^T \mathbf{b} dx - \mathbf{q}^{(e)} \right] = \mathbf{0} \quad (3.74)$$

As the virtual displacements are arbitrary, satisfaction of Eq.(3.74) implies

$$\left(\int_{l^{(e)}} \mathbf{B}^T \mathbf{D} \mathbf{B} dx \right) \mathbf{a}^{(e)} - \int_{l^{(e)}} \mathbf{N}^T \mathbf{b} dx = \mathbf{q}^{(e)} \quad (3.75)$$

Eq.(3.75) is a system of algebraic equations which can be written in the standard form

$$\mathbf{K}^{(e)} \mathbf{a}^{(e)} - \mathbf{f}^{(e)} = \mathbf{q}^{(e)} \quad (3.76a)$$

where

$$\boxed{\begin{aligned} \mathbf{K}^{(e)} &= \int_{l^{(e)}} \mathbf{B}^T \mathbf{D} \mathbf{B} dx \\ \mathbf{f}^{(e)} &= \int_{l^{(e)}} \mathbf{N}^T \mathbf{b} dx \end{aligned}} \quad (3.76b)$$

are respectively the stiffness matrix and the equivalent nodal force due to distributed loading for the element. Vector $\mathbf{q}^{(e)}$ in Eq.(3.76a) is the equilibrating nodal force vector for the element which is essential for the global assembly process.

Note that the derivation of $\mathbf{K}^{(e)}$ and $\mathbf{f}^{(e)}$ is *completely general*. Expressions (3.76) will frequently appear throughout the text and will be particularized for each element type studied.

The explicit form of $\mathbf{K}^{(e)}$ and $\mathbf{f}^{(e)}$ for the 2-noded axially loaded rod element is found by substituting into Eqs.(3.76b) the adequate expressions for \mathbf{B} , \mathbf{D} , \mathbf{N} and \mathbf{b} . In this case we have

$$\begin{aligned} \mathbf{N} &= [\mathbf{N}_1, \mathbf{N}_2] = [N_1, N_2] = \left[\frac{x_2 - x}{l^{(e)}}, \frac{x - x_1}{l^{(e)}} \right] \\ \mathbf{B} &= [\mathbf{B}_1, \mathbf{B}_2] = \left[\frac{dN_1}{dx}, \frac{dN_2}{dx} \right] = \left[-\frac{1}{l^{(e)}}, \frac{1}{l^{(e)}} \right] \end{aligned} \quad (3.77)$$

$$\mathbf{D} = [EA] \quad \text{and} \quad \mathbf{b} = \{b\}$$

Substituting Eqs.(3.77) into (3.76b) gives

$$\begin{aligned}\mathbf{K}^{(e)} &= \int_{l^{(e)}} \left\{ \begin{array}{c} -\frac{1}{l^{(e)}} \\ \frac{1}{l^{(e)}} \end{array} \right\} (EA) \left[-\frac{1}{l^{(e)}}, \frac{1}{l^{(e)}} \right] dx = \left(\frac{EA}{l} \right)^{(e)} \begin{bmatrix} 1 & -1 \\ -1 & 1 \end{bmatrix} \\ \mathbf{f}^{(e)} &= \int_{l^{(e)}} \left\{ \begin{array}{c} x_2 - x \\ x - x_1 \end{array} \right\} \left(\frac{b}{l} \right)^{(e)} dx = \frac{(bl)^{(e)}}{2} \begin{bmatrix} 1 \\ 1 \end{bmatrix}\end{aligned}\quad (3.78)$$

Note the coincidence of these expressions with those obtained in Eq.(3.56) by a more elaborate procedure.

We remark finally that the element stiffness matrix and the equivalent nodal force vector can be obtained from the corresponding sub-matrices and subvectors.

Thus, from Eqs.(3.77) and (3.76b) we have

$$\begin{aligned}\mathbf{K}^{(e)} &= \int_{l^{(e)}} \left\{ \begin{array}{c} \mathbf{B}_1^T \\ \mathbf{B}_2^T \end{array} \right\} \mathbf{D} [\mathbf{B}_1, \mathbf{B}_2] dx = \int_{l^{(e)}} \begin{bmatrix} \mathbf{B}_1^T \mathbf{D} \mathbf{B}_1 & \vdots & \mathbf{B}_1^T \mathbf{D} \mathbf{B}_2 \\ \dots\dots\dots & \dots & \dots\dots\dots \\ \mathbf{B}_2^T \mathbf{D} \mathbf{B}_1 & \vdots & \mathbf{B}_2^T \mathbf{D} \mathbf{B}_2 \end{bmatrix} dx \\ \mathbf{f}^{(e)} &= \int_{l^{(e)}} \left\{ \begin{array}{c} \mathbf{N}_1^T \\ \mathbf{N}_2^T \end{array} \right\} \mathbf{b} dx = \int_{l^{(e)}} \left\{ \begin{array}{c} \mathbf{N}_1^T \mathbf{b} \\ \mathbf{N}_2^T \mathbf{b} \end{array} \right\} dx\end{aligned}\quad (3.79)$$

Matrix $\mathbf{K}_{ij}^{(e)}$ relating nodes i and j of element e is

$$\mathbf{K}_{ij}^{(e)} = \int_{l^{(e)}} \mathbf{B}_i^T \mathbf{D} \mathbf{B}_j dx \quad ; \quad i, j = 1, 2 \quad (3.80)$$

$d \times d$ $(d \times t)$ $(t \times t)$ $(t \times d)$

and the equivalent nodal force vector of node i of element e is

$$\mathbf{f}_i^{(e)} = \int_{l^{(e)}} \mathbf{b} dx \quad i = 1, 2 \quad (3.81)$$

$(d \times 1)$ $(d \times d)$

Recall that d is the number of d.o.f. of each node (i.e. $d = 1$ for the axially loaded rod). For the particular case of the 2-noded rod element we have

$$\begin{aligned}K_{ij}^{(e)} &= \int_{l^{(e)}} \frac{dN_i}{dx} EA \frac{dN_j}{dx} dx = (-1)^{i+j} \left(\frac{EA}{l} \right)^{(e)} \\ f_i^{(e)} &= \int_{l^{(e)}} N_i b dx = \frac{(bl)^{(e)}}{2}\end{aligned}\quad (3.82)$$

from which the expressions of $\mathbf{K}^{(e)}$ and $\mathbf{f}^{(e)}$ of Eq.(3.78) can be obtained.

The computation of the element stiffness matrix $\mathbf{K}^{(e)}$ and the equivalent nodal force vector $\mathbf{f}^{(e)}$ from the nodal contributions $\mathbf{K}_{ij}^{(e)}$ and $\mathbf{f}_i^{(e)}$ is a simple and economical procedure and it also facilitates the organization of a computer program. We will be able to verify this on many occasions throughout the text.

3.9 SUMMARY OF THE STEPS FOR THE ANALYSIS OF A STRUCTURE USING THE FEM

Let us summarize the main steps to be followed in the finite element analysis of a structure.

Step 1. Discretize the structure into a mesh of finite elements.

Step 2. Compute for each element the stiffness matrix and the equivalent nodal force vector using expressions of the type

$$\begin{aligned} \mathbf{K}^{(e)} &= \int_{l^{(e)}} \mathbf{B}^T \mathbf{D} \mathbf{B} \, dx \quad ; \quad \mathbf{K}_{ij}^{(e)} = \int_{l^{(e)}} \mathbf{B}_i^T \mathbf{D} \mathbf{B}_j \, dx \\ \mathbf{f}^{(e)} &= \int_{l^{(e)}} \mathbf{N}^T \mathbf{b} \, dx \quad ; \quad \mathbf{f}_i^{(e)} = \int_{l^{(e)}} \mathbf{N}_i^T \mathbf{b} \, dx \end{aligned} \quad (3.83)$$

For two and three dimensional structures the element integrals are computed over the element area or volume.

Step 3. Assemble the stiffness matrix and the equivalent nodal force vector for each element into the global system

$$\mathbf{K} \mathbf{a} = \mathbf{f} \quad (3.84a)$$

$$\mathbf{K} = \mathbf{A}_e \mathbf{K}^{(e)} \quad ; \quad \mathbf{f} = \mathbf{A}_e \mathbf{f}^{(e)} \quad (3.84b)$$

where \mathbf{A}_e denotes the global assembly process of all the individual matrices and vectors for each element in the mesh.

Step 4. The nodal displacement values are computed by solving the equation system (3.84a) where the prescribed displacement must be adequately imposed, i.e.

$$\mathbf{a} = \mathbf{K}^{-1} \mathbf{f} \quad (3.85)$$

Also, the nodal reactions are obtained at the prescribed nodes.

Step 5. The strains and stresses are computed within each element from the nodal displacement values as

$$\boldsymbol{\varepsilon} = \mathbf{B} \mathbf{a} \quad ; \quad \boldsymbol{\sigma} = \mathbf{D} \mathbf{B} \mathbf{a} \quad (3.86)$$

Details of each of above steps and of the precise form of the element vectors and matrices will be given in the next chapters for each of the problems studied.

3.10 ADVANCED ROD ELEMENTS AND REQUIREMENTS FOR THE NUMERICAL SOLUTION

3.10.1 INTRODUCTION

The analysis of the simple axially loaded rod problem using 2-noded rod elements studied in the previous chapter is of big interest as it summarises the basic steps for the analysis of a structure by the FEM. However, a number of important questions still remain unanswered, such as: Can higher order rod elements be effectively used? What are their advantages versus the simpler 2-noded rod element? Can it be guaranteed that the numerical solution converges to the exact one as the mesh is refined? What are the conditions influencing the error in the numerical solution? The reader who faces the application of the FEM for the first time will certainly come across these and similar questions. In the following sections we will see that there are not definitive answers for many of the questions, and in some cases only some practical hints are possible. For simplicity we will mostly refer to the axially loaded rod problem as it allows a simple explanation of topics which are of general applicability to more complex problems.

3.11 ONE DIMENSIONAL C^0 ELEMENTS. LAGRANGE ELEMENTS

In the previous sections we introduced the basic concepts of the FEM using simple 2-noded one-dimensional elements with linear shape functions. Obviously, the polynomial interpolation guarantees that the axial displacement is continuous within the element and between adjacent elements. Elements satisfying this condition are termed “ C^0 continuous”. Additionally, we could require continuity of the first derivative of the displacement and the approximation is then called “ C^1 continuous”. In general, an element is “ C^m continuous” if the displacement field has continuous the $n - 1$ first derivatives. In Section 3.17.3 we will come back to this subject. In this section we will derive the shape functions for C^0 continuous 1D elements. These ideas will be very useful for deriving the shape functions of 2D elements.

The approximation of a displacement unknown in 1D elements can be written as

$$u(x) = \alpha_o + \alpha_1 x + \alpha_2 x^2 + \dots \quad (3.87)$$

where α_o , α_1 , etc., are constant parameters.

Let us choose a first degree polynomial

$$u(x) = \alpha_o + \alpha_1 x \quad (3.88)$$

The parameters α_o and α_1 can be obtained from the value of $u(x)$ at two element points. This requires the element associated with the interpolation (3.2) to have

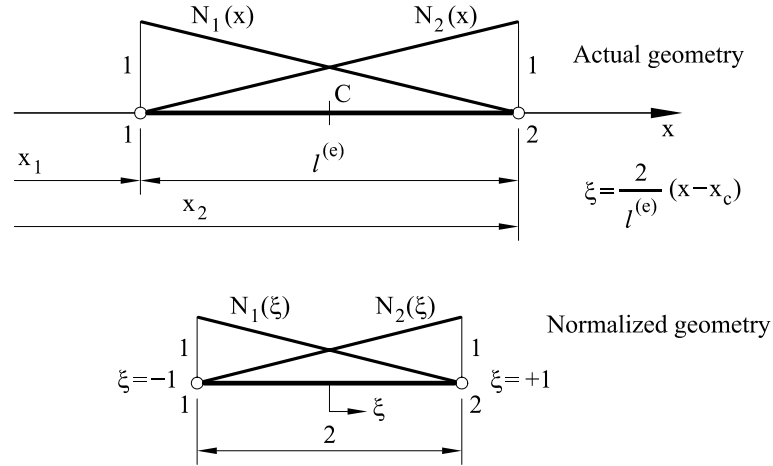


Fig. 3.8: Definition of the natural coordinate system ξ . Actual and normalized geometries for a 2-noded element

two nodes. For a 2-noded element of length $\ell^{(e)}$ with node 1 at $x = x_1$ and node 2 at $x = x_2$ (Figure 3.8), we have

$$\begin{aligned} u(x_1) &= u_1 = \alpha_o + \alpha_1 x_1 \\ u(x_2) &= u_2 = \alpha_o + \alpha_1 x_2 \end{aligned} \quad (3.89)$$

where u_1 and u_2 are the values of the axial displacement at the two nodes. Substituting the values of α_o and α_1 obtained from Eq.(3.89) into Eq.(3.88) gives

$$u(x) = N_1(x)u_1 + N_2(x)u_2 \quad (3.90a)$$

where

$$N_1(x) = \frac{(x_2 - x)}{\ell^{(e)}} \quad ; \quad N_2(x) = \frac{(x - x_1)}{\ell^{(e)}} \quad (3.90b)$$

are the element shape functions. Note the coincidence with the expressions obtained in Section 3.3 (see Eq.(3.12)).

The shape functions for C^o continuous 1D elements can be simply derived from the expressions of Lagrange polynomials. A $n - 1$ th degree Lagrange polynomial $\ell_i^n(x)$ is defined in terms of n points with coordinates x_1, x_2, \dots, x_n as follows

$$\ell_i^n(x) = (x - x_1)(x - x_2) \cdots (x - x_{i-1})(x - x_{i+1}) \cdots (x - x_n) \quad (3.91)$$

Note that $\ell_i^n(x_i) = y_i (\neq 0)$ and $\ell_i^n(x_j) = 0$ for $j = 1, 2, \dots, n (j \neq i)$. Therefore if the points coincide with the element nodes and the non-zero value y_i is normalized to the unity, the resulting Lagrange polynomial coincides with the shape function $N_i(x)$ of the corresponding 1D element. This explains why C^o continuous 1D elements are also called ‘‘Lagrange’’ elements.

The shape function N_i or a Lagrange element with n nodes can be obtained directly by the following expression

$$N_i(x) = \frac{\ell_i^n(x)}{\ell_i^n(x_i)} \quad (3.92a)$$

which can also be written as

$$N_i(x) = \prod_{j=1(j \neq i)}^n \left(\frac{x - x_j}{x_i - x_j} \right) \quad (3.92b)$$

For a two-noded element we find again that

$$\begin{aligned} N_1 &= \frac{x - x_2}{x_1 - x_2} = \frac{x_2 - x}{l^{(e)}} \\ N_2 &= \frac{x - x_1}{x_2 - x_1} = \frac{x - x_1}{l^{(e)}} \end{aligned} \quad (3.93)$$

A *natural coordinate* ξ is introduced for convenience as (Figure 3.8)

$$\xi = 2 \frac{x - x_c}{l^{(e)}} \quad (3.94)$$

where x_c is the cartesian coordinate of the element midpoint. Eq. (3.8) gives

$\xi = -1$ at the left-hand end of the element

$\xi = 0$ at the element mid point

$\xi = 1$ at the right-hand end of the element

Eq. (3.94) transforms the actual element geometry into a *normalized geometry* of length equal to 2. The shape functions can now be written in terms of the natural coordinate ξ . By analogy with Eq.(3.92b) we write

$$N_i(\xi) = \prod_{j=1(j \neq i)}^n \left(\frac{\xi - \xi_j}{\xi_i - \xi_j} \right) \quad (3.95)$$

For a linear Lagrange element with two nodes at $\xi = -1$ and $\xi = +1$ we obtain

$$\begin{aligned} N_1 &= \frac{\xi - \xi_2}{\xi_1 - \xi_2} = \frac{1}{2} (1 - \xi) \\ N_2 &= \frac{\xi - \xi_1}{\xi_2 - \xi_1} = \frac{1}{2} (1 + \xi) \end{aligned} \quad (3.96)$$

For a quadratic Lagrange element with three nodes at $\xi_1 = -1$, $\xi = 0$ and $\xi = +1$ (Figure 3.9) the shape functions are

$$\begin{aligned} N_1 &= \frac{(\xi - \xi_2)(\xi - \xi_3)}{(\xi_1 - \xi_2)} = \frac{1}{2} \xi(\xi - 1) \\ N_2 &= \frac{(\xi - \xi_1)(\xi - \xi_3)}{(\xi_2 - \xi_1)(\xi_2 - \xi_3)} = (1 - \xi^2) \\ N_3 &= \frac{(\xi - \xi_1)(\xi - \xi_2)}{(\xi_3 - \xi_1)(\xi_3 - \xi_2)} = \frac{1}{2} \xi(1 + \xi) \end{aligned} \quad (3.97)$$

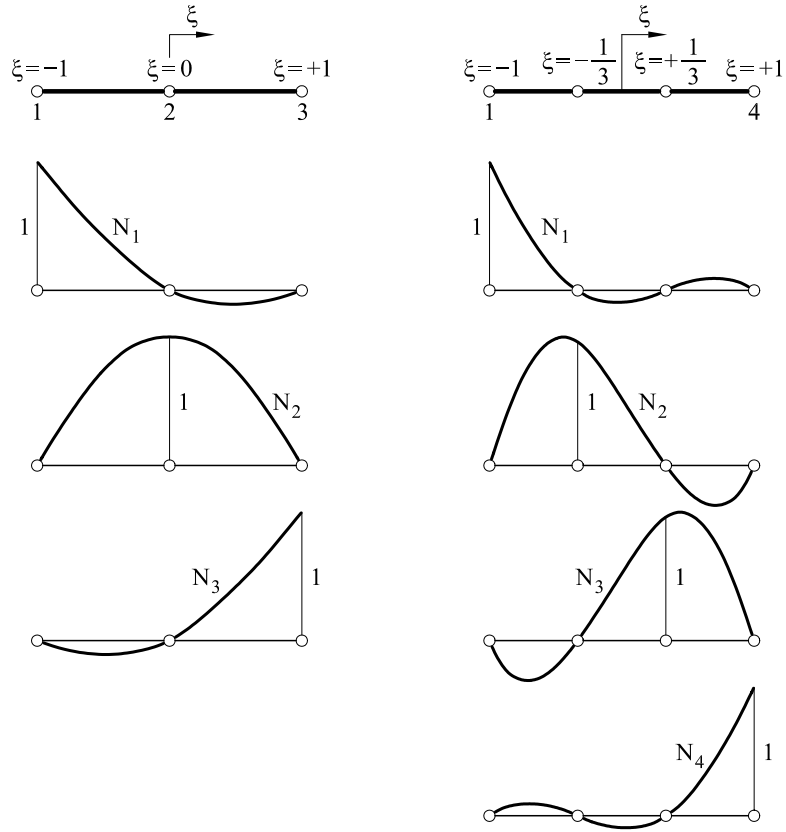


Fig. 3.9: Quadratic and cubic 1D elements with C^0 continuity

Finally, for a cubic element with four nodes at $\xi_1 = -1$, $\xi_2 = -1/3$, $\xi_3 = 1/3$ and $\xi_4 = +1$ (Figure 3.9) the shape functions are

$$\begin{aligned}
 N_1 &= \frac{(\xi - \xi_2)(\xi - \xi_3)(\xi - \xi_4)}{(\xi_1 - \xi_2)(\xi_1 - \xi_3)(\xi_1 - \xi_4)} = -\frac{9}{16} \left(\xi^2 - \frac{1}{9} \right) (\xi - 1) \\
 N_2 &= \frac{(\xi - \xi_1)(\xi - \xi_3)(\xi - \xi_4)}{(\xi_2 - \xi_1)(\xi_2 - \xi_3)(\xi_2 - \xi_4)} = \frac{27}{16} \left(\xi - \frac{1}{3} \right) (\xi^2 - 1) \\
 N_3 &= \frac{(\xi - \xi_1)(\xi - \xi_2)(\xi - \xi_4)}{(\xi_3 - \xi_1)(\xi_3 - \xi_2)(\xi_3 - \xi_4)} = -\frac{27}{16} \left(\xi + \frac{1}{3} \right) (\xi^2 - 1) \\
 N_4 &= \frac{(\xi - \xi_1)(\xi - \xi_2)(\xi - \xi_3)}{(\xi_4 - \xi_1)(\xi_4 - \xi_2)(\xi_4 - \xi_3)} = \frac{9}{16} (\xi + 1) \left(\xi^2 - \frac{1}{9} \right)
 \end{aligned} \tag{3.98}$$

The cartesian expressions of the above shape functions can be obtained from the transformation (3.94). However, only the normalized forms are necessary in practice.

The reader is encouraged to derive by himself the expressions of the shape functions of higher order 1D Lagrange elements.

The shape functions of C^1 continuous 1D elements will be derived in Chapter 7.

3.12 ISOPARAMETRIC FORMULATION AND NUMERICAL INTEGRATION

3.12.1 Introduction

We will now introduce two key concepts which have been essential for the development of the FEM. The first one is that of *isoparametric interpolation*. The basic idea is to interpolate the element geometry from the coordinates of the nodes. Such an interpolation is essential to obtain a general relationship between the natural and cartesian coordinates.

The second concept is that of *numerical integration*. In most cases the exact analytical computation of the element integrals is not possible and numerical integration is the only option to evaluate them in a simple and precise way.

The application of these two techniques to C^0 continuous 1D elements is presented in the next sections. However, the advantages of these procedures will become clearer when dealing with 2D and 3D elements.

3.12.2 The concept of parametric interpolation

Let us recall the displacement interpolation for a 2-noded axial rod element:

$$u(\xi) = N_1(\xi)u_1 + N_2(\xi)u_2 \quad (3.99)$$

Note that in Eq.(3.99) we have used the expression of the shape functions in terms of the natural coordinate ξ . With a few exceptions this will be the usual procedure throughout the text.

The axial strain is obtained from Eq.(3.99) as

$$\varepsilon = \frac{du}{dx} = \frac{dN_1(\xi)}{dx} u_1 + \frac{dN_2(\xi)}{dx} u_2 \quad (3.100)$$

The cartesian derivatives of the shape functions are therefore needed to compute the strain. This would be an easy task if the shape functions were expressed in terms of the cartesian coordinate x . However, as this will not generally be the case, some transformations are necessary. For the 1D problem we have

$$\begin{aligned} \frac{dN_1(\xi)}{dx} &= \frac{dN_1(\xi)}{d\xi} \frac{d\xi}{dx} = \frac{d}{d\xi} \left(\frac{1-\xi}{2} \right) \frac{d\xi}{dx} = -\frac{1}{2} \frac{d\xi}{dx} \\ \frac{dN_2(\xi)}{dx} &= \frac{dN_2(\xi)}{d\xi} \frac{d\xi}{dx} = \frac{d}{d\xi} \left(\frac{1+\xi}{2} \right) \frac{d\xi}{dx} = \frac{1}{2} \frac{d\xi}{dx} \end{aligned} \quad (3.101)$$

and the strain is obtained by

$$\varepsilon = -\frac{1}{2} \left(\frac{d\xi}{dx} \right) u_1 + \frac{1}{2} \left(\frac{d\xi}{dx} \right) u_2 \quad (3.102)$$

Eq.(3.102) involves the evaluation of $\frac{d\xi}{dx}$. This obviously requires an explicit relationship between ξ and x which can be obtained using a parametric interpolation of the element geometry. This expresses the coordinate of any point within the element in terms of the coordinates of m element points x_1, x_2, \dots, x_m by the following interpolation

$$x = \hat{N}_1(\xi)x_1 + \hat{N}_2(\xi)x_2 + \dots + \hat{N}_m(\xi)x_m \quad (3.103)$$

In Eq.(3.103) $\hat{N}_i(\xi)$ are *geometry interpolation functions* which satisfy the same requirements as the displacement shape functions; i.e. $\hat{N}_i(\xi)$ takes the value one at point i and zero at the other $m - 1$ points for which the coordinates are known. Hence, the expression of $\hat{N}_i(\xi)$ can be obtained simply by changing n for m in Eq.(3.95), where ξ_i are now the natural coordinates of the geometry interpolating points.

It is important to note that Eq. (3.103) yields precisely the relationship we are looking for between the coordinates ξ and x . This expression can also be interpreted as transformation between coordinates ξ and x , such that every point in the normalized space $[-1,1]$ is mapped onto another point in the cartesian space $[x_1, x_2]$. It is essential that this mapping be unique and this generally depends on the element geometry.

Example: 3.2 Parametric interpolation of a cubic polinomial.

- *Solution*

Let us consider the polynomial $y = x^3 - 2x^2 - x + 4$ plotted in Figure 3.10. Such a function can represent, for instance, the geometry of a curved beam or the boundary of a curved 2D element. We will assume that the coordinates of the three points at $x_1 = 0$, $x_2 = 1$, and $x_3 = 2$ are known.

The coordinates of the three points will be used to build up a quadratic approximation using a 3-noded 1D element. The relationship between the cartesian (x, y) coordinates and the natural coordinate ξ is obtained as a particular case of Eq.(3.103), i.e.

$$x = \sum_{i=1}^3 N_i(\xi)x_i = \frac{1}{2}\xi(\xi - 1)x_1 + (1 - \xi^2)x_2 + \frac{1}{2}\xi(\xi + 1)x_3 = 1 - \xi$$

$$y = \sum_{i=1}^3 N_i(\xi)y_i = \frac{1}{2}\xi(\xi - 1)y_1 + (1 - \xi^2)y_2 + \frac{1}{2}\xi(1 + \xi)y_3 = \xi^2 - \xi + 2$$

Figure 3.10 shows the approximating quadratic function. Note the error with respect to the “exact” cubic function. Also note that this error is much larger outside the interval $[0,2]$ which includes the three points selected.

The accuracy can be dramatically improved by using a cubic approximation in terms of the coordinates of four known points at $x_1 = 0$, $x_2 = 2/3$, $x_3 = 4/3$, and $x_4 = 2.0$, with $y(x_1) = 4.0$, $y(x_2) = 74/27$, $y(x_3) = 40/27$, and $y(x_4) = 2.0$, respectively. A cubic 1D element is now used giving

$$x = \sum_{i=1}^4 N_i(\xi)x_i \quad ; \quad y = \sum_{i=1}^4 N_i(\xi)y_i$$

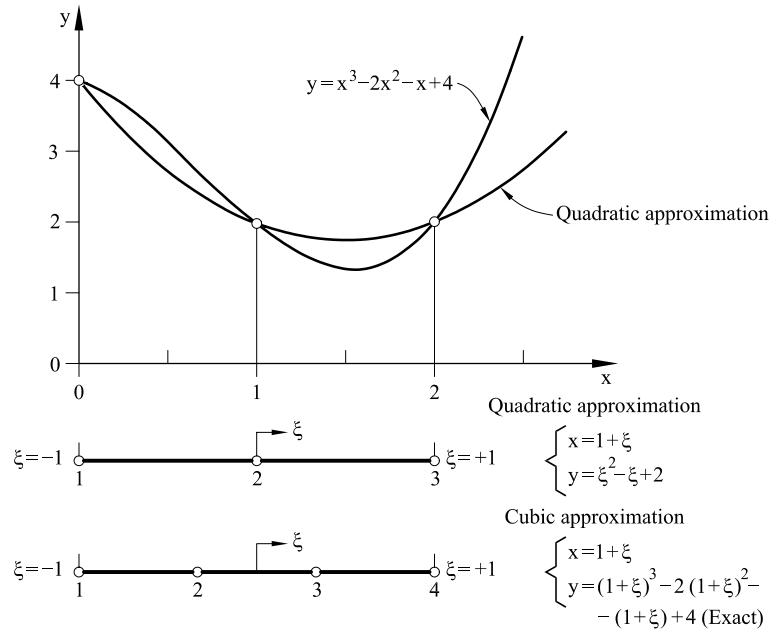


Fig. 3.10: Parametric interpolation of a cubic polynomial

where N_i are the cubic shape function of Eq.(3.97). After some algebra, the following is obtained (easily)

$$x = 1 + \xi \quad ; \quad y = (1 + \xi)^3 - 2(1 + \xi)^2 - (1 + \xi) + 4$$

As expected, the cubic field chosen exactly approximates the original cubic function.

Example 3.2 shows that important errors in the geometry approximation can occur unless a correct interpolation of the geometry is chosen. These errors are undesirable and should be avoided or, at least, minimized.

Two types of points must therefore be considered in an element: a) the points used for interpolating the displacement field (nodes) by the shape functions $N_i(\xi)$; and b) the points chosen to approximate the element geometry via the geometry interpolation function $\hat{N}_i(\xi)$. These two sets of points can coincide depending on the problem. Complex structures might require a higher order interpolation of the geometry, whereas a simple geometry can be exactly approximated using a linear field for \hat{N}_i , independently of the interpolation used for the displacement field.

If the number of geometry points m is greater than that of element nodes, the geometry interpolation functions \hat{N}_i will be polynomials of a higher order than the displacement shape functions, and the element is termed *superparametric*. If n coincides with the number of nodes, then $N_i \equiv \hat{N}_i$ and the element is *isoparametric*. Finally, if the number of geometry points is less than that of nodes, the element is called *subparametric*.

In practice it is usual to choose an isoparametric formulation. However, it is important to have a clear picture of the two other options which are useful in some cases.

The isoparametric concept originates from the work of Taig [T1,2] who derived the first 4-noded isoparametric quadrilateral. Irons [I3,4] extended these ideas to formulate high order isoparametric elements. In the following chapters we will extend this concept for 2D and 3D elements.

3.12.3 Isoparametric formulation of the two-noded rod element

The geometry of the linear rod element is expressed in terms of the coordinates of the two nodes as

$$x(\xi) = N_1(\xi)x_1 + N_2(\xi)x_2 \quad (3.104)$$

where N_1 and N_2 are the same linear shape functions used for interpolating the displacement field (see Eq.(3.96)).

From Eq.(3.104) we obtain

$$\frac{dx}{d\xi} = \frac{dN_1}{d\xi}x_1 + \frac{dN_2}{d\xi}x_2 = -\frac{1}{2}x_1 + \frac{1}{2}x_2 = \frac{l^{(e)}}{2} \quad (3.105)$$

and

$$dx = \frac{l^{(e)}}{2} d\xi \quad \text{y} \quad \frac{d\xi}{dx} = \frac{2}{l^{(e)}} \quad (3.106)$$

Substituting Eq.(3.106) into (3.101) gives

$$\begin{aligned} \frac{dN_1}{dx} &= \frac{2}{l^{(e)}} \frac{dN_1}{d\xi} = -\frac{1}{l^{(e)}} \\ \frac{dN_2}{dx} &= \frac{2}{l^{(e)}} \frac{dN_2}{d\xi} = \frac{1}{l^{(e)}} \end{aligned} \quad (3.107)$$

and from Eqs.(3.107) and (3.100)

$$\varepsilon = \left[-1/l^{(e)}, 1/l^{(e)} \right] \mathbf{a}^{(e)} = \mathbf{B} \mathbf{a}^{(e)} \quad (3.108a)$$

with

$$\mathbf{B} = \left[-1/l^{(e)}, 1/l^{(e)} \right] \quad (3.108b)$$

which naturally coincides with the expressions previously derived by a more direct procedure. The systematic approach chosen here is useful in order to understand the application of the isoparametric concept.

The stiffness matrix and the equivalent nodal force vector are expressed in the natural coordinate system combining Eqs.(3.106) and (3.83b) as

$$\mathbf{K}^{(e)} = \int_{-1}^{+1} \mathbf{B}^T (EA) \mathbf{B} \frac{l^{(e)}}{2} d\xi \quad , \quad \mathbf{f}^{(e)} = \int_{-1}^{+1} \mathbf{N}^T \mathbf{b} \frac{l^{(e)}}{2} d\xi \quad (3.109)$$

For homogeneous material and uniformly distributed loading the computation of the above integrals is simple, leading to the expressions (3.85).

3.12.4 Isoparametric formulation of the 3-noded quadratic rod element

We will now study the 3-noded rod element of Figure 3.9 with quadratic shape functions. The axial displacement is expressed by

$$u = N_1(\xi)u_1 + N_2(\xi)u_2 + N_3(\xi)u_3 \quad (3.110)$$

where the shape functions $N_1(\xi)$, $N_2(\xi)$ and $N_3(\xi)$ are given by Eq.(3.97).

The x coordinate of a point within the element is written in the isoparametric formulation as

$$x = N_1(\xi)x_1 + N_2(\xi)x_2 + N_3(\xi)x_3 \quad (3.111)$$

The axial strain is obtained by

$$\varepsilon = \frac{du}{dx} = \sum_{i=1}^3 \frac{dN_i}{d\xi} u_i = \left[\frac{dN_1}{d\xi} \frac{d\xi}{dx}, \frac{dN_2}{d\xi} \frac{d\xi}{dx}, \frac{dN_3}{d\xi} \frac{d\xi}{dx} \right] \begin{Bmatrix} u_1 \\ u_2 \\ u_3 \end{Bmatrix} = \mathbf{B} \mathbf{a}^{(e)} \quad (3.112)$$

From Eq.(3.97)

$$\frac{dN_1}{d\xi} = \xi - \frac{1}{2} ; \quad \frac{dN_2}{d\xi} = -2\xi ; \quad \frac{dN_3}{d\xi} = \xi + \frac{1}{2} \quad (3.113)$$

and the strain matrix \mathbf{B} is

$$\mathbf{B} = \left(\frac{d\xi}{dx} \right) \left[\left(\xi - \frac{1}{2} \right), -2\xi, \left(\xi + \frac{1}{2} \right) \right] \quad (3.114)$$

The derivative $\frac{dx}{d\xi}$ is computed from Eq.(3.111) as

$$\begin{aligned} \frac{dx}{d\xi} &= \frac{dN_1}{d\xi} x_1 + \frac{dN_2}{d\xi} x_2 + \frac{dN_3}{d\xi} x_3 = \left(\xi - \frac{1}{2} \right) x_1 - \\ &- 2\xi x_2 + \left(\xi + \frac{1}{2} \right) x_3 = \frac{l^{(e)}}{2} + \xi (x_1 + x_3 - 2x_2) \end{aligned} \quad (3.115)$$

and

$$\frac{d\xi}{dx} = \frac{2}{l^{(e)} + 2\xi(x_1 + x_3 - 2x_2)} \quad (3.116)$$

Eq.(3.116) provides a relationship between dx and $d\xi$ in terms of the three nodal coordinates. In the (usual) case that the central node is located at the element midpoint, we have

$$\frac{d\xi}{dx} = \frac{2}{l^{(e)}} \quad (3.117)$$

and

$$\frac{dx}{d\xi} = \frac{2}{l^{(e)}} \quad \text{y} \quad dx = \frac{l^{(e)}}{2} d\xi \quad (3.118)$$

In this latter case the strain matrix of Eq.(3.114) is simply

$$\mathbf{B} = \frac{2}{l^{(e)}} \left[\left(\xi - \frac{1}{2} \right), -2\xi, \left(\xi + \frac{1}{2} \right) \right] \quad (3.119)$$

The expression of \mathbf{B} for an arbitrary position of the central node is obtained by substituting Eq.(3.116) into (3.114).

The element stiffness matrix and the equivalent nodal force vector are obtained from the PVW as explained the 2-noded element. It can easily be found that the element stiffness matrix has once again the general form

$$\mathbf{K}^{(e)} = \int_{l^{(e)}} \mathbf{B}^T (EA) \mathbf{B} dx \quad (3.120)$$

Substituting the above expressions of dx and \mathbf{B} in terms of ξ into Eq.(3.120) leads to (in the case of the mid-node being central in the element)

$$\mathbf{K}^{(e)} = \int_{-1}^{+1} \frac{2}{l^{(e)}} \begin{Bmatrix} (\xi - \frac{1}{2}) \\ -2\xi \\ (\xi + \frac{1}{2}) \end{Bmatrix} (EA) \frac{2}{l^{(e)}} \left[(\xi - \frac{1}{2}), -2\xi, (\xi + \frac{1}{2}) \right] \frac{l^{(e)}}{2} d\xi \quad (3.121)$$

The computation of the above integral is straightforward if both E and A are constant over the element, giving

$$\mathbf{K}^{(e)} = \left(\frac{EA}{6l} \right)^{(e)} \begin{bmatrix} 14 & -16 & 2 \\ -16 & 32 & -16 \\ 2 & -16 & 14 \end{bmatrix} \quad (3.122)$$

The equivalent nodal force vector for a distributed loading of intensity b is

$$\mathbf{f}^{(e)} = \int_{l^{(e)}} \mathbf{N}^T \mathbf{b} dx = \int_{-1}^{+1} \begin{Bmatrix} \frac{1}{2}\xi(\xi - 1) \\ 1 - \xi^2 \\ \frac{1}{2}\xi(1 + \xi) \end{Bmatrix} b \frac{l^{(e)}}{2} d\xi \quad (3.123)$$

For a uniformly distributed loading

$$\mathbf{f}^{(e)} = \frac{(bl)^{(e)}}{6} \begin{Bmatrix} 1 \\ 4 \\ 1 \end{Bmatrix} \quad (3.124)$$

We note that in this case the central node absorbs four times more loading than the end nodes. This result which is not the obvious one, is a natural consequence of the PVW and the quadratic approximation chosen.

The expressions of $\mathbf{K}^{(e)}$ and $\mathbf{f}^{(e)}$ for an arbitrary position of the central node are obtained by making use of Eq.(3.116). Note that in this case rational polynomial terms in ξ are involved and, therefore, the analytical computation of the element integrals is not so simple.

The isoparametric formulation of higher order rod elements follows the rules explained for the quadratic element. The increasing complexity of the element integrals can be overcome by using numerical integration as explained in the next section.

3.13 NUMERICAL INTEGRATION

We have seen that in some cases the exact analytical computation of the integrals appearing in $\mathbf{K}^{(e)}$ and $\mathbf{f}^{(e)}$ can be difficult and sometimes impossible. This is typically the case for 2D and 3D isoparametric elements, due to the complexity of the rational terms involved in the integral expression. Numerical integration appears here as the only option to compute the element integrals in a simple and accurate way.

To enter into the mathematics of numerical integration falls outside the scope of this text. For simplicity we will only consider here the Gauss quadrature [R2] as this is the more popular numerical integration procedure used in the FEM. We will introduce here the basic ideas for 1D problems which will be extended for 2D and 3D problems in subsequent chapters.

Let us assume that the integral of a function $f(x)$ in the interval $[-1,1]$ is required

$$I = \int_{-1}^{+1} f(\xi) d\xi \quad (3.125)$$

The Gauss integration rule, or Gauss *quadrature*, expresses the value of the above integral as a sum of the products of the function values at a number of known points by prescribed weights. For a quadrature of order q th

$$I \simeq I_q = \sum_{i=1}^q f(\xi_i)W_i \quad (3.126)$$

where W_i is the weight corresponding to the i th sampling point located at $\xi = \xi_i$ and q the number of sampling points. A *Gauss quadrature of q th order integrates exactly a polynomial function of degree $2q - 1$* [R2]. The error in the computation of the integral is of the order $O(\Delta^{2q})$, where Δ is the spacing between the sampling points. The coordinates of the sampling points and the corresponding weights for the first six Gauss quadratures are shown in Table 3.3.

Note that the sampling points are all located within the normalized domain $[-1,1]$. This is useful for the computation of the element integrals expressed in terms of the natural coordinate ξ . The popularity of the Gauss quadrature derives from the fact that it requires the minimum number of sampling points to achieve a prescribed error in the computation of the integral. Thus, it minimizes the number of times the integrand function is computed. The reader can find further details in [R1,2] and [P13].

Example: 3.3 Applications of the Gauss quadrature.

- **Solution**

Let us consider the polynomial

$$f(x) = 1 + x + x^2 + x^3 + x^4$$

q	ξ_q	W_q
1	0.0	2.0
2	± 0.5773502692	1.0
3	± 0.774596697	0.5555555556
	0.0	0.8888888889
4	± 0.8611363116	0.3478548451
	± 0.3399810436	0.6521451549
5	± 0.9061798459	0.2369268851
	± 0.5384693101	0.4786286705
	0.0	0.5688888889
6	± 0.9324695142	0.1713244924
	± 0.6612093865	0.3607615730
	± 0.2386191861	0.4679139346
7	± 0.9491079123	0.1294849662
	± 0.7415311856	0.2797053915
	± 0.4058451514	0.3818300505
	0.0	0.4179591837
8	± 0.9602898565	0.1012285363
	± 0.7966664774	0.2223810345
	± 0.5255324099	0.3137066459
	± 0.1834346425	0.3626837834

Table 3.3: Coordinates and weights of Gauss quadratures

The exact integral of $f(x)$ over the interval $-1 \leq x \leq 1$ is

$$I = \int_{-1}^{+1} f(x) dx = 2 + \frac{2}{3} + \frac{2}{5} = 3.0666$$

- *First order Gauss quadrature:*

$$q = 1, \quad x_1 = 0, \quad W_1 = 2 \quad ; \quad I = W_1 f(x_1) = 2$$

- *Second order quadrature:*

$$q = 2 \quad \begin{cases} x_1 = -0.57735 & , & W_1 = 1 \\ x_2 = +0.57735 & , & W_2 = 2 \end{cases}$$

$$I = W_1 f(x_1) + W_2 f(x_2) = 0.67464 + 2.21424 = 2.8888$$

- *Third order quadrature:*

$$q = 3 \quad \begin{cases} x_1 = -0.77459 & , & W_1 = 0.5555 \\ x_2 = 0.57735 & , & W_2 = 0.8888 \\ x_3 = +0.77459 & , & W_3 = 0.5555 \end{cases}$$

$$\begin{aligned}
I &= W_1 f(x_1) + W_2 f(x_2) + W_3 f(x_3) = 0.7204 \times 0.5555 + \\
&+ 1.0 \times 0.8888 + 3.19931 \times 0.5555 = 3.0666 \quad \mathbf{Exact\ value}
\end{aligned}$$

We see that the exact integration of a fourth order polynomial requires a third order Gauss quadrature as expected.

3.14 STEPS FOR THE COMPUTATION OF MATRICES AND VECTORS FOR AN ISOPARAMETRIC ROD ELEMENT

We will now present the basic steps for computing the stiffness matrix and the equivalent nodal vector for an isoparametric rod element with n nodes. The steps have been arranged so as to facilitate their implementation within a computer program.

3.14.1 Interpolation of the axial displacement

The axial displacement within the element is expressed as

$$\begin{aligned}
u &= N_1 u_1 + N_2 u_2 + \dots + N_n u_n = \\
&= \sum_{i=1}^n N_i u_i = [N_1, N_2, \dots, N_n] \begin{Bmatrix} u_1 \\ u_2 \\ \vdots \\ u_n \end{Bmatrix} = \mathbf{N} \mathbf{a}^{(e)} \quad (3.127)
\end{aligned}$$

3.14.2 Geometry interpolation

The coordinate x is interpolated using the isoparametric form as

$$\begin{aligned}
x &= N_1 x_1 + N_2 x_2 + \dots + N_n x_n = \sum_{i=1}^n N_i x_i = \\
&= [N_1, N_2, \dots, N_n] \begin{Bmatrix} x_1 \\ x_2 \\ \dots \\ x_n \end{Bmatrix} = \mathbf{N} \mathbf{x}^{(e)} \quad (3.128)
\end{aligned}$$

3.14.3 Interpolation of the axial strain

The axial strain is expressed in terms of the nodal displacements as

$$\begin{aligned}\varepsilon &= \frac{du}{dx} = \frac{dN_1}{dx} u_1 + \frac{dN_2}{dx} u_2 + \dots + \frac{dN_n}{dx} u_n = \sum_{i=1}^n \frac{dN_i}{dx} u_i = \\ &= \left[\frac{dN_1}{dx}, \frac{dN_2}{dx}, \dots, \frac{dN_n}{dx} \right] \begin{Bmatrix} u_1 \\ u_2 \\ \vdots \\ u_n \end{Bmatrix} = \mathbf{B} \mathbf{a}^{(e)}\end{aligned}\quad (3.129)$$

The cartesian derivative of the shape functions is obtained by

$$\frac{dN_i}{dx} = \frac{dN_i}{d\xi} \frac{d\xi}{dx} \quad (3.130)$$

From Eq.(3.128) we deduce

$$\frac{dx}{d\xi} = \sum_{i=1}^n \frac{dN_i}{d\xi} x_i = J^{(e)} \quad (3.131)$$

and, therefore

$$dx = J^{(e)} d\xi \quad ; \quad \frac{d\xi}{dx} = \frac{1}{J^{(e)}} \quad (3.132)$$

and

$$\frac{dN_i}{dx} = \frac{1}{J^{(e)}} \frac{dN_i}{d\xi} \quad (3.133)$$

Substituting Eq.(3.133) into the expression of \mathbf{B} gives

$$\mathbf{B} = \left[\frac{dN_1}{dx}, \frac{dN_2}{dx}, \dots, \frac{dN_n}{dx} \right] = \frac{1}{J^{(e)}} \left[\frac{dN_1}{d\xi}, \frac{dN_2}{d\xi}, \dots, \frac{dN_n}{d\xi} \right] \quad (3.134)$$

We point out that $J^{(e)} = \frac{dx}{d\xi}$ is the Jacobian of the 1D coordinate transformation $x \rightarrow \xi$. In the following chapters we will find that for 2D and 3D problems $J^{(e)}$ is a matrix whose determinant relates the infinitesimal areas (for 2D) and volumes (for 3D) in the cartesian and natural coordinate systems.

3.14.4 Computation of the axial force

The axial force N is obtained in terms of the nodal displacements by

$$N = (EA) \varepsilon = \mathbf{D} \mathbf{B} \mathbf{a}^{(e)} \quad (3.135a)$$

with

$$\mathbf{D} = [EA] \quad (3.135b)$$

3.14.5 Element stiffness matrix

The PVW leads to the following general expression for the element stiffness matrix

$$\mathbf{K}^{(e)} = \int_{l^{(e)}} \mathbf{B}^T \mathbf{D} \mathbf{B} dx = \int_{-1}^{+1} \mathbf{B}^T \mathbf{D} \mathbf{B} J^{(e)} d\xi \quad (3.136)$$

From Eqs.(3.134) and (3.135b) we deduce

$$K_{ij}^{(e)} = \int_{-1}^{+1} \frac{1}{J^{(e)}} \frac{dN_i}{d\xi} (EA) \frac{dN_j}{d\xi} d\xi \quad (3.137)$$

The simplicity of the above integral depends on the expression of the shape functions and of $J^{(e)}$. In general, the computation of $\mathbf{K}^{(e)}$ is performed using the Gauss quadrature which evaluates (3.137) as exactly as possible. For a q th order quadrature we can write.

$$K_{ij}^{(e)} = \sum_{r=1}^q \left[\frac{1}{J^{(e)}} \frac{dN_i}{d\xi} (EA) \frac{dN_j}{d\xi} \right]_r W_r \quad (3.138)$$

where $[\cdot]_r$ denotes values computed at the sampling point $\xi = \xi_r$.

3.14.6 Equivalent nodal force vector

For a distributed loading of intensity $b(x)$ we have

$$\mathbf{f}^{(e)} = \int_{l^{(e)}} \mathbf{N}^T b dx = \int_{-1}^{+1} \mathbf{N}^T \cdot b J^{(e)} d\xi \quad (3.139)$$

The computation of Eq.(3.139) can be standardized by using numerical integration as

$$f_i^{(e)} = \sum_{r=1}^q [N_i b J^{(e)}]_r W_r \quad (3.140)$$

Example: 3.4 Compute the term $K_{11}^{(e)}$ of the stiffness matrix for the 3-noded rod element of Figure 3.9 using an isoparametric formulation and numerical integration.

- *Solution*

The term $K_{11}^{(e)}$ is obtained from Eq.(3.137) as

$$K_{11}^{(e)} = \int_{-1}^{+1} \frac{1}{J^{(e)}} \frac{dN_1}{d\xi} (EA) \frac{dN_1}{d\xi} d\xi$$

The expression of N_1 for the 3-noded rod element is (see Eq. (3.97))

$$N_1 = \frac{1}{2}(\xi - 1)\xi \quad \text{and} \quad \frac{dN_1}{d\xi} = \xi - \frac{1}{2}$$

Assuming that node 2 is centered in the element $J^{(e)} = \frac{l^{(e)}}{2}$.

Substituting $\frac{dN_1}{d\xi}$ and $J^{(e)}$ into $K_{11}^{(e)}$ we have

$$K_{11}^{(e)} = \int_{-1}^{+1} \frac{2EA}{l^{(e)}} \left(\xi - \frac{1}{2}\right)^2 d\xi$$

The integrand is a quadratic function and hence, the exact integral requires a Gauss quadrature of 2nd order ($q = 2$). From Eq.(3.138) and Table 3.1 we obtain

$$K_{11}^{(e)} = \sum_{r=1}^2 \left[\frac{2EA}{l^{(e)}} \left(\xi - \frac{1}{2} \right)^2 \right]_r W_r = \left[\frac{2EA}{l^{(e)}} \left(\xi - \frac{1}{2} \right)^2 \right]_{\xi=-\frac{\sqrt{3}}{3}} + \left[\frac{2EA}{l^{(e)}} \left(\xi - \frac{1}{2} \right)^2 \right]_{\xi=\frac{\sqrt{3}}{3}} = \frac{7}{3} \left(\frac{EA}{l} \right)^{(e)}$$

The same procedure can be followed for computing the rest of terms of $\mathbf{K}^{(e)}$.

3.15 BASIC ORGANIZATION OF A FINITE ELEMENT PROGRAM

The steps presented in the previous section for computing the stiffness matrix and the equivalent nodal force vector of the simple rod element are general and almost identical to those required for more complex 2D and 3D elements. Also, these steps define naturally the basic subroutines of a computer program for structural analysis using the FEM. Here we will just introduce the basic format of a finite element program for structural analysis.

Figure 3.11 shows the flow chart of a finite element program for the analysis of axially loaded rods. The first subroutine deals with the reading of the geometrical and mechanical data required for the analysis (subroutine INPUT). Then, the stiffness matrix and the equivalent nodal force vector are computed for each element in subroutines STIFFNESS and LOAD, respectively. The next step is the assembly and solution of the global system of algebraic equilibrium equations to obtain the nodal displacement values in subroutine SOLVE. Finally, the strains and stresses are computed at selected points within each element in subroutine STRESS. Note the analogy of the program skeleton with that of a program for matrix analysis of bar structures [L3], [L5].

3.16 SELECTION OF ELEMENT TYPE

The first task in the analysis of a structure by the FEM is to select the element to be used. This is an important decision and, moreover, not a simple one, as there are many elements available for solving the same structural problem, and each one has different advantages and disadvantages with regard to simplicity, accuracy, cost, etc.

In most cases, the selection of an element for a particular problem is made by the analyst responsible for the computations. This decision should be based on: 1) the characteristics of the structure to be analysed; 2) the elements available in commercial or in-house computer programs and the type of computer to be used;

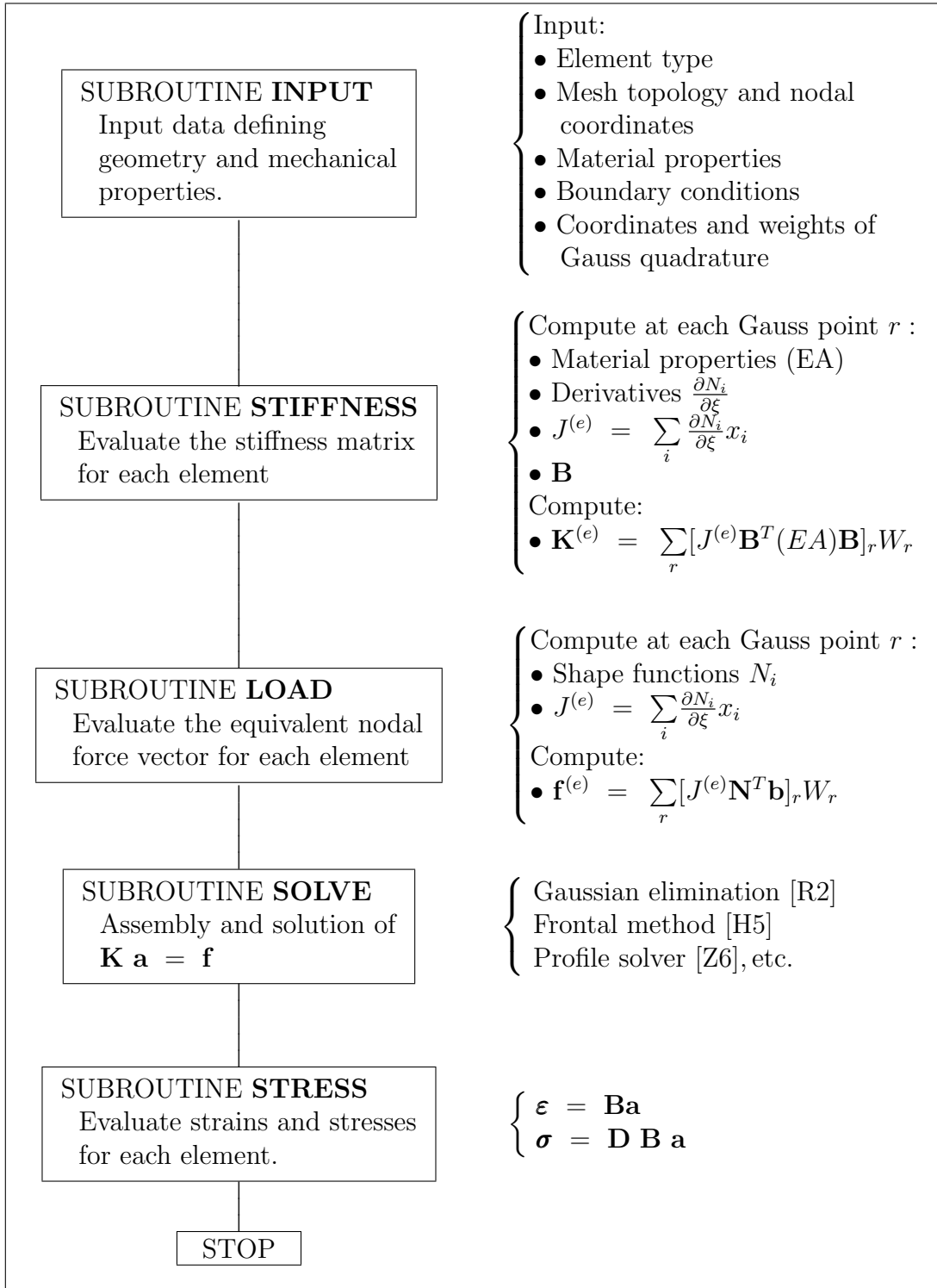


Fig. 3.11: Flow chart of a finite element program for analysis of axially loaded rods

and 3) the experience of the analyst in the solution of similar structures by the FEM.

Several rules for the selection of the best element for each particular structural

problem will be given throughout this text. Nevertheless a few rules of “thumb” can be summarized at this stage. These are:

1. The element chosen must be *robust*. This simply means that there should be no danger of obtaining a spurious solution due to intrinsic bad behaviour of the element under general geometrical or mechanical conditions. A test for robustness of the element is provided by the *patch test* studied in a next section.
2. The mesh should account for the probable stress gradients in the solution, i.e. the mesh should be finer in zones where stress gradients are expected to be higher. Here the use of error estimators and adaptive mesh refinement procedures is recommended.
3. The element should be as accurate as possible. The debate between using few elements of high order, or a finer mesh of simpler low order elements is still open in FEM practice. We note that the growing popularity of adaptive mesh refinement strategies, and the continuing increase in computer power is favouring the use of low order elements.

The choice of low or high order elements is schematically represented in Figure 3.12 showing the approximation of a third degree polynomial function representing the solution of an axial rod problem using different elements. Note that a large number of simple 2-noded elements is required, whereas a single 4-noded cubic element provides the exact solution.

An indicator to decide between two elements is the ratio between the accuracy and the number of nodal variables. This requires a definition of “accuracy”, which is not obvious if the exact solution is not known “a priori”. Another guideline is that in case of doubt between two elements of different order, the analyst should always choose the simplest one (which is generally the low order one).

A comparison between the quadratic and linear rod elements is presented next.

Example: 3.5 Solve the problem of Figure 3.2 using a single 3-noded quadratic rod element.

- *Solution*

Since we have only one element the global equilibrium equation is written from Eqs.(3.122) and (3.124) as

$$\frac{EA}{6l} \begin{bmatrix} 14 & -16 & 2 \\ -16 & 32 & -16 \\ 2 & -16 & 14 \end{bmatrix} \begin{Bmatrix} u_1 \\ u_2 \\ u_3 \end{Bmatrix} = \begin{Bmatrix} \frac{bl}{6} + R \\ \frac{2bl}{3} \\ \frac{bl}{6} + P \end{Bmatrix}, \quad u_1 = 0$$

Solving the above system with the condition $u_1 = 0$, gives

$$u_2 = \frac{3bl^2}{8EA} + \frac{Pl}{2A}, \quad u_3 = \frac{bl^2}{2EA} + \frac{Pl}{EA}$$

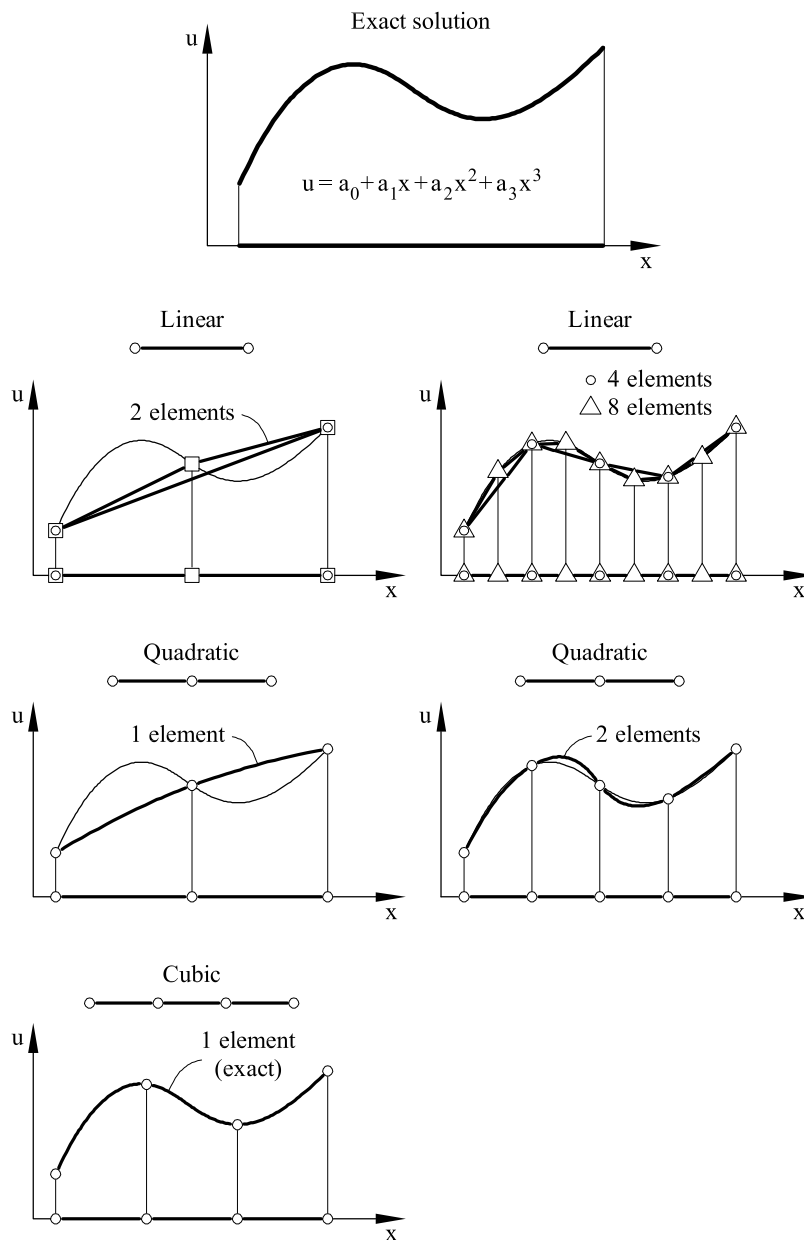


Fig. 3.12: Approximation of a cubic solution with different rod elements. For simplicity the finite element solution has been assumed to be exact at the nodes

It is easy to check that these values coincide with the exact solution (3.114) at the nodes. The displacement field within the element is

$$u = (1 - \xi^2)u_2 + \frac{1}{2}(1 + \xi)\xi u_3$$

Substituting the values for u_2 and u_3 and making the change of variable ($\xi = \frac{2x-l}{l}$) gives

$$u = \frac{1}{EA} \left(-\frac{bx^2}{2} + (P + bl)x \right)$$

which coincides with the exact solution (3.28). This could have been anticipated as the assumed displacement field contains the quadratic solution. The axial strain and stress fields within the element are

$$\varepsilon = \frac{1}{EA} (P + b(l-x))$$

$$\sigma = P + b(l-x)$$

which again coincide with the exact solution.

This example shows that the quadratic rod element has a better performance than the linear one (Figure 3.3). However, this is not a general rule in favour of quadratic elements, as in many cases (particularly for 3D problems) their greater accuracy is counterbalanced by an excessive computing cost.

3.17 REQUIREMENTS FOR CONVERGENCE OF THE SOLUTION

The finite element approximation must satisfy certain conditions which guarantee that as the mesh is refined the numerical solution converges to the exact values. It is very important that the elements satisfy these conditions which are the basis for the success of mesh refinement strategies.

3.17.1 Continuity condition

The displacement must be continuous *within* each element. This condition is automatically satisfied by using polynomial approximations for the displacement field. The issue of continuity of displacements *along the element interfaces* is treated in Section 3.19.1.

3.17.2 Derivativity condition

Obviously, the derivatives of the polynomial approximation should exist up to the order of the derivatives appearing in the element integrals.

For instance, for the axially loaded rod problem the element expressions derived from the PVW contain first order derivatives only. This requires that the shape functions should be at least first order polynomials.

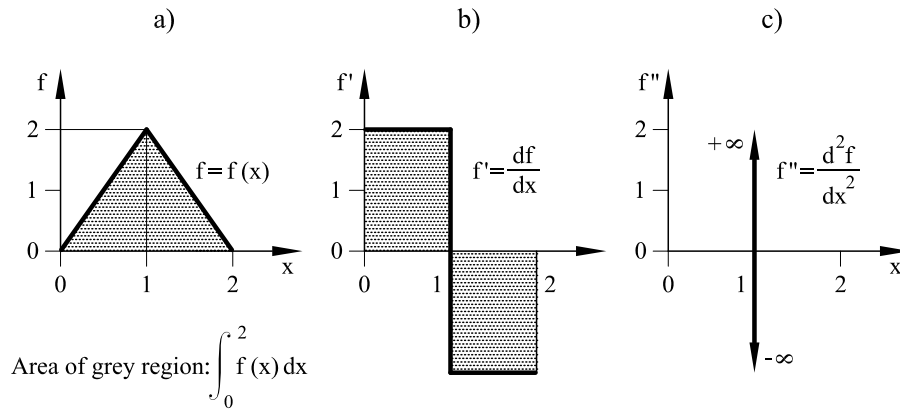


Fig. 3.13: Integral of a bilinear function and its two first derivatives

3.17.3 Integrability condition

Logically, the integrals appearing in the element expressions must have a primitive function. This condition can be explained by considering the simple example of Figure 3.13 where a continuous function $f(x)$ and its two first derivatives are represented. We see that the integral of $f(x)$ in the interval considered exists and it is equal to the area shown in the figure. Also, the integral of $f'(x)$ exists, although it is not a continuous function. Finally, we observe that the second derivative $f''(x)$ has two singular points, due to the discontinuity of $f'(x)$, and it is not integrable. Therefore, the general rule deduced from this simple example is the following. The derivative of a function is integrable if its $m - 1$ first derivatives are continuous (C^{m-1} continuity). It can be thus stated that if m th order derivatives of the displacement field appear in the PVW, the displacement field (and therefore the shape functions) must be C^{m-1} continuous. This condition ensures that the strains at the interface between elements are finite (even though they are indeterminate).

As an example let us consider the axial rod problem. The PVW (Eq.(3.3)) contains only first derivatives of u and hence just displacement continuity (C^0 continuity) is required. Such a continuity is guaranteed within each element by the polynomial approximation chosen, and between elements by the coincidence of the nodal interelemental values.

3.17.4 Rigid body condition

The displacement field chosen should not allow straining of an element to occur when the nodal displacements are caused by a rigid body displacement.

This physical condition is satisfied for a single element if the sum of the shape functions at any point is equal to one. To prove this, let us consider the simple 2-noded axially loaded rod element with equal prescribed nodal displacements \bar{u} .

Within the element we have

$$u = N_1 \bar{u} + N_2 \bar{u} = (N_1 + N_2) \bar{u} \quad (3.141)$$

and for $u = \bar{u}$ then $N_1 + N_2 = 1$ must be satisfied.

3.17.5 Constant strain condition

The displacement function has to be such that if nodal displacements are compatible with a constant strain field, such constant strain will in fact be obtained. Clearly, as elements get smaller, nearly constant strain conditions will prevail in them. It is therefore desirable that a finite size element should be able to reproduce a constant strain condition.

The constant strain criterion incorporates the rigid body requirement, as a rigid body displacement is a particular case of a constant (zero) strain field. Strictly both criteria need only be satisfied in the limit as the size of the elements tends to zero. However, satisfaction of these criteria on elements of finite size leads to a convergent and more accurate solution.

3.18 ASSESSMENT OF CONVERGENCE REQUIREMENTS. THE PATCH TEST

The patch test was first introduced by Irons [I5,I7] and has since then provided a necessary and sufficient condition for convergence. The test is based on selecting an arbitrary patch of elements and imposing upon it nodal displacements corresponding to any state of constant strain. If nodal equilibrium is achieved without imposing external nodal forces, and if a state of constant stress is obtained, then clearly the constant strain criterion of the previous section is satisfied and furthermore, displacement continuity is guaranteed, since no external work is lost through the interelement interfaces.

The patch test also includes the satisfaction of the rigid body condition by simply imposing a nodal displacement field corresponding to a zero strain value.

An alternative patch test is to prescribe a known linear displacement field at the boundary of the patch nodes only. It is then verified that the displacement solution at the interior nodes coincides with the exact values and that a constant strain field is obtained throughout the patch.

An interesting feature of the patch test is its ability to assess the convergence of elements with shape functions which are discontinuous along the element interfaces between adjacent elements. This issue will be discussed further in Section 3.19.1.

The application of the patch test to the simple 2-noded rod element is shown in the next example.

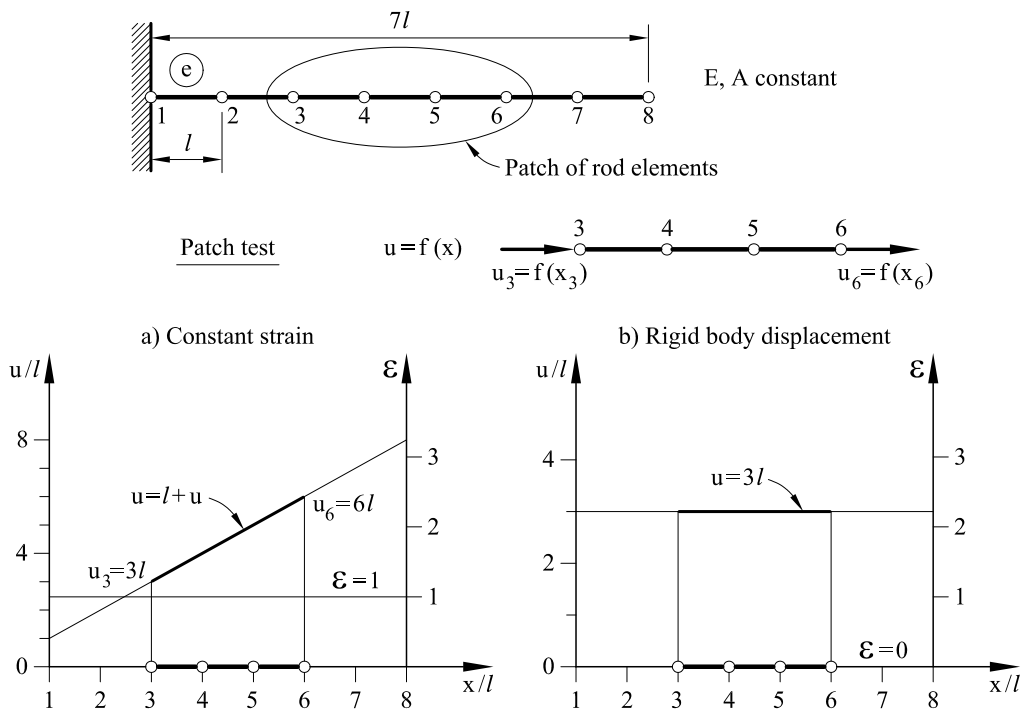


Fig. 3.14: Example of patch test in 2-noded rod elements

Example: 3.6 Apply the patch test to the three element patch of 2-noded rod elements shown in Figure 3.14. All elements have equal length and the same material properties.

- **Solution**

(a) *Constant strain condition*

We will assume a displacement field $u = l + x$ giving a constant strain field in the whole mesh, i.e. $\varepsilon = \frac{du}{dx} = 1$. The following displacements are prescribed at the end nodes of the patch:

$$\begin{aligned} u_3 &= l + 3l = 4l \\ u_6 &= l + 6l = 7l \end{aligned}$$

We now look for the solution for the nodal displacements u_4 and u_5 . The equation system to be solved is

$$\frac{EA}{l} \begin{bmatrix} 1 & -1 & 0 & 0 \\ -1 & 2 & -1 & 0 \\ 0 & -1 & 2 & -1 \\ 0 & 0 & -1 & 1 \end{bmatrix} \begin{Bmatrix} u_3 \\ u_4 \\ u_5 \\ u_6 \end{Bmatrix} = \begin{Bmatrix} R_3 \\ 0 \\ 0 \\ R_6 \end{Bmatrix} \quad \begin{matrix} u_3 = 4l \\ \\ \\ u_6 = 7l \end{matrix}$$

which gives $u_4 = 5l$ and $u_5 = 6l$. These values coincide with the exact ones given by the

prescribed field. It can also be checked that

$$\begin{aligned}\varepsilon^{(3)} &= -\frac{1}{l}u_3 + \frac{1}{l}u_4 = 1 \\ \varepsilon^{(4)} &= -\frac{1}{l}u_4 + \frac{1}{l}u_5 = 1 \\ \varepsilon^{(5)} &= -\frac{1}{l}u_5 + \frac{1}{l}u_6 = 1\end{aligned}$$

which corresponds to the exact constant field imposed. Therefore, the element satisfies the patch test.

(b) *Rigid body condition*

A particular case of the previous example is to study the performance of the patch subjected to a the constant displacement field $u = 3l$, corresponding to a rigid body movement of the patch. The FEM solution yields $u_4 = u_5 = 3l$, which is the correct answer giving a zero strain field over the patch.

3.19 OTHER REQUIREMENTS FOR THE FINITE ELEMENT APPROXIMATION

Next, we will consider some requirements which, in fact, are not strictly necessary for the convergence of the finite element solution. However, their fulfilment is always desirable since, otherwise, the convergence and accuracy of the solution can deteriorate in some cases.

3.19.1 Compatibility condition

The elements must be compatible. This implies that the displacement field for C^0 elements, or its first derivative field for C^1 elements, must be continuous along interelemental boundaries. This is a consequence of the more general integrability condition of Section 3.18.3. Elements satisfying the compatibility condition are termed *compatible* or *conforming*. These elements, when integrated exactly, always converge to the exact solution from the stiffer side.

The compatibility condition is usually satisfied when the displacement field is defined by a polynomial taking a unique value at the nodes. This, however, is not sufficient in some particular cases, such as in some C^1 thin plate bending elements based in Kirchhoff's theory where a discontinuity of the gradient of the deflection occurs at the element sides. These elements are termed *incompatible* or *non-conforming*. Incompatible elements can still converge to the exact solution if the patch test is satisfied. This guarantees that the compatibility condition is fulfilled in the limit as the mesh is refined.

It is interesting that non-conforming elements can be competitive in practice. The reason is that the interelemental discontinuities introduce a greater flexibility

in the element which tends to counterbalance the intrinsic rigidity of the finite element approximation. This leads in some occasions to very good solutions with relatively coarse meshes.

In summary, the non-conformity is an undesirable deficiency which, however, does not automatically invalidate an element. The patch test is the critical proof for acceptance of the element for practical purposes. Although incompatible elements can sometimes be very attractive, they should be looked upon with caution since they can have unexpected features. For instance, some incompatible solid elements show a spurious dependency with the Poisson's ratio which varies with the mesh size [N1].

3.19.2 Condition of complete polynomial

This condition can be explained by recalling that the finite element approximation can reproduce only a finite number of the Taylor expansion terms of the exact solution, which can be written in the vicinity of a point x_i as

$$u(x) = u(x_i) + \left(\frac{du}{dx}\right)_i (x - x_i) + \left(\frac{d^2u}{dx^2}\right)_i (x - x_i)^2 + \cdots + \left(\frac{d^nu}{dx^n}\right)_i (x - x_i)^n \quad (3.142)$$

It is obvious that the finite element approximation written as

$$\bar{u}(x) = a_o + a_1x + a_2x^2 + \cdots + a_mx^m \quad (3.143)$$

can only reproduce exact results up to the n th term of the Taylor expansion (3.142) when $\bar{u}(x)$ contains *all* the terms of the polynomial of m th degree. In such a case the approximation error is of the order Oh^{m+1} and this can be used to derive appropriate extrapolation rules (see Section 3.7).

Therefore, the finite element approximation depends on the higher complete polynomial included in the shape functions. The approximation will be "optimal" if the shape functions are complete polynomials. Unfortunately this is not always possible, and in many cases the shape functions contain incomplete polynomial terms which do not contribute to a higher approximation of the element.

Example: 3.7 Complete and incomplete polynomials and approximations.

- **Solution**

a) Complete approximations of 2nd degree.

$$1D : \bar{u}(x) = a_o + a_1x + a_2x^2$$

$$2D : \bar{u}(x, y) = a_o + a_1x + a_2y + a_3xy + a_4x^2 + a_5y^2$$

b) Incomplete approximations of 3rd degree.

$$1D : \bar{u}(x) = a_o + a_1x + a_2x^3$$

$$2D : \bar{u}(x, y) = a_o + a_1x + a_2y + a_3x^2 + a_4y^2 + a_5x^3$$

The terms of a complete polynomial of several variables can be deduced from the *Pascal triangle* [R2]. This subject will be treated when studying the shape functions of 2D and 3D elements.

In conclusion, it is desirable for the shape functions be complete polynomials, or, if this is not possible, that they contain to a small number of incomplete polynomials. Note that an incomplete approximation does not preclude the convergence of the element.

3.19.3 Stability condition

The analysis of a bar structure requires prescribing enough displacements to prevent the appearance of unstable mechanisms. Lack of stability is usually detected by the existence of one or more mechanisms which correspond to the same number of zero eigenvalues in the stiffness matrix and the associated so-called *rigid body modes*. The same concept applies to the stability of an element. In consequence, the stiffness matrix of an individual element (and also that of a patch of elements) must have the correct rank [R2]. This means that the number of zero eigenvalues of a single isolated element free of external constraints must be equal to the number of rigid body displacements of the element. The element is considered as stable if these zero eigenvalues disappear after prescribing the appropriate d.o.f. Element stability is generally guaranteed if the stiffness matrix is integrated exactly. However, the inexact computation of some terms of the stiffness matrix (by using reduced integration, for instance) can introduce undesirable internal mechanisms in addition to those of rigid body motion. These mechanisms should be avoided since they can lead to instability of the solution.

The existence of internal mechanisms is not always a reason to exclude an element as, in some cases, these mechanisms can not propagate themselves throughout the mesh. Therefore, eigenvalue tests must be performed to assess the existence of spurious mechanisms in an individual element, and also in patches of two or more element assemblies, in order to detect the capability of these mechanisms to propagate in a mesh.

3.19.4 Geometric invariance condition

An element should not have preferred directions. This means that the elements must have what is usually called “geometric-invariance”, also known as frame-invariance and geometric or spatial isotropy.

The lack of geometric-invariance is detected if different displacements or stresses are obtained when the element position is changed in space without changing the relative direction of the loading. In general, an element is geometric-invariant if all the displacement d.o.f. are interpolated with the same polynomial and this is not sensitive to the interchange of the coordinates. This can be achieved by using complete polynomial interpolations expressed in the natural coordinate system and an isoparametric formulation [C15].

Geometric-invariance can be lost in an element by under integration of some of the terms in the stiffness matrix, such as in the case of selective integration procedures. The lack of geometric-invariance is a defect to be avoided. However, this does not necessarily destroy the convergence of the element.

3.20 SOME REMARKS ON THE COMPATIBILITY AND EQUILIBRIUM OF THE SOLUTION

We should keep in mind that the finite element solution is approximate and in general does not satisfy the equilibrium and compatibility requirements of the exact solution. In most cases we will find that:

1. *The solution is compatible within the elements.* This is always guaranteed by using continuous polynomial approximations.
2. *The solution can be incompatible along the interelemental boundaries.* As previously explained interelemental continuity can be violated if the patch test is satisfied and this guarantees compatibility in the limit case of infinite refinement. Also, incompatible elements can sometimes produce excellent answers.
3. *Usually there is not equilibrium of stresses along interelemental boundaries.* Compatibility is always satisfied at the nodes, since they are the points where displacement continuity is enforced due to the polynomial form of the shape functions.
4. *Equilibrium of forces is satisfied at the nodes,* since these are the points where equilibrium is enforced during the assembly process and, therefore, at each node $\mathbf{K}\mathbf{a} - \mathbf{f} = 0$ it is satisfied.
5. *Usually there is not equilibrium of stresses along interelemental boundaries.* Nodal stresses σ can be directly obtained for each element in terms of the nodal displacements, or by extrapolating the values computed at the Gauss points within the element. Stresses at interface nodes are different for each element and the global stress field is discontinuous. A continuous stress field can be obtained by smoothing the discontinuous nodal values (for instance by simple nodal averaging) as shown in Figure 3.15. Also, the stresses computed at the free boundaries are usually not zero, although they are much smaller than the values inside the mesh. This incompatibility of the stress field is a consequence of the displacement formulation, where only displacement continuity is required and the stresses can be discontinuous. The stress discontinuity does not violate the convergence requirements and it is usually corrected as the mesh is refined.

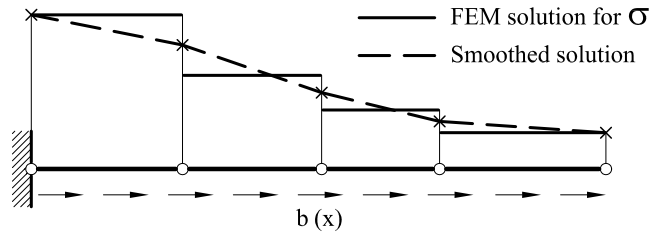


Fig. 3.15: Example of smothing of nodal stresses in linear rod elements

6. *The stresses are not in equilibrium within elements.* The finite element values approximates the exact solution in an average integral form (by means of the PVW) [Z15]. Therefore, the differential equations of equilibrium in stresses are only approximately satisfied pointwise. An exception to this rule is for elements with linear shape functions, where the strain and stress fields are constant and the equilibrium differential equations (involving first derivatives of stresses only) are automatically satisfied. This lack of equilibrium is also corrected as the mesh is refined and it does not preclude the convergence of the numerical solution.

3.21 CONVERGENCE REQUIREMENTS IN ISOPARAMETRIC ELEMENTS

Isoparametric elements are based on the interpolation of the geometry field in terms of the nodal coordinate values using the same shape functions as for the displacement field. The coordinate transformation changes the derivatives of any function by a jacobian relation. For 1D problems we have

$$\frac{du}{dx} = \frac{du}{d\xi} \left(\frac{dx}{d\xi} \right)^{-1} \quad (3.144)$$

Therefore the PVW can be expressed in terms of the natural coordinate ξ with the maximum order of differentiation unchanged.

It follows immediately that if the displacement shape functions are so chosen in the natural coordinate system as to observe the usual rules of convergence then convergence of isoparametric elements will occur.

Furthermore, C^0 isoparametric elements always satisfy the patch test. The proof of this is simple; let us prescribe the following linear displacement field

$$u = a_1 + a_2x \quad (3.145)$$

over a mesh of linear rod elements. The nodal displacements will take the values

$$u_i = a_1 + a_2x_i \quad ; \quad i = 1, 2 \quad (3.146)$$

Inside the element $u = \sum_{i=1}^2 N_i u_i$. Hence, making use of the prescribed field

$$u = \sum_{i=1}^2 N_i (a_1 + a_2 x_i) = a_1 \sum_{i=1}^2 N_i + a_2 \sum_{i=1}^2 N_i x_i \quad (3.147)$$

Since the element is isoparametric we have

$$x = \sum_{i=1}^2 N_i x_i \quad (3.148)$$

From Eqs.(3.147) and (3.148) we deduce that the displacement field will coincide with the prescribed one (3.145) if

$$\sum_{i=1}^2 N_i = 1 \quad (3.149)$$

is satisfied for any value of the natural coordinate ξ between -1 and $+1$. Note that Eq.(3.149) is the usual rigid body requirement for the shape functions (see Section 3.17.4). We conclude that the constant derivative condition is satisfied for C° isoparametric elements.

3.22 ERROR TYPES IN THE FINITE ELEMENT SOLUTION

We recall that the finite element solution is approximate. This automatically implies that some kind of error in the numerical solution is unavoidable. Next, we will study the more usual sources of error.

3.22.1 Discretization error

This error is intrinsic to the polynomial form of the finite element approximation. We showed in Section 3.19.2 that the error involved in the approximation is of the order of the first term in the Taylor expansion of the solution not included in the complete shape function polynomial. Strang and Fix [S14] proposed the following general expression to estimate this error for 1D problems

$$e(\text{error}) = u_{\text{approx}} - u_{\text{exact}} \leq Ch^{p+1} \text{Max} \left| \frac{\partial^{p+1} u_{\text{exact}}}{\partial x^{p+1}} \right| \quad (3.150)$$

where Max denotes the maximum value of the derivative over the element, C is a constant parameter depending on the element type, n is the maximum characteristic element dimension (i.e. the length in rod elements) and p the degree of the highest complete polynomial contained in the shape functions.

Eq.(3.150) shows that convergence is guaranteed if C and the $n+1$ th derivative of the solution are bounded. Note that in this case the error will tend to zero as the element size diminishes.

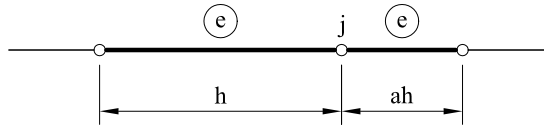


Fig. 3.16: Continuous rod elements of different sizes

The application of this concept to the 1D linear rod element gives for uniformly spaced meshes

$$e \propto h^2 \frac{\partial^2 u}{\partial x^2} \quad (3.151)$$

which implies that the error is proportional to the strain (or stress) gradient. Therefore, smaller elements should be used in zones where this gradient is expected to be higher. The reduction of the error by diminishing the element size is known in the mesh refinement literature as the *h method*.

The error can also be reduced by increasing the approximation order of the elements, while keeping their sizes constant. This results in a larger value of the exponent p in Eq.(3.150). This approach is known as the *p method* [Z15].

Eq.(3.150) assumed a mesh of equal element sizes. The effect of using elements of different sizes has been studied for the analysis of an axially loaded rod using linear elements of two different sizes. The error in the satisfaction of the differential equilibrium equation at the j th node is

$$e = -\frac{h}{3}(1-a) \left(\frac{\partial^3 u}{\partial x^3} \right)_j + \frac{h^2}{12} \left(\frac{1+a^3}{1+a} \right) \frac{\partial^4 u}{\partial x^4}(x_j) + \dots \quad (3.152)$$

where h and a are the lengths of two adjacent elements (see Figure 3.16). Eq.(3.155) shows that the error is of the order h^2 for a uniform mesh ($a \simeq 1$), whereas a higher error of order h is obtained when the element sizes are very different ($a \neq 1$). This indicates that drastic changes in the sizes of contiguous elements in a mesh should be avoided.

The same concepts apply for 2D and 3D problems. The estimation of the discretization error in two dimensions involves the Taylor expansion

$$u(x+h, y+k) = u(x, y) + \left[h \frac{\partial u}{\partial x} + k \frac{\partial u}{\partial y} \right] + \frac{1}{2!} \left[h^2 \frac{\partial^2 u}{\partial x^2} + 2hk \frac{\partial^2 u}{\partial x \partial y} + k^2 \frac{\partial^2 u}{\partial y^2} \right] + \dots \quad (3.153)$$

where u is the exact solution and h and k are a measure of the element sizes in the x and y directions respectively.

It can be shown that the discretization error for 2D linear elements, like the 3-noded triangle (Chapter 4), is proportional to the underlined term on the right-hand side of Eq.(3.67) [S14]. The second derivatives in Eqs.(3.153) can be related to strain (or stress) gradients. Thus, for a constant strain field the error is very small.

It is interesting that the discretization error can also be expressed in terms of the ratio $\frac{k}{h}$. This is a measure of the relative dimensions of the element and it is known as the *element aspect ratio*. For an equilateral element its aspect ratio should be equal to one. However, it will take a large value for a long triangular element. It is recommended to keep the element aspect ratio as close to unity as possible through the mesh.

3.22.2 Error in the geometry approximation

In many cases the interpolation of the geometry is unable to reproduce exactly the real shape. This can be due to a geometry approximation of a lower order than the exact one, or, what is more usual, to the ignorance of the exact analytical form of the geometry defined by the coordinates of a number of points. In both cases, there will be an error in the approximation of the geometry. This error can be reduced by refining the mesh, or by using higher order superparametric approximations. A compromise between these two options is sought in practice and usually isoparametric elements are used. This unavoidably introduces an error in the geometry approximation in some cases. An exception is the case of structures with linear boundaries where the geometry can always be exactly approximated.

3.22.3 Error in the computation of the element integrals

The exact numerical computation of the element integrals implies the use of an appropriate quadrature. Otherwise, an error occurs due to the underestimation of the integral value. In many cases, the exact numerical integration is not possible due to the rational terms appearing in the element integrals. Also, the approximation of the exact value may require a large number of integration points, which may be very expensive. In such cases, it is usual to accept a certain error in the computation of the element integrals.

Paradoxically enough, this error can, on occasions, be beneficial. Usually by subintegrating the rigidity terms the element becomes more flexible, and this balances the stiffening introduced by the approximation of the displacement and geometry fields. This explains why sometimes good results can be obtained with coarse meshes. In the following chapters we will see that the “reduced integration” quadrature is sometimes used to guarantee the correct solution. Note, however, that the inexact computation of the stiffness matrix can modify its correct rank and introduce spurious mechanisms. Reduced integration is therefore a technique which should be used with extreme care.

3.22.4 Errors in the solution of the global equation system

Three type of errors are typical in the solution of the global system of FEM equations using a direct solution method (i.e. Gaussian elimination, Choleski, Frontal

method, etc.): errors due to the *ill-conditioning* of the equations; truncation errors and round-off errors [R5].

The equation system $\mathbf{K}\mathbf{a} = \mathbf{f}$ is ill-conditioned if small changes in the terms of \mathbf{K} or \mathbf{f} induce large changes in the solution \mathbf{a} . The main reason for ill conditioning is the existence of an element, or a group of elements, of large stiffness connected to elements of much smaller stiffness. The behaviour of such a structure can be artificially altered and, unless the computer can store a sufficiently large number of digits, the stiffness matrix behaves as singular or quasi-singular. The error associated with ill-conditioning of the equation system therefore depends on the digit storage capacity of the computer, i.e. in the *truncation* and *round-off errors* which are the main contributors to the total error in the solution.

The *truncation error* is the most important. A computer using d digits to represent a number in simple precision can only store the first d digits of each term of \mathbf{K} and \mathbf{f} . It is then possible that essential information for the correct solution is lost by truncating a number.

The *round-off error* is due to the adjustment automatically performed by the computer on the last digit of each number during computations. Experience shows that this error is less important than the truncation error. Nevertheless, unnecessary round-off errors, such as those in some parameters like the coordinates and weights of the numerical quadrature, should be avoided by defining these parameters with the maximum number of digits allowed by the computer.

Example: 3.8 Study the influence of truncation error in the solution of the spring system shown in Figure 3.17.

- **Solution**

The stiffness matrix of the structure and its inverse are

$$\mathbf{K} = \begin{bmatrix} K_1 & -K_1 \\ -K_1 & K_1 + K_2 \end{bmatrix} \quad ; \quad \mathbf{K}^{-1} = \begin{bmatrix} \frac{1}{K_1} + \frac{1}{K_2} & \frac{1}{K_2} \\ \frac{1}{K_2} & \frac{1}{K_2} \end{bmatrix}$$

If $K_1 \gg K_2$, K_1 dominates in \mathbf{K} . However, K_2 dominates \mathbf{K}^{-1} and therefore the value of the solution. The computation of \mathbf{K}^{-1} is only correct if the terms in \mathbf{K} are evaluated in a way such that K_2 is not lost during the solution. Thus, if $K_1 = 50$ and $K_2 = 0.0023$ the computer must retain at least six digits and K_1 must be represented as 50.0000 so that the last digit of K_2 is retained in the term $K_1 + K_2$. If only four digits are retained the sum $K_1 + K_2$ will give 50.00 and \mathbf{K} will be singular. This problem is *ill conditioned* since the solution is sensitive to the changes (truncation) in the sixth digit of the term $K_1 + K_2$.

Also, if the system $\mathbf{K}\mathbf{a}=\mathbf{f}$ is solved using Gauss elimination, the elimination of the displacement u_1 changes the last diagonal term to $(K_1 + K_2) - K_1$. We see that information for a correct solution can again be lost if $K_1 \gg K_2$.

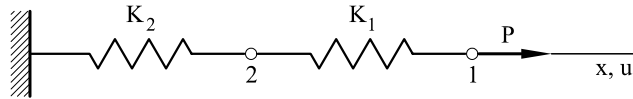


Fig. 3.17: Spring system with two degrees of freedom

A way to avoid truncation errors and to improve the solution is to use double precision throughout the solution process (i.e. for computing the terms of \mathbf{K} and \mathbf{f} and during the solution of the equation system).

An indicator of how sensitive the system $\mathbf{K}\mathbf{a} = \mathbf{f}$ is to truncation and round-off errors is the condition number of \mathbf{K} . An estimation of the number of significant figures exactly computed in the solution process is [B4]

$$s \approx t - \log_{10}[\text{cond}(\mathbf{K})] \quad (3.154)$$

where t is the maximum number of digits which can be stored by the computer and $\text{cond}(\mathbf{K})$ is the condition number of \mathbf{K} defined as

$$\text{cond}(\mathbf{K}) \simeq \frac{\lambda_{\max}}{\lambda_{\min}} \quad (3.155)$$

where λ_{\max} and λ_{\min} are respectively the larger and smaller eigenvalues of \mathbf{K} . Although Eq.(3.154) is only approximate, it indicates that the accuracy of the solution decreases as the condition number increases.

It is therefore desirable that the condition number of \mathbf{K} should be as low as possible. This can be achieved by an adequate scaling of the terms of \mathbf{K} [B4], [R2], [R6].

3.22.5 Errors associated with the constitutive equation

The survey of the error sources in the finite element solution of a structure would be incomplete without referring to the errors arising from a wrong definition of the material properties. The importance of the evaluation of the relevant parameters in the constitutive equation is obvious. For example, in a structure with homogeneous and isotropic material the displacements are proportional to the Young modulus, although the stresses are not affected by this value and they depend only on the Poisson's ratio. For a structure with orthotropic or anisotropic materials both the displacements and the stresses depend on the Young modulus and the Poisson's ratio. An incorrect definition of the material parameters can lead to larger errors than those induced by all the error sources mentioned in the previous sections.

Chapter 4

FEM ANALYSIS OF THE 2D POISSON EQUATION

4.1 INTRODUCTION

In this chapter the formulation of the FEM applied to the two-dimensional (2D) form of the Poisson equation is described.

Initially the main assumptions are presented; then, the FEM solution with the simple three-noded triangular element is presented.

4.2 STEADY-STATE POISSON EQUATION IN 2D

The steady-state Poisson equation for a 2D problem is

$$A(\phi): = \frac{\partial}{\partial x} \left(k_x \frac{\partial \phi}{\partial x} \right) + \frac{\partial}{\partial y} \left(k_y \frac{\partial \phi}{\partial y} \right) + Q = 0 \quad \text{in } \Omega \quad (4.1)$$

where $\phi(x, y)$ is the unknown function, k_x and k_y are the conductivities in the x and y directions and $Q(x, y)$ is a heat source over the domain Ω .

This equation can be obtained by improving flux balance in a differential domain (Figure 4.1). There exist two kinds of boundary conditions

$$B(\phi): \begin{cases} \text{Prescribed variable (Dirichlet condition)} \\ \phi - \bar{\phi} = 0 \quad \text{on } \Gamma_\phi \\ \\ \text{Prescribed normal heat flow (Neumann condition)} \\ q_n = \bar{q}_n + \alpha(\phi - \phi_a) \quad \text{on } \Gamma_q \end{cases} \quad (4.2a)$$

The normal flux q_n is obtained projecting the boundary flow over the boundary normal

$$q_n = \mathbf{n}^T \mathbf{q} = n_x q_x + n_y q_y$$

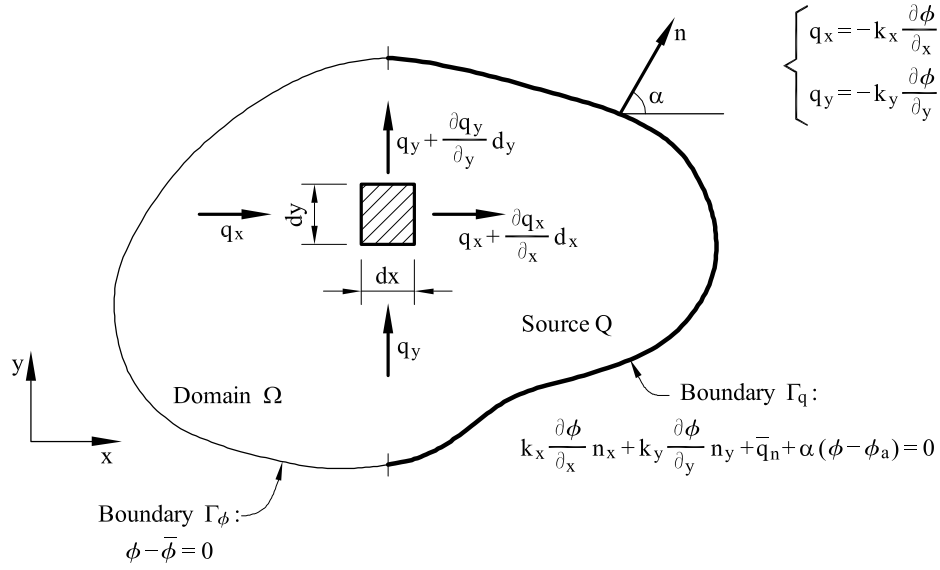


Figure 4.1: Problem definition for the Poisson equation in a 2D domain

Substituting $q_x = -k_x \frac{\partial \phi}{\partial x}$ and $q_y = -k_y \frac{\partial \phi}{\partial y}$ in the previous equations gives the prescribed heat flux condition along the boundary (Neumann condition) as follows:

$$k_x \frac{\partial \phi}{\partial x} n_x + k_y \frac{\partial \phi}{\partial y} n_y + \bar{q}_n + \alpha (\phi - \bar{\phi}_a) = 0 \quad \text{en } \Gamma_q \quad (4.2b)$$

where \bar{q}_n is the normal heat flow prescribed flow at the domain's boundary Γ_q (\bar{q}_n is positive if the flow is in the outgoing normal direction \mathbf{n}). The last term in (4.2b) express the heat flow at the boundary due the temperature difference in the boundary (ϕ) and the temperature of the external media (ϕ_a); α is the convection coefficient.

Note that

$$\Gamma = \Gamma_\phi \cup \Gamma_q \quad (4.3)$$

The boundary split in two zones Γ_ϕ and Γ_q is conceptual, because these conditions can appear in different zones along the boundary.

4.3 PROBLEM SOLUTION USING THE FINITE ELEMENT METHOD

We solve the problem defined by Eqs.(4.1) and (4.2) in a similar way as we did for the 1D case. First we apply the Galerkin's weighted residual (GWR) method on the Poisson equation that defines the balance of heat flow over the domain and the equation that defines the Neumann the boundary conditions.

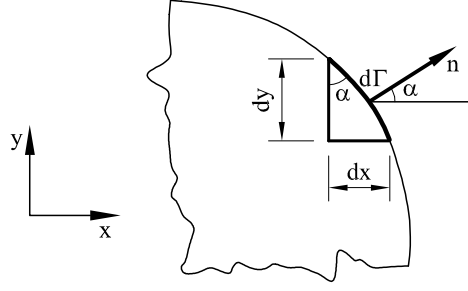


Figure 4.2: Normal vector to the boundary

4.3.1 Integral form of the GWR method

The equivalent integral form for the differential equations are obtained applying the GWR method. In this manner, multiplying the equations (4.1) and (4.2) by the weighted functions W and \bar{W} and integrating over the domain and the boundary Γ_q respectively gives:

$$\begin{aligned} & \iint_{\Omega} W \left[\frac{\partial}{\partial x} \left(k_x \frac{\partial \phi}{\partial x} \right) + \frac{\partial}{\partial y} \left(k_y \frac{\partial \phi}{\partial y} \right) + Q \right] dx dy + \\ & + \int_{\Gamma_q} \bar{W} \left[k_x \frac{\partial \phi}{\partial x} n_x + k_y \frac{\partial \phi}{\partial y} n_y + \bar{q}_n + \alpha(\phi - \phi_a) \right] d\Gamma = 0 \end{aligned} \quad (4.4)$$

The weak form is obtained integrating by parts the terms with second derivatives in (4.4)

$$\begin{aligned} & \iint_{\Omega} W \frac{\partial}{\partial x} \left(k_x \frac{\partial \phi}{\partial x} \right) dx dy = \int dy \int W \frac{\partial}{\partial x} \left(k_x \frac{\partial \phi}{\partial x} \right) dx = \\ & = - \iint_{\Omega} \frac{\partial W}{\partial x} k_x \frac{\partial \phi}{\partial x} dx dy + \int_{\Gamma=\Gamma_q+\Gamma_{\phi}} W k_x \frac{\partial \phi}{\partial x} dy \end{aligned} \quad (4.5)$$

A similar operation is applied for the integral of $\frac{\partial}{\partial y} \left(k_y \frac{\partial \phi}{\partial y} \right)$ to obtain:

$$\begin{aligned} & \iint_{\Omega} W \left[\frac{\partial}{\partial x} \left(k_x \frac{\partial \phi}{\partial x} \right) + \frac{\partial}{\partial y} \left(k_y \frac{\partial \phi}{\partial y} \right) + Q \right] dx dy = \\ & = - \iint_{\Omega} \left[\frac{\partial W}{\partial x} k_x \frac{\partial \phi}{\partial x} + \frac{\partial W}{\partial y} k_y \frac{\partial \phi}{\partial y} \right] dx dy + \iint_{\Omega} W Q dx dy + \\ & + \int_{\Gamma_q+\Gamma_{\phi}} W \left[k_x \frac{\partial \phi}{\partial x} dy + k_y \frac{\partial \phi}{\partial y} dx \right] \end{aligned} \quad (4.6)$$

Considering that (Figure 4.2)

$$\begin{aligned} dy &= d\Gamma \cos \alpha = d\Gamma n_x \\ dx &= d\Gamma \sin \alpha = d\Gamma n_y \end{aligned} \quad (4.7)$$

and adopting $\bar{W} = -W$ which eliminates the derivatives of in the Neumann boundary when substituting in (4.6) gives:

$$\begin{aligned}
& - \iint_{\Omega} \left[\frac{\partial W}{\partial x} k_x \frac{\partial \phi}{\partial x} + \frac{\partial W}{\partial y} k_y \frac{\partial \phi}{\partial y} \right] dx dy + \iint_{\Omega} W Q dx dy + \\
& + \int_{\underline{\Gamma_q + \Gamma_\phi}} W \left[k_x \frac{\partial \phi}{\partial x} n_x + k_y \frac{\partial \phi}{\partial y} n_y \right] d\Gamma - \\
& - \int_{\Gamma_q} W \left[k_x \frac{\partial \phi}{\partial x} n_x + k_y \frac{\partial \phi}{\partial y} n_y + \bar{q}_n + \alpha(\phi - \phi_a) \right] d\Gamma = 0
\end{aligned} \tag{4.8}$$

where the underlined terms are canceled together.

The resulting integral form is:

$$\begin{aligned}
& - \iint_{\Omega} \left[\frac{\partial W}{\partial x} k_x \frac{\partial \phi}{\partial x} + \frac{\partial W}{\partial y} k_y \frac{\partial \phi}{\partial y} \right] d\Omega + \iint_{\Omega} W Q d\Omega + \\
& + \int_{\Gamma_\phi} W \left[k_x \frac{\partial \phi}{\partial x} n_x + k_y \frac{\partial \phi}{\partial y} n_y \right] d\Gamma - \int_{\Gamma_q} W [\bar{q}_n + \alpha(\phi - \phi_a)] d\Gamma = 0
\end{aligned} \tag{4.9}$$

Recalling that

$$q_n = q_x n_x + q_y n_y = -k_x \frac{\partial \phi}{\partial x} n_x - k_y \frac{\partial \phi}{\partial y} n_y \tag{4.10}$$

and ordering the terms for ϕ the weak form is finally obtained. This equation allows to recover the C^0 continuity condition for W and ϕ :

$$\begin{aligned}
& \iint_{\Omega} \left[\frac{\partial W}{\partial x} k_x \frac{\partial \phi}{\partial x} + \frac{\partial W}{\partial y} k_y \frac{\partial \phi}{\partial y} \right] d\Omega + \int_{\Gamma_q} \alpha W \phi d\Gamma = \\
& = \iint_{\Omega} W Q d\Omega - \int_{\Gamma_q} W [\bar{q}_n - \alpha \phi_a] d\Gamma - \int_{\Gamma_\phi} W q_n d\Gamma
\end{aligned} \tag{4.11}$$

The weak form (4.11) is the starting expression for deriving the FEM equations.

4.3.2 FEM Discretization

The last integral in Eq.(4.11) is due the normal heat flow q_n crossing the boundary Γ_ϕ where ϕ is a known value. Note that the sign of the integral is negative, which means that the normal flux q_n takes heat from the domain toward outside the boundary. As in the 1D problem, this flux can be considered as a “reaction” that can be computed once the value of ϕ is solved over Ω .

Let us assume a discretization of the domain Ω using 2D finite elements with n nodes (Figure 4.3). The approximation of ϕ inside each element is defined as:

$$\phi \cong \hat{\phi} = \sum_{i=1}^n N_i^{(e)}(x, y) \phi_i^{(e)} \tag{4.12}$$

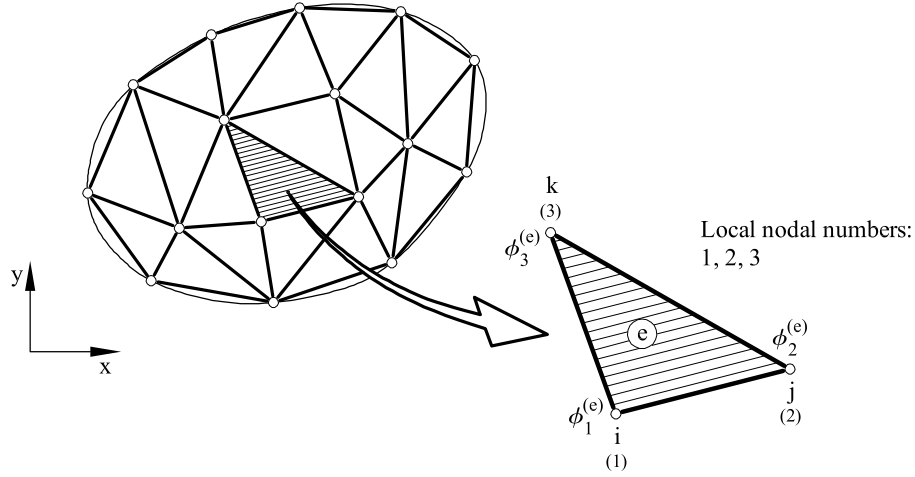


Figure 4.3: Discretization of a two-dimensional domain by tree-noded triangular elements.

where $N_i^{(e)}(x, y)$ are the 2D shape functions function and $\phi^{(e)}$ are the nodal values of the approximated solution.

The system of equations for the discretized domain is obtained substituting the approximation (4.12) into the weak form (4.11) and choosing N weighting functions W_i , where N is the total number of nodes in the mesh

$$\begin{aligned} & \iint_{\Omega} \left[\frac{\partial W_i}{\partial x} k_x \frac{\partial \hat{\phi}}{\partial x} + \frac{\partial W_i}{\partial y} k_y \frac{\partial \hat{\phi}}{\partial y} \right] d\Omega + \int_{\Gamma_q} \alpha W_i \hat{\phi} d\Omega = \\ & = \iint_{\Omega} W_i Q d\Omega - \int_{\Gamma_q} W_i [\bar{q}_n - \alpha \phi_a] d\Gamma - \int_{\Gamma_\phi} W_i q_n d\Gamma \quad i = 1, \dots, N \end{aligned} \quad (4.13)$$

The Galerkin form is obtained by making $W_i = N_i$. Assuming that all the functions that appear in (4.13) are integrable and having in mind the additive property of the integrals, the Galerkin form can be expressed as a function of the element contributions:

$$\begin{aligned} & \sum_e \iint_{\Omega^{(e)}} \left[\frac{\partial N_i^{(e)}}{\partial x} k_x \left(\sum_{j=1}^n \frac{\partial N_j^{(e)}}{\partial x} \phi_j^{(e)} \right) + \frac{\partial N_i^{(e)}}{\partial y} k_y \left(\sum_{j=1}^n \frac{\partial N_j^{(e)}}{\partial y} \phi_j^{(e)} \right) \right] d\Omega + \\ & + \sum_e \int_{\Gamma_q^{(e)}} \alpha N_i^{(e)} \left(\sum_{j=1}^n N_j^{(e)} \phi_j^{(e)} \right) d\Gamma = \\ & = \sum_e \iint_{\Omega^{(e)}} N_i^{(e)} Q d\Omega - \sum_e \int_{\Gamma_q^{(e)}} N_i^{(e)} [\bar{q}_n - \alpha \phi_a] d\Gamma - \sum_e \int_{\Gamma_\phi^{(e)}} N_i^{(e)} q_n d\Gamma \end{aligned} \quad (4.14)$$

where the sum applies are over all the elements discretizing the domain Ω . Expression (4.14) can be written in matrix form as

$$\mathbf{K}\mathbf{a} = \mathbf{f} \quad (4.15)$$

The terms of \mathbf{K} and \mathbf{f} are obtained by assembling the elemental contributions as usual. Because the shape function forms $N_i^{(e)}$ have a zero value outside the element (e), we deduce that:

$$\boxed{K_{ij}^{(e)} = \iint_{\Omega^{(e)}} \left(\frac{\partial N_i^{(e)}}{\partial x} k_x \frac{\partial N_j^{(e)}}{\partial x} + \frac{\partial N_i^{(e)}}{\partial y} k_y \frac{\partial N_j^{(e)}}{\partial y} \right) d\Omega + \int_{\Gamma_q^{(e)}} \alpha N_i^{(e)} N_j^{(e)} d\Gamma = K_{dij}^{(e)} + K_{cij}^{(e)}} \quad (4.16)$$

$$\boxed{f_i^{(e)} = \iint_{\Omega^{(e)}} N_i^{(e)} Q d\Omega - \int_{\Gamma_q^{(e)}} N_i^{(e)} [\bar{q}_n - \alpha \phi_a] d\Gamma - \int_{\Gamma_\phi^{(e)}} N_i^{(e)} q_n d\Gamma} \quad (4.17)$$

The terms $K_{dij}^{(e)}$ and $K_{cij}^{(e)}$ in (4.16) represent the elemental contributions due to the conductivity and convection in the element stiffness matrix, respectively. These terms are obtained by:

$$K_{dij}^{(e)} = \iint_{\Omega^{(e)}} \left[\frac{\partial N_i^{(e)}}{\partial x} k_x \frac{\partial N_j^{(e)}}{\partial x} + \frac{\partial N_i^{(e)}}{\partial y} k_y \frac{\partial N_j^{(e)}}{\partial y} \right] d\Omega \quad (4.18)$$

$$K_{cij}^{(e)} = \int_{\Gamma_q^{(e)}} \alpha N_i^{(e)} N_j^{(e)} d\Gamma \quad (4.19)$$

The independent computation of $K_{dij}^{(e)}$ and $K_{cij}^{(e)}$ simplifies the evaluation of the element stiffness matrix coefficients.

Similarly, the components of vector $f_i^{(e)}$ are:

$$f_i^{(e)} = f_{Q_i}^{(e)} + f_{c_i}^{(e)} + q_{n_i} \quad (4.20)$$

where

$$f_{Q_i}^{(e)} = \iint_{\Omega^{(e)}} N_i^{(e)} Q d\Omega \quad (4.21)$$

is the contribution of the heat source over the domain

$$f_{c_i}^{(e)} = - \int_{\Gamma_q^{(e)}} N_i^{(e)} [\bar{q}_n - \alpha \phi_a] d\Gamma \quad (4.22)$$

is the contribution of the heat flow through the Neumann boundary where the flow is prescribed and

$$q_{n_i}^{(e)} = - \int_{\Gamma_\phi^{(e)}} N_i^{(e)} q_n d\Gamma \quad (4.23)$$

is the “reaction” flow term over the boundary Γ_ϕ where the variable ϕ is prescribed. This flow is evaluated “*a posteriori*” once the nodal values of ϕ have been calculated.

Recall that the element boundary integral of (4.17) only contributes to the nodal force vector when the element has one or more sides over Γ_q or Γ_ϕ .

4.4 THREE-NODED TRIANGULAR ELEMENT

Let us assume a three-noded triangular element discretization over the domain, as shown in Figure 4.3.

Each element node has one degree of freedom (d.o.f.) which corresponds to the nodal unknown value of ϕ . The unknown variation is expressed by the following polynomial:

$$\phi(x, y) = \alpha_0 + \alpha_1 x + \alpha_2 y \quad (4.24)$$

To find the coefficients α_0 , α_1 and α_2 it is necessary to substitute the nodal coordinates into Eq.(4.24) as follows

$$\begin{aligned} \phi_1^{(e)} &= \alpha_0 + \alpha_1 x_1^{(e)} + \alpha_2 y_1^{(e)} \\ \phi_2^{(e)} &= \alpha_0 + \alpha_1 x_2^{(e)} + \alpha_2 y_2^{(e)} \\ \phi_3^{(e)} &= \alpha_0 + \alpha_1 x_3^{(e)} + \alpha_2 y_3^{(e)} \end{aligned} \quad (4.25)$$

Solving these equations and substituting the values of α_i we obtain

$$\begin{aligned} \phi(x, y) &= \frac{1}{2A^{(e)}} [(a_1^{(e)} + b_1^{(e)}x + c_1^{(e)}y)\phi_1^{(e)} + (a_2^{(e)} + b_2^{(e)}x + c_2^{(e)}y)\phi_2^{(e)} + \\ &+ (a_3^{(e)} + b_3^{(e)}x + c_3^{(e)}y)\phi_3^{(e)}] \end{aligned} \quad (4.26)$$

where

$$\begin{aligned} a_i^{(e)} &= x_j^{(e)}y_k^{(e)} - x_k^{(e)}y_j^{(e)} \\ b_i^{(e)} &= y_j^{(e)} - y_k^{(e)} \\ c_i^{(e)} &= x_k^{(e)} - x_j^{(e)} \end{aligned} \quad (4.27)$$

Indexes i, j, k go from 1 to 3 (Figure 4.3). Permuting the indexes allows to find the expression for each parameter.

The element area $A^{(e)}$ is obtained by the determinant of the coefficients in Eq.(4.25) as follows

$$2A^{(e)} = \begin{vmatrix} 1 & x_i^{(e)} & y_i^{(e)} \\ 1 & x_j^{(e)} & y_j^{(e)} \\ 1 & x_k^{(e)} & y_k^{(e)} \end{vmatrix} \quad (4.28)$$

Eq.(4.26) can be compacted as

$$\phi = \sum_{i=1}^3 N_i^{(e)} \phi_i^{(e)} = N_1^{(e)} \phi_1^{(e)} + N_2^{(e)} \phi_2^{(e)} + N_3^{(e)} \phi_3^{(e)} \quad (4.29)$$

which allows identifying the element shape functions by:

$$N_i^{(e)}(x, y) = \frac{1}{2A^{(e)}} (a_i^{(e)} + b_i^{(e)}x + c_i^{(e)}y); \quad i = 1, 2, 3 \quad (4.30)$$

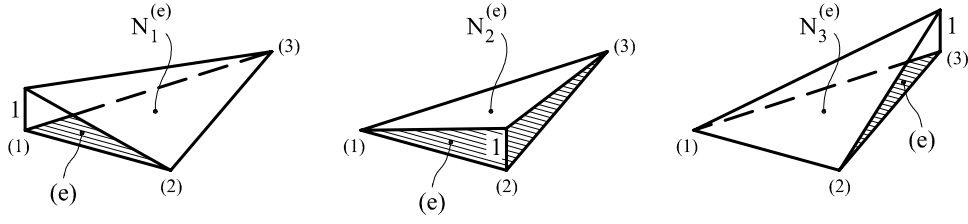


Figure 4.4: Shape functions for the three-noded triangular element.

In the 3-noded triangular element these shape functions are expressed by linear polynomials with coefficients depending on the nodal coordinates. The nodal shape functions take a unit value at the node and zero at the other nodes, as usual (Figure 4.4).

As for the 1D case, the *global* shape functions of a node has a unit value at the node and zero at any other node. Also, the influence domain for this function corresponds to all the elements surrounding the node.

4.4.1 Elemental stiffness matrix

From Eq.(4.30) we deduce

$$\frac{\partial N_i^{(e)}}{\partial x} = \frac{b_i}{2A^{(e)}}; \quad \frac{\partial N_i^{(e)}}{\partial y} = \frac{c_i}{2A^{(e)}} \quad (4.31)$$

Substituting Eqs.(4.30) and (4.31) into (4.18) and (4.19) gives

$$K_{d_{ij}}^{(e)} = \iint_{\Omega^{(e)}} \frac{1}{4A^{(e)2}} [k_x b_i b_j + k_y c_i c_j] d\Omega = \frac{1}{4A^{(e)}} [k_x b_i b_j + k_y c_i c_j] \quad (4.32)$$

and the $\mathbf{K}_d^{(e)}$ matrix is obtained by

$$\mathbf{K}_d^{(e)} = \frac{1}{4A^{(e)}} \begin{bmatrix} k_x b_1 b_1 + k_y c_1 c_1 & k_x b_1 b_2 + k_y c_1 c_2 & k_x b_1 b_3 + k_y c_1 c_3 \\ k_x b_2 b_1 + k_y c_2 c_1 & k_x b_2 b_2 + k_y c_2 c_2 & k_x b_2 b_3 + k_y c_2 c_3 \\ k_x b_3 b_1 + k_y c_3 c_1 & k_x b_3 b_2 + k_y c_3 c_2 & k_x b_3 b_3 + k_y c_3 c_3 \end{bmatrix}^{(e)} \quad (4.33)$$

The evaluation of the integral defined in (4.19) yields the convection stiffness matrix as

$$\mathbf{K}_c^{(e)} = \int_{\Gamma_q^{(e)}} \alpha \begin{bmatrix} N_1^{(e)} N_1^{(e)} & N_1^{(e)} N_2^{(e)} & N_1^{(e)} N_3^{(e)} \\ N_2^{(e)} N_1^{(e)} & N_2^{(e)} N_2^{(e)} & N_2^{(e)} N_3^{(e)} \\ N_3^{(e)} N_1^{(e)} & N_3^{(e)} N_2^{(e)} & N_3^{(e)} N_3^{(e)} \end{bmatrix}^{(e)} d\Gamma \quad (4.34)$$

It is important to note that the above integral is computed over the length of the sides of the triangular element laying on the Neumann boundary. Therefore the shape function for the third node which does not belong to a side takes a zero value over that side. This allows us to simplify expression (4.34) depending on the element's side where the boundary integral is computed.

Hence, for side 1-2, $N_3^{(e)} = 0$ and

$$K_{c_{12}}^{(e)} = \int_{l_{12}^{(e)}} \alpha \begin{bmatrix} N_1^{(e)} N_1^{(e)} & N_1^{(e)} N_2^{(e)} & 0 \\ N_2^{(e)} N_1^{(e)} & N_2^{(e)} N_2^{(e)} & 0 \\ 0 & 0 & 0 \end{bmatrix} d\Gamma \quad (4.35)$$

For side 2-3, $N_1^{(e)} = 0$ and

$$K_{c_{23}}^{(e)} = \int_{l_{23}^{(e)}} \alpha \begin{bmatrix} 0 & 0 & 0 \\ 0 & N_2^{(e)} N_2^{(e)} & N_2^{(e)} N_3^{(e)} \\ 0 & N_3^{(e)} N_2^{(e)} & N_3^{(e)} N_3^{(e)} \end{bmatrix} d\Gamma \quad (4.36)$$

For side 1-3, $N_2^{(e)} = 0$ and

$$K_{c_{13}}^{(e)} = \int_{l_{13}^{(e)}} \alpha \begin{bmatrix} N_1^{(e)} N_1^{(e)} & 0 & N_1^{(e)} N_3^{(e)} \\ 0 & 0 & 0 \\ N_1^{(e)} N_3^{(e)} & 0 & N_3^{(e)} N_3^{(e)} \end{bmatrix} d\Gamma \quad (4.37)$$

Considering that α is constant over the element sides, the above expressions can be integrated to obtain:

$$\int_{l_{ij}^{(e)}} N_i^{(e)} N_j^{(e)} d\Gamma = \begin{cases} l_{ij}^{(e)}/3; & i = j \\ l_{ij}^{(e)}/6; & i \neq j \end{cases} \quad (4.38)$$

where $l_{ij}^{(e)}$ is the length of the (e) element's side $i - j$; this gives:

$$K_{c_{12}}^{(e)} = \frac{\alpha l_{12}^{(e)}}{6} \begin{bmatrix} 2 & 1 & 0 \\ 1 & 2 & 0 \\ 0 & 0 & 0 \end{bmatrix}; \quad K_{c_{23}}^{(e)} = \frac{\alpha l_{23}^{(e)}}{6} \begin{bmatrix} 0 & 0 & 0 \\ 0 & 2 & 1 \\ 0 & 1 & 2 \end{bmatrix}; \quad K_{c_{13}}^{(e)} = \frac{\alpha l_{13}^{(e)}}{6} \begin{bmatrix} 2 & 0 & 1 \\ 0 & 0 & 0 \\ 1 & 0 & 2 \end{bmatrix} \quad (4.39)$$

The total element stiffness matrix is obtained as:

$$\mathbf{K}^{(e)} = \mathbf{K}_d^{(e)} + \mathbf{K}_{c_{12}}^{(e)} + \mathbf{K}_{c_{23}}^{(e)} + \mathbf{K}_{c_{13}}^{(e)} \quad (4.40)$$

We recall again that the contribution of matrices $\mathbf{K}_{c_{ij}}^{(e)}$ is only relevant if the element side $i - j$ belongs to the external Neumann boundary Γ_q . Also note that we have obtained explicit expressions for the element stiffness matrix due the linear form of the shape functions.

4.4.2 The equivalent nodal flux vector

The generic expression of $\mathbf{f}^{(e)}$ for the 3-noded triangular element is:

$$\mathbf{f}^{(e)} = \begin{Bmatrix} f_1^{(e)} \\ f_2^{(e)} \\ f_3^{(e)} \end{Bmatrix} \quad (4.41)$$

The heat source terms are deduced from Eq.(4.21)

$$\mathbf{f}_Q^{(e)} = \begin{Bmatrix} f_{Q_1}^{(e)} \\ f_{Q_2}^{(e)} \\ f_{Q_3}^{(e)} \end{Bmatrix} = \iint_{\Omega^{(e)}} \begin{Bmatrix} N_1^{(e)} \\ N_2^{(e)} \\ N_3^{(e)} \end{Bmatrix} Q d\Omega \quad (4.42)$$

For a constant value of Q over the element, it is easy to obtain:

$$\mathbf{f}_Q^{(e)} = \frac{QA^{(e)}}{3} \begin{Bmatrix} 1 \\ 1 \\ 1 \end{Bmatrix}$$

Hence, the total element flux is split in equal parts over the three nodes, as expected.

From equation (4.22) the nodal flux contribution due convection is evaluated as follows

$$\mathbf{f}_c^{(e)} = - \int_{\Gamma_q^{(e)}} \begin{Bmatrix} N_1^{(e)} \\ N_2^{(e)} \\ N_3^{(e)} \end{Bmatrix} [\bar{q}_n - \alpha\phi_a] d\Gamma \quad (4.43)$$

As for the convection stiffness matrix, the evaluation of the above integral requires to consider the element's side where the integral is computed. Therefore for each side we have:

Side 1-2 ($N_3^{(e)} = 0$)

$$\mathbf{f}_{c_{12}}^{(e)} = - \int_{l_{12}^{(e)}} \begin{Bmatrix} N_1^{(e)} \\ N_2^{(e)} \\ 0 \end{Bmatrix} [\bar{q}_n - \alpha\phi_a] d\Gamma \quad (4.44)$$

Side 1-3 ($N_2^{(e)} = 0$)

$$\mathbf{f}_{c_{13}}^{(e)} = - \int_{l_{13}^{(e)}} \begin{Bmatrix} N_1^{(e)} \\ 0 \\ N_3^{(e)} \end{Bmatrix} [\bar{q}_n - \alpha\phi_a] d\Gamma \quad (4.45)$$

Side 2-3 ($N_1^{(e)} = 0$)

$$\mathbf{f}_{c_{23}}^{(e)} = - \int_{l_{23}^{(e)}} \begin{Bmatrix} 0 \\ N_2^{(e)} \\ N_3^{(e)} \end{Bmatrix} [\bar{q}_n - \alpha\phi_a] d\Gamma \quad (4.46)$$

Assuming that \bar{q}_n , α and ϕ_a are constant over the side gives

$$\mathbf{f}_{c_{12}}^{(e)} = - \frac{l_{12}^{(e)}}{2} [\bar{q}_n - \alpha\phi_a] \begin{Bmatrix} 1 \\ 1 \\ 0 \end{Bmatrix} \quad (4.47)$$

with similar expressions for $\mathbf{f}_{c_{13}}^{(e)}$ and $\mathbf{f}_{c_{23}}^{(e)}$.

The last contributions to the nodal flux vector are the reactions at the boundary where ϕ is prescribed (Eq.4.23)). These fluxes are added directly to the boundary nodes and are evaluated “a posteriori” once the nodal values of ϕ have been computed.

Example 4.1 *Heat conduction into a square domain*

Solution

Consider the square domain shown in Figure 4.5. A known amount of heat is generated internally due to a heat source and conduction effects. The goal is to compute the temperature distribution over the domain.

We assume that $k_x = k_y = k = 2,0$ [cal/cm °C] and $Q = 2,4$ [cal/cm²s]. Due to symmetry conditions only an eighth section of the domain is analyzed. The boundary conditions are:

- Along the external boundary 4-6 $\alpha = 0, \bar{\phi} = 0$
- Along the boundaries 1-6 and 1-4, the symmetry condition implies that

$$\frac{\partial \phi}{\partial n} = 0$$

This means that the temperature gradient in the boundary’s normal direction is zero. The physical meaning of this condition corresponds to an isolated boundary. Because of the conditions applied, the heat flow only goes out the domain through the external side 1-4.

The analysis domain is discretized into a mesh of four 3-noded triangular elements as shown in Figure 4.5.

Because $\alpha = 0$

$$\mathbf{K}^{(e)} = \mathbf{K}_k^{(e)} = \frac{k}{4A^{(e)}} \begin{bmatrix} b_1b_1 + c_1c_1, & b_1b_2 + c_1c_2, & b_1b_3 + c_1c_3 \\ b_2b_1 + c_2c_1, & b_2b_2 + c_2c_2, & b_2b_3 + c_2c_3 \\ b_3b_1 + c_3c_1, & b_3b_2 + c_3c_2, & b_3b_3 + c_3c_3 \end{bmatrix}$$

with

$$\begin{aligned} b_i &= y_j^{(e)} - y_k^{(e)} \\ c_i &= x_k^{(e)} - x_j^{(e)} \end{aligned}$$

Following the element numbering shown in Figure 4.5b, for elements 1, 2 and 4 we have:

$$\mathbf{K}^{(1)} = \mathbf{K}^{(2)} = \mathbf{K}^{(4)} = \frac{2,0}{4 \frac{2,5^2}{2}} \begin{bmatrix} 6,25 & -6,25 & 0 \\ -6,25 & 6,25 + 6,25 & -6,25 \\ 0 & -6,25 & 6,25 \end{bmatrix} = \begin{bmatrix} 1 & -1 & 0 \\ -1 & 2 & -1 \\ 0 & -1 & 1 \end{bmatrix}$$

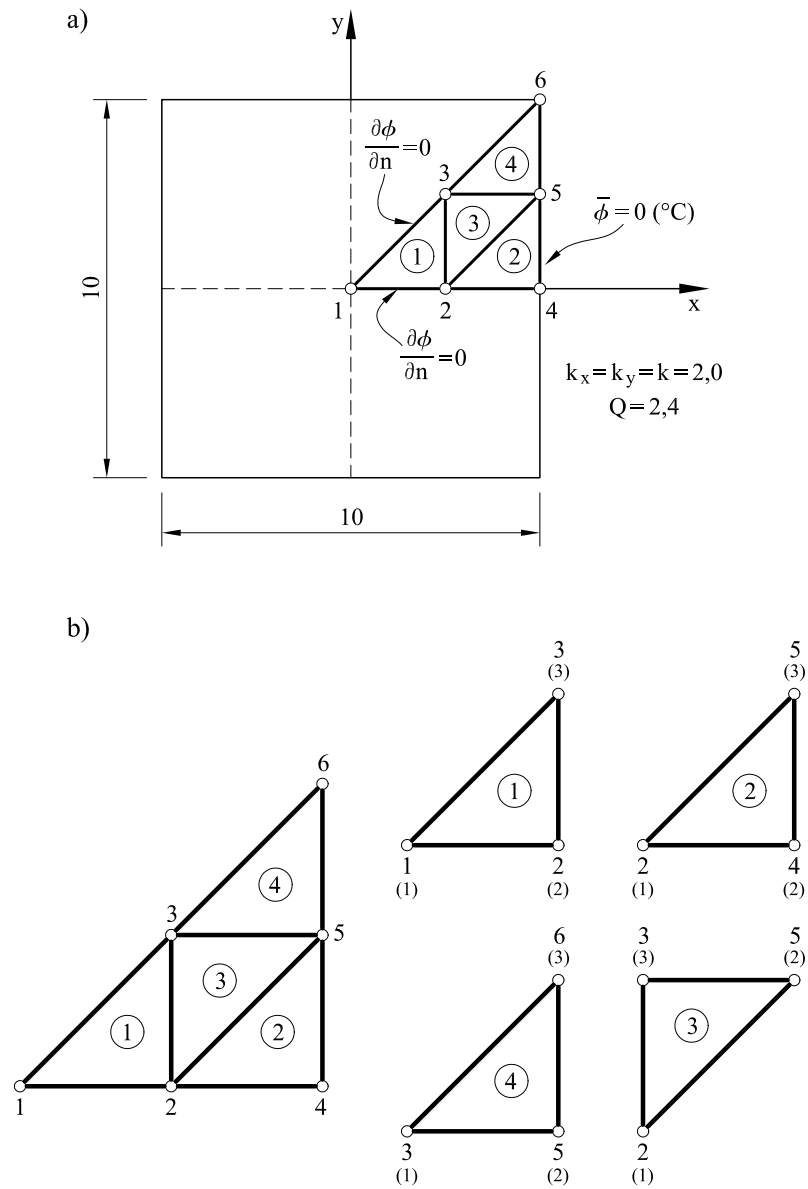


Figure 4.5: a) Heat conduction in a square domain. b) Mesh of 3-noded triangular elements using the symmetry simplification.

For the element number 3:

$$\mathbf{K}^{(3)} = \frac{2,0}{4 \frac{6,25}{2}} \begin{bmatrix} 6,25 & 0 & -6,25 \\ 0 & 6,25 & -6,25 \\ -6,25 & -6,25 & 12,50 \end{bmatrix} = \begin{bmatrix} 1 & 0 & -1 \\ 0 & 1 & -1 \\ -1 & -1 & 2 \end{bmatrix}$$

b_i	c_i
$b_1 = y_2^{(e)} - y_3^{(e)} = -2, 5$	$c_1 = x_3^{(e)} - x_2^{(e)} = 0$
$b_2 = y_3^{(e)} - y_1^{(e)} = 2, 5$	$c_2 = x_1^{(e)} - x_3^{(e)} = -2, 5$
$b_3 = y_1^{(e)} - y_2^{(e)} = 0$	$c_3 = x_2^{(e)} - x_1^{(e)} = 2, 5$

Table 4.1: Coefficients b_i and c_i for elements 1, 2 and 4

b_i	c_i
$b_1 = y_2^{(3)} - y_3^{(3)} = 0$	$c_1 = x_3^{(3)} - x_2^{(3)} = -2, 5$
$b_2 = y_3^{(3)} - y_1^{(3)} = 2, 5$	$c_2 = x_1^{(3)} - x_3^{(3)} = 0$
$b_3 = y_1^{(3)} - y_2^{(3)} = -2, 5$	$c_3 = x_2^{(3)} - x_1^{(3)} = 2, 5$

Table 4.2: Coefficients b_i and c_i for element 3

The elemental nodal flux vectors are

$$\mathbf{f}^{(e)} = \mathbf{f}_Q^{(e)} = \frac{QA^{(e)}}{3} \begin{Bmatrix} 1 \\ 1 \\ 1 \end{Bmatrix}$$

$$\mathbf{f}^{(e)} = \frac{2,4 \times 2,5^2}{3 \times 2} \begin{Bmatrix} 1 \\ 1 \\ 1 \end{Bmatrix} = 2,5 \begin{Bmatrix} 1 \\ 1 \\ 1 \end{Bmatrix}$$

Assembly of the global stiffness matrix

The first step is to identify the position of each coefficient of the elemental stiffness matrix \mathbf{K} through the correspondence between the local and global nodal numbers. From Figure 4.5 we deduce

$$\mathbf{K}^{(1)} = \begin{matrix} & \begin{matrix} 1 & 2 & 3 \end{matrix} \\ \begin{matrix} 1 \\ 2 \\ 3 \end{matrix} & \begin{pmatrix} K_{11}^{(1)} & K_{12}^{(1)} & K_{13}^{(1)} \\ K_{21}^{(1)} & K_{22}^{(1)} & K_{23}^{(1)} \\ K_{31}^{(1)} & K_{32}^{(1)} & K_{33}^{(1)} \end{pmatrix} \end{matrix}$$

$$\mathbf{K}^{(2)} = \begin{matrix} & \begin{matrix} 2 & 4 & 5 \end{matrix} \\ \begin{matrix} 2 \\ 4 \\ 5 \end{matrix} & \begin{pmatrix} K_{11}^{(2)} & K_{12}^{(2)} & K_{13}^{(2)} \\ K_{21}^{(2)} & K_{22}^{(2)} & K_{23}^{(2)} \\ K_{31}^{(2)} & K_{32}^{(2)} & K_{33}^{(2)} \end{pmatrix} \end{matrix}$$

$$\mathbf{K}^{(3)} = \begin{matrix} & \begin{matrix} 2 & 5 & 3 \end{matrix} \\ \begin{matrix} 2 \\ 5 \\ 3 \end{matrix} & \begin{pmatrix} K_{11}^{(3)} & K_{12}^{(3)} & K_{13}^{(3)} \\ K_{21}^{(3)} & K_{22}^{(3)} & K_{23}^{(3)} \\ K_{31}^{(3)} & K_{32}^{(3)} & K_{33}^{(3)} \end{pmatrix} \end{matrix}$$

$$\mathbf{K}^{(4)} = \begin{matrix} & \begin{matrix} 3 & 5 & 6 \end{matrix} \\ \begin{matrix} 3 \\ 5 \\ 6 \end{matrix} & \begin{pmatrix} K_{11}^{(4)} & K_{12}^{(4)} & K_{13}^{(4)} \\ K_{21}^{(4)} & K_{22}^{(4)} & K_{23}^{(4)} \\ K_{31}^{(4)} & K_{32}^{(4)} & K_{33}^{(4)} \end{pmatrix} \end{matrix}$$

The global stiffness matrix is:

$$\mathbf{K} = \begin{matrix} & \begin{matrix} 1 & 2 & 3 & 4 & 5 & 6 \end{matrix} \\ \begin{matrix} 1 \\ 2 \\ 3 \\ 4 \\ 5 \\ 6 \end{matrix} & \begin{pmatrix} K_{11}^{(1)} & K_{12}^{(1)} & K_{13}^{(1)} & 0 & 0 & 0 \\ & K_{22}^{(1)} + K_{11}^{(2)} + K_{11}^{(3)} & K_{23}^{(1)} + K_{13}^{(3)} & K_{12}^{(2)} & K_{13}^{(2)} + K_{12}^{(3)} & 0 \\ & & K_{33}^{(1)} + K_{33}^{(3)} + K_{11}^{(4)} & 0 & K_{32}^{(3)} + K_{12}^{(4)} & K_{13}^{(4)} \\ & & & K_{22}^{(2)} & K_{23}^{(2)} & 0 \\ \text{Symm.} & & & & K_{33}^{(2)} + K_{22}^{(3)} + K_{22}^{(4)} & K_{23}^{(4)} \\ & & & & & K_{33}^{(4)} \end{pmatrix} \end{matrix}$$

Finally the elemental nodal flow are assembled into the vector \mathbf{f} as follows

$$\underbrace{\begin{bmatrix} 1 & -1 & 0 & 0 & 0 & 0 \\ -1 & 4 & -2 & -1 & 0 & 0 \\ 0 & -2 & 4 & 0 & -2 & 0 \\ 0 & -1 & 0 & 2 & -1 & 0 \\ 0 & 0 & -2 & -1 & 4 & -1 \\ 0 & 0 & 0 & 0 & -1 & 1 \end{bmatrix}}_{\mathbf{K}} \underbrace{\begin{bmatrix} \phi_1 \\ \phi_2 \\ \phi_3 \\ \phi_4 \\ \phi_5 \\ \phi_6 \end{bmatrix}}_{\mathbf{a}} = \underbrace{\left\{ \begin{array}{l} f_1^{(1)} = 2, 5 \\ f_2^{(1)} + f_1^{(2)} + f_1^{(3)} = 7, 5 \\ f_3^{(1)} + f_3^{(3)} + f_1^{(4)} = 7, 5 \\ f_2^{(2)} = 2, 5 + R_4 \\ f_3^{(2)} + f_2^{(3)} + f_2^{(4)} = 7, 5 + R_5 \\ f_3^{(4)} = 2, 5 + R_6 \end{array} \right\}}_{\mathbf{f}} \begin{array}{l} \phi_4 = 0 \\ \phi_5 = 0 \\ \phi_6 = 0 \end{array}$$

where R_4 , R_5 y R_6 are the unknown fluxes at the nodes 4, 5 and 6 respectively. Note that the value of ϕ is known at those nodes ($\phi_4 = \phi_5 = \phi_6 = 0$).

Solution of the system of equations gives

$$\begin{aligned}\phi_1 &= 9,3748 \text{ }^\circ\text{C} \\ \phi_2 &= 6,8748 \text{ }^\circ\text{C} \\ \phi_3 &= 5,3123 \text{ }^\circ\text{C} \\ \phi_4 &= 0 \text{ }^\circ\text{C}; \quad R_4 = -9,3748 \text{ cal/s/cm}^2 \\ \phi_5 &= 0 \text{ }^\circ\text{C}; \quad R_5 = -18,124 \text{ cal/s/cm}^2 \\ \phi_6 &= 0 \text{ }^\circ\text{C}; \quad R_6 = -2,5 \text{ cal/s/cm}^2\end{aligned}$$

Let us compare the total flux generated in the domain (QA) with the flow that goes out through the domain boundary

$$\begin{aligned}R_4 + R_5 + R_6 &= 29,9988 \\ QA &= 30\end{aligned}$$

Hence, the total flux generated in the domain coincides with the total flux that goes out through the boundary. This proves the global equilibrium of nodal fluxes which is a consequence of the flux balance (equilibrium) approach followed in the FEM.

Chapter 5

FEM ANALYSIS OF THE 3D POISSON EQUATION

5.1 INTRODUCTION

In this chapter the formulation of the FEM applied to the 3D form of the Poisson equation is described. This chapter completes the study of problems with one variable per node.

5.2 STEADY-STATE POISSON EQUATION IN 3D

The steady-state Poisson equation for a three-dimensional (3D) problem is

$$A(\phi): = \frac{\partial}{\partial x} \left(k_x \frac{\partial \phi}{\partial x} \right) + \frac{\partial}{\partial y} \left(k_y \frac{\partial \phi}{\partial y} \right) + \frac{\partial}{\partial z} \left(k_z \frac{\partial \phi}{\partial z} \right) + Q = 0 \quad \text{in } \Omega \quad (5.1)$$

where $\phi(x, y, z)$ is the unknown function, k_x , k_y and k_z are the conductivities in the x , y , z directions and Q is a heat source over the domain Ω .

As for the 1D and 2D cases this equation is obtained by considering the balance of heat fluxes in a differential domain (Figure 5.1).

The boundary conditions are:

$$B(\phi): \begin{cases} \text{Prescribed variable condition (Dirichlet condition):} \\ \phi - \bar{\phi} = 0 \quad \text{on } \Gamma_\phi \\ \\ \text{Prescribed normal flux condition (Neumann condition):} \\ k_x \frac{\partial \phi}{\partial x} n_x + k_y \frac{\partial \phi}{\partial y} n_y + k_z \frac{\partial \phi}{\partial z} n_z + \bar{q}_n + \alpha(\phi - \bar{\phi}_a) = 0 \quad \text{on } \Gamma_q \end{cases} \quad (5.2)$$

As for the 2D case, \bar{q}_n is the prescribed flux in the normal direction to the boundary Γ_q , $\bar{\phi}_a$ is the external temperature, α is the convection coefficient and $\mathbf{n} = [n_x, n_y, n_z]^T$ is the unit normal to Γ_q and $\Gamma = \Gamma_\phi \cup \Gamma_q$.

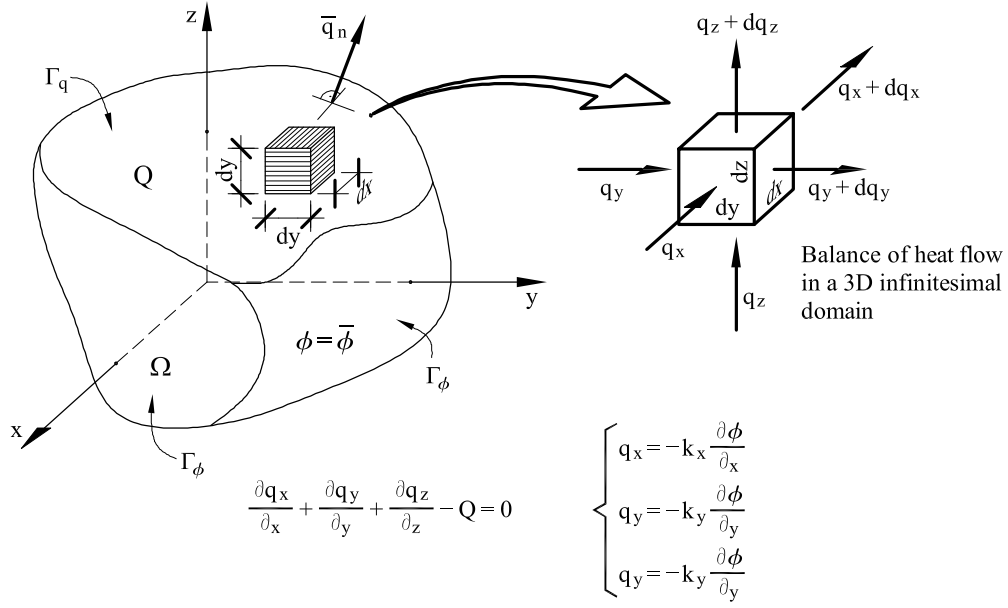


Figure 5.1: Three dimensional definition of the Poisson equation.

5.3 SOLUTION USING THE FINITE ELEMENT METHOD

5.3.1 Weak integral form

The equivalent integral form for the differential equations (5.1) and (5.2) are obtained applying the GWR method as

$$\begin{aligned}
 & \iiint_{\Omega} W \left[\frac{\partial}{\partial x} \left(k_x \frac{\partial \phi}{\partial x} \right) + \frac{\partial}{\partial y} \left(k_y \frac{\partial \phi}{\partial y} \right) + \frac{\partial}{\partial z} \left(k_z \frac{\partial \phi}{\partial z} \right) + Q \right] d\Omega + \\
 & + \iint_{\Gamma_q} \bar{W} \left[k_x \frac{\partial \phi}{\partial x} n_x + k_y \frac{\partial \phi}{\partial y} n_y + k_z \frac{\partial \phi}{\partial z} n_z + \bar{q}_n + \alpha(\phi - \phi_a) \right] d\Gamma = 0
 \end{aligned} \tag{5.3}$$

where W and \bar{W} are arbitrary weighting functions.

Integrating by parts the terms with second derivatives of ϕ in the first integral and choosing $\bar{W} = -W$ gives:

$$\begin{aligned}
 & - \iiint_{\Omega} \left(\frac{\partial W}{\partial x} k_x \frac{\partial \phi}{\partial x} + \frac{\partial W}{\partial y} k_y \frac{\partial \phi}{\partial y} + \frac{\partial W}{\partial z} k_z \frac{\partial \phi}{\partial z} \right) d\Omega + \\
 & + \iiint_{\Omega} W Q d\Omega + \iint_{\Gamma_q + \Gamma_\phi} W \left(k_x \frac{\partial \phi}{\partial x} n_x + k_y \frac{\partial \phi}{\partial y} n_y + k_z \frac{\partial \phi}{\partial z} n_z \right) d\Gamma \tag{5.4} \\
 & - \iint_{\Gamma_q} W \left[k_x \frac{\partial \phi}{\partial x} n_x + k_y \frac{\partial \phi}{\partial y} n_y + k_z \frac{\partial \phi}{\partial z} n_z + \bar{q}_n + \alpha(\phi - \phi_a) \right] d\Gamma = 0
 \end{aligned}$$

where the underlined terms cancel together.

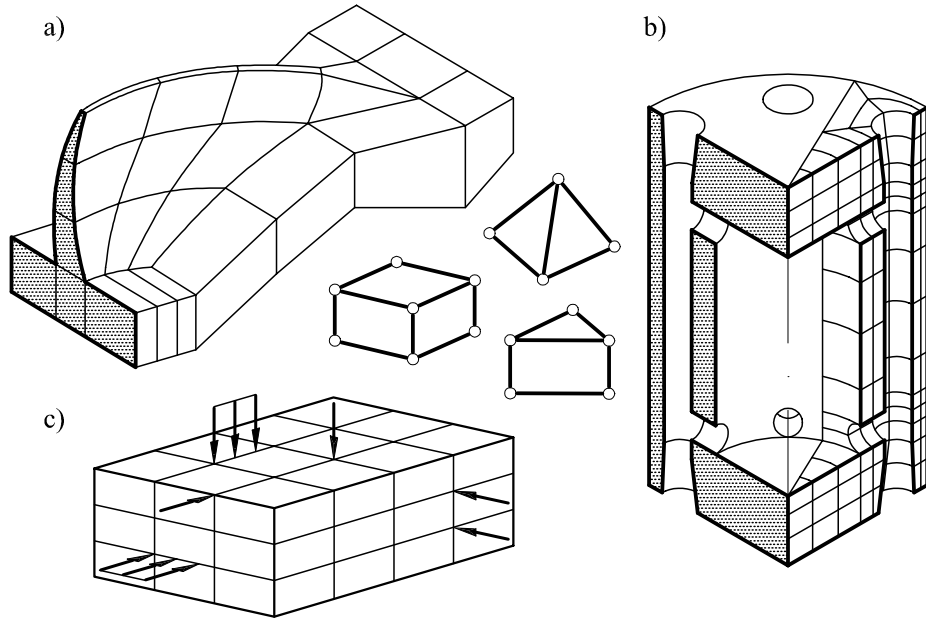


Figure 5.2: Solid domains discretized with finite elements.

Reordering the terms the weak form is finally expressed as

$$\begin{aligned}
 \iiint_{\Omega} \left[\frac{\partial W}{\partial x} k_x \frac{\partial \phi}{\partial x} + \frac{\partial W}{\partial y} k_y \frac{\partial \phi}{\partial y} + \frac{\partial W}{\partial z} k_z \frac{\partial \phi}{\partial z} \right] d\Omega + \iint_{\Gamma_q} W \alpha \phi d\Gamma = \\
 = \iiint_{\Omega} W Q d\Omega - \iint_{\Gamma_q} W [\bar{q}_n - \alpha \phi_a] d\Gamma - \iint_{\Gamma_\phi} W q_n d\Gamma
 \end{aligned} \tag{5.5}$$

In the above equation the use of the normal flux definition has been considered, i.e.

$$q_n = \mathbf{q}^T \mathbf{n} = q_x n_x + q_y n_y + q_z n_z = -k_x \frac{\partial \phi}{\partial x} n_x - k_y \frac{\partial \phi}{\partial y} n_y - k_z \frac{\partial \phi}{\partial z} n_z \tag{5.6}$$

The weak form (5.5) is the starting expression for deriving the FEM equations.

5.3.2 FEM Discretization

Consider the 3D domain discretizations shown in Figure 5.2 using finite elements with n nodes. The approximation of the unknown ϕ within each element is expressed as

$$\phi \cong \hat{\phi} = \sum_{j=1}^n N_j^{(e)}(x, y, z) \phi_j^{(e)} \tag{5.7}$$

where $N_j^{(e)}$ are the shape functions of the 3D element and $\phi_j^{(e)}$ are the nodal values of the approximation function.

Substituting the above approximation into the weak form (5.5) and selecting the same number of weighting functions as nodal unknowns, the approximate expression of the weak form is obtained

$$\begin{aligned}
& \iiint_{\Omega} \left[\frac{\partial W_i}{\partial x} k_x \frac{\partial \hat{\phi}}{\partial x} + \frac{\partial W_i}{\partial y} k_y \frac{\partial \hat{\phi}}{\partial y} + \frac{\partial W_i}{\partial z} k_z \frac{\partial \hat{\phi}}{\partial z} \right] d\Omega + \iint_{\Gamma_q} W_i \alpha \hat{\phi} d\Gamma = \\
& = \iint_{\Gamma_q} W_i [\bar{q}_n - \alpha \phi_a] d\Gamma - \iint_{\Gamma_\phi} W_i q_n d\Gamma \\
& \quad i = 1, 2, \dots, N
\end{aligned} \tag{5.8}$$

where N is total number of nodes in the mesh.

The Galerkin symmetric form is obtained by choosing $W_i = N_i$. Assuming that all the functions in the last expression can be integrated and using the additive property of the integral, the weak form can be expressed as the sum of the element contributions as

$$\begin{aligned}
& \sum_e \left\{ \iiint_{\Omega^{(e)}} \left[\frac{\partial N_i^{(e)}}{\partial x} k_x \left(\sum_{j=1}^n \frac{\partial N_j^{(e)}}{\partial x} \phi_j^{(e)} \right) + \frac{\partial N_i^{(e)}}{\partial y} k_y \left(\sum_{j=1}^n \frac{\partial N_j^{(e)}}{\partial y} \phi_j^{(e)} \right) + \right. \right. \\
& \quad \left. \left. + \frac{\partial N_i^{(e)}}{\partial z} k_z \left(\sum_{j=1}^n \frac{\partial N_j^{(e)}}{\partial z} \phi_j^{(e)} \right) \right] d\Omega + \iint_{\Gamma_q^{(e)}} N_i^{(e)} \alpha \left(\sum_{j=1}^n N_j^{(e)} \phi_j^{(e)} \right) d\Gamma \right\} = \\
& = \sum_e \left\{ \iiint_{\Omega^{(e)}} N_i^{(e)} Q d\Omega - \iint_{\Gamma_q^{(e)}} N_i^{(e)} (\bar{q} - \alpha \phi_a) d\Gamma - \iint_{\Gamma_\phi^{(e)}} N_i^{(e)} q d\Gamma \right\} \\
& \quad i = 1, 2, \dots, N
\end{aligned} \tag{5.9}$$

where the sum is performed over all the elements in the mesh.

The above integral expression can be interpreted as the i -th row of the algebraic equation system of the discretization, i.e.

$$K_{i1}\phi_1 + K_{i2}\phi_2 + \dots + K_{iN}\phi_N = f_i, \quad i = 1, 2, \dots, N \tag{5.10}$$

The global equation system is therefore written as

$$\mathbf{K}\mathbf{a} = \mathbf{f}$$

or

$$\begin{aligned}
& \begin{matrix} i = 1 \\ i = 2 \\ \vdots \\ \vdots \\ i = N \end{matrix} \underbrace{\begin{pmatrix} 1 & 2 & \dots & N \\ K_{11} & K_{12} & \dots & K_{1N} \\ K_{21} & K_{22} & \dots & K_{2N} \\ \vdots & \ddots & \ddots & \vdots \\ K_{N1} & K_{N2} & \dots & K_{NN} \end{pmatrix}}_{\mathbf{K}} \underbrace{\begin{Bmatrix} \phi_1 \\ \phi_2 \\ \vdots \\ \phi_N \end{Bmatrix}}_{\mathbf{a}} = \underbrace{\begin{Bmatrix} f_1 \\ f_2 \\ \vdots \\ f_N \end{Bmatrix}}_{\mathbf{f}} \tag{5.11}
\end{aligned}$$

As for the 1D and 2D cases, the \mathbf{K} matrix and the \mathbf{f} vector can be obtained by assembling the stiffness matrices $\mathbf{K}^{(e)}$ and the elemental nodal flux vectors $\mathbf{f}^{(e)}$ for each element given by:

$$\mathbf{K}^{(e)} = \begin{bmatrix} K_{11}^{(e)} & \cdots & K_{1n}^{(e)} \\ \vdots & \ddots & \vdots \\ K_{n1}^{(e)} & \cdots & K_{nn}^{(e)} \end{bmatrix} \quad (5.12)$$

$$\mathbf{f}_1^{(e)} = \begin{Bmatrix} f_1^{(e)} \\ \vdots \\ f_n^{(e)} \end{Bmatrix} \quad (5.13)$$

where n is the number of nodes in the element and

$$\begin{aligned} K_{ij}^{(e)} &= \overbrace{\iiint_{\Omega^{(e)}} \left(\frac{\partial N_i^{(e)}}{\partial x} k_x \frac{\partial N_j^{(e)}}{\partial x} + \frac{\partial N_i^{(e)}}{\partial y} k_y \frac{\partial N_j^{(e)}}{\partial y} + \frac{\partial N_i^{(e)}}{\partial z} k_z \frac{\partial N_j^{(e)}}{\partial z} \right) d\Omega}^{K_{dij}^{(e)}} + \\ &+ \underbrace{\iint_{\Gamma_q^{(e)}} \alpha N_i^{(e)} N_j^{(e)} d\Gamma}_{K_{cij}^{(e)}} = K_{kij}^{(e)} + K_{cij}^{(e)} \end{aligned} \quad (5.14)$$

$K_{dij}^{(e)}$ is the conduction stiffness term and $K_{cij}^{(e)}$ is the convection stiffness term. The second integral only appears in the Neumann boundary part where the convection condition is prescribed.

For the flux vector

$$f_i^{(e)} = \underbrace{\iiint_{\Omega^{(e)}} N_i^{(e)} Q d\Omega}_{f_{Q_i}^{(e)}} - \underbrace{\iint_{\Gamma_q^{(e)}} N_i^{(e)} (\bar{q} - \alpha \phi_a) d\Gamma}_{f_{c_i}^{(e)}} - q_{n_i}^{(e)} \quad (5.15)$$

where $f_{Q_i}^{(e)}$ is the nodal flux term related to the heat source Q , $f_{c_i}^{(e)}$ is the nodal flux term related to the prescribed heat flux at the Neumann boundary and $q_{n_i}^{(e)} = \iint_{\Gamma_q^{(e)}} N_i^{(e)} q_n d\Gamma$ is the reaction flux in the node where the value of ϕ is prescribed. Again, the term $f_{c_i}^{(e)}$ will be considered only in nodes that belong to the Neumann boundary.

In the next section the above expressions will be particularized the four-noded tetrahedral element.

5.4 FOUR-NODED TETRAHEDRAL ELEMENT

In this section the four-noded tetrahedral element will be considered. This element is also known as the linear tetrahedron (Figure 5.3).

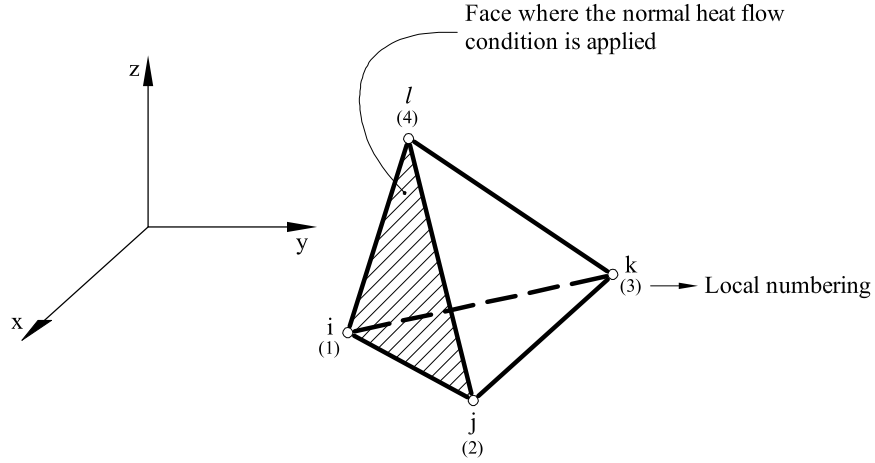


Figure 5.3: Four-noded tetrahedral element.

The linear tetrahedron is the simplest 3D element, similarly as the three-noded triangular element is the simplest element for 2D problems. Both element families have similar properties.

The approximation of the unknown field inside each tetrahedron is expressed by the following linear polynomial interpolation

$$\phi^{(e)} = \alpha_0 + \alpha_1 x + \alpha_2 y + \alpha_3 z \quad (5.16)$$

From the above expression we can deduce

$$\begin{aligned} \phi_1^{(e)} &= \alpha_0 + \alpha_1 x_1^{(e)} + \alpha_2 y_1^{(e)} + \alpha_3 z_1^{(e)} \\ \phi_2^{(e)} &= \alpha_0 + \alpha_1 x_2^{(e)} + \alpha_2 y_2^{(e)} + \alpha_3 z_2^{(e)} \\ \phi_3^{(e)} &= \alpha_0 + \alpha_1 x_3^{(e)} + \alpha_2 y_3^{(e)} + \alpha_3 z_3^{(e)} \\ \phi_4^{(e)} &= \alpha_0 + \alpha_1 x_4^{(e)} + \alpha_2 y_4^{(e)} + \alpha_3 z_4^{(e)} \end{aligned} \quad (5.17)$$

Solving this equation system and substituting the expression for α_i into Eq.(5.16) and reordering terms yields:

$$\phi = \sum_{i=1}^4 N_i^{(e)}(x, y, z) \phi_i^{(e)} = N_1^{(e)}(x, y, z) \phi_1^{(e)} + \dots + N_4^{(e)}(x, y, z) \phi_4^{(e)} \quad (5.18)$$

where

$$N_i^{(e)}(x, y, z) = \frac{1}{6\Omega^{(e)}} (a_i^{(e)} + b_i^{(e)}(x) + c_i^{(e)}y + d_i^{(e)}z) \quad (5.19)$$

with

$$\begin{aligned} a_i^{(e)} &= \begin{vmatrix} x_j^{(e)} & y_j^{(e)} & z_j^{(e)} \\ x_k^{(e)} & y_k^{(e)} & z_k^{(e)} \\ x_l^{(e)} & y_l^{(e)} & z_l^{(e)} \end{vmatrix}; & b_i^{(e)} &= - \begin{vmatrix} 1 & y_j^{(e)} & z_j^{(e)} \\ 1 & y_k^{(e)} & z_k^{(e)} \\ 1 & y_l^{(e)} & z_l^{(e)} \end{vmatrix} \\ c_i^{(e)} &= \begin{vmatrix} x_j^{(e)} & 1 & z_j^{(e)} \\ x_k^{(e)} & 1 & z_k^{(e)} \\ x_l^{(e)} & 1 & z_l^{(e)} \end{vmatrix}; & d_i^{(e)} &= - \begin{vmatrix} x_j^{(e)} & y_j^{(e)} & 1 \\ x_k^{(e)} & y_k^{(e)} & 1 \\ x_l^{(e)} & y_l^{(e)} & 1 \end{vmatrix} \end{aligned} \quad (5.20)$$

The rest of the constants can be obtained by rotating the indexes (i, j, k, l) using the right-hand rule

The element volume $\Omega^{(e)}$ can be found from the following determinant

$$6\Omega^{(e)} = \begin{vmatrix} 1 & x_i^{(e)} & y_i^{(e)} & z_i^{(e)} \\ 1 & x_j^{(e)} & y_j^{(e)} & z_j^{(e)} \\ 1 & x_k^{(e)} & y_k^{(e)} & z_k^{(e)} \\ 1 & x_l^{(e)} & y_l^{(e)} & z_l^{(e)} \end{vmatrix} \quad (5.21)$$

The three dimensional shape functions forms are hyper-planes and $N_i^{(e)}$ can not be visualized as for the 2D problem. Note however that, as usual, the shape function $N_i^{(e)}$ take a unit value at the node and zero at the rest of the nodes.

Another difficulty related to 3D elements is the visualization of the results. There are some methodologies to help with this task, like the previous subdivision in hexahedra followed by an automatic division in tetrahedra.

From the shape functions expression we deduce:

$$\frac{\partial N_i^{(e)}}{\partial x} = \frac{b_i}{6\Omega^{(e)}}; \quad \frac{\partial N_i}{\partial y} = \frac{c_i}{6\Omega^{(e)}}; \quad \frac{\partial N_i}{\partial z} = \frac{d_i}{6\Omega^{(e)}} \quad (5.22)$$

Substituting into $\mathbf{K}_{ij}^{(e)}$ gives

$$K_{d_{ij}}^{(e)} = \frac{1}{36\Omega^{(e)}}(k_x b_i b_j + k_y c_i c_j + k_z d_i d_j) \quad (5.23)$$

and

$$\mathbf{K}_d^{(e)} = \frac{1}{36\Omega^{(e)}} \begin{bmatrix} k_x b_1 b_1 + k_y c_1 c_1 + k_z d_1 d_1 & \dots & k_x b_1 b_4 + k_y c_1 c_4 + \dots + k_z d_1 d_4 \\ k_x b_2 b_1 + k_y c_2 c_1 + k_z d_2 d_1 & \dots & k_x b_2 b_4 + k_y c_2 c_4 + \dots + k_z d_2 d_4 \\ k_x b_3 b_1 + k_y c_3 c_1 + k_z d_3 d_1 & \dots & k_x b_3 b_4 + k_y c_3 c_4 + \dots + k_z d_3 d_4 \\ k_x b_4 b_1 + k_y c_4 c_1 + k_z d_4 d_1 & \dots & k_x b_4 b_4 + k_y c_4 c_4 + \dots + k_z d_4 d_4 \end{bmatrix} \quad (5.24)$$

is the conductivity stiffness matrix for the element.

The general expression for the element convection stiffness matrix is

$$\mathbf{K}_c^{(e)} = \iint_{\Gamma_q^{(e)}} \begin{bmatrix} N_1^{(e)} N_1^{(e)} & \dots & N_1^{(e)} N_4^{(e)} \\ \vdots & \ddots & \vdots \\ N_4^{(e)} N_1^{(e)} & \dots & N_4^{(e)} N_4^{(e)} \end{bmatrix} \alpha d\Gamma \quad (5.25)$$

The tetrahedron boundaries correspond to the element faces (Figure 5.3). In that way the shape function $N_i^{(e)}$ will have a null value if the i -th node does not belong to the face where the integral is evaluated. From the shape function expression it is easy to obtain:

$$K_{c_{ij}}^{(e)} = \iint_{\Gamma_q^{(e)}} \alpha N_i^{(e)} N_j^{(e)} d\Gamma = \begin{cases} \frac{\alpha A^{(e)}}{6}; & i = j \\ \frac{\alpha A^{(e)}}{12}; & i \neq j \end{cases} \quad (5.26)$$

where $A^{(e)}$ is the tetrahedron's face area where the convection boundary is prescribed.

As an example, for the face 1-2-4 of the tetrahedron shown in Figure 5.3, $N_3^{(e)} = 0$ and

$$\mathbf{K}_{c_{124}}^{(e)} = \iint_{\Gamma_{q_{124}}^{(e)}} \alpha \begin{bmatrix} N_1^{(e)} N_1^{(e)} & N_1^{(e)} N_2^{(e)} & 0 & N_1^{(e)} N_4^{(e)} \\ N_2^{(e)} N_1^{(e)} & N_2^{(e)} N_2^{(e)} & 0 & N_2^{(e)} N_4^{(e)} \\ 0 & 0 & 0 & 0 \\ N_4^{(e)} N_1^{(e)} & N_4^{(e)} N_2^{(e)} & 0 & N_4^{(e)} N_4^{(e)} \end{bmatrix} d\Gamma \quad (5.27)$$

If α is constant over the face 1-2-4

$$\mathbf{K}_{c_{124}}^{(e)} = \frac{\alpha A_{124}^{(e)}}{6} \begin{bmatrix} 1 & 1/2 & 0 & 1/2 \\ 1/2 & 1 & 0 & 1/2 \\ 0 & 0 & 0 & 0 \\ 1/2 & 1/2 & 0 & 1 \end{bmatrix} \quad (5.28)$$

The same procedure is followed to evaluate $\mathbf{K}_c^{(e)}$ over the other faces of the tetrahedron.

As a conclusion, the element stiffness matrix can be written as:

$$\mathbf{K}^{(e)} = \mathbf{K}_d^{(e)} + \mathbf{K}_{c_{123}}^{(e)} + \mathbf{K}_{c_{124}}^{(e)} + \mathbf{K}_{c_{134}}^{(e)} + \mathbf{K}_{c_{234}}^{(e)} \quad (5.29)$$

The equivalent nodal flux vector for a uniformly distributed heat source is

$$\mathbf{f}_Q^{(e)} = \begin{Bmatrix} f_{Q_1}^{(e)} \\ f_{Q_2}^{(e)} \\ f_{Q_3}^{(e)} \\ f_{Q_4}^{(e)} \end{Bmatrix} = \iiint_{\Omega} \begin{Bmatrix} N_1^{(e)} \\ N_2^{(e)} \\ N_3^{(e)} \\ N_4^{(e)} \end{Bmatrix} Q d\Omega \quad (5.30)$$

If Q is constant over the element

$$\mathbf{f}_Q^{(e)} = \frac{Q\Omega^{(e)}}{4} \begin{Bmatrix} 1 \\ 1 \\ 1 \\ 1 \end{Bmatrix} \quad (5.31)$$

Note that in this case the total flux over the element is uniformly distributed in all the element's nodes, similarly as for the 3-noded triangle.

The vector associated to the ijl face where the normal flux is prescribed (Figure 5.3) is

$$\mathbf{f}_{c_{ijl}}^{(e)} = - \iint_{\Gamma_{q_{ijl}}^{(e)}} (\bar{q}_n - \alpha\phi_a) \begin{Bmatrix} N_i^{(e)} \\ N_j^{(e)} \\ N_k^{(e)} \\ N_l^{(e)} \end{Bmatrix} d\Gamma = - \iint_{A_{ijl}^{(e)}} (\bar{q}_n - \alpha\phi_a) \begin{Bmatrix} N_i^{(e)} \\ N_j^{(e)} \\ 0 \\ N_l^{(e)} \end{Bmatrix} d\Gamma \quad (5.32)$$

where $A_{ijl}^{(e)}$ is the ijl side area where $N_k^{(e)} = 0$. If \bar{q}_n , α and ϕ_a are constant over the face, then

$$\mathbf{f}_{c_{ijl}}^{(e)} = -\frac{A_{ijl}^{(e)}}{3}(\bar{q}_n - \alpha\phi_a) \begin{Bmatrix} 1 \\ 1 \\ 0 \\ 1 \end{Bmatrix} \quad (5.33)$$

In a similar form, the expression for $\mathbf{f}_c^{(e)}$ can be obtained for the other faces where the normal flux is prescribed.

As a conclusion, the element equivalent flux vector can be written as:

$$\mathbf{f}^{(e)} = \mathbf{f}_Q^{(e)} + \mathbf{f}_{c_{123}}^{(e)} + \mathbf{f}_{c_{124}}^{(e)} + \mathbf{f}_{c_{134}}^{(e)} + \mathbf{f}_{c_{234}}^{(e)} \quad (5.34)$$

where

$$\mathbf{f}_{234} = -\frac{A_{234}^{(e)}}{3}(\bar{q}_n - \alpha\phi_a) \begin{Bmatrix} 0 \\ 1 \\ 1 \\ 1 \end{Bmatrix}, \quad \text{etc.} \quad (5.35)$$

Chapter 6

MATRIX FORMULATION FOR THE FEM SOLUTION OF THE POISSON EQUATION

6.1 INTRODUCTION

In previous sections the Poisson equation has been analysed for 1D, 2D and 3D problems with the FEM. In this section, the FEM solution will be presented in a general form using a matrix formulation. This approach is useful to treat in a similar manner many other problems solved with the FEM.

6.2 MATRIX FORMULATION OF THE POISSON EQUATION

The heat flow balance equation over an infinitesimal domain for 1D, 2D or 3D problems can be expressed in a matrix form as

$$\nabla^T \mathbf{q} - Q = 0 \quad (6.1)$$

where ∇ is the gradient vector operator and \mathbf{q} is flux vector given by

$$\begin{aligned} 1\text{D: } \nabla &= \left[\frac{\partial}{\partial x} \right], \quad \mathbf{q} = [q] \\ 2\text{D: } \nabla &= \left[\frac{\partial}{\partial x}, \frac{\partial}{\partial y} \right]^T, \quad \mathbf{q} = [q_x, q_y]^T \\ 3\text{D: } \nabla &= \left[\frac{\partial}{\partial x}, \frac{\partial}{\partial y}, \frac{\partial}{\partial z} \right]^T, \quad \mathbf{q} = [q_x, q_y, q_z]^T \end{aligned} \quad (6.2)$$

The extended form of Eq.(6.1) corresponds to the heat flow balance equation obtained in previous chapters. For example, Eq.(6.1) has the following form for 2D problems:

$$\left[\frac{\partial}{\partial x}, \frac{\partial}{\partial y} \right] \begin{Bmatrix} q_x \\ q_y \end{Bmatrix} - Q = \frac{\partial q_x}{\partial x} + \frac{\partial q_y}{\partial y} - Q = 0 \quad (6.3)$$

The gradient vector is defined as

$$\mathbf{g} = \nabla \phi \quad (6.4)$$

where

$$\begin{aligned}
1\text{D: } \mathbf{g} &= [g] = \left[\frac{\partial \phi}{\partial x} \right] \\
2\text{D: } \mathbf{g} &= [g_x, g_y]^T = \left[\frac{\partial \phi}{\partial x}, \frac{\partial \phi}{\partial y} \right]^T \\
3\text{D: } \mathbf{g} &= [g_x, g_y, g_z]^T = \left[\frac{\partial \phi}{\partial x}, \frac{\partial \phi}{\partial y}, \frac{\partial \phi}{\partial z} \right]^T
\end{aligned} \tag{6.5}$$

The relationship between the heat flow vector and the gradient vector is defined by Fourier's law

$$\mathbf{q} = -\mathbf{D}\mathbf{g} = -\mathbf{D}\nabla\phi \tag{6.6}$$

where \mathbf{D} is the conductivity matrix given by

$$\begin{aligned}
1\text{D: } \mathbf{D} &= [k] \\
2\text{D: } \mathbf{D} &= \begin{bmatrix} k_x & 0 \\ 0 & k_y \end{bmatrix} \\
3\text{D: } \mathbf{D} &= \begin{bmatrix} k_x & 0 & 0 \\ 0 & k_y & 0 \\ 0 & 0 & k_z \end{bmatrix}
\end{aligned} \tag{6.7}$$

Substituting Eq.(6.6) into (6.1) the matrix form of the flux balance equation is obtained as

$$\boxed{\nabla^T(\mathbf{D}\nabla\phi) + Q = 0 \quad \text{en } \Omega} \tag{6.8}$$

Expanding this equation, the usual form of the Poisson equation is obtained. For 2D problems

$$\left[\frac{\partial}{\partial x}, \frac{\partial}{\partial y} \right] \begin{bmatrix} k_x & 0 \\ 0 & k_y \end{bmatrix} \left\{ \begin{array}{c} \frac{\partial \phi}{\partial x} \\ \frac{\partial \phi}{\partial y} \end{array} \right\} + Q = \frac{\partial}{\partial x} \left(k_x \frac{\partial \phi}{\partial x} \right) + \frac{\partial}{\partial y} \left(k_y \frac{\partial \phi}{\partial y} \right) + Q = 0 \tag{6.9}$$

The boundary conditions can be described in a general way as follows.

Prescribed variable condition

$$\phi - \bar{\phi} = 0 \quad \text{on } \Gamma_\phi \tag{6.10}$$

Prescribed flux condition

$$\mathbf{n}^T \mathbf{D}\nabla\phi + \bar{q}_n + \alpha(\phi - \phi_q) = 0 \quad \text{on } \Gamma_q \tag{6.11}$$

where \mathbf{n} is the external normal to the boundary Γ_q and the rest of the terms have the usual meaning.

6.3 WEAK INTEGRAL FORM

The equivalent weak integral form of the balance equation and the boundary conditions can be obtained from the GWR method as

$$\int_{\Omega} W[\nabla^T \mathbf{D} \nabla \phi + Q] + \oint_{\Gamma_q} \bar{W}[\mathbf{n}^T \mathbf{D} \nabla \phi + \bar{q}_n + \alpha(\phi - \phi_a)] d\Gamma = 0 \quad (6.12)$$

Integrating by parts the term with second derivatives in the first integral and selecting $\bar{W} = -W$, the weak form is obtained as

$$-\int_{\Omega} (\nabla^T W) \mathbf{D} \nabla \phi d\Omega + \int_{\Omega} W Q d\Omega - \int_{\Gamma_q} W[\bar{q}_n - \alpha(\phi - \phi_a)] d\Gamma + \int_{\Gamma_{\phi}} W \mathbf{n}^T \mathbf{D} \nabla \phi d\Omega = 0 \quad (6.13)$$

Having in mind the definition of the heat flow and selecting $W = \delta\phi$ as the virtual variation of the unknown and $\nabla = \delta\mathbf{g}$ as the *virtual gradient vector*, the weak form can be rewritten as

$$\int_{\Omega} \delta\mathbf{g}^T \mathbf{q} d\Omega + \int_{\Omega} \delta\phi Q d\Omega - \int_{\Gamma_q} \delta\phi[\bar{q}_n - \alpha(\phi - \phi_a)] d\Gamma - \int_{\Gamma_{\phi}} \delta\phi q_n d\Gamma = 0 \quad (6.14)$$

Eq.(6.14) can be named as the *virtual variation principle* and it is equivalent to the virtual work principle for solid mechanics. The virtual field $\delta\phi$ satisfies the boundary conditions at the Dirichlet boundary. Therefore if $\phi = 0$ on Γ_{ϕ} then also $\delta\phi = 0$ on Γ_{ϕ} and the last integral in (6.14) can be omitted.

The integral expression in (6.13) (or the equivalent one in (6.14)) is the starting point for deriving the FEM discretized equations.

6.4 MATRIX FORM OF THE FEM EQUATIONS

The finite element approximation is expressed for a n -noded element in matrix form as

$$\phi = \sum_{i=1}^n N_i^{(e)} \phi_i^{(e)} = [N_1^{(e)}, N_2^{(e)}, \dots, N_n^{(e)}] \begin{Bmatrix} \phi_1^{(e)} \\ \phi_2^{(e)} \\ \vdots \\ \phi_n^{(e)} \end{Bmatrix} = \mathbf{N}^{(e)} \mathbf{a}^{(e)} \quad (6.15)$$

with

$$\begin{aligned} \mathbf{N}^{(e)} &= [N_1^{(e)}, N_2^{(e)}, \dots, N_n^{(e)}] \\ \mathbf{a}^{(e)} &= [\phi_1^{(e)}, \phi_2^{(e)}, \dots, \phi_n^{(e)}]^T \end{aligned} \quad (6.16)$$

The $\mathbf{N}^{(e)}$ matrix is the *shape function matrix* and $\mathbf{a}^{(e)}$ is the *nodal variable vector* for the element.

The gradient vector is expressed as a function of the elemental nodal variables by

$$\mathbf{g} = \nabla\phi = [\nabla\mathbf{N}^{(e)}] \mathbf{a}^{(e)} = [\nabla\mathbf{N}^{(e)}] \mathbf{a}^{(e)} = \mathbf{B}_i^{(e)} \mathbf{a}^{(e)} \quad (6.17)$$

where $\mathbf{B}^{(e)}$ is the gradient matrix for the element defined by

$$\begin{aligned} \mathbf{B}^{(e)} &= \nabla\mathbf{N}^{(e)} = \nabla[N_1^{(e)}, N_2^{(e)}, \dots, N_n^{(e)}] = \\ &= [\nabla N_1^{(e)}, \nabla N_2^{(e)}, \dots, \nabla N_n^{(e)}] = [\mathbf{B}_1^{(e)}, \mathbf{B}_2^{(e)}, \dots, \mathbf{B}_n^{(e)}] \end{aligned} \quad (6.18)$$

where $\mathbf{B}_i^{(e)} = \nabla N_i^{(e)}$ is the gradient matrix for the i -th node of element e . Note that $\mathbf{B}^{(e)}$ is formed by as many $\mathbf{B}_i^{(e)}$ sub-matrices as nodes has the element. For example, for a 3-noded triangular element

$$\mathbf{B}^{(e)} = \left[\begin{array}{c|c|c} \frac{\partial N_1^{(e)}}{\partial x} & \frac{\partial N_2^{(e)}}{\partial x} & \frac{\partial N_3^{(e)}}{\partial x} \\ \hline \frac{\partial N_1^{(e)}}{\partial y} & \frac{\partial N_2^{(e)}}{\partial y} & \frac{\partial N_3^{(e)}}{\partial y} \end{array} \right]; \quad \mathbf{B}_i^{(e)} = \left[\begin{array}{c} \frac{\partial N_i^{(e)}}{\partial x} \\ \frac{\partial N_i^{(e)}}{\partial y} \end{array} \right] = \frac{1}{2A^{(e)}} \left\{ \begin{array}{c} b_i^{(e)} \\ c_i^{(e)} \end{array} \right\} \quad (6.19)$$

The heat flux vector is expressed in terms of the nodal variables as:

$$\mathbf{q} = -\mathbf{D}\mathbf{g} = -\mathbf{D}\mathbf{B}^{(e)} \mathbf{a}^{(e)} \quad (6.20)$$

Substituting Eqs.(6.17) and (6.18) into the integral expression ((6.13)) and selecting the Galerkin form with $W_i = \delta\phi = N_i$ the discretized equations system is obtained in the standard form $\mathbf{K}\mathbf{a} = \mathbf{f}$. The \mathbf{K} matrix and the \mathbf{f} vector are obtained by assembling the element contributions as usual.

The element stiffness matrix expression is

$$\mathbf{K}^{(e)} = \int_{\Omega^{(e)}} \mathbf{B}^{(e)T} \mathbf{D}\mathbf{B}^{(e)} d\Omega + \int_{\Gamma_q^{(e)}} \alpha [\mathbf{N}^{(e)}]^T \mathbf{N}^{(e)} d\Gamma \quad (6.21)$$

with

$$K_{ij}^{(e)} = \int_{\Omega^{(e)}} [\mathbf{B}_i^{(e)}]^T \mathbf{D}\mathbf{B}_j^{(e)} d\Omega + \int_{\Gamma_q^{(e)}} \alpha N_i^{(e)} N_j^{(e)} d\Gamma \quad (6.22)$$

The expression for $\mathbf{K}^{(e)}$ holds for 1, 2 and 3 dimensional problems. For each case the integrals are computed over the corresponding elemental domain and the element boundaries belonging to the external Neumann boundary where the normal flux is prescribed.

The equivalent nodal flux vector can be written in matrix form as:

$$\mathbf{f}^{(e)} = \int_{\Omega^{(e)}} [\mathbf{N}^{(e)}]^T Q d\Omega - \oint_{\Gamma_q^{(e)}} [\mathbf{N}^{(e)}]^T [\bar{q}_n - \alpha\phi_a] - \mathbf{r}^{(e)} \quad (6.23)$$

with

$$f_i^{(e)} = \int_{\Omega^{(e)}} N_i^{(e)} Q d\Omega - \oint_{\Gamma_q^{(e)}} N_i^{(e)} [\bar{q}_n - \alpha\phi_a] d\Gamma - q_{n_i}^{(e)} \quad (6.24)$$

As usual, the integrals are evaluated over the corresponding elemental domain.

The $\mathbf{r}^{(e)}$ vector corresponds to the unknown “reaction” flux in the nodes where the ϕ variable is prescribed. These fluxes are computed “a posteriori” once the solution for the nodal value of ϕ is found.

It is important to note that the matrix formulation provides a general framework for solving any Poisson problem in 1D, 2D and 3D. The matrix formulation presented in this section is applied in similar way to solid mechanics and fluid mechanics problems solved using the FEM.

6.5 THE MATRIX EQUILIBRIUM EQUATIONS OBTAINED FROM THE NODAL FLUXES

The usual procedure to obtain the global equations system is applying the concept of nodal flux balance (equilibrium). The process is similar to using Kirchhoff’s law in electrical networks or in hydraulic networks. Expressing the fluxes in the element “sides” as a function of the nodal variables and the external actions via the balance equilibrium equation for each element, and imposing flux balance at all nodes yields the global equilibrium equations as $\mathbf{K}\mathbf{a} = \mathbf{f}$. The “flux addition” procedure allows to obtain \mathbf{K} and \mathbf{f} by assembling the expressions for $\mathbf{K}^{(e)}$ and $\mathbf{f}^{(e)}$ for each element.

The flux balance expression will be described for the 1D and 2D elements shown in Figure 6.1.

6.5.1 One dimensional 2-noded element

We will start with the simplest 1D element under a uniform flux Q and two nodal fluxes $q_1^{(e)}$ y $q_2^{(e)}$ applied at nodes 1 and 2 respectively.

Let us consider the global flux balance expression over the element written in the weak integral form, or the equivalent expression derived from the virtual variation principle

$$\int_{I^{(e)}} \delta \mathbf{g}^T q dx + \int_{I^{(e)}} \delta \phi Q dx - \delta \phi_1^{(e)} q_1^{(e)} - \delta \phi_2^{(e)} q_2^{(e)} = 0 \quad (6.25)$$

The negative signs in the above equation are due the flux definition for $q_1^{(e)}$ and $q_2^{(e)}$ which go out the element (the heat goes out the element).

Note that $\delta \phi$ are virtual variations of ϕ and $\delta \mathbf{g}$ is the virtual gradient field ($\delta \mathbf{g} = \nabla \delta \phi$).

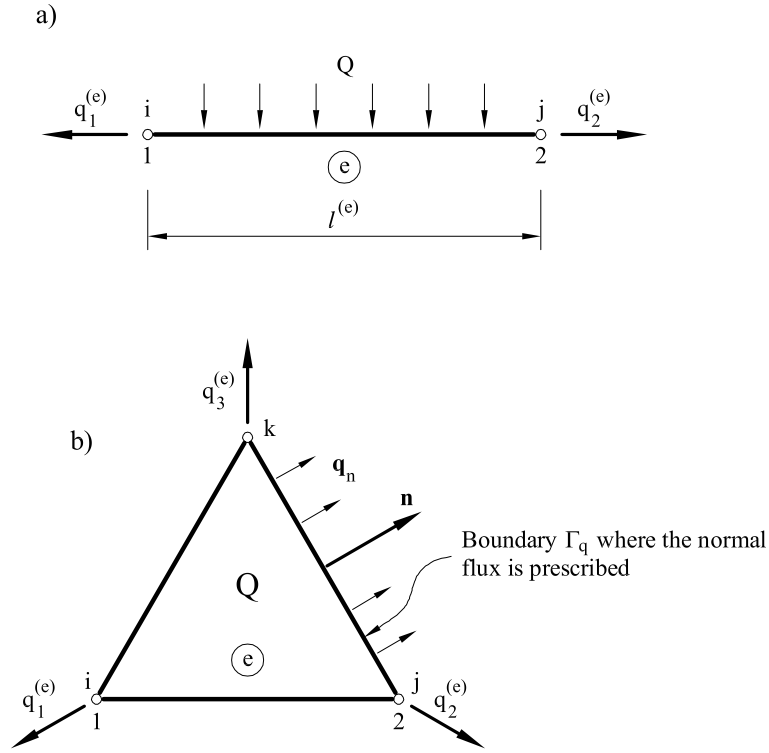


Figure 6.1: Flux balance in a 1D 2-noded element (a) and in a 2D 3-noded triangle (b)

Eq.(6.25) allows expressing the “virtual work” produced by the nodal fluxes in terms of the elemental variables as:

$$[\delta \mathbf{a}^{(e)}]^T \mathbf{q}^{(e)} = \int_{l^{(e)}} \delta g q d\Omega + \int_{l^{(e)}} \delta \phi Q d\Omega \quad (6.26)$$

with

$$\delta \mathbf{a}^{(e)} = [\delta \phi_1^{(e)}, \delta \phi_2^{(e)}]^T, \quad \mathbf{q}^{(e)} = [q_1^{(e)}, q_2^{(e)}]^T \quad (6.27)$$

where $\mathbf{q}^{(e)}$ is the so called vector of the interelemental balancing nodal fluxes.

Let us substitute the FEM approximation into Eq.(6.26). The ϕ and $\delta \phi$ fields can be expressed inside each element in a matrix form by

$$\phi = \sum_{i=1}^2 N_i^{(e)} \phi_i^{(e)} = \mathbf{N}^{(e)} \mathbf{a}^{(e)} \quad (6.28)$$

$$\delta \phi = \sum_{i=1}^2 N_i^{(e)} \delta \phi_i^{(e)} = \mathbf{N}^{(e)} \delta \mathbf{a}^{(e)} \quad (6.29)$$

with

$$\mathbf{N}^{(e)} = [N_1^{(e)}, N_2^{(e)}], \quad \mathbf{a}^{(e)} = [\phi_1^{(e)}, \phi_2^{(e)}]^T \quad (6.30)$$

and

$$\delta \mathbf{a}^{(e)} = [\delta \phi_1^{(e)}, \delta \phi_2^{(e)}]^T \quad (6.31)$$

The virtual gradient is expressed in terms of the nodal virtual variables by

$$\delta g = \nabla \delta \phi = [\nabla \mathbf{N}^{(e)}] \delta \mathbf{a}^{(e)} = \mathbf{B}^{(e)} \delta \mathbf{a}^{(e)} \quad (6.32)$$

with

$$\nabla = \left[\frac{\partial}{\partial x} \right], \quad \mathbf{B}^{(e)} = [B_1^{(e)}, B_2^{(e)}], \quad B_i^{(e)} = \left[\frac{\partial N_i^{(e)}}{\partial x} \right] \quad (6.33)$$

Substituting the above expression into (6.26) and extracting $\delta \mathbf{a}^{(e)}$ in the second term gives

$$[\delta \mathbf{a}^{(e)}]^T \mathbf{q}^{(e)} = [\delta \mathbf{a}^{(e)}]^T \left\{ - \left[\int_{l^{(e)}} [\mathbf{B}^{(e)}]^T \mathbf{D} \mathbf{B}^{(e)} d\Omega \right] \mathbf{a}^{(e)} + \int_{l^{(e)}} [\mathbf{N}^{(e)}]^T Q d\Omega \right\} \quad (6.34)$$

Having in mind that the virtual variables $\delta \phi_i^{(e)}$ are arbitrary, the above equation must be true for any value of $\delta \mathbf{a}^{(e)}$; this gives

$$\boxed{\mathbf{q}^{(e)} = - \left[\int_{l^{(e)}} [\mathbf{B}^{(e)}]^T \mathbf{D} \mathbf{B}^{(e)} dx \right] \mathbf{a}^{(e)} + \int_{l^{(e)}} [\mathbf{N}^{(e)}]^T Q dx} \quad (6.35)$$

or

$$\boxed{\mathbf{q}^{(e)} = -\mathbf{K}^{(e)} \mathbf{a}^{(e)} + \mathbf{f}^{(e)}} \quad (6.36)$$

where

$$\mathbf{K}^{(e)} = \int_{l^{(e)}} [\mathbf{B}^{(e)}]^T \mathbf{D} \mathbf{B}^{(e)} dx \quad (6.37)$$

$$\mathbf{f}^{(e)} = \int_{l^{(e)}} [\mathbf{N}^{(e)}]^T Q dx \quad (6.38)$$

are the elemental stiffness matrix and the nodal flux vector due the uniform distributed Q source.

Eq.(6.36) is the *flux balance* equation for the element and express the equilibrium (balance) between the interelemental balancing nodal fluxes, the nodal flux dues the Q source and the fluxes due the gradient of ϕ inside the element.

Note the analogy between Eq.(6.36) and the equation expression the equilibrium of nodal forces for a discrete system (Eq.(1.6)). This analogy also holds for the assembling process.

Eq.(6.36) is the key to obtain the global equilibrium equation in terms of the nodal variables. The process is similar to that explained for discrete systems. For each node the equilibrium of fluxes is considered taking into account the contribution from all the elements sharing the node.

Therefore the expression for balance of nodal fluxes is written as

$$\sum_e q_i^{(e)} = q_j^{\text{ext}} \quad j = 1, 2, \dots, N \quad (6.39)$$

where the sum is over all the elements that share the node with global number j , q_j^{ext} is the external flux that goes into the j node (in general $q_j^{\text{ext}} = 0$) and N is the total number of nodes in the mesh.

Expressing the values of $q_i^{(e)}$ in terms of the nodal variables $\mathbf{a}^{(e)}$ and the external fluxes $\mathbf{f}^{(e)}$ via Eq.(6.36), the global system of equations is obtained in the usual form $\mathbf{K}\mathbf{a} = \mathbf{f}$. The stiffness matrix \mathbf{K} and the nodal flux vector \mathbf{f} are assembled from the element contributions following the same rules as for the discrete systems.

It is important to understand that this assembling process coincides with that explained in the previous chapter using the weak integral form and the additive properties of the integrals defined over the analysis domain.

To clarify this concept the assembling process will be repeated for the three-noded triangular element.

6.5.2 2D three-noded triangular element

Consider the three-noded triangular element shown in Figure 6.1b. The element is subjected to a uniform distributed source Q , to the normal fluxes through the boundaries sides Γ_q and to the interelemental fluxes. The flux balance expression for all the fluxes and the inner gradients can be expressed by the virtual variation principle as:

$$\iint_{\Omega^{(e)}} [\delta \mathbf{g}^{(e)}]^T \mathbf{q} d\Omega + \iint_{\Omega^{(e)}} \delta \phi Q d\Omega - \int_{\Gamma_q^{(e)}} \delta \phi \bar{q}_n d\Gamma - [\delta \mathbf{a}^{(e)}]^T \mathbf{q}^{(e)} = 0 \quad (6.40)$$

where

$$\delta \mathbf{g}^{(e)} = [\delta g_x, \delta g_y]^T = \nabla(\delta \phi) \quad (6.41)$$

$$\mathbf{q} = [q_x, q_y]^T = -\mathbf{D}\mathbf{g} = -\mathbf{D}\nabla\phi, \quad \nabla = \left\{ \begin{array}{c} \frac{\partial}{\partial x} \\ \frac{\partial}{\partial y} \end{array} \right\} \quad (6.42)$$

$$\delta \mathbf{a}^{(e)} = [\delta \phi_1^{(e)}, \delta \phi_2^{(e)}, \delta \phi_3^{(e)}]^T \quad (6.43)$$

$$\mathbf{q}^{(e)} = [q_1^{(e)}, q_2^{(e)}, q_3^{(e)}]^T \quad (6.44)$$

In the above expressions $q_i^{(e)}$ is the interelemental nodal flux that goes out through the i -th node. This flux can be expressed as the sum of the fluxes in the x and y directions.

It is important to note that the third integral in the expression (6.40) only should be considered if the element has sides on the Neumann boundary where the flux is prescribed to \bar{q}_n . For elements laying in the interior domain, the fluxes along the sides cancel out in the assembly process, as these fluxes are identical but with opposite sign for the two elements sharing a side. Also, if any convection with the external environment exist it is necessary to add the term $\alpha(\phi - \phi_a)$ to \bar{q}_n . For simplicity reasons we do not consider this term here.

The FEM discretization is written in matrix form as

$$\phi = \sum_{i=1}^3 N_i^{(e)} \phi_i^{(e)} = \mathbf{N}^{(e)} \mathbf{a}^{(e)} \quad (6.45)$$

$$\mathbf{g} = \mathbf{B}^{(e)} \mathbf{a}^{(e)}, \quad \delta \mathbf{g} = \mathbf{B}^{(e)} \delta \mathbf{a}^{(e)} \quad (6.46)$$

$$\mathbf{q} = -\mathbf{D} \mathbf{g} = -\mathbf{D} \mathbf{B}^{(e)} \mathbf{a}^{(e)} \quad (6.47)$$

with

$$\mathbf{N}^{(e)} = [N_1^{(e)}, N_2^{(e)}, N_3^{(e)}] \quad (6.48)$$

$$\mathbf{B}^{(e)} = [\mathbf{B}_1^{(e)}, \mathbf{B}_2^{(e)}, \mathbf{B}_3^{(e)}], \quad \mathbf{B}_i^{(e)} = \nabla N_i^{(e)} = \begin{bmatrix} \frac{\partial N_i^{(e)}}{\partial x} \\ \frac{\partial N_i^{(e)}}{\partial y} \end{bmatrix} \quad (6.49)$$

$$\mathbf{D} = \begin{bmatrix} k_x & 0 \\ 0 & k_y \end{bmatrix} \quad (6.50)$$

Substituting these expressions into the integral form and extracting $\delta \mathbf{a}^{(e)}$ we obtain

$$\begin{aligned} [\delta \mathbf{a}^{(e)}]^T \mathbf{q}^{(e)} &= [\delta \mathbf{a}^{(e)}]^T \left\{ \left[- \iint_{\Omega^{(e)}} [\mathbf{B}^{(e)}]^T \mathbf{D} \mathbf{B}^{(e)} d\Omega \right] \mathbf{a}^{(e)} + \right. \\ &\quad \left. + \left[\iint_{\Omega^{(e)}} [\mathbf{N}^{(e)}]^T Q d\Omega - \oint_{\Gamma_q^{(e)}} [\mathbf{N}^{(e)}]^T \bar{q}_n d\Gamma \right] \right\} \end{aligned} \quad (6.51)$$

This gives

$$\mathbf{q}^{(e)} = -\mathbf{K}^{(e)} \mathbf{a}^{(e)} + \mathbf{f}^{(e)} \quad (6.52)$$

with

$$K_{ij}^{(e)} = \iint_{\Omega^{(e)}} [\mathbf{B}_i^{(e)}]^T \mathbf{D} \mathbf{B}_j^{(e)} d\Omega \quad (6.53)$$

$$f_i^{(e)} = \iint_{\Omega^{(e)}} N_i^{(e)} Q d\Omega - \oint_{\Gamma_q^{(e)}} N_i^{(e)} \bar{q}_n d\Gamma$$

The assembling process follows the usual steps of imposing the equilibrium of nodal fluxes as

$$\sum_e q_i^{(e)} = q_j^{\text{ext}} \quad j = 1, 2, \dots, N \quad (6.54)$$

Substituting in (6.54) the expressions for $q_i^{(e)}$ from Eq.(6.53) we obtain the global equation systems of equations in matrix form $\mathbf{K} \mathbf{a} = \mathbf{f}$ where matrix \mathbf{K} and vector \mathbf{f} are formed by assembling the contributions if $\mathbf{K}^{(e)}$ and $\mathbf{f}^{(e)}$ for each element in the standard way.

Chapter 7

SHAPE FUNCTIONS FOR 2D AND 3D ELEMENTS WITH C^0 CONTINUITY

7.1 INTRODUCTION

This chapter extends the concepts previously studied for the analysis of 2D problems with the FEM using triangular and quadrilateral elements. The use of higher order elements with arbitrary geometry including curved sides is now considered. The isoparametric formulation and numerical integration is mandatory in these cases. These topics are explained in Chapter 8.

The chapter is organized as follows. In the first sections we detail the systematic derivation of the shape functions for rectangular and triangular elements of different order of approximation. Next, some rules for the analytical computation of the element integrals over rectangles and straight side triangles are given. The same topics are then explained for 3D elements of tetrahedral and prismatic shape.

7.2 DERIVATION OF THE SHAPE FUNCTIONS FOR C^0 TWO DIMENSIONAL ELEMENTS

Next, we will derive next the shape functions for different triangular and rectangular elements with C^0 continuity. The possibilities of distorting these elements into arbitrary shapes including curved sides will be treated in Chapter 8 using the concept of isoparametric interpolation.

7.2.1 Complete polynomials in two dimensions. Pascal's triangle

We recall that the chosen displacement field can only reproduce exactly a polynomial solution of an order equal to or less than that of the complete polynomial contained in the shape functions. Consequently, the finite element solution will improve as the degree of such a complete polynomial increases.

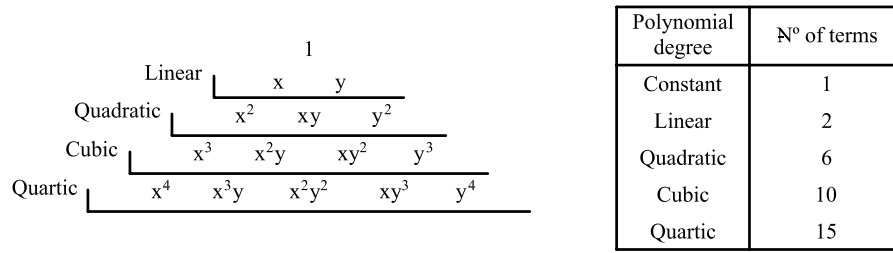


Fig. 7.1: Pascal's triangle in two dimensions

A 2D complete polynomial of n th degree can be written as

$$f(x, y) = \sum_{i=1}^p \alpha_i x^j y^k \quad ; \quad j + k \leq n \quad (7.1)$$

where the number of terms is

$$p = (n + 1)(n + 2)/2 \quad (7.2)$$

For a linear polynomial ($p = 3$)

$$f(x, y) = \alpha_1 + \alpha_2 x + \alpha_3 y \quad (7.3a)$$

and for a quadratic polynomial ($p = 6$)

$$f(x, y) = \alpha_1 + \alpha_2 x + \alpha_3 y + \alpha_4 xy + \alpha_5 x^2 + \alpha_6 y^2 \quad (7.3b)$$

The terms of a 2D complete polynomial can be readily identified by means of the *Pascal's triangle* (Figure 7.1).

The shape functions of many elements contain incomplete polynomial terms. For instance, the 4-noded rectangle includes the term $\alpha_4 xy$ from the quadratic polynomial (Section 7.3.1). These terms involve nodal variables which in general do not contribute to increasing the order of the approximation. This should be taken into account when designing a new element.

7.2.2 Shape functions of C^0 rectangular elements. Natural coordinates in two dimensions

A local coordinate system ξ, η is defined for each element in order to facilitate the derivation of the shape functions. Such a *natural* or *intrinsic* coordinate system is normalized so that the element sides are located at $\xi = \pm 1$ and $\eta = \pm 1$ as shown in Figure 7.2. The natural coordinate ξ was introduced for 1D rod elements in Chapter 2. It is easy to deduce from Figure 7.2 that

$$\xi = \frac{x - x_c}{a} \quad ; \quad \eta = \frac{y - y_c}{b} \quad (7.4)$$

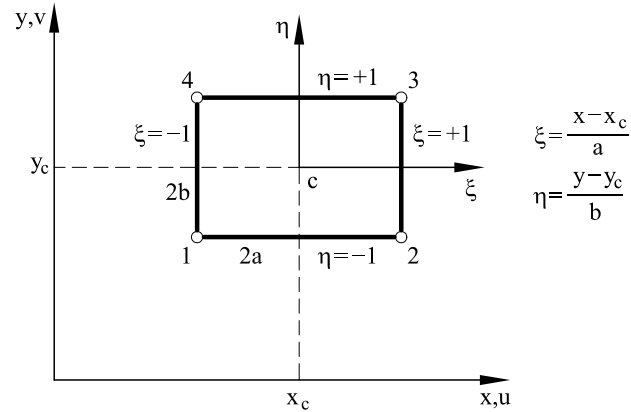


Fig. 7.2: Geometry of a generic rectangular element. Cartesian and natural coordinates

where x_c and y_c are the coordinates of the element centroid. Thus

$$\frac{d\xi}{dx} = \frac{1}{a} \quad ; \quad \frac{d\eta}{dy} = \frac{1}{b} \quad (7.5)$$

The differential of area in both systems is related by

$$dx \, dy = ab \, d\xi \, d\eta \quad (7.6)$$

The integration of a function $f(x, y)$ over a rectangular element can be expressed in the natural coordinate system by

$$\iint_{A^{(e)}} f(x, y) \, dx \, dy = \int_{-1}^{+1} \int_{-1}^{+1} g(\xi, \eta) ab \, d\xi \, d\eta \quad (7.7)$$

The shape functions when expressed in the natural coordinates must satisfy the same requirements as in cartesian coordinates. Therefore, the shape functions of C^0 continuous elements must satisfy:

a) Condition of nodal compatibility

$$N_i(\xi_j, \eta_j) = \begin{cases} 1 & i = j \\ 0 & i \neq j \end{cases} \quad (7.8)$$

b) Rigid body condition

$$\sum_{i=1}^n N_i(\xi, \eta) = 1 \quad (7.9)$$

Two element families can be clearly identified within the C^0 continuous rectangular elements, i.e. the Lagrange family and the Serendipity family. The derivation of the shape functions for each of these two element families is presented next.

7.3 LAGRANGE RECTANGULAR ELEMENTS

The shape functions of Lagrange elements can be obtained by the simple product of the two one dimensional (1D) Lagrange polynomials corresponding to the natural coordinates ξ and η of the node. Thus, if $l_I^i(\xi)$ is the Lagrange polynomial of order I in the ξ direction for node i and $l_J^i(\eta)$ is the Lagrange polynomial of order J in the η direction for node i , the shape function of node i is

$$N_i(\xi, \eta) = l_I^i(\xi) l_J^i(\eta) \quad (7.10)$$

The 1D Lagrange polynomials for each node can be obtained by Eq.(3.9) which can be indistinctly used for the coordinates ξ or η . Figure 7.3 shows some of the more popular Lagrange rectangular elements. Note that the number of nodes in each of the two directions ξ and η are the same along any nodal line. This is a particular feature of Lagrange elements.

The polynomial terms contained in the shape functions can be directly obtained from the Pascal's triangle as shown in Figure 7.3. Note that the shape functions are not complete polynomials and all contain some incomplete polynomial terms.

The derivation of the shape functions for the more popular Lagrange rectangular elements is presented next.

7.3.1 Four-noded Lagrange rectangle

This is the simplest element of the Lagrange family. We will derive its shape functions again using natural coordinates (Figure 7.4).

Let us consider a generic node i . The 1D shape functions corresponding to the local directions ξ and η coincide with the shape functions of the 2-noded bar element. Thus, it is easy to find

$$l_1^i(\xi) = \frac{1}{2}(1 + \xi\xi_i) \quad ; \quad l_1^i(\eta) = \frac{1}{2}(1 + \eta\eta_i) \quad (7.11)$$

where ξ_i and η_i take the values given in the table of Figure 7.4. The shape function of any node can be written in compact form as

$$N_i(\xi, \eta) = l_1^i(\xi)l_1^i(\eta) = \frac{1}{4}(1 + \xi\xi_i)(1 + \eta\eta_i) \quad (7.12)$$

Figure 4.16 shows in graphic form the shape function of node 1. It is easy to verify that the shape functions (7.12) satisfy the conditions (7.8) and (7.9).

7.3.2 Nine-noded quadratic Lagrange rectangle

The shape functions of the 9-noded Lagrange rectangle (Figure 7.5) are obtained by the product of two 1D quadratic polynomials in ξ and η . These

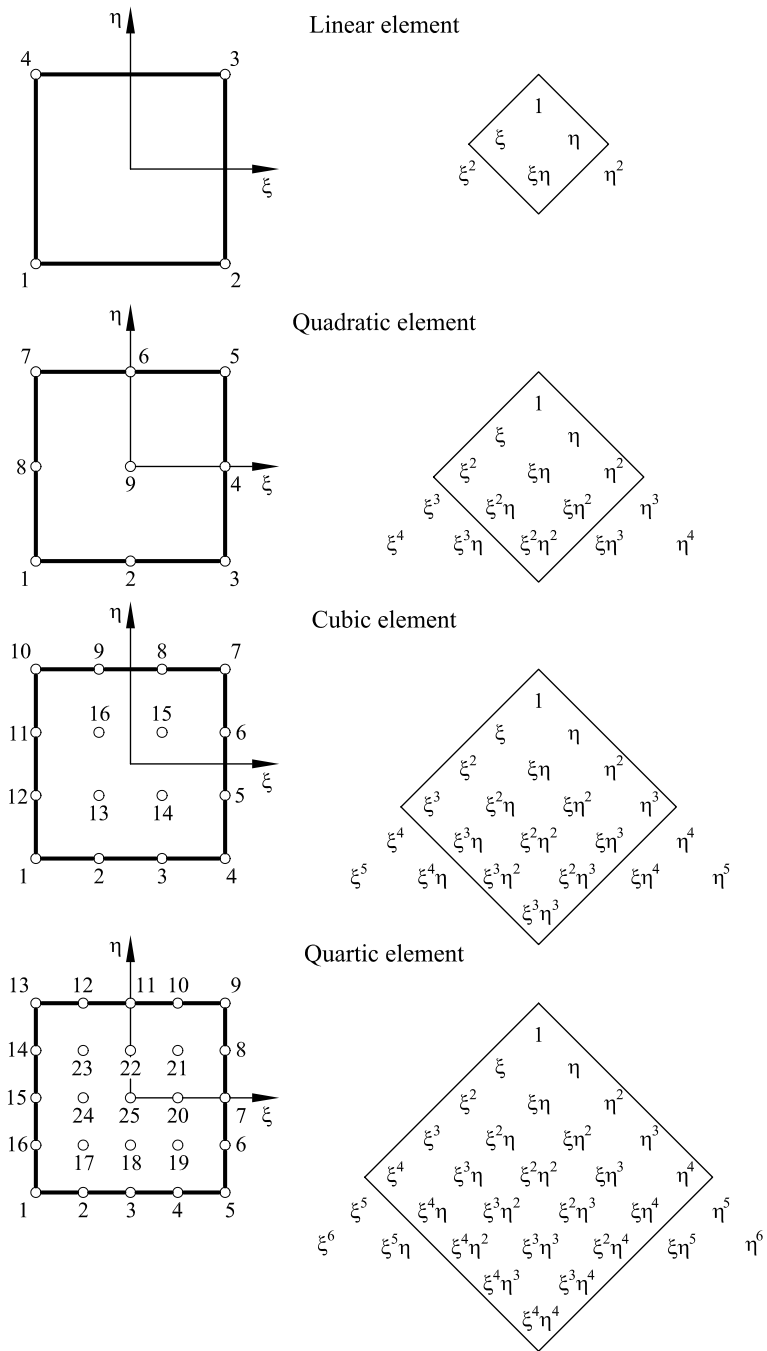


Fig. 7.3: Some Lagrange rectangular elements. Polynomial terms contained in the shape functions

polynomials are obtained from the shape functions of the quadratic rod element (Eq.(3.11)). Thus, for node 1

$$l_2^1(\xi) = \frac{1}{2}(\xi - 1)\xi \quad ; \quad l_2^1(\eta) = \frac{1}{2}(\eta - 1)\eta \quad (7.13)$$

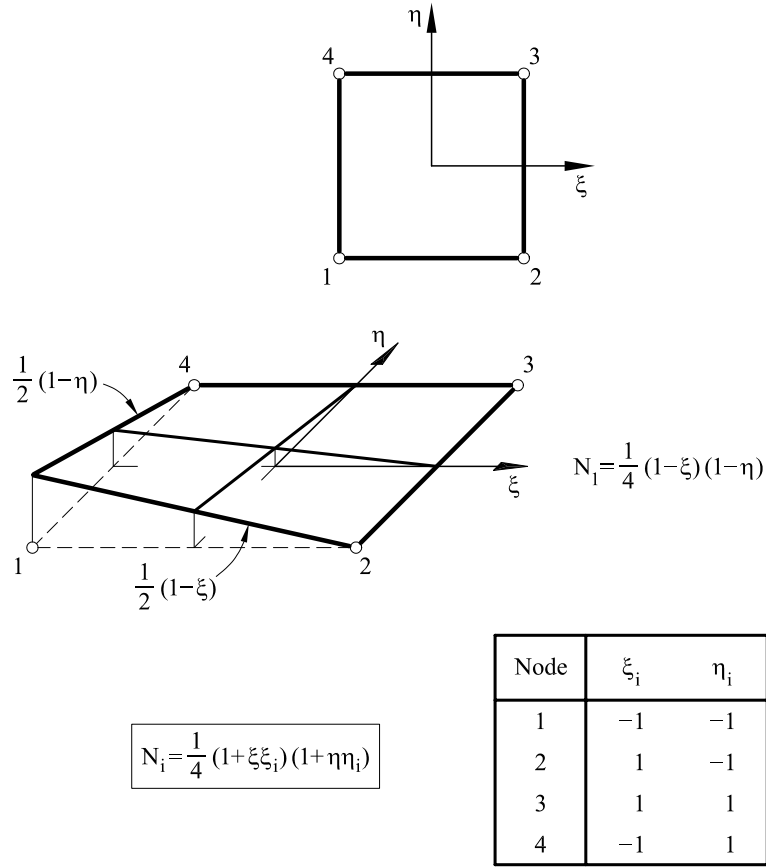


Fig. 7.4: Four-noded Lagrange rectangular element

and the shape function is

$$N_2(\xi, \eta) = l_2^1(\xi)l_2^1(\eta) = \frac{1}{4}(\xi - 1)(\eta - 1)\xi \eta \quad (7.14)$$

Following a similar procedure for the rest of the nodes, the shape functions can be written in compact form as

a) Corner nodes

$$N_i = \frac{1}{4}(\xi^2 + \xi\xi_i)(\eta^2 + \eta\eta_i) \quad ; \quad i = 1, 3, 5, 7 \quad (7.15)$$

b) Mid-side nodes

$$N_i = \frac{1}{2}\eta_i^2(\eta^2 - \eta\eta_i)(1 - \xi^2) + \frac{1}{2}\xi_i^2(\xi^2 - \xi\xi_i)(1 - \eta^2) \quad ; \quad i = 2, 4, 6, 8 \quad (7.16)$$

c) Central node

$$N_9(\xi, \eta) = (1 - \xi^2)(1 - \eta^2) \quad (7.17)$$

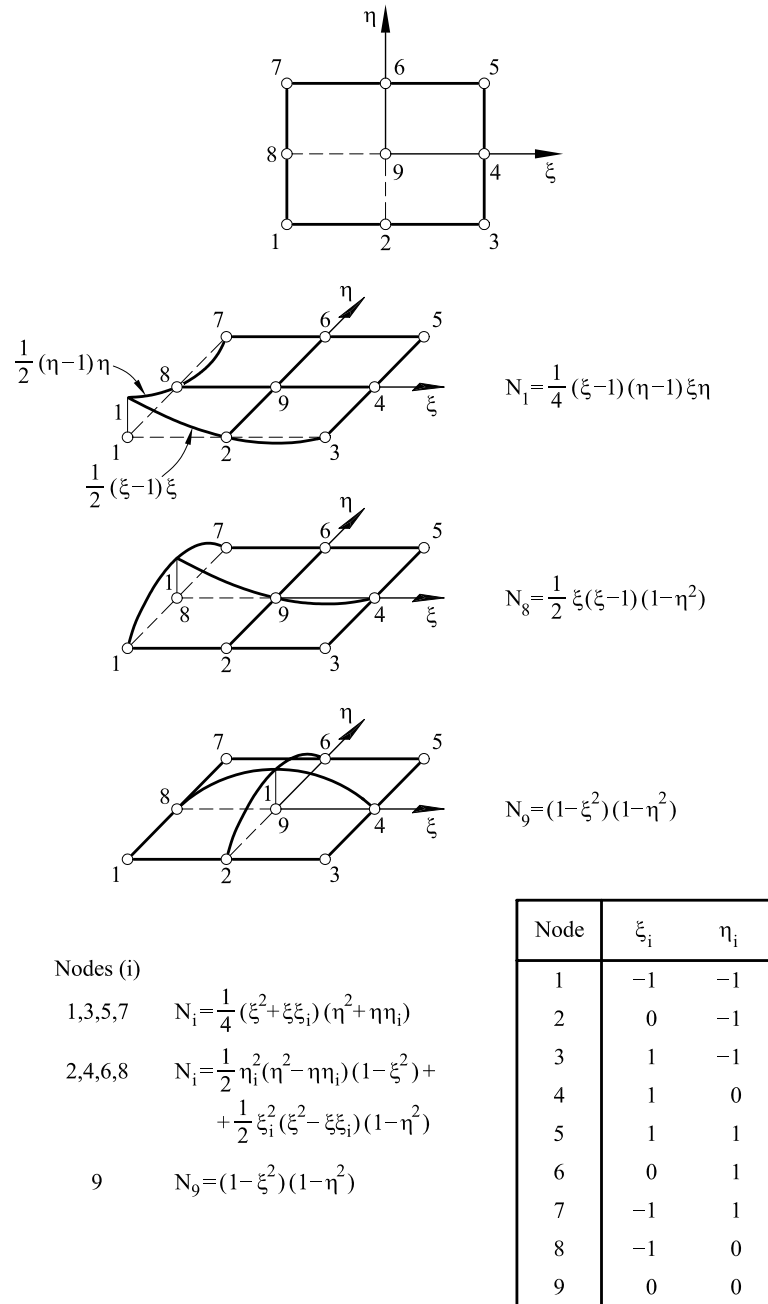


Fig. 7.5: Nine-noded quadratic Lagrange rectangle

We can verify that these shape functions satisfy Eqs.(7.8) and (7.9).

Figure 7.5 shows the shape function of three characteristic nodes. These functions contain the polynomial terms shown in Figure 7.3. Note that the 9-noded Lagrange rectangle contains all the terms of a complete quadratic polynomial plus three additional terms of the cubic and quartic polynomials (x^2y, xy^2, x^2y^2). Therefore, the approximation is simply of quadratic order.

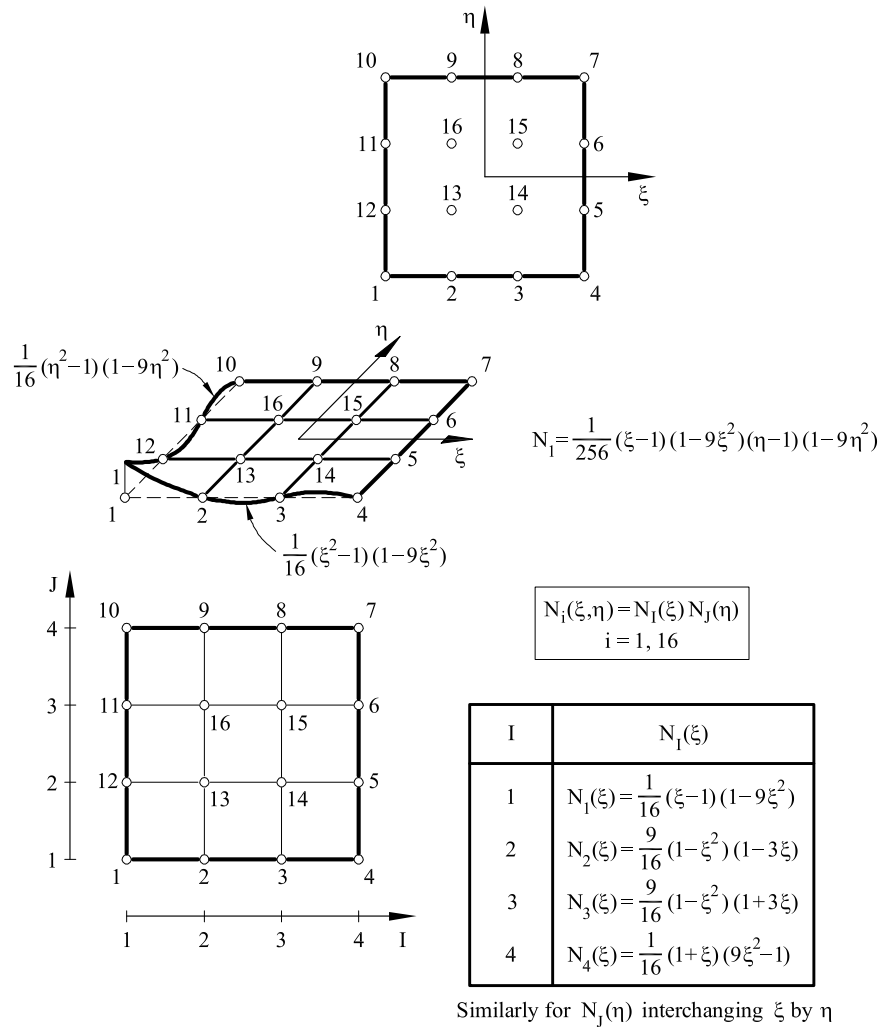


Fig. 7.6: Sixteen-noded cubic Lagrange rectangular element. Shape functions in natural coordinates

7.3.3 Sixteen-noded cubic Lagrange rectangle

This element has four nodes in each of the two directions ξ and η . The shape functions are obtained by the product of two cubic 1D Lagrange polynomials in the ξ and η directions deduced from Eq.(3.12). Figure 7.6 shows the resulting expressions of the shape functions. Figure 7.3 shows that the shape functions are *complete cubic* polynomials and contain the following additional terms: x^3y , x^2y^2 , xy^3 , x^3y^2 , x^2y^3 and x^3y^3 from the quartic, quintic and sextic polynomials. The shape functions satisfy Eqs.(7.8) and (7.9).

7.3.4 Other Lagrange rectangular elements

The shape functions of higher order Lagrange rectangular elements with 5, 6, 7, etc. nodes in each of the ξ and η directions are obtained by the product of

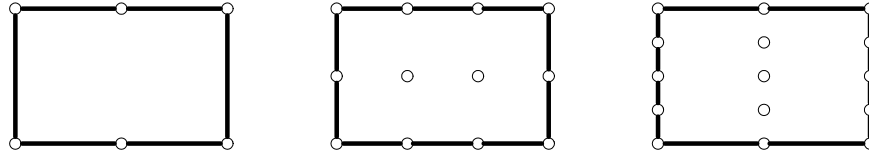


Fig. 7.7: Lagrange rectangular elements with different number of nodes along each local direction

fourth, fifth, sixth, etc. degree 1D Lagrange polynomials in ξ and η , similar to the linear, quadratic and cubic elements previously studied. It is easy to verify that the shape functions of a Lagrange element with n nodes in each of the two local directions ξ and η contain a complete n th degree polynomial and $n(n + 1)/2$ terms of incomplete polynomials of a higher degree which can be deduced from the Pascal's triangle.

Lagrange elements can have different number of nodes in each local direction ξ or η (Figure 7.7). The shape functions in this case are obtained by the product of the adequate 1D polynomials in ξ and η corresponding to the number of nodes in each direction. The shape functions now contain a complete 2D polynomial of a degree equal to the smallest degree of the two 1D polynomials in each local direction. Therefore, the degree of approximation of the element does not change by simply increasing the number of nodes in one of the two local directions only. This explains why these elements are not very popular and they are only occasionally used as a transition between elements of two different orders.

7.4 SERENDIPITY RECTANGULAR ELEMENTS

Serendipity elements are obtained as follows. First the number of nodes defining a 1D polynomial of a given degree along each side is chosen. Then, the minimum number of nodes *within* the element is added so that a complete and symmetrical 2D polynomial *of the same degree* as the 1D polynomial chosen along the sides is obtained. Figure 7.8 shows some of the more popular Serendipity elements and the polynomial terms contained in the shape functions. Note that the simplest element of the Serendipity family, i.e. the 4-noded rectangle, coincides with the same element of the Lagrange family. Also note that the quadratic and cubic elements of 8 and 12 nodes, respectively, do not have interior nodes, whereas the 17 node element requires a central node to guarantee the complete quartic approximation, as is explained next.

The derivation of the shape functions of Serendipity elements are not as straightforward as those of Lagrange elements. In fact, some ingenuity is needed and this explains the name Serendipity, after the ingenuous discoveries of the Prince of Serendip quoted in the romances of Horacio Walpole in the eighteenth century.

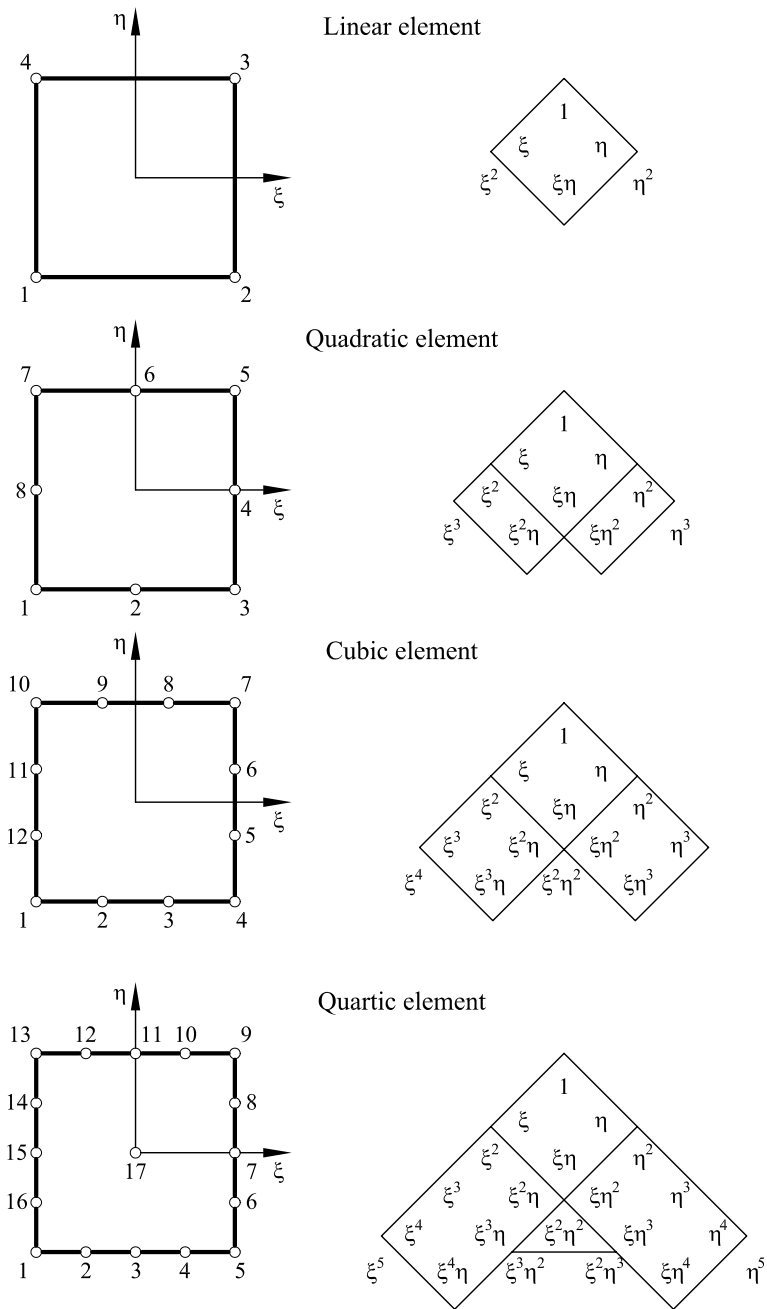


Fig. 7.8: Some Serendipity elements and terms contained in their shape functions

7.4.1 Eighth-noded quadratic Serendipity rectangle

The shape functions of the side nodes are readily obtained as the product of a second degree polynomial in ξ (or η) and another one in η (or ξ). It can be checked that this product contains the required complete quadratic terms

(Figure 7.9). For these nodes we obtain

$$\begin{aligned} N_i(\xi, \eta) &= \frac{1}{2}(1 + \xi\xi_i)(1 - \eta^2) \quad ; \quad i = 4, 8 \\ N_i(\xi, \eta) &= \frac{1}{2}(1 + \eta\eta_i)(1 - \xi^2) \quad ; \quad i = 2, 6 \end{aligned} \quad (7.18)$$

Unfortunately this strategy can not be applied for the corner nodes, since in this case the product of two quadratic polynomials will yield a zero value at the center and thus the criterion of Eq.(7.9) would be violated. Consequently, a different procedure is followed as detailed below.

Step 1. The shape function of the corner node is initially assumed to be bi-linear, i.e. for node 1 (Figure 7.9) we have

$$N_1^L = \frac{1}{4}(1 - \xi)(1 - \eta) \quad (7.19)$$

This shape function is equal to one at the corner node and takes the value zero at all the other nodes, except for the two nodes 2 and 8 adjacent to node 1 where it takes the value 1/2.

Step 2. The shape function is made zero at node 2 by subtracting from the bi-linear function one half of the quadratic shape function (7.19) of node 2:

$$\bar{N}_1(\xi, \eta) = N_1^L - \frac{1}{2}N_2 \quad (7.20)$$

Step 3. Function \bar{N}_1 still takes the value 1/2 at node 8. Hence, the final step is to subtract from \bar{N}_1 one half of the quadratic shape function of node 8 (Eq.(7.18)), i.e.

$$N_1(\xi, \eta) = N_1^L - \frac{1}{2}N_2 - \frac{1}{2}N_8 \quad (7.21)$$

It can be verified that the resulting function N_1 satisfies the conditions (7.8) and (7.9) and contains the desired (quadratic) polynomial terms. Therefore, it is the shape function of node 1 we are looking for.

Following the same procedure for the rest of the corner nodes yields the following general expression

$$N_i(\xi, \eta) = \frac{1}{4}(1 + \xi\xi_i)(1 + \eta\eta_i)(\xi\xi_i + \eta\eta_i - 1) \quad ; \quad i = 1, 3, 5, 7 \quad (7.22)$$

Figure 7.9 shows that the shape functions of the 8-noded Serendipity element contain a complete quadratic polynomial and two terms x^2y and xy^2 of the cubic polynomial. Therefore, this element has the same approximation as the 9-noded Lagrange element *and it has a node less*. This makes the 8-noded quadrilateral in principle more competitive for practical purposes (see Section 8.1.2 for further details).

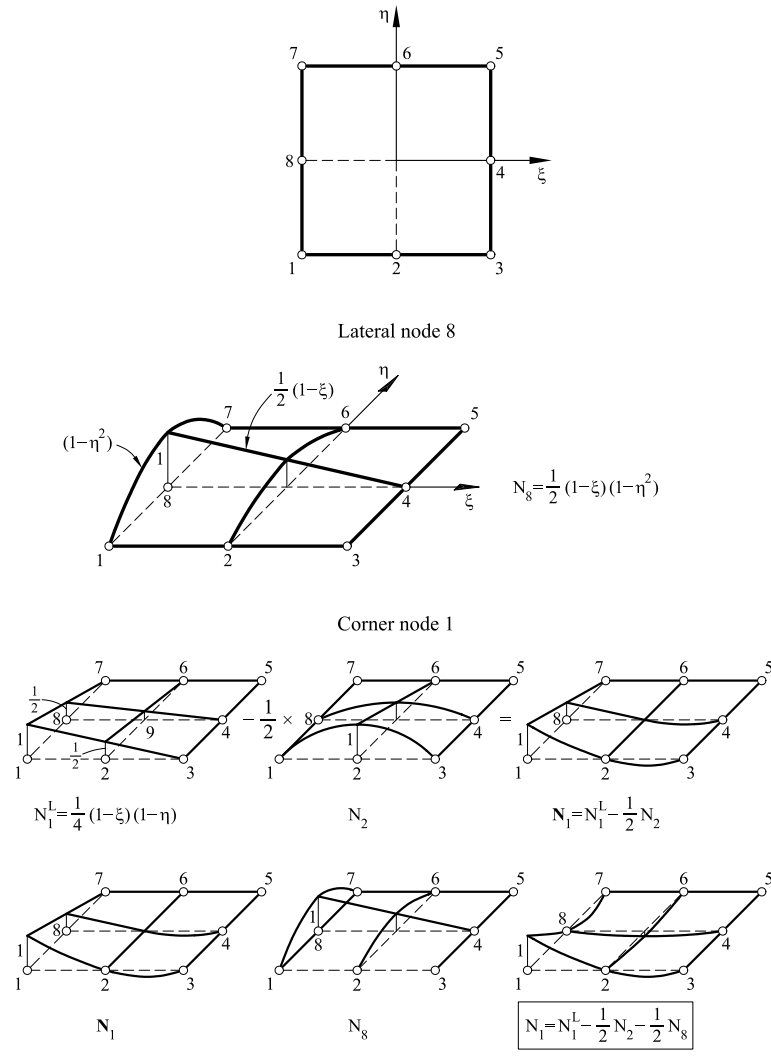


Fig. 7.9: 8-noded quadratic Serendipity rectangle. Derivation of the shape functions for a mid-side node and a corner node

7.4.2 Twelve-noded cubic Serendipity rectangle

This element has four nodes along each side and a total of twelve side nodes which define the twelve term polynomial approximation shown in Figure 7.8. The shape functions are derived following the same procedure explained for the 8-noded element. Thus, the shape functions for the side nodes are obtained by the simple product of two Lagrange cubic and linear polynomials. For the corner nodes the starting point is again the bilinear approximation. This initial shape function is forced to take a zero value at the two side nodes adjacent to the corner node by subtracting the shape functions of those nodes weighted by the factors 2/3 and 1/3. Figure 7.10 shows the expression of the shape functions which can be derived by the reader as an exercise.

It is simple to check that the element satisfies conditions (7.8) and (7.9).

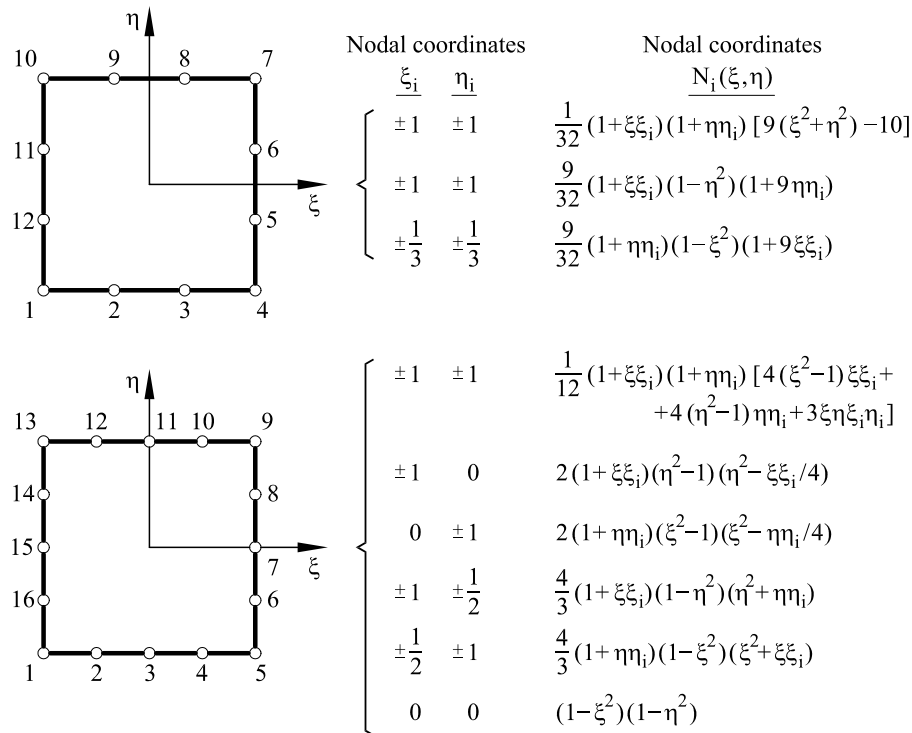


Fig. 7.10: Shape functions for the cubic (12 nodes) and quartic (17 nodes) Serendipity rectangles

Figure 7.8 shows that the shape functions contain a complete cubic approximation plus two terms (x^3y, xy^3) of the quartic polynomial. This element compares very favourably with the 16-noded Lagrange element, since both have a cubic approximation but the Serendipity element has fewer nodes (12 nodes versus 16 nodes for the cubic Lagrange rectangle).

7.4.3 Seventeen-noded quartic Serendipity rectangle

The quartic Serendipity rectangle has five nodes along each side and a total of seventeen nodes (sixteen side nodes plus a central node, Figure 7.10). The central node is necessary to introduce the “bubble” function $(1 - \xi^2)(1 - \eta^2)$, contributing the term $\xi^2\eta^2$ to complete a quartic approximation as shown in Figure 7.8.

The derivation of the shape functions follows a procedure similar to that for the 8 and 12 node Serendipity elements. The shape functions for the side nodes are obtained by the product of a quartic and a linear polynomial. An exception are nodes 3, 7, 11 and 15 for which the function $1/2 (1 - \xi^2)(1 - \eta^2)$ is subtracted from that product so that the resulting shape function takes a zero value at the central node. The starting point for the corner nodes is the bilinear function to which a proportion of the shape functions of the side nodes is subtracted so that the resulting shape function takes a zero value at

these nodes. Finally, the shape function for the central node coincides with the bubble function. Figure 7.10 shows the shape functions for this element.

Figure 7.8 shows that the shape functions contain a complete quartic approximation plus two additional terms (x^4y and yx^4) from the quintic polynomial. The corresponding quartic Lagrange element has 25 nodes (Figure 7.2) and hence the 17-noded Serendipity rectangle is in principle more competitive for practical purposes.

7.5 SHAPE FUNCTIONS FOR C^o CONTINUOUS TRIANGULAR ELEMENTS

The shape functions for the more popular C^o continuous triangular elements are *complete polynomials* whose terms can be readily identified by the Pascal's triangle. This also defines the position of the nodes within the element. We recall, for instance, that the shape function of the 3-noded triangle is linear. Similarly, the six and ten-noded triangles define the following complete quadratic and cubic approximations

6-noded triangle

$$\phi = \alpha_o + \alpha_1x + \alpha_2y + \alpha_3xy + \alpha_4x^2 + \alpha_5y^2 \quad (7.23)$$

10-noded triangle

$$\phi = \alpha_o + \alpha_1x + \alpha_2y + \alpha_3xy + \alpha_4x^2 + \alpha_5y^2 + \alpha_6x^3 + \alpha_7x^2y + \alpha_8xy^2 + \alpha_9y^3 \quad (7.24)$$

The α_i parameters are obtained by the same procedure as described for the 3-noded triangle in Chapter 4. This method has obvious difficulties for high order elements and it is simpler to apply the technique based on area coordinates that is explained below.

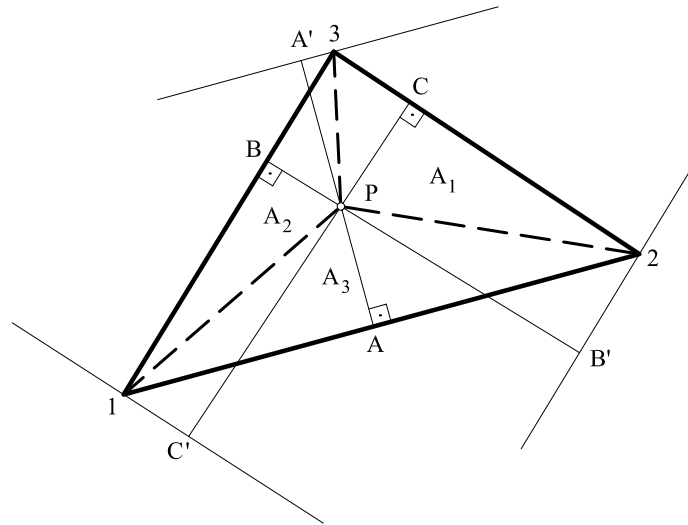
7.5.1 Area coordinates

Let us join a point P within a triangle of area A with the three vertices 1, 2, 3 (Figure 7.11). This defines three sub-areas A_1, A_2 and A_3 corresponding to the triangles $P13, P12$ and $P23$, respectively (note that $A_1 + A_2 + A_3 = A$). The area coordinates are defined as

$$L_1 = \frac{A_1}{A} \quad ; \quad L_2 = \frac{A_2}{A} \quad ; \quad L_3 = \frac{A_3}{A} \quad (7.25)$$

Obviously

$$L_1 + L_2 + L_3 = \frac{A_1 + A_2 + A_3}{A} = \frac{A}{A} = 1 \quad (7.26)$$



$$\text{Área (A)} = A_1 + A_2 + A_3$$

$$L_1 = \frac{A_1}{A} = \frac{CP}{CC'} \quad L_2 = \frac{A_2}{A} = \frac{BP}{BB'} \quad L_3 = \frac{A_3}{A} = \frac{AP}{AA'}$$

Fig. 7.11: Area coordinates for a triangle

The position of point P can be defined by any two of these three coordinates. The area coordinates of a node can be interpreted as the ratio between the distance from point P to the opposite side divided by the distance from the node to that side (Figure 7.11). Thus, area coordinates of the centroid are $L_1 = L_2 = L_3 = 1/3$. Area coordinates are also known as barycentric, triangular, and trilinear coordinates and they are typical of geometry treatises [F3]. In the FEM context area coordinates have proved to be very useful for deriving the shape functions of triangular finite elements.

Area coordinates are also of interest to define a parametric interpolation of the element geometry. For a straight side triangle the following relationship between the area and cartesian coordinates can be written

$$\begin{aligned} x &= L_1x_1 + L_2x_2 + L_3x_3 \\ y &= L_1y_1 + L_2y_2 + L_3y_3 \end{aligned} \tag{7.27}$$

This equation system is completed with Eq.(7.26) so that L_1 , L_2 and L_3 can be obtained in terms of the cartesian coordinates by

$$L_i = \frac{1}{2A^{(e)}}(a_i + b_ix + c_iy) \tag{7.28}$$

where $A^{(e)}$ is the area of the triangle and a_i, b_i, c_i coincide with the values given in Eq.(4.27) for the 3-noded triangle. It is concluded that *the area coordinates coincide precisely with the shape functions of the 3-noded triangular element.*

7.5.2 Derivation of the shape functions for C^o continuous triangles

The shape functions for triangles containing complete M th degree polynomials can be obtained in terms of the area coordinates as follows. Let us consider a node i characterized by the position (I, J, K) where I, J and K are the powers of the area coordinates L_1, L_2 and L_3 , respectively in the expression of the shape function of the node. Thus, $I + J + K = M$ and the shape function of node i is given by

$$N_i = l_I^i(L_1) l_J^i(L_2) l_K^i(L_3) \quad (7.29)$$

where $l_I^i(L_1)$ is the 1D Lagrange I th degree polynomial in L_1 which takes the value one at node i (Eq.(3.6a)), i.e.

$$l_I^i(L_1) = \prod_{\substack{j=1, I \\ j \neq i}} \frac{(L_1 - L_1^j)}{(L_1^i - L_1^j)} \quad (7.30)$$

with identical expressions for $l_J^i(L_2)$ and $l_K^i(L_3)$. In Eq.(7.30) L_1^i is the value of L_1 at node i .

The main difficulty in applying Eq.(7.29) is to deduce the values of I, J, K for each node. This can be done simply by noting that: a) the shape function of a corner node depends on a single area coordinate only and thus the corresponding I, J or K power for that node is equal to M ; b) all nodes located on the lines $L_1 = \text{constant}$ have the same value for I and the same occurs with L_2 and J and L_3 and K ; and c) the values of I, J and K associated with L_1, L_2 and L_3 , respectively, decrease progressively from the maximum value for the lines $L_i = 1$ at the corner nodes, to a value equal to zero at the lines $L_i = 0$ which coincide with the opposite side to each corner node i (Figure 7.12).

This procedure will be clarified next with some examples of its application.

7.5.3 Shape functions for the 3-noded linear triangle

The shape functions of the 3-noded triangle are linear polynomials ($M = 1$). The area coordinates and the values of I, J, K for each node can be seen in Figure 7.12.

Node 1

Position $(I, J, K) : (1, 0, 0)$

Area coordinates: $(1, 0, 0)$

$$N_1 = l_1^1(L_1) = L_1 \quad (7.31)$$

It is straight-forward find $N_2 = L_2$ and $N_3 = L_3$ as expected.

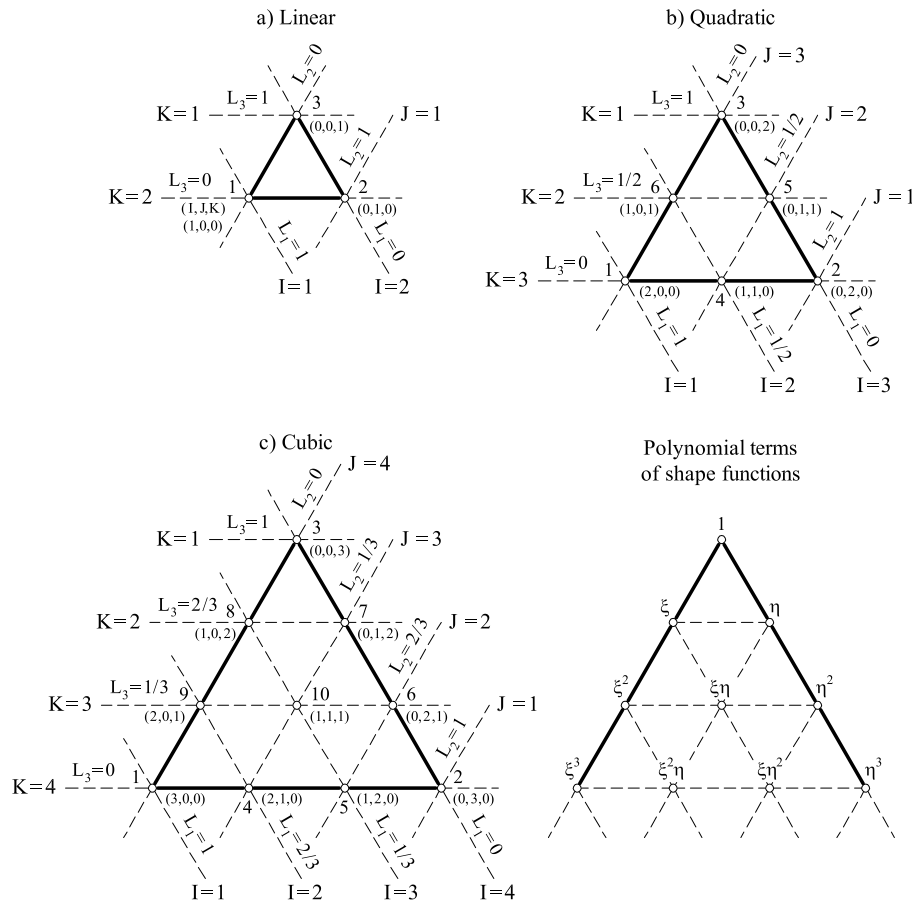


Fig. 7.12: Linear, quadratic and cubic triangular elements. Area coordinates and values of (I, J, K) for each node

7.5.4 Shape functions for the six-noded quadratic triangle

The shape functions for this element are complete quadratic polynomials ($M = 2$). The area coordinates and the values of I, J and K at each node are shown in Figure 7.12.

Node 1

Position $(I, J, K) : (2, 0, 0)$

Area coordinates: $(1, 0, 0)$

$$N_1 = l_2^1(L_1) = \frac{(L_1 - 1/2)L_1}{(1 - 1/2) 1} = (2L_1 - 1)L_1 \quad (7.32)$$

Node 4

Position $(I, J, K) : (1, 1, 0)$

Area coordinates: $(1/2, 1/2, 0)$

$$N_4 = l_1^2(L_1) l_1^2(L_2) = \frac{L_1}{1/2} \frac{L_2}{1/2} = 4L_1L_2 \quad (7.33)$$

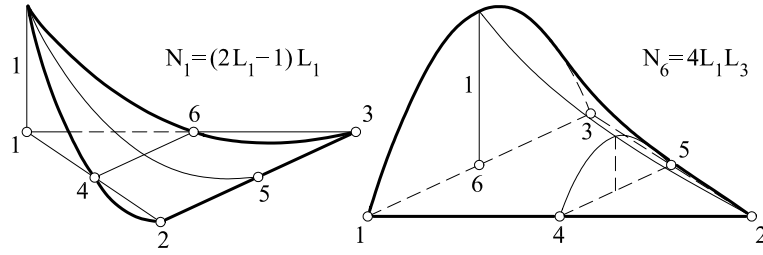


Fig. 7.13: Shape functions of a corner node and a side node for a quadratic triangle

Following the same procedure for the rest of nodes we find (that)

$$\begin{aligned} N_1 &= (2L_1 - 1)L_1 & ; & & N_2 &= (2L_2 - 1)L_2 & ; & & N_3 &= (2L_3 - 1)L_3 \\ N_4 &= 4L_1L_2 & ; & & N_5 &= 4L_2L_3 & ; & & N_6 &= 4L_1L_3 \end{aligned} \quad (7.34)$$

Figure 7.13 shows two characteristic shape functions for this element.

7.5.5 Shape functions for the ten-noded cubic triangle

The shape functions for this element are complete cubic polynomials ($M = 3$). Figure 7.12 shows the area coordinates and the values of I, J and K at each node:

Node 1

Position $(I, J, K) : (3, 0, 0)$

Area coordinates: $(1, 0, 0)$

$$N_1 = l_3^1(L_1) = \frac{(L_1 - 2/3)(L_1 - 1/3)L_1}{(1 - 2/3)(1 - 1/3)1} = \frac{1}{2}L_1(3L_1 - 1)(3L_1 - 2) \quad (7.35)$$

Node 4

Position $(I, J, K) : (2, 1, 0)$

Area coordinates: $(2/3, 1/3, 0)$

$$N_4 = l_2^2(L_1)l_1^2(L_2) = \frac{(L_1 - 1/3)L_1}{(2/3 - 1/3)2/3} \cdot \frac{L_2}{1/3} = \frac{9}{2}(3L_1 - 1)L_1L_2 \quad (7.36)$$

The same procedure applied to the rest of the nodes gives

$$\begin{aligned} N_1 &= \frac{1}{2}L_1(3L_1 - 1)(3L_1 - 2) & ; & & N_2 &= \frac{1}{2}L_2(3L_2 - 1)(3L_2 - 2) \\ N_3 &= \frac{1}{2}L_3(3L_3 - 1)(3L_3 - 2) & ; & & N_4 &= \frac{9}{2}(3L_1 - 1)L_1L_2 \\ N_5 &= \frac{9}{2}(3L_2 - 1)L_1L_2 & ; & & N_6 &= \frac{9}{2}(3L_2 - 1)L_2L_3 \\ N_7 &= \frac{9}{2}(3L_3 - 1)L_2L_3 & ; & & N_8 &= \frac{9}{2}(3L_3 - 1)L_3L_1 \\ N_9 &= \frac{9}{2}(3L_2 - 1)L_3L_1 & ; & & N_{10} &= 27L_1L_2L_3 \end{aligned} \quad (7.37)$$

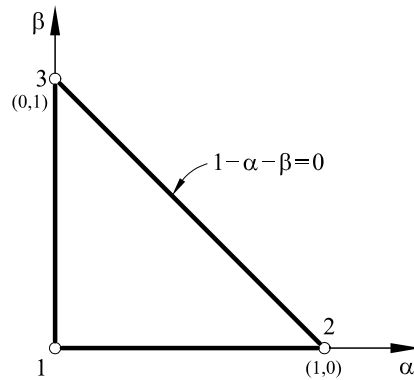


Fig. 7.14: Natural coordinates for a triangular element

A similar technique can be employed to derive the shape functions of higher order triangular elements.

7.5.6 Natural coordinates for triangles

It is very convenient to define a normalized coordinate system α, β (also called natural coordinate system), such that the element has the sides over the lines $\alpha = 0, \beta = 0$ and $1 - \alpha - \beta = 0$ as shown in Figure 7.14. The shape functions for the 3-noded triangle can then be written as

$$N_1 = 1 - \alpha - \beta \quad ; \quad N_2 = \alpha \quad , \quad N_3 = \beta \quad (7.38)$$

It is deduced that the area coordinates L_2 and L_3 coincide with the natural coordinates α and β , respectively and $L_1 = 1 - \alpha - \beta$.

These coincidences allow us to express the shape functions of triangular elements in terms of the natural coordinates. This is particularly useful for deriving isoparametric triangular elements.

7.6 ANALYTIC COMPUTATION OF INTEGRALS OVER RECTANGLES AND STRAIGHT SIDE TRIANGLES

The integration of polynomials over 2D elements can be difficult and, in general, numerical integration is used. However, some interesting analytical expressions in terms of the local cartesian coordinates \bar{x}, \bar{y} shown in Figure 7.15 exist for rectangles and straight side triangles. A typical integral term such as

$$\bar{C}_{ij} = D \iint_{A^{(e)}} \bar{x}^m \bar{y}^n dA \quad (7.39)$$

can be directly integrated by the following expressions:

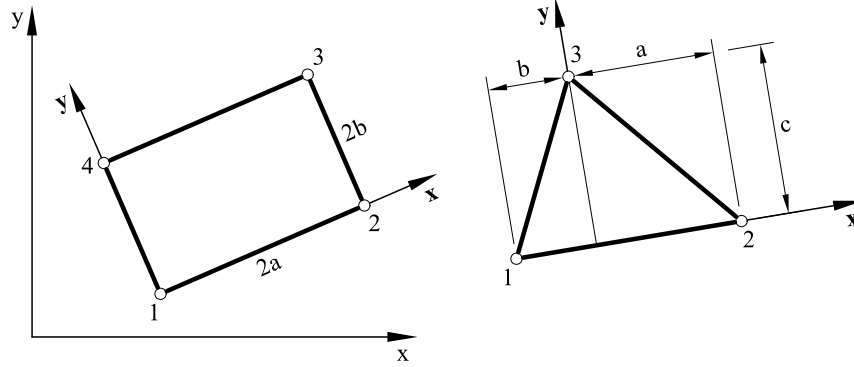


Fig. 7.15: Local coordinate system \bar{x} , \bar{y} for the analytical computation of integrals over triangular and rectangular elements

Straight side triangular element

$$\bar{C}_{ij} = D c^{n+1} \left[a^{m+1} - (-b)^{m+1} \right] \frac{m!n!}{(m+n+2)!} \quad (7.40)$$

Rectangular element

$$\bar{C}_{ij} = D \frac{(2a)^{m+1} (2b)^{n+1}}{(m+1)(n+1)} \quad (7.41)$$

In the above m and n are integers and a, b and c are typical element dimensions (Figure 7.15). Once $\bar{\mathbf{K}}$ and $\bar{\mathbf{f}}$ have been found in the local coordinate system \bar{x}, \bar{y} using the above expressions, they can be transformed into the global axes using the standard relationship (see Chapter 1)

$$\mathbf{K}_{ij} = \mathbf{T}^T \bar{\mathbf{K}}_{ij} \mathbf{T} \quad , \quad \mathbf{f}_i = \mathbf{T}^T \bar{\mathbf{f}}_i \quad (7.42)$$

where \mathbf{T} is the 2×2 coordinate transformation matrix

$$\mathbf{T} = \begin{bmatrix} \cos(\bar{x}x) & \cos(\bar{x}y) \\ \cos(\bar{y}x) & \cos(\bar{y}y) \end{bmatrix} \quad (7.43)$$

with $(\bar{x}x)$ being the angle between the local \bar{x} axis and the global x axis, etc.

Other simple analytical forms in terms of area coordinates can be found for area integrals over straight side triangles. A typical stiffness matrix term involves the cartesian derivatives of the shape functions. This is expressed in terms of area coordinates by the standard chain rule

$$\frac{\partial N_1(L_1, L_2, L_3)}{\partial x} = \frac{\partial N_1}{\partial L_1} \frac{\partial L_1}{\partial x} + \frac{\partial N_1}{\partial L_2} \frac{\partial L_2}{\partial x} + \frac{\partial N_1}{\partial L_3} \frac{\partial L_3}{\partial x} \quad (7.44)$$

As the element sides are assumed to be straight, Eq.(7.28) leads to

$$\frac{\partial L_i}{\partial x} = \frac{b_i}{2A^{(e)}} \quad \text{and} \quad \frac{\partial L_i}{\partial y} = \frac{c_i}{2A^{(e)}} \quad (7.45)$$

where b_i and c_i are given by Eq.(4.27). Combining Eqs.(7.44) and (7.45) gives

$$\frac{\partial N_i}{\partial x} = \frac{1}{2A^{(e)}} \sum_{i=1}^3 b_i \frac{\partial N_i}{\partial L_i} \quad ; \quad \frac{\partial N_i}{\partial y} = \frac{1}{2A^{(e)}} \sum_{i=1}^3 c_i \frac{\partial N_i}{\partial L_i} \quad (7.46)$$

Thus, the element integrals can be easily expressed in terms of area coordinates and they can be directly computed by the following expressions

$$\iint_{A^{(e)}} L_1^k L_2^l L_3^m dA = 2A^{(e)} \frac{k! l! m!}{(2+k+l+m)!} \quad (7.47a)$$

$$\oint_{l^{(e)}} L_i^k L_j^l ds = l^{(e)} \frac{k! l!}{(1+k+l)!} \quad (7.47b)$$

If one of the area coordinates is missing in the integrand, the corresponding power is omitted in the denominator of Eqs.(7.47) and it is made equal to a unit value in the numerator.

The use of the natural coordinates α and β does not introduce any additional difficulty. Exact expressions for the integrals over straight side triangles can be found as

$$I = \iint_{A^{(e)}} \alpha^m \beta^n dA = \frac{2A^{(e)} \Gamma(m+1) \Gamma(n+1)}{\Gamma(3+m+n)} \quad (7.48)$$

where Γ is the Gamma function [R2]. When m and n are positive integers

$$I = 2A^{(e)} \frac{m! n!}{(2+m+n)!} \quad (7.49)$$

Note that this is just a particular case of Eq.(7.47a) when one of the area coordinates is missing. Similarly, it is deduced from (7.47b) that

$$\oint_{l^{(e)}} \alpha^m ds = l^{(e)} \frac{m!}{(2+m)!} \quad (7.50)$$

For curved side elements the computation of the cartesian derivatives of the shape functions requires a parametric formulation. This generally introduces rational terms in the integrals and makes the use of numerical integration unavoidable.

Example: 7.1 Compute the stiffness matrix $K_{11}^{(e)}$ for an orthotropic quadratic triangle with straight sides and unit thickness.

- **Solution**

The first step is to obtain the cartesian derivatives of the shape function N_1 expressed in terms of the area coordinates as

$$\begin{aligned}\frac{\partial N_1}{\partial x} &= \frac{\partial N_1}{\partial L_1} \frac{\partial L_1}{\partial x} + \frac{\partial N_1}{\partial L_2} \frac{\partial L_2}{\partial x} + \frac{\partial N_1}{\partial L_3} \frac{\partial L_3}{\partial x} \\ \frac{\partial N_1}{\partial y} &= \frac{\partial N_1}{\partial L_1} \frac{\partial L_1}{\partial y} + \frac{\partial N_1}{\partial L_2} \frac{\partial L_2}{\partial y} + \frac{\partial N_1}{\partial L_3} \frac{\partial L_3}{\partial y}\end{aligned}$$

From Eq.(7.32) we deduce

$$\frac{\partial N_1}{\partial L_1} = 4L_1 - 1 \quad ; \quad \frac{\partial N_1}{\partial L_2} = \frac{\partial N_1}{\partial L_3} = 0$$

and from Eq.(7.45)

$$\frac{\partial L_i}{\partial x} = \frac{b_i}{2A^{(e)}} \quad ; \quad \frac{\partial L_i}{\partial y} = \frac{c_i}{2A^{(e)}}$$

Therefore

$$\frac{\partial N_1}{\partial x} = \frac{b_1}{2A^{(e)}}(4L_1 - 1) \quad ; \quad \frac{\partial N_1}{\partial y} = \frac{c_1}{2A^{(e)}}(4L_1 - 1)$$

and

$$\mathbf{B}_1 = \frac{(4L_1 - 1)}{2A^{(e)}} \begin{bmatrix} b_1 & 0 \\ 0 & c_1 \\ c_1 & b_1 \end{bmatrix}$$

Matrix $\mathbf{K}_{11}^{(e)}$ is thus obtained by

$$\begin{aligned}\mathbf{K}_{11}^{(e)} &= \iint_{A^{(e)}} \mathbf{B}_1^T \mathbf{D} \mathbf{B}_1 t dA = \frac{t}{(2A^{(e)})^2} \begin{bmatrix} b_1 & 0 & b_1 \\ 0 & c_1 & c_1 \end{bmatrix} \begin{bmatrix} d_{11} & d_{12} & 0 \\ d_{12} & d_{22} & 0 \\ 0 & 0 & d_{33} \end{bmatrix} \times \\ &\times \begin{bmatrix} b_1 & 0 \\ 0 & c_1 \\ c_1 & b_1 \end{bmatrix} \iint_{A^{(e)}} (4L_1 - 1)^2 dA\end{aligned}$$

We deduce from Eq.(7.47a)

$$\iint_{A^{(e)}} (4L_1 - 1)^2 dA = 2A^{(e)} \left[\frac{16 \cdot 2!}{4!} - \frac{8 \cdot 1!}{3!} + \frac{1}{2} \right] = A^{(e)}$$

which leads to

$$\mathbf{K}_{11}^{(e)} = \frac{1}{4A^{(e)}} \begin{bmatrix} b_1^2 d_{11} + c_1^2 d_{33} & b_1 c_1 (d_{33} + d_{12}) \\ b_1 c_1 (d_{33} + d_{12}) & b_1^2 d_{33} + c_1^2 d_{22} \end{bmatrix}$$

The rest of the $\mathbf{K}_{ij}^{(e)}$ matrices are obtained following an identical procedure. The complete expression of the stiffness matrix for the quadratic triangle can be found in [C15] and [W2].

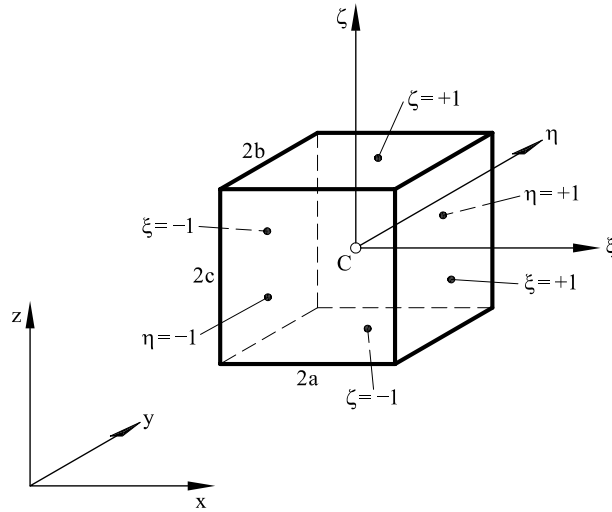


Fig. 7.16: Natural coordinate system for a right prism

7.7 SHAPE FUNCTIONS FOR 3D ELEMENTS

We will study next the derivation of two families of 3D solid elements: hexahedra and tetrahedra of different orders. In common with 2D solid elements, 3D hexahedra can be of Lagrange or Serendipity types. The shape functions of hexahedra elements are obtained for a right prismatic geometry in terms of the three natural coordinates following similar rules as for 2D rectangles. The extension of hexahedra elements to model arbitrary 3D geometries of irregular shapes, including curved surfaces, is straightforward using an isoparametric formulation (Chapter 8).

The shape functions for Lagrange right prisms are simply obtained by the product of three Lagrange polynomials in 1D. The derivation of 3D Serendipity prismatic elements is more cumbersome, although again the same rules given for the 2D case apply (Chapter 8).

Like triangles, the shape functions for tetrahedra are complete polynomials and they are more easily expressed in terms of volume and natural coordinates.

7.8 RIGHT PRISMS

Let us consider a right prism with the natural coordinates ξ, η, ζ defined as shown in Figure 7.16. For an element with edges $2a \times 2b \times 2c$ we have

$$\xi = \frac{(x - x_c)}{a} ; \quad \eta = \frac{(y - y_c)}{b} ; \quad \zeta = \frac{(z - z_c)}{c} \quad (7.51)$$

where (x_c, y_c, z_c) are the coordinates of the element centroid. From Eq.(7.51) it is deduced that

$$\frac{d\xi}{dx} = \frac{1}{a} ; \quad \frac{d\eta}{dy} = \frac{1}{b} ; \quad \frac{d\zeta}{dz} = \frac{1}{c} \quad (7.52)$$

and a differential of volume is expressed by

$$dx dy dz = abc d\xi d\eta d\zeta \quad (7.53)$$

The integration of a function $f(x, y, z)$ over the element is expressed in the natural coordinate system as

$$\iiint_{V^{(e)}} f(x, y, z) dV = \int_{-1}^{+1} \int_{-1}^{+1} \int_{-1}^{+1} f(\xi, \eta, \zeta) abc d\xi d\eta d\zeta \quad (7.54)$$

Since the element is a right prism, the cartesian derivatives of the shape functions are directly obtained by

$$\frac{\partial N_i}{\partial x} = \frac{1}{a} \frac{\partial N_i}{\partial \xi} ; \quad \frac{\partial N_i}{\partial y} = \frac{1}{b} \frac{\partial N_i}{\partial \eta} ; \quad \frac{\partial N_i}{\partial z} = \frac{1}{c} \frac{\partial N_i}{\partial \zeta} \quad (7.55)$$

The shape functions must satisfy the standard conditions

$$N_i(\xi_j, \eta_j, \zeta_j) = \begin{cases} 1 & \text{if } i = j \\ 0 & \text{if } i \neq j \end{cases} \quad (7.56a)$$

and

$$\sum_{i=1}^n N_i(\xi, \eta, \zeta) = 1 \quad (7.56b)$$

7.8.1 Right prisms of the Lagrange family

The shape functions of Lagrange right prisms are obtained by multiplying three 1D polynomial Lagrange polynomials as

$$N_i(\xi, \eta, \zeta) = l_I^i(\xi) l_I^i(\eta) l_I^i(\zeta) \quad (7.57)$$

where $l_I^i(\xi)$ is the Lagrange polynomial of I th degree passing by node i , etc. For the same reasons mentioned in Section 7.3.4 it is usual, to choose the same polynomial approximation in each of the three directions ξ, η and ζ .

The terms contained in the shape functions of prismatic elements are deduced from the Pascal's tetrahedron. Figure 7.17 shows the linear and quadratic elements of this family whose shape functions are derived next.

Linear right prism of the Lagrange family

The simplest Lagrange prismatic element is the 8-noded linear prism shown in Figure 7.17.

The shape function of a node is obtained by multiplying the three linear polynomials in ξ, η and ζ , corresponding to the node. In general form

$$N_i(\xi, \eta, \zeta) = \frac{1}{8} (1 + \xi_i \xi) (1 + \eta_i \eta) (1 + \zeta_i \zeta) \quad (7.58)$$

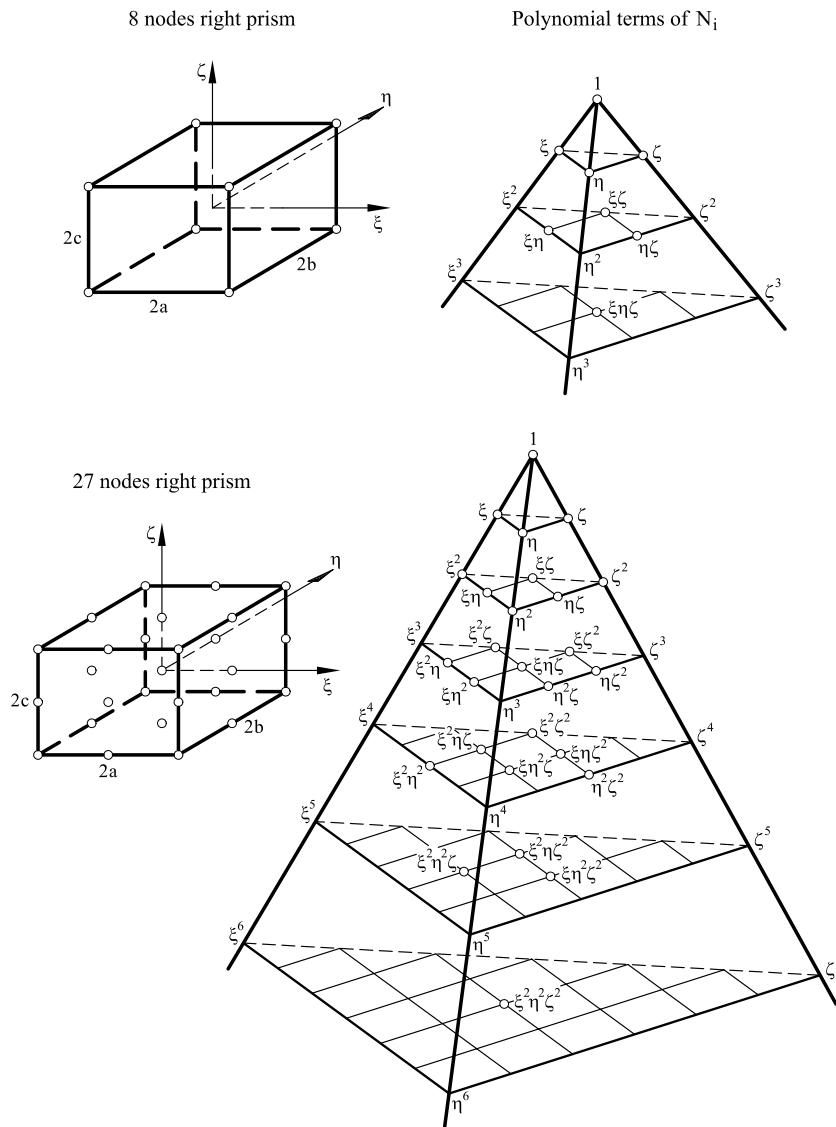


Fig. 7.17: Linear and quadratic right prisms of the Lagrange family. Polynomial terms contained in the shape functions deduced from the Pascal's tetrahedron

Note that:

1. The shape functions contain a complete linear polynomial in ξ, η, ζ and the incomplete quadratic and cubic terms $\xi\eta, \xi\zeta, \eta\xi$ and $\xi\eta\zeta, \xi\eta\zeta$ (see Figure 7.18).
2. The shape functions satisfy the conditions (7.56).

The linear hexahedron is a popular element due to the small number of nodal variables, which is attractive for practical 3D analysis.

The linear hexahedron performs very well for problems with uniform gradients, whereas its accuracy is poor for problems where strains gradient changes occur.

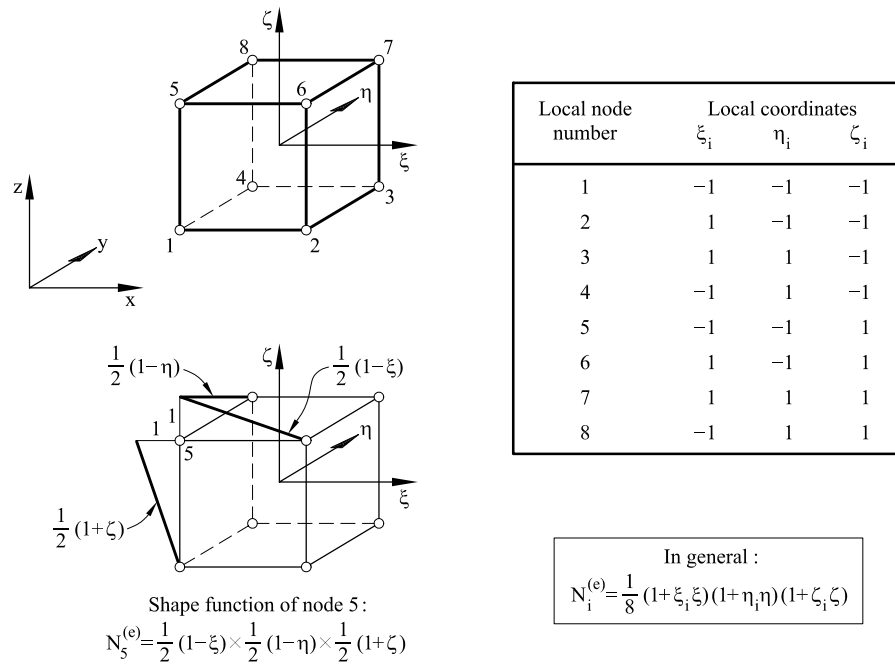


Fig. 7.18: Shape functions for the linear right prism

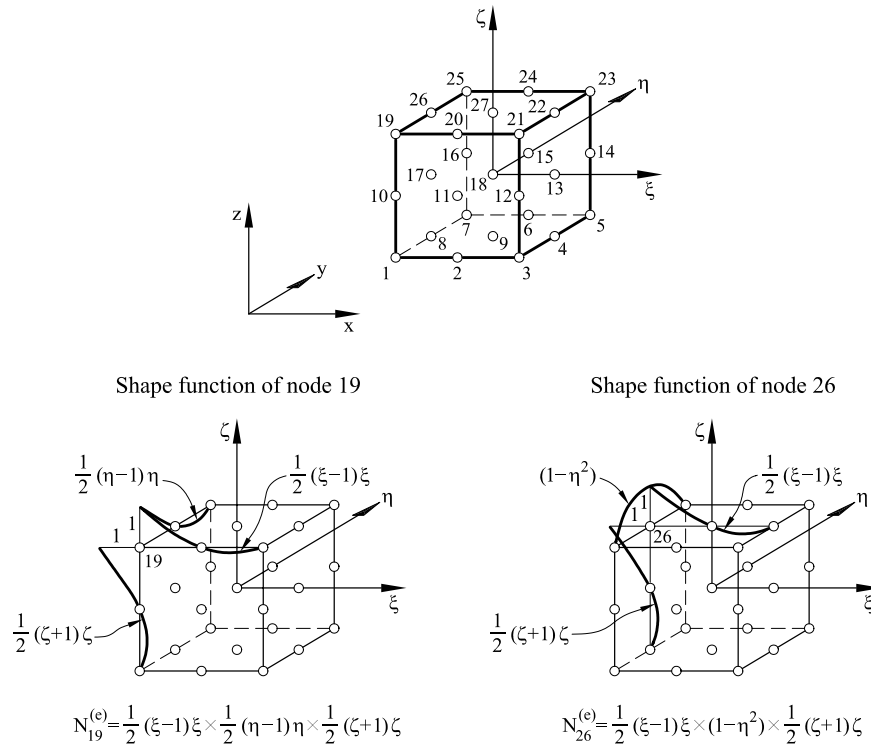


Fig. 7.19: Quadratic right prism of the Lagrange family. Shape functions for a corner node and a mid-side node

Quadratic right prism of the Lagrange family

The quadratic Lagrange prism has 27 nodes (see Figure 7.19). The shape functions are obtained by the product of three 1D quadratic Lagrange polynomials. Figure 7.19 shows the derivation of the shape functions for a corner node and a mid-side node. It is simple to extrapolate this procedure to obtain the following general expressions

Corner nodes

$$N_i = \frac{1}{8}(\xi^2 + \xi\xi_i)(\eta^2 + \eta\eta_i)(\zeta^2 + \zeta\zeta_i) \quad ; \quad i = \begin{matrix} 1,3,5,7 \\ 19,21,23,25 \end{matrix} \quad (7.59)$$

Mid-side nodes

$$N_i = \frac{1}{4}\eta_i^2(\eta^2 - \eta\eta_i)\zeta^2(\zeta^2 - \zeta\zeta_i)(1 - \xi^2) + \frac{1}{4}\zeta_i^2(\zeta^2 - \zeta\zeta_i) + \xi_i^2(\xi^2 - \xi\xi_i)(1 - \eta^2) + \frac{1}{4}\xi_i^2(\xi^2 - \xi\xi_i)\eta_i^2(\eta^2 - \eta\eta_i)(1 - \zeta^2) \quad ; \quad i = \begin{matrix} 2,4,6,8 \\ 10,12,14,16 \\ 20,22,24,26 \end{matrix} \quad (7.60)$$

Face nodes

$$N_i = \frac{1}{2}(1 - \xi^2)(1 - \eta^2)(\zeta + \zeta_i\zeta^2) + \frac{1}{2}(1 - \eta^2)(1 - \zeta^2)(\xi + \xi_i\xi^2) + \frac{1}{2}(1 - \xi^2)(1 - \zeta^2)(\eta + \eta_i\eta^2) \quad ; \quad i = \begin{matrix} 9,11,13 \\ 15,17,27 \end{matrix} \quad (7.61)$$

Central internal node

$$N_{18} = (1 - \xi^2)(1 - \eta^2)(1 - \zeta^2) \quad (7.62)$$

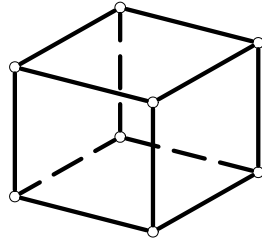
Other hexahedral elements of the Lagrange family

The next members of the Lagrange family are the 64-noded cubic prism (4 nodes along each edge) and the 125-noded quartic prism. Their shape functions are obtained by the product of three 1D cubic and quartic polynomials respectively. These elements in their right form are in general not competitive versus the analogous Serendipity element which involve lower nodal variables.

7.8.2 Serendipity prisms

Serendipity prisms are obtained by extension from the corresponding 2D rectangular Serendipity elements. Figure 7.20 shows the first two elements in the family, i.e. the 8- and 20-noded right prisms. Note that the 8-noded prism is common to the Lagrange and Serendipity families and hence its shape functions coincide with those given in (7.58).

Serendipity right prism of 8 nodes



Terms of N_i

$$1, \xi, \eta, \zeta, \xi\eta, \xi\zeta, \zeta\eta, \xi\eta\zeta$$

Serendipity right prism of 20 nodes

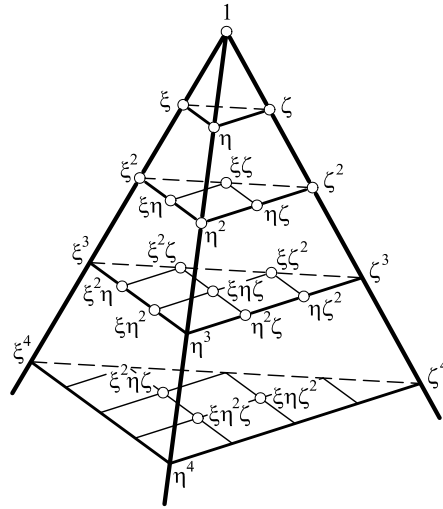
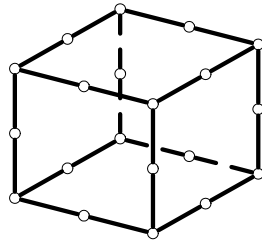


Fig. 7.20: 8-noded and 20-noded Serendipity prisms. Polynomial terms contained in the shape functions deduced from the Pascal's tetrahedron

20-noded quadratic Serendipity prism

The shape functions are obtained using similar criteria as for the 8-noded rectangle (Section 7.4.1). The shape functions for the side nodes are obtained by multiplying a 1D quadratic Lagrange polynomial and two 1D linear polynomials expressed in the natural coordinates. For the corner nodes, a two step procedure is followed. The first step involves the derivation of the trilinear function corresponding to the node. This function is subsequently modified so that it takes a zero value at the side nodes, by subtracting one half of the values of the shape function of the side nodes adjacent to the relevant corner node under consideration. See Section 7.4.1 for details.

Figure 7.21 shows the derivation of the shape function for a side node (20) and a corner node (13). The element shape functions are written in compact form as

Corner nodes

$$N_i = \frac{1}{8}(1 + \xi_i\xi)(1 + \eta_i\eta)(1 + \zeta_i\zeta)(\xi_i\xi + \eta_i\eta + \zeta_i\zeta - 2) \quad ; \quad i = \begin{matrix} 1, 3, 5, 7 \\ 13, 15, 17, 19 \end{matrix} \quad (7.63)$$

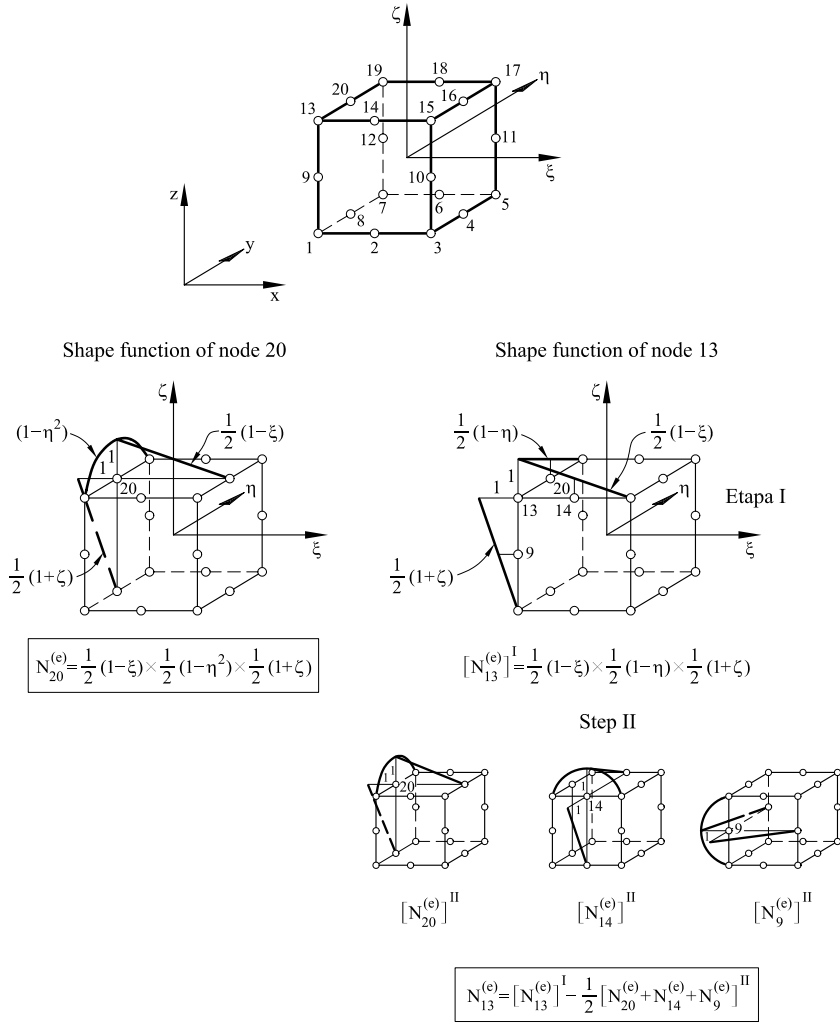


Fig. 7.21: 20-noded quadratic Serendipity prism. Shape functions for a side node and a corner node

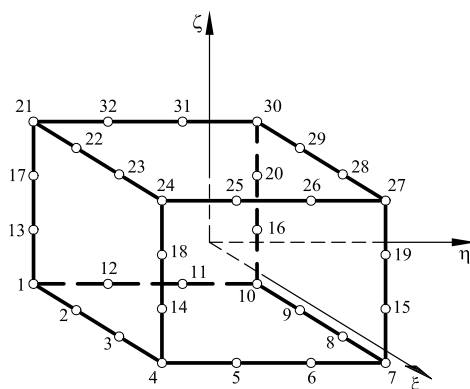
Side nodes

$$\begin{aligned}
 N_i &= \frac{1}{4}(1 - \xi^2)(1 + \eta_i\eta)(1 + \zeta_i\zeta) & ; & \quad i = 2, 6, 14, 18 \\
 &= \frac{1}{4}(1 - \eta^2)(1 + \zeta_i\zeta)(1 + \xi_i\xi) & ; & \quad i = 4, 8, 16, 20 \\
 &= \frac{1}{4}(1 - \zeta^2)(1 + \eta_i\eta)(1 + \xi_i\xi) & ; & \quad i = 9, 10, 11, 12
 \end{aligned} \tag{7.64}$$

Note that:

1. The shape functions contain a complete quadratic polynomial plus the terms $\xi\eta^2$, $\xi^2\eta$, $\xi^2\zeta$, $\xi\cdot\zeta^2$, $\zeta^2\eta$, $\eta^2\zeta$, $\xi\eta\zeta$, $\xi^2\eta\zeta$, $\xi\eta^2\zeta$ and $\xi\eta\zeta^2$. The shape functions satisfy the conditions in (7.56).
2. The 20-noded Serendipity prism has the same quadratic approximation as the 27-noded Lagrange prism. This means savings of 21 nodal vari-

Serendipity right prism of 32 nodes



Shape functions

$$\begin{aligned}
 N_i &= \frac{9}{64} (1+\xi\xi_i)(1+\eta\eta_i)(1+\zeta\zeta_i) \left(-\frac{19}{9} + \xi^2 + \eta^2 + \zeta^2\right) & i &= \begin{cases} 1, 4, 7, 10 \\ 21, 24, 27, 30 \end{cases} \\
 N_i &= \frac{81}{64} (1-\xi^2) \left(\frac{1}{9} + \xi\xi_i\right) (1+\eta\eta_i) (1+\zeta\zeta_i) & i &= \begin{cases} 2, 3, 8, 9 \\ 22, 23, 28, 29 \end{cases} \\
 N_i &= \frac{81}{64} (1+\xi\xi_i) (1-\eta^2) \left(\frac{1}{9} + \eta\eta_i\right) (1+\zeta\zeta_i) & i &= \begin{cases} 5, 6, 11, 12 \\ 25, 26, 31, 32 \end{cases} \\
 N_i &= \frac{81}{64} (1+\xi\xi_i) (1+\eta\eta_i) \left(\frac{1}{9} + \zeta\zeta_i\right) (1-\zeta^2) & i &= \begin{cases} 13, 14, 15, 16 \\ 17, 18, 19, 20 \end{cases}
 \end{aligned}$$

Fig. 7.22: Shape functions for the 32-noded cubic Serendipity prism

ables per element, which explains the popularity of the 20-noded right prism for practical applications.

32-noded cubic Serendipity prism

This element has 8 corner nodes and 24 nodes along the edges as shown in Figure 7.22. The 12 face nodes define a cubic polynomial over each face as for the corresponding quadrilateral element (see Section 7.4.2). The shape functions for the side nodes are obtained by multiplying a 1D cubic Lagrange polynomial and two 1D linear polynomials expressed in the natural coordinates. For the corner nodes the starting point is the trilinear shape function, from which a proportion of the shape functions of the side nodes are subtracted so that the final shape function takes a zero value at these nodes. The reader is invited to derive the expressions of the shape functions for this element shown in Figure 7.22.

The shape functions contain a complete cubic polynomial (20 terms) plus the following twelve terms: $\xi^3\eta$, $\xi\eta^3$, $\eta^3\zeta$, $\eta\zeta^3$, $\xi\zeta^3$, $\zeta^3\xi$, $\xi^2\eta\zeta$, $\xi\eta^2\zeta$, $\xi\eta\zeta^2$, $\xi^3\eta\zeta$, $\xi\eta^3\zeta$, $\xi\eta\zeta^3$. Therefore, the cubic Serendipity prism has the same approximation as the analogous 64-noded Lagrangian prism, but with a substantial reduction

in the number of nodal variables. This element is less popular however than the 20-noded prism.

Example: 7.2 Compute the matrix $\mathbf{K}_{11}^{(e)}$ for the 8-noded right prism of Figure 7.8 for a homogeneous isotropic material.

- *Solution*

The cartesian derivatives of the shape function N_1 are obtained using Eqs.(7.58) as (note that the element sides are straight)

$$\frac{\partial N_1}{\partial x} = \frac{\partial N_1}{\partial \xi} \frac{\partial \xi}{\partial x} = \frac{1}{a} \frac{\partial}{\partial \xi} \left[\frac{1}{8} (1 - \xi)(1 - \eta)(1 - \zeta) \right] = -\frac{1}{8a} (1 - \eta)(1 - \zeta)$$

and

$$\frac{\partial N_1}{\partial y} = \frac{\partial N_1}{\partial \eta} \frac{\partial \eta}{\partial y} = -\frac{1}{8b} (1 - \xi)(1 - \zeta)$$

$$\frac{\partial N_1}{\partial z} = \frac{\partial N_1}{\partial \zeta} \frac{\partial \zeta}{\partial z} = -\frac{1}{8c} (1 - \xi)(1 - \eta)$$

The strain matrix \mathbf{B}_1 is

$$\mathbf{B}_1 = \frac{1}{8} \begin{bmatrix} -\frac{1}{a}(1 - \eta)(1 - \zeta) & 0 & 0 \\ 0 & -\frac{1}{b}(1 - \xi)(1 - \zeta) & 0 \\ 0 & 0 & -\frac{1}{c}(1 - \xi)(1 - \eta) \\ -\frac{1}{b}(1 - \xi)(1 - \zeta) & -\frac{1}{a}(1 - \eta)(1 - \zeta) & 0 \\ -\frac{1}{c}(1 - \xi)(1 - \eta) & 0 & -\frac{1}{a}(1 - \eta)(1 - \zeta) \\ 0 & -\frac{1}{c}(1 - \zeta)(1 - \eta) & -\frac{1}{b}(1 - \xi)(1 - \zeta) \end{bmatrix}$$

Matrix $\mathbf{K}_{11}^{(e)}$ is obtained by

$$\mathbf{K}_{11}^{(e)} = \iiint_{V^{(e)}} \mathbf{B}_1^T \mathbf{D} \mathbf{B}_1 dV = \int_{-1}^{+1} \int_{-1}^{+1} \int_{-1}^{+1} \mathbf{B}_1^T \mathbf{D} \mathbf{B}_1 abc d\xi d\eta d\zeta$$

Denoting $\bar{\xi} = 1 - \xi$, $\bar{\eta} = 1 - \eta$ and $\bar{\zeta} = 1 - \zeta$ we can write

$$\mathbf{D} \mathbf{B}_1 = \frac{1}{8} \begin{bmatrix} d_{11} & d_{12} & d_{13} & & & & \\ d_{12} & d_{22} & d_{23} & & \mathbf{0} & & \\ d_{13} & d_{23} & d_{33} & & & & \\ & & & d_{44} & & & \\ \mathbf{0} & & & & d_{55} & & \\ & & & & & d_{66} & \end{bmatrix} \begin{bmatrix} -\frac{1}{a}\bar{\eta}\bar{\zeta} & 0 & 0 \\ 0 & -\frac{1}{b}\bar{\xi}\bar{\zeta} & 0 \\ 0 & 0 & -\frac{1}{c}\bar{\xi}\bar{\eta} \\ -\frac{1}{b}\bar{\xi}\bar{\zeta} & -\frac{1}{a}\bar{\eta}\bar{\zeta} & 0 \\ -\frac{1}{c}\bar{\xi}\bar{\eta} & 0 & -\frac{1}{a}\bar{\eta}\bar{\zeta} \\ 0 & -\frac{1}{c}\bar{\xi}\bar{\eta} & -\frac{1}{b}\bar{\xi}\bar{\zeta} \end{bmatrix} =$$

$$= \frac{1}{8} \begin{bmatrix} -\frac{d_{11}}{a}\bar{\eta}\bar{\zeta} & -\frac{d_{12}}{b}\bar{\xi}\bar{\zeta} & -\frac{d_{13}}{c}\bar{\xi}\bar{\eta} \\ -\frac{d_{12}}{a}\bar{\eta}\bar{\zeta} & -\frac{d_{22}}{b}\bar{\xi}\bar{\zeta} & -\frac{d_{23}}{c}\bar{\xi}\bar{\eta} \\ -\frac{d_{13}}{a}\bar{\eta}\bar{\zeta} & -\frac{d_{23}}{b}\bar{\xi}\bar{\zeta} & -\frac{d_{33}}{c}\bar{\xi}\bar{\eta} \\ -\frac{d_{44}}{b}\bar{\xi}\bar{\zeta} & -\frac{d_{44}}{a}\bar{\eta}\bar{\zeta} & 0 \\ -\frac{d_{55}}{c}\bar{\xi}\bar{\eta} & 0 & -\frac{d_{55}}{a}\bar{\eta}\bar{\zeta} \\ 0 & -\frac{d_{66}}{c}\bar{\zeta}\bar{\eta} & -\frac{d_{66}}{b}\bar{\xi}\bar{\zeta} \end{bmatrix}$$

Multiplying the previous equation by \mathbf{B}_1^T gives

$$\mathbf{B}_1^T \mathbf{D} \mathbf{B}_1 =$$

$$= \frac{1}{64} \begin{bmatrix} \left(\frac{d_{11}}{a^2}\bar{\eta}_1 + \frac{d_{44}}{b^2}\bar{\xi}_2 + \frac{d_{55}}{c^2}\bar{\xi}_1 \right) & \left(d_{12} + d_{44} \right) \frac{\bar{\xi}_3}{ab} & \left(d_{13} + d_{55} \right) \frac{\bar{\xi}_4}{ac} \\ & \left(\frac{d_{22}}{b^2}\bar{\xi}_2 + \frac{d_{44}}{a^2}\bar{\eta}_1 + \frac{d_{66}}{c^2}\bar{\xi}_1 \right) & \left(d_{23} + d_{66} \right) \frac{\bar{\xi}_5}{bc} \\ \text{Symmetrical} & & \left(\frac{d_{33}}{c^2}\bar{\xi}_1 + \frac{d_{55}}{a^2}\bar{\eta}_1 + \frac{d_{66}}{b^2}\bar{\xi}_2 \right) \end{bmatrix}$$

with $\bar{\xi}_1 = \bar{\xi}\bar{\eta}$, $\bar{\xi}_2 = \bar{\xi}^2\bar{\zeta}^2$, $\bar{\xi}_3 = \bar{\xi}\bar{\eta}\bar{\zeta}^2$, $\bar{\xi}_4 = \bar{\xi}\bar{\eta}^2\bar{\zeta}$, $\bar{\xi}_5 = \bar{\xi}^2\bar{\eta}\bar{\zeta}$, $\bar{\eta}_1 = \bar{\eta}^2\bar{\zeta}^2$.

Taking into account that

$$\int_{-1}^{+1} \bar{\xi}^2 d\xi = \int_{-1}^{+1} \bar{\eta}^2 d\eta = \int_{-1}^{+1} \bar{\zeta}^2 d\zeta = \frac{8}{3}$$

$$\int_{-1}^{+1} \bar{\xi} d\xi = \int_{-1}^{+1} \bar{\eta} d\eta = \int_{-1}^{+1} \bar{\zeta} d\zeta = 2$$

we finally obtain

$$\mathbf{K}_{11}^{(e)} = \frac{V^{(e)}}{8} \begin{bmatrix} \frac{1}{9} \left(\frac{d_{11}}{a^2} + \frac{d_{44}}{b^2} + \frac{d_{55}}{c^2} \right) & \frac{1}{6ab} (d_{12} + d_{44}) & \frac{1}{6ac} (d_{13} + d_{55}) \\ & \frac{1}{9} \left(\frac{d_{22}}{b^2} + \frac{d_{44}}{a^2} + \frac{d_{66}}{c^2} \right) & \frac{1}{6bc} (d_{23} + d_{66}) \\ & \text{Symmetrical} & \frac{1}{9} \left(\frac{d_{33}}{c^2} + \frac{d_{55}}{a^2} + \frac{d_{66}}{b^2} \right) \end{bmatrix}$$

The rest of the $\mathbf{K}_{ij}^{(e)}$ matrices are obtained following a similar procedure.

7.9 STRAIGHT EDGED TETRAHEDRA

Straight edged tetrahedral elements are a direct 3D extension of straight sided triangles. Their shape functions are also complete polynomials whose terms can easily be deduced from the Pascal's tetrahedron as shown in Figure 7.23.

The shape functions of tetrahedral elements can be written in terms of volume coordinates and/or natural coordinates. *The volume coordinates* are identified by L_1, L_2, L_3 and L_4 and have a similar meaning to the area coordinates in triangles. Each coordinate L_i is now defined as the ratio between the volume of the tetrahedron formed by a point inside the element P and the face opposite node i , and the total volume (see Figure 7.24). Thus

$$L_i = \frac{\text{Volume } Pjkl}{V^{(e)}} \quad ; \quad i = 1, 2, 3, 4 \quad (7.65)$$

Obviously, the following expression holds

$$L_1 + L_2 + L_3 + L_4 = 1 \quad (7.66)$$

Volume coordinates can be used to define a linear interpolation of the element geometry as

$$x = \sum_{i=1}^4 L_i x_i, \quad y = \sum_{i=1}^4 L_i y_i, \quad z = \sum_{i=1}^4 L_i z_i \quad (7.67)$$

Eqs. (7.65) and (7.66) allow us to eliminate L_i in terms of the cartesian coordinates as

$$L_i = \frac{l}{6V^{(e)}} (a_i + b_i x + c_i y + d_i z) = N_i \quad (7.68)$$

where a_i, b_i, c_i, d_i coincide with the values given in Eq.(5.20) for the shape functions of the linear tetrahedron.

Eq.(7.68) allows us to obtain the cartesian derivatives of the volume coordinates as

$$\frac{\partial L_i}{\partial x} = \frac{l}{6V^{(e)}} b_i \quad ; \quad \frac{\partial L_i}{\partial y} = \frac{l}{6V^{(e)}} c_i \quad ; \quad \frac{\partial L_i}{\partial z} = \frac{l}{6V^{(e)}} d_i \quad (7.69)$$

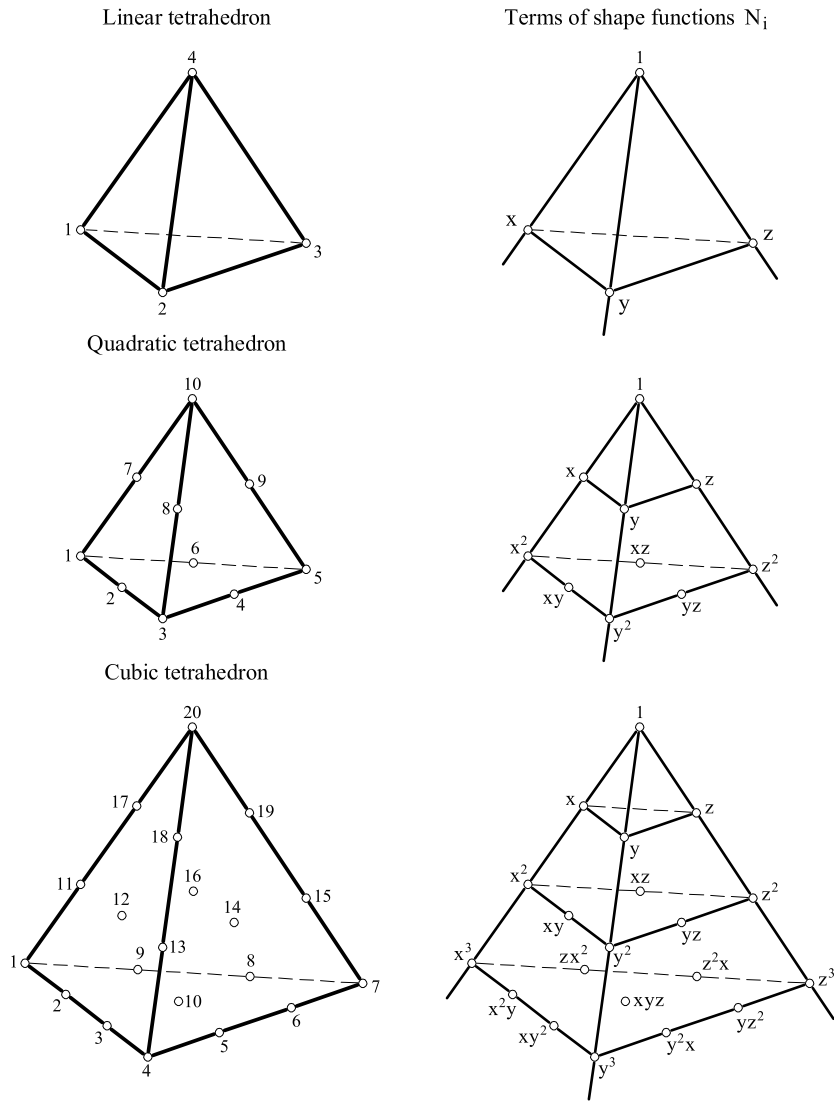


Fig. 7.23: Straight edged tetrahedral elements: linear (4 nodes), quadratic (10 nodes), cubic (20 nodes). Polynomial terms contained in the shape functions

The *natural coordinates* α, β, γ define a normalized straight tetrahedron with faces for $\alpha = 0, \beta = 0, \gamma = 0$ and $1 - \alpha - \beta - \gamma = 0$ (Figure 7.25). For a tetrahedron with edges a, b, c we have

$$\alpha = \frac{x - x_i}{a} \quad ; \quad \beta = \frac{y - y_i}{b} \quad ; \quad \gamma = \frac{z - z_i}{c} \tag{7.70}$$

where i is the node taken as origin of the natural coordinate system. It is deduced from Eq.(7.70)

$$\frac{d\alpha}{dx} = \frac{1}{a} \quad ; \quad \frac{d\beta}{dy} = \frac{1}{b} \quad ; \quad \frac{d\gamma}{dz} = \frac{1}{c} \tag{7.71}$$

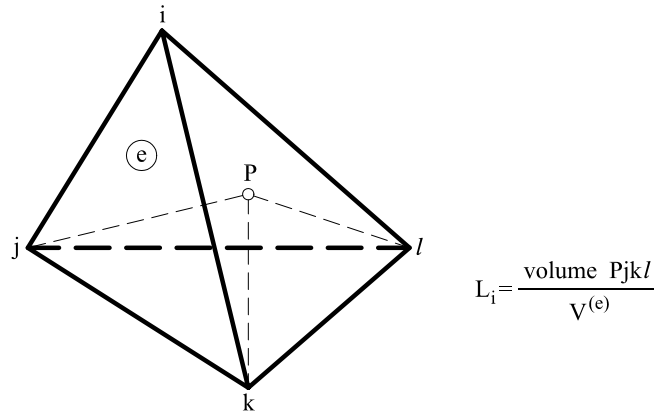


Fig. 7.24: Volume coordinates in a tetrahedron

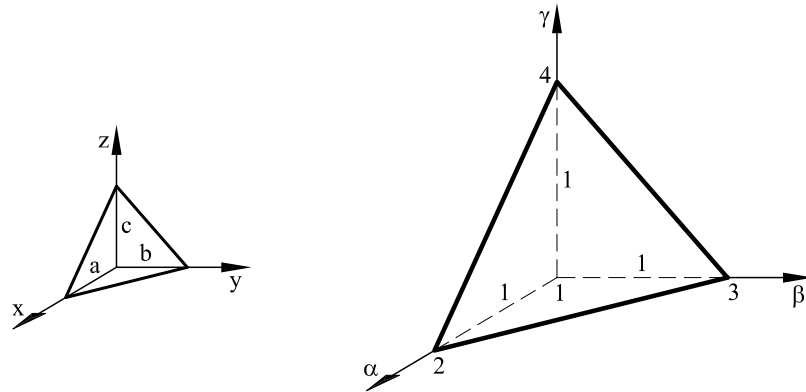


Fig. 7.25: Natural coordinate system α, β, γ in a tetrahedron

A differential of volume can be expressed as

$$dx \, dy \, dz = abc \, d\alpha \, d\beta \, d\gamma \quad (7.72)$$

The integral of a function $f(x, y, z)$ over the element can be written in the natural coordinate system as

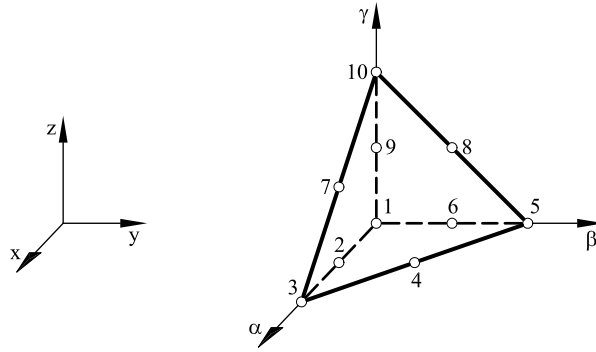
$$\iiint_{V^{(e)}} f(x, y, z) \, dx \, dy \, dz = \int_0^1 \int_0^{1-\alpha} \int_0^{1-\beta-\gamma} f(\alpha, \beta, \gamma) abc \, d\alpha \, d\beta \, d\gamma \quad (7.73)$$

The shape functions of the linear tetrahedron can be expressed simply in terms of the natural coordinates α, β, γ as

$$N_1 = 1 - \alpha - \beta - \gamma ; \quad N_2 = \alpha ; \quad N_3 = \beta ; \quad N_4 = \gamma \quad (7.74)$$

Note that the shape functions in the natural coordinate system satisfy Eqs.(7.56). Also from Eqs.(7.74) and (7.71) we obtain

$$\frac{\partial N_i}{\partial x} = \frac{1}{a} \frac{\partial N_i}{\partial \alpha} ; \quad \frac{\partial N_i}{\partial y} = \frac{1}{b} \frac{\partial N_i}{\partial \beta} ; \quad \frac{\partial N_i}{\partial z} = \frac{1}{c} \frac{\partial N_i}{\partial \gamma} \quad (7.75)$$



Local node numbers	Coordinates				Natural coordinates		
	I	J	K	L	α_i	β_i	γ_i
1	2	0	0	0	0	0	0
2	1	1	0	0	1/2	0	0
3	0	2	0	0	1	0	0
4	0	1	1	0	1/2	1/2	0
5	0	0	2	0	0	1	0
6	1	0	1	0	0	1/2	0
7	0	1	0	1	1/2	0	1/2
8	0	0	1	1	0	1/2	1/2
9	1	0	0	1	0	0	1/2
10	0	0	0	2	0	0	1

Fig. 7.26: 10-noded quadratic tetrahedron. Generalized coordinates I, J, K, L and natural coordinates α, β, γ for each node

The relationship between the volume and natural coordinates is readily deduced from Eqs.(7.68) and (7.74) as

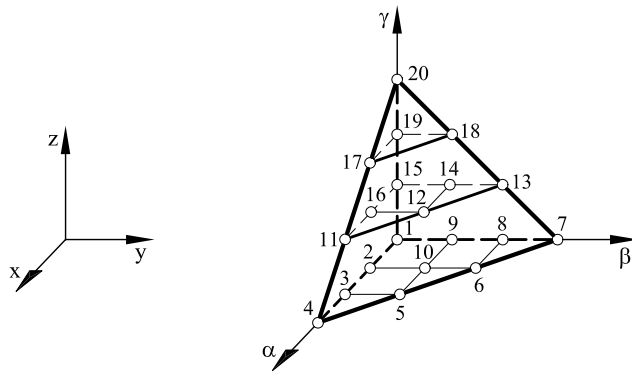
$$L_1 = 1 - \alpha - \beta - \gamma; \quad L_2 = \alpha; \quad L_3 = \beta \quad L_4 = \gamma \quad (7.76)$$

Volume coordinates allow us to express the element shape functions of tetrahedral elements by the product of four 1D Lagrange polynomials, in a similar way as explained for triangular elements. Thus the shape function of a node i with generalized coordinates (I, J, K, L) is given by

$$N_i = l_I^i(L_1) l_J^i(L_2) l_K^i(L_3) l_L^i(L_4) \quad (7.77)$$

where the value of the generalized coordinates $I, J, K,$ and L coincides with the power of each volume coordinate in the expression of N_i . There $I+J+K+L = M$ where M is the degree of the complete polynomial contained in N_i . Also, $l_I^i(L_j)$ is the Lagrange polynomial of I th degree in L_j passing by node i (see Eq.(3.5)). Figures 7.26 and 7.27 show the values of the generalized coordinates I, J, K, L for two typical tetrahedral elements.

The expression of the shape functions in terms of natural coordinates α, β, γ is straightforward by making use of the transformations (7.76).



Local node numbers	Coordinates				Natural Coordinates		
	I	J	K	L	α_i	β_i	γ_i
1	3	0	0	0	0	0	0
2	2	1	0	0	1/3	0	0
3	1	2	0	0	2/3	0	0
4	0	3	0	0	1	0	0
5	0	2	1	0	2/3	1/3	0
6	0	1	2	0	1/2	2/3	0
7	0	0	3	0	0	1	0
8	1	0	2	0	0	2/3	0
9	2	0	1	0	0	1/3	0
10	1	1	1	0	1/3	1/3	0
11	0	2	0	1	2/3	0	1/3
12	0	1	1	1	1/3	1/3	1/3
13	0	0	2	1	0	2/3	1/3
14	1	0	1	1	0	1/3	1/3
15	2	0	0	1	0	0	1/3
16	1	1	0	1	1/3	0	1/3
17	0	1	0	2	1/3	0	2/3
18	0	0	1	2	0	1/3	2/3
19	1	0	0	2	0	0	2/3
20	0	0	0	3	0	0	1

Fig. 7.27: 20-noded cubic tetrahedron. Generalized coordinates I, J, K, L and natural coordinates for each node

7.9.1 Shape functions for the 10-noded quadratic tetrahedron

The nodal values of the generalized coordinates I, J, K, L and of the natural coordinates are shown in Figure 7.26. The values of the volume coordinates L_i are deduced from Eq.(7.76). The shape functions are derived next using Eq.(7.77).

Node 1

Position $(I, J, K, L) : (2, 0, 0, 0)$. Volume coordinates : $(1, 0, 0, 0)$

$$N_1 = l_2^1(L_1) = \frac{\left(L_1 - \frac{1}{2}\right)L_1}{1 - \frac{1}{2}} = (2L_1 - 1)L_1 \quad (7.78)$$

Node 2

Position $(I, J, K, L) : (1, 1, 0, 0)$. Volume coordinates : $(\frac{1}{2}, \frac{1}{2}, 0, 0)$

$$N_2 = l_1^2(L_1) l_1^2(L_2) = \frac{L_1}{\frac{1}{2}} \frac{L_2}{\frac{1}{2}} = 4L_1 L_2 \quad (7.79)$$

The same procedure gives

$$\begin{aligned} N_3 &= (2L_2 - 1) & ; & & N_7 &= 4 L_2 L_4 \\ N_4 &= 4L_2 L_3 & ; & & N_8 &= 4 L_3 L_4 \\ N_5 &= (2 L_3 - 1)L - 3 & ; & & N_9 &= 4 L_1 L_4 \\ N_6 &= 4 L_1 L_3 & ; & & N_{10} &= (2 L_4 - 1) L_4 \end{aligned} \quad (7.80)$$

The expression of N_i in terms of the natural coordinates is obtained using Eq.(7.76). The cartesian form of N_i for a *straight edged* tetrahedron is directly obtained from Eq.(7.68).

The shape functions of this element contain all the terms of a quadratic polynomial (Figure (7.23)) and they satisfy Eqs.(7.56).

7.9.2 Shape functions for the 20-noded quadratic tetrahedron

The nodal values of the generalized coordinates I, J, K, L and α, β, γ are shown in Figure 7.27. From Eqs.(7.77) we obtain:

Node 1

Position $(I, J, K, L) : (3, 0, 0, 0)$. Volume coordinates : $(3, 0, 0, 0)$

$$N_1 = l_3^1(L_1) = \frac{\left(L_1 - \frac{2}{3}\right)\left(L_1 - \frac{1}{3}\right)L_1}{\left(1 - \frac{2}{3}\right)\left(1 - \frac{1}{3}\right)1} = \frac{1}{2}L_1(3L_1 - 1)(3L_1 - 2) \quad (7.81)$$

Node 2

Position $(I, J, K, L) : (2, 1, 0, 0)$. Volume coordinates : $(\frac{2}{3}, \frac{1}{3}, 0, 0)$

$$N_2 = l_2^2(L_1) L_1^2(L_2) = \frac{\left(L_1 - \frac{1}{3}\right)L - 1}{\left(\frac{2}{3} - \frac{1}{3}\right)\frac{2}{3}} \frac{L_2}{\frac{1}{3}} = \frac{9}{2}(3L_1 - 1)L_1 L_2 \quad (7.82)$$

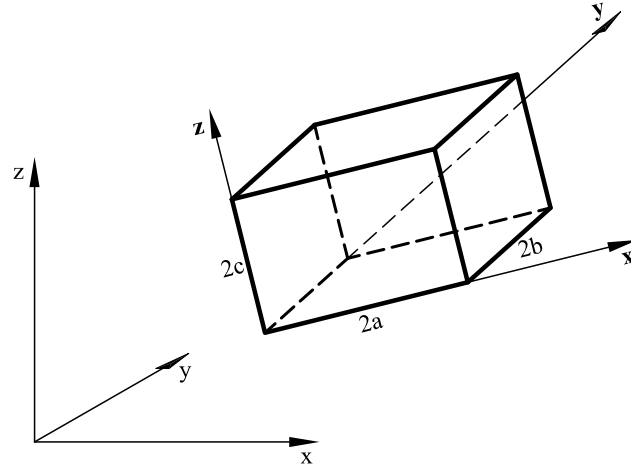


Fig. 7.28: Local coordinate system $\bar{x}\bar{y}\bar{z}$ for the analytical computation of volume integrals over right prisms

Following a similar procedure gives

$$\begin{aligned}
 N_3 &= \frac{9}{2}(3L_2 - 1)L_1L_2 & ; & \quad N_9 = \frac{9}{2}(3L_1 - 1)L_1L_3 & \quad ; & \quad N_{15} = \frac{9}{2}(3L_1 - 1)L_1L_4 \\
 N_4 &= \frac{1}{2}L_2(3L_2 - 1)(3L_2 - 2) & ; & \quad N_{10} = 27 L_1 L_2L_3 & \quad ; & \quad N_{16} = 27L_1L_2L_4 \\
 N_5 &= \frac{9}{2}(3L_2 - 1)L_2 L_3 & ; & \quad N_{11} = \frac{9}{2}(3L_2 - 1)L_2 L_4 & \quad ; & \quad N_{17} = \frac{9}{2}(3L_4 - 1)L_4 L_2 \\
 N_6 &= \frac{9}{2}(3L_3 - 1)L_3 L_2 & ; & \quad N_{12} = 27 L_2 L_3 L_4 & \quad ; & \quad N_{18} = \frac{9}{2}(3L_4 - 1)L_4 L_3 \\
 N_7 &= \frac{1}{2}L_3(3L_3 - 1)(3L_3 - 2) & ; & \quad N_{13} = \frac{9}{2}(3L_3 - 1)L_3 L_4 & \quad ; & \quad N_{19} = \frac{9}{2}(3L_4 - 1)L_4 L_1 \\
 N_8 &= \frac{9}{2}(3L_3 - 1)L_3L_1 & ; & \quad N_{14} = 27L_1L_3L_4 & \quad ; & \quad N_{20} = \frac{1}{2}L_4(3L_4 - 1)(3L_4 - 2)
 \end{aligned} \tag{7.83}$$

Eqs.(7.76) allows us to express N_i in terms of the natural coordinates. The cartesian form of N_i for a straight edged tetrahedron is obtained substituting Eq.(7.68) into above expressions. Note that the shape functions are complete cubic polynomials and they satisfy Eq.(7.56).

7.10 COMPUTATION OF THE ELEMENT INTEGRALS

7.10.1 Analytical computation of element integrals

In general, the computation of the element integrals is carried out via numerical integration. Useful analytical rules can, however, be derived for straight edged tetrahedra or right prisms as shown below.

Volume integrals over right prisms can be computed exactly using the local coordinate system $\bar{x}\bar{y}\bar{z}$ shown in Figure 7.28. For instance, the integral over a face with $\bar{x} = constant$, is first obtained by Eq.(7.41) and then a simple line

integral in the \bar{z} direction is performed. The resulting local stiffness matrix $\bar{\mathbf{K}}$ is next transformed to the global axes xyz by a transformation similar to Eq.(7.42) taking into account the third cartesian axis. This procedure is not applicable to non-regular or hexahedra curved sides for which the use of an isoparametric formulation and numericaly integration is essential.

The integrals over straight-sided tetrahedra have simpler expressions. Thus, the volume integral of a polynomial term expressed in volume coordinates is given by

$$\iiint_{V^{(e)}} L_1^k L_2^l L_3^m L_4^n dV = 6V^{(e)} \frac{k! l! m! n!}{(k+l+m+n+3)!} \quad (7.84)$$

Similarly, the surface integrals over the element faces can be obtained by Eqs.(7.40) or (7.38).

The use of natural coordinates does not introduce any additional difficulty. The volume integrals are computed by

$$\iiint_{V^{(e)}} \alpha^k \beta^l \gamma^m dV = 6V^{(e)} \frac{k! l! m!}{(k+l+m+3)!} \quad (7.85)$$

and the surface integrals can be obtained by Eq.(7.48). Recall that if any of the coordinates is missing in the integrals of Eqs.(7.84) and (7.85) then the corresponding power is made equal to one in the numerator and to zero in the denominator of the corresponding right-hand side.

Curved-side tetrahedra require an isoparametric formulation and numerical integration (Chapter 8).

Example: 7.3 Compute the submatrix $\mathbf{K}_{11}^{(e)}$ of a 20-noded quadratic tetrahedron with straight sides.

- **Solution**

We compute first the cartesian derivatives of the shape function N_1 expressed in terms of volume coordinates. For instance,

$$\frac{\partial N_1}{\partial x} = \frac{\partial N_1}{\partial L_1} \frac{\partial L_1}{\partial x} + \frac{\partial N_1}{\partial L_2} \frac{\partial L_2}{\partial x} + \frac{\partial N_1}{\partial L_3} \frac{\partial L_3}{\partial x} + \frac{\partial N_1}{\partial L_4} \frac{\partial L_4}{\partial x}$$

Since $N_1 = L_1(2L_1 - 1)$ we have from Eq.(7.68)

$$\frac{\partial N_1}{\partial x} = (4L_1 - 1) \frac{b_i}{6V^{(e)}}$$

Following a similar procedure gives

$$\frac{\partial N_1}{\partial y} = (4L_1 - 1) \frac{c_i}{6V^{(e)}} \quad \text{and} \quad \frac{\partial N_1}{\partial z} = (4L_1 - 1) \frac{d_i}{6V^{(e)}}$$

The strain matrix \mathbf{B}_1 is written as

$$\mathbf{B}_1 = \frac{(4L_1 - 1)}{6V^{(e)}} \begin{bmatrix} b_i & 0 & 0 \\ 0 & c_i & 0 \\ 0 & 0 & d_i \\ c_i & b_i & 0 \\ d_i & 0 & b_i \\ 0 & d_i & c_i \end{bmatrix} = \frac{(4L_1 - 1)}{6V^{(e)}} \bar{\mathbf{B}}_1$$

and matrix $\mathbf{K}_{11}^{(e)}$ is given by

$$\mathbf{K}_{11}^{(e)} = \iiint_{V^{(e)}} \mathbf{B}_1^T \mathbf{D} \mathbf{B}_1 dV = \frac{1}{36(V^{(e)})^2} \bar{\mathbf{B}}_1^T \mathbf{D} \bar{\mathbf{B}}_1 \iiint_{V^{(e)}} (4L_1 - 1)^2 dV$$

Making use of Eq.(7.84) gives finally

$$\mathbf{K}_{11}^{(e)} = \frac{1}{60V^{(e)}} \begin{bmatrix} (d_{11}b_1^2 + d_{44}c_1^2 + d_{55}d_1^2) & b_1c_1(d_{12} + d_{44}) & (d_{13}b_1d_1 + d_{55}d_1c_1) \\ & (d_{22}c_1^2 + d_{44}b_1^2 + d_{66}d_1^2) & c_1d_1(d_{23} + d_{66}) \\ \text{Symmetrical} & & (d_{33}d_1^2 + d_{55}b_1^2 + d_{66}c_1^2) \end{bmatrix}$$

The rest of the $\mathbf{K}_{ij}^{(e)}$ matrices are obtained in a similar manner.

Chapter 8

2D AND 3D ISOPARAMETRIC ELEMENTS

8.1 ISOPARAMETRIC QUADRILATERAL ELEMENTS

We recall that the term “isoparametric” means that the standard shape functions are used to interpolate the element geometry in terms of the nodal coordinates. Thus, the geometry of a 2D isoparametric quadrilateral with n nodes is expressed as

$$x = \sum_{i=1}^n N_i(\xi, \eta) x_i \quad ; \quad y = \sum_{i=1}^n N_i(\xi, \eta) y_i \quad (8.1)$$

where $N_i(\xi, \eta)$ are the standard displacement shape functions. Eqs.(8.1) relate the cartesian and the natural coordinates at each point. Such a relationship must be unique and this is satisfied if the Jacobian matrix of the coordinate transformation $x, y \rightarrow \xi, \eta$ has a constant sign over the element [S14].

It can be shown that this condition is satisfied for linear quadrilateral elements if all internal angles between two element sides are greater than 180° [S14]. For quadratic elements it is additionally required that the side nodes are located within the “middle third” of the distance between adjacent corners [J5]. There are no practical rules for higher order quadrilateral elements and the constant sign of the Jacobian is the only possible verification in this case. Figure 8.1 shows some examples of 2D isoparametric elements.

Most of the ideas of the isoparametric formulation originated from the work of Taig [T1, T2], who derived 4-noded isoparametric quadrilaterals. These concepts were generalized to more complex 2D and 3D elements by Irons [I2,7].

Eq.(8.1) allows us to obtain a relationship between the derivatives of the shape functions with respect to the cartesian and the natural coordinates. In general, N_i is expressed in terms of the natural coordinates ξ and η and the chain rule of derivation yields

$$\begin{aligned} \frac{\partial N_i}{\partial \xi} &= \frac{\partial N_i}{\partial x} \frac{\partial x}{\partial \xi} + \frac{\partial N_i}{\partial y} \frac{\partial y}{\partial \xi} \\ \frac{\partial N_i}{\partial \eta} &= \frac{\partial N_i}{\partial x} \frac{\partial x}{\partial \eta} + \frac{\partial N_i}{\partial y} \frac{\partial y}{\partial \eta} \end{aligned} \quad (8.2)$$

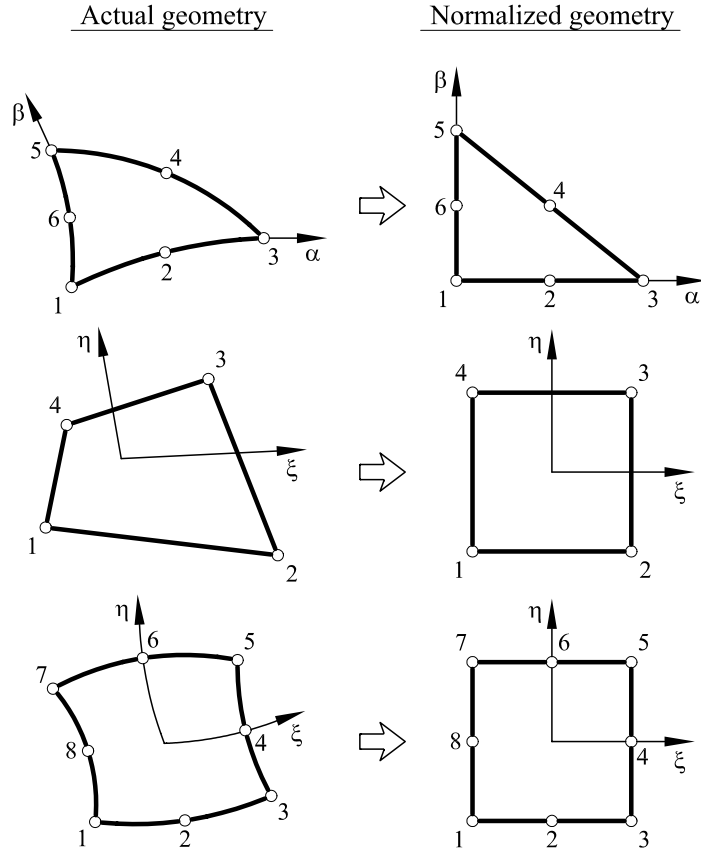


Fig. 8.1: Some two-dimensional isoparametric elements

In matrix form

$$\begin{Bmatrix} \frac{\partial N_i}{\partial \xi} \\ \frac{\partial N_i}{\partial \eta} \end{Bmatrix} = \underbrace{\begin{bmatrix} \frac{\partial x}{\partial \xi} & \frac{\partial y}{\partial \xi} \\ \frac{\partial x}{\partial \eta} & \frac{\partial y}{\partial \eta} \end{bmatrix}}_{\mathbf{J}^{(e)}} \begin{Bmatrix} \frac{\partial N_i}{\partial x} \\ \frac{\partial N_i}{\partial y} \end{Bmatrix} = \mathbf{J}^{(e)} \begin{Bmatrix} \frac{\partial N_i}{\partial x} \\ \frac{\partial N_i}{\partial y} \end{Bmatrix} \quad (8.3)$$

where $\mathbf{J}^{(e)}$ is the *Jacobian matrix* of the transformation between the cartesian and natural coordinates. The superindex e in \mathbf{J} denotes that this matrix is always computed at element level. We deduce from Eq.(8.3)

$$\begin{Bmatrix} \frac{\partial N_i}{\partial x} \\ \frac{\partial N_i}{\partial y} \end{Bmatrix} = \left[\mathbf{J}^{(e)} \right]^{-1} \begin{Bmatrix} \frac{\partial N_i}{\partial \xi} \\ \frac{\partial N_i}{\partial \eta} \end{Bmatrix} = \frac{1}{|\mathbf{J}^{(e)}|} \begin{bmatrix} \frac{\partial y}{\partial \eta} & -\frac{\partial y}{\partial \xi} \\ -\frac{\partial x}{\partial \eta} & \frac{\partial x}{\partial \xi} \end{bmatrix} \begin{Bmatrix} \frac{\partial N_i}{\partial \xi} \\ \frac{\partial N_i}{\partial \eta} \end{Bmatrix} \quad (8.4)$$

where $|\mathbf{J}^{(e)}|$ is the determinant of the Jacobian matrix. This determinant also relates the differential of area in the two coordinate systems, i.e.

$$dx \, dy = \left| \mathbf{J}^{(e)} \right| d\xi \, d\eta \quad (8.5)$$

The terms of the Jacobian matrix are computed using the isoparametric approximation (8.1), i.e.

$$\frac{\partial x}{\partial \xi} = \sum_{i=1}^n \frac{\partial N_i}{\partial \xi} x_i \quad ; \quad \frac{\partial x}{\partial \eta} = \sum_{i=1}^n \frac{\partial N_i}{\partial \eta} x_i; \text{ etc.} \quad (8.6)$$

and

$$\mathbf{J}^{(e)} = \sum_{i=1}^n \begin{bmatrix} \frac{\partial N_i}{\partial \xi} x_i & \frac{\partial N_i}{\partial \xi} y_i \\ \frac{\partial N_i}{\partial \eta} x_i & \frac{\partial N_i}{\partial \eta} y_i \end{bmatrix} \quad (8.7)$$

For a rectangular element

$$\mathbf{J}^{(e)} = \begin{bmatrix} a & 0 \\ 0 & b \end{bmatrix} \quad \text{and} \quad |\mathbf{J}^{(e)}| = ab \quad (8.8)$$

8.1.1 Stiffness matrix and load vector of isoparametric quadrilateral

Substituting the cartesian derivatives of the shape functions from Eq.(8.4) into (6.19) yields the general form of the gradient matrix for an isoparametric quadrilateral element in terms of the natural coordinates by

$$\mathbf{B}_i(\xi, \eta) = \begin{Bmatrix} \frac{\partial N_i}{\partial x} \\ \frac{\partial N_i}{\partial y} \end{Bmatrix} = \frac{1}{|\mathbf{J}^{(e)}|} \begin{Bmatrix} \bar{b}_i \\ \bar{c}_i \end{Bmatrix} \quad (8.9)$$

where

$$\bar{b}_i = \frac{\partial y}{\partial \eta} \frac{\partial N_i}{\partial \xi} - \frac{\partial y}{\partial \xi} \frac{\partial N_i}{\partial \eta} \quad ; \quad \bar{c}_i = \frac{\partial x}{\partial \xi} \frac{\partial N_i}{\partial \eta} - \frac{\partial x}{\partial \eta} \frac{\partial N_i}{\partial \xi} \quad (8.10)$$

The element stiffness matrix for a 2D Poisson element can be written in the normalized natural coordinate space as

$$\begin{aligned} K_{ij}^{(e)} &= \int \int_{A^{(e)}} \mathbf{B}_i^T \mathbf{D} \mathbf{B}_j \, dx dy = \int_{-1}^{+1} \int_{-1}^{+1} \mathbf{B}_i^T(\xi, \eta) \mathbf{D} \mathbf{B}_j(\xi, \eta) |\mathbf{J}^{(e)}| \, d\xi \, d\eta = \\ &= \int_{-1}^{+1} \int_{-1}^{+1} (k_x \bar{b}_i \bar{b}_j + k_y \bar{c}_i \bar{c}_j) \frac{1}{|\mathbf{J}^{(e)}|} \, d\xi \, d\eta = \\ &= \int_{-1}^{+1} \int_{-1}^{+1} G_{ij} \, d\xi \, d\eta \end{aligned} \quad (8.11a)$$

with

$$G_{ij} = (k_x \bar{b}_i \bar{b}_j + k_y \bar{c}_i \bar{c}_j) \frac{1}{|\mathbf{J}^{(e)}|} \quad (8.11b)$$

Eq.(8.11a) shows that the integrand of $\mathbf{K}_{ij}^{(e)}$ contains rational functions in ξ and η . An exception to this rule is when the determinant of the Jacobian matrix is constant. This only occurs for rectangular elements (and for straight side triangles). In these cases the element integrals contain simple polynomials and the analytical expressions of Section 7.6 can be applied. However, for general quadrilateral shapes the analytical integration of $\mathbf{K}_{ij}^{(e)}$ is difficult (and in most cases impossible!) and the only option is to use numerical integration.

A similar procedure will be followed to compute the equivalent nodal force vectors for isoparametric elements. For example, for the case of a heat source

$$f_i^{(e)} = \iint_{A^{(e)}} N_i Q \, dx \, dy = \int_{-1}^{+1} \int_{-1}^{+1} N_i Q \left| \mathbf{J}^{(e)} \right| t \, d\xi \, d\eta \quad (8.12)$$

Numerical integration is also typically used to compute integrals such as that of Eq.(8.12).

Example: 8.1 Formulate an isoparametric quadrilateral of 4 nodes.

Solution

The actual and normalized geometries of the element are shown in the Figure 8.2 below.

The isoparametric description of the geometry is written as

$$\mathbf{x} = \begin{Bmatrix} x \\ y \end{Bmatrix} = \sum_{i=1}^4 N_i(\xi, \eta) \begin{Bmatrix} x_i \\ y_i \end{Bmatrix} \quad (8.13)$$

where $N_i(\xi, \eta) = \frac{1}{4}(1 + \xi\xi_i)(1 + \eta_i\eta)$.

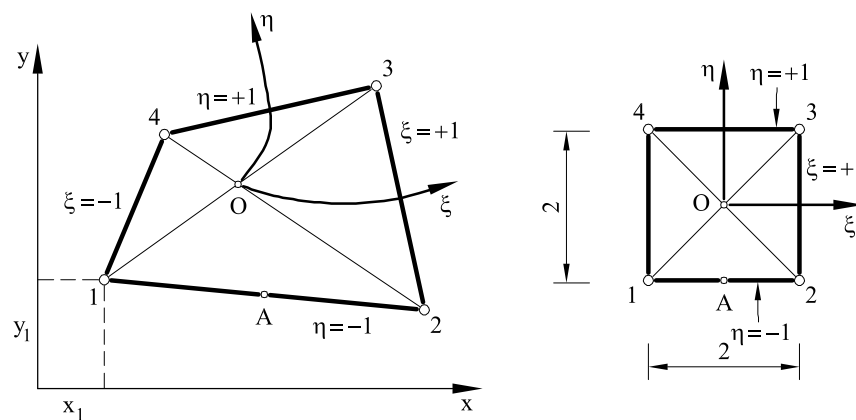


Fig. 8.2: Four-noded isoparametric quadrilateral. Actual and normalized geometry

The above expression maps the natural coordinates of each element point on to the cartesian space. For instance, the cartesian position of the central point O with natural coordinates (0,0) is

$$\mathbf{x}_O = \sum_{i=1}^4 N_i(0,0) \begin{Bmatrix} x_i \\ y_i \end{Bmatrix} = \frac{1}{4} \begin{Bmatrix} x_1 + x_2 + x_3 + x_4 \\ y_1 + y_2 + y_3 + y_4 \end{Bmatrix} \quad (8.14a)$$

Point A at the center of side 1–2 with natural coordinates (0,-1) is located in the cartesian space at

$$\mathbf{x}_A = \sum_{i=1}^4 N_i(0,-1) \begin{Bmatrix} x_i \\ y_i \end{Bmatrix} = \frac{1}{2} \begin{Bmatrix} x_1 + x_2 \\ y_1 + y_2 \end{Bmatrix} \quad (8.14b)$$

We can observe that the isoparametric description is useful to express all the element expressions in the natural coordinate system.

The Jacobian matrix of Eq.(8.7) is given by

$$\mathbf{J}^{(e)} = \sum_{i=1}^4 \begin{bmatrix} \frac{\xi_i}{4}(1 + \eta\eta_i)x_i & \frac{\xi_i}{4}(1 + \eta\eta_i)y_i \\ \frac{\eta_i}{4}(1 + \xi\xi_i)x_i & \frac{\eta_i}{4}(1 + \xi\xi_i)y_i \end{bmatrix} \quad (8.15)$$

The cartesian derivatives of the shape functions are obtained from Eq.(8.4) as

$$\begin{Bmatrix} \frac{\partial N_i}{\partial x} \\ \frac{\partial N_i}{\partial y} \end{Bmatrix} = \frac{1}{|\mathbf{J}^{(e)}|} \sum_{j=1}^4 \begin{bmatrix} \frac{\eta_j}{4}(1 + \xi\xi_j)y_j & -\frac{\xi_j}{4}(1 + \eta\eta_j)y_j \\ -\frac{\eta_j}{4}(1 + \xi\xi_j)x_j & \frac{\xi_j}{4}(1 + \eta\eta_j)x_j \end{bmatrix} \begin{Bmatrix} \frac{\xi_i}{4}(1 + \eta\eta_i) \\ \frac{\eta_i}{4}(1 + \xi\xi_i) \end{Bmatrix} \quad (8.16)$$

From above equations we deduce

$$\begin{Bmatrix} \frac{\partial N_i}{\partial x} \\ \frac{\partial N_i}{\partial y} \end{Bmatrix} = \begin{Bmatrix} \hat{b}_i \\ \hat{c}_i \end{Bmatrix} \quad (8.17a)$$

with

$$\hat{b}_i = \frac{\alpha_1^i + \alpha_2^i\xi + \alpha_3^i\eta + \alpha_4^i\xi\eta}{\beta_1^i + \beta_2^i\xi + \beta_3^i\eta + \beta_4^i\xi\eta}, \quad \hat{c}_i = \frac{\alpha_5^i + \alpha_6^i\xi + \alpha_7^i\eta + \alpha_8^i\xi\eta}{\beta_5^i + \beta_6^i\xi + \beta_7^i\eta + \beta_8^i\xi\eta} \quad (8.17b)$$

where $\alpha_1^i \dots \alpha_8^i, \beta_1^i \dots \beta_8^i$ are nodal parameters depending on the nodal coordinates.

Clearly, the element strain matrix and the stiffness matrix now contains rational polynomials making exact integration over an arbitrary quadrilateral domain is extremely difficult. This problem can be overcome by using numerical integration (Section 8.3).

The above equations simplify considerably for rectangular shapes. For a rectangle of size $2a \times 2b$ we have

$$\mathbf{J}^{(e)} = \begin{bmatrix} a & 0 \\ 0 & b \end{bmatrix}, \quad |\mathbf{J}^{(e)}| = ab \quad \text{and} \quad dx dy = ab d\xi d\eta \quad (8.18)$$

The cartesian derivatives of the shape functions are now simply given by

$$\begin{pmatrix} \frac{\partial N_i}{\partial x} \\ \frac{\partial N_i}{\partial y} \end{pmatrix} = \begin{pmatrix} \frac{\xi_i}{4b}(1 + \eta\eta_i) \\ \frac{\eta_i}{4a}(1 + \xi\xi_i) \end{pmatrix} \quad (8.19)$$

The element stiffness matrix is expressed in the natural system by

$$\mathbf{K}_{ij}^{(e)} = \int_{-1}^{+1} \int_{-1}^{+1} \mathbf{B}_i^T \mathbf{D} \mathbf{B}_i ab d\xi d\eta \quad (8.20)$$

The integral expression of $\mathbf{K}_{ij}^{(e)}$ now contains polynomial expressions in ξ, η, ξ^2, η^2 and $\xi\eta$ which can be directly computed noting that

$$\int_{-1}^{+1} \int_{-1}^{+1} C[1, \xi, \eta, \xi^2, \eta^2, \xi\eta] d\xi d\eta = C \left[4, 0, 0, \frac{4}{3}, \frac{4}{3}, 0 \right] \quad (8.21)$$

where C is a constant parameter.

8.1.2 A comparison between the 8- and 9-noded isoparametric quadrilaterals

It is interesting to assess the circumstances under which the linearly distorted 8 and 9-noded quadrilaterals can fully represent any quadratic cartesian expansion. The straight-sided element geometry is exactly approximated by the bilinear (subparametric) interpolation

$$\mathbf{x} = \sum_{i=1}^4 N_i \mathbf{x}_i \quad (8.22)$$

where $N_i = \frac{1}{4}(1 + \xi\xi_i)(1 + \eta\eta_i)$ are the shape functions of the 4-noded rectangle.

We wish to be able to reproduce

$$u = \alpha_1 + \alpha_2 x + \alpha_3 y + \alpha_4 x^2 + \alpha_5 xy + \alpha_6 y^2 \quad (8.23)$$

Noting that the bilinear form contains terms such as $1, \xi, \eta$ and $\xi\eta$ and by substituting Eq.(8.22) into (8.23) the above can be written as

$$u = \beta_1 + \beta_2 \xi + \beta_3 \eta + \beta_4 \xi^2 + \beta_5 \xi\eta + \beta_6 \eta^2 + \beta_7 \eta^2 + \beta_8 \xi^2 + \beta_9 \xi^2 \eta^2 \quad (8.24)$$

where β_1 to β_9 depend on the values of α_1 to α_6 .

We shall now try to match the terms arising from the quadratic expansion of the 8-noded Serendipity shown in Figure 7.8. Noting the terms occurring in the Pascal's triangle of Figure 7.8, the interpolation can be written as

$$u = b_1 + b_2 \xi + b_3 \eta + b_4 \xi^2 + b_5 \xi\eta + b_6 \eta^2 + b_7 \xi\eta^2 + b_8 \xi^2 \eta \quad (8.25)$$

It is evident that for arbitrary values of η_1 to η_9 it is impossible to match the coefficients b_1 to b_8 due to the absence of the term $\xi^2\eta^2$ in Eq.(8.25).

For the 9-noded Lagrange element (Figure 7.5) the expansion similar to Eq.(8.24) gives

$$u = b_1 + b_2\xi + b_3\eta + b_4\xi^2 + b_5\xi\eta + b_6\eta^2 + b_7\xi\eta^2 + b_8\xi^2\eta + b_9\xi^2\eta^2 \quad (8.26)$$

and the matching of the coefficients in Eqs.(8.24) and (8.26) can be made directly.

We conclude that the 9-noded elements can better represent quadratic cartesian polynomials on linearly distorted shapes and therefore are generally preferable in modelling smooth solutions. Figure 8.3 shows an example of this for the analysis, with 8- and 9-node elements, respectively of a simple beam solution where exact answers are quadratic. With no distortion both elements with a full (3×3) integration rule give exact results but when distorted only the 9-node element does so, the 8-noded element giving a significant stress fluctuation.

A similar argument leads to the conclusion that in 3D, again only 27-noded Lagrangian elements are capable of reproducing fully a quadratic function in cartesian coordinates when trilinearity distorted.

8.2 ISOPARAMETRIC TRIANGULAR ELEMENTS

The isoparametric interpolation for triangular elements is written as

$$x = \sum_{i=1}^n N_i(L_1, L_2, L_3) x_i \quad ; \quad y = \sum_{i=1}^n N_i(L_1, L_2, L_3) y_i \quad (8.27)$$

The computation of the cartesian derivatives of N_i and the Jacobian matrix is immediate for straight side triangles (see Example 8.2) giving

$$\mathbf{J}^{(e)} = \begin{bmatrix} x_2 - x_1 & y_2 - y_1 \\ x_3 - x_1 & y_3 - y_1 \end{bmatrix}^{(e)} \quad \text{and} \quad |\mathbf{J}^{(e)}| = 2A^{(e)} \quad (8.28)$$

The computation of the element integrals in this case is simple via the analytic expressions of Section 7.6.

For curved side triangles it is convenient to use the natural coordinates α and β defined in Figure 7.14. This implies that L_2 and L_3 will be replaced by α and β , respectively, and L_1 by $1 - \alpha - \beta$ in all expressions. The computation of the cartesian derivatives of N_i follows precisely the steps described in the previous section, simply changing the coordinates ξ and η for α and β , respectively. For instance

$$\begin{Bmatrix} \frac{\partial N_i}{\partial x} \\ \frac{\partial N_i}{\partial y} \end{Bmatrix} = \frac{1}{|\mathbf{J}^{(e)}|} \begin{bmatrix} \frac{\partial y}{\partial \beta} & -\frac{\partial y}{\partial \alpha} \\ -\frac{\partial x}{\partial \beta} & -\frac{\partial x}{\partial \alpha} \end{bmatrix} \begin{Bmatrix} \frac{\partial N_i}{\partial \alpha} \\ \frac{\partial N_i}{\partial \beta} \end{Bmatrix} \quad (8.29)$$

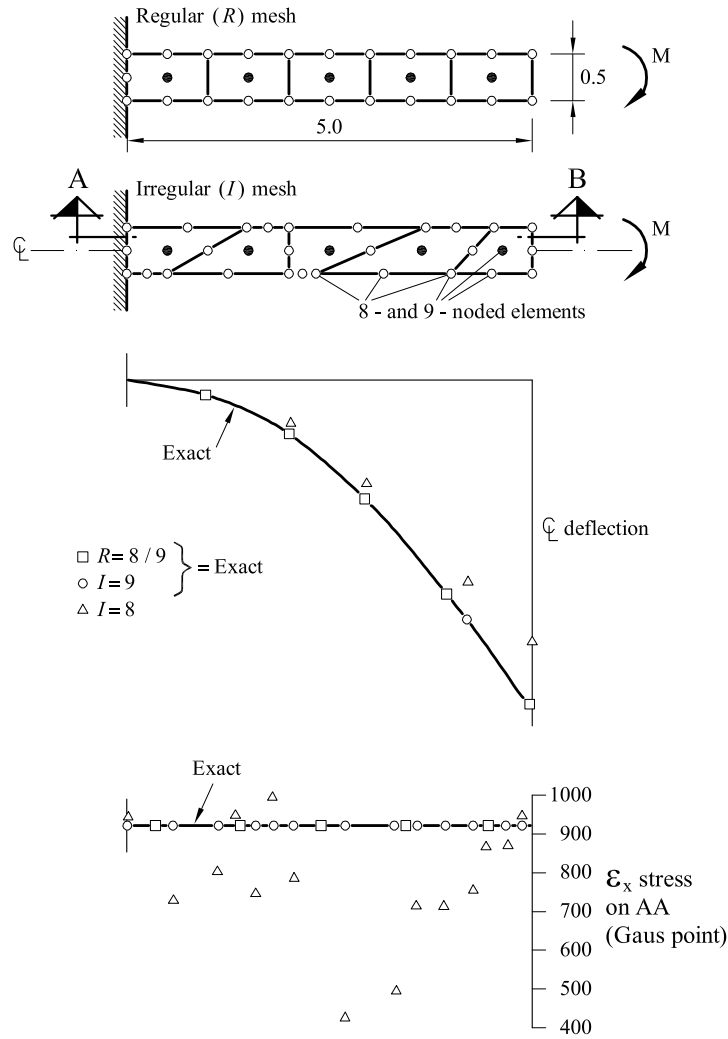


Fig. 8.3: Quadratic Serendipity and Lagrangian 8- and 9-noded elements in regular and distorted form. Elastic deflection of a beam under constant moment. Note poor results of 8-noded element

$$\mathbf{J}^{(e)} = \sum_{i=1}^n \begin{bmatrix} \frac{\partial N_i}{\partial \alpha} x_i & \frac{\partial N_i}{\partial \alpha} y_i \\ \frac{\partial N_i}{\partial \beta} x_i & \frac{\partial N_i}{\partial \beta} y_i \end{bmatrix} \quad (8.30)$$

$$\frac{\partial x}{\partial \alpha} = \sum_{i=1}^n \frac{\partial N_i(\alpha, \beta)}{\partial \alpha} x_i \quad ; \quad \frac{\partial x}{\partial \beta} = \sum_{i=1}^n \frac{\partial N_i(\alpha, \beta)}{\partial \beta} x_i \quad ; \quad \text{etc.} \quad (8.31)$$

The element stiffness matrix is obtained by an expression analogous to Eq.(8.11a) by

$$K_{ij}^{(e)} = \int_0^1 \int_0^{1-\beta} \mathbf{B}_i^T \mathbf{D} \mathbf{B}_j \left| \mathbf{J}^{(e)} \right| d\alpha d\beta = \int_0^1 \int_0^{1-\beta} G_{ij}(\alpha, \beta) d\alpha d\beta \quad (8.32)$$

where all the terms in \mathbf{B}_i and \mathbf{G}_{ij} are deduced from Eqs. (8.11) simply substituting ξ and η for α and β , respectively.

For curved side triangles the integrand of Eq.(8.32) is a rational polynomial and numerical integration is needed.

Example: 8.2 Derive the expression of the Jacobian matrix for an isoparametric triangle with straight sides.

Solution

As the element sides are straight, a linear interpolation for the geometry will suffice, i.e.

$$\begin{aligned} x &= L_1x_1 + L_2x_2 + L_3x_3 \\ y &= L_1y_1 + L_2y_2 + L_3y_3 \end{aligned} \quad (8.33)$$

where x_i, y_i $i = 1, 2, 3$ are the coordinates of the three vertex nodes.

Recall that $L_1 = 1 - L_2 - L_3$. Substituting this into the above gives

$$\begin{aligned} x &= x_1 + (x_2 - x_1)L_2 + (x_3 - x_1)L_3 \\ y &= y_1 + (y_2 - y_1)L_2 + (y_3 - y_1)L_3 \end{aligned} \quad (8.34)$$

The Jacobian matrix is obtained from

$$\begin{Bmatrix} \frac{\partial N_i}{\partial L_2} \\ \frac{\partial N_i}{\partial L_3} \end{Bmatrix} = \begin{bmatrix} \frac{\partial x}{\partial L_2} & \frac{\partial y}{\partial L_2} \\ \frac{\partial x}{\partial L_3} & \frac{\partial y}{\partial L_3} \end{bmatrix} \begin{Bmatrix} \frac{\partial N_i}{\partial x} \\ \frac{\partial N_i}{\partial y} \end{Bmatrix} = \mathbf{J}^{(e)} \begin{Bmatrix} \frac{\partial N_i}{\partial x} \\ \frac{\partial N_i}{\partial y} \end{Bmatrix} \quad (8.35)$$

The Jacobian matrix is deduced from the above two equations as

$$\mathbf{J}^{(e)} = \begin{bmatrix} \frac{\partial x}{\partial L_2} & \frac{\partial y}{\partial L_2} \\ \frac{\partial x}{\partial L_3} & \frac{\partial y}{\partial L_3} \end{bmatrix} = \begin{bmatrix} x_2 - x_1 & y_2 - y_1 \\ x_3 - x_1 & y_3 - y_1 \end{bmatrix} \quad (8.36)$$

The cartesian derivatives are obtained by (noting that $|\mathbf{J}^{(e)}| = 2A^{(e)}$)

$$\begin{Bmatrix} \frac{\partial N_i}{\partial x} \\ \frac{\partial N_i}{\partial y} \end{Bmatrix} = \frac{1}{2A^{(e)}} \begin{bmatrix} y_3 - y_1 & y_1 - y_2 \\ x_1 - x_3 & x_2 - x_1 \end{bmatrix} \begin{Bmatrix} \frac{\partial N_i}{\partial L_2} \\ \frac{\partial N_i}{\partial L_3} \end{Bmatrix} \quad (8.37)$$

Let us verify the above expression for the simple 3-noded triangle. For instance, for $i = 1$, $\frac{\partial N_1}{\partial L_2} = \frac{\partial N_1}{\partial L_3} = -1$ (as $N_1 = L_1 = 1 - L_2 - L_3$) and

$$\begin{Bmatrix} \frac{\partial N_1}{\partial x} \\ \frac{\partial N_1}{\partial y} \end{Bmatrix} = \frac{1}{2A^{(e)}} \begin{Bmatrix} y_2 - y_3 \\ x_3 - x_2 \end{Bmatrix} \quad (8.38)$$

Note the coincidence with the expression obtained using Eqs.(4.30) directly.

The expression for the cartesian derivatives obtained is completely general for straight side triangles of any approximation order (i.e. quadratic, cubic, etc.).

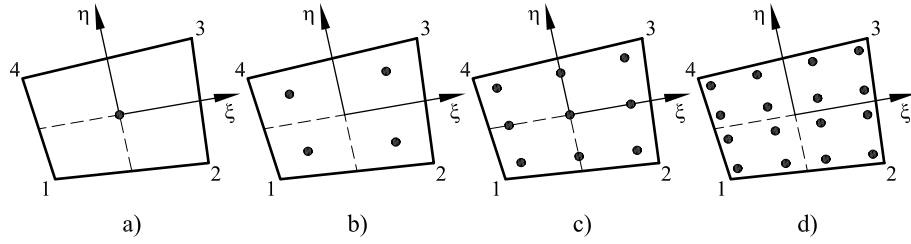


Fig. 8.4: Gauss quadratures over quadrilateral elements, a) 1×1 , b) 2×2 , c) 3×3 , d) 4×4 integration points

8.3 NUMERICAL INTEGRATION IN TWO DIMENSIONS

It has been shown in the previous section that all element integrals can be written in the natural coordinate space making use of the isoparametric formulation. The numerical integration by a Gauss quadrature will be considered next.

8.3.1 Numerical integration in quadrilateral domains

The integral of a term $g(\xi, \eta)$ over the normalized isoparametric quadrilateral domain can be evaluated using a 2D Gauss quadrature by

$$\int_{-1}^{+1} \int_{-1}^{+1} g(\xi, \eta) d\xi d\eta = \int_{-1}^{+1} d\xi \left[\sum_{q=1}^{n_q} g(\xi, \eta_q) W_q \right] = \sum_{p=1}^{n_p} \sum_{q=1}^{n_q} g(\xi_p, \eta_q) W_p W_q \quad (8.39)$$

where n_p and n_q are the number of integration points along each natural coordinate ξ and η respectively; ξ_p and η_q are the natural coordinates of the p th integration point and W_p, W_q are the corresponding weights.

The coordinates and weights for each natural direction are directly deduced from those given in Table 3.3 for the 1D case. Recall that a 1D quadrature of q th order integrates *exactly* a polynomial of degree $q \leq 2n - 1$. Figure 8.4 shows the more usual quadratures for quadrilateral elements.

Example: 8.3 Integrate numerically the function $f(\xi, \eta) = \xi^2 \eta^2$ over a rectangular element with dimensions $2a \times 2b$.

Solution

Since the element is rectangular $|\mathbf{J}^{(e)}| = ab$ (see Eq.(8.18)).

The integrand is a quadratic function in ξ and η and hence a 2×2 quadrature is

needed (Figure 8.4b). Thus

$$\begin{aligned} I &= \iint_A \xi^2 \eta^2 dA = ab \int_{-1}^{+1} \int_{-1}^{+1} \xi^2 \eta^2 = ab \sum_{p=1}^2 \sum_{q=1}^2 (\xi^2 \eta^2)_{p,q} W_p W_q = \\ &= ab \left[\left(-\frac{\sqrt{3}}{3}\right)^2 \left(-\frac{\sqrt{3}}{3}\right)^2 + \left(-\frac{\sqrt{3}}{3}\right)^2 \left(\frac{\sqrt{3}}{3}\right)^2 + \left(\frac{\sqrt{3}}{3}\right)^2 \left(-\frac{\sqrt{3}}{3}\right)^2 + \left(\frac{\sqrt{3}}{3}\right)^2 \left(\frac{\sqrt{3}}{3}\right)^2 \right] = \frac{4}{9} ab \end{aligned}$$

which is the exact solution.

8.3.2 Numerical integration over triangles

The Gauss quadrature for triangles is written as

$$\int_0^1 \int_0^{1-L_3} f(L_1, L_2, L_3) dL_2 dL_3 = \sum_{p=1}^{n_p} f(L_{1p}, L_{2p}, L_{3p}) W_p \quad (8.40)$$

where n_p is the number of integration points: L_{1p}, L_{2p}, L_{3p} and W_p are the area coordinates and the corresponding weight for the p th integration point.

Figure 8.5 shows the more usual coordinates and weights; the term “accuracy” in the figure refers to the highest degree polynomial which is exactly integrated by each quadrature. Figure 8.5 is also of direct application for computing the integrals defined in terms of the natural coordinates α and β , simply recalling that $L_2 = \alpha, L_3 = \beta$ and $L_1 = 1 - \alpha - \beta$.

It is important to note that the weights in Figure 8.5 are normalized so that their sum is $1/2$. In many references this value is changed to the unity and this requires the sum of Eq.(5.91) to be multiplied by $1/2$ so that the element area is correctly computed in those cases.

Example: 8.4 Compute the area of a triangular element with straight sides by numerical integration.

Solution

$$A^{(e)} = \iint_{A^{(e)}} dx dy = \int_0^1 \int_0^{1-\beta} |J^{(e)}| d\alpha d\beta = |J^{(e)}| \sum_p W_p = \frac{|J^{(e)}|}{2} \quad (8.41)$$

which corresponds with the value obtained in Eq.(8.28).

For further information on numerical integration over triangular domains see refs. [C15], [C19], [D10], [H20] y [Z6].

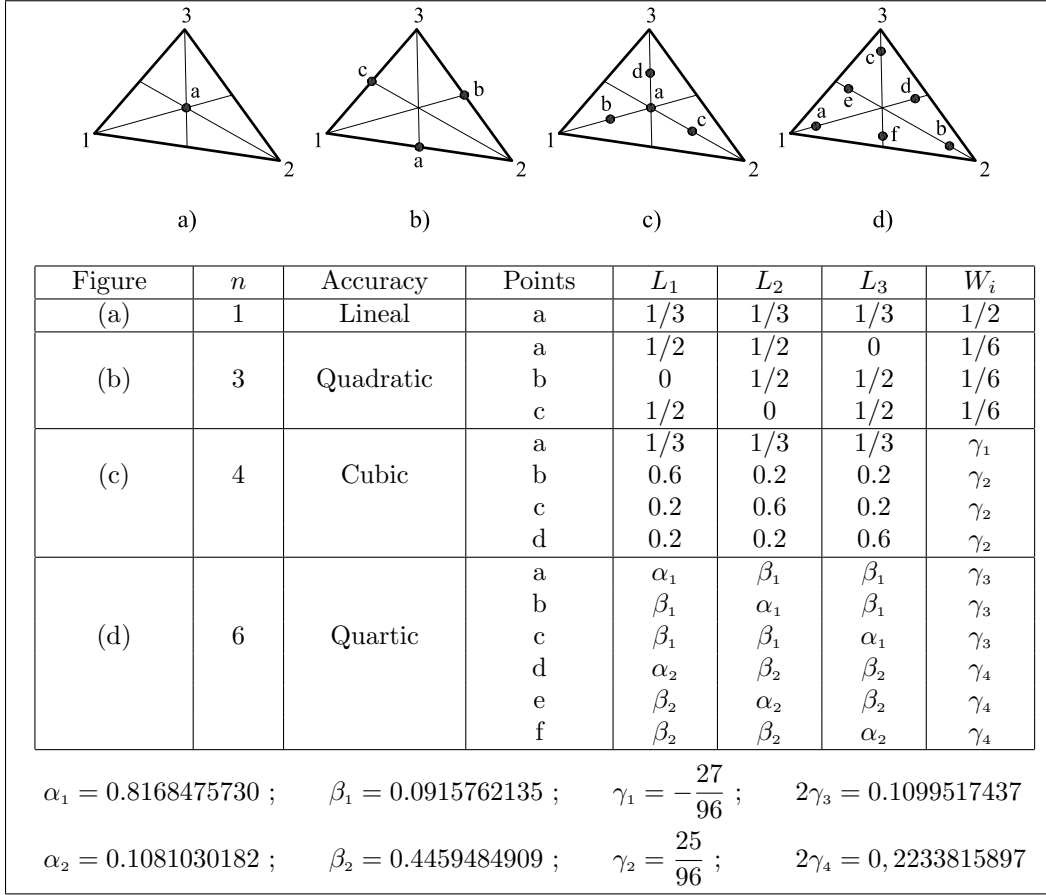


Fig. 8.5: Coordinates and weights for the Gauss quadrature in triangular elements

8.4 NUMERICAL INTEGRATION OF THE ELEMENT MATRICES AND VECTORS

The stiffness matrix of an isoparametric quadrilateral element is computed using numerical integration as

$$\begin{aligned}
 K_{ij}^{(e)} &= \iint_{A^{(e)}} \mathbf{B}_i^T \mathbf{D} \mathbf{B}_j dx dy = \int_{-1}^{+1} \int_{-1}^{+1} \mathbf{B}_i^T \mathbf{D} \mathbf{B}_j \left| \mathbf{J}^{(e)} \right| d\xi d\eta = \\
 &= \sum_{p=1}^{n_p} \sum_{q=1}^{n_q} \left[\mathbf{B}_i^T \mathbf{D} \mathbf{B}_j \left| \mathbf{J}^{(e)} \right| \right]_{p,q} W_p W_q = \sum_{p=1}^{n_p} \sum_{q=1}^{n_q} [G_{ij}]_{p,q} W_p W_q
 \end{aligned} \tag{8.42}$$

where G_{ij} is given in Eq.(8.11b). For a triangular element we deduce from Eq.(8.32)

$$\mathbf{K}_{ij}^{(e)} = \int_0^1 \int_0^{1-\beta} \mathbf{B}_i^T \mathbf{D} \mathbf{B}_j \left| \mathbf{J}^{(e)} \right| d\alpha d\beta = \sum_{p=1}^{n_p} [\mathbf{B}_i^T \mathbf{D} \mathbf{B}_j \left| \mathbf{J}^{(e)} \right|]_p W_p = \sum_{p=1}^{n_p} [G_{ij}]_p \tag{8.43}$$

where the position of the integration points and the corresponding weights is obtained from Figure 8.5.

The numerical integration of the stiffness matrix requires the evaluation of the Jacobian $\mathbf{J}^{(e)}$ and its determinant, the strain matrix \mathbf{B}_i and the constitutive matrix \mathbf{D} at each integration point. Similarly, the numerical integration of the equivalent nodal flux vector due to a heat source for isoparametric quadrilateral elements gives

$$f_{b_i}^{(e)} = \int_{-1}^{+1} \int_{-1}^{+1} N_i Q \left| \mathbf{J}^{(e)} \right| d\xi d\eta = \sum_{p=1}^{n_p} \sum_{q=1}^{n_q} \left(N_i Q \left| \mathbf{J}^{(e)} \right| \right)_{p,q} W_p W_q \quad (8.44)$$

For triangular elements the double sum is replaced by the single sum of Eq.(8.43).

The computation of the equivalent nodal flux vector due to surface fluxes deserves a special comment. Let us recall that this vector has the following expression (see Eq.(4.57))

$$f_i^{(e)} = \oint_{l^{(e)}} N_i (\alpha \phi_a - \bar{q}_n) dS \quad (8.45)$$

where $l^{(e)}$ is the loaded element boundary. In general this boundary represents a line $\xi = \text{constant}$ or $\eta = \text{constant}$ in the natural coordinate space (see Figure 8.6). Therefore, the differential of length over the side $\eta = 1$ for an isoparametric quadrilateral element is computed by

$$\begin{aligned} (ds)_{\eta=1} &= (dx^2 + dy^2)_{\eta=1} = \left[\sqrt{\left(\frac{dx}{d\xi} \right)_{\eta=1}^2 + \left(\frac{dy}{d\xi} \right)_{\eta=1}^2} \right] d\xi = \\ &= \left[\sqrt{\left(\sum_{i=1}^n \frac{dN_i}{d\xi} x_i \right)_{\eta=1}^2 + \left(\sum_{i=1}^n \frac{dN_i}{d\xi} y_i \right)_{\eta=1}^2} \right] d\xi = c(\xi) d\xi \end{aligned} \quad (8.46)$$

Substituting Eq.(8.46) into (8.45) yields a line integral which is a function of the natural coordinate ξ only. This is computed using a 1D quadrature by

$$f_i^{(e)} = \oint_{l^{(e)}} N_i (\alpha \phi_a - \bar{q}_n) c(\xi) d\xi = \int_{-1}^{+1} g(\xi) d\xi = \sum_{p=1}^{n_p} g(\xi_p) W_p \quad (8.47)$$

For three-noded triangles and four-noded quadrilaterals, $f_i^{(e)}$ has the following expression for a uniform boundary flux

$$f_i^{(e)} = \frac{l^{(e)}}{2} (\alpha \phi_a - \bar{q}_n) \quad (8.48)$$

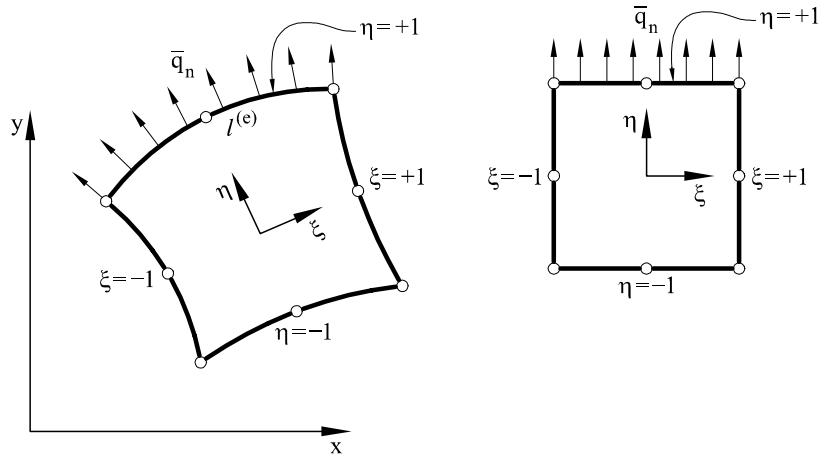


Fig. 8.6: Normal flux across a boundary of a 2D element

8.5 COMPUTER PROGRAMMING OF $\mathbf{K}^{(e)}$ AND $\mathbf{f}^{(e)}$

Previous sections provided all the necessary expressions for programming the computation of the stiffness matrix and the equivalent nodal force vector for each element. The basic steps involved in programming the computation of $\mathbf{K}^{(e)}$ and $\mathbf{f}^{(e)}$ for quadrilateral elements are given next.

Figure 8.7 shows the flow diagram for computing of $\mathbf{K}^{(e)}$ as deduced from Eq. (8.42).

The evaluation of the constitutive matrix \mathbf{D} can be taken out of the numerical integration loop if the material properties are homogeneous over the element. The case of \mathbf{D} variable is treated simply by using a standard interpolation within the element in terms of the nodal values as

$$\mathbf{D} = \sum_{i=1}^n N_i \mathbf{D}_i \quad (8.49)$$

Eq.(8.49) is used to obtain the values of \mathbf{D} at the Gauss points within the numerical integration loop.

Figure 8.8 shows the flow chart for computing the flux vector $\mathbf{f}^{(e)}$ for the case of a heat source Q as deduced from Eq.(8.44).

The computation of the heat source Q can be taken out from the numerical integration loop if it is constant over the element. A variable heat source can be accounted for by interpolating the known nodal values, in the same way as was done for matrix D in Eq. (8.49).

The flow charts in Figures 8.7 and 8.8 are completely general and applicable to most problems solved with the FEM.

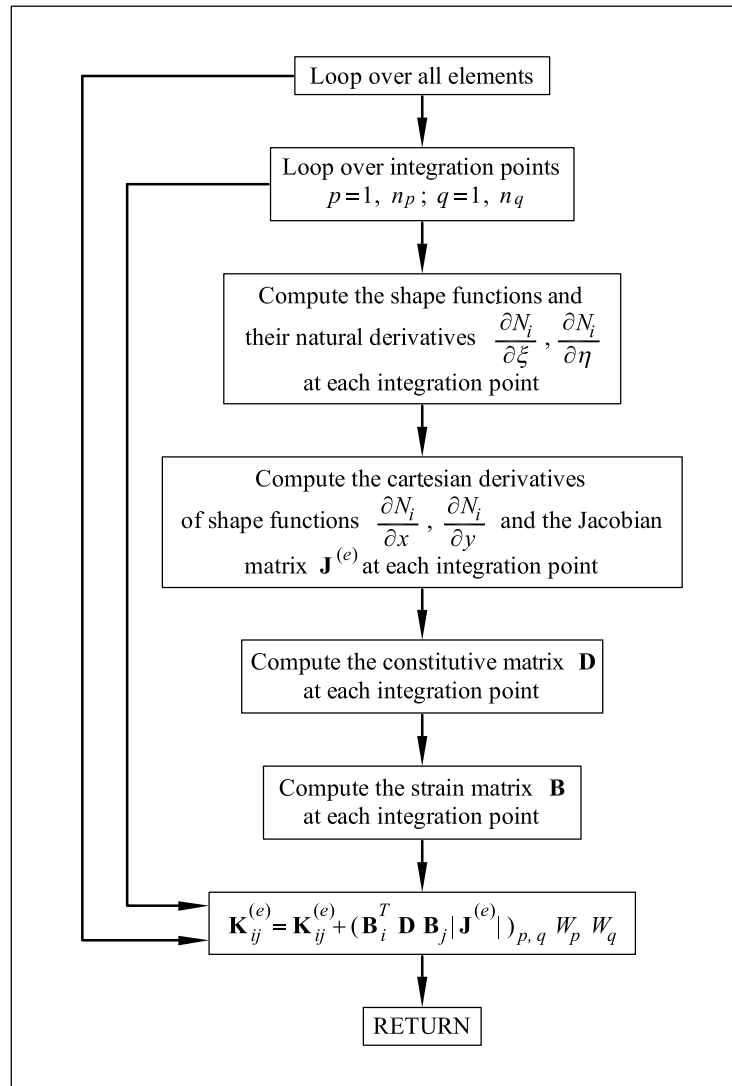


Fig. 8.7: Flow chart for the computation of $\mathbf{K}^{(e)}$

8.6 OPTIMAL POINTS FOR COMPUTING GRADIENT FLUXES

The gradient (and the fluxes) are obtained from the derivatives of the unknown function ϕ . Therefore, their approximation is always of a lower order than that for ϕ . In general, if the shape functions are complete polynomials of p th degree the approximation for the fluxes will be a polynomial of degree $p - 1$ or $p - 2$, depending if they are obtained as first or second derivatives of the ϕ field, respectively.

It can be proved that the fluxes from the finite element solution can be considered a least square interpolation of the exact flux field [Z6]. Naturally, the exact flux field is unknown. However, an enhanced stress distribution can be found by the following property of the Gauss quadrature: A n th degree

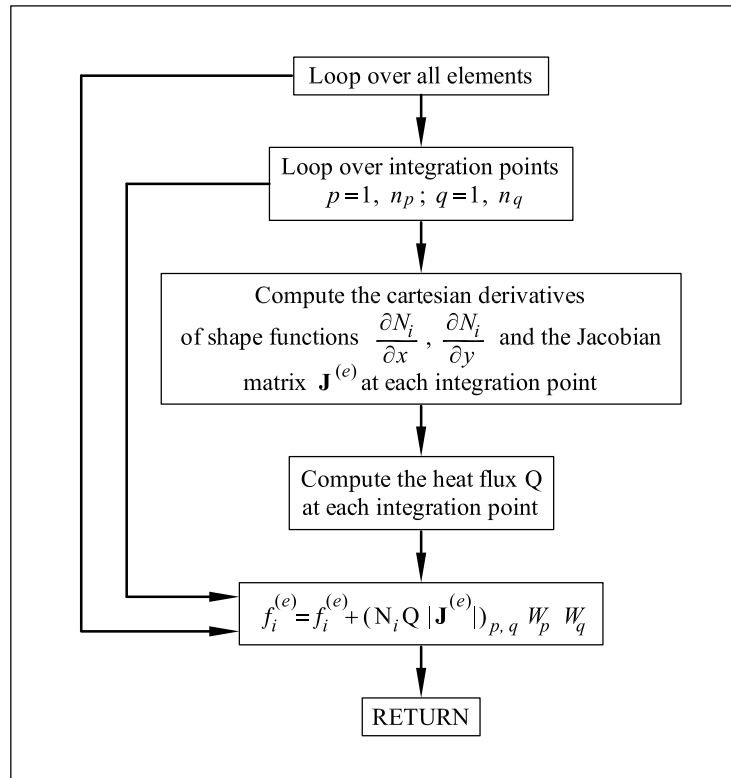


Fig. 8.8: Flow diagram for computing $\mathbf{f}^{(e)}$ for the case of body forces

polynomial and a $n - 1$ th degree polynomial, obtained by least square fitting of the first one, take the same values at the points of the Gauss quadrature of order n th. Hence, we can obtain an approximation of the fluxes and the gradients that is one order higher higher by computing these at the Gauss points. This important property will be clarified with the following two examples.

Example: 8.5 Verify that a second degree polynomial, and a first degree polynomial obtained by least square smoothing of the another, take the same values at the points of the Gauss quadrature of order 2.

Solution

Let us consider the second degree polynomial ($n = 2$)

$$f(x) = 1 + x + x^2$$

We will now obtain a first degree polynomial ($n = 1$) which approximates $f(x)$ in the least square sense; i.e. find a polynomial

$$g(x) = a + bx$$

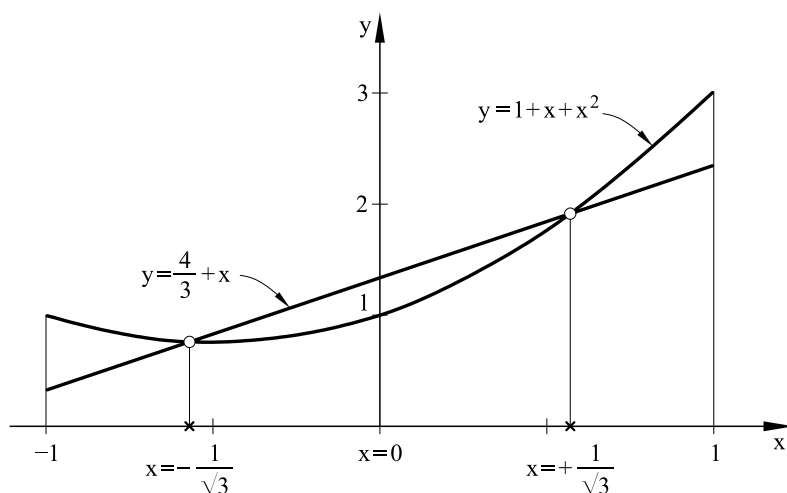


Fig. 8.9: Least square approximation of a quadratic polynomial by a linear one. Intersection of both polynomials at the points of the Gauss quadrature of order 2

such that it minimizes the functional

$$M = \int_{-1}^{+1} [f(x) - g(x)]^2 dx = \int_{-1}^{+1} [(1-a) + (1-b)x + x^2]^2 dx$$

be a minimum.

The parameters a and b are obtained by making

$$\begin{aligned} \frac{\partial M}{\partial a} = 0 &\implies \int_{-1}^{+1} -2[(1-a) + (1-b)x + x^2] dx = 0 \\ \frac{\partial M}{\partial b} = 0 &\implies \int_{-1}^{+1} -2x[(1-a) + (1-b)x + x^2] dx = 0 \end{aligned}$$

which gives $a = \frac{4}{3}$ y $b = 1$.

Figure 8.9 shows the two polynomials $f(x)$ and $g(x)$. Note that both polynomials take the same values at the points of the Gauss quadrature of order 2.

Example: 8.6 Verify that a cubic polynomial and a quadratic one obtained by least square smoothing of the former, take same values at the points of the 3rd order Gauss quadrature.

Solution

Let us consider the third degree polynomial ($n = 3$)

$$f(x) = 1 + x + x^2 + x^3$$

We will obtain the second degree polynomial $g(x) = a + bx + cx^2$, such that

$$M = \int_{-1}^{+1} [f(x) - g(x)]^2 dx = \int_{-1}^{+1} [(1-a) + (1-b)x + (1-c)x^2 + x^3]^2 dx$$

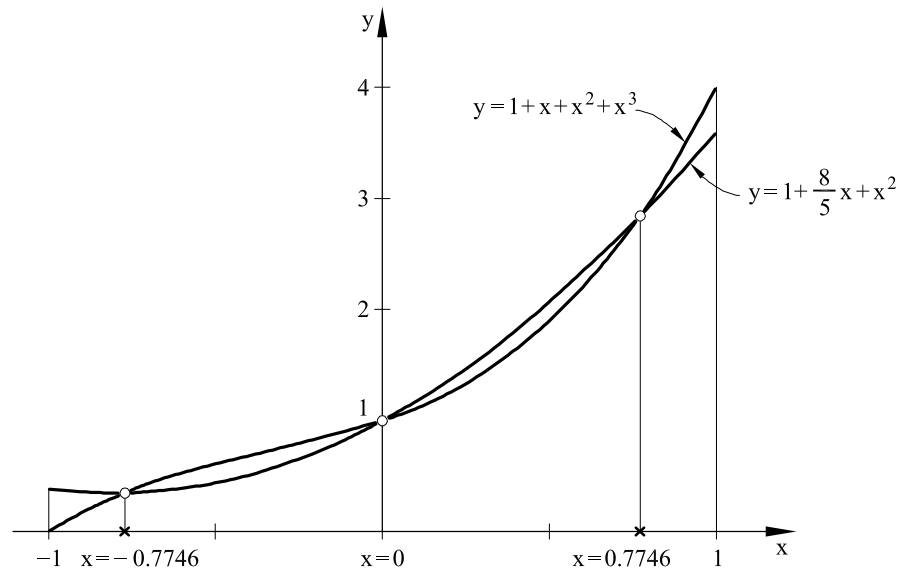


Fig. 8.10: Least square interpolation of a cubic polynomial by a quadratic one. Intersection of both polynomials at the points of the Gauss quadrature of order 3

is a minimum.

The three constants a, b , and c are obtained by solving the following system

$$\begin{aligned} \frac{\partial M}{\partial a} = 0 &\implies 1 - a + \frac{1 - c}{3} = 0 \\ \frac{\partial M}{\partial b} = 0 &\implies \frac{1 - b}{3} + \frac{1}{5} = 0 \\ \frac{\partial M}{\partial c} = 0 &\implies \frac{1 - a}{3} + \frac{1 - c}{5} = 0 \end{aligned}$$

which gives

$$a = 1 \quad ; \quad b = \frac{8}{5} \quad y \quad c = 1$$

Figure 8.10 shows that the exact and interpolating polynomials take the same values at the three points of the 3rd order Gauss quadrature (i.e. $\xi = 0$ and $\xi = \pm\sqrt{3/3}$).

The following conclusions can be drawn from what is explained:

1. If the *exact* distribution of the gradient \mathbf{g} (and the flux \mathbf{q}) field is a polynomial of n th degree and the approximate finite element solution is a polynomial of $n - 1$ th degree, the computation of \mathbf{q} (or \mathbf{g}) at the points of the Gauss quadrature of n th order gives the *exact* values.
2. The evaluation of \mathbf{q} or \mathbf{g} at the Gauss quadrature points chosen for the integration of $\mathbf{K}^{(e)}$ yields a solution of *one approximation order higher* than at any other point within the element.

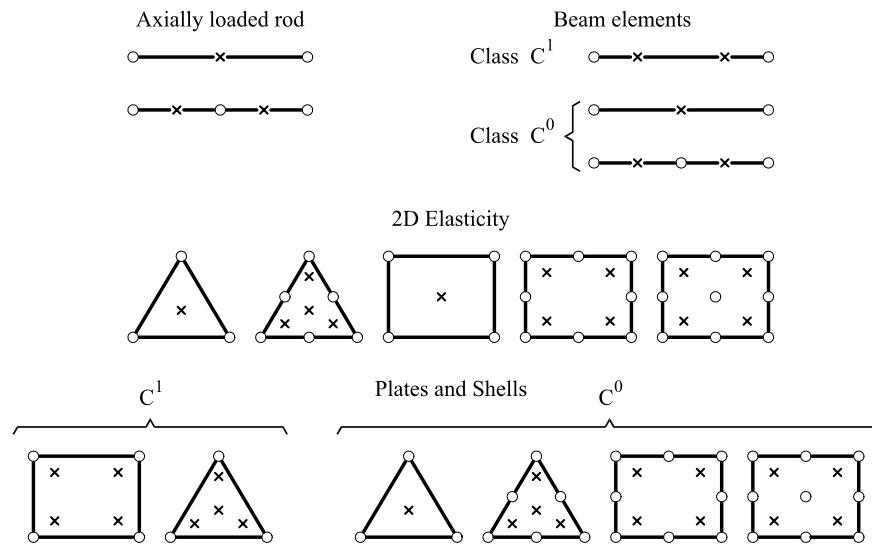


Fig. 8.11: Optimal points for computation of the gradients and the fluxes in some 1D and 2D elements

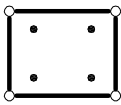
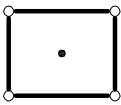
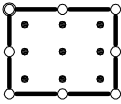
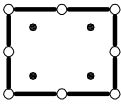
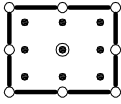
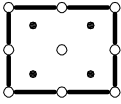
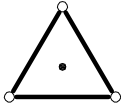
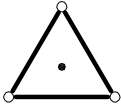
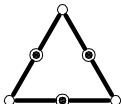
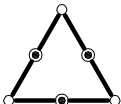
The evaluation of gradients and fluxes at the so called “optimal” quadrature points is therefore of higher accuracy than at any other element point. The nodal stress values can subsequently be obtained from a local or global smoothing of the Gauss point values.

The above concepts are rigorously true for 1D elements. For 2D and 3D elements the sampling of the gradients and the fluxes at the “optimal” Gauss quadrature points leads also to a substantial improvement in the results. Figure 8.11 shows the optimal points for computation of gradients and fluxes for some 1D and 2D elements. Extrapolation to the 3D case is simple.

These concepts extend naturally for elasticity problems (Chapter 9) where the Gauss point and optimal for the sampling of the strains $\boldsymbol{\varepsilon}$ and the stresses $\boldsymbol{\sigma}$. Figure 8.12 shows an example of the analysis of a cantilever beam analyzed with 8-noded Serendipity rectangles. The accuracy of the shear stress sampled at the 2×2 Gauss points is noticeable.

8.7 SELECTION OF THE QUADRATURE ORDER

The number of integration points is selected according to the degree of the polynomials appearing in the element integrals. Isoparametric elements contain rational terms within the integrals and exact integration is not longer possible. The alternative is to choose a quadrature order which integrates exactly the same expression for a rectangular or straight side triangular element. This quadrature is termed in practice *full integration* or *standard integration*. Remember that in these cases the Jacobian matrix is constant and the element integrals have a simple analytical form.

Exact	Minimum
 2×2	 1×1*
 3×3	 2×2
 3×3	 2×2
 n=1	 n=1
 n=3	 n=3

* Produces two propagable mechanisms (Fig. 5.29a)

Fig. 8.12: Exact and minimum quadrature rules for some rectangular and straight side triangular elements

The minimum quadrature order for the stiffness matrix should preserve the convergence rate of the element. This is achieved by choosing a quadrature which integrates exactly all the complete polynomial terms contained in the shape functions. For rectangular elements this quadrature is of lower order than that required for the exact integration of the element stiffness matrix and, thus, some economy is obtained. Figure 8.12 shows the exact and minimum quadratures for some popular rectangular and triangular elements. Note that both quadratures coincide for triangles.

Some authors associate the name “minimum quadrature” to that which guarantees that the element can reproduce in the limit a constant gradient (or strain) field [Z6,15]. This implies that the quadrature chosen should evaluate exactly the element area (or volume), which simply requires the exact computation of the following integral

$$A^{(e)} = \iint_{A^{(e)}} dA = \iint_{A^{(e)}} |J^{(e)}| d\xi d\eta$$

In rectangles and straight side triangles this condition is too weak as it requires a single point quadrature which generally violates the minimum requirement for preserving the element convergence as described above (with the exception of 3-noded triangles).

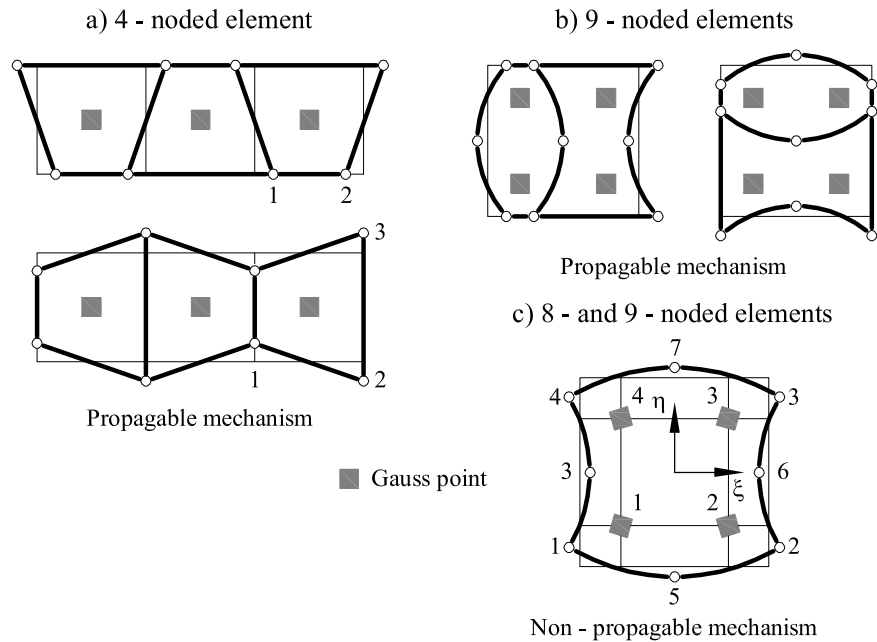


Fig. 8.13: a) Propagable mechanisms in the 4-noded rectangle with a single integration point, b) Mechanisms in the 8-noded and 9-noded quadrilaterals induced by reduced 2×2 quadrature. The mechanism in the 8-noded element are not propagable in a mesh

Extreme care must also be taken so that a lower order quadrature does not introduce internal mechanisms in the element. These mechanisms appear when the interpolation field for the main variables field generates a gradient (or strain) field which vanishes at the integration points, thus yielding a singular stiffness matrix. Sometimes these mechanisms are compatible between adjacent elements and lead to the singularity of the global stiffness matrix and, consequently, to an incorrect solution. A typical example of this situation is the two mechanisms induced by the reduced one point quadrature in the four-noded rectangle for 2D elasticity problems as shown in Figure 8.13a. This mechanism invalidates this reduced quadrature for practical purposes unless some stabilization techniques are used.

In some cases, the mechanisms induced by the reduced integration of the stiffness matrix can not propagate in the mesh, and this preserves the correctness of the solution. This happens for the single mechanism originated by the 2×2 reduced quadrature in the eight-noded rectangle for 2D elasticity problems, as shown in Figure 8.13b. Unfortunately this is not the case for the 9-noded Lagrangian as the reduced integration introduces three mechanisms (Figure 8.13) Two of which are propagable and can pollute the solution and hence it is not recommended practice.

Note that the minimum quadrature points coincide in most cases with the optimum points for the computation of fluxes (or stresses). This can be easily verified by comparing the minimum and optimum quadratures shown in Fig-

ures 8.9 and 8.10, respectively. This important coincidence is shown clearly in the analysis of a cantilever beam using 8-noded Serendipity rectangles. Figure 8.14 shows that the shear force distribution within each element is parabolic and, therefore, far from the correct linear solution. However, the tangential stresses at the 2×2 Gauss quadrature coincide with the exact values and the simple linear interpolation of the stresses gives the exact shear force distribution.

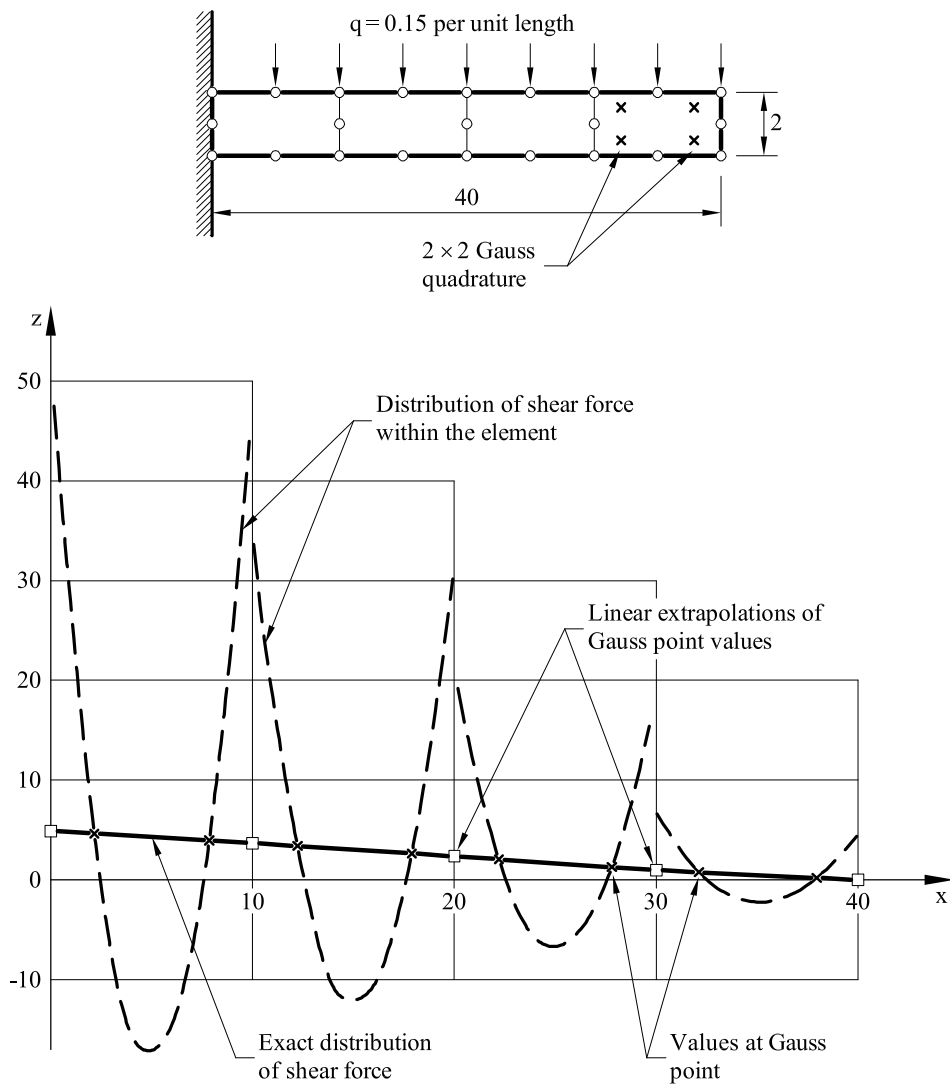


Fig. 8.14: Cantilever beam analyzed with four 8-noded Serendipity rectangles. Linear extrapolation of the shear force values from the transverse sections corresponding to the 2×2 Gauss quadrature

8.8 THE PATCH TEST FOR 2D ELEMENTS

Application of the patch test to triangular and quadrilateral elements follows the general lines described in Section 3.9 for 1D elements. Here once again the test is a necessary and sufficient condition for the convergence of the element.

The application of the patch test to a 2D element can take the following three different modalities.

Patch test A. A known linear field \mathbf{u}^p is prescribed at all nodes of a patch of 2D elements, where \mathbf{Q}^p are prescribed temperatures in a heat conduction problem, or prescribed displacements in an elasticity problems, etc. For each internal node j in the patch we verify that (Figure 8.13)

$$\mathbf{K}_{ij}\mathbf{a}_j^p - \mathbf{f}_j^p = \mathbf{0} \quad (8.50)$$

where \mathbf{a}_j^p is the nodal unknown vector corresponding to the known field and \mathbf{f}_j^p is a vector resulting from any external flux (or force) required to satisfy the governing differential equations for the known solution. Generally, in problems expressed in cartesian coordinates $\mathbf{f}_j^p = 0$.

Patch test B. Only the values of \mathbf{u}^p corresponding to the boundaries of the patch are inserted only and \mathbf{a}_i is found as (Figure 8.13)

$$\mathbf{a}_i = \mathbf{K}_{ii}^{-1}(\mathbf{f}_i^p - \mathbf{K}_{ij}\mathbf{u}_j) \quad i \neq j \quad (8.51)$$

and compared against the exact value.

Patch tests A and B also involve the computation of the fluxes (stresses) within the elements and the comparison with the expected “exact” values (Figure 8.15).

Satisfaction of patch tests A and B is a *necessary condition* for convergence of the element.

Patch test C. The assembled matrix system of the whole patch is written as

$$\bar{\mathbf{K}}\bar{\mathbf{a}} = \bar{\mathbf{f}}^p \quad (8.52)$$

where the bar denotes the patch values and $\bar{\mathbf{f}}^p$ represents prescribed boundary forces corresponding to the known solution. The solution for $\bar{\mathbf{a}}$ is sought after fixing the minimum number of degrees of freedom necessary to eliminate the singularity of the stiffness equation (i.e. one temperature for the heat conduction problem or the displacements for 2D elasticity problems) and it is compared with the known solution.

Patch test C allows us to detect any singularity in the stiffness matrix. This test is therefore an assessment of the *stability* of the finite element solution and hence provides not only a necessary but a sufficient condition for convergence.

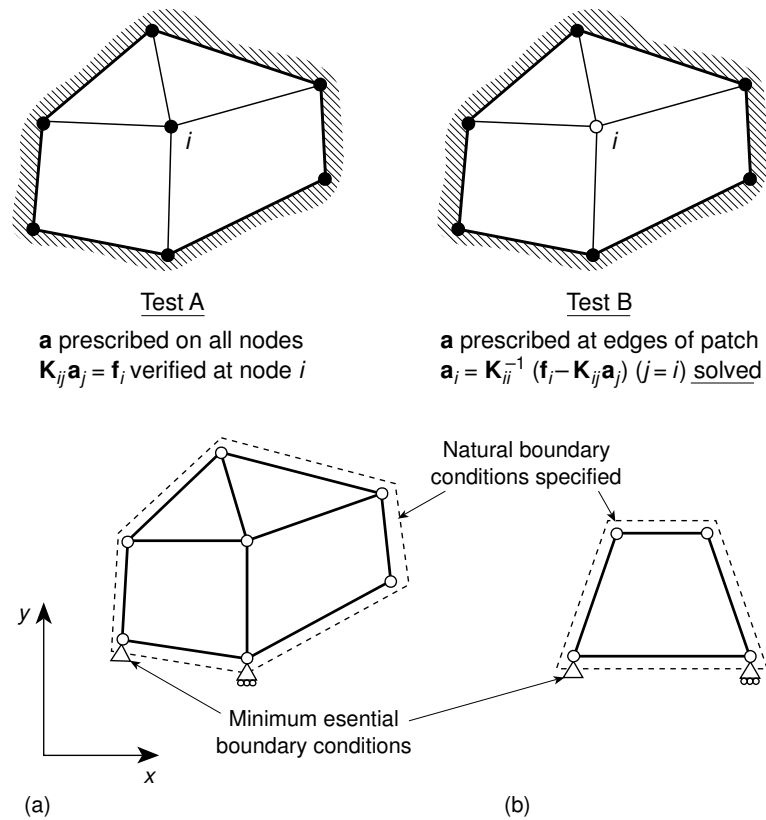


Fig. 8.15: Patch tests of form A , B and C

When the patch is reduced to just one element the C test is termed the *single-element test*. This test is one requirement of a good finite element formulation as, on occasion, a larger patch may not reveal the intrinsic instabilities of a single element. A typical example is the 8-noded isoparametric element for elasticity problems with reduced 2×2 Gauss quadrature. Here the singular deformation mode of a single element disappears when several elements are assembled. The satisfaction of the single-element test is not a sufficient condition for convergence and the test of at least one internal element boundary needs to be tested to assess sufficiency.

8.9 3D ISOPARAMETRIC ELEMENTS

3D elements with arbitrary geometry, as those shown in Figure 8.16, can be easily derived using an isoparametric formulation. The element geometry is defined in terms of the nodal coordinates, whereas the element integrals are performed over normalized cubes or tetrahedra using simple transformations.

Let us consider first the case of hexahedral elements. The coordinates of a

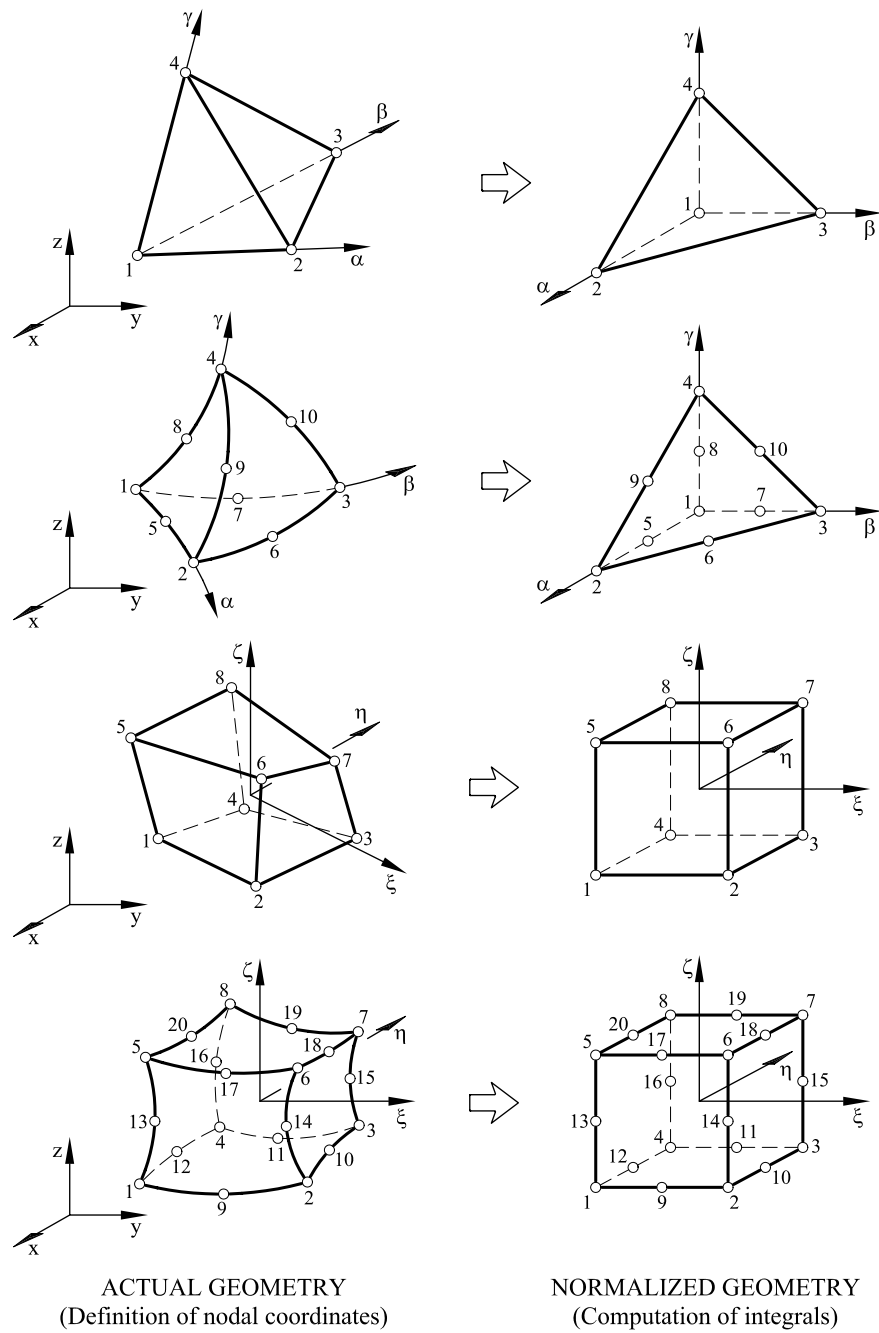


Fig. 8.16: 3D isoparametric elements. Actual and normalized geometries

point within a n -noded element are expressed in isoparametric form as

$$\mathbf{x} = \begin{Bmatrix} x \\ y \\ z \end{Bmatrix} = \sum_{i=1}^n \mathbf{N}_i \begin{Bmatrix} x_i \\ y_i \\ z_i \end{Bmatrix} = \mathbf{N} \mathbf{x}^{(e)} \quad (8.53)$$

with

$$\mathbf{N} = [\mathbf{N}_1, \mathbf{N}_2, \dots, \mathbf{N}_n] \quad ; \quad \mathbf{N}_i = \begin{bmatrix} N_i \\ N_i \\ N_i \end{bmatrix} \quad ; \quad N_i = f(\xi, \eta, \zeta) \quad (8.54)$$

where N_i are the shape functions used for the displacement field.

Eq.(8.53) relates the cartesian and the natural coordinates. This relationship is uniquely defined if the sign of the determinant of the Jacobian transformation $x, y, z \rightarrow \xi, \eta, \zeta$ is positive over the element. This is usually fulfilled except for very distorted element shapes.

The cartesian derivatives of the shape functions are computed following the same procedure as explained for 2D elements. The chain rule of derivation gives

$$\begin{Bmatrix} \frac{\partial N_i}{\partial \xi} \\ \frac{\partial N_i}{\partial \eta} \\ \frac{\partial N_i}{\partial \zeta} \end{Bmatrix} = \begin{bmatrix} \frac{\partial x}{\partial \xi} & \frac{\partial y}{\partial \xi} & \frac{\partial z}{\partial \xi} \\ \frac{\partial x}{\partial \eta} & \frac{\partial y}{\partial \eta} & \frac{\partial z}{\partial \eta} \\ \frac{\partial x}{\partial \zeta} & \frac{\partial y}{\partial \zeta} & \frac{\partial z}{\partial \zeta} \end{bmatrix} \begin{Bmatrix} \frac{\partial N_i}{\partial x} \\ \frac{\partial N_i}{\partial y} \\ \frac{\partial N_i}{\partial z} \end{Bmatrix} = \mathbf{J}^{(e)} \frac{\partial \mathbf{N}_i}{\partial \mathbf{x}} \quad (8.55)$$

where $\mathbf{J}^{(e)}$ is the Jacobian matrix. Using Eq.(8.53) gives

$$\mathbf{J}^{(e)} = \sum_{i=1}^n \begin{bmatrix} \frac{\partial N_i}{\partial \xi} x_i & \frac{\partial N_i}{\partial \xi} y_i & \frac{\partial N_i}{\partial \xi} z_i \\ \frac{\partial N_i}{\partial \eta} x_i & \frac{\partial N_i}{\partial \eta} y_i & \frac{\partial N_i}{\partial \eta} z_i \\ \frac{\partial N_i}{\partial \zeta} x_i & \frac{\partial N_i}{\partial \zeta} y_i & \frac{\partial N_i}{\partial \zeta} z_i \end{bmatrix} \quad (8.56)$$

The cartesian derivatives of N_i are computed as

$$\nabla N_i = \begin{Bmatrix} \frac{\partial N_i}{\partial x} \\ \frac{\partial N_i}{\partial y} \\ \frac{\partial N_i}{\partial z} \end{Bmatrix} = \left[\mathbf{J}^{(e)} \right]^{-1} \begin{Bmatrix} \frac{\partial N_i}{\partial \xi} \\ \frac{\partial N_i}{\partial \eta} \\ \frac{\partial N_i}{\partial \zeta} \end{Bmatrix} \quad (8.57)$$

The volume differential is expressed as

$$dx \, dy \, dz = \left| \mathbf{J}^{(e)} \right| d\xi \, d\eta \, d\zeta \quad (8.58)$$

The strain matrix of an isoparametric prismatic element can be expressed in terms of natural coordinates using Eq.(8.57) as

$$\mathbf{B}_i(\xi, \eta, \zeta) = \nabla N_i = \begin{Bmatrix} \bar{b}_i \\ \bar{c}_i \\ \bar{d}_i \end{Bmatrix} \quad (8.59)$$

with

$$\begin{Bmatrix} \bar{b}_i \\ \bar{c}_i \\ \bar{d}_i \end{Bmatrix} = \sum_{k=1}^3 \begin{Bmatrix} \bar{J}_{1k}^{(e)} \\ \bar{J}_{2k}^{(e)} \\ \bar{J}_{3k}^{(e)} \end{Bmatrix} \frac{\partial N_i}{\partial \xi_k} \quad (8.60)$$

where $\bar{J}_{ij}^{(e)}$ is the term ij of the inverse Jacobian matrix $[\mathbf{J}^{(e)}]^{-1}$, $\xi_1 = \xi$, $\xi_2 = \eta$ and $\xi_3 = \zeta$.

The general form of the stiffness matrix of a 3D isoparametric hexahedral element is therefore

$$\begin{aligned} K_{ij}^{(e)} &= \iiint_{V^{(e)}} \mathbf{B}_i^T \mathbf{D} \mathbf{B}_j dV = \\ &= \int_{-1}^{+1} \int_{-1}^{+1} \int_{-1}^{+1} \mathbf{B}_i^T(\xi, \eta, \zeta) \mathbf{D} \mathbf{B}_j(\xi, \eta, \zeta) \left| \mathbf{J}^{(e)} \right| d\xi d\eta d\zeta = \\ &= \int_{-1}^{+1} \int_{-1}^{+1} \int_{-1}^{+1} G_{ij}(\xi, \eta, \zeta) d\xi d\eta d\zeta \end{aligned} \quad (8.61a)$$

with

$$G_{ij} = \mathbf{B}_i^T \mathbf{D} \mathbf{B}_j \left| \mathbf{J}^{(e)} \right| \quad (8.61b)$$

where $\bar{b}_{ij} = \bar{b}_i \bar{b}_j$, $\bar{c}_{ij} = \bar{c}_i \bar{c}_j$ and $\bar{d}_{ij} = \bar{d}_i \bar{d}_j$, with $\bar{b}_i, \bar{c}_i, \bar{d}_i$ as given in Eq.(7.84) and d_{ij} are the terms of the constitutive matrix \mathbf{D} of Eq.(6.7). Matrix \mathbf{G} will typically contain rational polynomials arising from the Jacobian inverse contributions. Numerical integration is therefore the recommended option in these cases.

Isoparametric tetrahedral elements follow a similar procedure. The geometry interpolation is once again defined by Eq.(8.53) with N_i expressed in terms of volume or natural coordinates. The computation of the cartesian derivatives of N_i for straight side tetrahedra is immediate from Eqs.(8.57). The element integrals are directly expressed in terms of volume or natural coordinates. Natural coordinates are more convenient for curved tetrahedra. The derivation of the stiffness matrix follows the same steps explained for hexahedral elements simply substituting the coordinates ξ, η, ζ for α, β, γ , respectively. The resulting stiffness matrix has the form

$$K_{ij}^{(e)} = \int_0^1 \int_0^{1-\alpha} \int_0^{1-\alpha-\beta} G_{ij}(\alpha, \beta, \gamma) d\alpha d\beta d\gamma \quad (8.62)$$

where $\mathbf{G}(\alpha, \beta, \gamma)$ is deduced from Eq.(7.61b).

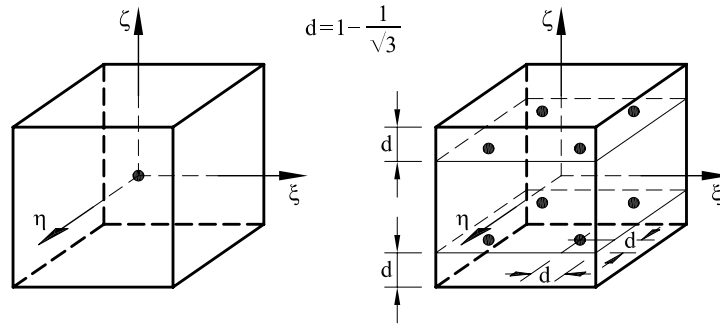


Fig. 8.17: Gauss quadratures of $1 \times 1 \times 1$ and $2 \times 2 \times 2$ points in hexahedral elements

8.10 NUMERICAL INTEGRATION IN THREE DIMENSIONS

8.10.1 Hexahedral elements

Let us consider the integration of a function $f(x, y, z)$ over a hexahedral isoparametric element. The following transformations are required

$$\begin{aligned} \iiint_{V^{(e)}} f(x, y, z) dx dy dz &= \int_{-1}^1 \int_{-1}^1 \int_{-1}^1 f(\xi, \eta, \zeta) |\mathbf{J}^{(e)}| d\xi d\eta d\zeta = \\ &= \int_{-1}^{+1} \int_{-1}^{+1} \int_{-1}^{+1} g(\xi, \eta, \zeta) d\xi d\eta d\zeta \end{aligned} \quad (8.63)$$

The use of a Gauss quadrature leads to

$$\begin{aligned} \int_{-1}^{+1} \int_{-1}^{+1} \int_{-1}^{+1} g(\xi, \eta, \zeta) d\xi d\eta d\zeta &= \int_{-1}^{+1} \int_{-1}^{+1} \sum_{p=1}^{n_p} W_p g(\xi_p, \eta, \zeta) d\eta d\zeta = \\ &= \int_{-1}^{+1} \sum_{q=1}^{n_q} \sum_{p=1}^{n_p} W_p W_q g(\xi_p, \eta_q, \zeta) d\zeta = \\ &= \sum_{r=1}^{n_r} \sum_{q=1}^{n_q} \sum_{p=1}^{n_p} W_p W_q W_r g(\xi_p, \eta_q, \zeta_r) \end{aligned} \quad (8.64)$$

where n_p, n_q and n_r are the integration points via the ξ, η, ζ directions, respectively, ξ_p, η_q, ζ_r are the coordinates of the integration point (p, q, r) and W_p, W_q, W_r are the weights for each natural direction.

The local coordinates and weights for each quadrature are deduced from Table 3.3 for the 1D case. We recall that a q th order quadrature integrates exactly a 1D polynomial of degree $2q - 1$. This rule helps us to identify the number of integration point in each natural directions. Figure 8.17 shows the sampling points for the $1 \times 1 \times 1$ and $2 \times 2 \times 2$ quadratures.

8.10.2 Tetrahedral elements

A Gauss quadrature for tetrahedral elements formulated in terms of volume coordinates is written as

$$\int_0^1 \int_0^{1-L_1} \int_0^{1-L_1-L_2} f(L_1, L_2, L_3, L_4) dL_1 dL_2 dL_3 = \sum_{i=1}^{n_p} f(L_{1_i}, L_{2_i}, L_{3_i}, L_{4_i}) W_i \quad (8.65)$$

Figure 8.18 shows the position of the integration points and the corresponding weights for the linear, quadratic and cubic quadratures.

Note that the weights in Figure 8.18 have been normalized so that their sum is 1/6. In this manner, the element volume is computed exactly. Thus

$$\begin{aligned} V^{(e)} &= \int \int \int_{V^{(e)}} dV = \int_{-1}^{+1} \int_{-1}^{+1} \int_{-1}^{+1} |\mathbf{J}^{(e)}| d\xi d\eta d\zeta = \\ &= |\mathbf{J}^{(e)}| \int_{-1}^{+1} \int_{-1}^{+1} \int_{-1}^{+1} d\xi d\eta d\zeta = \\ &= |\mathbf{J}^{(e)}| \sum_{i=1}^{n_p} W_i = 6V^{(e)} \sum_{i=1}^{n_p} W_i = \mathbf{V}^{(e)} \end{aligned} \quad (8.66)$$

8.11 NUMERICAL INTEGRATION OF THE ELEMENT MATRICES

8.11.1 Isoparametric hexahedral elements

Combining Eqs.(8.61) and (8.64) yields the stiffness matrix of an isoparametric hexahedral element as

$$\begin{aligned} K_{ij}^{(e)} &= \iiint_{V^{(e)}} \mathbf{B}_i^T \mathbf{D} \mathbf{B}_j dx dy dz = \int_{-1}^{+1} \int_{-1}^{+1} \int_{-1}^{+1} \mathbf{B}_i^T \mathbf{D} \mathbf{B}_j |\mathbf{J}^{(e)}| d\xi d\eta d\zeta = \\ &= \sum_{p=1}^{n_p} \sum_{q=1}^{n_q} \sum_{r=1}^{n_r} \left[\mathbf{B}_i^T \mathbf{D} \mathbf{B}_j \Big|_{\mathbf{J}^{(e)}} \right]_{p,q,r} W_p W_q W_r = \\ &= \sum_{p=1}^{n_p} \sum_{q=1}^{n_q} \sum_{r=1}^{n_r} [G_{ij}]_{p,q,r} W_p W_q W_r \end{aligned} \quad (8.67)$$

where \mathbf{G}_{ij} was given in Eq.(8.61b).

The computation of the equivalent nodal force vectors involving volume integrals follows an identical procedure. For the nodal flux vector

$$\begin{aligned} f_i^{(e)} &= \int \int \int_{V^{(e)}} N_i Q dx dy dz = \int_{-1}^{+1} \int_{-1}^{+1} \int_{-1}^{+1} N_i Q |\mathbf{J}^{(e)}| d\xi d\eta d\zeta = \\ &= \sum_{p=1}^{n_p} \sum_{q=1}^{n_q} \sum_{r=1}^{n_r} \left[N_i Q \Big|_{\mathbf{J}^{(e)}} \right]_{p,q,r} W_p W_q W_r \end{aligned} \quad (8.68)$$

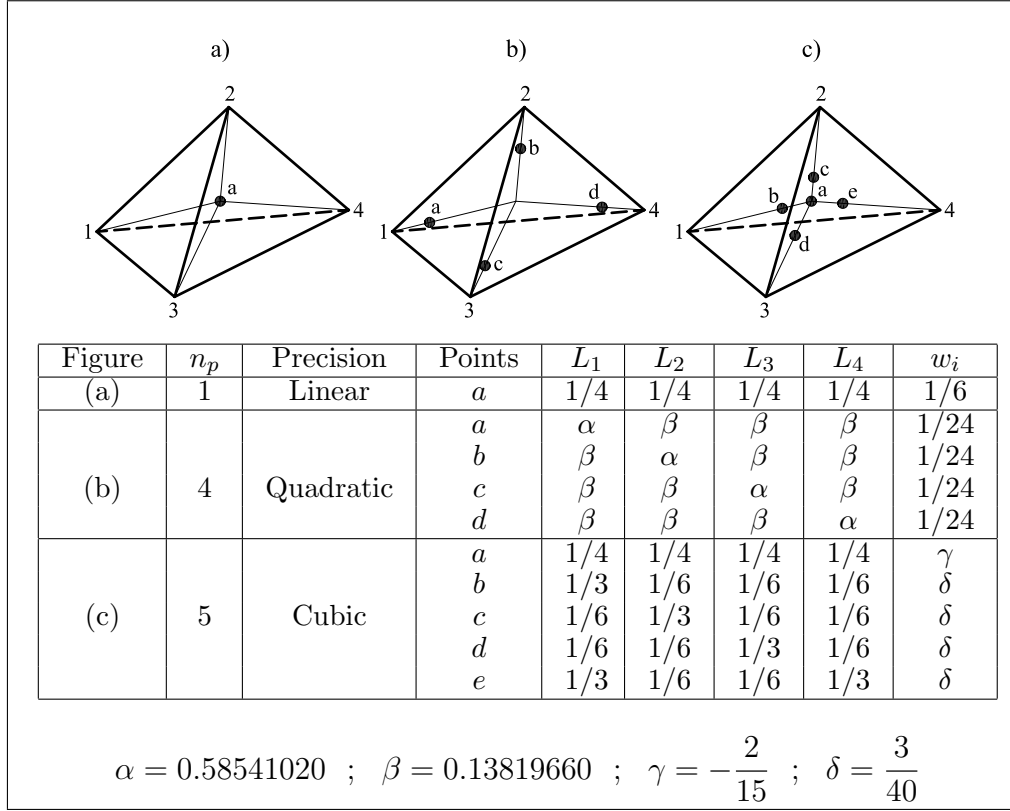


Fig. 8.18: Coordinates and weights for the Gauss quadrature in tetrahedra

The case of surface fluxes is somewhat more complicated. To explain the process let us assume that a distributed flux t_n acts *orthogonally* to the element face corresponding to $\zeta = +1$ defined by nodes 5 to 8 (Figure 8.19). The computation of the equivalent nodal vector for this case requires evaluating the term $\mathbf{t} dA$ where \mathbf{t} contains the global components of the surface flux acting on the element face and dA is the area differential. Thus, if \mathbf{n} is the unit normal to the face we have

$$\mathbf{t} = t_n \mathbf{n} \quad \text{with} \quad \mathbf{n} = [n_x, n_y, n_z]^T \quad (8.69)$$

Vector \mathbf{n} is obtained by the cross product of vectors \vec{V}_1 and \vec{V}_2 tangent to the lines $\eta = \text{constant}$ and $\xi = \text{constant}$ over the face, respectively. Thus

$$\vec{V}_1 = \left(\frac{\partial x}{\partial \xi} \mathbf{i} + \frac{\partial y}{\partial \xi} \mathbf{j} + \frac{\partial z}{\partial \xi} \mathbf{k} \right)_{\zeta=+1} d\xi$$

$$\vec{V}_2 = \left(\frac{\partial x}{\partial \eta} \mathbf{i} + \frac{\partial y}{\partial \eta} \mathbf{j} + \frac{\partial z}{\partial \eta} \mathbf{k} \right)_{\zeta=+1} d\eta \quad (8.70)$$

Eq.(8.70) shows that the components of \vec{V}_1 and \vec{V}_2 coincide with the terms in the first and second row of the Jacobian matrix of Eq.(8.56).

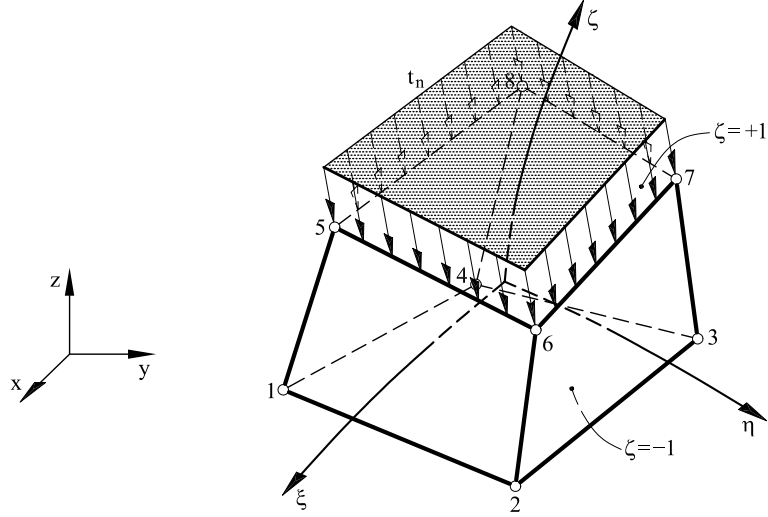


Fig. 8.19: Normal flux acting on a face of a hexahedral element

The unit normal vector is

$$\mathbf{n} = \frac{\vec{V}_1 \times \vec{V}_2}{|\vec{V}_1 \times \vec{V}_2|} \quad (8.71)$$

Noting that $dA = |\vec{V}_1 \times \vec{V}_2|$ gives

$$\mathbf{n} = \frac{1}{dA} \begin{Bmatrix} J_{12}J_{23} - J_{22}J_{13} \\ J_{21}J_{13} - J_{11}J_{23} \\ J_{11}J_{32} - J_{21}J_{12} \end{Bmatrix}_{\zeta=+1}^{(e)} d\xi d\eta = \frac{1}{dA} \mathbf{j}^{(e)} d\xi d\eta \quad (8.72)$$

where the $J_{ij}^{(e)}$ terms are deduced from Eq.(8.56).

The final expression of the equivalent nodal force vector is

$$\begin{aligned} f_{t_i}^{(e)} &= \iint_{A^{(e)}} N_i t_n dA = \int_{-1}^{+1} \int_{-1}^{+1} N_i t_n \mathbf{j}^{(e)} d\xi d\eta = \\ &= \sum_{p=1}^{n_p} \sum_{q=1}^{n_q} [N_i \mathbf{j}^{(e)} t_n]_{p,q} W_p W_q \end{aligned} \quad (8.73)$$

where $\mathbf{j}^{(e)}$ is deduced from Eq.(8.72). Also note that in Eq.(8.73) $N_i = N_i(\xi, \eta, \zeta = +1)$.

8.11.2 Isoparametric tetrahedral elements

The element stiffness matrix and the equivalent nodal force vector for isoparametric tetrahedra are computed by

$$K_{ij}^{(e)} = \sum_{p=1}^{n_p} [G_{ij}(\alpha, \beta, \gamma)]_p W_p \quad (8.74a)$$

$$f_i^{(e)} = \sum_{p=1}^{n_p} \left[N_i Q | \mathbf{J}^{(e)} | \right]_p W_p \quad (8.74b)$$

where

$$G_{ij} = \mathbf{B}_i^T(\alpha, \beta, \gamma) \mathbf{D} \mathbf{B}_j(\alpha, \beta, \gamma) | \mathbf{J}^{(e)} |$$

For the case of surface fluxes we have

$$f_{t_i}^{(e)} = \sum_{p=1}^{n_p} \left[N_i \mathbf{j}^{(e)} t_n \right]_p W_p \quad (8.75)$$

where the different terms have the same meaning as for hexahedra.

8.11.3 Selection of the quadrature order

The selection of the quadrature order for hexahedral and tetrahedral elements follows the same rules given for 2D solid elements. The full (exact) quadrature for linear and quadratic prisms is $2 \times 2 \times 2$ and $3 \times 3 \times 3$, respectively. These quadratures are also recommended for distorted shapes.

The reduced $1 \times 1 \times 1$ and $2 \times 2 \times 2$ quadratures induce spurious modes in the 8-noded and 27-noded elements, respectively. The performance of the 20-noded Serendipity elements generally improves with the $2 \times 2 \times 2$ reduced quadrature. However, this quadrature must be used with extreme care as it can lead to spurious mechanisms in certain problems, in a similar way as for 2D quadrilaterals.

For linear and quadratic tetrahedra the 1 and 4 points quadratures yield exact integration. Cubic tetrahedra require a quadrature of quartic precision for the exact integration of all the stiffness matrix terms.

The subroutines for computing $\mathbf{K}^{(e)}$ and $\mathbf{f}^{(e)}$ follow precisely the same steps as for 2D elements.

8.12 PERFORMANCE OF 3D SOLID ELEMENTS

3D solid elements behave in general terms very similarly to their analogous 2D elements. Hexahedral elements are more accurate than tetrahedra of the same order. Low order elements like the 8-noded hexahedron or 4-noded tetrahedron require fine meshes for problems with high gradients and higher order elements give more satisfactory results in these cases.

The 27-noded Lagrange element performs better than the 20-noded Serendipity one for representing a quadratic function on trilinearly distorted shapes. The reasons are similar to those given to explain the better performance of the 9-noded element when linearly distorted. The performance of the 20-noded Serendipity element in those cases can be improved by using $2 \times 2 \times 2$ reduced integration. However, great care should be taken when using a reduced quadrature for the quadratic Serendipity element.

Despite its highest cost the 27-noded Lagrange element is therefore generally preferable for modelling smooth solutions on distorted geometries.

We emphasize that mesh generation is one of the crucial problems for practical 3D analysis. Here, tetrahedral elements are by far the more versatile option for the discretization of complex 3D geometries. Much research on the development of efficient mesh generators for tetrahedral and hexahedral elements has been carried out in recent years. This issue is of even greater importance if adaptive refinement strategies are used.

Chapter 9

2D SOLIDS. LINEAR TRIANGULAR AND RECTANGULAR ELEMENTS

9.1 INTRODUCTION

This chapter initiates the application of the FEM to structures which satisfy the assumptions of two-dimensional (2D) elasticity (i.e. plane stress or plane strain). Many of the concepts in this chapter will be useful when dealing with other structural problems in subsequent chapters. Therefore, this chapter is introductory to the application of the FEM to continuous 2D and 3D structures.

There are a wide number of structures of practical interest which can be analyzed following the assumptions of 2D elasticity. All these structures have a sort of prismatic geometry. Depending on the relative dimensions of the prism and the loading type, the following two categories can be distinguished:

Plane stress problems. A prismatic structure is under plane stress if one of its dimensions (thickness) is much smaller than the other two and all the loads are contained in the middle plane of the structure (Figure 9.1). Amongst the structural problems that can be included in the plane stress category we find the analysis of deep beams, plates and walls under in-plane loading, buttress dams, etc.

Plane strain problems. A prismatic structure is under plane strain if one of its dimensions (length) is larger than the other two and all the loads are uniformly distributed along its length and they act orthogonally to the longitudinal axis (Figure 9.2). Amongst the structures which follow the plane strain assumption we can list containing walls, gravity dams, pressurised pipes, and also many problems of geotechnical engineering (tunnels, foundations, etc.).

One of the main advantages of 2D elasticity theory is that it allows the study of plane stress and plane strain problems in a unified manner. We should recall however that each problem conceptually represents a class of very different structural types.

2D elasticity theory provides a mathematical model by which the behaviour

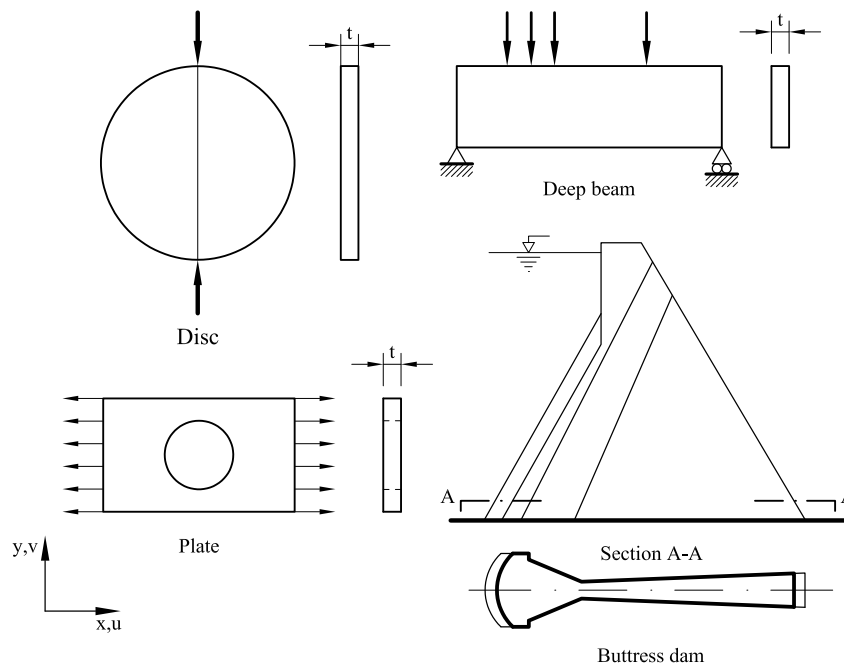


Fig. 9.1: Examples of plane stress problems

of a real 3D structure is represented by that of a 2D solid. The finite element method allows us to obtain an approximation to the “exact” solution of the 2D elasticity equations using 2D solid elements. The accuracy of the finite element solution will depend on the element type and the quality of the mesh chosen.

The chapter starts with a brief description of the basic concepts of 2D elasticity theory. Then the finite element solution using simple 3-noded triangles and 4-noded quadrilaterals is presented. Most of the finite element expressions are completely general and applicable to any other 2D solid element types. The general derivation of the element shape functions and the formulation of higher order triangular and quadrilateral elements and of isoparametric elements are studied in the next chapter.

9.2 TWO DIMENSIONAL ELASTICITY THEORY

Next, we present the concepts of 2D elasticity theory needed for the application of the FEM.

9.2.1 Displacement field

Both the plane stress and plane strain assumptions imply that the transverse sections to the longitudinal axis z deform in the same manner and also that the longitudinal displacement is negligible. Therefore, only a generic 2D transverse

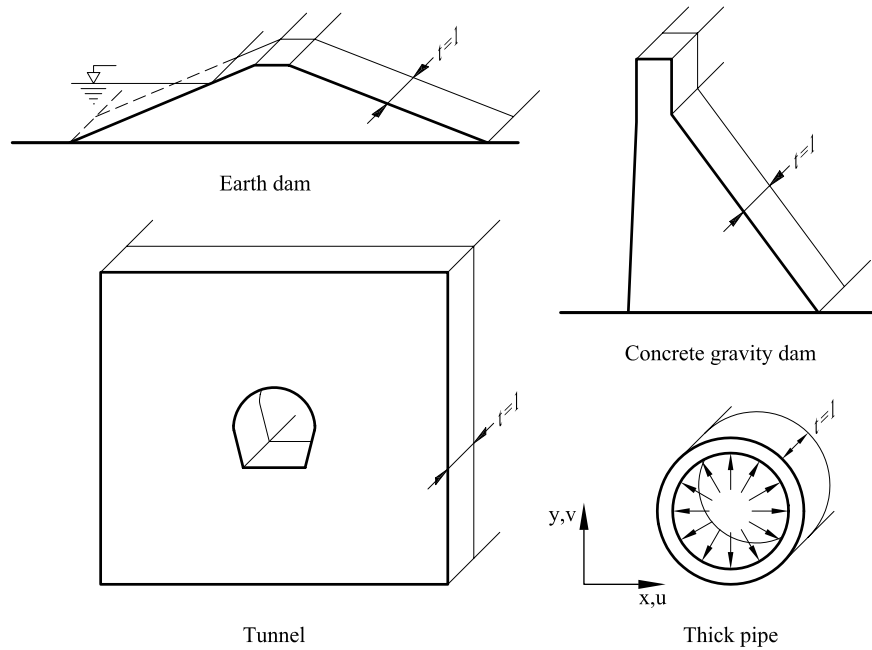


Fig. 9.2: Examples of plane strain problems

section defined in the plane $x - y$ needs to be considered for the analysis (Figures 9.1 and 9.2). The displacement field of the generic section is defined by the displacements in the x and y directions of all its points. The displacement vector is defined as

$$\mathbf{u}(x, y) = \begin{Bmatrix} u(x, y) \\ v(x, y) \end{Bmatrix} \quad (9.1)$$

where $u(x, y)$ and $v(x, y)$ are the displacements of the point in directions x and y , respectively.

9.2.2 Strain field

The displacement field (9.1) allows the corresponding strains to be derived from standard elasticity theory [T6]. This gives

$$\begin{aligned} \varepsilon_x &= \frac{\partial u}{\partial x} \\ \varepsilon_y &= \frac{\partial v}{\partial y} \\ \gamma_{xy} &= \frac{\partial u}{\partial y} + \frac{\partial v}{\partial x} \\ \gamma_{xz} &= \gamma_{yz} = 0 \end{aligned} \quad (9.2)$$

The longitudinal strain ε_z is assumed to be zero in the plane strain case. Conversely, ε_z is not zero in plane stress situations, although the conjugate stress σ_z is assumed to be zero. Therefore, ε_z need not be considered for either

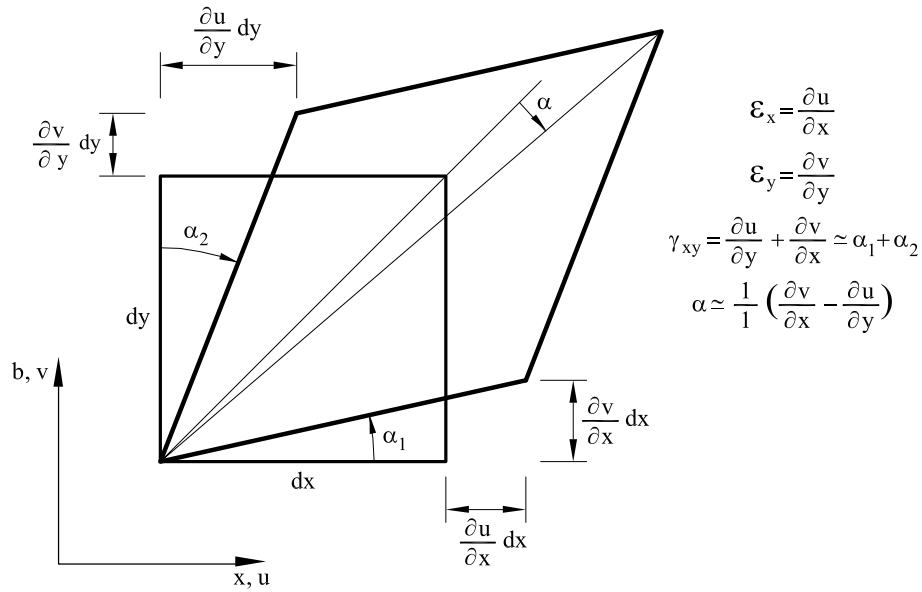


Fig. 9.3: Deformation of an infinitesimal 2D domain and definition of strains

plane stress or plane strain problems as the *work performed* by the longitudinal strains (i.e. $\sigma_z \epsilon_z$) is always zero. Consequently, the *strain vector* is defined in cases simply as

$$\boldsymbol{\epsilon} = [\epsilon_x, \epsilon_y, \gamma_{xy}]^T \quad (9.3)$$

The graphical meaning of the strains for 2D problems is shown in Figure 9.3.

9.2.3 Stress field

It is deduced from Eq.(9.2) that the shear stresses τ_{xz} and τ_{yz} are zero. Also, for the same reasons as explained above, the longitudinal stress σ_z does not contribute to the internal work and the stress vector is defined for both plane stress and plane strain cases as (Figure 9.3)

$$\boldsymbol{\sigma} = [\sigma_x, \sigma_y, \tau_{xy}]^T \quad (9.4)$$

9.2.4 Stress-strain relationship

The relationship between stresses and strains is derived from 3D elasticity theory [T6] using the assumptions stated above (i.e. $\sigma_z = 0$ for plane stress, $\epsilon_z = 0$ for plane strain, and $\gamma_{xz} = \gamma_{yz} = 0$ in both cases). After some simple algebra (see Example 4.1) the following matrix relationship can be obtained

$$\boldsymbol{\sigma} = \mathbf{D} \boldsymbol{\epsilon} \quad (9.5)$$

where \mathbf{D} is the elastic material matrix (or constitutive matrix)

$$\mathbf{D} = \begin{bmatrix} d_{11} & d_{12} & 0 \\ d_{21} & d_{22} & 0 \\ 0 & 0 & d_{33} \end{bmatrix} \quad (9.6)$$

It can be proved from the Maxwell-Betti theorem that \mathbf{D} is always symmetrical [T6] and $d_{12} = d_{21}$. For isotropic elasticity we have

$$\begin{array}{ll} \textit{Plane stress} & \textit{Plane strain} \\ d_{11} = d_{22} = \frac{E}{1 - \nu^2} & d_{11} = d_{22} = \frac{E(1 - \nu)}{(1 + \nu)(1 - 2\nu)} \\ d_{12} = d_{21} = \nu d_{11} & d_{12} = d_{21} = d_{11} \frac{\nu}{1 - \nu} \\ d_{33} = \frac{E}{2(1 + \nu)} = G & d_{33} = \frac{E}{2(1 + \nu)} = G \end{array} \quad (9.7)$$

where E is the Young modulus and ν the Poisson's ratio.

For an orthotropic material with principal orthotropy directions along the 1, 2, 3 axes, matrix \mathbf{D} has the following expression [T6]:

$$\mathbf{D} = \frac{1}{1 - \nu_{xy}\nu_{yx}} \begin{array}{c} \textit{Plane-stress} \\ \left[\begin{array}{ccc} E_1 & \nu_{21}E_1 & 0 \\ \nu_{12}E_2 & E_2 & 0 \\ 0 & 0 & (1 - \nu_{12}\nu_{21})G_{12} \end{array} \right] \end{array} \quad (9.8a)$$

$$\mathbf{D} = \frac{1}{ad - bc} \begin{array}{c} \textit{Plane strain} \\ \left[\begin{array}{ccc} aE_1 & bE_1 & 0 \\ cE_2 & dE_2 & 0 \\ 0 & 0 & (ad - bc)G_{12} \end{array} \right] \end{array} \quad (9.8b)$$

where

$$\frac{1}{G_{12}} \simeq \frac{1 + \nu_{21}}{E_1} + \frac{1 + \nu_{12}}{E_2} \quad (9.9a)$$

and

$$\begin{array}{ll} a = 1 - \nu_{23}\nu_{32} & ; \quad b = \nu_{12} + \nu_{32}\nu_{13} \\ c = \nu_{21} + \nu_{yz}\nu_{31} & ; \quad d = 1 - \nu_{13}\nu_{31} \end{array} \quad (9.9b)$$

The symmetry of \mathbf{D} requires

$$\frac{E_2}{E_1} = \frac{\nu_{12}}{\nu_{21}}(\textit{plane stress}) \quad \text{and} \quad \frac{E_2}{E_1} = \frac{b}{c}(\textit{plane strain}) \quad (9.10)$$

If the orthotropy directions 1, 2 are inclined at an angle ϕ with respect to the global axes of the structure 1, 2 (Figure 9.4) the constitutive relationship is derived as follows. First, the strains in local axes 1, 2 are expressed in terms of the global strains by

$$\boldsymbol{\varepsilon}' = \mathbf{T}\boldsymbol{\varepsilon} \quad (9.11)$$

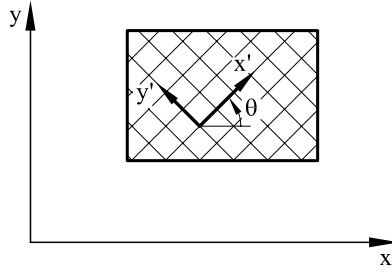


Fig. 9.4: Orthotropic material with principal orthotropy directions 1, 2

with [C15]

$$\mathbf{T} = \begin{bmatrix} \cos^2\phi & \sin^2\phi & \sin\phi \cos\phi \\ \sin^2\phi & \cos^2\phi & -\sin\phi \cos\phi \\ -2\sin\phi \cos\phi & 2\sin\phi \cos\phi & \cos^2\phi - \sin^2\phi \end{bmatrix} \quad (9.12)$$

The global stresses are related to those in the local axes by [T6]

$$\boldsymbol{\sigma} = \mathbf{T}^T \boldsymbol{\sigma}' \quad (9.13)$$

The stress-strain relationship in the local axes is written as

$$\boldsymbol{\sigma}' = \mathbf{D}' \boldsymbol{\varepsilon}' \quad (9.14)$$

where \mathbf{D}' is given by Eq.(9.8).

Finally, from Eqs.(9.1), (9.13) and (9.14) we obtain

$$\boldsymbol{\sigma} = \mathbf{T}^T \mathbf{D}' \mathbf{T} \boldsymbol{\varepsilon} = \mathbf{D} \boldsymbol{\varepsilon} \quad (9.15)$$

with

$$\mathbf{D} = \mathbf{T}^T \mathbf{D}' \mathbf{T} \quad (9.16)$$

It is easy to check that matrix \mathbf{D} is also symmetrical.

The d_{ij} coefficients for anisotropic elasticity can be found in references [H2] and [L1].

If the solid is subjected to initial strains such as thermal strains, the constitutive relationship (9.5) must be modified. The total strain $\boldsymbol{\varepsilon}$ is now equal to the sum of the elastic ($\boldsymbol{\varepsilon}^e$) and the initial ($\boldsymbol{\varepsilon}^0$) strains, whereas in Eq.(9.5) *all* the strains were considered to be elastic. Since the stresses are proportional to the elastic strains, the constitutive equation is now written as

$$\boldsymbol{\sigma} = \mathbf{D} \boldsymbol{\varepsilon}^e = \mathbf{D}(\boldsymbol{\varepsilon} - \boldsymbol{\varepsilon}^0) \quad (9.17)$$

For the case of initial strains due to thermal effects and isotropic material, vector $\boldsymbol{\varepsilon}^0$ has the following expressions

$$\begin{array}{cc}
\textit{Plane stress} & \textit{Plane strain} \\
\boldsymbol{\varepsilon}^0 = \begin{Bmatrix} \alpha\Delta T \\ \alpha\Delta T \\ 0 \end{Bmatrix} & \boldsymbol{\varepsilon}^0 = (1 + \nu) \begin{Bmatrix} \alpha\Delta T \\ \alpha\Delta T \\ 0 \end{Bmatrix}
\end{array} \quad (9.18)$$

where α is the thermal expansion coefficient and ΔT is the temperature increment at each point.

The difference between the values of $\boldsymbol{\varepsilon}^0$ for plane stress and plane strain is due to the different assumptions for σ_z and ε_z in each case (see Examples 4.2 and 4.3).

For anisotropic materials, the initial strains due to thermal effects are considered first in the principal directions of the material and then are transformed to global axes to find the global components of $\boldsymbol{\varepsilon}^0$. In these cases the tangential strain τ_{xy}^0 is not longer zero [H2], [Z6].

The solid can also be initially subjected to stresses defined by a vector $\boldsymbol{\sigma}^0$. These *initial stresses* can have different sources. For instance, if a part of the material is removed from a deformed structure under a set of loads, then automatically a new deformation is originated due to the existence of initial stresses. The total stresses in the new equilibrium configuration are obtained by the sum of the initial ones and those originated in the deformation process. For the more general case

$$\boldsymbol{\sigma} = \mathbf{D}(\boldsymbol{\varepsilon} - \boldsymbol{\varepsilon}^0) + \boldsymbol{\sigma}^0 \quad (9.19)$$

where

$$\boldsymbol{\sigma}^0 = [\sigma_x^0, \sigma_y^0, \tau_{xy}^0]^T \quad (9.20)$$

is the initial stress vector. A practical example of initial stresses is the analysis of a tunnel in geotechnical engineering, where the equilibrium of the excavated zone depends on the initial stresses in the zone before the excavation. Initial stresses are also very common in welded mechanical parts and here they are usually termed “residual” stresses.

Example: 9.1 Find the constitutive equation for an isotropic elastic material under plane stress and plane strain conditions.

- **Solution**

The starting point is the constitutive equation for 3D isotropic elasticity [T6]

$$\begin{aligned}
\varepsilon_x &= \frac{(\sigma_x - \nu\sigma_y - \nu\sigma_z)}{E}; \quad \varepsilon_y = \frac{(\sigma_y - \nu\sigma_x - \nu\sigma_z)}{E}; \quad \varepsilon_z = \frac{(\sigma_z - \nu\sigma_x - \nu\sigma_y)}{E} \\
\gamma_{xy} &= \frac{2(1 + \nu)}{E} \tau_{xy} \quad ; \quad \gamma_{xz} = \frac{2(1 + \nu)}{E} \tau_{xz} \quad ; \quad \gamma_{yz} = \frac{2(1 + \nu)}{E} \tau_{yz}
\end{aligned}$$

These equations will be now simplified using the plane stress and plane strain assumptions.

Plane stress: $\sigma_z = 0; \gamma_{xz} = \gamma_{yz} = 0$

Substituting the plane stress conditions into the above equations we have

$$\begin{aligned}\varepsilon_x &= \frac{1}{E}(\sigma_x - \nu\sigma_y), \quad \varepsilon_y = \frac{1}{E}(\sigma_y - \nu\sigma_x), \quad \gamma_{xy} = \frac{2(1+\nu)}{E}\tau_{xy} \\ \varepsilon_z &= -\frac{\nu}{E}(\sigma_x + \sigma_y) \quad ; \quad \tau_{xz} = \tau_{yz} = 0\end{aligned}$$

These equations yield the relationship between $\sigma_x, \sigma_y, \tau_{xy}$ and the corresponding strains as

$$\sigma_x = \frac{E}{1-\nu^2}(\varepsilon_x + \nu\varepsilon_y); \quad \sigma_y = \frac{E}{1-\nu^2}(\varepsilon_y + \nu\varepsilon_x); \quad \tau_{xy} = \frac{E}{(1+\nu)}\gamma_{xy}$$

from which the coefficients of **D** in Eq.(9.6) can be deduced.

Substituting the expressions of σ_x and σ_y for ε_z we find that

$$\varepsilon_z = -\nu(\varepsilon_x + \varepsilon_y)$$

Therefore, the longitudinal strain ε_z can be obtained “a posteriori” in terms of ε_x and ε_y .

Plane strain: $\varepsilon_z = 0; \gamma_{xz} = \gamma_{yz} = 0$

From the general equations relating strains and stresses we have

$$\begin{aligned}\varepsilon_x &= \frac{1}{E}(\sigma_x - \nu\sigma_y - \nu\sigma_z); \quad \varepsilon_y = \frac{1}{E}(\sigma_y - \nu\sigma_x - \nu\sigma_z) = 0 \\ \varepsilon_z = 0 &= \frac{1}{E}(\sigma_z - \nu\sigma_x - \nu\sigma_y) \quad ; \quad \gamma_{xy} = \frac{2(1+\nu)}{E}\tau_{xy} \quad ; \quad \tau_{xz} = \tau_{yz} = 0\end{aligned}$$

From the condition $\varepsilon_z = 0$ we find $\sigma_z = \nu(\sigma_x + \sigma_y)$. Substituting this value into the other equations we find

$$\begin{aligned}\sigma_x &= \frac{E(1-\nu)}{(1+\nu)(1-2\nu)}\left(\varepsilon_x + \frac{\nu}{1-\nu}\varepsilon_y\right) \\ \sigma_y &= \frac{E(1-\nu)}{(1+\nu)(1-2\nu)}\left(\varepsilon_y + \frac{\nu}{1-\nu}\varepsilon_x\right) \\ \tau_{xy} &= \frac{E}{2(1+\nu)}\gamma_{xy}\end{aligned}$$

from which the expression (9.6) for **D** can be obtained.

The same procedure can be used for orthotropic or anisotropic materials taking as a starting point the corresponding expressions of 3D elasticity [T6].

Example: 9.2 Find the initial strain vectors due to thermal effects for 2D isotropic elasticity.

- **Solution**

The main assumption is that the total strains are the sum of the elastic and the thermal ones. Also, it is assumed that a thermal expansion (or contraction) originates axial strains of value $\alpha\Delta T$, where α is the thermal expansion coefficient and ΔT the temperature increment. With these assumptions the total strains for 3D isotropic elasticity can be written as (see first equation of Example 4.1).

$$\begin{aligned}\varepsilon_x &= \varepsilon_x^e + \varepsilon_x^0 = \frac{1}{E}(\sigma_x - \nu\sigma_y - \nu\sigma_z) + \alpha\Delta T \\ \varepsilon_y &= \varepsilon_y^e + \varepsilon_y^0 = \frac{1}{E}(\sigma_y - \nu\sigma_x - \nu\sigma_z) + \alpha\Delta T \\ \varepsilon_z &= \varepsilon_z^e + \varepsilon_z^0 = \frac{1}{E}(\sigma_z - \nu\sigma_x - \nu\sigma_y) + \alpha\Delta T \\ \gamma_{xy} &= \frac{2(1+\nu)}{E}\tau_{xy} \quad ; \quad \gamma_{xz} = \frac{2(1+\nu)}{E}\tau_{xz} \quad ; \quad \gamma_{yz} = \frac{2(1+\nu)}{E}\tau_{yz}\end{aligned}$$

Plane stress $\sigma_z = \gamma_{xz} = \gamma_{yz} = 0$

Substituting these conditions into above equations we have

$$\begin{aligned}\varepsilon_x &= \frac{1}{E}(\sigma_x - \nu\sigma_y) + \alpha\Delta T \quad ; \quad \varepsilon_y = \frac{1}{E}(\sigma_y - \nu\sigma_x) + \alpha\Delta T \\ \varepsilon_z &= -\frac{\nu}{E}(\sigma_x + \sigma_y) + \alpha\Delta T \quad ; \quad \gamma_{xy} = \frac{2(1+\nu)}{E}\tau_{xy} \quad ; \quad \tau_{xz} = \tau_{yz} = 0\end{aligned}$$

Solving for σ_x , σ_y and τ_{xy} gives

$$\begin{aligned}\sigma_x &= \frac{E}{1-\nu^2} \left[(\varepsilon_x - \varepsilon_x^0) + \nu(\varepsilon_y - \varepsilon_y^0) \right] \\ \sigma_y &= \frac{E}{1-\nu^2} \left[(\varepsilon_y - \varepsilon_y^0) + \nu(\varepsilon_x - \varepsilon_x^0) \right] \\ \tau_{xy} &= \frac{E}{2(1+\nu)} \gamma_{xy}\end{aligned}$$

which can be written in the form $\boldsymbol{\sigma} = \mathbf{D}(\boldsymbol{\varepsilon} - \boldsymbol{\varepsilon}^0)$, with $\boldsymbol{\varepsilon}^0 = \alpha\Delta T[1, 1, 0]^T$ being the initial strain vector and \mathbf{D} the matrix given in (9.6) and (9.7).

Plane strain $\varepsilon_z = \gamma_{xz} = \gamma_{yz} = 0$

From the general expressions we find

$$\begin{aligned}\varepsilon_x &= \frac{1}{E}(\sigma_x - \nu\sigma_y - \nu\sigma_z) + \alpha\Delta T \\ \varepsilon_y &= \frac{1}{E}(\sigma_y - \nu\sigma_x - \nu\sigma_z) + \alpha\Delta T \\ 0 &= \frac{1}{E}(\sigma_z - \nu\sigma_x - \nu\sigma_y) + \alpha\Delta T \\ \gamma_{xy} &= \frac{2(1+\nu)}{E}\tau_{xy} \quad ; \quad \tau_{xz} = \tau_{yz} = 0\end{aligned}$$

From the third equation we find that

$$\sigma_z = \nu(\sigma_x + \sigma_y) - E \alpha \Delta T$$

Substituting this value into the first two equations yields

$$\begin{aligned}\varepsilon_x &= \frac{1}{E} \left[(1 - \nu^2)\sigma_x - \nu(1 + \nu)\sigma_y \right] + (1 + \nu)\alpha\Delta T \\ \varepsilon_y &= \frac{1}{E} \left[(1 - \nu^2)\sigma_y - \nu(1 + \nu)\sigma_x \right] + (1 + \nu)\alpha\Delta T \\ \gamma_{xy} &= \frac{2(1 + \nu)}{E} \tau_{xy}\end{aligned}$$

Solving for σ_x, σ_y and τ_{xy} gives

$$\begin{aligned}\sigma_x &= \frac{E(1 - \nu)}{(1 + \nu)(1 - 2\nu)} \left[(\varepsilon_x - (1 + \nu)\alpha\Delta T) + \frac{\nu}{1 - \nu}(\varepsilon_y - (1 + \nu)\alpha\Delta T) \right] \\ \sigma_y &= \frac{E(1 - \nu)}{(1 + \nu)(1 - 1\nu)} \left[(\varepsilon_y - (1 + \nu)\alpha\Delta T) + \frac{\nu}{1 - \nu}(\varepsilon_x - (1 + \nu)\alpha\Delta T) \right] \\ \tau_{xy} &= \frac{E}{2(1 + \nu)} \gamma_{xy}\end{aligned}$$

which can be written in matrix form as $\boldsymbol{\sigma} = \mathbf{D}(\boldsymbol{\varepsilon} - \boldsymbol{\varepsilon}^0)$, where

$$\boldsymbol{\varepsilon}^0 = (1 + \nu)\alpha\Delta T[1, 1, 0]^T$$

is the initial strain vector and \mathbf{D} the matrix given in Eqs.(9.6) and (9.7).

Example: 9.3 Explain the meaning of the initial strains for the bar in Figure 9.5 subjected to a uniform temperature increase.

- **Solution**

Let us assume first that the bar is clamped at one end and free at the other end (Figure 9.5a). Under a uniform temperature increment the bar will increase in length by the amount

$$\Delta l = \alpha \Delta T l$$

and the corresponding “initial” strain is

$$\varepsilon_x^0 = \frac{\Delta l}{l} = \alpha \Delta T$$

Since the bar is free to move horizontally, the total elongation is equal to that produced by the thermal increment and, therefore, the elastic strain is equal to zero, i.e.

$$\varepsilon_x^e = \varepsilon_x - \varepsilon_x^0 = \alpha \Delta T - \alpha \Delta T = 0$$

Thus, from Eq.(9.17) it is deduced that the stresses in the deformed bar are zero.

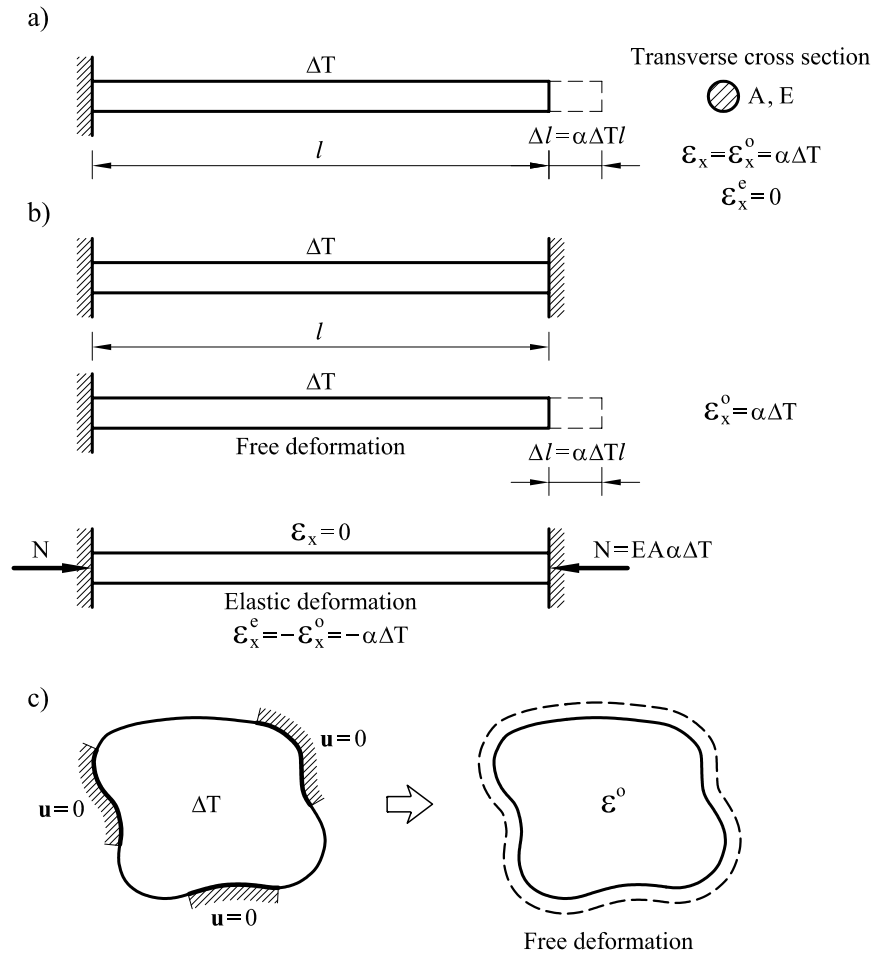


Fig. 9.5: Interpretation of initial thermal strains, a) Clamped/free bar, b) Fully clamped bar, c) 2D solid

Let us consider now the fully clamped bar of Figure 9.5b. To compute the initial strains let us assume that the bar points are free to move horizontally. Under these conditions the “initial” elongation of the bar will coincide with that of the clamped/free bar of Figure 9.5a, i.e. $\varepsilon_x^o = \alpha\Delta T$. However, since the bar points have the horizontal displacement restrained (due to the two clamped ends), the “elastic strain” is now

$$\varepsilon_x^e = \varepsilon_x - \varepsilon_x^o = 0 - \alpha\Delta T = -\alpha\Delta T$$

and by using Eq.(9.17) it is deduced that the bar is subjected to a uniform axial force of value $N = -\alpha EA\Delta T$.

Therefore, the initial thermal strains can be interpreted as the strains induced in the constraint-free body by a temperature increment occurring in some points (Figure 9.5c). Satisfaction of the kinematic (displacement) boundary conditions provides the values of the actual (total) strains. The difference between total and initial strains yields the “elastic” strains responsible for the stresses in the body.

It is also deduced from this example that a thermal increment produces no stresses in a body which can move freely in space.

9.2.5 Virtual work expression

PVW is written for 2D elasticity problems as

$$\begin{aligned} \iint_A (\delta\varepsilon_x \sigma_x + \delta\varepsilon_y \sigma_y + \delta\gamma_{xy} \tau_{xy}) t \, dA &= \iint_A (\delta u b_x + \delta v b_y) t \, dA + \\ &+ \oint_l (\delta u t_x + \delta v t_y) t \, ds + \sum_i (\delta u_i U_i + \delta v_i V_i) \end{aligned} \quad (9.21)$$

The second term in Eq.(9.21) represents the virtual work of the forces per unit area b_x, b_y ; the surface tractions t_x, t_y ; and the point loads U_i, V_i , respectively. The first term represents the work performed by the stresses $\sigma_x, \sigma_y, \tau_{xy}$ over the virtual strains $\delta\varepsilon_x, \delta\varepsilon_y$ y $\delta\gamma_{xy}$. A and l denote respectively the area and the boundary of the transverse section of the solid and t its thickness. For plane stress problems t is the actual thickness of the solid. For plane strain situations the analysis domain is a unit slice and it is usual to take t equal to one.

Eq.(9.21) can be written in matrix form as

$$\iint_A \delta\boldsymbol{\varepsilon}^T \boldsymbol{\sigma} t \, dA = \iint_A \delta\mathbf{u}^T \mathbf{b} t \, dA + \oint_l \delta\mathbf{u}^T \mathbf{t} t \, ds + \sum_i \delta\mathbf{u}_i^T \mathbf{q}_i \quad (9.22)$$

where

$$\begin{aligned} \delta\boldsymbol{\varepsilon} &= [\delta\varepsilon_x, \delta\varepsilon_y, \delta\gamma_{xy}]^T & ; & & \delta\mathbf{u} &= [\delta u, \delta v]^T & ; & & \mathbf{b} &= [b_x, b_y]^T \\ \mathbf{t} &= [t_x, t_y]^T & ; & & \delta\mathbf{u}_i &= [\delta u_i, \delta v_i]^T & ; & & \mathbf{q}_i &= [U_i, V_i]^T \end{aligned} \quad (9.23)$$

The above equations show that the PVW integrals involve up to first derivatives of the displacements only. Hence, C^0 continuous elements can be used. This requirement holds for all elasticity elements (i.e. 2D/3D solids and axisymmetric solids).

Eq.(9.22) is the starting point to derive the discretized finite element equations as described in the next section.

9.3 FINITE ELEMENT FORMULATION. THREE-NODED SOLID TRIANGULAR ELEMENT

We will study first the simple 3-noded solid triangular element. This is considered to be the first element used for the analysis of structural problems. Prior to the finite element era, Courant successfully used linear polynomial approximations over triangular regions to solve differential equations in 2D domains [C6]. Some years later Turner *et al.* [T12] in their classic paper proposed the discretization of 2D solid domains into simple triangles as a way to

analyze solids using matrix structural techniques. This explains why the 3-noded triangle is sometimes known as the Turner element. This element soon became very popular among engineers and it was widely used in the analysis of many structures in aeronautical and civil engineering [A10,11], [C18]. We note the impact of this element in the study of gravity dams and tunnels for practical civil engineering applications [Z12]. The key to the success of the 3-noded triangle is its simplicity which allows the assimilation of the FEM and the standard matrix method for bar structures known to most structural engineers. Conversely, it has limited accuracy due to the linear displacement approximation yielding constant strain and stress fields. Hence, fine meshes are required to capture accurate solutions in zones of high displacement gradients. This is however not a serious problem due to its versatile geometry, which is also very adequate for adaptive mesh refinement, as shown in Chapter 15. In summary, the 3-noded triangular element has the ideal features to introduce the application of the FEM to the analysis of 2D solids.

9.3.1 Discretization of the displacement field

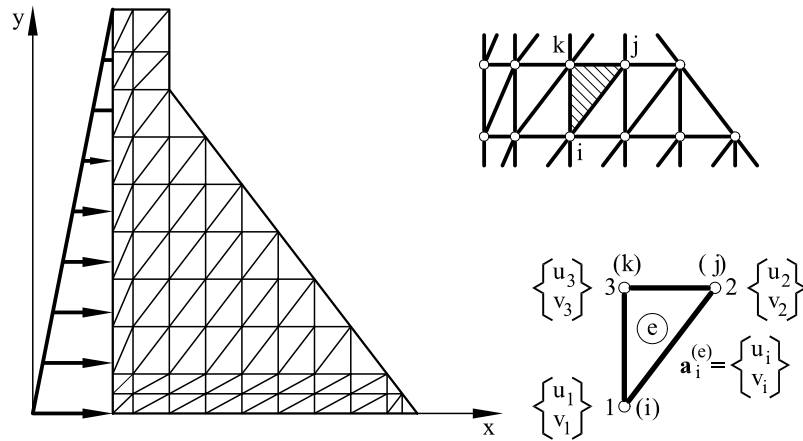
Figure 9.6 shows the transverse section of a solid analyzed under the assumptions of plane elasticity. As usual the first step is the discretization of the analysis domain as a mesh of finite elements. Figure 9.6 shows the mesh of 3-noded triangles chosen. The accuracy of the finite element solution can obviously be improved by using a finer mesh.

A typical 3-noded solid triangular element is characterized by the numbering of its nodes and their coordinates x, y . The three nodes have a global numbering i, j, k which corresponds to the local numbers 1, 2, 3 respectively. It is convenient to use the local numbering to compute the element matrices and vectors and to use the correspondance between local and global numbering (Figure 9.5) for the assembly process, as in the matrix analysis of bar structures [L3].

Let us consider an individual triangle like that shown in Figure 9.6. The two cartesian displacements of an arbitrary point within the element can be expressed in terms of the nodal displacements as

$$\begin{aligned} u &= N_1u_1 + N_2u_2 + N_3u_3 \\ v &= N_1v_1 + N_2v_2 + N_3v_3 \end{aligned} \tag{9.24}$$

where (u_i, v_i) and N_i are the horizontal and vertical displacements and the shape function of node i , respectively. There is not a fundamental reason to choose the same approximation for the vertical and horizontal displacements. However, the same interpolation for both displacements is typically used in practice.



Element	Node		Nodal variables		Nodal coordinates	
	Local	Global	Local	Global	Local	Global
ⓔ	1	i	u_1	u_i	x_1	x_i
	2	j	v_1	v_i	y_1	y_i
	3	k	u_2	u_j	x_2	x_j
Area: $A^{(e)}$			v_2	v_j	y_2	y_j
			u_3	u_k	x_3	x_k
			v_3	v_k	y_3	y_k

Fig. 9.6: Discretization of a structure in 3-noded solid triangular elements

Eq.(9.24) is written in matrix form as

$$\mathbf{u} = \begin{Bmatrix} u \\ v \end{Bmatrix} = \begin{bmatrix} N_1 & 0 & N_2 & 0 & N_3 & 0 \\ 0 & N_1 & 0 & N_2 & 0 & N_3 \end{bmatrix} \begin{Bmatrix} u_1 \\ v_1 \\ u_2 \\ v_2 \\ u_3 \\ v_3 \end{Bmatrix} \quad (9.25)$$

or

$$\mathbf{u} = \mathbf{N} \mathbf{a}^{(e)} \quad (9.26)$$

where

$$\mathbf{u} = \begin{Bmatrix} u \\ v \end{Bmatrix} \quad (9.27)$$

is the displacement vector of a point,

$$\mathbf{N} = [\mathbf{N}_1, \mathbf{N}_2, \mathbf{N}_3] \quad ; \quad \mathbf{N}_i = \begin{bmatrix} N_i & 0 \\ 0 & N_i \end{bmatrix} \quad (9.28)$$

are the shape function matrices of the element and the i th node, respectively, and

$$\mathbf{a}^{(e)} = \begin{Bmatrix} \mathbf{a}_1^{(e)} \\ \mathbf{a}_2^{(e)} \\ \mathbf{a}_3^{(e)} \end{Bmatrix} \quad \text{with} \quad \mathbf{a}_i^{(e)} = \begin{Bmatrix} u_i \\ v_i \end{Bmatrix} \quad (9.29)$$

are the nodal displacement vectors of the element and of i th node, respectively.

Note that \mathbf{N} and $\mathbf{a}^{(e)}$ contain as many matrices \mathbf{N}_i and vectors $\mathbf{a}_i^{(e)}$ as element nodes. This is a general rule which applies in all cases, as will be seen throughout this book.

The shape functions for the 3-noded triangular element can be found as follows.

The three nodes define a linear displacement field which can be written as

$$\begin{aligned} u &= \alpha_1 + \alpha_2 x + \alpha_3 y \\ v &= \alpha_4 + \alpha_5 x + \alpha_6 y \end{aligned} \quad (9.30)$$

Since we have assumed the same interpolation for u and v , it is sufficient to derive the shape function for one of the two displacements. Thus, for instance, the nodal horizontal displacement values are deduced from Eq.(9.30) as

$$\begin{aligned} u_1 &= \alpha_1 + \alpha_2 x_1 + \alpha_3 y_1 \\ u_2 &= \alpha_1 + \alpha_2 x_2 + \alpha_3 y_2 \\ u_3 &= \alpha_1 + \alpha_2 x_3 + \alpha_3 y_3 \end{aligned} \quad (9.31)$$

Solving for α_1, α_2 and α_3 and substituting into Eq.(9.30) yields

$$u = \frac{1}{2A^{(e)}} \left[(a_1 + b_1 x + c_1 y)u_1 + (a_2 + b_2 x + c_2 y)u_2 + (a_3 + b_3 x + c_3 y)u_3 \right] \quad (9.32a)$$

where $A^{(e)}$ is the element area and

$$a_i = x_j y_k - x_k y_j \quad , \quad b_i = y_j - y_k \quad , \quad c_i = x_k - x_j \quad ; \quad i, j, k = 1, 2, 3 \quad (9.32b)$$

Comparing Eqs.(9.32) and (9.24) the expression for the shape functions is found to be as

$$N_i = \frac{1}{2A^{(e)}} (a_i + b_i x + c_i y) \quad , \quad i = 1, 2, 3 \quad (9.33)$$

The form of the linear shape functions is shown in Figure 9.7. It can be checked that the shape function N_i takes the value one at node i and zero at the other two nodes.

9.3.2 Discretization of the strain field

Substituting Eq.(9.24) into (9.2) gives the three characteristic strains as

$$\begin{aligned} \varepsilon_x &= \frac{\partial u}{\partial x} = \frac{\partial N_1}{\partial x} u_1 + \frac{\partial N_2}{\partial x} u_2 + \frac{\partial N_3}{\partial x} u_3 \\ \varepsilon_y &= \frac{\partial v}{\partial y} = \frac{\partial N_1}{\partial y} v_1 + \frac{\partial N_2}{\partial y} v_2 + \frac{\partial N_3}{\partial y} v_3 \\ \gamma_{xy} &= \frac{\partial u}{\partial y} + \frac{\partial v}{\partial x} = \frac{\partial N_1}{\partial y} u_1 + \frac{\partial N_1}{\partial x} v_1 + \frac{\partial N_2}{\partial y} u_2 + \frac{\partial N_2}{\partial x} v_2 + \frac{\partial N_3}{\partial y} u_3 + \frac{\partial N_3}{\partial x} v_3 \end{aligned} \quad (9.34)$$

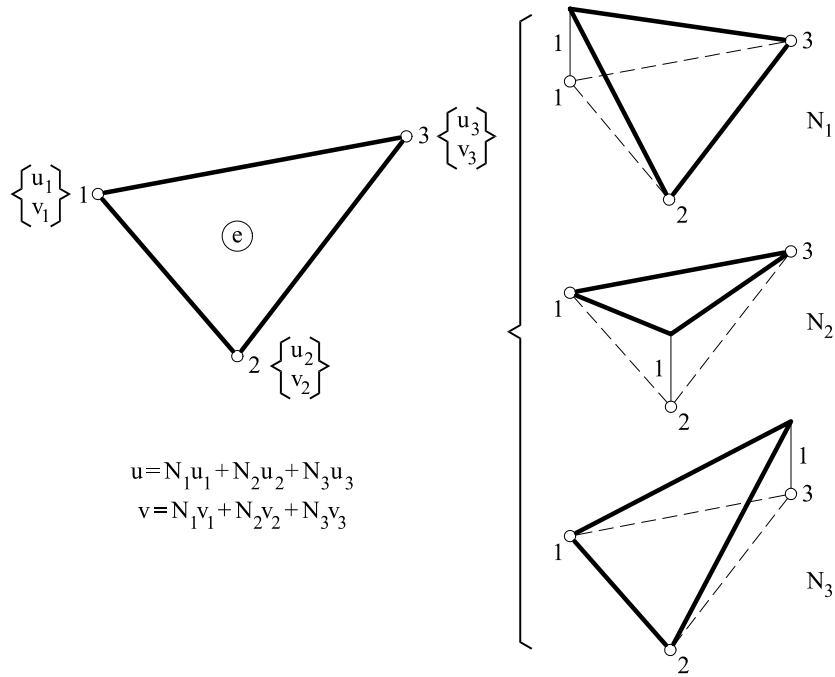


Fig. 9.7: Shape functions for the 3-noded solid triangular element

In matrix form

$$\boldsymbol{\varepsilon} = \begin{Bmatrix} \frac{\partial u}{\partial x} \\ \frac{\partial v}{\partial y} \\ \frac{\partial u}{\partial y} + \frac{\partial v}{\partial x} \end{Bmatrix} = \begin{bmatrix} \frac{\partial N_1}{\partial x} & 0 & \vdots & \frac{\partial N_2}{\partial x} & 0 & \vdots & \frac{\partial N_3}{\partial x} & 0 \\ 0 & \frac{\partial N_1}{\partial y} & \vdots & 0 & \frac{\partial N_2}{\partial y} & \vdots & 0 & \frac{\partial N_3}{\partial y} \\ \frac{\partial N_1}{\partial y} & \frac{\partial N_1}{\partial x} & \vdots & \frac{\partial N_2}{\partial y} & \frac{\partial N_2}{\partial x} & \vdots & \frac{\partial N_3}{\partial y} & \frac{\partial N_3}{\partial x} \end{bmatrix} \begin{Bmatrix} u_1 \\ v_1 \\ u_2 \\ v_2 \\ u_3 \\ v_3 \end{Bmatrix} \quad (9.35)$$

or

$$\boldsymbol{\varepsilon} = \mathbf{B}\mathbf{a}^{(e)} \quad (9.36)$$

where

$$\mathbf{B} = [\mathbf{B}_1, \mathbf{B}_2, \mathbf{B}_3] \quad (9.37)$$

is the element strain matrix, and

$$\mathbf{B}_i = \begin{bmatrix} \frac{\partial N_i}{\partial x} & 0 \\ 0 & \frac{\partial N_i}{\partial y} \\ \frac{\partial N_i}{\partial y} & \frac{\partial N_i}{\partial x} \end{bmatrix} \quad (9.38)$$

is the strain matrix of node i .

Note that \mathbf{B} contains as many \mathbf{B}_i matrices as element nodes. This is also a general property. Particularizing Eqs.(9.37) and (9.38) for the 3-noded triangle we obtain (using Eq.(9.33))

$$\mathbf{B} = \frac{1}{2A^{(e)}} \begin{bmatrix} b_1 & 0 & \vdots & b_2 & 0 & \vdots & b_3 & 0 \\ 0 & c_1 & \vdots & 0 & c_2 & \vdots & 0 & c_3 \\ c_1 & b_1 & \vdots & c_2 & b_2 & \vdots & c_3 & b_3 \end{bmatrix} \quad (9.39)$$

and, therefore

$$\mathbf{B}_i = \frac{1}{2A^{(e)}} \begin{bmatrix} b_i & 0 \\ 0 & c_i \\ c_i & b_i \end{bmatrix} \quad (9.40)$$

We note that the expression of \mathbf{B}_i in Eq.(9.38) is completely general and applicable to any 2D solid element.

9.3.3 Discretization of the stress field

The discretized expression of the stress field within the element is obtained by substituting Eq.(9.36) into (9.5) as

$$\boldsymbol{\sigma} = \mathbf{D}\boldsymbol{\varepsilon} = \mathbf{D}\mathbf{B}\mathbf{a}^{(e)} \quad (9.41)$$

If initial strains and stresses are considered we deduce from Eq.(9.17)

$$\boldsymbol{\sigma} = \mathbf{D}(\boldsymbol{\varepsilon} - \boldsymbol{\varepsilon}^0) + \boldsymbol{\sigma}^0 = \mathbf{D}\mathbf{B}\mathbf{a}^{(e)} - \mathbf{D}\boldsymbol{\varepsilon}^0 + \boldsymbol{\sigma}^0 \quad (9.42)$$

Note that the strain matrix for the 3-noded triangle is constant (Eq.(9.40)). *This implies that both the strain and stress fields are constant within the element.* This is a consequence of the linear displacement interpolation chosen which, naturally, has constant first derivatives. Therefore, a finer mesh will be needed in zones where stress gradients are higher, so that the stress field is accurately approximated.

9.3.4 Discretized equilibrium equations

The discretized equilibrium equations for the 3-noded triangle will be derived by applying the PVW to an individual element. We note that the expressions derived hereafter are completely general and applicable to any 2D solid element.

Let us assume that the following *external* forces act on the element (Figure 9.8): a) distributed forces \mathbf{b} acting per unit area (body forces), and b) distributed forces \mathbf{t} acting along the element sides belonging to a boundary line (surface tractions).

Note that the surface tractions due to the interaction of adjacent elements are excluded "a priori" they cancel themselves out during the assembly process.

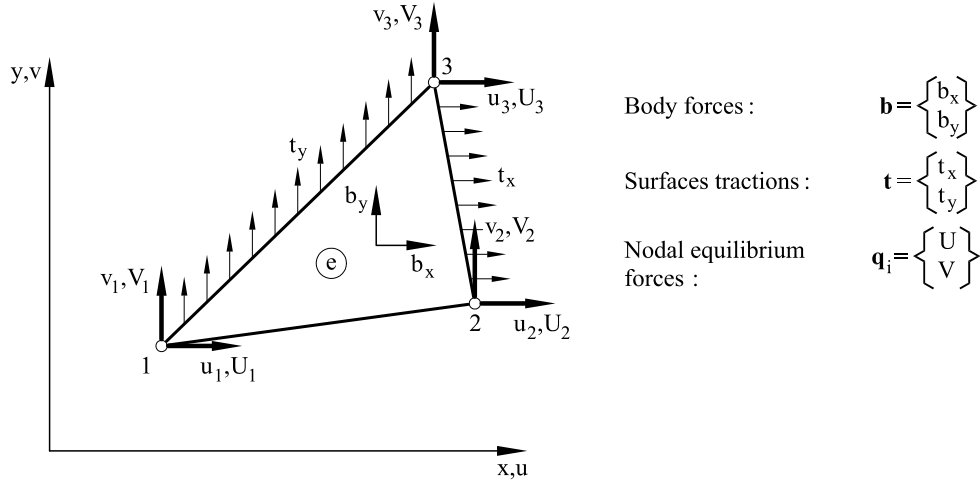


Fig. 9.8: Forces acting on a 3-noded solid triangle. The sides 13 and 23 belong to the external boundary

As usual in the FEM, the equilibrium of the forces acting on the element is enforced point wise at the nodes only. We must therefore define nodal point loads which will balance the external forces and the internal forces due to the element deformation. These “equilibrating nodal forces” are obtained by applying the PVW to an individual element as

$$\begin{aligned} \iint_{A^{(e)}} \delta \boldsymbol{\varepsilon}^T \boldsymbol{\sigma} t dA &= \iint_{A^{(e)}} \delta \mathbf{u}^T \mathbf{b} t dA + \oint_{l^{(e)}} \delta \mathbf{u}^T \mathbf{t} t ds + \\ &+ \sum_{i=1}^3 \delta u_i U_i + \sum_{i=1}^3 \delta v_i V_i \end{aligned} \quad (9.43)$$

where δu_i and δv_i are the nodal virtual displacements and U_i and V_i the corresponding equilibrating nodal forces. The virtual work performed by these forces can be obtained from Eq.(9.43) as

$$\iint_{A^{(e)}} \delta \boldsymbol{\varepsilon}^T \boldsymbol{\sigma} t dA - \iint_{A^{(e)}} \delta \mathbf{u}^T \mathbf{b} t dA - \oint_{l^{(e)}} \delta \mathbf{u}^T \mathbf{t} t ds = [\delta \mathbf{a}^{(e)}]^T \mathbf{q}^{(e)} \quad (9.44)$$

For the 3-noded triangular element

$$\begin{aligned} \delta \mathbf{a}^{(e)} &= [\delta u_1, \delta v_1, \delta u_2, \delta v_2, \delta u_3, \delta v_3]^T \\ \mathbf{q}^{(e)} &= [U_1, V_1, U_2, V_2, U_3, V_3]^T \end{aligned} \quad (9.45)$$

Next we interpolate the virtual displacements in terms of the nodal values. Following the same procedure as for deriving Eqs.(9.26) and (9.36) we obtain

$$\delta \mathbf{u} = \mathbf{N} \delta \mathbf{a}^{(e)} \quad ; \quad \delta \boldsymbol{\varepsilon} = \mathbf{B} \delta \mathbf{a}^{(e)} \quad (9.46a)$$

and

$$\delta \mathbf{u}^T = [\delta \mathbf{a}^{(e)}]^T \mathbf{N}^T \quad ; \quad \delta \boldsymbol{\varepsilon}^T = [\delta \mathbf{a}^{(e)}]^T \mathbf{B}^T \quad (9.46b)$$

Substituting the last equations into Eq.(9.44) gives

$$[\delta \mathbf{a}^{(e)}]^T \left[\iint_{A^{(e)}} \mathbf{B}^T \boldsymbol{\sigma} t dA - \iint_{A^{(e)}} \mathbf{N}^T \mathbf{b} t dA - \oint_{l^{(e)}} \mathbf{N}^T \mathbf{t} t ds \right] = [\delta \mathbf{a}^{(e)}]^T \mathbf{q}^{(e)} \quad (9.47)$$

Since the virtual displacements are arbitrary it is finally deduced that

$$\iint_{A^{(e)}} \mathbf{B}^T \boldsymbol{\sigma} t dA - \iint_{A^{(e)}} \mathbf{N}^T \mathbf{b} t dA - \oint_{l^{(e)}} \mathbf{N}^T \mathbf{t} t ds = \mathbf{q}^{(e)} \quad (9.48)$$

Eq.(9.48) yields the equilibrating nodal forces $\mathbf{q}^{(e)}$ in terms of the nodal forces due to the element deformation (first integral), the body forces (second integral) and the surface tractions (third integral). Substituting the stresses in terms of the nodal displacements from Eq.(9.42) gives

$$\iint_{A^{(e)}} \mathbf{B}^T (\mathbf{D} \mathbf{B} \mathbf{a}^{(e)} - \mathbf{D} \boldsymbol{\varepsilon}^0 + \boldsymbol{\sigma}^0) t dA - \iint_{A^{(e)}} \mathbf{N}^T \mathbf{b} t dA - \oint_{l^{(e)}} \mathbf{N}^T \mathbf{t} t ds = \mathbf{q}^{(e)} \quad (9.49)$$

and

$$\begin{aligned} & \left[\iint_{A^{(e)}} \mathbf{B}^T \mathbf{D} \mathbf{B} t dA \right] \mathbf{a}^{(e)} - \iint_{A^{(e)}} \mathbf{B}^T \mathbf{D} \boldsymbol{\varepsilon}^0 t dA + \\ & + \iint_{A^{(e)}} \mathbf{B}^T \boldsymbol{\sigma}^0 t dA - \iint_{A^{(e)}} \mathbf{N}^T \mathbf{b} t dA - \oint_{l^{(e)}} \mathbf{N}^T \mathbf{t} t ds = \mathbf{q}^{(e)} \end{aligned} \quad (9.50)$$

or

$$\mathbf{K}^{(e)} \mathbf{a}^{(e)} - \mathbf{f}^{(e)} = \mathbf{q}^{(e)} \quad (9.51)$$

where

$$\boxed{\mathbf{K}^{(e)} = \iint_{A^{(e)}} \mathbf{B}^T \mathbf{D} \mathbf{B} t dA} \quad (9.52)$$

is the element stiffness matrix, and

$$\boxed{\mathbf{f}^{(e)} = \mathbf{f}_\varepsilon^{(e)} + \mathbf{f}_\sigma^{(e)} + \mathbf{f}_b^{(e)} + \mathbf{f}_t^{(e)}} \quad (9.53)$$

is the equivalent nodal force vector for the element where

$$\mathbf{f}_\varepsilon^{(e)} = \iint_{A^{(e)}} \mathbf{B}^T \mathbf{D} \boldsymbol{\varepsilon}^0 t dA \quad (9.54)$$

$$\mathbf{f}_\sigma^{(e)} = - \iint_{A^{(e)}} \mathbf{B}^T \boldsymbol{\sigma}^0 t dA \quad (9.55)$$

$$\mathbf{f}_b^{(e)} = \iint_{A^{(e)}} \mathbf{N}^T \mathbf{b} t dA \quad (9.56)$$

$$\mathbf{f}_t^{(e)} = \oint_{l^{(e)}} \mathbf{N}^T \mathbf{t} t ds \quad (9.57)$$

are the equivalent nodal force vectors due to initial strains, initial stresses, body forces and surface tractions, respectively.

The expressions for the element stiffness matrix and the equivalent nodal force vectors given by Eqs.(9.52) - (9.57) are completely general and, therefore,

they are applicable to any 2D solid element. The particularization of these expressions for the 3-noded triangular element is given in the next section.

The global equilibrium equations for the whole mesh are obtained by establishing that the nodes are in equilibrium, similarly as for 1D problems; i.e. the sum of all the equilibrating nodal forces at a node balance the external point loads and

$$\sum_e \mathbf{q}_i^{(e)} = \mathbf{p}_j \quad (9.58)$$

where \mathbf{p}_j represents the vector of external point loads acting at node j and the sum refers to all elements sharing the node. Eq.(9.58) is identical to that studied in Chapter 1 for bar structures. The equilibrium equations for the whole mesh can thus be obtained following identical procedures as explained for bar structures. The global equilibrium equation is written in matrix form as

$$\mathbf{K}\mathbf{a} = \mathbf{f} \quad (9.59)$$

where \mathbf{K} and \mathbf{f} are the global stiffness matrix and the equivalent nodal force vector for the whole mesh. Both \mathbf{K} and \mathbf{f} are assembled from the element contributions in the standard manner.

We note once more that the equilibrating nodal forces due to the surface traction along the element interface cancel themselves out during the assembly process. Therefore, *only the surface tractions acting on the external boundaries of the structure must be considered in the analysis.*

9.3.5 Stiffness matrix and equivalent nodal force vectors for the 3-noded solid triangular element

Stiffness matrix

Eq.(9.52) can be written for the 3-noded triangle using (9.37) as

$$\begin{aligned} \mathbf{K}^{(e)} &= \iint_{A^{(e)}} \begin{Bmatrix} \mathbf{B}_1^T \\ \mathbf{B}_2^T \\ \mathbf{B}_3^T \end{Bmatrix} \mathbf{D} [\mathbf{B}_1, \mathbf{B}_2, \mathbf{B}_3] t dA = \\ &= \iint_{A^{(e)}} \begin{bmatrix} \mathbf{B}_1^T \mathbf{D} \mathbf{B}_1 & \mathbf{B}_1^T \mathbf{D} \mathbf{B}_2 & \mathbf{B}_1^T \mathbf{D} \mathbf{B}_3 \\ \cdot \cdot & \mathbf{B}_2^T \mathbf{D} \mathbf{B}_2 & \mathbf{B}_2^T \mathbf{D} \mathbf{B}_3 \\ \text{Sym.} & \cdot \cdot & \mathbf{B}_3^T \mathbf{D} \mathbf{B}_3 \end{bmatrix} t dA \quad (9.60) \end{aligned}$$

A typical element stiffness submatrix, $\mathbf{K}_{ij}^{(e)}$, linking nodes i and j of the element can be obtained as

$$\mathbf{K}_{ij}^{(e)} = \iint_{A^{(e)}} \mathbf{B}_i^T \mathbf{D} \mathbf{B}_j t dA \quad (9.61)$$

Substituting Eqs.(9.6) and (9.40) into Eq.(9.61) gives

$$\mathbf{K}_{ij}^{(e)} = \iint_{A^{(e)}} \frac{1}{2A^{(e)}} \begin{bmatrix} b_j & 0 & c_j \\ 0 & c_j & b_j \end{bmatrix} \begin{bmatrix} d_{11} & d_{12} & 0 \\ d_{21} & d_{22} & 0 \\ 0 & 0 & d_{33} \end{bmatrix} \frac{1}{2A^{(e)}} \begin{bmatrix} b_j & 0 \\ 0 & c_j \\ c_j & b_j \end{bmatrix} t dA \quad (9.62)$$

Since the integrand of Eq.(9.62) is constant we can easily obtain

$$\mathbf{K}_{ij}^{(e)} = \left(\frac{t}{4A} \right)^{(e)} \begin{bmatrix} b_i b_j d_{11} + c_i c_j d_{33} & b_i c_j d_{12} + b_j c_i d_{33} \\ c_i b_j d_{21} + b_i c_j d_{33} & b_i b_j d_{33} + c_i c_j d_{22} \end{bmatrix} \quad (9.63)$$

The form of $\mathbf{K}_{ij}^{(e)}$ for plane stress and plane strain situations is simply obtained by introducing the adequate values of the coefficients d_{ij} from Eq.(9.7). Note that $\mathbf{K}_{ij}^{(e)}$ is always symmetrical as $d_{12} = d_{21}$.

Equivalent nodal force vectors

a) *Body forces*

$$\mathbf{f}_b^{(e)} = \iint_{A^{(e)}} \mathbf{N}^T \mathbf{b} t dA = \iint_{A^{(e)}} \begin{Bmatrix} \mathbf{N}_1^T \mathbf{b} \\ \mathbf{N}_2^T \mathbf{b} \\ \mathbf{N}_3^T \mathbf{b} \end{Bmatrix} t dA \quad (9.64)$$

The nodal contribution of vector $\mathbf{f}_b^{(e)}$ is

$$\mathbf{f}_{b_i}^{(e)} = \iint_{A^{(e)}} \mathbf{N}_i^T \mathbf{b} t dA \quad (9.65)$$

If the body forces \mathbf{b} are uniformly distributed over the element we obtain using Eq.(9.33)

$$\mathbf{f}_{b_i} = \frac{(At)^{(e)}}{3} \begin{Bmatrix} bx \\ by \end{Bmatrix} \quad (9.66)$$

i.e. the total force acting over the element is split into equal parts between the three nodes of the triangle, as expected.

A particular case of body force is self weight with gravity acting in the direction of the y -axis. In this case $b_x = 0$ and $b_y = -\rho g$ where ρ and g are the material density and the value of the gravity constant, respectively.

b) *Surface loads*

$$\mathbf{f}_t^{(e)} = \oint_{l^{(e)}} \mathbf{N}^T \mathbf{t} t ds \quad (9.67)$$

For a node i belonging to a loaded external boundary we have

$$\mathbf{f}_{t_i}^{(e)} = \oint_{l^{(e)}} \mathbf{N}_i^T \mathbf{t} t ds = \oint_{l^{(e)}} \begin{Bmatrix} N_i t_x \\ N_i t_y \end{Bmatrix} t ds \quad (9.68)$$

We note that the shape function of a node not belonging to the loaded boundary takes a zero value. Thus, if the element side 1-2 is loaded with uniformly distributed tractions t_x and t_y , vector $\mathbf{f}_t^{(e)}$ is simply

$$\mathbf{f}_t^{(e)} = \frac{(l_{12} t)^{(e)}}{2} \begin{Bmatrix} t_x \\ t_y \\ t_x \\ t_y \\ 0 \\ 0 \end{Bmatrix} \quad (9.69)$$

where $l_{12}^{(e)}$ is the side length. Eq.(9.69) shows that the traction force acting along the element side is distributed into equal parts between the two side nodes. The expressions of $\mathbf{f}_t^{(e)}$ for loaded sides 1-3 and 2-3 are

$$\mathbf{f}_t^{(e)} = \frac{(l_{13}t)^{(e)}}{2} \begin{Bmatrix} t_x \\ t_y \\ 0 \\ 0 \\ t_x \\ t_y \end{Bmatrix} ; \quad \mathbf{f}_t^{(e)} = \frac{(l_{23}t)^{(e)}}{2} \begin{Bmatrix} 0 \\ 0 \\ t_x \\ t_y \\ t_x \\ t_y \end{Bmatrix} \quad (9.70)$$

c) Forces due to initial strains

Substituting Eq.(9.37) into (9.54) gives

$$\mathbf{f}_\varepsilon^{(e)} = \iint_{A^{(e)}} \mathbf{B}^T \mathbf{D} \varepsilon^0 t dA = \iint_{A^{(e)}} \begin{Bmatrix} \mathbf{B}_1^T \mathbf{D} \varepsilon^0 \\ \mathbf{B}_2^T \mathbf{D} \varepsilon^0 \\ \mathbf{B}_3^T \mathbf{D} \varepsilon^0 \end{Bmatrix} t dA \quad (9.71)$$

and the equivalent nodal force of node i due to the initial strains is

$$\mathbf{f}_{\varepsilon_i}^{(e)} = \iint_{A^{(e)}} \mathbf{B}_i^T \mathbf{D} \varepsilon^0 t dA \quad (9.72)$$

If ε^0 is constant over the element we obtain using Eqs.(9.6) and (9.40)

$$\begin{aligned} \mathbf{f}_{\varepsilon_i}^{(e)} &= \iint_{A^{(e)}} \frac{1}{2A^{(e)}} \begin{bmatrix} b_i & 0 & c_i \\ 0 & c_i & b_i \end{bmatrix} \begin{bmatrix} d_{11} & d_{12} & 0 \\ d_{21} & d_{22} & 0 \\ 0 & 0 & d_{33} \end{bmatrix} \begin{Bmatrix} \varepsilon_x^0 \\ \varepsilon_y^0 \\ \gamma_{xy}^0 \end{Bmatrix} t dA = \\ &= \frac{t^{(e)}}{2} \begin{Bmatrix} b_i(d_{11}\varepsilon_x^0 + d_{12}\varepsilon_y^0) + c_i d_{33} \gamma_{xy}^0 \\ c_i(d_{21}\varepsilon_x^0 + d_{22}\varepsilon_y^0) + b_i d_{33} \gamma_{xy}^0 \end{Bmatrix} \end{aligned} \quad (9.73)$$

For initial thermal strains, the expressions (9.18) for ε^0 should be used.

d) Forces due to initial stresses

Substituting Eq.(9.37) into (9.55) gives

$$\mathbf{f}_\sigma^{(e)} = - \iint_{A^{(e)}} \mathbf{B}^T \boldsymbol{\sigma}^0 t dA = - \iint_{A^{(e)}} \begin{Bmatrix} \mathbf{B}_1^T \boldsymbol{\sigma}^0 \\ \mathbf{B}_2^T \boldsymbol{\sigma}^0 \\ \mathbf{B}_3^T \boldsymbol{\sigma}^0 \end{Bmatrix} t dA \quad (9.74)$$

and the equivalent nodal force of node i due to the initial stresses is

$$\mathbf{f}_{\sigma_i}^{(e)} = - \iint_{A^{(e)}} \mathbf{B}_i^T \boldsymbol{\sigma}^0 t dA \quad (9.75)$$

For $\boldsymbol{\sigma}^0$ being constant over the element, we obtain using Eqs.(9.20) and (9.40)

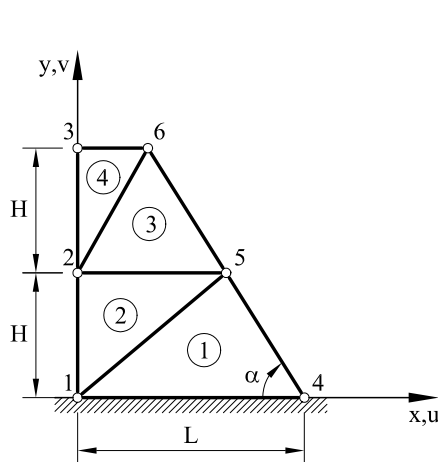
$$\mathbf{f}_{\sigma_i}^{(e)} = - \iint_{A^{(e)}} \frac{1}{2A^{(e)}} \begin{bmatrix} b_i & 0 & c_i \\ 0 & c_i & b_i \end{bmatrix} \begin{Bmatrix} \sigma_x^0 \\ \sigma_y^0 \\ \tau_{xy}^0 \end{Bmatrix} t dA = - \frac{t^{(e)}}{2} \begin{Bmatrix} b_i \sigma_x^0 + c_i \tau_{xy}^0 \\ c_i \sigma_y^0 + b_i \tau_{xy}^0 \end{Bmatrix} \quad (9.76)$$

The above expressions allow us to compute the matrices and vectors for the simple 3-noded triangle for 2D elasticity applications. Some comments and examples showing the behaviour of this element are given in Sections 9.5 and 9.6.

An example that illustrates the assembly and solution process is presented below.

Example: 9.4 Analyze the plane structure of the figure below under self weight.

- *Solution*



Mesh topology

Element	Nodal connections		
1	1	4	5
2	1	5	2
3	2	6	3
4	2	6	3

Plane strain situation

$$\mathbf{u}_1 = \mathbf{u}_4 = \mathbf{0}$$

The assembly process is similar to that for matrix analysis of bar structures. The global system of equations has the following form

$$\begin{array}{cccccc}
 & 1 & 2 & 3 & 4 & 5 & 6 \\
 \begin{array}{l} 1 \\ 2 \\ 3 \\ 4 \\ 5 \\ 6 \end{array} & \left[\begin{array}{cccccc}
 (\mathbf{K}_{11}^{(1)} + \mathbf{K}_{11}^{(2)}) & \mathbf{K}_{13}^{(2)} & \mathbf{0} & \mathbf{K}_{12}^{(1)} & (\mathbf{K}_{13}^{(1)} + \mathbf{K}_{12}^{(2)}) & \mathbf{0} \\
 & (\mathbf{K}_{33}^{(2)} + \mathbf{K}_{11}^{(3)} + \mathbf{K}_{11}^{(4)}) & \mathbf{K}_{13}^{(4)} & \mathbf{0} & (\mathbf{K}_{32}^{(2)} + \mathbf{K}_{12}^{(3)}) & (\mathbf{K}_{13}^{(3)} + \mathbf{K}_{12}^{(4)}) \\
 & & \mathbf{K}_{33}^{(4)} & \mathbf{0} & \mathbf{0} & \mathbf{K}_{32}^{(4)} \\
 & \text{Symm.} & & \mathbf{K}_{22}^{(1)} & \mathbf{K}_{23}^{(1)} & \mathbf{0} \\
 & & & & (\mathbf{K}_{33}^{(1)} + \mathbf{K}_{22}^{(2)} + \mathbf{K}_{22}^{(3)}) & \mathbf{K}_{23}^{(3)} \\
 & & & & & (\mathbf{K}_{22}^{(4)} + \mathbf{K}_{33}^{(3)})
 \end{array} \right] & \begin{Bmatrix} \mathbf{a}_1 \\ \mathbf{a}_2 \\ \mathbf{a}_3 \\ \mathbf{a}_4 \\ \mathbf{a}_5 \\ \mathbf{a}_6 \end{Bmatrix} & = & \begin{Bmatrix} \mathbf{r}_1 + \mathbf{f}_1^{(1)} + \mathbf{f}_1^{(2)} \\ (\mathbf{f}_3^{(2)} + \mathbf{f}_1^{(3)} + \mathbf{f}_1^{(4)}) \\ \mathbf{f}_3^{(4)} \\ \mathbf{r}_4 + \mathbf{f}_2^{(1)} \\ (\mathbf{f}_3^{(1)} + \mathbf{f}_2^{(2)} + \mathbf{f}_2^{(3)}) \\ \mathbf{f}_3^{(3)} + \mathbf{f}_2^{(4)} \end{Bmatrix}
 \end{array}$$

where $\mathbf{K}_{ij}^{(e)}$ is obtained from Eq.(9.63) and $\mathbf{f}_i^{(e)}$ from Eq.(9.64) with $b_x = 0$ and $b_y = -\rho g$. In both cases $t = 1$ should be taken.

The above system can be solved in the usual way by eliminating the rows and columns corresponding to the prescribed displacements \mathbf{a}_1 and \mathbf{a}_4 . Once the nodal displacements have been obtained the corresponding reactions \mathbf{r}_1 and \mathbf{r}_4 can be computed.

Finally, the constant strains and stresses within each element can be found “a posteriori” from the known nodal displacements by Eqs.(9.36) and (9.41), respectively.

The reader is encouraged to repeat this exercise by him/herself.

9.4 THE FOUR NODED SOLID RECTANGULAR ELEMENT

9.4.1 Basic formulation

The 4-noded solid rectangle is the simplest of the quadrilateral solid element family. This element was developed soon after the 3-noded solid triangle of the previous section. However, its irregular behaviour has motivated much research which we will summarize here.

Figure 9.9 shows a deep beam discretized in a mesh of 4-noded rectangles. Let us consider an isolated element with the local coordinate system r and s shown in Figure 9.9. The four nodal displacements define a four-term polynomial interpolation for the displacement field. The simplest interpolation satisfying the condition of interelement compatibility and geometric invariance is

$$\begin{aligned}
 u(x, y) &= \alpha_1 + \alpha_2 r + \alpha_3 s + \alpha_4 rs \\
 v(x, y) &= \alpha_5 + \alpha_6 r + \alpha_7 s + \alpha_8 rs
 \end{aligned} \tag{9.77}$$

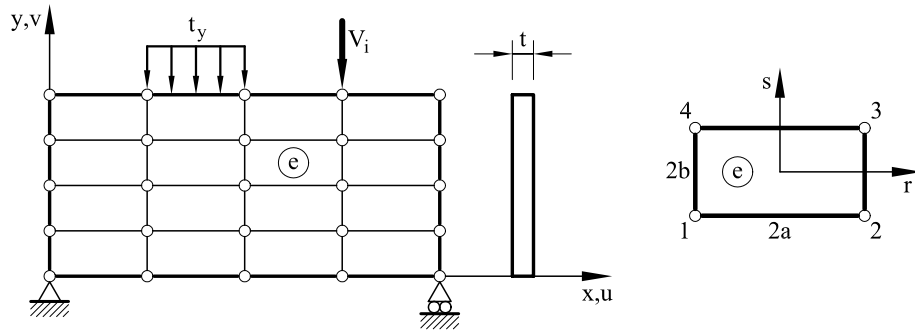


Fig. 9.9: Discretization of a deep beam with 4-noded solid rectangular elements. Definition of the local axes r and s for an element

Eq.(9.77) implies a linear distribution of u and v along each element side, thus guaranteeing continuity of the displacement field between adjacent elements. Note that the displacements vary as an incomplete quadratic polynomial within the element. The four constants α_i for each displacement component are obtained from the following conditions expressed in the local system r, s .

$$\begin{aligned}
 u &= u_1 & \text{and} & & v &= v_1 & \text{for} & & r &= -a & , & & s &= -b \\
 u &= u_2 & \text{and} & & v &= v_2 & \text{for} & & r &= -a & , & & s &= -b \\
 u &= u_3 & \text{and} & & v &= v_3 & \text{for} & & r &= a & , & & s &= b \\
 u &= u_4 & \text{and} & & v &= v_4 & \text{for} & & r &= a & , & & s &= b
 \end{aligned} \tag{9.78}$$

Substituting these conditions into Eq.(9.77) and solving for the α_i parameter, Eq.(9.77) can be rewritten as follows (note that only the α_i parameters for one of the two displacements are needed, as the same interpolation is used for u and v)

$$u = \sum_{i=1}^4 N_i u_i \quad ; \quad v = \sum_{i=1}^4 N_i v_i \tag{9.79}$$

The shape functions N_i are

$$\begin{aligned}
 N_1 &= \frac{1}{4} \left(1 - \frac{r}{a}\right) \left(1 - \frac{s}{b}\right) & ; & & N_2 &= \frac{1}{4} \left(1 + \frac{r}{a}\right) \left(1 - \frac{s}{b}\right) \\
 N_3 &= \frac{1}{4} \left(1 + \frac{r}{a}\right) \left(1 + \frac{s}{b}\right) & ; & & N_4 &= \frac{1}{4} \left(1 - \frac{r}{a}\right) \left(1 + \frac{s}{b}\right)
 \end{aligned} \tag{9.80}$$

Eqs.(9.79) can be rewritten in matrix form as

$$\mathbf{u} = \begin{Bmatrix} u \\ v \end{Bmatrix} = \begin{bmatrix} N_1 & 0 & \vdots & N_2 & 0 & \vdots & N_3 & 0 & \vdots & N_4 & 0 \\ 0 & N_1 & \vdots & 0 & N_2 & \vdots & 0 & N_3 & \vdots & 0 & N_4 \end{bmatrix} \begin{Bmatrix} u_1 \\ v_1 \\ u_2 \\ v_2 \\ u_3 \\ v_3 \\ u_4 \\ v_4 \end{Bmatrix} = \mathbf{N} \mathbf{a}^{(e)} \quad (9.81)$$

where

$$\mathbf{N} = [\mathbf{N}_1, \mathbf{N}_2, \mathbf{N}_3, \mathbf{N}_4] \quad ; \quad \mathbf{N}_i = \begin{bmatrix} N_i & 0 \\ 0 & N_i \end{bmatrix} \quad (9.82)$$

$$\mathbf{a}^{(e)} = \begin{Bmatrix} \mathbf{a}_1^{(e)} \\ \mathbf{a}_2^{(e)} \\ \mathbf{a}_3^{(e)} \\ \mathbf{a}_4^{(e)} \end{Bmatrix} \quad ; \quad \mathbf{a}_i^{(e)} = \begin{Bmatrix} u_i \\ v_i \end{Bmatrix}$$

are the shape function matrix and the displacement vector for the element and the node i , respectively.

The element strain matrix is obtained from Eqs.(9.2) and (9.79) as

$$\boldsymbol{\varepsilon} = \sum_{i=1}^4 \mathbf{B}_i \mathbf{a}_i^{(e)} = [\mathbf{B}_1, \mathbf{B}_2, \mathbf{B}_3, \mathbf{B}_4] \begin{Bmatrix} \mathbf{a}_1^{(e)} \\ \mathbf{a}_2^{(e)} \\ \mathbf{a}_3^{(e)} \\ \mathbf{a}_4^{(e)} \end{Bmatrix} = \mathbf{B} \mathbf{a}^{(e)} \quad (9.83)$$

where \mathbf{B}_i is given by precisely the same expression (9.40) derived for the 3-noded triangle. For the computation of \mathbf{B}_i note that

$$\frac{\partial N_i}{\partial x} = \frac{\partial N_i}{\partial r} \quad \text{and} \quad \frac{\partial N_i}{\partial y} = \frac{\partial N_i}{\partial s} \quad (9.84)$$

The expression of the \mathbf{B} matrix is shown in Box 4.1.

The stiffness matrix and the equivalent nodal force vectors for the element are obtained via the PVW as previously explained for the linear triangle. The element stiffness matrix is

$$\begin{aligned} \mathbf{K}^{(e)} &= \iint_{A^{(e)}} \mathbf{B}^T \mathbf{D} \mathbf{B} t \, dr \, ds = \\ &= \iint_{A^{(e)}} \begin{bmatrix} \mathbf{B}_1^T \mathbf{D} \mathbf{B}_1 & \mathbf{B}_1^T \mathbf{D} \mathbf{B}_2 & \mathbf{B}_1^T \mathbf{D} \mathbf{B}_3 & \mathbf{B}_1^T \mathbf{D} \mathbf{B}_4 \\ \vdots & \mathbf{B}_2^T \mathbf{D} \mathbf{B}_2 & \mathbf{B}_2^T \mathbf{D} \mathbf{B}_3 & \mathbf{B}_2^T \mathbf{D} \mathbf{B}_4 \\ \text{Sym.} & \vdots & \mathbf{B}_3^T \mathbf{D} \mathbf{B}_3 & \mathbf{B}_3^T \mathbf{D} \mathbf{B}_4 \\ & & & \mathbf{B}_4^T \mathbf{D} \mathbf{B}_4 \end{bmatrix} t \, dr \, ds \quad (9.85) \end{aligned}$$

Box 4.1 shows that the strain matrix contains linear terms in r and s . Therefore, the integrand of Eq.(9.85) contains quadratic terms. However, the

$$\mathbf{B} = \left[\begin{array}{cc|cc|cc|cc} -b_2 & 0 & b_2 & 0 & b_1 & 0 & -b_1 & 0 \\ 0 & -a_2 & 0 & -a_1 & 0 & a_1 & 0 & a_2 \\ -a_2 & b_2 & -a_1 & b_2 & a_1 & b_1 & a_2 & b_1 \end{array} \right]$$

$$a_1 = \frac{1}{4b} \left(1 + \frac{r}{a}\right) \quad , \quad a_2 = \frac{1}{4b} \left(1 - \frac{r}{a}\right)$$

$$b_1 = \frac{1}{4a} \left(1 + \frac{1}{b}\right) \quad , \quad b_2 = \frac{1}{4a} \left(1 - \frac{1}{b}\right)$$

$$\mathbf{K}^{(e)} = \left[\begin{array}{cccccccc} 2a_{11} & a_{36} & c_{41} & b_{36} & -a_{14} & -a_{36} & c_{14} & b_{63} \\ & 2a_{35} & b_{63} & c_{25} & -a_{36} & -a_{25} & b_{36} & c_{52} \\ & & 2a_{14} & -a_{36} & c_{14} & b_{36} & -a_{14} & a_{63} \\ & & & 2a_{25} & b_{63} & c_{52} & a_{36} & -a_{52} \\ & & & & 2a_{14} & a_{36} & c_{41} & b_{63} \\ \text{Symmetric} & & & & & 2a_{25} & b_{63} & c_{25} \\ & & & & & & 2a_{11} & -b_{36} \\ & & & & & & & 2a_{25} \end{array} \right]$$

$$a_{ij} = a_i + a_j \quad , \quad b_{ij} = a_i - a_j \quad , \quad c_{ij} = a_i - 2a_j$$

$$a_1 = \frac{td_{11}}{6a} \quad , \quad a_2 = \frac{tad_{22}}{6b} \quad , \quad a_3 = \frac{td_{12}}{4} \quad , \quad a_4 = \frac{tad_{33}}{6b} \quad , \quad a_5 = \frac{tbd_{33}}{6a} \quad , \quad a_6 = \frac{td_{33}}{4}$$

Box 9.1 Strain and stiffness matrices for a 4-noded solid rectangular element of dimensions $2a \times 2b$

simplicity of the element geometry allows an explicit integration of all terms. The resulting expression for $\mathbf{K}^{(e)}$ is also shown in Figure 9.9.

In the same way, the equivalent nodal force vectors for the element are obtained by Eqs.(9.54)-(9.57) using the new expressions for \mathbf{N}_i and \mathbf{B}_i . It is interesting that the nodal contributions of a uniformly distributed load over the element (see Eq.(9.65)) are

$$\mathbf{f}_{b_i}^{(e)} = \frac{(tA)^{(e)}}{4} \left\{ \begin{array}{c} b_x \\ b_y \end{array} \right\} \quad (9.86)$$

i.e. the total force is distributed in equal parts between the four nodes, like for the 3-noded triangle.

Similarly, a uniformly distributed traction acting over a side is distributed in equal parts between the two side nodes.

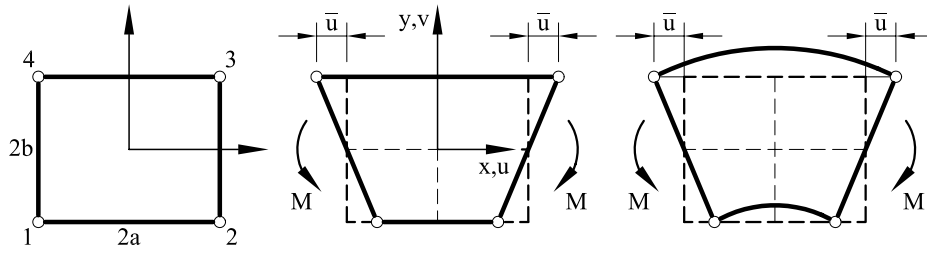


Fig. 9.10: 4-noded solid rectangle subjected to pure bending, a) Initial geometry, b) Element distortion, c) Correct deformation of a beam segment in pure bending

9.4.2 Some remarks on the behaviour of the 4-noded solid rectangle

Both the 3-noded solid triangle and the 4-noded solid rectangle perform excellently in problems where traction (or compression) is important. Conversely, the accuracy of both elements strongly deteriorates in situations where bending movements are involved, and very fine meshes are needed to obtain accurate solutions in these cases (see Section 4.7).

The fact that the 4-noded solid rectangle cannot be used to model bending dominated fields has a very instructive explanation. Let us consider the behaviour of an isolated element subjected to pure bending (Figure 9.10). The exact solution from beam theory is [T6]

$$\begin{aligned} u(r, s) &= \frac{M}{EI} r s \\ v(r, s) &= \frac{M a^2}{2EI} \left(1 - \frac{r^2}{a^2}\right) + \frac{M b^2}{2EI} \left(1 - \frac{s^2}{b^2}\right) \end{aligned} \quad (9.87)$$

Since the element sides are straight, the 4-noded rectangle can only represent the following bending mode (Figure 9.10)

$$u = \bar{u} r s \quad ; \quad v = 0 \quad (9.88)$$

It is obvious from the above that the element cannot correctly reproduce the quadratic distribution of vertical displacements for the pure bending case. This leads to excessive stiffness, which is a natural consequence of the inability of the element sides to be curved.

Additionally it is deduced from Eq.(9.87) that

$$\gamma_{xy} = \frac{\partial u}{\partial y} + \frac{\partial v}{\partial x} = 0$$

i.e. the “exact” shear strain vanishes and only normal strains (and stresses) exist.

The shear strain field for the element is obtained from Eq.(9.88) as

$$\gamma_{xy} = \bar{u} r \quad (9.89)$$

i.e. the element has an “excess” of shear strain. This introduces an undesirable additional stiffness which contributes to the poor ability of the element to reproduce bending modes. Similar results are obtained for bending moments acting on the horizontal sides simply by changing the coordinate r for s in Eq.(9.89).

The deficiencies of the 4-noded solid rectangle also show for more irregular quadrilateral shapes. These drawbacks are usually overcome in practice by using very fine meshes. Other alternatives are possible, however, and some are presented in the following sections.

Reduced integration of the shear stiffness terms

Eq.(9.89) clearly shows that the shear strain is zero at the element center only. Therefore, the excess of shear strain can be eliminated by sampling the shear strain at the element center ($r = s = 0$). This is simply achieved by using a reduced one point Gauss quadrature for the shear terms in the stiffness matrix. For this purpose the element stiffness matrix is split into two parts as

$$\mathbf{K}^{(e)} = \mathbf{K}_a^{(e)} + \mathbf{K}_s^{(e)} \quad (9.90)$$

where $\mathbf{K}_a^{(e)}$ and $\mathbf{K}_s^{(e)}$ include the “axial” and “shear” contributions, respectively given by

$$\mathbf{K}_{a_{ij}}^{(e)} = \iint_{A^{(e)}} \mathbf{B}_{a_i}^T \mathbf{D}_a \mathbf{B}_{a_j} t dA \quad ; \quad \mathbf{K}_{s_{ij}}^{(e)} = \iint_{A^{(e)}} \mathbf{B}_{s_i}^T \mathbf{D}_t \mathbf{B}_{s_j} t dA \quad (9.91)$$

with

$$\mathbf{B}_{a_i} = \begin{bmatrix} \frac{\partial N_i}{\partial x} & 0 \\ 0 & \frac{\partial N_i}{\partial y} \end{bmatrix} \quad ; \quad \mathbf{B}_{s_i} = \begin{bmatrix} \frac{\partial N_i}{\partial y} & \frac{\partial N_i}{\partial x} \end{bmatrix} \quad (9.92)$$

$$\mathbf{D}_a = \begin{bmatrix} d_{11} & d_{12} \\ d_{12} & d_{22} \end{bmatrix} \quad ; \quad \mathbf{D}_s = [d_{33}]$$

Matrix $\mathbf{K}_a^{(e)}$ is integrated exactly, either analytically or via a 2×2 Gauss quadrature, whereas a single integration point is used for $\mathbf{K}_s^{(e)}$. This “selected integration” technique also improves the behaviour of 4-noded quadrilaterals of arbitrary shape.

The reduced integration of $\mathbf{K}_s^{(e)}$ can also be interpreted as a simple procedure to mitigate the excessive influence of the shear terms in the element stiffness matrix. A disadvantage of reduced integration is that it produces a quadrilateral element that is not geometric-invariant (Section 3.10.4), although it passes the patch test and, therefore, it converges to the exact solution [3.3, Cook]. In Chapter 7 we will study the application of reduced integration to alleviate the influence of the transverse shear stiffness in Timoshenko beam elements. However, reduced integration of the stiffness matrix terms should always be looked upon with extreme caution, as they can lead to internal

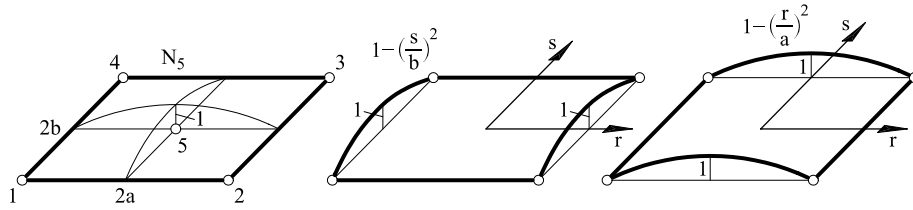


Fig. 9.11: Four node rectangle, a) Addition of a central node, b) Shape functions for the incompatible modes

mechanisms and to the violation of the patch test in some cases. Reduced integration procedures will be further considered in Chapters 9-12 when dealing with plates and shells.

Addition of internal modes

A method to enhance the flexibility of the 4-noded rectangle is to add to the original interpolation internal displacement modes which vanish at the element boundaries. The simplest mode is a “bubble” function associated with an extra central node (Figure 9.11a). The displacement field is expressed as

$$u = \sum_{i=1}^5 N_i u_i \quad ; \quad v = \sum_{i=1}^5 N_i v_i \quad (9.93)$$

where N_1, N_2, N_3, N_4 are the linear functions of (9.80) and

$$N_5 = \left[1 - \left(\frac{r}{a}\right)^2\right] \left[1 - \left(\frac{s}{b}\right)^2\right] \quad (9.94)$$

The internal d.o.f u_5 and v_5 (also called hierarchical d.o.f [C23]) can be eliminated after the element stiffness matrix is obtained. Note that u_5 and v_5 are not absolute displacements and they represent the difference between the total displacements of the central node and the bilinear field defined by the four corner displacements. For instance, the horizontal displacement of the central node is given by

$$u_5 = u(0,0) = \left(\sum_{i=1}^4 N_i u_i \right)_{0,0} + u_5 \quad (9.95)$$

The behaviour of the modified 4-noded solid element can be improved by using a reduced single point quadrature for the shear terms as described in the previous section.

Addition of incompatible modes

The 4-noded rectangle can also be improved by adding to the original displacement field the displacement modes $1 - \left(\frac{r}{a}\right)^2$ and $1 - \left(\frac{s}{b}\right)^2$ which are needed

to reproduce the exact solution (9.87) (Figure 9.11b). The new displacement field is

$$\begin{aligned} u &= \sum_{i=1}^4 N_i u_i + \left[1 - \left(\frac{r}{a}\right)^2\right] u_5 + \left[1 - \left(\frac{s}{b}\right)^2\right] u_6 \\ v &= \sum_{i=1}^4 N_i v_i + \left[1 - \left(\frac{r}{a}\right)^2\right] v_5 + \left[1 - \left(\frac{s}{b}\right)^2\right] v_6 \end{aligned} \quad (9.96)$$

The additional generalized d.o.f. u_5, v_5, u_6, v_6 (also called “nodells” d.o.f.) are internal to each element and can be eliminated by static condensation. However, the displacements along the interelemental boundaries are discontinuous and the element is incompatible. Incompatible 4-noded quadrilaterals formulated in this way fail to pass the patch test under constant stress (or constant strain) states unless they are rectangular.

Fortunately, the element satisfies the patch test for arbitrary quadrilateral shapes if the shear stiffness terms are evaluated using a reduced single point Gauss quadrature, whereas the rest of the stiffness terms can be exactly integrated [C15,T3]. The resulting element is geometrically invariant and does not have spurious mechanisms. Box 9.2 shows the stiffness matrix for an homogeneous and isotropic element with reduced integration after eliminating the internal incompatible d.o.f. by static condensation [C15], [F11].

The incompatible modes technique can also be successfully applied to 4-noded quadrilaterals of arbitrary shape. More information can be found in [C15] and [Z6].

Use of an assumed strain field

Another procedure to enhance the performance of the 4-noded quadrilateral is to impose over the element an assumed strain field compatible with the condition $\gamma_{xy} = 0$ for the pure bending case.

Dvorkin and Vassolo [D13] have proposed the following assumed strain field

$$\varepsilon_x = \alpha_1 + \alpha_2 x + \alpha_3 y ; \quad \varepsilon_y = \alpha_4 + \alpha_5 x + \alpha_6 y ; \quad \gamma_{xy} = \alpha_7 \quad (9.97)$$

The α_i parameters are expressed in terms of the nodal displacements by sampling the assumed strains at a number of element points and equaling their values with those given by the strains deduced from the original displacement field. This leads to a substitute strain matrix from which the element stiffness matrix can be directly obtained. More information on this element can be found in [D13].

9.5 PERFORMANCE OF THE 3-NODED SOLID TRIANGLE AND THE 4-NODED SOLID RECTANGLE

The 3-noded triangle and the 4-noded rectangle perform reasonably well under pure tension or compression dominated situations. In general the 4-noded

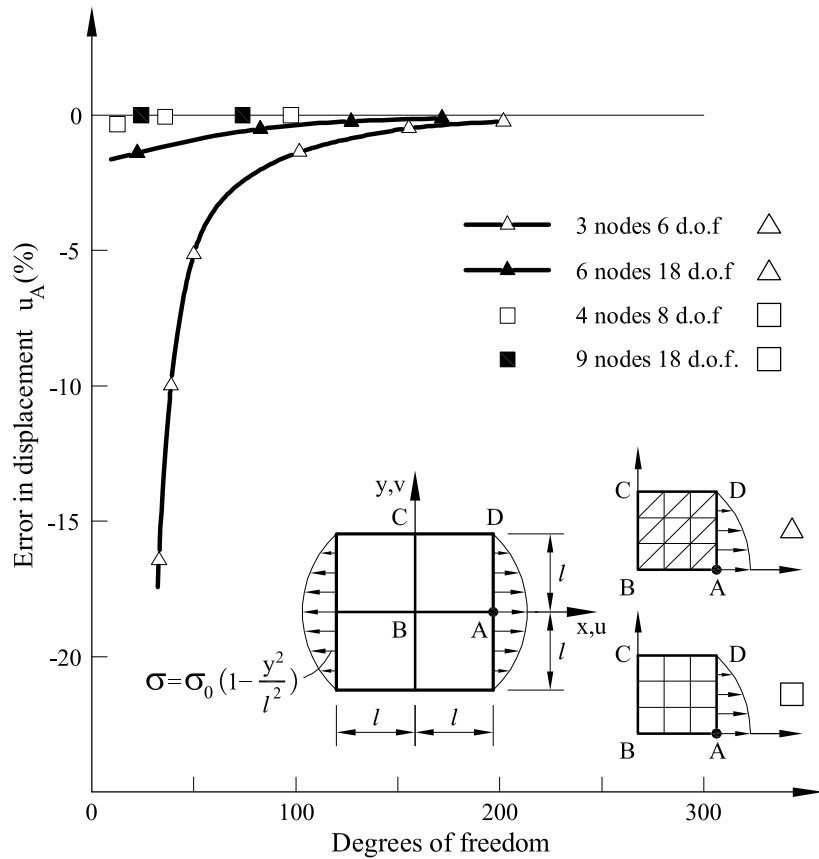


Fig. 9.12: Square plate under parabolic traction. Analysis with 3- and 6-noded triangles and 4 and 9-noded rectangles

mation for the displacement field. This also allows curved sided elements to be derived using an isoparametric formulation as described in the next chapter.

9.6 GENERAL PERFORMANCE OF TRIANGULAR AND RECTANGULAR ELEMENTS

Figures 9.12 and 9.13 show two examples which lead us to draw some interesting conclusions on the behaviour of rectangular and triangular elements. The first example is the analysis of a square plate under a parabolic traction acting symmetrically on two opposite sides. Different meshes of 3 and 6-noded triangles and 4 and 9-noded rectangles are used for the analysis. The numerical results for the horizontal displacement of the central point on the loaded side show that the 3-noded triangle is the less accurate of all elements studied. Nevertheless 1% error with respect to the “exact” analytical solution is obtained using a fine mesh (Figure 9.12).

The accuracy increases notably for the same number of d.o.f. when 6-noded triangles are used and, even more, when either the 4- or the 8-noded

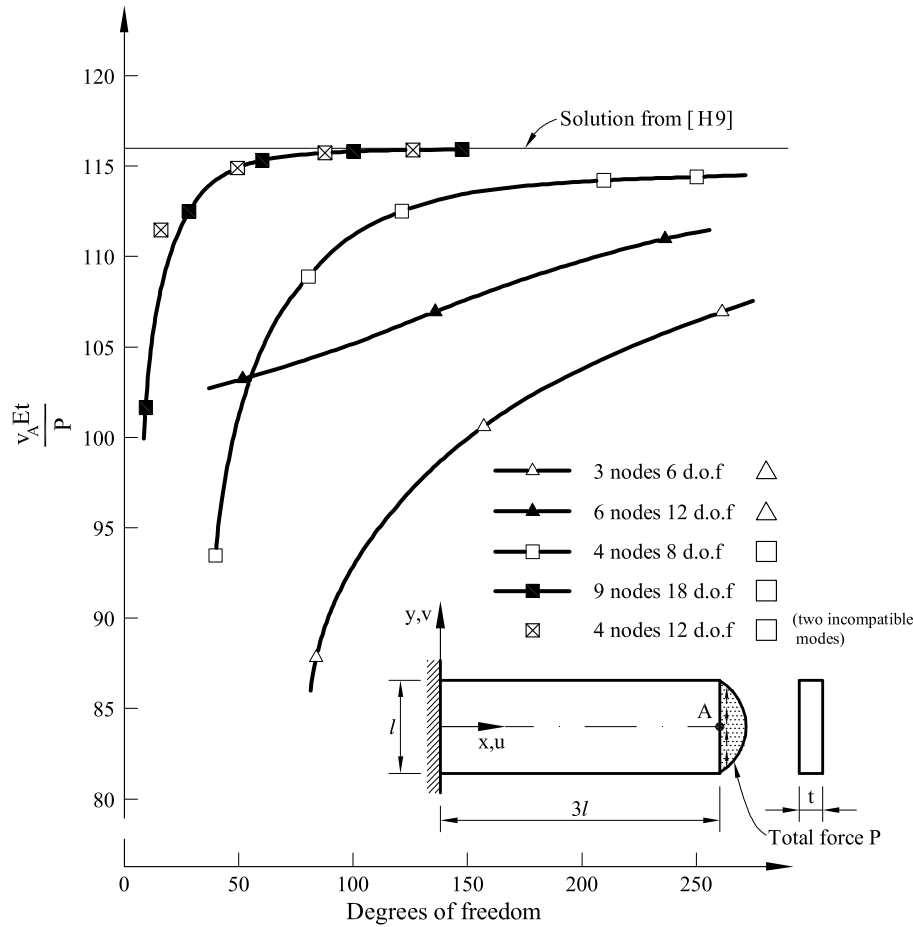


Fig. 9.13: Cantilever deep beam under parabolic edge load ($\nu = 0.2$). Analysis with 3- and 6-noded triangles, 4- and 9-noded rectangles and the 4-noded rectangle with two incompatible modes

rectangles are used, as shown in Figure 9.12 [G3], [Y1]. Similarly good results are obtained with the 8-noded rectangle.

The second example is a cantilever deep beam under a parabolic edge load (Figure 9.13). The analysis is performed using the same elements as in the previous example and, in addition, the 4-noded rectangle is enhanced with two incompatible modes studied in Section 9.4.2. Results plotted in Figure 9.13 show clearly the poor accuracy of the 3-noded triangle for bending dominated problems. The solution improves slightly for the quadratic triangular element. The 4-noded rectangle has an over stiff behaviour, as expected from its inability to reproduce pure bending situations. The solution improves however when finer meshes are used. Note the excellent performance of the incompatible 4-noded rectangle and also of the 9-noded Lagrange rectangle. Similar good results are obtained using the 8-noded quadratic Serendipity rectangle.

These results can be generalized to other situations. Typically, rectangles are more accurate than triangles for the same number of degrees of freedom. However, triangular elements are more versatile due to their better ability to

model complex geometries with unstructured meshes using automatic mesh generators.

As a rule, low order elements are simpler to use, although finer meshes are needed in zones where high stress gradients exist. Higher order elements are more competitive in these regions.

9.7 CONCLUDING REMARKS

This chapter has presented the basic concepts for the analysis of 2D solids with the FEM. The steps followed in the formulation of the kinematic variables, the strain and stress fields, the equilibrium expression via the PVW and the discretization process are completely general and will repeatedly appear when considering the finite element analysis of any other structure. The study of this chapter is therefore essential as a general introduction to the analysis of continuous structures with the FEM.

The procedure for deriving the element stiffness matrix and the equivalent nodal force vector from the PVW has been detailed. The expressions of the different matrices and vectors have general applicability to any element type. The particular form of these matrices for the 3-noded linear triangle and the 4-noded rectangle has been given. The linear triangle has limited accuracy for coarse meshes although its simplicity and versatility make it probably the most popular element for practical analysis of 2D solids with arbitrary geometry. The basic 4-noded rectangle has some limitations when it comes to capturing pure bending modes. These deficiencies can be overcome by “ad hoc” procedures such as reduced integration, the addition of internal nodes and the use of an assumed strain field.

The derivation of higher order triangular and quadrilateral elements of arbitrary shape follows the concept studied in previous chapters for the Poisson equation. The basic ingredients are: a systematic procedure to obtain the shape functions, the use of an isoparametric formulation and numerical integration. These topics will be studied in the course on computational structural mechanics.

REFERENCIAS

- A1 ABAQUS, Versión 4.8, Users Manual, Hibbit, Karlsson and Sorensen Inc., 1989.
- A2 Abel, J.F. y Desai, C.S., “Comparison of finite elements for plate bending”, *Journal of Structural Divison*, ASCE, Vol. **98**, ST9, pp. 2143–48, 1972.
- A3 ADINA versión 5.0 Users Manual. Adina R & D, Massachusetts, USA, Noviembre 1989.
- A4 Adini, A. y Clough, R.W., “Analysis of plate bending by the finite element method”, Nat. Sci. Found, G7337, 1961,
- A5 Ahmad, S., Irons, B.M. y Zienkiewicz, O.C., “Curved thick shell and membrane elements with particular reference to axisymmetric problems”, *Proc. 2nd Conf. Matrix Methods in structural Mech*, Air Force Inst. of Technol., Wright–Patterson A.F. Base, Ohio, 1968.
- A6 Ahmad, S., “*Curved finite elements in the analysis of solid shell and plate structures*”, Ph.D. Thesis, Univ. of Wales, Swansea, 1969,
- A7 Allman, D.L., “A compatible triangular element including vertex rotations for plane elasticity analysis”, *RAE Rep. TR820826*, Farnborough, Hants., 1982.
- A8 Alwar, R.S. y Ramachandran, K.N., “Theoretical and photoelastic analysis of thick slabs subjected to highly localised loads”, *Building Science*, Vol. **7**, pp. 159–66, 1972.
- A9 ANSYS, Users Manual Revision 4.4, Swanson Analysis Systems Inc. 1989.
- A10 Argyris, J.H. y Kelsey, S. *Energy theorems and structural analysis*, Butterworth, 1960.
- A11 Argyris, J.H., “Matrix displacement analysis of anisotropic shells by triangular elements”, *J. Roy. Aero. Soc.*, Vol. **69**, pp. 801–5, 1965.
- A12 Argyris, J.H., Fried, I. y Scharpf, D.W., “The TUBA family of plate elements for the matrix displacement method”, *Aeronautical Journal of the Royal Aeron. Society*, Vol. **72**, pp. 701–9, 1968.
- A13 Arnold, D.N. y Falk, S.N., “An uniformly accurate finite element method for the Mindlin-Reissner plate”, Preprint 307, Inst. for Mathematics and its Applicat., Univ. of Minnesota, Abril, 1987.
- A14 Arnold, D.N. y Falk, R.S., “Edge effects in the Reissner-Mindlin plate theory”, *Proc. Symposium an Analytical and Computational Models for Shells*, ASME, Winter Annual Meeting, San Francisco, California, Diciembre, 1990.
- A15 Arnold, D.N. y Falk, R.S., “The boundary layer for the Reissner-Mindlin plate”

a publicarse en *SIAM, J. Math.*, 1991.

- A16 Ashwell, D.G., Sabir, A.B. y Roberts, T.M., “Further studies in the application of curved finite elements to circular arches”, *Int. Journ. Mech. Science*, Vol. **13**, 6, pp. 507–17, 1971.
- A17 Ashwell, D.G., “Strain elements with applications to arches, rings and cylindrical shells”, en *Finite elements for thin shells and curved members*, Eds. D.G. Ashwell y R.H. Gallagher, John Wiley, pp. 91–111, 1976.
- A18 Ashwell, D.G. y Gallagher, R.H., (eds.), *Finite element method for thin shells and curved members*, J. Wiley, 1976.
- A19 Atamaz-Sibai, W. y Hinton, E., “Adaptive mesh refinement with the Morley plate element”, *Proc. of NUMETA 90 Conference*, Swansea, Enero 1990, Vol. **2**, pp. 1049–57, Elsevier Appl. Science, London, 1990.
- A20 Atamaz-Sibai, W., Hinton, E. y Selman, A., “Adaptive mesh refinement with the Mindlin-Reissner elements”, *Proc. of 2nd Int. Conf. an Computer Aided Analysis and Design of Concrete Structures.*, Zell-an-see, Austria, Abril 1990, Pineridge Press, 1990.
- A21 Ayad, R., Batoz, J.L., Dhatt, G. y Katili, I., “A study of recent triangular elements for thin and thick plates”. en *European Conf. on New Advances in Computational Structural Mechanics*, . P Lavedeze and O.C. Zienkiewicz (Eds.), pp. 471–9, Giens, Abril, 1991.
- B1 Baldwin, J.T., Razzaque, A. y Irons, B.M., “Shape functions subroutine for an isoparametric thin plate element”, *Int. J. Num. Meth. Engng.*, Vol. **7**, pp. 431, 1973.
- B2 Bares, R., *Tablas para el cálculo de placas y vigas pared*, Ed. Gustavo Gili, Barcelona, 1964.
- B3 Bathe, K.J., “ADINA - A finite element program for automatic dynamic incremental non linear analysis”, Rep. 82448-1, Dept. Mech Engng., MIT, 1978.
- B4 Bathe, K.J., *Finite element procedures in engineering analysis*, Prentice Hall, Inc., 1982.
- B5 Bathe, K.J. y Dvorkin, E.N., “ A four node plate bending element based on Mindlin/Reissner plate theory and mixed interpolation”, *Int. J. Numer. Meth. Eng.*, Vol. **21**, pp. 367–383, 1985.
- B6 Bathe, K.J. y Dvorkin, E.N., “A formulation of general shell elements. The use of mixed interpolation of tensorial components, *Int. J. Meth. Engng.* Vol. **22**, pp. 697–722, 1986.
- B7 Bathe, K.J., Bucalem, M.L. and Brezzi, F., “Displacement and stress convergence of our MITC plate bending elements”, *Eng. Comput.*, Vol. **7**,

4, pp. 291–303, 1990.

- B8 Batoz, J.L., Bathe, K.J. y Ho, L.W., “A study of three node triangular plate bending elements”, *Int. J. Num. Meth. Eng.*, Vol. **15**, pp. 1771–812, 1980.
- B9 Batoz, J.L., “An explicit formulation for an efficient triangular plate bending element”, *Int. J. Num. Meth. Engng.*, Vol. **18**, pp. 1077–89, 1982.
- B10 Batoz, J.L. y Ben Tahor, M., “Evaluation of a new quadrilateral thin plate bending element”, *Int. J. Num. Meth. Engng.*, Vol. **18**, pp. 1655–77. 1982.
- B11 Batoz, J.L., Lardeur, P.A. “A discrete shear triangular nine dof element for the analysis of thick to very thin plates”, *Int. J. Num. Meth. Engng.*, Vol. **28**, pp. 5, 1989.
- B12 Batoz, J.L. y Dhatt, G., “ A state of the art on the discrete Kirchhoff plate bending elements”, en *Calcul des Structures et Intelligence Artificielle*, J.M. Fonet, P. Ladeveze y R. Ohayon (Eds.), Ed. Pluralis, 1988.
- B13 Batoz, J.L. y Dhatt, G., *Modelisation des structures par éléments finis*, Vol. **1: Solides elastiques, Vol. **2: Poutres et plaques**, Hermes, Paris, 1990.**
- B14 Batoz, J.L. y Katili, I., “A new reliable and efficient discrete shear triangular plate bending element with incompatible modes”, Public. Interna, Univ. de Tecnología de Compiegne, 1991
- B15 Bazeley, G.P., Cheung, Y.K., Irons, B.M. y Zienkiewicz, O.C., “Triangular elements bending-conforming and non conforming solution”, *Proc. Conf. Matrix Meth in Struct. Mech.*, Air Force Inst. of Tech., Wright Patterson A.F. Base, Ohio, 1965.
- B16 Bell, K., “ A refined triangular plate bending finite element”, *Int. J. Num. Meth. Engng.*, Vol. **1**, pp. 101-22. 1969.
- B17 Belytschko T., Tsay C.S. y Liu W.K., “A stabilization matrix for the bi-linear Mindlin plate element”, *Comp. Methods Appl. Mech. Eng.*, Vol. **29**, pp. 313-327, 1981.
- B18 Belytschko, T. y Tsay, C.S., “A stabilization procedure for the quadrilateral plate element with one point quadrature”, *Int. J. Num. Meth. Engng.*, Vol. **19**, pp. 405–19, 1983.
- B19 Belytschko, T., Stolarski, H. y Carpenter, N., “A C_0 Triangular plate element with one point quadrature”, *Int. J. Num. Meth, Engng.*, Vol. **20**, pp. 787–802, 1984.
- B20 Belytschko, T., Liu, W.H., Shou-Jen Ong, J. y Lam, D., “Implementation and application of a 9–node Lagrange shell element with spurious mode control”, *Comp. and Struct.*, Vol. **20**, pp. 1–3, 121–8, 1985
- B21 Bergan, P.G. y Felippa, C.A., “A triangular membrane element with rotational degrees of freedom”, *Comp. Meth. Appl. Mech. Engng.*.

- B22 Blanco, E., *Estudio numérico y experimental de la influencia de distintos parámetros en la respuesta de tableros oblicuos de puentes de sección transversal losa*, Tesis Doctoral, E.T.S. de Ingenieros de Caminos, Univ. Politécnica de Catalunya, 1988.
- B23 Bogner, F.K., Fox, R.L. y Schmit, L.A., “The generation of interelement compatible stiffness and mass matrices by the use of interpolation formulae”, *Proc. Conf. Matrix Methods in Struct. Mech.*, Air Force Inst. of Tech., Wright Patterson A. F. Base, Ohio, 1965.
- B24 Bogner, F.K., Fox, R.L. y Schmit, L.A., “A cylindrical shell discrete element”, *AIAA Journal*, Vol. **5**, 4, pp. 745–50, 1967.
- B25 Bonet, J. y Peraire, J., “An alternate digital tree algorithm for geometric searching and intersection problems”, *Int. J. Num. Meth, Engng.*, Vol. **31**, pp. 1–17, 1991.
- B26 Brezzi, F., Fortin, M. y Stenberg, R., “Error analysis of mixed interpolated elements for Reissner-Mindlin plates”, *Mathematical Models and Methods in Appl. Sciences*, Vol. **1**, 2 pp. 125–51, 1991.
- B27 Budiansky, B. y Sanders, J.L. Jr., “On the best first order linear shell theory”, *Progress in Applied Mech.*, MacMillan, New York, 1963.
- B28 Bugada, G. *Utilización de técnicas de estimación de error y generación automática de mallas en procesos de optimización estructural*, Tesis Doctoral, E.T.S. de Ingenieros de Caminos Canales y Puertos de Barcelona, Universidad Politécnica de Cataluña, 1990.
- B29 Bugada, G., Oliver, J. y Oñate, E., “Utilización de técnicas de control de errores y generación automática de mallas en la optimización estructural”, *I Congreso de Métodos Numéricos en Ingeniería*, Las Palmas de Gran Canaria, Junio, 1990, G. Winter y M. Galante, (Eds.), SEMNI, Barcelona, 1990.
- B30 Bugada, G., Oliver, J., “Automatic adaptive remeshing for structural shape optimization”, en *European Conf. on New Advances in Computational Structural Mechanics*, P. Ladeveze y O.C. Zienkiewicz (Eds.) pp. 25–33, Giens, Abril, 1991.
- B31 Bugada, G., ‘FLAVIA. Programa para visualización gráfica en 2 y 3 dimensiones’, Publicación Centro Internacional de Métodos Numéricos en Ingeniería, Barcelona, 1992.
- C1 Cantin, G. y Clough, R.W., “A curved cylindrical shell finite element”, *AIAA Journal*, Vol. **6**, pp. 1057–62, 1968.
- C2 Cantin, G., Loubignac, G. y Touzot, G., “An iterative algorithm to build continous stress and displacement solutions”, *Int. J. Num. Meth. Eng.*, Vol. **12**, pp. 1493–1506, 1978.
- C3 Carpenter, N., Belytschko, T. y Stolarski, H., “Locking and shear scaling factors

- in C_0 bending elements”, *Comput. and Struct.*, Vol. **22**, pp. 39–52, 1986.
- C4 Carpenter, N., Stolarski, H. y Belytschko, T., “Improvements in 3 node triangular shell elements”, *Int. J. Num. Meth. Engng.*, Vol. **23**, pp. 1643–67, 1986.
- C5 Casteleiro, M., Oñate, E., Huerta, A., Roig, J. y Alonso, E., “Three dimensional analysis of no tension materials”, *4th. Int. Conf. on Rock Mech.*, Melbourne, Australia, 1983.
- C6 Cervera, M., Oliver, Herrero, E. y Oñate E., “A computational model for progressive cracking in large dams due to swelling of concrete”, *Int. Journal of Fracture*, Vol. **35**, n^o1,2,3, pp 573–85, 1990.
- C7 Cervera, M., Oliver, J. y Galindo, M., “Simulación numérica de patologías en presas de hormigón”, *Monografía N^o 4*, Centro Internacional de Métodos Numéricos en Ingeniería, Barcelona, 1991.
- C8 Clough, R.W., “The finite element method in plane stress analysis”, *Proc. 2nd A.S.C.E. Conf. in Electronic Computation*, Pittsburgh, Pa., Sept. 1960.
- C9 Clough, R.W. y Tocher, J.L., “Finite element stiffness matrices for analysis of plates in bending”, *Proc. Conf. Matrix Meth. in Struct. Mech.*, AFIT, Wright-Patterson, Air Force Base, Ohio, pp. 515-45. 1965.
- C10 Clough, R.W. y Rashid, Y., “Finite element analysis of axisymmetric solids”, *Journal of Engng. Mechanics Division*, ASCE, Vol. **91**, EMI, pp. 71–85, 1965.
- C11 Clough, R.W. y Felippa, C.A., “A refined quadrilateral element for analysis of plate bending”, *Proc. 2d Conf. Mat. Meth. Struct. Mech.*, AFIT, Wright-Patterson, Air Force Base, Ohio, pp. 399–440, 1968.
- C12 Clough, R.W., “Comparison of three dimensional finite elements”, *Proceedings Symposium on Applications of Finite Element Methods in Civil Engineering*, Vanderbilt Univ., Nashville, Tenn., (publicado por ASCE), pp. 1–26, 1969.
- C13 Clough, R.W. y Wilson, E.L., “Dynamic finite element analysis of arbitrary thin shells”, *Comp. and Struct.*, Vol. **1**, pp. 35, 1971.
- C14 Connor, J. y Brebbia, C., “A stiffness matrix for a shallow rectangular shell element”, *Journal of Engng. Mech. Div.*, ASCE, Vol. **93**, pp. 43–65, 1967.
- C15 Cook, R.D., Malkus, D.S. y Plesha, M.E., , *Concepts and application of finite element analysis*, 4^a ed., John Wiley and Sons, 1989.
- C16 Courant, R., “Variational methods for the solution of problems of equilibrium and vibration”, *Bull. Am. Math. Soc.*, Vol. **49**, pp. 1–23, 1943.
- C17 Cowper, G.R., Kosko, E., Lindberg, G.M. y Olson, D.M., “A high precision triangular plate bending element”, *Report LR-514, National Aeronautical Establishment*, National Research Council of Canada, Ottawa, 1968.

- C18 Cowper, G.R., Lindberg, G.M. y Olsen, M.D., “A shallow finite element of triangular shape”, *Int. J. Solids and Struct.*, Vol. **6**, 8, pp. 1133–56, 1970.
- C19 Cowper, G.R., “Gaussian quadrature formulae for triangles”, *Int. J. Num. Meth. Engng.*, Vol. **7**, pp. 405–8, 1973.
- C20 Crisfield, M.A., y Puthli, R.S., “Approximations in the non linear analysis of thin plate structures”, en *Finite elements in non linear mechanics*, (Ed. P. Bergan *et al.*), Vol. **1**, Tapir, Trondheim, Noruega, pp. 373–92, 1978.
- C21 Crisfield, M.A., “A four-noded thin-plate bending element using shear constrains. A modified version of Lyon’s element”, *Comp. Meth. Appl. Mech. Eng.*, Vol. **38**, pp. 93–120, 1983
- C22 Crisfield, M.A., “A quadratic Mindlin element using shear constraints”, *Comput and Struct.*, Vol. **18**, pp. 833–52, 1984.
- C23 Crisfield, M.A., *Finite element and solution procedures for structural analysis, Vol. I: Linear analysis*, Pineridge Press, 1986.
- CH1 Chan, A.S.L. y Firmin, A., “The analysis of cooling towers by the matrix finite element method”, *Aeronaut. J.*, Vol. **74**, pp. 826–35, 1970.
- CH2 Cheung, Y.K., King. I.P. y Zienkiewicz, O.C., “Slab bridges with arbitrary shape and support condition - A general method of analysis based or finite elements”, *Proc. Inst. Civil Engng.*, Vol. **40**, pp. 9–36, 1968.
- CH3 Cheung, Y.K., “Finite strip analysis of elastic slabs”, *Proc. Am. Soc. Civil Eng.*, Vol. **94**, pp. 1365–78, 1968.
- CH4 Cheung, Y.K., “The finite strip method in the analysis of elastic plates with two opposite simple supported ends”, *Proc. Inst. Civil Engng*, Vol. **40**, pp. 1–7, 1968
- CH5 Cheung, Y.K., “Analysis of box girder bridges by the finite strip method”, *Am. Conc. Inst. Public.*, SP 26, pp. 357–78, 1969.
- CH6 Cheung, Y.K., “Folded plate structures by the finite strip method”, *Am. Soc. Civil Eng.*, Vol. **96**, pp. 2963–79, 1969.
- CH7 Cheung, Y.K., “The analysis of cylindrical orthotropic curved bridge decks”, *Pub. Int. Ass. Struct. Engng.*, Vol. **29**, pp. 41–52, 1969.
- CH8 Cheung, Y.K., *The finite strip method in structural analysis*, Pergamon Press, 1976.
- D1 Dawe, D.J., “Shell analysis using a simple facet element”, *J. Strain Analysis*, Vol. **7**, pp. 266–70, 1972.
- D2 Dawe, D.J., “Some higher order elements for arches and shells”, en *Finite elements for thin shells and curved members*, (Ed.) D.G. Ashwell y R.H.

- Gallagher, J. Wiley, pp. 131–53, 1976.
- D3 Dawe, D.J., “Curved finite elements for the analysis of shallow and deep arches”, *Comput. and Struct.*, Vol. **4**, pp. 559–82, 1979.
- D4 Delpak, R., *Role of the curved parametric element in linear analysis of thin rotational shells*, Ph.D Thesis, Dept. Civil Engineering and Building, The Polytechnic of Wales, 1975.
- D5 Dhatt, G., “Numerical analysis of thin shells by curved triangular elements based an discrete Kirchhoff hypothesis”, *Proc. ASCE Symp. on Applications of FEM in Civil Engng.*, Vanderbilt Univ., Nashville, Tenn., pp. 13–14, 1969.
- D6 Dhatt, G., “An efficient triangular shell element”, *AIAA J.*, Vol. **8**, pp. 2100-2, 1970.
- D7 Dhatt, G. y Venkatasubby, S., “Finite element analysis of containment vessels”, *Proc. First Conf. an Struct. Mech. in Reactor Tech.*, Vol. **5**, Paper J3/6, Berlin, 1971.
- D8 Dill, E.H., “A triangular finite element for thick plates”, *Computational Mechanics Vol. III*, S.N. Atluri *et al.* (eds.), Springer Verlag, 1988.
- D9 Donea J. y Lamain, L.G., “A modified representation of transverse shear in C_0 quadrilateral plate elements”, *Comp. Meth. Appl. Mech. Engng.*, Vol. **63**, pp. 183–207, 1987.
- D10 Dumavanet, D.A., “High degree efficient symmetrical Gaussian quadrature rules for the triangle”, *Int. J. Num. Meth. Engng.*, Vol. **21**, Vol. **7**, 1985.
- D11 Dupuis, G. y Goël, J.J., “A curved finite element for thin elastic shells,”, *Int. J. Solids and Struct.*, Vol. **6**, 11, pp. 1413–28, 1970.
- D12 Dvorkin, E.N. y Bathe, K.J., “A continuum mechanics based four node shell element for general non-linear analysis”, *Eng. Comp.*, Vol. **1**, pp. 77–88, 1984.
- D13 Dvorkin, E.N. y Vassolo, S.I. “A quadrilateral 2D finite element based on mixed interpolation of tensorial components”, *Eng. Comput.*, Vol. **6**, pp. 217–24, 1989.
- F1 Felippa, C.A. y Bergan, P.G., “A triangular plate bending element based on energy orthogonal free formulation”, *Comp. Meth. Appl. Mech. Engng.*, Vol. **61**, pp. 129–60, 1981
- F2 FEMGEM/FEMVIEW, The Finite Element Pre and Post–processor, User Manual, Femview Limited, Leicester, U.K., 1991.
- F3 Ferrers, N.M., *An elementary treatise on trilinear coordinates, the method of reciprocal polars and the theory of projections*, MacMillan , London, 1961.
- F4 Flügge, N., *Stresses in shells*, Springer-Verlag, 1962.

- F5 Fong, H.M., “Interactive graphics and commercial finite element codes”, *Mechanical Engng.*, 106(6), pp. 18–27, 1989.
- F6 Fraeijs de Veubeke, B., “Bending and stretching of plates”, *Proc. Conf. Matrix Meth. in Structural Mech.*, Air Force Inst. of Tech., Wright Patterson, Air Force Base, Ohio, 1965.
- F7 Fraeijs de Veubeke, B., “A conforming finite element for plate bending”, *Int. J. Solids and Struct.*, Vol. 4, pp. 95–108, 1968.
- F8 Fried, I. y Yang, S.K., “Triangular nine degrees of freedom C_0 plate bending element of quadratic accuracy”, *Quart. Appl. Math.*, Vol. 31, pp. 303–312, 1973.
- F9 Fried, I., “Residual balancing technique in the generation of plate bending finite element”, *Comput. and Struct.*, Vol. 4, pp. 771–78, 1974.
- F10 Fried, I., “Shear in C_0 and C_1 plate bending elements”, *Int. J. Solids and Struct.*, Vol. 9, pp. 449–60, 1973.
- F11 Fröier, M., Nilsson, L. y Samuelsson, A., “The rectangular plane stress element by Turner, Pian y Wilson”, *Int. J. Num. Meth. Engng.*, Vol. 8, 2, pp. 433–7, 1974.
- G1 Gallagher, R.H., “The development and evaluation of matrix methods for thin shell structural analysis”, *Ph. D. Thesis*, State Univ. New York, Buffalo, 1966.
- G2 Gallagher, R.H., “Shell elements”, *World Conf. on Finite Element Methods in Structural Mech.*, E1–E35, Bournemouth, Dorset, Inglaterra, Oct., 1975.
- G3 Gallagher, R.H., *Finite Element Analysis Fundamentals*, Prentice–Hall, Englewood Cliffs, N.J., 1975.
- G4 Giannini, M. y Miles, G.A., “A curved element approximation in the analysis of axisymmetric thin shells”, *Int. J. Num. Meth. Eng.*, Vol. 2, pp. 459–70, 1970.
- G5 Gould, P.L., *Finite Element Analysis of shells of Revolutions*, Pittman Pub. Co., Marsfield, MA, 1985.
- G6 Grafton, P.E. y Strome, D.R., “Analysis of axi-symmetric shells by the direct stiffness method”, *A.I.A.A.J.*, Vol. 1, pp. 2342–7, 1963.
- H1 Harvey, J.W. y Kelsey, S., “Triangular plate elements with enforced continuity”, *A.I.A.A.J.*, Vol. 9, pp. 1026–6, 1971.
- H2 Hearmon, R.F.S., *An introduction to applied anisotropic elasticity*, Oxford Univ. Press, 1961.
- H3 Hinton, E. y Cambell, J.S., “Local and global smoothing of discontinuous element functions using a least square method”, *Int. J. Num. Meth. Eng.*, Vol. 8, pp.

461–80, 1979.

- H4 Hinton, E. y Owen, D.R.J., *Finite element programming*, Academic Press, 1979.
- H5 Hinton, E. y Owen, D.R.J., *Introduction to finite element computations*, Pineridge Press, 1980.
- H6 Hinton, E. y Huang, H.C., “A family of quadrilateral Mindlin plate element with substitute shear strain fields”, *Comp. and Struct.*, Vol. **23**, pp. 409–431, 1986.
- H7 Hinton, E. y Owen, D.R.J., *Finite element software for plates and shells*, Pineridge Press, 1988.
- H8 Hinton, E., Özakça, M. y Rao, N.V.R., “Adaptive analysis of thin shells using facet elements”, Internal Report Civil Engng Dpt., Univ. College of Swansea, CR/950/90, Abril, 1990.
- H9 Hooley, R.F y Hibbert, P.D., “Bounding plane stress solutions by finite elements”, *Journal Struct. Division*, ASCE, Vol. **92**, ST1, pp. 39–48, 1966.
- H10 Horrigmoe, G. y Bergan, P.G., “Non linear analysis of free form shells by flat finite elements”, *Comp. Meth. Appl. Mech. Engng.*, Vol. **16**, pp. 11-35, 1979.
- H11 Hrenikoff, A., “Solution of problems in elasticity by the framework method”, *J. Appl. Mech.*, Vol. **18**, pp. 169–75, 1991.
- H12 Huang, H.C. y Hinton, E., “A nine node Lagrangian Mindlin plate element with enhanced shear interpolation”, *Engng. Comput.*, Vol. **1**, pp. 369–79, 1984.
- H13 Huang, H.C. y Hinton, E., “Lagrangean and Serendipity plate and shell elements through thick and thin”, in *Finite element methods for plate and shell structures*, T.J.R. Hughes y E. Hinton (Eds.) Pineridge Press, 1986.
- H14 Huang, H.C. y Hinton, E., “A new nine node degenerated shell element with enhanced membrane and shear interpolation”, *Int. J. Num. Meth. Eng.*, Vol. **22**, pp. 73–92, 1986.
- H15 Huang, H.C., *Static and dynamic of plates and shells*, Springer-Verlag, 1989.
- H16 Huerta, A., Casteleiro, M. y Alonso, E., “Non linear numerical analysis of earth dam constructions”, in *Numerical Methods for non Linear Problems*, C. Taylor, E. Hinton, R. Owen y E. Oñate (Eds.), Pineridge Press, 1984.
- H17 Hughes, T.J.R., Taylor, R.L. y Kanoknukulchai W. , “A simple and efficient element for plate bending”, *Int. J. Num. Meth. Eng.*, Vol. **11**, pp. 1529–43, 1977.
- H18 Hughes, T.J.R. y Cohen, M., “The Heterosis finite element for plate bending”, *Comput. and Struct.*, Vol. **9**, pp. 445–50, 1978.

- H19 Hughes, T.J.R., Taylor, R.L., y Tezduyar, T.E., “Finite elements based upon Mindlin plate theory with particular reference to the four node bilinear isoparametric element”, *J. Appl. Mech.*, Vol. **46**, pp. 587–596, 1981.
- H20 Hughes, T.J.R. y Taylor, R.L., “The linear triangular plate bending element”, *Proc. of 4th MAFELAP Conf.*, Brunel Univ., Uxbridge, 1981, (Edited by J.R. Whiteman), pp. 127–42, Academic Press, 1982.
- H21 Hughes, T.R.J., “*The finite element method. Linear Static and Dynamic analysis*”, Prentice Hall, 1987.
- I1 I-DEAS, General capabilities, P-0100, Structural Dynamics Research Corporation, Milford, Ohio, USA, 1991.
- I2 Irons, B.M., “Numerical integration applied to finite element method”, *Conf. Use of Digital Computer in Struct. Eng.*, Univ. Newcastle, 1966.
- I3 Irons, B.M., “Engineering application of numerical integration in stiffness method”, *A.I.A.A.J.*, Vol. **14**, pp. 2035–7, 1966.
- I4 Irons, B.M., “A conforming quartic triangular element for plate bending”, *Int. J. Num. Meth. Engng.*, Vol. **1**, pp. 29–46, 1969.
- I5 Irons, B.M. y Razzaque, A., “Experience with the patch test for convergence of finite element method”, *Mathematical Foundations of the Finite Element Method*, pp. 557–87, (Ed. A.R. Aziz), Academic Press, 1972.
- I6 Irons, B.M., “The semiloof shell element”, *Finite elements for thin shells and curved members*, Cap. **11**, pp. 197–222 (Eds.) D.G. Ashwell y R.H. Gallagher, J. Wiley, 1976.
- I7 Irons, B.M. y Ahmad, S., *Techniques of finite elements*, Ellis Harwood, Chichester, 1980.
- J1 Jirousek, J., “A family of variable section curved beam and thick shell or membrane-stiffening isoparametric elements”, *Int. J. Num. Meth. Eng.*, Vol. **17**, pp. 171–86, 1981.
- J2 Jones, R.E. y Strome, D.R., “Direct stiffness method of analysis of shells of revolution using curved elements”, *A.I.A.A.J.*, Vol. **4**, pp. 1519–25, 1965.
- J3 Jones, R.E. y Strome, D.R., “A survey of analysis of shells by the displacement method”, *Proc. Conf on Matrix Methods in Struct. Mech.*, Air Force Inst. of Tech., Wright-Patterson, Air Force Base, Ohio, 1965.
- J4 Jordan, F.F., “Stresses and deformations of the thin-walled pressurized torus”, *J. Aerospace Science*, Vol. **29**, pp. 213–25, 1962.
- J5 Jordan, W.B., “The plane isoparametric structural element”, *General Electric Co., Report KAPL-M-7112*, Schenectady, New York, 1970.
- K1 Kabir, A.F. y Scordelis, A.C., “CURDI—Computer program for curved bridges

- and flexible bents”, *Internal Report, Dept. Civil Engineering, Univ. of California, Berkeley, Septiembre, 1979.*
- K2 Kantorovitch, L.V. y Krylov, V.I., *Approximate methods of higher analysis*, J. Wiley, 1958.
- K3 Klein, S., A study of the matrix displacement method as applied to shells of revolution, *Proc. Conf. on Matrix Methods in Struct. Mech.*, Air Force Inst. of Tech., Wright Patterson Air Force Base, Ohio, Oct. 1965.
- K4 Koiter, W.T., “A consistent first approximation in the general theory of thin elastic shells”, *First IUTAM Sympos.*, (Ed. W.T. Koiter), North Holland, Vol. **2**, 1960.
- K5 Kraus, H., *Thin elastic shells*, J. Wiley, 1967.
- L1 Lekhnitskii, S.G., *Theory of elasticity of an anisotropic elastic body*, Holden Day, San Francisco, 1963.
- L2 Lim, P.T.K., Kilford, J.T. y Moffatt, K.R., “Finite element analysis of curved box girder bridges”, en *Developments in Bridge Design and Constructions*, (Ed. K.C. Rockey *et al.*), Crosby Lockwood, London, pp. 264–86, 1971.
- L3 Livesley, R.K., “*Matrix methods in structural analysis*”, 2nd ed., Pergamon Press, 1975.
- L4 Loo, Y.C. y Cusens, Y.A.R., *The finite strip method in bridge engineering*, Viewpoint, 1978.
- L5 Loubignac, B., Cantin, G. and Touzot, G., “Continuous stresses formulation in finite element analysis”, *A.I.A.A. J.*, Vol. **15**, pp. 1645–49, 1977.
- L6 Lyons, L.P.R., “*A general finite element system with special reference to the analysis of cellular structures*”, Ph D. Thesis, Imp. College of Science and Technol., Londres, 1977.
- M1 Mackerle, J. y Fredriksson B., *Handbook of Finite Element Software*, Chartwell-Bratt Ltd., Bromley, U.K., 1990.
- M2 MacNeal, R.H., “A simple quadrilateral shell element”, *Comp. and Struct.*, Vol. **8**, pp. 175–83, 1978.
- M3 MacNeal, R.H., y Harder, R.L., “A proposed standard set of problems to test finite element accuracy”, *Finite Elements in Analysis and Design*, Vol. **1**, pp. 3–20, 1985.
- M4 Malkus, D.S. y Hughes, T.J.R., “Mixed finite element methods-reduced and selective integration techniques: A unification of concepts”, *Comp. Meth. Appl. Mech. Eng.*, , Vol. **15**, pp. 63–81, 1978.
- M5 Marguerre, K., “Zur thorie der Gekrummten platte grosser formanderung”, *Proc. 5th. Int. Congress Appl. Mech.*, J. Wiley, Londres, pp. 98–101, 1938.

- M6 Mc. Henry, D., “A lattice analogy for the solution of plane stress problems”, *J. Inst. Civ. Engng.*, Vol. **21**, pp. 59–82, 1943.
- M7 Melosh R.J., “A stiffness matrix for the analysis of thin plates in bending”, *Journal of Aerospace Science*, Vol. **28**, 1, pp. 34–42, 1961.
- M8 Melosh, R.J., “Basis of derivation of matrices for the direct stiffness method”, *A.I.A.A.J.*, Vol. **1**, **7**, pp. 1631–37, 1963.
- M9 Miquel, J., Botello, S., Buil, J. y Oñate, E., “La presa bóveda de Talvachia. Análisis estático y dinámico”, *Monografía n^o 6*, Centro Internacional de Métodos Numéricos en Ingeniería, Barcelona, 1991.
- M10 Mindlin, R.D., “Influence of rotatory inertia and shear in flexural motions of isotropic elastic plates”, *J. Appl. Mech.*, Vol. **18**, pp. 31–38, 1951.
- M11 Moan, T. y Soreide, T., “The analysis of stiffened plates considering non linear material and geometrical behaviour”, *World Congress on Finite Elements in Structural Mechanics*, (Ed. J. Robinson), Robinson & Assoc., Verwood, pp. 14.1–14.28, 1975.
- M12 Morley, L.S.D., “The triangular equilibrium element in the solution of plate bending problems”, *Aero Quart.*, Vol. **19**, pp. 149–69, 1968.
- M13 Morley, L.S.D., “On the constant moment plate bending element”, *J. Strain Analysis*, Vol. **6**, pp. 10–4, 1971.
- M14 Morley, L.S.D., “Finite element criteria for some shells”, *Int. J. Num. Meth. Engng.*, Vol. **20**, pp. 587–92, 1984.
- M15 Morris, A.J., “A deficiency in current finite elements for thin shell applications”, *Int. J. Solids Struct.*, Vol. **9**, pp. 331–45, 1973.
- M16 MSC/DYNA, Users Manual Demonstration Manual and Theoretical Manual. The McNeal–Schwendler Corporation, Los Angeles, 1989.
- N1 Narayanaswani, R. “Dependence of plate bending finite element deflections and eigenvalues on Poisson’s ratio”, *A.I.A.A.J.*, Vol. **12**. pp. 1420–21, 1974.
- N2 NASTRAN, “Theoretical Manual”, MacNeal, R.H. (Ed.), McNeal–Schwendler Corp., Los Angeles, 1972.
- N3 Nguyen, V.P., “Automatic mesh generation with tetraedon elements”, *Int. J. Num. Meth. Engng.*, Vol. **18**, pp. 273–89, 1982.
- N4 Noor, A., “Bibliography of books and monographs on finite element technology”, *Appl. Mech. Rev.*, Vol. **44**, 6, pp. 307–17, June, 1991.
- N5 Novozhilov, V.V., *Theory of thin shells.*, P. Noordhoff, 1959.
- N6 Nygard, M.K., *The free formulation for non linear finite elements with applications to shells*, Ph. D. Thesis, Univ. Trondheim, Norway, 1986.

- O1 Oliver, J., “Un sencillo procedimiento para evitar la singularidad de elementos de lámina plana coplanares”, Comunicación Privada, E.T.S Ing.de Caminos, Barcelona, 1982.
- O2 Oliver, J., Cervera, M., Oñate, E. y Herrero, E., “A case study of gravity dam subjected to severe internal actions: Description and numerical simulations”, Publicado en *Sixth Congress on Large Dams, Commission Internationale des Grands Barrages*, San Francisco, C.29, pp. 1387–409, 1988.
- O3 Oliver, J., “Modelado de la fisuración en estructuras de hormigón”, *Publicación de Investigación PI-3*, Centro Internacional de Métodos Numéricos de Ingeniería, Barcelona, 1990.
- O4 Oñate, E., “*Comparisons of finite strip methods for the analysis of box girder bridges*”, M. Sc. Thesis, Civil, Eng. Dpt., Univ. College of Swansea, 1976.
- O5 Oñate, E., Hinton, E. y Glover, N., “Techniques for improving the performance of isoparametric shell elements”, *Applied Numerical Modelling*, C. Brebbia y E. Alarcón (eds.), Pentech Press, 1979.
- O6 Oñate, E. y Suárez, B., “The finite strip for the analysis of plate, bridge and axisymmetric shell problems”, in *Finite element software for plate and shell analysis*, E. Hinton y D.R.J. Owen (Eds.), Pineridge Press, Swansea, 1984.
- O7 Oñate, E. y Suárez, B., “A comparison of the linear, quadratic and cubic Mindlin strip element for the analysis of thick and thin plates”, *Computers and Struct.*, Vol. **17**, pp. 427–39, 1983.
- O8 Oñate, E. y Suárez, B., “An unified approach for the analysis of bridges, plates and axisymmetric shells using the linear Mindlin strip element”, *Computer and Struct.*, Vol. **17**, 3, pp. 407–26, 1986.
- O9 Oñate, E., Oliver, J. y Bugeda, G., “Finite element analysis of the non linear response of concrete dams subjected to internal loading”, *Finite Element Methods for Non Linear Problems*, Europe–US Symposium, Trondheim, Norway, 1985, P. Bergan et al. (Eds.), Springer–Verlag, 1985.
- O10 Oñate, E., Suárez, B. y Zienkiewicz, O.C., “Una metodología para obtener elementos de placa de Reissner-Mindlin basados en campo de deformaciones de cortante impuestas”, *Actas del I Congreso sobre Métodos Numéricos en Ingeniería*, Las Palmas de Gran Canaria, Junio 1990, (Eds.) G. Winter y M. Galante, SEMNI, Barcelona, 1990.
- O11 Oñate, E., Zienkiewicz, O.C., Suárez, B. y Taylor, R.L., “A methodology for deriving shear constrained Reissner-Mindlin plate elements”, *Int. Journal Numerical Methods Eng.*, 1992.
- O12 Oñate, E. y Castro, J., “Derivation of plate elements based on assumed shear strain fields” en *Recent advances on Computational Structural mechanics*, P. Ladeveze and O.C. Zienkiewicz (Eds.), Elsevier Pub, 1991.
- O13 Oñate, E., Castro, J. y Kreiner, R., “Error estimation and mesh adaptivity

techniques for plate and shell problems”, en *The 3rd. International Conference on Quality Assurance and Standards in Finite Element Methods*, Stratford-upon-Avon, England, 10–12 September, 1991.

- O14 Oñate, E., y Castro, J., “Adaptive mesh refinement techniques for structural problems”, en *The Finite Element Method in the 1990's, A book dedicated to O.C. Zienkiewicz*, E. Oñate, J. Periaux and A. Samuelsson (Eds.) Springer-Verlag/CIMNE, Barcelona, 1991.
- O15 Oñate, E. y Castro, J., “Elementos de placa y láminas basados en campos de deformaciones impuestas”, Publicación del centro Internacional de Metodos Numéricos en Ingeniería, 1991.
- O16 Oñate, E. “Error estimation and mesh adaptivity techniques for structural and fluid flow problems”, Publicado en *Mecánica Computacional*, Vol. XII, S. Idelshon (Ed.), MECOM, Santa Fe, Argentina, 1991.
- O17 Oñate, E., Castro, J. y Bugeda, G., “Adaptive remeshing strategies for structural analysis”, A publicarse en *Int. J. Num Meth. Engng.*, 1992.
- P1 Palaninathan, R. y Chadracharan, P.S., “Curved beam element stiffness matrix formulation”, *Comp. Struct.*, Vol. **21**, pp. 663–9, 1983.
- P2 Pammaer, Z. y Szabo, L., “Stereo decomposition subroutines for three dimensional plotter programs”, *Int. J. Num. Meth. Engng.*, Vol. **17**, pp. 1571–75, 1981.
- P3 Papadopoulos, P. y Taylor, R.L., “A triangular element based on Reissner-Mindlin plate theory”, *Int. J. Num. Meth, Engng.*, Vol. **5**, pp. 1029–51, 1990.
- P4 Parisch, H., “A critical survey of the 9 noded degenerate shell element with special emphasis on thin shell application and reduced integration”, *Comp. Meth. Appl. Mech. Engng.*, Vol. **20**, pp. 323–50, 1979.
- P5 PATRAN Plus Users Manual, PDA Engineering, PATRAN Division, Costa Mesa, California, USA, 1991.
- P6 Pawsey, S.E., y Clough, R.W., “Improved numerical integration of thick shell elements”, *Int. J. Num. Meth. Engng.*, Vol. **3**, pp. 545–86, 1971.
- P7 Peiró, J. *A finite element procedure for the solution of the Euler equations on unstructured meshes*, Ph.D. Thesis, Civil Eng. Dpt., Univ. College of Swansea, U.K., 1989.
- P8 Peraire, J., Vahdati, M., Morgan, K. y Zienkiewicz, O.C., “Adaptive remeshing for compressible flow computation”, *J. Comp. Phys.*, Vol. **72**, pp 449–66, 1987.
- P9 Percy, J.H., Pian, T.M.H., Klein, S., y Navaratna, D.R., “Application of matrix displacement method to linear elastic analysis of shells of revolution”, *A.I.A.A.J.*, Vol. **3**, pp. 2138–45, 1965.

- P10 Pissanetzky, S., “Kubik: An automatic three dimensional mesh generator”, *Int. J. Num. Meth. Engng.*, Vol. **17**, pp. 255–69, 1987.
- P11 Popov, E.R., Penzien, J. y Liu, Z.A., “Finite element solution for axisymmetric shells”, *Proc. Am. Soc. Civil Eng.*, EM, pp. 119–45, 1964.
- P12 Perruchoud, M. y Frey, F., “How to modelize beams of slab–beam structures in a simple way”, Dpt. Genie Civil, Ecole Polytechnique Federale de Lausanne, Rapport Interne IREM90/3, Abril, 1990.
- P13 Pres, W.H., Flannery, B.P., Teukolsky, S.A., Vetterling, W.T., *Numerical Recipes. The art of Scientific Computing*, Cambridge Univ. Press, 1986.
- P14 Przemienieck, J.S., *Theory of matrix structural analysis*, Mc Graw Hill, New York, 1968.
- P15 Pugh, E.D.L., Hinton, E. y Zienkiewicz, O.C., “A study of quadrilateral plate bending elements with reduced integration”, *J. Appl. Mech.*, Vol. **12**, pp. 1059–1079, 1978.
- R1 Radau, *Journal of Math.*, Vol. **3**, p. 283, 1880.
- R2 Ralston, A., *Introducción al análisis numérico*, Limusa–Wiley, 1970.
- R3 Razzaque, A., *Finite Element analysis of plates and shells*, Ph.D. Thesis, Civil Eng. Dpt, Univ. of Wales, Swansea, 1972.
- R4 Reissner, E., “The effect of transverse shear deformation on the bending of elastic plates”, *J. Appl. Mech.*, Vol. **12** pp. 69–76, 1945.
- R5 Rosanoff, R.A. y Ginisburg, T.A., “Matrix error analysis for engineers”, *Proc. First Conf. on Matrix Meth in Struct. Mech.*, Wright-Patterson, Air Force B., Ohio, 1965.
- R6 Rosanoff, R.A., Gloudemann, J.F. y Levy, S., “ Numerical conditioning of stiffness matrix formulations for frame structures”, *Proc. Second Conf. on Matrix Meth. in Struct. Mech.*, Wright–Patterson, AFB, Ohio, 1968 (AFFDL-TR-68-150. Dec, 1969: AD-703-685 N.T.T.S) pp. 1029–60.
- R7 Rossow, M.P. y Chen, K.C., “Computational efficiency of plate elements”, ASCE, 103, St2, pp. 447–51, 1977.
- S1 SAMCEF, “User’s manual”, Samtech Ltd., Lieja, Bélgica, 1991.
- S2 Samuelsson, A., “The global constant strain condition and the patch test”, Ch. **3**, 46–68, *Energy Methods in Finite Element Analysis*, (EdS.) R. Glowinski, E.Y. Rodin y O.C. Zienkiewicz, J. Wiley, 1979.
- S3 Sanders Jr., J.L. y Liepins, A., “Toroidal membrane under internal pressure”, *A.I.A.A.J.*, Vol. **1**, pp. 2105–10, 1963.
- S4 Sander, G., “Bornes superieures et infereures dans l’analyse matricielle des plaques en flexion-torsion”, *Bull Soc. Royale des Sc. de Liege*, Vol. **33**, pp.

456–94, 1964.

- S5 Selman, A., Hinton, E. y Atamaz–Sibai, W., “Edge effects in Mindlin–Reissner plates using adaptive mesh refinement”, Internal Report, Civil Engng. Dpt., Univ. College of Swansea, CR/1948/90, Abril 1990.
- S6 Simó, J.C. y Fox, D.D., “On a stress resultant geometrically exact shell model. Part I: Formulations and optimal parametrizations”, *Computer Methods in Applied Mech and Engng.*, Vol. **72**, pp. 267–304, 1989.
- S7 Simó, J.C., Fox, D.D. y Rifai, M.S., “On a stress resultant geometrically exact shell model. Part II. The linear theory: Computational aspects”, *Computer Methods in Applied Mech and Engng.*, Vol. **73**, pp. 53–92, 1989.
- S8 Simó, J.C. y Hughes, T.J.R., “On the variational formulations of assumed strain methods”, *J. Appl. Mech.*, Vol. **53**, 1, pp.51–4, 1986.
- S9 Specht, B., “Modified shape function for three noded plate bending element passing the patch test”, *Int. J. Num. Meth. Engng.*, Vol. **26**, pp. 705–15, 1988.
- S10 Stanley, G.M., *Continuum based shell elements*, Ph. D. Thesis, Dpt. Appl. Mechanics, Stanford Univ., 1985.
- S11 Stenberg, R. y Vihinen, T., “Calculations with some linear elements for Reissner Mindlin plates”, *European Conf. on New advances in Computational Structural Mechanics*, . P Lavedeze and O.C. Zienkiewicz (Eds.), pp. 505–11, Giens, Abril, 1991
- S12 Stolarski, H. y Belytschko, T. “Membrane locking and reduced integration for curved elements”, *J. Appl. Mech.*, Vol. **49**, pp. 172–6. 1982.
- S13 Stolarski, H., Belytschko, T., Carpenter, N. y Kennedy, J.M., “A simple triangular curved shell element”, *Eng. Comput.*, Vol. **1**, 3, pp. 210–8, 1984.
- S14 Strang, S. y Fix, G.J., *An analysis of the finite element method*, Prentice Hall, 1973.
- S15 Stricklin, J.A., Navaratna, D.R. y Pian, T.H.H., “Improvements in the analysis of shells of revolution by matrix displacement method: Curved elements”, *A.I.A.A.J.*, Vol. **4**, pp. 2069–72, 1966.
- S16 Stricklin, J.A., Haisler, W., Tisdale, P. y Gunderson, R., “A rapidly converging triangular plate element”, *A.I.A.A.J.*, Vol. **7**, pp. 180-1, 1969.
- S17 Suárez, B., *La formulación de bandas finitas de Reissner-Mindlin para análisis de placas, puentes y láminas de revolución*, Tesis Doctoral, E.T.S. de Ingenieros de Caminos, Univ. Politécnica de Catalunya, 1982.
- S18 Suárez, B. y Oñate, E., “Aplicación del método de la banda finita a estructuras laminares prismáticos de espesor variable”, Publicación interna, Centro. Int. de Met. Num. en Ingeniería, Barcelona, 1992.

- S19 Suárez, B. y Martel, E., “Análisis de la presa de Santa Coloma por el método de elementos finitos”, Pub. IT-26, Cent. Int. de Met. Num. en Ing., Barcelona, 1991.
- S20 Suárez, B., y Martel, E., “Análisis del edificio de turbinas de una central hidroeléctrica”, Pub. Cent. Int. de Met. Num. en Ing., Barcelona, 1991.
- T1 Taig, I.C. y Kerr, R.I., “Some problems in the discrete element representation of aircraft structures”, en *Matrix Methods of Structural Analysis*, (Ed. B.M. Fraeijs de Veubeke), Pergamon Press, 1964.
- T2 Taig, O.C., *Structural analysis by the matrix displacement method*, Electric Aviation report, No. 5017, 1961.
- T3 Taylor, R.L., Beresford, P.J. y Wilson, E.L., “A non conforming element for stress analysis”, *Int. J. Num. Meth. Engng.*, Vol. **10**, pp. 1211-20, 1976.
- T4 Taylor, R.L., Zienkiewicz, O.C., Simo, J.C. y Chan, A.H.C., “The patch test - A condition for assessing FEM convergence”, *Int. J. Numer. Meth. Eng.*, Vol. **22**, pp. 32-62, 1986.
- T5 Tessler, A. y Hughes, T.J.R., “An improved treatment of transverse shear in the Mindlin type four quadrilateral element”, *Comp. Meth. in Appl. Mech. and Engng.*, Vol. **39**, pp. 311-35, 1983.
- T6 Timoshenko, S.P. y Goodier, J.N., *Teoría de la elasticidad*, Edic. Urmo, 1968.
- T7 Timoshenko, S.P., *Resistencia de Materiales, Partes I y II*, Espasa-Calpe, 1970.
- T8 Timoshenko S.P. y Woinowsky-Krieger S., *Teoría de Placas y Láminas*, Ediciones Urmo, Bilbao, 1970.
- T9 Timoshenko, S.P., y Young, D.M., *Theory of Structures*, 2d Edition. Mc GrawHill, 1965.
- T10 Timoshenko, S.P. y Gere, J.H., *Mecánica de Materiales*, Unión Tipográfica Editorial Hispano-Americana, 1974.
- T11 Tocher, J.L., *Analysis of plates using triangular elements*, Ph. D. Thesis, Dept. of Civil Engineering, University of California at Berkeley, 1962.
- T12 Turner, M.J., Clough, R.W., Martin, H. y Topp, L.J., “Stiffness and deflection analysis of complex structures”, *J. Aeron. Sci.*, Vol. **23**, pp. 805-23, 1956.
- T13 Tocher, J.L., y Kapur. K.K., “Comment on basis for derivation of matrices for the direct stiffness method”, *A.I.A.A.J.*, Vol. **6**, pp. 1215-16, 1965.
- V1 Vlasov, V.Z., General theory of shells and its application to engineering, *NASA TTF-99*, 1964.
- W1 Washizu, K., *Variational methods in elasticity and plasticity*, Pergamon Press, 1975.

- W2 Weaver, W. (Jr.) y Johnston, P.R., *Finite elements for structural analysis*, Prentice Hall, 1984.
- W3 Wempner, G.A., “Finite elements, finite rotations and small strains of finite shells”, *Int. J. Solids Struct.*, Vol. **5**, pp. 117–53, 1964.
- W4 Wempner, G.A., Oden, J.T. y Kross, D.A., “Finite elements analysis of thin shells”, *Eng. Mech. Div. Proc. ASCE*, Vol. **94**, (EMS), pp. 1273–94, 1968.
- W5 Wilson, E.L., “Structural analysis of axisymmetric solids”, *A.I.A.A.J.*, Vol. **3**, pp. 2269–74, 1965.
- W6 Wilson, E.L., Taylor, R.L., Doherty, W.P. y Ghabussi, T., “Incompatible displacement models” en *Numerical and Computer Methods in Structural Mechanics*, (Eds.) S.T. Fenves, *et al.*, Academic Press, 1973.
- W7 Wilson, E.L., “Finite elements for foundations, joints and fluids”, *Proc. Conf. on Numerical Methods in Soil and Rock Mechanics*, Univ. of Kalsruhe, J. Wiley, 1977.
- W8 Willam, K.J. y Scordelis, A.C., “Cellular structures of arbitrary plan geometry”, *J. Struct. Div.*, ASCE, pp. 1377–442, 1972.
- W9 Wood, R.D., *The application of finite element methods to geometrically non linear analysis*, Ph. D. Thesis, Univ. of Wales, Swansea, 1973.
- W10 Wood, R.D. y Zienkiewicz, O.C., “Geometrically non linear finite element analysis of beams, frames, arches and axisymmetric shells”, *Comp. Struct.*, Vol. **7**, pp. 725–35, 1977.
- W11 Wong, C.C.K. y Vardy, A.E., “Finite prism analysis of plates and shells”, *Int. Journ. Num. Meth. Engng.*, Vol. **21**, pp. 529–41, 1985.
- Y1 Yang, T.Y., *Finite Element Structural Analysis*, Prentice Hall, 1986.
- Z1 Zienkiewicz, O.C. y Cheung, Y.K., “The finite element method for analysis of elastic isotropic and isotropic slabs”, *Proc. Inst. Civ. Engng.*, Vol. **28**, pp. 471–88. 1964.
- Z2 Zienkiewicz, O.C., Kalliappan, S. y King, I.P., “Stress analysis of rock as a no tension material”, *Geotechnique*, Vol. **18**, PP. 56, 1968.
- Z3 Zienkiewicz, O.C., Too, J. y Taylor, R.L., “Reduced integration techniques in general analysis of plates and shells”, *Int. J. Num. Meth. Eng.*, Vol. **3**, pp. 275–90, 1971.
- Z4 Zienkiewicz, O.C. y Too, J. “The finite element prism in analysis of thick simply supported bridges”, *Proc. Inst. Civ. Eng.*, Vol. **53**, pp. 147–72, 1972.
- Z5 Zienkiewicz, O.C., Bauer, J., Morgan, K. y Oñate, E., “A simple and efficient shell element for axisymmetric shells”, *Int. J. Num. Meth. Engng.*, Vol. **11**,

pp. 1545–1559, 1977.

- Z6 Zienkiewicz, O.C., *El Método de los Elementos Finitos*, 3^{era} Edición, Ed. Reverté, Barcelona, 1979.
- Z7 Zienkiewicz, O.C. y Morgan, K., *Finite Elements and Approximations*, Ed. J. Wiley, 1980.
- Z8 Zienkiewicz, O.C., Qu, S., Taylor, R.L. y Nakazawa, S., “The Patch test for mixed formulations”, *Int. J. Num. Meth. Eng.*, Vol. **23**, pp. 1873–1883, 1986.
- Z9 Zienkiewicz, O.C. y Lefebvre, D., “Three field mixed approximation and the plate bending problem”, *Comm. Appl. Numer. Meth.*, Vol. **3**, pp. 301–9, 1987.
- Z10 Zienkiewicz, O.C. y Zhu, J.Z., “A simple error estimator and adaptive procedure for practical engineering analysis”, *Int. J. Num. Meth. Engng.*, Vol. **24**, pp. 337–57, 1987.
- Z11 Zienkiewicz, O.C. y Lefebvre, D., “A robust triangular plate bending element of the Reissner-Mindlin type”, *Int. J. Num. Meth. Eng.*, Vol. **26**, pp. 1169–84, 1988.
- Z12 Zienkiewicz, O.C. and Zhu, J.Z. “Error estimates and adaptive refinement for plate bending problems”, *Int. J. Num. Meth. Engng.*, Vol. **28**, pp. 2839–543, 1989.
- Z13 Zienkiewicz, O.C. y Zhu, J.Z., “The three R 's of engineering analysis and error estimation and adaptivity”, *Comp. Meth. in Appl. Mech and Engng.*, Vol. **82**, pp. 95–113, 1990.
- Z14 Zienkiewicz, O.C., Taylor, R.L., Papadopoulos P. y Oñate, E., “Plate bending elements with discrete constraints: New Triangular Elements”, *Computer and Struct.*, Vol. **35**, pp. 4, 505–2, 1990.
- Z15 Zienkiewicz, O.C. y Taylor, R.L. *The Finite Element Method*, 4^a Ed., Mc Graw Hill, Vol. I, 1989, Vol. II, 1991.
- Z16 Zienkiewicz, O.C. y Zhu, J.Z. “Superconvergent derivative recovery techniques and a posteriori error estimations in the finite element method. Part I: A General superconvergent recovery technique”, Internal report CR/671/91, Univ. College of Swansea, U.K., 1991, A publicarse en *Int. J. Num. Meth. Engng.*
- Z17 Zienkiewicz, O.C. y Zhu, J.Z., “Superconvergent derivative recovery techniques and a posteriori error estimations in the finite element method. Part II: The Zienkiewicz-Zhu a posteriori error estimator”, Internal report CR/672/91, Univ. College of Swansea, U.K., 1991. A publicarse en *Int. J. Meth. Engng.*